DESERTIFICATION AND REHABILITATION

EDITED BY: Xian Xue, Atsushi Tsunekawa and Caroline King-Okumu
PUBLISHED IN: Frontiers in Environmental Science and
Frontiers in Earth Science

frontiers Research Topics

ISSN 1664-8714
ISBN 978-2-88976-720-5
DOI 10.3389/978-2-88976-720-5

About Frontiers

Frontiers is more than just an open-access publisher of scholarly articles: it is a pioneering approach to the world of academia, radically improving the way scholarly research is managed. The grand vision of Frontiers is a world where all people have an equal opportunity to seek, share and generate knowledge. Frontiers provides immediate and permanent online open access to all its publications, but this alone is not enough to realize our grand goals.

Frontiers Journal Series

The Frontiers Journal Series is a multi-tier and interdisciplinary set of open-access, online journals, promising a paradigm shift from the current review, selection and dissemination processes in academic publishing. All Frontiers journals are driven by researchers for researchers; therefore, they constitute a service to the scholarly community. At the same time, the Frontiers Journal Series operates on a revolutionary invention, the tiered publishing system, initially addressing specific communities of scholars, and gradually climbing up to broader public understanding, thus serving the interests of the lay society, too.

Dedication to Quality

Each Frontiers article is a landmark of the highest quality, thanks to genuinely collaborative interactions between authors and review editors, who include some of the world's best academicians. Research must be certified by peers before entering a stream of knowledge that may eventually reach the public - and shape society; therefore, Frontiers only applies the most rigorous and unbiased reviews.
Frontiers revolutionizes research publishing by freely delivering the most outstanding research, evaluated with no bias from both the academic and social point of view. By applying the most advanced information technologies, Frontiers is catapulting scholarly publishing into a new generation.

What are Frontiers Research Topics?

Frontiers Research Topics are very popular trademarks of the Frontiers Journals Series: they are collections of at least ten articles, all centered on a particular subject. With their unique mix of varied contributions from Original Research to Review Articles, Frontiers Research Topics unify the most influential researchers, the latest key findings and historical advances in a hot research area! Find out more on how to host your own Frontiers Research Topic or contribute to one as an author by contacting the Frontiers Editorial Office: frontiersin.org/about/contact

DESERTIFICATION AND REHABILITATION

Topic Editors:
Xian Xue, Northwest Institute of Eco-Environment and Resources, Chinese Academy of Sciences (CAS), China
Atsushi Tsunekawa, Tottori University, Japan
Caroline King-Okumu, The Borders Institute (TBI), Kenya

Citation: Xue, X., Tsunekawa, A., King-Okumu, C., eds. (2022). Desertification and Rehabilitation. Lausanne: Frontiers Media SA. doi: 10.3389/978-2-88976-720-5

Table of Contents

frontiers | Frontiers in Environmental Science

EDITORIAL
published: 08 July 2022
doi: 10.3389/fenvs.2022.874963

Editorial: Desertification and Rehabilitation

Xian Xue[1], *Atsushi Tsunekawa*[2] *and Caroline King-Okumu*[3,4]*

[1]Northwest Institute of Eco-Environment Resources, Chinese Academy of Sciences (CAS), Beijing, China, [2]Arid Land Research Center, Tottori University, Tottori, Japan, [3]The Borders Institute (TBI), Africa, Nairobi, Kenya, [4]GeoData Institute, School of Geography and Environmental Science, Faculty of Environmental and Life Sciences, University of Southampton, Southampton, United Kingdom

Keywords: climate change, human activities, degradation, restoration, rehabilitation, sustainable development

Editorial on the Research Topic

Desertification and Rehabilitation

INTRODUCTION

Desertification, resulting from climatic variability and irrational human activities, is currently one of the most important environmental problems. Because desertification has brought poverty, famine, and displacement, hindering the improvement of eco-environment and social-economy in the developing countries and regions, it has attracted the attention of the whole world. Since 1994, when the United Nations Convention to Combat Desertification (UNCCD) was established, all kinds of battles against desertification have been conducted worldwide with hopes to bring about a positive change.

Nevertheless, a large number of questions concerning desertification still remain, depending on the different contexts and objectives of national strategies (Xue et al., 2015; Muñoz-Rojas et al., 2021). The large gap between sciences and policies concerning the rehabilitation of the desertified land requires urgent attention in many countries. To design effective land restoration and rehabilitation strategies and achieve the global goals for sustainable development, including Land Degradation Neutrality, a systemic and comprehensive understanding of desertification and rehabilitation is necessary (see discussions in: Wang et al., 2015; Kong et al., 2021; Xue, 2022). Following a brief conceptual overview and an introduction to the context and planning of Chinese national investments in land rehabilitation, this Editorial introduces fifteen collected contributions to this debate from interested scientists in China.

Due to the scale of the land degradation, desertification and drought challenges in China, it accounts for a large portion of the total area of degraded land globally (Alexander et al., 2019)[1]. The achievement of the global target for land degradation neutrality and the objectives of the UN Decade on Ecosystem Restoration will depend on significant progress to be made in China. The Chinese Government is investing heavily in the achievement of its ecological objectives, and reporting substantial achievements (PRC, 2021). For example, from 2015 to 2018, the net area of land restored in China was calculated to account for about one fifth of the global total. On this basis, the 2021 Chinese Voluntary National Review stated that China had restored more land than any other country (PRC, 2021 p28). The role of Chinese scientists, and their commentaries on this achievement should

[1]See: https://knowledge.unccd.int/glo/global-land-outlook-glo.

OPEN ACCESS

Edited by:
Ioan Cristian Ioja,
University of Bucharest, Romania

Reviewed by:
Alexandru-Ionut Petrisor,
Ion Mincu University of Architecture and Urbanism, Romania
Mihai Razvan Nita,
University of Bucharest, Romania

****Correspondence:***
Caroline King-Okumu
caroking@yahoo.com

Specialty section:
This article was submitted to Land Use Dynamics, a section of the journal Frontiers in Environmental Science

Received: *13 February 2022*
Accepted: *02 May 2022*
Published: *08 July 2022*

Citation:
Xue X, Tsunekawa A and King-Okumu C (2022) Editorial: Desertification and Rehabilitation. Front. Environ. Sci. 10:874963. doi: 10.3389/fenvs.2022.874963

therefore be of considerable interest to the international-science-policy community (Kong et al., 2021).

CONCEPTUAL FRAMINGS OF DESERTIFICATION, DEGRADATION, REHABILITATION AND RESTORATION

According to the UNCCD, "desertification" means land degradation in arid, semi-arid and dry sub-humid areas resulting from various factors, including climatic variations and human activities; "land" means the terrestrial bio-productive system (that comprises soil, vegetation, other biota, and the ecological and hydrological processes that operate within the system); and "land degradation" means reduction or loss of the biological or economic productivity and complexity in that terrestrial system. More recently, the millennium ecosystem assessment has defined measures of productivity (or loss of productivity) in terms of ecosystem services. The Paris Agreement has captured emerging understanding of the complexity of food-related aspects of the terrestrial system.

According to the United Nations Convention for Combatting Desertification (Article 1b)[2], "Combating desertification" includes activities which are part of the integrated development of land for sustainable development which are aimed at: (i) prevention and/or reduction of land degradation; (ii) rehabilitation of partly degraded land; and (iii) reclamation of desertified land. Rehabilitation aims to improve to some degree a degraded site by re-establishing associated ecosystem functions such as trophic interactions, water, and nutrient cycles (Gurr et al., 2014). The goals are determined by what society wants and needs, the level of degradation, and the economic, political, and social environment (Gurr et al., 2014). Dryland ecologists observe a distinction between the limited objectives of ecosystem rehabilitation versus the more ambitious agenda for ecological restoration (Aronson et al., 1999; Alexander et al., 2016).

Rehabilitation is used to refer to restoration activities that may fall short of fully restoring the biotic community to its pre-degradation state, including natural regeneration and emergent ecosystems (Fisher et al., 2018 p6). The Society for Ecological Restoration (SER) defines standards for rehabilitation as follows (Gann et al., 2019):

Rehabilitation–management actions that aim to reinstate a level of ecosystem functioning on degraded sites, where the goal is renewed and ongoing provision of ecosystem services rather than the biodiversity and integrity of a designated native reference ecosystem.

Alexander et al. (2016) observe the focus of rehabilitation activities on functionality and the delivery of targeted services more than on reinstating the pre-disturbance system condition in all its biological complexity (as restoration does). They maintain that rehabilitation may in fact be the only option in situations where degradation has passed a point of no return, where species have become extinct, or where seed and soil biota have all been lost. Furthermore, rehabilitation is more in line with the immediate aspirations of the public and decision-makers.

Globally, it appears that there will be some challenges to be faced over the coming years in order for policy-makers to be able to monitor and report successes achieved in relation to land restoration targets. Rehabilitation is more feasible to monitor than restoration. This can be done in terms of emerging economic environmental accounts that capture the stocks and flows of ecosystem services of value to the human population, including provisioning services and selected supporting and regulating services that are measurable in many parts of the developing world through the emerging systems for water accounting alongside other aspects of natural capital accounting (UNEP, 2021a; UNEP, 2021b).

A range of case studies of successful rehabilitation are available from the Intergovernmental Panel on Biodiversity and Ecosystem Services, whereas the case studies of success in restoration were fewer (IPBES, 2019). The Hunshandak Sandland, Inner Mongolia, China, was one of the few case study examples of restoration success presented in this assessment.

Dryland ecologists have frequently observed that for the most degraded areas, rehabilitation is a more feasible objective and a necessary first step toward restoration (Aronson et al., 1999). According to Le Floc'h et al. (1999):

"The main objective of ecological rehabilitation is to pilot trajectories of disturbed ecosystems so that they may recover their main functions, including productivity, via intensive interventions of relatively short duration. Rehabilitated ecosystems should become autonomous and have sufficient resilience to recover after moderate disturbances."

Aronson et al. (1999) observed that thereafter, it could be possible either to proceed toward full restoration or else to "pilot" the systems in question in other directions according to local needs and priorities and, of course, the potentialities of local climate and soils. But until that first level of reparation is achieved, nothing else, longterm, is realistically possible. They argued that this, in a nutshell, was the situation of almost all the populous dryland regions in the world by the early 1990s.

In 2020, the international community has launched a UN Decade for Ecosystem Restoration in pursuit of the ambitious agenda of Ecosystem Restoration and are calling upon governments to invest commensurately (UNEP, 2021b). To track progress of efforts to restore degraded ecosystems for the United Nations Decade on Ecosystem Restoration, a Framework for Ecosystem Restoration Monitoring has been established[3]. Already, all governments have made a commitment to achieve a universal global goal to neutralize land degradation. Many governments have published targets and strategies for achievement of this within their countries, and a number have voluntarily reviewed their progress so far (Sewell et al., 2020)[4].

[2]Available in all 5 UN Languages including Chinese and English from: https://www.unccd.int/convention/about-convention.

[3]https://www.fao.org/national-forest-monitoring/ferm/en/.

[4]See: https://knowledge.unccd.int/ldn/ldn-monitoring/sdg-indicator-1531 and also https://landportal.org/book/sdgs/1531/sdgs-indicator-1531 and https://trends.earth/docs/en/ and all VNRs at: https://sustainabledevelopment.un.org/vnrs/.

For decades, whereas, ecological restoration has been recognized as a challenging objective, requiring massive investment over a long period of time, scientists have considered that rehabilitation is a feasible and realistic first step that can be taken toward it and which can be pursued across a wider area (Aronson et al., 1999; Wang et al., 2015). For example, they have argued that 100 million hectares could be rehabilitated immediately for the same cost or less than what it would take to fully restore 1,000 ha (see p316 in Aronson et al., 1999).

From both ecological and economic perspectives, rehabilitation is still recognized as often the most pragmatic response to be taken in cases where all stakeholders can agree that land degradation has occurred (Alexander et al., 2016). Rehabilitation is also still considered the first step that can be taken and achieved rapidly toward full-scale restoration to follow over the longer term. Scientists across the developing world remain aware of the relevance and value of the differentiated objective of ecological rehabilitation (Tlili et al., 2018; Tlili et al., 2020), as a contribution to the global agenda for ecosystem restoration. Not only does it positively support and move beyond the agenda for land degradation neutrality, but it also builds in greater feasibility, measurability and achievability for decision-makers who are also committed to the achievement of ecological restoration, recovery and the creation of a new green economy.

A further differentiation of terms between restoration, rehabilitation and reclamation has been highlighted recently by the SER (Gerwing et al., 2021) which observes that when rehabilitation occurs on mined lands or post-industrial sites, it is sometimes, but not always, called reclamation; suggesting that reclamation could be considered as conceptually nested within rehabilitation. In practice, the delineation between these two terms, as well as their relationship to ecological restoration, is unclear.

BACKGROUND TO DESERTIFICATION AND REHABILITATION DEBATES IN CHINA

According to the Chinese Voluntary National Review of the Sustainable Development Goals/SDGs (PRC, 2021 p28), in China:

"Desertification has been checked across 10 million hectares, leading to a drop in both area and intensity of desertification in three consecutive monitoring periods. Compared with 2011, the area of rocky desertification has shrunk by 1.932 million hectares; the sediment in the Yangtze River basin is down by more than 40%; 61.4% of the rocky desertification areas are covered by vegetation. From 2015 to 2018, net restored land in China accounted for about one fifth of the global total, ranking first in the world."

Reported positive changes are particularly concentrated in the North-Central part of China and Northeast (**Figure 1**).

On August 15, 2005, Xi Jinping, then secretary of the CPC Zhejiang Provincial Committee shared his vision that "Lucid waters and lush mountains are as good as mountains of gold and silver." In 2017, this vision was written into the report of the 19th CPC National Congress and the revised CPC Constitution as a guiding principle for coordinated development and conservation. It also informed a report on the national targets for land degradation neutrality in China (PRC, 2017). Also in 2017, to advance global efforts to control desertification, China hosted CoP 13 of the United Nations Convention to Combat Desertification. This was the first CoP China has ever hosted in the UN environmental field. Through this and subsequent CoPs, the Chinese experience and solutions were shared with other Parties.

In 2021, the Chinese government has issued policies on accelerating the establishment of a sound, green, low carbon and circular economic system and on establishing a mechanism for realizing the value of ecosystem products, as part of the effort to put in place a policy system to promote green development. The Chinese VNR (PRC, 2021) also highlights China's *14th Five-year Plan for National Economic and Social Development and Vision 2035 which* covers the immediate next 5 years and also outlines a medium-term vision. It is essentially compatible with the SDGs which integrate economic, social and environmental dimensions and cover five key elements: People, Planet, Prosperity, Peace and Partnership. During the 14th Five-year Plan period, China will strive to achieve high-quality development, balanced social progress and harmony between man and nature through economic growth, innovation, improvement in people's well-being and ecological conservation.

The role of science in enabling effective monitoring and understanding of processes taking place in the rehabilitated ecosystems is critical (Xue et al., 2015; Xue, 2022). Chinese scientists have raised many questions about the feasibility of extensive afforestation in arid and semi-arid areas and the negative effects of afforestation on soil water, groundwater levels, and surface runoff. As increased drought has been considered to contribute to the degradation of the water environment, scientists have investigated the increasing demands for water that are created by the expansion of the afforestation area. A second question that is, frequently raised concerns the impact of grazing exclusion and ecological migration on the stability and diversity of rangeland ecosystems and the local cultural traditions: Can the no-grazing-induced increase in the vegetation cover be considered to signify the reversal of degraded rangeland?

Alongside these, a new battle against deserts (not desertification) is raging in modern China. This involves a struggle to transform the natural or semi-natural land such as dune fields by planting tree species where nature did not intend that they should grow. However, scientists have observed that this can be counter-productive—resulting in increased erosion rather than stablization of mobile sand dunes (Wang et al., 2015). These three issues directly affect the sustainability of desertification control in China.

There is a need for decision-makers to maintain the balance of the coupled human-environmental system while making full use of their human capability as leaders to formulate policies and measures. Although land degradation and restoration are chronic long-term processes, government planning horizons must plan and budget in shorter-term phases. Where designed and implemented effectively, these can support a rapid recovery in vegetation cover and biomass. In light of this, a recent commentary by researchers at the Chinese Academy of Sciences (Xue, 2022) focuses on goals and principles that could guide and inform better policy and planning, by improving the available understanding of the concepts, assessment criteria, and causes of desertification in China. Until they do this, the target for Zero Net Land Degradation (ZNLD) cannot be achieved in China or globally.

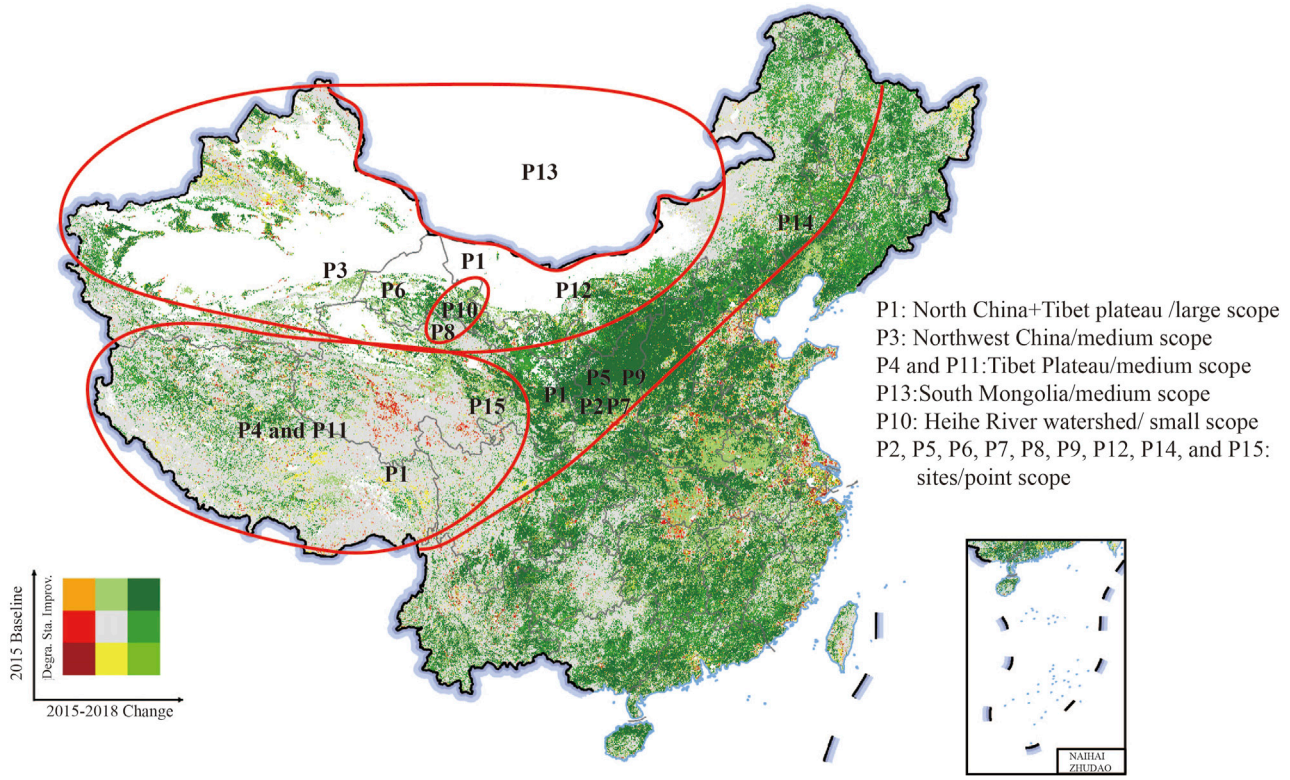

FIGURE 1 | Reported dynamics of land restoration in China (2018) and location of papers in this issue (prepared by Xian Xue from original map provided by Li et al. (2021), and presented in PRC (2021)).

TABLE 1 | Overview of papers included in this Special Issue.

Author name	Climate/ecological conditions	Landcover/land use/Ecosystems	Features under observation	Methods of observation
Wang et al.	Arid, semi arid and sub-humid	All vegetation	NDVI	RS
Zou et al.	Semi-arid	Forest	Methods approach	Field observation, and experiment
Guojing et al.	Arid and semi-arid	Forest	Plants	data and documents analysis
Huang et al.	Alpine	Grassland	Plant and soil	Field observation
Zhang et al.	Semi-Arid	Sandy land	Fungi	Field observation
Cui et al.	Arid	Sandy land and Gobi	Soil water	Field observation
Gu et al.	Semi-Arid	Agro-pastoral ecotone	Plant and soil	Field observation
Wang et al.	Arid	Oasis and desert	Soil water	Field observation
Li et al.	Semi-Arid	Sandy land	Erosion	Experiment
Song et al.	Arid	Oasis and desert	Land cover	RS
Zhang and Sun	Alpine	Grassland	Plant	Field observation
Qu et al.	Arid	Grassland	Litter	Field observation
Kim et al.	Arid	Gobi desert	Erosion	RS
Wang et al.	Sub-humid	Agro-pasture ecotone	Cellulose decomposer	experiment
Zhu and Wang	Alpine	Grassland	Plant	Field observation

OVERVIEW OF THE SPECIAL ISSUE CONTRIBUTIONS

Researchers from the Chinese Academy of Sciences have led the preparation of this Special Issue in Frontiers in Earth Science to share with international scientific community some of the high-quality research from different fields of research that is, ongoing in China on desertification and restoration (**Figure 1**; **Table 1**).

The papers range from broadscale overviews of the effectiveness of land restoration practices, as observed using remote sensing techniques, to finer scaled studies conducted at the field level and in the laboratories of the Chinese Academy of Sciences. Some of the studies involve experiments designed and conducted to increase the available knowledge of plants, soils and hydrological responses under the effects of rehabilitation or degradation processes.

The contributions help the scientific community to better understand the dynamics of land degradation, desertification and rehabilitation. Insights address current issues and solutions to improve the ongoing national investments in land restoration and rehabilitation to enable economic growth, innovation, improvement in people's well-being and ecological conservation.

They contribute to understanding China's policies and measures for neutralizing land degradation and raise questions for the future. For example, one of the papers analyses over half a century (7 decades) of investments in afforestation in Northwest China. They also highlight questions relating to the effects on ecosystems and livelihoods that have been achieved through fencing and grazing prohibition measures adopted in the North-eastern grasslands of the Qinghai-Tibet Plateau. Such measures have been carried out in Northern China, especially Inner Mongolia. However, as yet, these could not be fully evaluated. Furthermore, the papers reflect on questions concerning the effects of land restoration policies on hydrological conditions in the drier regions. For example, the article on the dynamics of soil-water content in the desert-oasis ecotone shows that some of the practices currently being implemented for ecological restoration purposes may in fact be exacerbating soil-water deficits and drought risks.

We conclude that further research on these questions will require close collaboration between geographers, ecologists, and social scientists to ensure a multi-angle analysis of sustainable degraded land restoration policies. This learning could help to achieve the anticipated transitions through ongoing investments in land rehabilitation and restoration.

AUTHOR CONTRIBUTIONS

All authors listed have made a substantial, direct, and intellectual contribution to the work and approved it for publication.

REFERENCES

Alexander, S., Aronson, J., Whaley, O., and Lamb, D. (2016). The Relationship between Ecological Restoration and the Ecosystem Services Concept. *Ecol. Soc.* 21, 34. doi:10.5751/es-08288-210134

Aronson, J., Dhillion, S., and Floc'H, E. L. (1999). Dryland Restoration and Rehabilitation. *Arid Soil Res. Rehabilitation* 13, 315–317. doi:10.1080/089030699263203

Fisher, J., Montanarella, L., and Scholes, R. (2018). "Chapter 1: Benefits to People from Avoiding Land Degradation and Restoring Degraded Land," in *The IPBES Assessment Report on Land Degradation and Restoration*. Editors L. Montanarella, R. Scholes, and A. Brainich (Bonn, Germany: Secretariat of the Intergovernmental Panel on Biodiversity and Ecosystem Services IPBES).

Gann, G. D., Mcdonald, T., Walder, B., Aronson, J., Nelson, C. R., Jonson, J., et al. (2019). International Principles and Standards for the Practice of Ecological Restoration. Second Edition. *Restor. Ecol.* 27, S1–S46. doi:10.1111/rec.13035

Gerwing, T. G., Hawkes, V. C., Gann, G. D., and Murphy, S. D. (2021). Restoration, Reclamation, and Rehabilitation: on the Need for, and Positing a Definition of, Ecological Reclamation. *Restor. Ecol.*, e13461. doi:10.1111/rec.13461

Gurr, G. M., Johnson, A. C., and Liu, J. (2014). "Land Use: Restoration and Rehabilitation," in *Encyclopedia of Agriculture and Food Systems*, Vol. 4, 139–147.

IPBES (2019). *Assessment Report on Land Degradation and Restoration*. Nairobi, Kenya: Intergovernmental Panel on Biodiversity and Ecosystem Services.

Kong, Z. H., Stringer, L. C., Paavola, J., and Lu, Q. (2021). Situating China in the Global Effort to Combat Desertification. *Land* 10 (7), 702. doi:10.3390/land10070702

Le Floc'h, E., Neffati, M., Chaieb, M., Floret, C., and Pontanier, R. (1999). Rehabilitation Experiment at Menzel Habib, Southern tunisia. *Arid Soil Res. Rehabilitation* 13, 357–368.

Li, X. S., Qi, L., and Xiaoxia, J. (2021). Harnessing Big Earth Data to Facilitate Land Degradation Neutrality Goals—Practices and Prospects. *Bull. Chin. Acad. Sci.* 36, 896–903. (in Chinese).

Muñoz-Rojas, M., Hueso-Gonzalez, P., Branquinho, C., and Baumgartl, T. (2021). Restoration and Rehabilitation of Degraded Land in Arid and Semiarid Environments: Editorial. *Land Degrad. Dev.* 32, 3–6. doi:10.1002/ldr.3640

PRC (2017). *China National Committee to Implement the UNCCD (CCICCD) China Final National Report of the Voluntary Land Degradation Neutrality (LDN) Target Setting Programme December 2017*. People's Republic of China.

PRC (2021). *China's VNR Report on Implementation of the 2030 Agenda for Sustainable Development*. Beijing: Ministry of Foreign Affairs of the People's Republic of China June 2021.

S. Alexander, U. Kang, and J. Xiosha (Editors) (2019). *The Global Land Outlook, Northeast Asia Thematic Report* (Bonn, Germany: United Nations Convention to Combat Desertification).

Sewell, A., Esch, S. V. D., and Löwenhardt, H. (2020). *Goals and Commitments for the Restoration Decade: A Global Overview of Countries' Restoration Commitments under the Rio Conventions and Other Pledges*. The Hague: PBL Netherlands Environmental Assessment Agency.

Tlili, A., Ghanmi, E., Ayeb, N., Louhaichi, M., Neffati, M., and Tarhouni, M. (2020). Revegetation of Marginal Saline Rangelands of Southern Tunisia Using Pastoral Halophytes. *Afr. J. Range Forage Sci.* 37, 151–157. doi:10.2989/10220119.2020.1720293

Tlili, A., Tarhouni, M., Cerdà, A., Louhaichi, M., and Neffati, M. (2018). Comparing Yield and Growth Characteristics of Four Pastoral Plant Species under Two Salinity Soil Levels. *Land Degrad. Dev.* 29, 3104–3111. doi:10.1002/ldr.3059

UNEP (2021a). "Ecosystem Restoration Playbook," in *UN Decade on Ecosystem Restoration*.

UNEP (2021b). *State of Finance for Nature 2021*. Nairobi: United Nations Environment Programme.

Wang, T., Xue, X., Zhou, L., and Guo, J. (2015). Combating Aeolian Desertification in Northern China. *Land Degrad. Dev.* 26, 118–132. doi:10.1002/ldr.2190

Xue, X. (2022). "Chapter 7 Goals and Principles for Combating Aeolian Desertification," in *Combating Aeolian Desertificaiton in Northeast Asia*. Editors T. Wang, A. Tsunekawa, X. Xue, and Y. Kurosaki (Singapore: SpringerNature).

Xue, X., Liao, J., Hsing, Y., Huang, C., and Liu, F. (2015). Policies, Land Use, and Water Resource Management in an Arid Oasis Ecosystem. *Environ. Manag.* 55, 1036–1051. doi:10.1007/s00267-015-0451-y

Conflict of Interest: The authors declare that the research was conducted in the absence of any commercial or financial relationships that could be construed as a potential conflict of interest.

frontiers in Environmental Science

ORIGINAL RESEARCH
published: 30 June 2020
doi: 10.3389/fenvs.2020.00088

Increasing Precipitation Interval Has More Impacts on Litter Mass Loss Than Decreasing Precipitation Amount in Desert Steppe

Hao Qu[1], Xueyong Zhao[1,2], Jie Lian[2], Xia Tang[2], Xinyuan Wang[3] and Eduardo Medina-Roldán[4]**

[1] Urat Desert-Grassland Research Station, Northwest Institute of Eco-Environment and Resources, Chinese Academy of Sciences, Lanzhou, China, [2] Naiman Desertification Research Station, Northwest Institute of Eco-Environment and Resources, Chinese Academy of Sciences, Lanzhou, China, [3] Ecological Environmental Supervision and Administration Bureau of Gansu Province, Lanzhou, China, [4] Health and Environmental Science Department, Xi'an Jiaotong Liverpool University, Suzhou, China

OPEN ACCESS

Edited by:
Xian Xue,
Northwest Institute of Eco-Environment and Resources (CAS), China

Reviewed by:
Guodong Han,
Inner Mongolia Agricultural University, China
Jianshuang Wu,
Chinese Academy of Agricultural Sciences, China

***Correspondence:**
Hao Qu
quhao@lzb.ac.cn
Eduardo Medina-Roldán
eduardo.medina-roldan@xjtlu.edu.cn

Specialty section:
This article was submitted to Soil Processes, a section of the journal Frontiers in Environmental Science

Received: 08 February 2020
Accepted: 29 May 2020
Published: 30 June 2020

Citation:
Qu H, Zhao X, Lian J, Tang X, Wang X and Medina-Roldán E (2020) Increasing Precipitation Interval Has More Impacts on Litter Mass Loss Than Decreasing Precipitation Amount in Desert Steppe. Front. Environ. Sci. 8:88. doi: 10.3389/fenvs.2020.00088

Litter mass loss and nutrient release are key links in the material cycling and energy flowing in ecosystems and of special ecological significance in maintaining ecosystem stability, improving soil structure, and promoting vegetation restoration in the arid and semi-arid regions. Furthermore, litter mass loss could be affected by the change in precipitation patterns. However, currently, most studies on the response of litter mass loss to precipitation pattern change focus on the precipitation amount much more than the precipitation frequency. Therefore, we conducted a 3-year manipulative research in a desert steppe to assess the effects of decreasing precipitation amount and increasing precipitation interval on the litter mass loss of *Stipa klemenzii* and their relationships with litter chemical traits [contents of carbon (C), nitrogen (N), phosphorus (P), potassium (K), lignin and ash, C/N ratio, and lignin/N ratio] and abiotic factors (light intensity and temperature and humidity of soil and air). The results showed that (1) both treatments have negative effects on litter mass loss; (2) for abiotic factors, both treatments affected only soil moisture; for biotic factors, both treatments decreased the litter lignin contents; the increased precipitation interval treatment decreased the litter N and K contents, but increased the litter C/N ratio and lignin/N ratio; (3) the main control of litter mass loss was due to our manipulation of drought regime and its effects on the soil decomposition environment, rather than to other factors such as litter quality or light intensity; (4) compared to decreased precipitation amount, increased precipitation interval has more impact on litter mass loss, and this was caused by the increased litter C/N ratio in increased precipitation interval treatment. We speculated that increased precipitation interval was a harsher abiotic factor for the decomposer, and more research on this should be conducted in the future.

Keywords: litter decomposition, precipitation patterns, arid region, C/N ratio, lignin content

INTRODUCTION

Recently, global climate change has altered precipitation pattern and extended time intervals between precipitation events (Easterling et al., 2000; Intergovernmental Panel on Climate Change [IPCC], 2014). In arid and semi-arid regions, precipitation is the most important source of water (Easterling et al., 2000), and its spatial and temporal distribution determines plant colonization and growth, biomass production and distribution, litter mass loss, and nutrient release (Hobbie et al., 2001; Salinas et al., 2011). This, in turn, restricts the formation and development of vegetation communities and affects climate change by changing the cycle of carbon and water (Davidson and Janssens, 2006; Bonan et al., 2013). However, the phenomenon of extreme drought is frequent, represented by an increase in the interval of precipitation events or decreasing amount of precipitation (Min et al., 2011; Intergovernmental Panel on Climate Change [IPCC], 2014; Knapp et al., 2017).

Among the biogeochemical cycles affected by precipitation, litter mass loss and nutrient release are key links in the material and energy cycle within an ecosystem and play a decisive role in soil properties and plant productivity (Zhang et al., 2013). Moreover, a small change in the rate of decomposition can significantly affect soil carbon budget, soil fertility status, and land-atmosphere carbon exchange (Currie et al., 2010; Potthast et al., 2012; Wang et al., 2014). Previous studies showed that more than 90% of nitrogen and phosphorus required for plant growth were derived from the nutrient release during litter decomposition (Chapin et al., 2002), indicating that litter decomposition is important for maintaining ecosystem nutrient balance (Aerts et al., 2003). Compared with other ecosystems, the soils in drylands are very poor in organic matter, and the element cycling and energy flow are slow (Poulter et al., 2014). Thus, plant biomass product is strongly dependent on leaf litter decomposition (Killingbeck, 1996). Therefore, in the arid and semi-arid regions, there is a special ecological significance of litter decomposition in maintaining ecosystem stability, improving soil structure, and promoting vegetation restoration (Cornwell et al., 2008).

Litter decomposition is a complex process, which is controlled by both biotic and abiotic factors (Berg and McClaugherty, 2003; Jacotot et al., 2019). Among abiotic factors, precipitation is the most important factor affecting litter decomposition and nutrient release (Pucheta et al., 2006; Brandt et al., 2007). First, precipitation can directly accelerate the decomposition of litter by nutrient leaching (Clein and Schimel, 1994; Franklin et al., 2020). Second, precipitation can also affect decomposition and nutrient release from litter by affecting the activities of soil microbes and soil animals (Berg, 1986; Clein and Schimel, 1994). Third, precipitation can indirectly affect the rate of decomposition by changing the chemical composition of litter (Pastor and Post, 1988; Austin and Vitousek, 2000). Because rainfall and high temperatures are mostly synchronous in arid and semi-arid regions, this is conducive to higher activity of soil microbes, thus accelerating the decomposition of litter (Wang et al., 2013). However, there are significant variations in the availability of water in reality, which in turn makes the biotic and abiotic functions significantly different, leading to differences in the effects of precipitation on litter decomposition (Austin et al., 2004). Some researchers have stated that drought can reduce litter decomposition rate in arid and semi-arid ecosystems. For instance, Whitford et al. (1995) conducted water removal and addition experiments in the Chihuahuan Desert. They found that the decomposition of litter had different responses to dry and wet treatments and that only the water removal treatment reduced the decomposition rate of litter. In the Patagonian steppe, reducing precipitation by 30% in the rainless season significantly reduced the decomposition rate of *Stipa speciosa* litter (Yahdjian et al., 2006). However, other studies have suggested that reducing precipitation had little effect on the decomposition of litter in arid and semi-arid regions, because microorganisms in these areas can adjust their own C/N to ensure the decomposition of litter (Parton et al., 2007).

The effect of precipitation on the decomposition of litter can also vary as a result of changes in the amount of annual precipitation, but observations on this aspect are not consistent either (McCulley et al., 2005). Some studies have found that the decomposition rate of litter is positively correlated with precipitation in areas with high precipitation, but in areas with annual precipitation below 300 mm, the decomposition rate is not related to actual precipitation (Austin and Vitousek, 2000; Epstein et al., 2002). Other studies have pointed that when the precipitation is less than 100 mm (the soil is in extreme drought for most of the time) the decomposition of litter is basically controlled by precipitation (Jacobson and Jacobson, 1998). Finally, when precipitation is larger than 200 mm, the soil water content can sustain substantial soil microbial activity, so that the influence of pulsed precipitation on the decomposition of litter is reduced (Xu and Hirata, 2005). Furthermore, most studies on the response of litter mass loss and nutrient release to precipitation changes focus on the change in the net amount of precipitation, but fewer consider changes of precipitation frequency (Beier et al., 2012).

Thus, climate change plays an important role in controlling decomposition of litter (Aerts, 1997). Compared with other factors, precipitation has a great spatial and temporal variability in arid and semi-arid areas. This makes it complex to predict climate change effects on litter decomposition in arid and semi-arid regions. Therefore, we manipulated extreme drought conditions (decreased precipitation amount and increased precipitation interval) in an arid ecosystem for more than 3 years to evaluate the impacts of climate change on litter decomposition. We hypothesized that (1) leaf litter that under extreme drought conditions will decompose slower than litter under natural condition due to precipitation is conductive to litter mass loss by increasing the soil moisture (Clein and Schimel, 1994); (2) compared to the decrease in total precipitation amount, increase in precipitation intervals will have more negative impact on the litter mass loss due to the latter being harsher on the living conditions of the decomposer (Allison et al., 2013).

MATERIALS AND METHODS

Experimental Site and Materials

The study was conducted on the Urat Desert-Grassland Research Station of the Chinese Academy of Sciences, a 340-ha fenced desert steppe station located in Urat Houqi County (106°58′ E, 41°25′ N, altitude ∼1,520 m), the western part of Inner Mongolia, China, a transitional area from grassland to desert (**Figure 1**). The average annual air temperature is 3.7–4.6°C. The annual mean sunshine duration is 3,110–3,300 h, and the frost-free period is ∼126 days. The annual precipitation is 100–150 mm, whereas the annual evapotranspiration is 3,032–3,179 mm, and the wetting coefficient is from 0.15 to 0.30 (Qu et al., 2014).

The vegetation is dominated by *Stipa klemenzii*, a perennial gramineous plant, which is mainly distributed in northern central Asia and represents the main vegetation type of the desert steppe. Other species in the desert steppe include *Achnatherum splendens*, *Peganum harmala*, *Salsola collina*, *Allium mongolicum*, *Allium polyrhizum*, *Corispermum macrocarpum*, *Bassia dasyphylla*, *Setaria viridis*, *Reaumuria songarica*, and *Oxytropis aciphylla*.

We selected leaf litter (as it accounts for > 60% of total litter, and its decomposition rate is faster than that of other litters, Huysen et al., 2013) of the dominated species *S. klemenzii* as the experimental litter material. *Stipa klemenzii* is a short herb, usually 1.5–13.5 cm high. It is drought tolerant and plays a vital role in environmental protection, and the conservation of water and soil in the dessert steppe (Qu et al., 2019).

Experimental Platform

The Urat Desert-Grassland Research Station is equipped with an experimental platform for studying the response of ecosystems to extreme drought (**Figure 2**). It is a standard experiment setup in six major grassland ecosystems in the United States since 2012. Since 2014, China and the United States have conducted a network research to study the response of grassland ecosystems to the extreme drought.

The experimental platform uses a canopy to reduce or exclude the rainwater. This type of shelter has been used by many other ecological peers (Knapp et al., 2017) and is technically feasible. There is a shelter area of 36 m^2, and the top of the shelter is arched to facilitate the flow of the intercepted water and reduce the damage of the wind. The shelter is made of transparent acrylic plastic plate with easy disassembly, high light transmission, and high UV penetration, which completely shields the precipitation and avoids the influence of light.

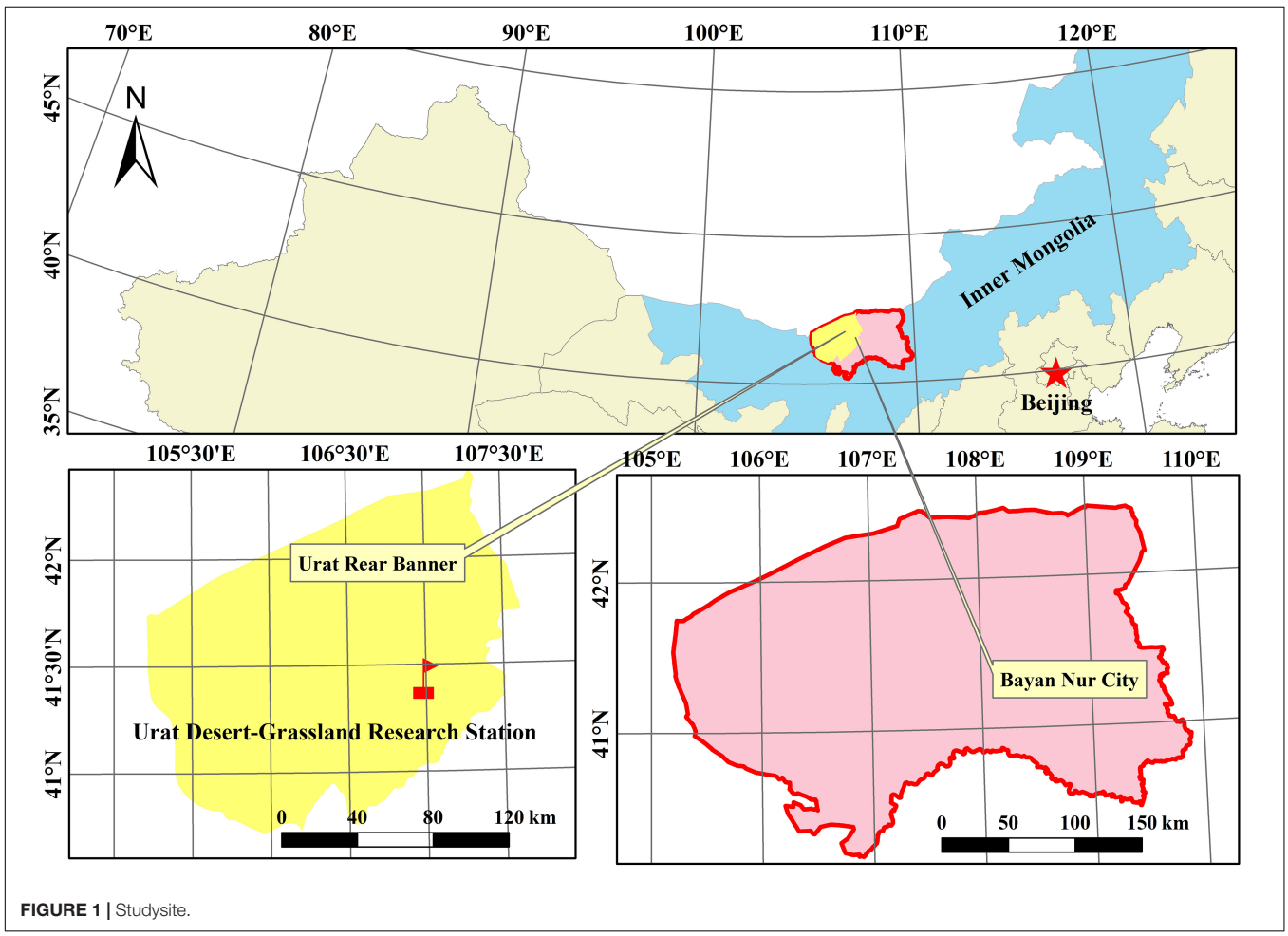

FIGURE 1 | Studysite.

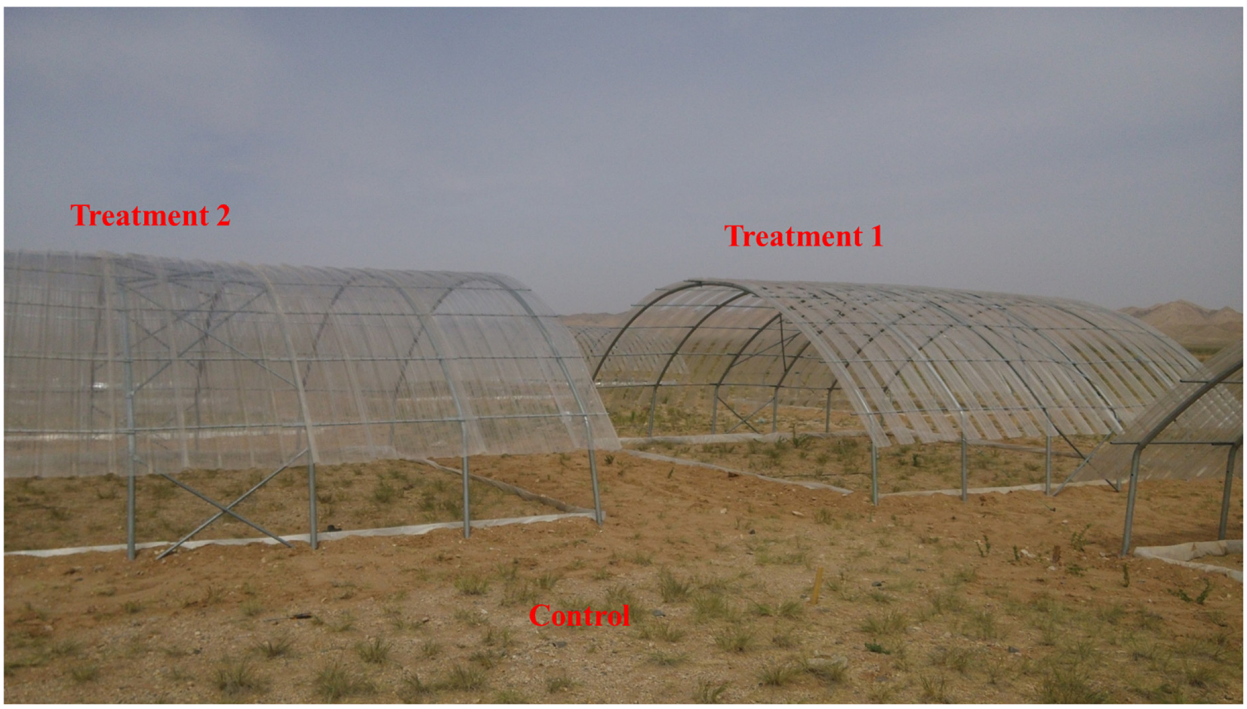

FIGURE 2 | Experimental platform for studying the response of ecosystems to extreme drought.

There are 12 sets of experimental facilities in Urat Desert-Grassland Research station, and there are also six natural precipitation control plots with the same area. Therefore, there are 18 plots in total and each covering 36 m^2. Every plot is separated by 5 m; the surrounding area is deeply digging 1–1.5 m and separated by a 6-m-long plastic baffle to prevent mutual interference of moisture lateral movement. The 4 × 4-m^2 area in the center of each plot is the experimental area, and the surrounding 1 m is a buffer zone to facilitate sample collection during the experiment and reduce the marginal effect. The experimental platform has good controllability and can conveniently carry out the precipitation interval processing of different durations.

Experimental Design

Based on the same experimental approach to that setup in the United States and the historical precipitation situation, we set our precipitation modification experiment with three treatments: a natural background precipitation control, and two extreme drought treatments: (1) decreased precipitation amount by two-thirds of that in the growing season (May 1–August 31) and (2) increased precipitation interval in the early stage of growth season (May 1–June 30). There were six repetitions of each treatment; thus, there are 18 experimental plots in total.

The litter bag method (Knacker et al., 2003; Githaiga et al., 2019) was used for estimating litter decomposition dynamics. We used a litter bag size of 15 × 10 cm and a mesh size of 1 × 1 mm. The experiment was conducted for 3 years, and the field collection of leaf litter was completed in the autumn of 2015. All the collected litter was cleaned and dried at 65°C until constant weight. Based on previous experience in the study area (Qu et al., 2019), we placed 10 g leaf litter of *S. klemenzii* in every nylon bag. Litter bags were equipped with zippers to prevent the litter from leaking out and then were placed into the precipitation interval experimental platform on April 1, 2016. According to a previous study, the decomposition of litter is faster in the initial stage and slower in the later stage (Qu et al., 2010); thus, samples were taken every 2 months in the first year (June, August, October, and December in 2016) and then every 3 months in the rest of the experimental period (March, June, September, and December in 2017 and 2018), and six litter bags were sampled each time in each plot. Therefore, there are 12 sampling times in total. The total of litter bags placed was 3 (treatments) × 6 (plots) × 6 (replicates) × 12 (sampling times) = 1,296; all litter bags are placed on the ground surface.

Data Collection

Abiotic Factors

The soil surface temperature, soil humidity, and light intensity were measured every 10 days at the same time (11:00 AM) during the experimental period and determined using geothermometers (HH82; Exphil Calibration Labs, Bohemia, NY, United States) and hygrometers (TRIME-FM;, IMKO, GmbH, Ettlingen, Germany) and illuminometer (Testo 545, Schwarzwald, Germany), respectively. The data of precipitation (**Supplementary Table S1**), air temperature, and air humidity were provided by the standard weather station in the experimental field. The differences in air temperature

(**Supplementary Figure S1A**), air humidity (**Supplementary Figure S1B**), soil temperature (**Supplementary Figure S1C**), and light intensity (**Supplementary Figure S2**) among control and different treatments were not significant ($P > 0.05$). However, the soil humidity of control, decreased precipitation amount treatment, and increased precipitation interval treatment showed different trends during the experimental period (**Supplementary Figure S1D**).

Mass Loss

The sampled litter bags were carefully washed with clean water every time to remove the mud and debris and then dried at 65°C to constant weight to calculate the mass loss. The litter mass was determined as ash free dry mass (AFDM) after the combustion of samples at 550°C in a muffle furnace for 4 h, and all litter chemical traits were calculated on the basis of AFDM (Duan et al., 2013).

The leaf litter mass loss was measured by Equation (1):

$$\text{Mass loss (\%)} = (\text{W0} - \text{W1})/\text{W0} \times 100$$

where W0 is the initial litter weight (10 g), and W1 refers to the measured weight after each sampling.

Leaf Litter Traits

The leaf litter traits were measured three times during the experiment period (initial, after 1 year of decomposition, and by the end of the experiment, respectively). The total carbon content (C) and total nitrogen content (N) of leaf litters were measured by using an elemental analyzer (vario MACRO cube; Elementar, Langenselbol, Germany). The phosphorus (P) and potassium (K) contents were determined with an inductively coupled plasma emission spectrometer after digestion of samples in concentrated nitric acid. The lignin content was determined by gravimetry using hot sulfuric acid digestion (Flora et al., 1996). The ash content was determined by a muffle furnace with litter samples burning at 550°C to constant weight.

Statistical Analysis

Data were examined to determine if they satisfied the assumptions of parametric statistics. SPSS version 20.0 (SPSS Inc., Chicago, IL, United States) was used to perform analysis of variance (ANOVA). If the data did not meet the prerequisites for ANOVA, conversion of logarithmic was conducted. We used two approaches to analyze our mass loss data. First, to test whether the drought treatments affected mass loss differently, we conducted a repeated-measurement ANOVA. Second, to test the importance of the different factors on mass loss (e.g., factors related to our treatments such as soil moisture, see below), we used a model selection approach. We analyzed controls of litter mass loss using mixed linear effect models to test out hypotheses whether the main control on mass loss was due either to our treatment manipulation (and variables related to it, mainly soil moisture) or to variables partially related to the treatments (litter quality, represented by the lignin/N ratio), or variables not related to the experimental manipulation (represented by light intensity). We built models that included only the effect of either our factors or litter quality or light intensity at once, and a full model. We compared the plausibility of each model by the Akaike's information criterion (AIC). Given that our data acquisition for litter chemistry variables was limited to three particular sampling dates, we used environmental and litter-bag mass data close to those dates for our analysis of controls on decomposition. Additionally, because some variables covary with time for these sampling dates on a "non-causal basis" (see below), we included sampling time as a factor in our analysis to avoid spurious results on the effects on those variables and mass loss. For instance, both litter mass and light intensity decreased monotonically with time, but light did it only as a result of our particular selection of sampling dates (two spring dates and a winter sampling date with much lower intensity values). For all mixed models, the drought treatments were the between-subjects factor; time of sampling was the repeated variable (fix effects), and plot was treated as the random factor (within subjects). Other covariates were used as fixed factors in the model selection approach. *Post hoc* Tukey test was performed after the ANOVA to differentiate among drought treatments if applicable. All data were transformed. These analyses were carried out with R using the nlme library (Pinheiro et al., 2013). All statistical tests were conducted at a 5% significance level.

RESULTS

Mass Loss of Leaf Litter

The mass loss of *S. klemenzii* leaf litter in control was significantly more than that in increased precipitation interval treatment for every sampling ($P < 0.05$), and the difference with decreased precipitation amount treatment was not significant in the initial stage of experiment ($P > 0.05$), whereas after the sixth sampling, the litter in control was decomposed significantly faster than that in increased precipitation interval treatment ($P < 0.05$). The difference of mass loss between the litter in decreased precipitation amount treatment and in increased precipitation interval treatment was not significant in the first sampling ($P > 0.05$); with the experiment continued, the litter in decreased precipitation amount treatment was decomposed significantly faster than that in increased precipitation interval treatment ($P < 0.05$), whereas their differences were not significant in the seventh, eighth, and ninth sampling ($P > 0.05$), however, the litter in decreased precipitation amount treatment was decomposed significantly faster than that in increased precipitation interval treatment again since the 10th sampling to the end of the experiment ($P < 0.05$). The mass losses of *S. klemenzii* litter after 3 years were 21.0% (control) > 18.1% (decreased precipitation amount treatment) > 14.0% (increased precipitation interval treatment) (**Figure 3**).

Changes of Leaf Litter Traits With Decomposition

The initial leaf litter C content of the *S. klemenzii* was between 462.72 and 465.47 g/kg. After 1 year of the experiment, litter C contents of different treatments were between 478.78 and 502.23 g/kg, and the differences were not significant among treatments or with the initial ($P > 0.05$). There was no obvious

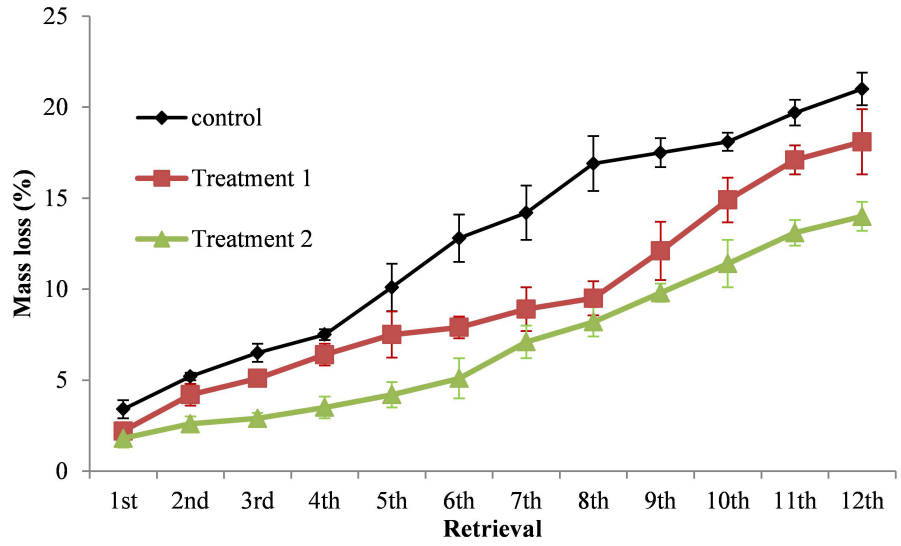

FIGURE 3 | Comparative leaf litter mass loss of different extreme drought treatments at different retrieval times. Bar heights are means ± 1 SE for the error bars. Treatment 1, decreased precipitation amount by 2/3 in the growth season (May 1–August 31); Treatment 2, increased precipitation interval in the early stage of growth season (May 1–June 30); control, natural precipitation.

change of the leaf litter C contents of different treatments to the end of the experiment, and the differences among the treatments and in different periods were not significant ($P > 0.05$) (**Figure 4A**).

The initial leaf litter N content was between 6.31 and 6.66 g/kg. After 1 year of the experiment, the N contents of all the control, decreased precipitation amount treatment, and increased precipitation interval treatment were decreased significantly ($P < 0.05$), whereas the differences among different treatments were not significant ($P > 0.05$). By the end of the experiment, the differences of the N contents compared with those in the first year of the experiment were not significant ($P > 0.05$), whereas the N content of increased precipitation interval treatment was significantly lower than that of the control and the decreased precipitation amount treatment ($P < 0.05$) (**Figure 4B**).

The initial leaf litter P content was between 1.12 and 1.19 g/kg. And not similar to the C and N contents, the P content was increased with the experiment time, and by the end of the experiment, the P contents in the control, decreased precipitation amount treatment, and increased precipitation interval treatment were significantly higher than that in the initial, respectively ($P < 0.05$). However, the differences of P contents among the control, decreased precipitation amount treatment, and increased precipitation interval treatment were not significant during the whole experiment ($P > 0.05$) (**Figure 4C**).

The initial leaf litter K content was between 7.12 and 7.15 g/kg. After 1 year of the experiment, the K content in decreased precipitation amount treatment was 6.69 g/kg, significantly higher than that in control and increased precipitation interval treatment, and the K content in increased precipitation interval treatment was significantly higher than that in decreased precipitation amount treatment ($P < 0.05$). By the end of the experiment, the K content in increased precipitation interval treatment was decreased obviously and significantly lower than that in the control and decreased precipitation amount treatment ($P < 0.05$), the differences between control and decreased precipitation amount treatment were not significant ($P > 0.05$). The initial K content of the control was significantly higher than the contents after 1 year and by the end of the experiment ($P < 0.05$), and the difference of the K contents between that after 1 year and by the end of the experiment was not significant ($P > 0.05$) (**Figure 4D**).

The initial leaf litter lignin content was between 427.45 and 429.95 g/kg. After 1 year of the experiment, the lignin content in the control and increased precipitation interval treatment was increased significantly to 481.84 and 535.73 g/kg, respectively, whereas the lignin content in decreased precipitation amount treatment was decreased to 418.78 g/kg. Thus, the lignin contents in control and increased precipitation interval treatment were significantly higher than that in decreased precipitation amount treatment ($P < 0.05$). By the end of the experiment, the lignin contents in decreased precipitation amount treatment and increased precipitation interval treatment were decreased significantly to 314.24 and 324.61 g/kg, respectively, significantly lower than that in the control (457.22 g/kg) ($P < 0.05$). The lignin content after 1 year of the experiment in increased precipitation interval treatment was significant higher than that in the initial and by the end of the experiment, and the lignin content by the end of the experiment in decreased precipitation amount treatment was significantly lower than that in control and increased precipitation interval treatment ($P < 0.05$) (**Figure 4E**).

The initial leaf litter ash content was between 25.53 and 26.82 g/kg. After 1 year of the experiment, there was no obvious change of the ash contents in the control and the two treatments,

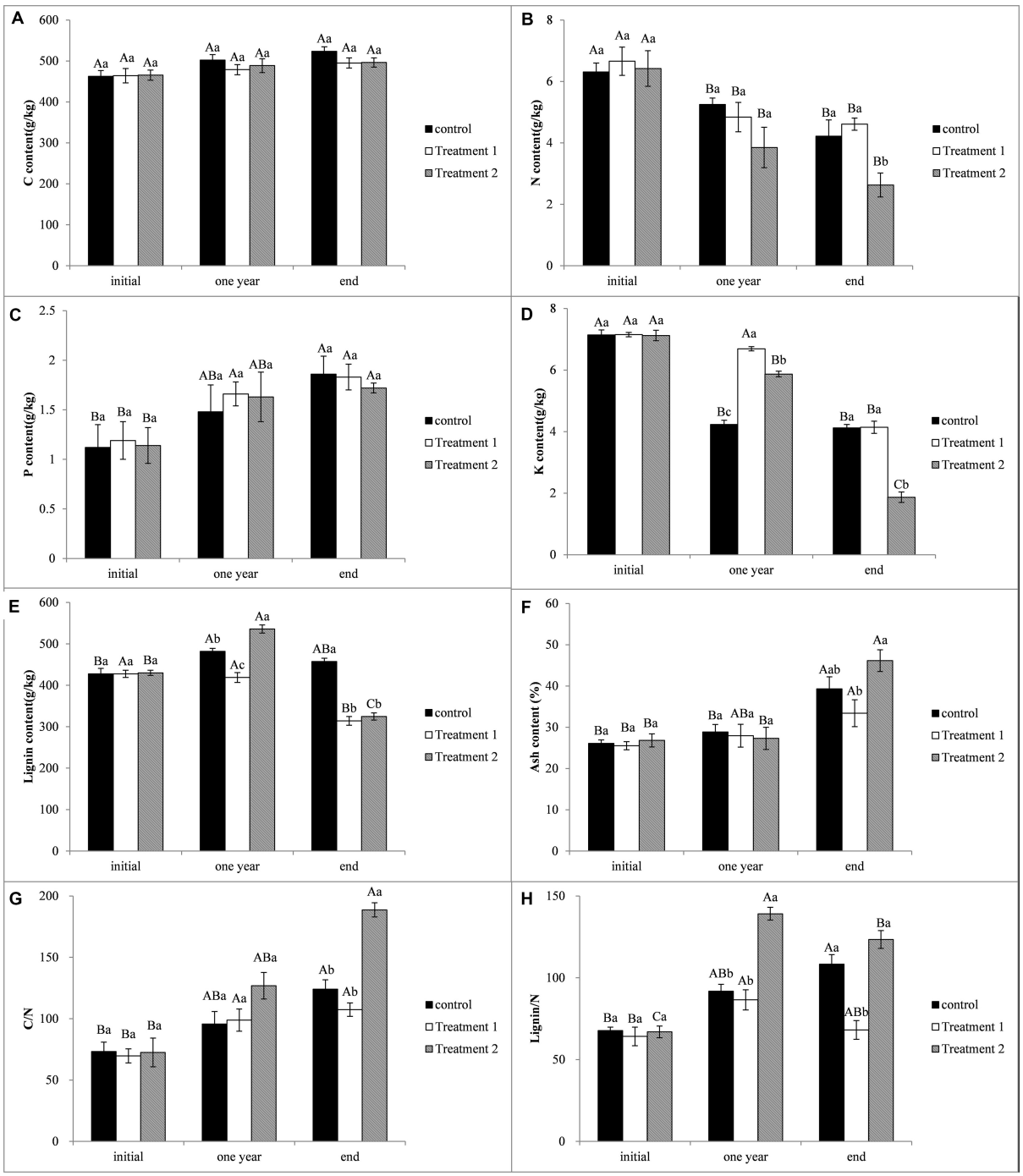

FIGURE 4 | Initial traits of *Stipa klemenzii* leaf litter. **(A)** C content; **(B)** N content; **(C)** P content; **(D)** K content; **(E)** Lignin content; **(F)** Ash content; **(G)** C/N ratio; **(H)** Lignin/N ratio. Bar heights (means) ± error bars (1 SE). Mean values with different lowercase letters are significantly different among the different treatments at $P < 0.05$; mean values with different uppercase letters are significantly different among the different retrieval times at $P < 0.05$. Treatment 1, decreased precipitation amount by 2/3 in the growth season (May 1–August 31); Treatment 2, increased precipitation interval in the early stage of growth season (May 1–June 30); control, natural precipitation.

and the differences were not significant ($P > 0.05$). By the end of the experiment, the ash contents of control and increased precipitation interval treatment were increased significantly, and the ash content in decreased precipitation amount treatment was significantly lower than that in increased precipitation interval treatment ($P < 0.05$) (**Figure 4F**).

The initial C/N of the *S. klemenzii* leaf litter was between 69.70 and 73.33. With the experiment continued, the C/N showed an

increased trend, and all the C/N ratios in the control and the two treatments by the end of the experiment were significantly higher than that in the initial. And the C/N in the increased precipitation interval treatment was 188.72 by the end of the experiment, significantly higher than that in the control (124.11) and the decreased precipitation amount treatment (107.39, $P < 0.05$) (**Figure 4G**).

The initial lignin/N ratio of the *S. klemenzii* leaf litter was between 64.18 and 67.78. After 1 year of the experiment, all the lignin/N ratios in the control and the two treatments were increased, and the lignin/N in the increased precipitation interval treatment was significantly higher than that in control and decreased precipitation amount treatment ($P < 0.05$). By the end of the experiment, the lignin/N ratios in decreased precipitation amount treatment and increased precipitation interval treatment were decreased, whereas that in the control increased, and the lignin/N ratio in the decreased precipitation amount treatment was 68.16, significantly lower than that in the control (108.35) and increased precipitation interval treatment (123.43) ($P < 0.05$) (**Figure 4H**).

Effects of Treatments on Litter Mass Loss, Litter Traits, and Abiotic Factors

The repeated-measurement ANOVA was performed to test the significance of the extreme drought treatments, sampling times, and their interactions on litter mass losses. Results showed that the litter mass losses were affected by the extreme drought treatments (D), sampling times (T), and the $T \times D$ interaction. The litter C, N, K, and lignin contents; C/N ratio; and lignin/N ratio were related to sampling times, drought treatments, and the $T \times D$ interaction. The litter P contents were affected only by sampling times (**Table 1**).

Our linear mixed-model analysis showed that our treatment and its effects on soil environment were the main factor explaining variation on litter mass. In this way, the models with either only our rainfall treatments or treatments plus soil moisture showed that our manipulation was highly significant on mass litter, and these models had the lowest AICs [-224.2 with 11 degrees of freedom (df), and -222.6 with 12 df, respectively]. In contrast, models including either only lignin/N ratio or light intensity had the lowest AICs (-194.4 with 6 df and -190.8 with 6 df), and the effect litter mass was significant only for the model including litter chemistry, not for that with light intensity.

DISCUSSION

Many studies evaluating the impact of precipitation manipulation on litter decomposition in terrestrial ecosystems have been conducted (Chapin et al., 2002; Aerts et al., 2003; Currie et al., 2010; Zhang et al., 2013). However, the main drivers of litter mass loss in the extreme drought condition are yet not fully understood, even though drylands accounted for 41% of the global land area (Poulter et al., 2014). In our study, we conducted a simulation test in order to answer the question: as two of the most common phenomena in precipitation patterns under global climate change, is increased precipitation interval equivalent to decreased precipitation amount at litter mass loss?

The first hypothesis was supported by our findings, leaf litter under extreme drought conditions decomposed slower than litter under natural condition and showed decreased precipitation amount treatment < increased precipitation interval treatment < control after 3 years, and their differences in most samples (especially the later samples) are significant (**Figure 3**). The analysis also indicated that the main effect on litter mass loss is related to our treatments (and their effects on soil moisture are most important) and secondarily to litter chemistry and almost nothing to light intensity, suggesting that precipitation is conductive to litter mass loss. This is in line with many studies dealing with litter decomposition that reported significant reductions in litter mass loss with precipitation reduction (Sardans et al., 2008; Araujo and Austin, 2015; Bastida et al., 2017). And this negative

TABLE 1 | Results of the repeated-measurement ANOVAs on the response of variables to the imposed drought treatments (D), time of sampling (T), and their interaction ($T \times D$).

	D			*T*			*T* × *D*		
	***F*-value**	***df* (numerator, denominator)**	**Significance**	***F*-value**	***df* (numerator, denominator)**	**Significance**	***F*-value**	***df* (numerator, denominator)**	**Significance**
Variable									
Mass loss	806.3	2, 12	***	1510.1	12, 144	***	14.1	24, 144	***
Litter chemistry									
Carbon	8.9	2, 12	**	52.0	2, 24	***	3.41	4, 24	*
Nitrogen	49.5	2, 12	***	203.1	2, 24	***	15.1	4, 24	***
Phosphorous	1.0	2, 12	NS	66.9	2, 24	***	1.0	4, 24	NS
Potassium	233.8	2, 12	***	4384.7	2, 24	***	621.4	4, 24	***
Lignin	310.0	2, 12	***	828.4	2, 24	***	265.9	4, 24	***
C/N ratio	45.7	2, 12	***	202.2	2, 24	***	13.8	4, 24	***
Lignin/N ratio	74.0	2, 12	***	123.2	2, 24	***	22.4	4, 24	***

*ANOVAs were modeled as linear mixed models with drought treatments and time as fixed factors and experimental plot as a random factor. NS, not significant. *P < 0.05, **P < 0.01, ***P < 0.001.*

impact was directly attributed to the decreased biomass and activity of soil microbial communities caused by decreased precipitation and the subsequent reduction in soil and litter moisture under drought conditions, which were important to litter mass loss (Baldrian et al., 2013; Maynard et al., 2018).

The second hypothesis was also supported by our study; compared to decreased precipitation amount, increased precipitation interval has more impact on the litter mass loss; the former decomposed 4.1% more than did the latter after 3 years, and the difference was significant (**Figure 3**). This may be because the infrequent rainfall events induce lower litter moisture compared to smaller but more frequent ones (Jolya et al., 2019), and litter moisture is a very important factor as we illustrated above (Baldrian et al., 2013). We also found that the C/N ratio was increased in increased precipitation interval treatment, but it was not found in decreased precipitation amount treatment (**Figure 4G**). This is in agreement with previous research that reported litter mass loss showed a negative relationship with the C/N ratio (Zhou et al., 2015), because microbes transitioned from C to N limitation when the C/N ratio of plants increased (Averill and Waring, 2018). These results indicated that increased precipitation interval was harsher on the living conditions of the decomposer than decreased precipitation amount (Allison et al., 2013), because the altered abiotic environment would select for more drought-resistant microbial communities (Yuste et al., 2011). It also should be noticed that the lignin contents were lower in both extreme drought treatments than that in control (**Figure 4E**); this is inconsistent with a previous study that found litter with lower lignin content will decompose faster because lignin is difficult to decompose (Zhou et al., 2012; Qu et al., 2019). However, similar with Prieto et al. (2019), the potential positive effect of lower lignin content in our study may be overwhelmed by climate-induced reductions in litter decomposition in the extreme drought treatments.

CONCLUSION

We conclude that the main control of litter mass loss was due to our manipulation of drought regime and its effects on the soil decomposition environment, rather than to other factors such as litter quality or light intensity. We found that as two of the most common phenomena in precipitation patterns under global climate change, both increased precipitation interval and decreased precipitation amount have negative effects on litter mass loss in the desert steppe because of the reduced soil and litter humidity. However, the effects of the two treatments on litter mass loss are different, compared to decreased precipitation amount, the litter mass loss under increased precipitation interval is less significant. Furthermore, we found that the C/N ratio of litters in the increased precipitation interval treatment was significantly higher than that in the control, but this is not observed in the decreased precipitation amount treatment. This indicated that increased precipitation interval can prevent litter mass loss by increasing the C/N ratio; therefore, it is harsher on the living conditions of the decomposer than decreased precipitation amount treatment. Based on this, we proposed that more studies should focus on the decomposer change in relation to litter mass loss in extreme drought conditions in the future.

DATA AVAILABILITY STATEMENT

All datasets generated for this study are included in the article/**Supplementary Material**.

AUTHOR CONTRIBUTIONS

HQ: conceptualization, methodology, and writing – original draft preparation. XZ: conceptualization and methodology. JL: visualization and investigation. XT: supervision. XW and EM-R: software, reviewing, and editing. All authors contributed to the article and approved the submitted version.

FUNDING

This work was supported by the National Natural Science Foundation of China (41877540), the Visiting Scholar Research Program of China Scholarship Council (201804910131), the Key Research and Development Plan of Ning Xia Province, China (2020BBF02003), the National Key Research and Development Plan of China (2016YFC0500506), and the Second Tibetan Plateau Scientific Expedition and Research program (2019QZKK0305).

ACKNOWLEDGMENTS

We thank all members of Naiman Desertification Research Station and Urat Desert-Grassland Research Station, Chinese Academy of Sciences (CAS), for their help in field and laboratory work.

SUPPLEMENTARY MATERIAL

The Supplementary Material for this article can be found online at: https://www.frontiersin.org/articles/10.3389/fenvs.2020.00088/full#supplementary-material

FIGURE S1 | Air temperature **(A)**, air humidity **(B)** and soil temperature **(C)**, soil humidity **(D)** of different extreme drought treatments during the experimental period. Values were assigned as mean ± SE. The soil surface temperature and soil humidity were measured every 10 days at the same time (11:00 AM) during the experimental period. The data of air temperature and air humidity were provided by the standard weather station in the experimental field. Jul-16: July 2016. Treatment 1, decreased precipitation amount by 2/3 in the growth season (May 1–August 31); Treatment 2, increased precipitation interval in the early stage of growth season (May 1–June 30); control, natural precipitation.

FIGURE S2 | Light intensity of different extreme drought treatments during the experimental period. Values were assigned as mean ± SE. The data were measured every 10 days at the same time (11:00 AM) during the experimental period. Jul-16: July 2016. Treatment 1: decreased precipitation amount by 2/3 in the growth season (May 1–August 31); Treatment 2: increased precipitation interval in the early stage of growth season (May 1–June 30); control, natural precipitation.

REFERENCES

Aerts, R. (1997). Climate, leaf litter chemistry and leaf litter decomposition in terrestrial ecosystems: a triangular relationship. *Oikos* 79, 439–449. doi: 10.2307/3546886

Aerts, R., Caluwede, H., and Beltman, B. (2003). Plant community mediated vs. nutritional controls on litter decomposition rates in grasslands. *Ecology* 84, 3198–3208. doi: 10.1890/02-0712

Allison, S. D., Lu, Y., Weihe, C., Goulden, M. L., Martiny, A. C., Treseder, K. K., et al. (2013). Microbial abundance and composition influence litter decomposition response to environmental change. *Ecology* 94, 714–725. doi: 10.1890/12-1243.1

Araujo, P. I., and Austin, A. T. (2015). A shady business: pine afforestation alters the primary controls on litter decomposition along a precipitation gradient in Patagonia, Argentina. *J. Ecol.* 103, 1408–1420. doi: 10.1111/1365-2745.12433

Austin, A. T., and Vitousek, P. M. (2000). Precipitation, decomposition and litter decomposability of *Metrosideros polymorpha* in native forests on Hawai'i. *J. Ecol.* 88, 129–138. doi: 10.1046/j.1365-2745.2000.00437.x

Austin, A. T., Yahdjian, L., Stark, J. M., Belnap, J., Porporato, A., Norton, U., et al. (2004). Water pulses and biogeochemical cycles in arid and semiarid ecosystems. *Oecologia* 141, 221–235. doi: 10.2307/40005683

Averill, C., and Waring, B. (2018). Nitrogen limitation of decomposition and decay: how can it occur? *Glob. Chang. Biol.* 24, 1417–1427. doi: 10.1111/gcb.13980

Baldrian, P., Šnajdr, J., Merhautová, V., Dobiášová, P., Cajthaml, T., and Valášková, V. (2013). Responses of the extracellular enzyme activities in hardwood forest to soil temperature and seasonality and the potential effects of climate change. *Soil Biol. Biochem.* 56, 60–68. doi: 10.1016/j.soilbio.2012.01.020

Bastida, F., Torres, I. F., Andrés-Abellán, M., Baldrian, P., López-Mondéjar, R., Vítrovskı, T., et al. (2017). Differential sensitivity of total and active soil microbial communities to drought and forest management. *Glob. Chang. Biol.* 23, 4185–4203. doi: 10.1111/gcb.13790

Beier, C., Beierkuhnlein, C., Wohlgemut, T., Penuelas, J., Emmett, B., Körner, C., et al. (2012). Precipitation manipulation experiments-challenges and recommendations for the future. *Ecol. Lett.* 15, 899–911. doi: 10.1111/j.1461-0248.2012.01793.x

Berg, B. (1986). Nutrient release from litter and humus in coniferous forest soils-a mini review. *Scand. J. Forest Res.* 1, 359–369. doi: 10.1080/02827588609382428

Berg, B., and McClaugherty, C. (2003). *Plant Litter Decomposition, Humus Formation, carbon Sequestration*. New York, NY: Springer-Verlag Press.

Bonan, G. B., Hartman, M. D., Parton, W. J., and Wieder, W. R. (2013). Evaluating litter decomposition in earth system models with long-term litterbag experiments: an example using the community land model version 4 (CLM4). *Glob. Chang. Biol.* 19, 957–974. doi: 10.1111/gcb.12031

Brandt, L. A., King, J. Y., and Milchunas, D. G. (2007). Effects of ultraviolet radiation on litter decomposition depend on precipitation and litter chemistry in a shortgrass steppe ecosystem. *Glob. Chang. Biol.* 13, 2193–2205. doi: 10.1111/j.1365-2486.2007.01428.x

Chapin, F. S., Matson, P. A., and Mooney, H. A. (2002). *Principles of Terrestrial Ecosystem Ecology*. New York, NY: Springer-Verlag Press.

Clein, J. S., and Schimel, J. P. (1994). Reduction in microbial activity in birch litter due to repeated drying and rewetting events. *Soil Biol. Biochem.* 26, 403–406. doi: 10.1016/0038-0717(94)90290-9

Cornwell, W. K., Cornelissen, J. H. C., Amatangelo, K., Dorrepaal, E., Eviner, V. T., Godoy, O., et al. (2008). Plant species traits are the predominant control on litter decomposition rates within biomes worldwide. *Ecol. Lett.* 11, 1065–1071. doi: 10.1111/j.1461-0248.2008.01219.x

Currie, W. S., Harmon, M. E., Burke, I. C., Hart, S. C., Parton, W. J., and Silver, W. (2010). Cross-biome transplants of plant litter show decomposition models extend to a broader climatic range but lose predictability at the decadal time scale. *Glob. Chang. Biol.* 16, 1744–1761. doi: 10.1111/j.1365-2486.2009.02086.x

Davidson, E. A., and Janssens, I. A. (2006). Temperature sensitivity of soil carbon decomposition and feedbacks to climate change. *Nature* 440, 165–173. doi: 10.1038/nature04514

Duan, J. C., Wang, S. P., Zhang, Z. H., Xu, G., Luo, C., Chang, X., et al. (2013). Non-additive effect of species diversity and temperature sensitivity of mixed litter decomposition in the alpine meadow on tibetan plateau. *Soil Biol. Biochem.* 57, 841–847. doi: 10.1016/j.soilbio.2012.08.009

Easterling, D. R., Meehl, G. A., Parmesan, C., Changnon, S. A., Karl, T. R., and Mearns, L. O. (2000). Climate extremes: observations, modeling, and impacts. *Science* 28, 2068–2074. doi: 10.1126/science.289.5487.2068

Epstein, H. E., Burke, I. C., and Lauenroth, W. K. (2002). Regional patterns of decomposition and primary production rates in the U.S. great plains: regional ecological analysis. *Ecology* 83, 320–327. doi: 10.2307/2680016

Flora, A. R., Amalia, V. D. S., Berg, B., Alfani, A., and Fioretto, A. (1996). Lignin decomposition in decaying leaves of *Fagus sylvatica* L. and needles of Abies alba Mill. *Soil Biol. Biochem.* 28, 101–106. doi: 10.1016/0038-0717(95)00120-4

Franklin, H. M., Carroll, A. R., Chen, C. R., Maxwell, P., and Burford, M. A. (2020). Plant source and soil interact to determine characteristics of dissolved organic matter leached into waterways from riparian leaf litter. *Sci. Total Environ.* 703:134530. doi: 10.1016/j.scitotenv.2019.134530

Githaiga, M. N., Frouws, A. M., Kairo, J. G., and Huxham, M. (2019). Seagrass removal leads to rapid changes in fauna and loss of carbon. *Front. Ecol. Evol.* 7:62. doi: 10.3389/fevo.2019.00062

Hobbie, S. E., Schimel, J. P., Trumbore, S. E., and Randerson, J. A. (2001). Controls over carbon storage and turnover in high latitude soils. *Glob. Chang. Biol.* 6, 196–210. doi: 10.1046/j.1365-2486.2000.06021.x

Huysen, T. L., Harmon, H. E., Perakis, S. S., and Chen, H. (2013). Decomposition and nitrogen dynamics of 15N-labeled leaf, root, and twig litter in temperate coniferous forests. *Oecologia* 173, 1563–1573. doi: 10.1007/s00442-013-2706-8

Intergovernmental Panel on Climate Change [IPCC] (2014). *Intergovernmental Panel on Climate Change*. doi: 10.1016/B978-0-12-375067-9.00128-5

Jacobson, K. M., and Jacobson, P. J. (1998). Rainfall regulates decomposition of buried cellulose in the Namib Desert. *J. Arid Environ.* 38, 571–583. doi: 10.1006/jare.1997.0358

Jacotot, A., Marchand, C., and Allenbach, M. (2019). Increase in growth and alteration of C:N ratios of avicennia marina and *Rhizophora stylosa* subject to elevated CO2 concentrations and longer tidal flooding duration. *Front. Ecol. Evol.* 7:98. doi: 10.3389/fevo.2019.00098

Jolya, F. X., Weibela, A. K., Coulisb, M., and Throopa, H. L. (2019). Rainfall frequency, not quantity, controls isopod effect on litter decomposition. *Soil Biol. Biochem.* 135, 154–162. doi: 10.1016/j.soilbio.2019.05.003

Killingbeck, K. T. (1996). Nutrients in senesced leaves: keys to the search for potential resorption and resorption proficiency. *Ecology* 77, 1716–1727. doi: 10.2307/2265777

Knacker, T., Forstera, B., Rombkea, J., and Frampton, G. K. (2003). Assessing the effects of plant protection products on organic matter breakdown in arable fields-litter decomposition test systems. *Soil Biol. Biochem.* 35, 1269–1287. doi: 10.1016/S0038-0717(03)00219-0

Knapp, A. K., Ciais, P., and Smith, M. D. (2017). Reconciling inconsistencies in precipitation-productivity relationships: implications for climate change. *New Phytol.* 214, 41–47. doi: 10.1111/nph.14381

Maynard, D. S., Covey, K. R., Crowther, T. W., Sokol, N. W., Morrison, E. W., Frey, S. D., et al. (2018). Species associations overwhelm abiotic conditions to dictate the structure and function of wood-decay fungal communities. *Ecology* 99, 801–811. doi: 10.1002/ecy.2165

McCulley, R. L., Burke, I. C., Nelson, J. A., Lauenroth, W. K., Knapp, A. K., and Kelly, E. F. (2005). Regional patterns in carbon cycling across the great plains of North America. *Ecosystems* 8, 106–121. doi: 10.1007/s10021-004-0117-8

Min, S., Zhang, X., Zwiers, F. W., and Hegerl, G. C. (2011). Human contribution to more-intense precipitation extremes. *Nature* 470, 378–381. doi: 10.1038/nature09763

Parton, W., Silver, W. L., Burke, I. C., Grassens, L., Harmon, M. E., and Currie, W. S. (2007). Global-scale similarities in nitrogen re-lease patterns during long-term decomposition. *Science* 315, 361–364. doi: 10.1126/science.1134853

Pastor, J., and Post, W. M. (1988). Response of northern forests to CO2-induced climate change. *Nature* 334, 55–57. doi: 10.1038/334055a0

Pinheiro, J., Bates, D., DebRoy, S., and Sarkar, D. (2013). *nlme: Linear and Nonlinear Mixed Effects Models. R Package Version 3.1-111*. Vienna: R Foundation.

Potthast, K., Hamer, U., and Makeschin, H. F. (2012). Land-use change in a tropical mountain rainforest region of southern Ecuador affects soil microorganisms and nutrient cycling. *Biogeochemistry* 2012, 151–167. doi: 10.2307/23359735

Poulter, B., Frank, D., Ciais, P., Myneni, R. B., Andela, N., Bi, J., et al. (2014). Contribution of semi-arid ecosystems to interannual variability of the global carbon cycle. *Nature* 509, 600–603. doi: 10.1038/nature13376

Prieto, I., Almagro, M., Bastida, F., and Querejeta, J. I. (2019). Altered leaf litter quality exacerbates the negative impact of climate change on decomposition. *J. Ecol.* 107, 2364–2382. doi: 10.1111/1365-2745.13168

Pucheta, E., Llanos, M., and Meglioli, C. (2006). Litter decomposition in a sandy monte desert of western argentina: influences of vegetation patches and summer rainfall. *Austral Ecol.* 31, 808–816. doi: 10.1111/j.1442-9993.2006.01635.x

Qu, H., Pan, C. C., Zhao, X. Y., Lian, J., Wang, S. K., Wang, X. Y., et al. (2019). Initial lignin content is an indicator of predicting leaf litter decomposition and the mixed effects of two perennial gramineous plants in a desert steppe: a 5-year long-term study. *Land Degrad. Dev.* 30, 1645–1654. doi: 10.1002/ldr.3343

Qu, H., Zhao, X. Y., Wang, S. K., Huang, W. D., and Mao, W. (2014). Effects of different vegetation communities on soil carbon and nitrogen contents in Urat desert steppe. *Pratacul. Sci.* 31, 355–360. doi: 10.11829/j.issn.1001-0629.2013-0249

Qu, H., Zhao, X. Y., Zhao, H. L., and Wang, S. K. (2010). Research progress of litter decomposition in terrestrial ecosystems. *Pratacult. Sci.* 27, 44–51.

Salinas, N., Malhi, Y., Meir, P., Silman, M., Cuesta, R. R., Huaman, J., et al. (2011). The sensitivity of tropical leaf litter decomposition to temperature: results from a large-scale leaf translocation experiment along an elevation gradient in Peruvian forests. *New Phytol.* 189, 967–977. doi: 10.2307/29783383

Sardans, J., Peñuelas, J., and Estiarte, M. (2008). Changes in soil enzymes related to C and N cycle and in soil C and N content under prolonged warming and drought in a Mediterranean shrubland. *Appl. Soil Ecol.* 39, 223–235. doi: 10.1016/j.apsoil.2007.12.011

Wang, H., Liu, S. R., Wang, J. X., Shi, Z. M., Lu, L. H., Guo, W. F., et al. (2013). Dynamics and speciation of organic carbon during decomposition of leaf litter and fine roots in four subtropical plantations of China. *Forest Ecol. Manag.* 300, 43–52. doi: 10.1016/j.foreco.2012.12.015

Wang, Y. K., Chang, S. X., Fang, S. Z., and Tian, Y. (2014). Contrasting decomposition rates and nutrient release patterns in mixed vs singular species litter in agroforestry systems. *J. Soil Sediment* 14, 1071–1081. doi: 10.1007/s11368-014-0853-0

Whitford, W. G., Martínez-Turanzas, G., and Martínez-Meza, E. (1995). Persistence of desertified ecosystems: explanations and implications. *Environ. Monit. Assess.* 37, 319–332. doi: 10.1007/BF00546898

Xu, X., and Hirata, E. (2005). Decomposition patterns of leaf litter of seven common canopy species in a subtropical forest: N and P dynamics. *Plant Soil* 273, 279–289. doi: 10.1007/s11104-004-8069-5

Yahdjian, L., Sala, O. E., and Austin, A. T. (2006). Differential controls of water input on litter decomposition and nitrogen dynamics in the Patagonian steppe. *Ecosystems* 9, 128–141. doi: 10.1007/s10021-004-0118-7

Yuste, J. C., Peñuelas, J., Estiarte, M., Garcia-Mas, J., Mattana, S., Ogaya, R., et al. (2011). Drought-resistant fungi control soil organic matter decomposition and its response to temperature. *Glob. Chang. Biol.* 17, 1475–1486. doi: 10.1111/j.1365-2486.2010.02300.x

Zhang, B., Wang, H. L., Yao, S. H., and Bi, L. D. (2013). Litter quantity confers soil functional resilience through mediating soil biophysical habitat and microbial community structure on an eroded bare land restored with mono *Pinus massoniana*. *Soil Biol. Biochem.* 57, 556–567. doi: 10.1016/j.soilbio.2012.07.024

Zhou, H. C., Tam, N. F., Lin, Y. M., Wei, S. D., and Li, Y. Y. (2012). Changes of condensed tannins during decomposition of leaves of *Kandelia obovata* in a subtropical mangrove swamp in China. *Soil Biol. Biochem.* 44, 113–121. doi: 10.1016/j.soilbio.2011.09.015

Zhou, W. J., Sha, L. Q., Schaefer, D. A., Zhang, Y. P., Song, Q. H., Tan, Z. H., et al. (2015). Direct effects of litter decomposition on soil dissolved organic carbon and nitrogen in a tropical rainforest. *Soil Biol. Biochem.* 81, 255–258. doi: 10.1016/j.soilbio.2014.11.019

Conflict of Interest: The authors declare that the research was conducted in the absence of any commercial or financial relationships that could be construed as a potential conflict of interest.

frontiers in Earth Science

ORIGINAL RESEARCH
published: 31 July 2020
doi: 10.3389/feart.2020.00231

Rainwater Use Process of *Caragana intermedia* in Semi-Arid Zone, Tibetan Plateau

Yajuan Zhu[1]* *and Guojie Wang*[2]

[1] Institute of Desertification Studies, Chinese Academy of Forestry, Beijing, China, [2] Oregon State University Agriculture Program at Eastern Oregon University, Oregon State University, La Grande, OR, United States

Summer rain is changeable in the semi-arid climate and is the limiting factor to the survival and growth of sand-fixing vegetation, especially in the Tibetan Plateau. *Caragana intermedia* is the dominant sand-binding shrub on a sand dune in the northeast Tibetan Plateau. Stable hydrogen and oxygen isotopes of xylem water, soil water, and groundwater were examined to study the rainwater uptake process by *C. intermedia* in mid-summer. Soil water content was monitored continuously before and after a 13.9-mm rain. Contribution of each water source was analyzed by the MixSIAR model. The results showed that the surface soil water (0−10 cm) was replenished by rainwater through increasing soil water content and reducing its stable isotope. *Caragana intermedia* mainly used surface soil water (0−10 cm) replenished by rainwater one day after the rain, accounting for about 60% of its total water source. As water availability decreased in upper soil layers, it used soil water at deeper levels (10−150 cm), the same water source as that one day before the rain. The rapid and efficient uptake of rainwater by *C. intermedia* reflected its response to summer rain, which is an adaptive strategy to the semi-arid environment. Therefore, *C. intermedia* could survive on a sand dune by shallow soil water replenished from rainwater in the Tibetan Plateau.

Keywords: desertification restoration, δD, $\delta^{18}O$, sand-fixing vegetation, water source

OPEN ACCESS

Edited by:
Xian Xue,
Northwest Institute of Eco-Environment and Resources (CAS), China

Reviewed by:
Jian Sun,
Chinese Academy of Sciences, China
Xueyong Zhao,
Northwest Institute of Eco-Environment and Resources (CAS), China

***Correspondence:**
Yajuan Zhu
zhuyj@caf.ac.cn;
zhuyajuan8005@sohu.com

Specialty section:
This article was submitted to Hydrosphere, a section of the journal Frontiers in Earth Science

Received: *09 January 2020*
Accepted: *29 May 2020*
Published: *31 July 2020*

Citation:
Zhu Y and Wang G (2020) Rainwater Use Process of Caragana intermedia in Semi-Arid Zone, Tibetan Plateau. Front. Earth Sci. 8:231. doi: 10.3389/feart.2020.00231

INTRODUCTION

In drylands, water is an important restricting factor for the growth, survival, and reproduction of plant species (Hou et al., 2013), where precipitation is low and changeable, potential evaporation is high, and drought is frequent. Based on the prediction of the climate change model, the extreme precipitation in the arid and semi-arid zones would increase in frequency under global warming. Moreover, total water resource would decrease and thus result in negative influence on the ecosystem (IPCC, 2013). Precipitation reduction combined with warming will modify water sources used by trees (Grossiord et al., 2017). Therefore, the reliance on rainwater in the growing season is important for plant phenology (flowering and fruit maturation) in semi-arid zones (Xia and Wan, 2012). Water use adaptation of plant species affects many ecological processes including plant growth, population regeneration, vegetation dynamics, and ecosystem water cycle. For most plant species, stable isotopes of hydrogen and oxygen usually do not fractionate when root systems absorb water from soil and plants transport water from root systems to branches. Therefore, the

water source of a plant could be determined by comparing δD and $\delta^{18}O$ of sap water and its possible water sources (Ehleringer, 1993). The possible water sources for plants in different seasons were rainwater (Zhou et al., 2015), snow melt (Yang et al., 2011), soil water, and/or groundwater (Kray et al., 2012; Song et al., 2014; Su et al., 2014; Liu et al., 2015; Barbeta and Peñuelas, 2017).

Precipitation is a driving factor of soil water availability in drylands, where small rain (2−5 mm) is the most common occurrence. Its contribution to total precipitation is quite constant for years. The importance of small rain is significantly related to mean annual precipitation and air temperature, which was most at the coolest and driest sites. However, large rain above 30 mm varies significantly among years and is a major source of annual variability in ecological functioning (Loik et al., 2004). Generally, snow in winter and early spring and large rain in summer could infiltrate to a deeper soil depth if their duration time is longer than small rain (Schwinning and Sala, 2004). The uptake of precipitation by plant species is related to its seasonal distribution (Yang et al., 2011). Many woody plants primarily used shallow soil water replenished by rainwater in spring and summer, such as *Senecio filaginoides* and *Mulinum spinosum* in the Patagonian steppe (Kowaljow and Fernández, 2011) and *Haloxylon ammodendron* in Gurbantonggut Desert (Dai et al., 2015). However, some woody plants mainly used deeper soil water replenished by snow in winter or early spring and large rain in summer, such as *Sarcobatus vermiculatus* in Colorado (Kray et al., 2012), *Nitraria sibirica* in Gurbantonggut Desert (Zhou et al., 2015) and *Caragana microphylla* in the Inner Mongolia steppe (Zheng et al., 2015).

Rain amount not only affects the depth and time of water infiltration into soil (Yang et al., 2014) but also affects the contribution of rainwater to plant growth (Duan et al., 2008). The interspecific difference of rain amount that plants use is related to their life forms (Dodd et al., 1998; Antunes et al., 2018). Annual plants initially use small rain (2−5 mm). Perennial grasses or herbs and small shrubs use light rain (10−20 mm). However, shrubs or trees might use heavy rain (65.3 mm) (Cheng et al., 2006). Water is absorbed primarily by root systems; therefore, the duration of soil water use depends on root distribution especially in arid zones (Zhou et al., 2015). Shallow-rooted plants with fine root systems are sensitive to small rain (Zhou et al., 2018). Deep-rooted plants or plants with a tap root respond to large rain after a few days (Li et al., 2007). However, some woody plants have dimorphic root systems and thus they can change water sources in different periods and use shallow soil water after precipitation but extract deeper soil water, even groundwater, during drought (Weltzin and Tissue, 2003). Thus, they can benefit from small or large rain allowing the plant to access water sources in different seasons based on availability (Kowaljow and Fernández, 2011; Zhou et al., 2015).

In the semi-arid zone of the Tibetan Plateau with 250−500 mm annual precipitation, water is the limiting factor for vegetation restoration in land desertification. Plants in different habitats may have different water use strategies based on water availability. For shrubs on interdunes, deep soil water replenished by groundwater is available, such as *Salix cheilophila* and *Salix psammophila* (Zhu et al., 2016). However, shrubs on sand dunes may rely on soil water replenished by rainwater, such as *Caragana intermedia*. Our earlier research indicated older *C. intermedia* (9- and 25-year-old) used deeper soil water in summer than younger *C. intermedia* (5-year-old) to adapt to the semi-arid climate (Jia et al., 2012). Moreover, this shrub had a dynamic water use strategy to access different depths of soil water and groundwater (Zhu, 2016). In this study, rainwater uptake of *C. intermedia* was investigated by stable hydrogen and oxygen isotopes before and after a summer rain. Our purpose was to evaluate the response of *C. intermedia* to summer rain and the contribution of rainwater to its water sources. This study will help to evaluate its stability on sand dunes under a semi-arid climate and give theoretical support to desertification restoration in the Tibetan Plateau.

MATERIALS AND METHODS

Site Description

A field survey was conducted in Shazhuyu Town, Gonghe County, Qinghai Province (36°16′N, 100°16′E, and elevation 2874 m), located in the northeast Tibetan Plateau. The area has a temperate climate in a semi-arid zone. The average annual air temperature is 2.4°C, and the average air temperature is 12.6°C from May to September. The average annual precipitation is 246.3 mm, mainly occurring in summer and autumn. The average monthly precipitation was 29.3, 51.5, 70.5, 39.8, and 41.8 mm from May to September. The average annual potential evaporation is 1716.1 mm. There are only 91 frost-free days per year. The main soil type is aeolian sand, containing 6.86% clay, 8.93% silt, and 84.21% sand, with the pH of 8.61 (Li et al., 2016). The contents of soil organic matter, nitrogen, phosphorus, and potassium on the surface (0−5 cm) are 2.29−3.49, 0.35−0.55, 0.21−0.44, and 11.84−14.82 $g \cdot kg^{-1}$, respectively (Li et al., 2015). The natural vegetation is dominated by grassland (*Achnatherum splendens*). Shrub land is distributed on sand dunes and river banks (*Artemisia arenaria*, *Nitraria sibirica*, and *Caragana tibetica*). Sand-fixing shrubs in *Caragana* and *Salix* were planted between oasis and sand dunes to protect farms, roads, and villages.

Plant Species

Caragana intermedia Kuang et H.C.Fu (*Caragana liouana* Zhao Y. Chang & Yakovlev) is a leguminous shrub with a height of 1.5 m (Flora of China, 1993). The branches are yellowish gray–green. The leaves are pinnate with 6−16 foliolate. The leaflet blades are elliptic to obovate–elliptic, with sizes of 3−10 mm × 4−6 mm, whitish green, and villous in both surfaces. The corolla is yellow and 2−2.5 cm long. The pod is flat, lanceolate to oblong–lanceolate, with size of 2.5−3.5 cm × 6−7 mm. It mainly distributes on fixed and semi-fixed sand dunes in Gansu, North Hebei, Inner Mongolia, Ningxia, Shaanxi, and west Shanxi. It was used widely in sand-fixing and water and soil conservation in North China. It was introduced in the 1980s from Ordos City of Inner Mongolia to control land desertification on the Tibetan Plateau. This shrub blooms in May, and its legume matures in July

in our study site. *Caragana intermedia* were seeded with the density of one plant per 1 m^2, after the straw checkerboard was constructed on moving sand dunes in the spring of 2000. The root system of *C. intermedia* is 1.30 m deep (Jia et al., 2012). A few grasses and herbs grew in the *C. intermedia* community, including *Leymus secalinus*, *Bassia dasyphylla*, and *Chenopodium foetidum*.

Field Sample and Lab Measurements

Field samples were taken in July 2016. On July 13, 20 *C. intermedia* plants were selected randomly to measure their height and crown diameter. The mean plant height of *C. intermedia* was 1.51 ± 0.22 m, with the mean crown diameter of 1.42 ± 0.19 m (E–W) and 1.63 ± 0.25 m (S–N), which was defined as standard plant. Four plots with 5 m × 5 m size were set randomly in the *C. intermedia* community for field sampling. Twig samples were taken from four plants per plot which were similar to the standard plant. Lignified, 2-year-old twigs 5 cm in length and 3–5 mm in diameter were clipped from the sunny side of four shrubs on July 13, 15, 19, and 27, which was one day before and 1, 5, and 13 days after the rain (13.9 mm) on July 14. The bark was removed because the phloem water is isotopically enriched by photosynthesis and the samples of xylem were kept in 8-mL glass vials (National Scientific Company, Rockwood, TN, United States). Rainwater was collected in July in Shazhuyu Town. Groundwater was replaced by well water and collected on July 17 from a well with a 5-m water table, which was located 1 km north of the study site and not bailed during the previous 2 months. Three replicates of rainwater and groundwater were kept in 8-mL glass vials, respectively. All vials were immediately sealed with Parafilm® (Alcan Packaging, Chicago, IL, United States) and kept in a 16-L medical cooler containing dry ice.

Soil samples were collected at the middle point of each plot using a soil auger with 6.99 cm diameter (AMS Inc., American Falls, ID, United States). Soil sampling depths were 10, 25, 50, 75, 100, and 150 cm, based on the rooting depth of *C. intermedia*. Some soil samples with four replicates were kept and stored as similar to xylem samples. Other soil samples with four replicates were kept in aluminum cans. Wet soil mass was measured by an electronic balance (± 0.01 g) and dried at 105°C for 24 h, and dry soil mass was measured, then soil water content (g kg^{-1}) was calculated as the loss of water.

Soil and xylem samples were stored frozen (−18°C) in the laboratory. Water in soil and xylem samples was extracted by the LI-2000 water vacuum extract system (LICA United Technology Limited, Beijing, China). Rainwater and groundwater samples were filtered prior to analysis. The δD and $\delta^{18}O$ of water samples were measured with a Flash 2000 HT elemental analyzer and a Finnigan MAT 253 mass spectrometer (Thermo Fisher Scientific Co., Ltd., Bremen, Germany) in the Stable Isotope Ecology Laboratory, Department of Earth System Science, Tsinghua University. The measurement accuracy for stable hydrogen and oxygen isotope was ±1 and ±0.2%, respectively. Each water sample was measured three times, and their mean was used for analysis.

Statistical Analysis

Soil water content, δD, and $\delta^{18}O$ were expressed as mean ± SE. One-sample Kolmogorov–Smirnov test and log transformations were used to check and satisfy normality, then one-way ANOVA in SPSS 19.0 (IBM Corp., Armonk, NY, United States) was applied to analyze the effects of time and depth on soil water content. If there was a significant effect ($P < 0.05$), Duncan's multiple-range test was applied to analyze the difference between times or depths. The water use ratio to different sources was analyzed by the MixSIAR Bayesian isotope mixing model (v2.1.3) (Stock et al., 2018). The input data of the model were δD and $\delta^{18}O$ of xylem water, soil water in three layers (0−10, 10−50, and 50−150 cm), and groundwater. The discrimination value was set to 0 for both isotopes, because isotopes usually do not fractionate during plant uptake water (Ehleringer, 1993). Parameter configuration was referred to Ma and Song (2016), including run length of Markov Chain Monte Carlo occurrence, the error options of "residual error" and "process error." Trace plots and the diagnostic tests Gelman–Rubin, Heidelberger–Welch, and Geweke were applied to define if the model converged or not. The estimated median proportion was analyzed for comparisons, which was the median source contribution for each water source. The contribution of rainwater was assumed to be present at surface soil water (0−10 cm).

RESULTS

Soil Water Dynamics Before and After the Rain

Soil water content in the *C. intermedia* community was significantly influenced by sampling date ($P < 0.001$) and soil depth ($P < 0.001$). One day before the rain and on day one and day five afterward, soil water content was significantly higher at 10−50 cm than at 75−150 cm. Thirteen days after the rain, soil water content was significantly higher at 10 cm than at 25−150 cm. Soil water content at 0−25 cm was significantly higher one day after the rain than on other days (**Figure 1**).

The δD and $\delta^{18}O$ of groundwater were similar to some soil water (150 cm), indicating that groundwater replenished deep soil water (**Figure 2**). On July 15, one day after the rain, the δD and $\delta^{18}O$ of surface soil water (10 cm) were similar to rainwater on July 14 (13.9 mm) (**Figure 3**). On July 27, the δD and $\delta^{18}O$ of surface soil water were similar to rainwater on July 22 (10.1 mm), indicating rainwater replenished surface soil water.

Water Sources of *Caragana intermedia*

The $\delta^{18}O$ of xylem water in *C. intermedia* was located under the local meteoric water line (**Figure 2**), indicating its water source was influenced by isotope enrichment which resulted from evaporation. The δD and $\delta^{18}O$ of xylem water of *C. intermedia* were similar to those of groundwater, indicating it extracted some groundwater.

One day before the rain, the δD and $\delta^{18}O$ of xylem water of *C. intermedia* were similar to soil water at 25 cm and 75 − 150 cm

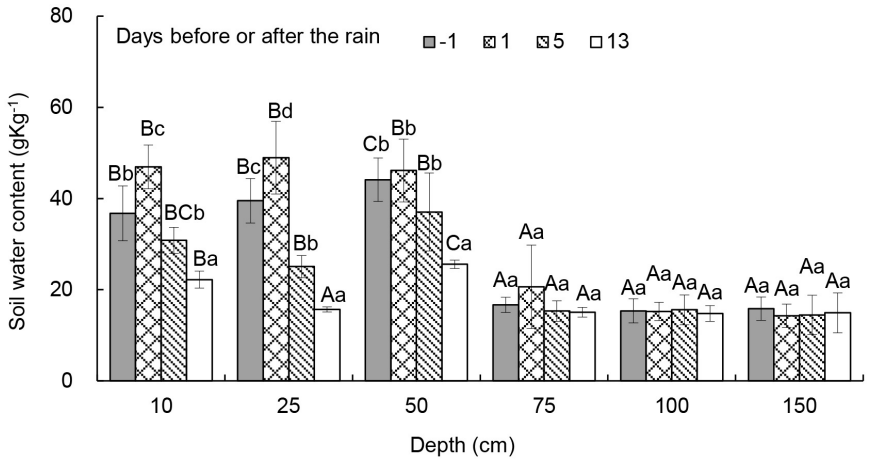

FIGURE 1 | Soil water content in the *Caragana intermedia* community 1 day before and 1, 5, and 13 days after the rain on July 14, 2016. Different uppercase letters mean significant difference between days; different lowercase letters mean significant difference between depths.

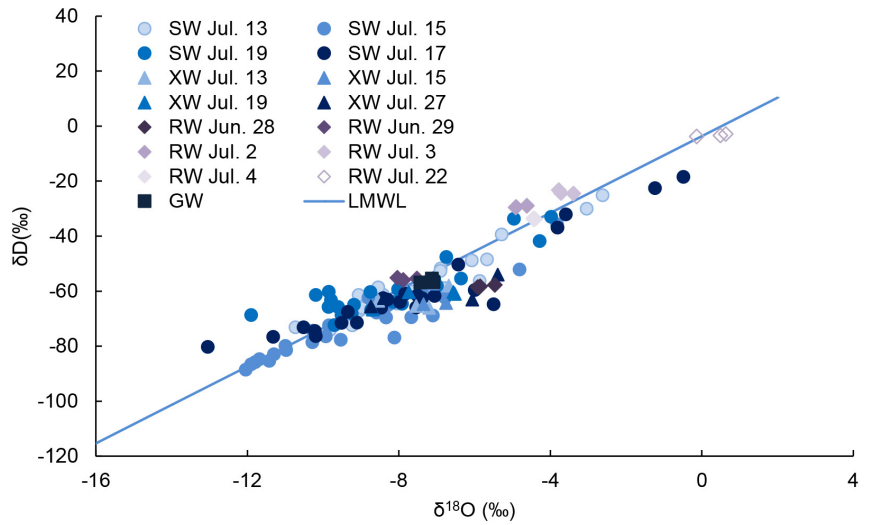

FIGURE 2 | The δD and $\delta^{18}O$ of xylem water (XW) of *Caragana intermedia*, soil water (SW), rainwater (RW), and groundwater (GW) in July 2016. LMWL is the local meteoric water line ($\delta D = 6.977 \times \delta^{18}O - 3.668$, $R^2 = 0.849$, $P < 0.001$).

(**Figures 3A,B**). One day after the rain, the δD and $\delta^{18}O$ of xylem water of *C. intermedia* were similar to soil water at 10 − 25 cm and groundwater (**Figures 3C,D**). Five days after the rain, the δD and $\delta^{18}O$ of xylem water of *C. intermedia* were similar to soil water at 25−100 cm and groundwater (**Figures 3E,F**). After 2 weeks, the δD and $\delta^{18}O$ of *C. intermedia* xylem water were similar to soil water at 25−150 cm and groundwater (**Figures 3G,H**).

The Contribution of Different Water Sources

Caragana intermedia changed its main water source before and after the rain. It mainly used 10−150 cm soil water and groundwater one day before the rain, accounting for 96.3% of the total water source (**Figure 4**). One day after the rain, it mainly used 0−50 cm soil water and groundwater, accounting for 93.4% of its total water source. With the time elapsed after the rain, the water source of this shrub moved into deeper soil profiles. Five days after the rain, the water source of this shrub returned to pre-rain status and mainly used 10−150 cm soil water and groundwater, accounting for 94.5% of its total water source. Two weeks after the rain, this shrub mainly used 10−150 cm soil water and groundwater, accounting for 91.6% of its total water source. The contribution of 0−10 cm surface soil water (replenished by rainwater) was 59.9% of its total water source one day after the rain. Moreover, *C. intermedia* always used groundwater before and after the rain, accounting for 18.5−21.3% of its total water source.

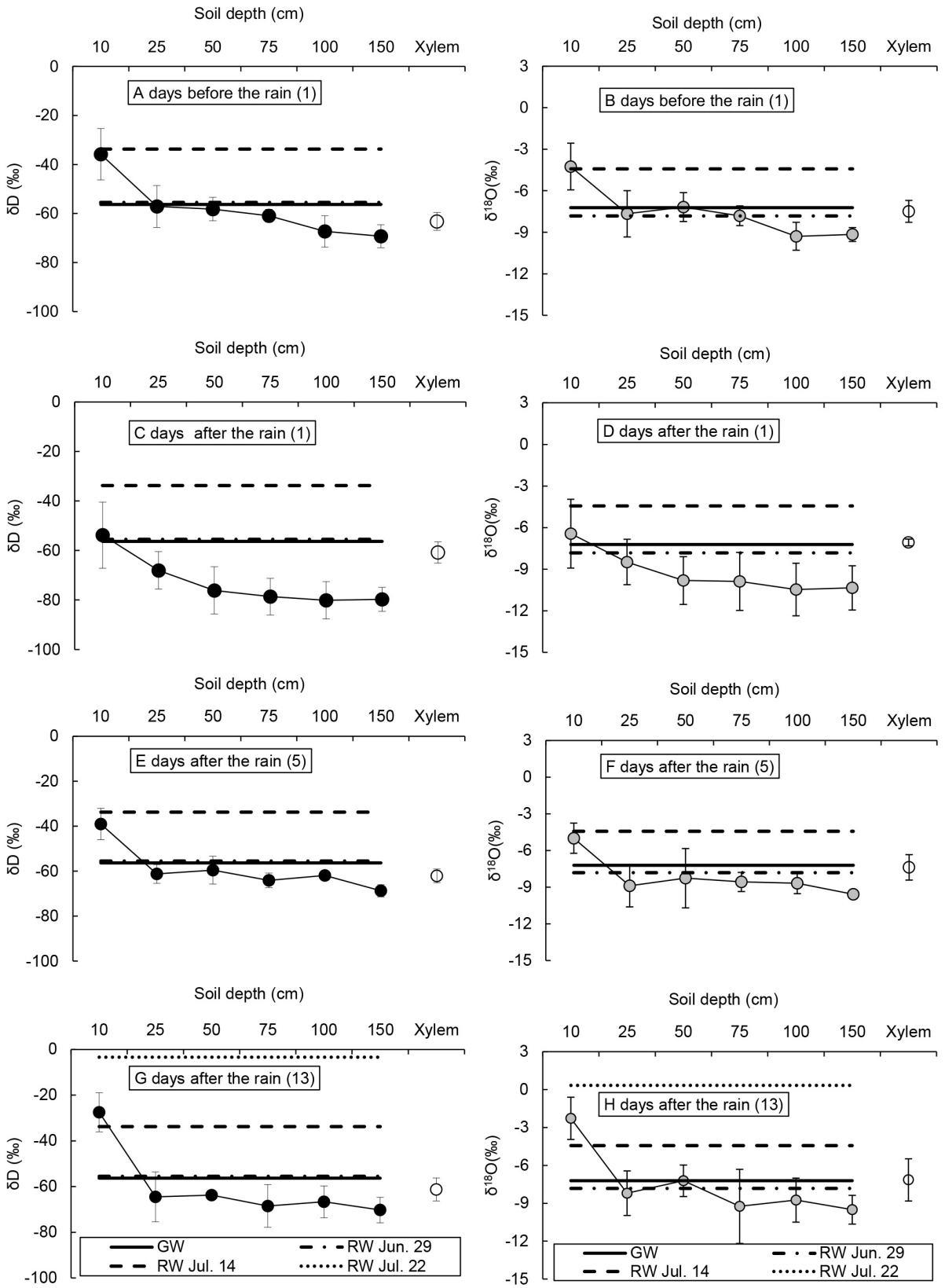

FIGURE 3 | The δD **(A,C,E,G)** and $\delta^{18}O$ **(B,D,F,H)** of xylem water and soil water of the *Caragana intermedia* community, rainwater (RW), and groundwater (GW) in the summer of 2016.

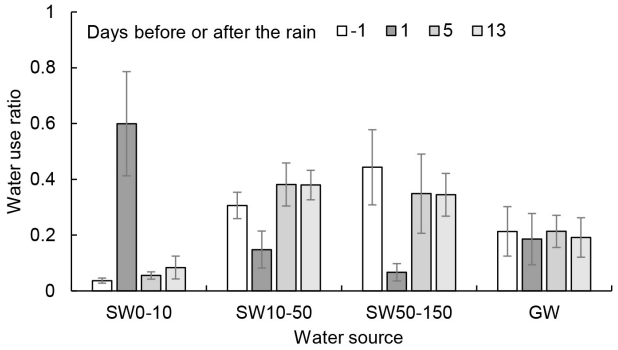

FIGURE 4 | Water use ratio (mean ± SD) of *Caragana intermedia* to different layers of soil water (SW) and groundwater (GW).

DISCUSSION

Our research showed that shallow soil water was replenished by rainwater in the *C. intermedia* community. One day after the rain, soil water content was increased at shallow depths (0−25 cm) than one day before the rain. Moreover, rainwater decreased the δD and $\delta^{18}O$ of surface soil water. However, 5 days after the rain, soil water content at shallow depths was restored; meanwhile, the δD and $\delta^{18}O$ of shallow soil water recovered to those one day before the rain. Therefore, the 13.9 mm rain had influence on soil water of sand dunes only for one day. Soil water depletion and isotope enrichment at shallow depths resulted from evaporation, rainwater infiltration, and plant consumption, similarly on sand dunes in Gurbantonggut Desert (Dai et al., 2015) and Tengger Desert (Huang and Zhang, 2015).

Caragana intermedia was responsive to summer rain and used rainwater one day after the rain. The contribution of 0−10 cm surface soil water replenished by rainwater accounted for approximately 60% of its total water source. When soil water was depleted in the shallow profile, *C. intermedia* used deeper soil water (10−150 cm). The rapid uptake of surface soil water replenished by rainwater was an adaptation for the growth of *C. intermedia*. It not only maximized the extraction of shallow soil water before evaporation loss but also had the opportunity for uptake nutrients in shallow soil (Antunes et al., 2018). *Caragana intermedia* used some groundwater before and after the rain, accounting for about 20% of its total water source. The consistent uptake of groundwater in summer may be important for the survival, especially the maintenance of metabolic activity of fine roots in shallow soil during drought (Antunes et al., 2018). For *C. intermedia*, summer rain is a changeable water source under a semi-arid climate, however, groundwater is a relatively reliable water source. The ability to use both rainwater and groundwater ensures the stability of the *C. intermedia* community on sand dune. Therefore, *C. intermedia* has a resource-dependent water use function adapted to a semi-arid climate. Other *Caragana* species also used rain in arid and semiarid zones. For example, *C. microphylla* in the Inner Mongolia steppe used summer rain, accounting for 42.65–63.92% of its water source (Zheng et al., 2015). After a 9.5 mm rainfall in southeast Tengger Desert, *Caragana korshinskii* mainly used water from deeper soil layers (100–150 cm) with soil moisture infiltration (Huang and Zhang, 2015). However, *C. korshinskii* used surface soil water replenished by rainwater in spring and autumn on sand dune in the Tibetan Plateau (Zhu, 2016). Therefore, *Caragana* shrubs appear to have different water use strategies based on water availability to adapt to drylands.

Many shrubs or trees use soil water replenished by precipitation in different seasons in drylands. Some shrubs use surface soil water replenished by rainwater in spring or summer. For example, rainwater accounted for 42.6% of xylem water of *Nitraria tangutorum* in July in Golmud, Tibetan Plateau (Duan et al., 2008). The proportion of surface pulse water to total water uptake was 29−38 and 22−32% for *Senecio filaginoides* and *Mulinum spinosum* in early summer in the Patagonia steppe, respectively (Kowaljow and Fernández, 2011). *Sarcobatus vermiculatus* used precipitation from soil layers after large rainfall in Colorado (Kray et al., 2012). *Artemisia ordosica* intensively depended on shallow soil water (10−20 cm) after a 9.5 mm summer rain in southeast Tengger Desert (Huang and Zhang, 2015). In interdunes in the Tibetan Plateau, *Salix psammophila* and *Salix cheilophila* depended on 0−25 cm shallow soil water replenished by rainwater in spring and summer, respectively (Zhu et al., 2016). In the Heihe River Basin of northwest China, *Nitraria sphaerocarpa* used summer rainwater more rapidly than *Reaumuria soongorica* (Zhang et al., 2017). Xerophytic shrubs relied on 10 cm top soil water in spring and summer in semi-arid coastal dune systems of southwest Spain (Antunes et al., 2018). In addition, other shrubs use soil moisture replenished by snow in winter or early spring. For example, *Pinus edulis* and *Juniperus osteosperma* utilized winter-derived shallow moisture during spring in South Utah (West et al., 2007). *Nitraria sibirica* mainly used water from snow melt in Gurbantonggut Desert (Zhou et al., 2015). In early spring after snow melt, *Haloxylon ammodendron* on interdune primarily used shallow soil water (0−40 cm) in Gurbantonggut Desert (Dai et al., 2015). Therefore, plants could survive in drylands depending on soil water replenished by precipitation in the growing season.

CONCLUSION

In the Tibetan Plateau, surface soil water (0−10 cm) on sand dune was replenished and its hydrogen and oxygen isotopes were reduced by a 13.9 mm rain. *Caragana intermedia* was rapidly responsive to rainfall and mainly used surface soil water one day after the rain. The contribution of rainwater to *C. intermedia* was approximately 60% of its total water source. With the decrease in soil water availability at shallow depths, this shrub was able to access soil water at deeper depths (25−150 cm). The rapid uptake of summer rain of *C. intermedia* is an adaptation to a semi-arid climate, which may benefit nutrient uptake and its survival. Therefore, summer rain is an important water source to maintain the stability of sand-fixing vegetation on sand dune in the Tibetan Plateau.

DATA AVAILABILITY STATEMENT

The raw data supporting the conclusions of this article will be made available by the authors, without undue reservation. Requests to access the datasets should be directed to YZ, zhuyajuan8005@sohu.com.

AUTHOR CONTRIBUTIONS

YZ designed this study, collected the sample, analyzed the data, prepared the figures, and wrote the main manuscript. GW contributed to improve the manuscript. Both authors reviewed the manuscript.

FUNDING

This study was financially supported by the Fundamental Research Funds for the Central Non-profit Research Institute of Chinese Academy of Forestry (CAFZC2017M006) and the National Natural Science Foundation of China (41301095).

ACKNOWLEDGMENTS

The authors thank Ms. Anne Nyren and Mr. Paul Nyren from North Dakota State University for the contribution in refining the manuscript. We thank the two reviewers for their valuable suggestions.

REFERENCES

Antunes, C., Díaz-Barradas, M. C., Zunzunegui, M., Vieira, S., and Máguas, C. (2018). Water source partitioning among plant functional types in a semi-arid dune ecosystem. *J. Veg. Sci.* 29, 671–683. doi: 10.1111/jvs.12647

Barbeta, A., and Peñuelas, J. (2017). Relative contribution of groundwater to plant transpiration estimated with stable isotopes. *Sci. Rep.* 7:10580.

Cheng, X., An, S., Li, B., Chen, J., Lin, G., Liu, Y., et al. (2006). Summer rain pulse size and rainwater uptake by three dominant desert plants in a desertified grassland ecosystem in northwestern China. *Plant Ecol.* 184, 1–12. doi: 10.1007/s11258-005-9047-6

Dai, Y., Zheng, X.-J., Tang, L.-S., and Li, Y. (2015). Stable oxygen isotopes reveal distinct water use patterns of two *Haloxylon* species in the Gurbantonggut Desert. *Plant Soil* 389, 73–87. doi: 10.1007/s11104-014-2342-z

Dodd, M. B., Lauenroth, W. K., and Welker, J. M. (1998). Differential water resource use by herbaceous and woody plant life forms in a short grass steppe community. *Oecologia* 117, 504–512. doi: 10.1007/s004420050686

Duan, D.-Y., Ouyang, H., Song, M.-H., and Hu, Q.-W. (2008). Water sources of dominant species in three alpine ecosystems on the Tibetan Plateau. *China. J. Integr. Plant Biol.* 50, 257–264. doi: 10.1111/j.1744-7909.2007.00633.x

Ehleringer, J. R. (1993). "Carbon and water relations in desert plants: an isotopic perspective," in *Stable Isotope and Plant Carbon-Water Relations*, eds J. R. Ehleringer, A. E. Hall, and G. D. Farquhar (San Diego: Academic Press), 155–172. doi: 10.1016/b978-0-08-091801-3.50018-0

Flora of China (1993). *Caragana Intermedia*. Avaliable at: http://foc.iplant.cn/content.aspx?TaxonId=250094187 (accessed January 9, 2020).

Grossiord, C., Sevanto, S., Dawson, T. E., Adams, H. D., Collins, A. D., Dickman, L. T., et al. (2017). Warming combined with more extreme precipitation regimes modifies the water sources used by trees. *New Phytol.* 213, 584–596. doi: 10.1111/nph.14192

Hou, Y., Zhou, G., Xu, Z., Liu, T., and Zhang, X. (2013). Interactive effects of warming and increased precipitation on community structure and composition in an annual forb dominated desert steppe. *PLoS One* 8:e70114. doi: 10.1371/journal.pone.0070114

Huang, L., and Zhang, A. (2015). Stable isotopic analysis on water utilization of two xerophytic shrubs in a revegetated desert area: tengger desert, China. *Water* 7, 1030–1045. doi: 10.3390/w7031030

IPCC (2013). *Climate Change 2013. The Physical Science Basis*. New York, NY: Cambridge University Press.

Jia, Z., Zhu, Y., and Liu, L. (2012). Different water use strategies of juvenile and adult *Caragana intermedia* plantations in the Gonghe Basin, Tibet Plateau. *PLoS One* 7:e45902. doi: 10.1371/journal.pone.0045902

Kowaljow, E., and Fernández, R. J. (2011). Different utilization of a shallow-water pulse by six shrub species in the Patagonian steppe. *J. Arid Environ.* 75, 211–214. doi: 10.1016/j.jaridenv.2010.10.004

Kray, J. A., Cooper, D. J., and Sanderson, J. S. (2012). Groundwater use by native plants in response to changes in precipitation in an intermountain basin. *J. Arid Environ.* 83, 25–34. doi: 10.1016/j.jaridenv.2012.03.009

Li, Q., Jia, Z., Zhu, Y., Wang, Y., Li, H., Yang, D., et al. (2015). Spatial heterogeneity of soil nutrients after the establishment of *Caragana intermedia* plantation on sand dunes in alpine sandy land of the Tibet Plateau. *PLoS One* 10:e124456. doi: 10.1371/journal.pone.0124456

Li, S., Romero-Saltos, H., Tsujimura, M., Sugimoto, A., Sasaki, L., Davaa, G., et al. (2007). Plant water sources in the cold semiarid ecosystem of the upper Kherlen River catchment in Mongolia: a stable isotope approach. *J. Hydrol.* 333, 109–117. doi: 10.1016/j.jhydrol.2006.07.020

Li, S., Wang, X. Q., Gao, Q., Bao, Y., and Yin, S. (2016). Influence of soil heterogeneity based on vegetation recovery in alpine sandy land. *Forest Res.* 29, 553–559.

Liu, S., Chen, Y., Chen, Y., Friedman, J. M., Hati, J. H. A., and Fang, G. (2015). Use of ^{2}H and ^{18}O stable isotopes to investigate water sources for different ages of *Populus euphratica* along the lower Heihe River. *Ecol. Res.* 30, 581–587. doi: 10.1007/s11284-015-1270-6

Loik, M. E., Breshears, D. D., Lauenroth, W. K., and Belnap, J. (2004). A multi-scale perspective of water pulses in dryland ecosystems: climatology and ecohydrology of the western USA. *Oecologia* 141, 269–281. doi: 10.1007/s00442-004-1570-y

Ma, Y., and Song, X. F. (2016). Using stable isotopes to determine seasonal variations in water uptake of summer maize under different fertilization treatments. *Sci. Total Environ.* 550, 471–483. doi: 10.1016/j.scitotenv.2016.01.148

Schwinning, S., and Sala, O. E. (2004). Hierarchy of responses to resource pulses in arid and semi-arid ecosystems. *Oecologia* 141, 211–220. doi: 10.1007/s00442-004-1520-8

Song, L., Zhu, J., Li, M., and Yu, Z. (2014). Water utilization of *Pinus sylvestris* var. *mongolica* in a sparse wood grassland in the semiarid sandy region of Northeast China. *Trees* 28, 971–982. doi: 10.1007/s00468-014-1010-5

Stock, B. C., Jackson, A., Ward, E. J., Parnell, A. C., Phillips, D. I., and Semmens, B. X. (2018). Analyzing mixing systems using a new generation of Bayesian tracer mixing models. *PeerJ* 6: e5096. doi: 10.7717/peerj.5096

Su, H., Li, Y., Liu, W., Xu, H., and Sun, J. O. (2014). Changes in water use with growth in *Ulmus pumila* in semiarid sandy land of northern China. *Trees* 28, 41–52. doi: 10.1007/s00468-013-0928-3

Weltzin, J. F., and Tissue, D. T. (2003). Resource pulses in arid environments – patterns of rain, patterns of life. *New Phytol.* 157, 171–173. doi: 10.1046/j.1469-8137.2003.00672.x

West, A. G., Hultine, K. R., Burtch, K. G., and Ehleringer, J. R. (2007). Seasonal variation in moisture use in a piñon-juniper woodland. *Oecologia* 153, 787–798. doi: 10.1007/s00442-007-0777-0

Xia, J., and Wan, S. (2012). The effects of warming-shifted plant phenology on ecosystem carbon exchange are regulated by precipitation in a semi-arid grassland. *PLoS One* 7:e32088. doi: 10.1371/journal.pone.0032088

Yang, H., Auerswald, K., Bai, Y., and Han, X. (2011). Complementarity in water sources among dominant species in typical steppe ecosystems of inner mongolia. *China Plant Soil* 340, 141–155. doi: 10.1007/s11104-010-0307-4

Yang, W. B., Tang, J. N., Liang, H. R., Dang, H. Z., and Li, W. (2014). Deep soil water infiltration and its dynamic variation in the shifting sandy land of typical deserts in China. *Sci. China Earth Sci.* 57, 1816–1824. doi: 10.1007/s11430-014-4882-8

Zhang, C., Li, X., Wu, H., and Wang, P. (2017). Differences in water-use strategies along an aridity gradient between two coexisting desert shrubs (*Reaumuria soongorica* and *Nitraria sphaerocarpa*): isotopic approaches with physiological evidence. *Plant Soil* 419, 169–187. doi: 10.1007/s11104-017-3332-8

Zheng, X. R., Zhao, G. Q., Li, X. Y., Li, L., Wu, H. W., Zhang, S. Y., et al. (2015). Application of stable hydrogen isotope in study of water sources for *Caragana microphylla* bushland in Nei Mongol. *Chin. J. Plant Ecol.* 39, 184–196. doi: 10.17521/cjpe.2015.0018

Zhou, H., Zhao, W., Zheng, X., and Li, S. (2015). Root distribution of *Nitraria sibirica* with seasonally varying water sources in a desert habitat. *J. Plant Res.* 128, 613–622. doi: 10.1007/s10265-015-0728-5

Zhou, Y., Boutton, T. W., Wu, X. B., Wright, C. L., and Dion, A. L. (2018). Rooting strategies in a subtropical savanna: a landscape-scale three-dimensional assessment. *Oecologia* 186, 1127–1135. doi: 10.1007/s00442-018-4083-9

Zhu, Y. (2016). "Water use strategy of four desert shrubs in Gonghe Basin, Qinghai-Tibetan Plateau," in *Water Stress in Plants*, eds I. M. Rahman, Z. A. Begum, and H. Hasegawa (Croatia: InTech), 81–98. doi: 10.5772/63195

Zhu, Y., Wang, G., and Li, R. (2016). Seasonal dynamics of water use strategy of two salix shrubs in alpine sandy land, Tibetan Plateau. *PLoS One* 11:e0156586. doi: 10.1371/journal.pone.0156586

Conflict of Interest: The authors declare that the research was conducted in the absence of any commercial or financial relationships that could be construed as a potential conflict of interest.

frontiers in Environmental Science

ORIGINAL RESEARCH
published: 11 September 2020
doi: 10.3389/fenvs.2020.528732

Isolation of Efficient Cellulose Decomposer in Sandy Cropland and Its Application in Straw Turnover in Agro-Pasture Ecotone of Northern China

Shaokun Wang[1], Xueyong Zhao[1]*, Balt Suvdantsetseg[2] and Jie Lian[1]*

[1] *Urat Desert-Grassland Research Station, Naiman Desertification Research Station, Northwest Institute of Eco-Environment and Resources, Chinese Academy of Sciences, Lanzhou, China,* [2] *Sustainable Development Institute for Western Region of Mongolia, Ulaanbaatar, Mongolia*

Slow organic material and nutrient turnover is one of the limiting processes in arid and semiarid ecosystems, and cellulose decomposers play an important role in straw turnover and nutrient return in cropland ecosystem in drylands. In order to moderate the limiting effect of material turnover, a highly efficient cellulose decomposing fungus was screened from 85 cellulose decomposing fungi and we named the isolated fungus as NMCel-crop1 in the sandy cropland of Horqin Sandy Land in a semiarid agro-pasture ecotone in northern China. This fungal decomposer was identified as *Rhizomucor variabilis* by using morphological and rDNA-ITS molecular methods. The optimized temperature for expressing its carboxymethyl cellulose (CMC) enzyme activity ranges from 40 to 55°C. The CMC enzyme activity was significantly and highly produced by the NMCel-crop1 than that *in situ* soil in the cropland, and the filter paper decomposition rate was 82% in 7 days. The field straw decomposition experiment showed that the decomposition rate of maize straw infected by NMCel-crop1 reached at 92.5% in 1 year, which was 26% higher than that without infection. Straw turnover accelerated by NMCel-crop1 significantly increased soil organic carbon (SOC) and total nitrogen (TN) by 34.08 and 14.26%, respectively, indicating that the selected highly efficient decomposing fungus could accelerate straw turnover rate and increase SOC and nitrogen content and promote soil fertility and soil health in the sandy cropland, as well as potentially improve crop productivity and quality in the sustainable agriculture management of the arid and semiarid sandy cropland.

Keywords: cellulose decomposer, CMC enzyme activity, sandy cropland, straw turnover, agro-pasture ecotone

OPEN ACCESS

Edited by:
Atsushi Tsunekawa, Tottori University, Japan

Reviewed by:
Rentao Liu, Ningxia University, China
Takeshi Taniguchi, Tottori University, Japan

****Correspondence:***
Shaokun Wang
wangsk@lzb.ac.cn
Xueyong Zhao
zhaoxy@lzb.ac.cn

Specialty section:
This article was submitted to Land Use Dynamics, a section of the journal Frontiers in Environmental Science

Received: *13 February 2020*
Accepted: *17 August 2020*
Published: *11 September 2020*

Citation:
Wang S, Zhao X, Suvdantsetseg B and Lian J (2020) Isolation of Efficient Cellulose Decomposer in Sandy Cropland and Its Application in Straw Turnover in Agro-Pasture Ecotone of Northern China. Front. Environ. Sci. 8:528732. doi: 10.3389/fenvs.2020.528732

INTRODUCTION

The boundary line of the agricultural and pastoral area is approximately consistent with the 400-mm isohyet in China. The land use in the southeast part of the isohyet is cropping dominant, and the northwest part is pasture dominant. The agro-pasture transitional ecotone is in between the agricultural and pastoral area, in which both cropping is expanding and grazing intensified spatially

and temporally. The agro-pasture transitional ecotone of northern China starts from Hulun Buir of western Great Khingan, southward to Tongliao and Chifeng of Inner Mongolia, then goes to northern Hebei, Shanxi, and Shaanxi provinces, and ends up at eastern Gansu province (Zhao et al., 2002). The annual precipitation of the transitional ecotone is ranging from 300 to 450 mm. Precipitation, which fluctuates significantly, is the main limiting factor for both cropping and grazing in this area. The vegetation changes variably in consequence with the precipitation, which makes this transitional area a very vulnerable ecotone (Zhao et al., 2003).

Horqin Sandy Land is located in the southeast part of Inner Mongolia, which is one of the most vulnerable and most typical areas for ecological and environmental study in semiarid agro-pasture transitional ecotone. During the recent few decades, a large area of grassland has been converted into farmland year by year in this region, mostly due to the rapid growth of population and their aspiration for better life. Therefore, maize (*Zea mays* L.) became the best choice for cropping, because of its higher productivity and higher price. However, maize consumes much more water than the local plants, and the overuse of water for irrigation resulted in desertification of this vulnerable sandy land ecosystem (Zhao et al., 2015; Wang et al., 2016a).

Straw turnover is a conservational management to enhance the soil fertility in agricultural sustainable maintenance (Kassam et al., 2009). However, the low precipitation and temperature makes the straw decompose much slower in winter and spring, retaining a large amount of undecomposed cellulose in and/or upon the surface soil of the cropland in Horqin sandy cropland. The undecomposed straw residual will lead to pest and virus breakouts in this area. So many farmers prefer burning the maize straw after harvest, which causes heavy air pollution, consequently causing respiratory infections and also waste of organic resource in the semiarid area (Qu et al., 2012; Zhang et al., 2014). Cellulose is one of the most renewable bioenergy materials, producing alcohol, carbohydrate, single-cell protein, and organic fertilizer during its enzymatic decomposition procedure (Lynd et al., 2002). Therefore, the efficient treatment and suitable utilization of cellulose could not only supplement bioenergy shortage but also relieve environmental pollution from agricultural waste, especially in dryland areas. It is an efficient and environmentally friendly approach to decompose cellulose by cellulolytic decomposers (Panagiotou et al., 2003). Cellulose decomposers play a very important role in sandy farmland ecosystems. They participate actively in straw turnover, nutrient uptake, and pest control (Jin, 2004; Wang et al., 2016b; Jaiswal et al., 2017). The cellulose decomposers isolated from terrestrial ecosystems are mostly fungi, and most of them could be categorized into *Trichoderma*, *Penicillium*, *Aspergillus*, and *Fusarium* (Panagiotou et al., 2003; Wen et al., 2005; Lu et al., 2011; Wang et al., 2015a). The study on the functional cellulose decomposers and their ecological service are fundamental and essential in sustainable agricultural management in drylands (Qin and Wei, 2007). However, it is seldom reported on the isolation of efficient cellulosed decomposers in semiarid sandy cropland. The purpose of this study is to isolate several highly efficient cellulose decomposers in Horqin sandy cropland. We hypothesized that isolation of highly efficient cellulose decomposers in Horqin sandy cropland soil could not only enrich soil functional microbial bank and accelerate maize straw turnover but also promote sustainable agricultural development in the agro-pasture ecotone of northern China.

MATERIALS AND METHODS

Study Area

This study was conducted in Naiman Desertification Research Station of the Chinese Academy of Sciences (NDRS), which is located in Naiman County in the southwestern part of the Horqin Sandy Land, Inner Mongolia, northern China (120°55′E, 42°41′N; 360 m a.s.l.) (**Figure 1**). The climate in this area is characterized as a temperate, semiarid continental monsoon, with a hot summer and cold winter. The mean annual precipitation is 366 mm, with 70–80% falls during the general plant growing season from June to September. The annual mean open-pan evaporation is around 1935 mm, five times greater than annual precipitation. The annual mean temperature is around 6.4°C, ranging from a monthly maximum of 23.5°C in July to a monthly minimum of −16.8°C in January. The annual mean wind velocity ranges from 3.6 to 4.1 m/s, and the dominant wind is southwest in summer and autumn and northwest in winter and spring. The zonal soil is classified as sandy chestnut, which is sandy in texture, light yellow in color, and loose in structure and is vulnerable to wind erosion (Zhao et al., 2003; Wang et al., 2016b). The original landscape was dominated by sandy grassland with scattered trees (mostly elms, *Ulmus* spp.). However, the grassland has been replaced by farmland, due to the increase in population and development of irrigation. Maize (*Z. mays* L.) monoculture dominates the cultivated land because of its higher productivity and easier management (Wang et al., 2016a).

Experimental Design

Soil Collection

We collected soil samples for isolating cellulose decomposers in the comprehensive observation cropland field in NDRS. This long-term observation field was established in 1997, covering 20,000 m^2 and planting maize since then. This field is a typical irrigated sandy cropland in Horqin sandy cropland. We randomly set up 10 quadrats (1 m × 1 m) in the observation field, took five replications of soil cores at a depth of 0–20 cm in each quadrat and mixed as a pooled sample. Every pooled sample was sieved (<2 mm) to remove rocks and plant material and stored separately in sterilized ziplock bags at 4°C, prepared for laboratory isolation of cellulose decomposers. The soil collection was conducted in early August. The basic characteristics of the observation field are shown in **Table 1**.

Culturable Medium for Cellulose Decomposing Fungi Isolation

The medium used for isolating and selecting efficient cellulose-decomposing fungi includes carboxymethyl cellulose (CMC) medium, PDA medium, Congo Red CMC medium, litter medium, and liquid medium (peptone: 2.6 g; yeast extract: 1.3 g;

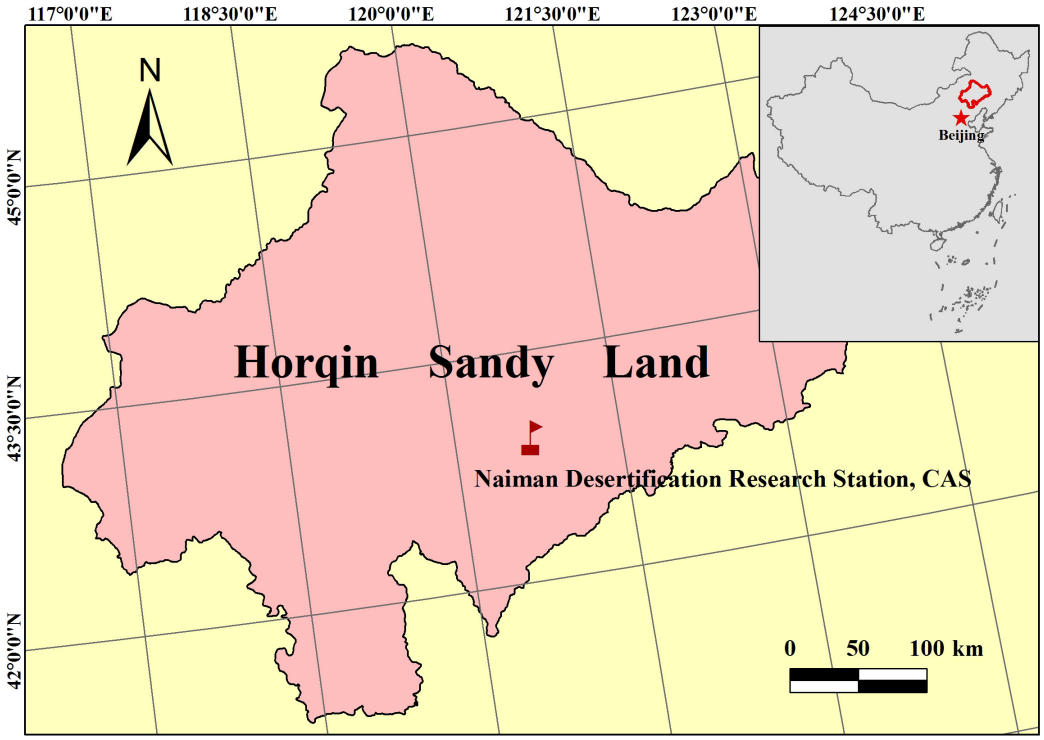

FIGURE 1 | Study area of Naiman Desertification Research Station (NDRS), in the southeastern part of Inner Mongolia, typical area in agro-pasture ecotone of northern China.

litter powder: 5 g; $MgSO_4 \cdot 7H_2O$: 0.8 g; KH_2PO_4: 2 g; NaCl: 0.1 g; H_2O: 1,000 mL). The detailed recipe for each medium was shown in Wang et al. (2015b).

Procedures for Isolation and Screening

Isolation: 10 g fresh soil was mixed into 90 ml sterilized water until the soil was totally suspended. 1 ml supernate was added into 9 ml sterilized water and shaken to produce 1 and 10% soil microbial suspensions. 1-ml suspensions were transferred into CMC medium plates with five replicates for both 1 and 10% suspensions, separately. The plates were incubated at 30°C for 10–15 days until different colonies grew big enough to be picked for purification.

Purification: Separated colonies were picked and transferred into PDA medium plates and incubated at 30°C for 3–5 days. Colonies without any infection were selected as purified fungi for advanced screening.

Screening for efficient cellulose-decomposing fungi: Pure colonies were transferred into litter medium plates at 30°C for 5–10 days. Pure colonies with long mycelium and abundant spore were chosen as cellulose-decomposing fungi. Separated colonies were scraped by vaccinating lancet, placed into Congo Red CMC medium plates, and incubated at 30°C for 10 days to select efficient cellulose decomposing fungi. Colonies with faster growth and larger transparent rings in the Congo Red CMC medium plates were screened as highly efficient cellulose decomposing fungi. The selected fungal strains were stored in Congo Red CMC medium tubes for morphological and molecular identification and further experiment.

TABLE 1 | Characteristics of the cropland.

Crop	Species	*Zea mays* L.
	Yield (g/m^2)	998.37 ± 38.32
	Aboveground biomass (g/m^2)	2288.73 ± 156.71
	Underground biomass (g/m^2)	77.45 ± 9.16
Soil	pH	8.20 ± 0.21
	C ($g.kg^{-1}$)	7.56 ± 0.30
	N ($g.kg^{-1}$)	0.85 ± 0.04
	P ($mg.kg^{-1}$)	28.76 ± 4.01
	K ($mg.kg^{-1}$)	95.31 ± 7.83
	Bulk density ($g.cm^{-3}$)	1.41 ± 0.11
Microbe	Bacteria abundance (10^3 /g. dry soil)	1032.44 ± 50.97
	Actinomycete abundance (10^3 /g. dry soil)	495.20 ± 44.16
	Fungi abundance (10^3 /g. dry soil)	21.07 ± 3.38
	Soil Microbial biomass carbon ($mg\ kg^{-1}$)	462.17 ± 35.08

Data were from the long-term observation database in NDRS (http://nmd.cern.ac.cn/meta/metaData).

Morphological and Molecular Identification

Morphology

The selected fungal strains were transferred into PDA medium plates and incubated at 30°C for 3–5 days. Microscopic

examination was performed to observe the characteristics of the mycelium and spore for each strain. "Manual of Fungi Taxa Identification" (Wei, 1979) and "Illustrated Genera of Imperfect Fungi" (Barnett and Hunter, 1998) were used for the fungi taxa identification.

Molecular Identification

DNA was extracted from a small portion of the selected fungi mycelium (Zhang et al., 2008). Universal primers of ITS1 (5′-TCCGTAGGTGAACCTGCGG-3′) and ITS 4 (5′-TCCTCCGCTTATTGATATGC-3′) were used for PCR. PCR reaction system (50 μL): dd H_2O 30 μL, PCR buffer 5 μL, dNTP 5 μL, $MgCl_2$ 2 μL, formamide 2 μL, ITS1 1.5 μL, rTaq enzyme 1 μL, template DNA 2 μL. PCR reaction condition: 94°C for 5 min, 94°C for 40 s, 55°C for 40 s, 72°C for 1 min, 72°C for 10 min, 38 cycles. The target PCR products with a clear strip were sequenced in Nuosai Gene. The DNA sequences were aligned with the GenBank database in National Center for Biotechnology Information (NCBI)[1] to determine the taxa of the selected fungus. Molecular Evolutionary Genetics Analysis 7 (MEGA 7) was used to build a phylogenetic Minimum Evolution (ME) tree based on the DNA sequences that are similar with the target DNA sequence in NCBI, and the evolutionary distances were computed using the p-distance method (Nei and Kumar, 2000).

CMC Enzyme Activity

Carboxymethyl cellulose enzyme activity from the supernate was determined at different temperature gradient (20, 25, 30, 70°C).

A small amount of the final selected fungus was taken and dipped into the conical flasks with the liquid medium. The flasks were shaken (150 r/min) at 30°C for 7 days and then centrifuged at 4,000 r/min for 15 min. The supernate was used for determining the CMC enzyme activity. 0.5 ml of supernate was placed into a tube with 1.5 ml citrate buffer (0.05 mol/l, pH 5.0, containing 0.5% CMC-Na). The tube was water-bathed at different temperature gradients (20, 25, 30, 35, 40, 45, 50, 55, 60, 65, 70°C) for 30 min. Then, 1 ml dinitrosalicylic acid (DNS) was added into the tube which was boiled at 100°C for 5 min. The volume was remained constant at 5 ml when the tube cooled at room temperature. The absorbance was determined at 540 nm in a spectrophotometer. The glucose content was calculated based on the standard curve (Fang et al., 2007; Bayer et al., 2013; Sun et al., 2017).

CMC enzyme activity $X = m/(V.t).n$ (Equation 1)

where m represents glucose content, V represents supernate volume (0.5 mL), t represents reaction time (30 min), and n represents dilution ratio (5/0.5).

A 10 g fresh soil was diluted into 90 ml sterilized water, shaken for 15 min at 150 r/min, and 0.5 ml of the soil supernate was used to determine soil CMC enzyme activity (Guan, 1986).

Decomposition Ability

A small piece of the strain was taken and incubated in the liquid medium conical flask for 24 h. Then, five pieces of filter paper were put into the flask, shaken (150 r/min), and incubated at 30°C for 10 days. Weight loss was determined every day until the weight did not change significantly (Yao and Huang, 2006).

Decomposition rate $D = ((m_0\text{-}m_i)/m_0) \times 100\%$ (Equation 2)

where m_0 is the original weight of the filter paper, while m_i is the weight at the ith day.

Straw Decomposition in Field Experiment

The maize straw was cut into small pieces (<5 cm) after harvest, and the straw pieces were oven dried at 70°C for 24 h to a constant weight. The maize straw carbon and nitrogen contents were 451.6 ± 6.6 and 7.73 ± 0.26, respectively, and its C:N ratio was 58.42 ± 1.64. 10-g straw pieces were sealed in a 20 cm × 25 cm nylon net bag (net hole are 2 mm × 2 mm). The net bags were soaked with straw in the liquid medium and incubated with the selected cellulose-decomposing fungi for 30 min. Meanwhile, net bags of straw without decomposer infection were set as control. The control net bags were soaked in the liquid medium without any microbes for 30 min to minimize the influence of the liquid medium for straw decomposition. Then, 20 net bags with and without the decomposing fungi were buried at 10 cm deep in the cropland soil, respectively. The net bags were set randomly 20 m away from each other in the comprehensive observation cropland field in NDRS in early October. We collected five net bags with the impact of the selected cellulose decomposing fungi, as well as five control net bags in early December (frozen season, 60th day), next early May (seeding season, the 200th day), next mid August (growing season, 300th day), and next early October (harvest season, 360th day), respectively. The straws in the net bags were cleaned and then oven-dried at 70°C for 24 h. The mycelia from NMCel-crop1 were observed in all of the net bags added with the selected decomposing fungi, suggesting that NMCel-crop1 fungi were present in all the decomposing stages. The maize straw mass loss rate is calculated as 1-D (D refers to the decomposition rate in Eq. 2) (Qu et al., 2011). A modified "Olson" litter mass loss model (Eq. 3) was used to predict straw turnover.

$R = \frac{x}{x_0} = e^{-(kt)^{\alpha}}$ (Equation 3) (Olson, 1963; Liu et al., 2006)

where R is the percentage of remaining mass; x_0 is the initial litter mass, and x is the litter mass at the time of t; k represents the litter turnover rate (higher k means faster decomposition rate); α is a correction factor.

Meanwhile, soils were carefully collected under net bags (≤1 cm both with and without selected decomposers) and bare soil at a depth of 0–10 cm was collected as control at the end of the straw decomposition experiment. The soil organic carbon (SOC) and total nitrogen (TN) were analyzed to calculate the nutrient return in the field. SOC was measured by the dichromate oxidation method of Walkley and Black (Nelson and Sommers, 1982), and TN was determined by the Kjeldahl procedure (Institute of Soil Sciences CAS, 1978).

Data Analysis

Origin 8.0 (OriginLab, United States), SPSS 17.0 (IBM SPSS Statistics, United States), and Microsoft excel 2016 (Microsoft, United States) were used to analyze the descriptive statistical data and significance tests. Significant differences were assessed by one-way ANOVA and LSD tests at $p < 0.05$. All the descriptive data were expressed as means ± SE.

[1] https://www.ncbi.nlm.nih.gov

TABLE 2 | Diameter of hydrolytic ring of the selected five strains.

Strains	Diameter(cm)
NMCel-crop1	2.1 ± 0.3 a
NMCel-crop2	1.5 ± 0.2 b
NMCel-crop3	1.5 ± 0.1 b
NMCel-crop4	1.2 ± 0.2 c
NMCel-crop5	1.1 ± 0.1 c

Values (mean ± SE) with different letters within a column are significantly different at $p < 0.05$.

RESULTS

Isolation

The results showed that 85 cellulose-decomposing fungi were detected in the CMC medium plates, 11 of which were purified from the isolation due to the different colors and shapes of the colony. Five strains grew much faster after prescreening in the litter medium plates. These five screened strains were numbered as NMCel-crop1, NMCel-crop2, NMCel-crop3, NMCel-crop4, and NMCel-crop5. Advanced screening showed that NMCel-crop1 grew much faster, and the diameter of hydrolytic ring was significantly larger than the other four strains in the Congo Red CMC medium plates (**Table 2**). Therefore, NMCel-crop1 was selected as the highly efficient cellulose decomposing fungus.

Identification

From the microscopic images (**Figure 2**), we could clearly see that there are no separation in the hypha, and single sporangiophores emerge at the end of each hypha. Spherical sporangia, with a great number of spores, appear at the top of sporangiophores. The morphological characteristics illustrated that NMCel-crop1 could be assigned in the Mucoraceae family. DNA sequencing analysis showed that the length of the extracted DNA is 1048 bp, with 38.26% of the G + C base. Blast alignment of the DNA sequence in the NCBI GenBank database indicated that the strain is mostly associated with the known fungus sequence (FJ227892.1: *Rhizomucor variabilis var. regularior isolate 80*, genetic similarity = 99.49%) (**Figure 3**). The NMCel-crop1 fungus was identified as the species of *R. variabilis* in the genus of *Rhizomucor* and family of Mucoraceae.

CMC Enzyme Activity

Carboxymethyl cellulose enzyme activity from the supernate was determined at different temperature gradients (20, 25, 30, 70°C). The CMC enzyme activity increased gradually from 20 to 40°C, then increased smoothly, and got to its peak at 50°C. It decreased sharply from 55°C (**Figure 4**). Therefore, the optimized temperature for the NMCel-crop1 fungus to fulfill its decomposing ability is 50°C. The CMC enzyme activity produced by the NMCel-crop1 fungus (0.43 ± 0.03 mg/ml·min) was significantly higher than that from the sandy cropland soil (0.05 ± 0.01 mg/ml·min) ($p < 0.001$).

Decomposition Ability

The change in filter paper mass loss, decomposed by the NMCel-crop1 fungus, showed that it decomposed very slowly in the first 3 days ($D < 20\%$). From the 3rd to 6th days, the filter paper weight lost very fast from 20 to 80% and almost lost at a rate of 20% per day. Then, after the 7th day ($D = 82.03 \pm 2.46\%$), the mass did not change significantly (**Figure 5**).

Straw Decomposition in the Field Experiment

The result from the field experiment (**Figure 6**) showed that straw was decomposed very fast at the first decomposing stage (harvest to frozen seasons, 0–60 day) by 42.27 ± 3.91% infected by NMCel-crop1 fungus, which was 11.47% higher than bare soil, and then became much slower in the frozen season from early December to early May (60–200 day), 9.03% infected by the NMCel-crop1 fungus, and 4.47% in bare soil. When it became warmer, the straw decomposition rate was much faster again. The decomposition rate reached 83.69 ± 2.50% infected by the NMCel-crop1 fungus, 20% higher than bare soil at the end of the growing season in mid August. The daily decomposition rate did not show a statistical difference between NMCel-crop1 fungus (0.28%/day) and bare soil (0.26%/day) at the 3rd decomposing stage (seeding season to growing season, 200–300 day). After the growing season (300–400 day), the straw mass loss was still going on when infected by the NMCel-crop1 fungus, but it slowed down in bare soil. The straw mass loss reached 92.49% infected by the NMCel-crop1 fungus, 26% higher than that in bare soil after 1 year buried in the sandy cropland soil. The residual of the straw remained less than

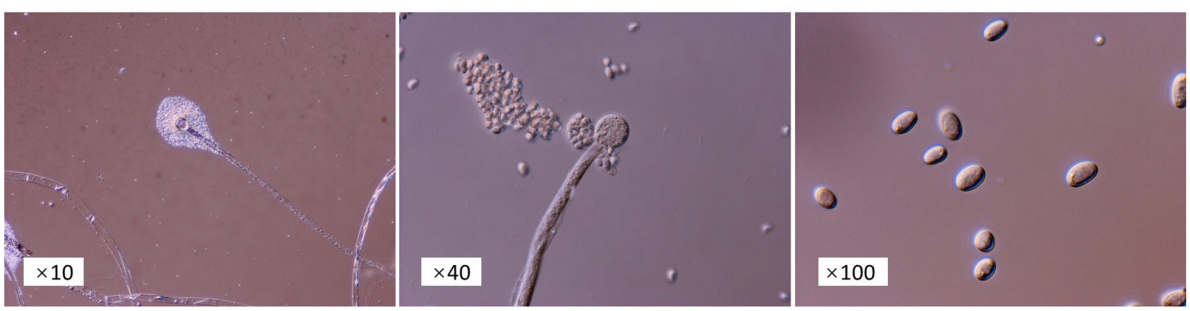

FIGURE 2 | Microscopic morpha of NMCel-crop1 magnified at 10, 40, and 100 times.

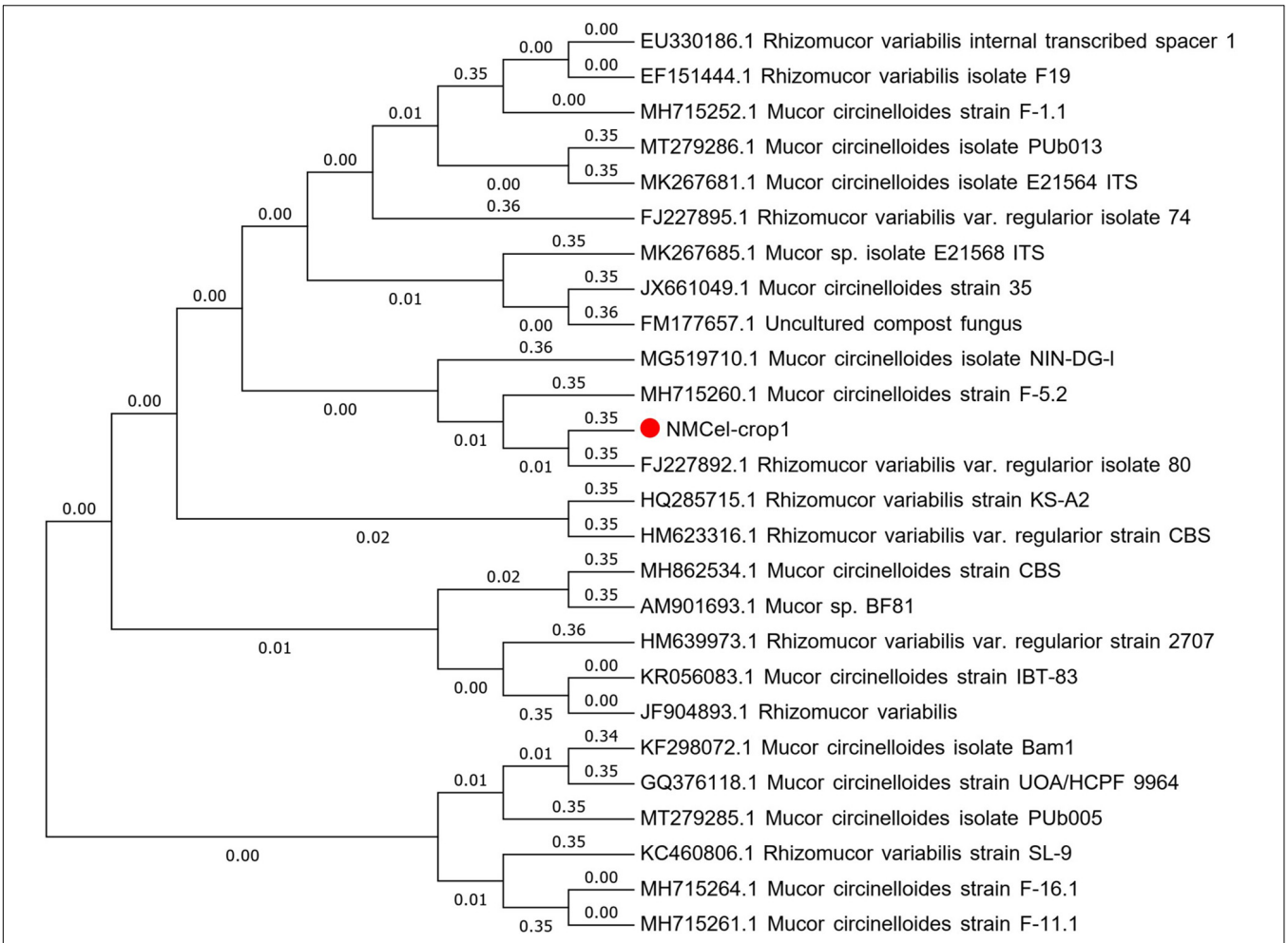

FIGURE 3 | Phylogenetic Minimum-Evolution (ME) tree of NMCel-crop1 and its related strains.

10% infected by the NMCel-crop1 fungus, which significantly accelerated the straw turnover in the semiarid sandy cropland. The modified "Olson" mass loss model was made to predict maize straw turnover both in bare soil and that affected by the NMCel-crop1 fungus in the field. It clearly showed that the observed mass loss rate could be well fitted in the model ($R^2 > 0.9$) and the litter turnover rate k was much higher in the model affected by NMCel-crop1 than that in bare soil (**Table 3**), indicating that the maize straw turnover rate was much fast with the help of the NMCel-crop1 fungus than that in natural bare soil.

To evaluate the quantitative nutrient return in the cropland soil, SOC and TN were collected and analyzed at the end of the field experiment. The result showed that maize straw turnover increased SOC significantly. SOC was 20.16 and 34.08% significantly higher in soils under the net bag with (WD) the selected decomposer compared with that in soils without the selected decomposer (ND) and the control soil (CK), respectively. Soil TN did not show a statistical difference between ND and CK. However, TN was significantly higher in WD than that in ND and CK. SOC and nitrogen ratio (C:N) increased significantly by 13.06 and 16.80% in ND and WD than that in CK. The C:N ratio did not show a significant difference between ND and WD. The results indicated that our selected decomposing fungus could not

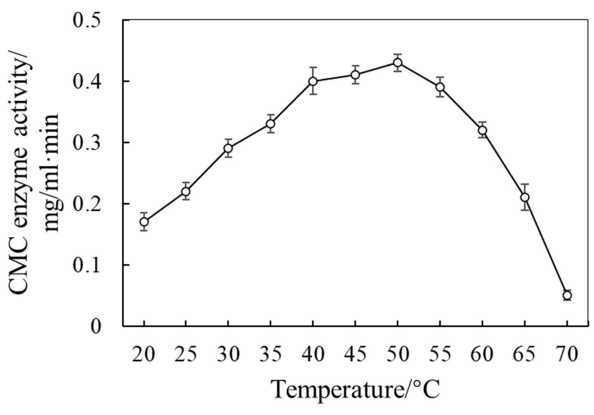

FIGURE 4 | CMC enzyme activity at different temperature gradients.

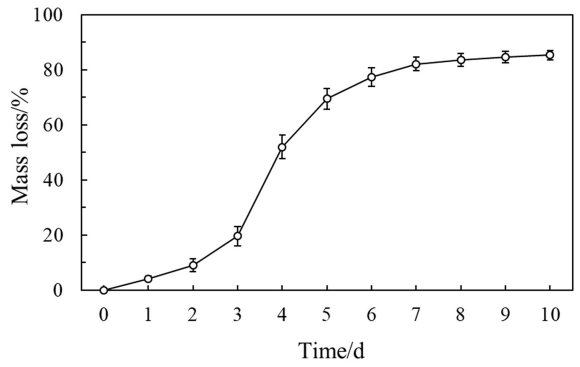

FIGURE 5 | Mass loss of the filter paper decomposed by the NMCel-crop1 fungus.

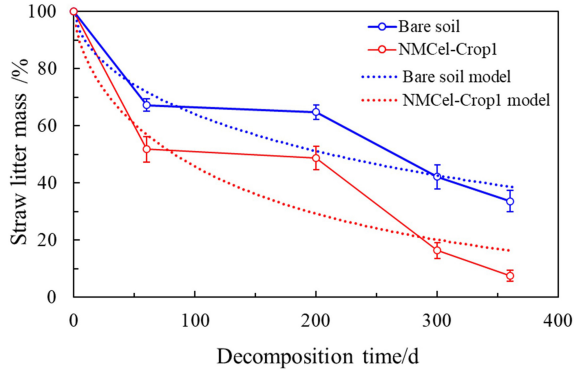

FIGURE 6 | Straw decomposition rate accelerated by the NMCel-crop1 fungus in the field experiment.

TABLE 3 | Modified "Olson" mass loss model in the field decomposition experiment.

Modified "Olson" mass loss model	Bare soil	NMCel-crop1
$R = \frac{x}{x_0} = e^{-(kt)^{\alpha}}$	$\alpha = 0.597$ $k = 0.883$ $R^2 = 0.915$	$\alpha = 0.653$ $k = 2.386$ $R^2 = 0.906$

only accelerate the straw turnover rate but also could increase SOC and nitrogen content and potentially promote soil fertility and soil health in the sandy cropland.

DISCUSSION

We have isolated and selected abundant and highly efficient cellulose decomposers, some of which contributed to litter decomposition by 50% in 30 days in the former work in Horqin sandy grassland (Wang et al., 2015a). However, the cellulose decomposers detected in the sandy cropland was much less (Wang et al., 2016a) and could not isolate highly efficient cellulose decomposers for a long time. That is why we optimized the isolation, purification, and screening procedures to obtain this highly efficient cellulose-decomposing fungus (*R. variabilis*) for promoting straw turnover and nutrient cycling in semiarid sandy cropland maintenance in Horqin sandy cropland.

Soil organic carbon is an important component to soil fertility and water holding capacity. Soil nitrogen is a major nutrient element that influences plant growth and biogeochemical cycle in terrestrial ecosystems. The SOC and nitrogen ratio (C:N) has been used as a key factor to evaluate soil health in agriculture ecosystem (Al-Kaisi et al., 2005; Kibblewhite et al., 2008; Swangjang, 2015; Liu et al., 2018). Our result showed that straw turnover accelerated by the selected efficient decomposing fungus significantly increased SOC, TN, and C:N ratio in the sandy cropland (**Figure 7**), indicating that our selected decomposer (NMCel-crop1) could be magnified and demonstrated to accelerate straw turnover and increase soil nutrient in Horqin sandy cropland and other semiarid regions.

Generally speaking, the soil C:N ratio ranging from 15 to 25% indicates that the soil is in good health. The higher soil C:N ratio indicates that the soil has greater ability to immobilize additional nitrogen input (Livesley et al., 2016). In our experimental site, the C:N ratio in the bare soil was 14.74, mostly due to low SOC in sandy soil, as well as high chemical fertilizer input of agricultural management. Straw turnover significantly increased soil C:N ratio to 16.66 because of increased carbon input. Highly efficient cellulose-decomposing fungus (NMCel-crop1) addition promoted the soil C:N ratio at 17.21, indicating that maize absorbed more immobilized nitrogen during the growing season.

The selected highly efficient cellulose-decomposing fungus could produce CMC enzyme at 50°C and even higher (**Figure 4**), which is almost the maximum soil temperature recorded in Naiman Desertification Research Station[2], as well as in most of other deserts in Asia and in Africa (Zhao, 2012). The result indicated that the selected cellulose-decomposing fungus could also be potentially magnified and used in the arid and semiarid areas to accelerate litter decomposition, where the litter decomposed rate is slow.

Carboxymethyl cellulose enzyme activity from the supernate was determined at different temperature gradient (20, 25, 30, 70°C). The CMC enzyme activity increased gradually from 20 to 40°C, then increased smoothly, and got to its peak at 50°C. It decreased sharply from 55°C (**Figure 4**). Therefore, the optimized temperature for the NMCel-crop1 fungus to fulfill its decomposing ability is 50°C, and the optimized range for litter decomposition should be 40–55°C. The CMC enzyme activity produced by the NMCel-crop1 fungus (0.43 ± 0.03 mg/ml·min) was significantly higher than that from the sandy cropland soil (0.05 ± 0.01 mg/ml·min) ($p < 0.001$).

Many species in *Rhizomucor* genus are key fungi for fermentation in the food industry, and some of them are pathogenic fungi for skin disease. They play a very important role in alcoholic fermentation, sugar production, and lipid enzymolysis. Research showed that *Rhizomucor pusillus* could catalyze different carbon source substrates into small particles, such as glycerinum, lactic acid, and xylitol, which are very important products in the food industry (Millati et al., 2005).

[2]http://nmd.cern.ac.cn/meta/metaData

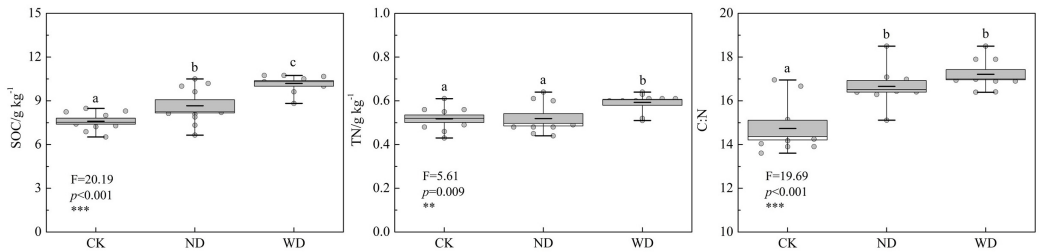

FIGURE 7 | Influence of straw turnover (with and without efficient cellulose decomposer) on soil organic carbon (SOC), total nitrogen (TN), and carbon and nitrogen ratio (C:N) in the field decomposition experiment. CK: bare soil without straw; ND: soil under straw net bags without selected decomposing fungi; WD: soil under straw net bags with selected decomposing fungi. Different letters represent significant difference among the treatments at $p < 0.05$.

Chadha et al. (2004) isolated a fungus (*R. pusillus*) with high phosphatase activity from the compost, and it could be used to regulate the composition of livestock fodder. Several species of *Rhizomucor* was isolated from soils in a semiarid area of southern Africa. These fungal species had high tolerance in excess nitrite and could survive under extreme drought stress (Seabi et al., 1999). Another species of *Rhizomucor* (*Rhizomucor miehei*) could produce lipase, which could be used in dairy products (Soltani et al., 2019) and also in biofuel industry (Rodrigues and Fernandez-Lafuente, 2010; Adnan et al., 2018). Some of the *R. miehei* could also produce mannose enzyme in strong acid and high-temperature environments (Li et al., 2017). Reports about *R. variabilis* were mostly focused on medical science. They are pathogenic fungi for many skin diseases (Lu et al., 2009; Tomita et al., 2011; Patil et al., 2013). Recently, a few reports on food production indicated that *R. variabilis* showed highly alkali resistance to produce lipase (Bancerz et al., 2015, 2018). Researchers isolated *R. variabilis* from mushroom (Ke et al., 2016) and corncob (Xu et al., 2017). These fungi were sensitive to nitrogen variations and beneficial for protecting crop from rot disease. Our research firstly recruited new fungal species into soil functional microbe banks in semiarid sandy cropland and tested their highly efficient litter decomposition function.

Soil microorganisms work collaboratively to regulate soil health and maintain the sustainable production in agricultural cropland (Chapin et al., 2002; Acostamartínez et al., 2010; Jaiswal et al., 2017). Cellulose decomposers are mainly responsible for crop straw decomposition and acceleration of its turnover in the agricultural ecosystem. Crop straw turnover could promote soil microbial activity and increase soil fertility, so that less chemical fertilizer would be applied and high-quality agricultural products could be produced in green agricultural development. Therefore, straw turnover became an effective practice in sustainable agricultural management (Roper and Gupta, 1995; Wei et al., 2017). However, in the cold and semiarid agro-pasture ecotone, such as Horqin Sandy Land, the precipitation is low and so is the temperature, especially in winter and spring. The straw decomposed very slowly after harvest, and the organic material could not return to the soil rapidly, leading to a waste of organic resource and even pest disease in the coming year. In the natural field condition of Horqin sandy cropland, the maize straw decomposition rate is only 35% from its harvest to the next seeding season, and it reaches 66% in a whole year, and 1/3 of the maize straw could not be decomposed. The straw residual is mostly lignin and/or polycellulose, and the residual could hardly be decomposed. We isolated and selected this highly efficient cellulose decomposing fungus (*R. variabilis*) from soils *in situ* in Horqin sandy cropland and magnified and accelerated straw turnover. The application of the decomposing microbial agents significantly increased the straw decomposition rate by 50% from its harvest to the next seeding season, and reached to >90% in 1 year. The maize straw could mainly return into soil as organic matter in a year. The application of this fungus could reduce the chemical fertilizer application and produce healthy crop products in a sustainable agricultural management system in the arid and semiarid agro-pasture area.

CONCLUSION

Five cellulose-decomposing fungi were isolated, and one of them was selected as a highly efficient cellulose decomposer in sandy cropland of the agro-pasture ecotone in northern China. This selected cellulose-decomposing fungus was identified as *R. variabilis*. The optimized temperature for expressing its CMC enzyme activity ranges from 40 to 55°C. The CMC enzyme activity produced by the selected fungus was 0.43 mg/ml·min, which was significantly higher than that from sandy cropland soil. It has high ability to decompose cellulose material, not only in laboratory test but also in the field experiment. Straw turnover accelerated by NMCel-crop1 could significantly increase SOC and TN input, indicating that the selected highly efficient decomposing fungi could potentially promote soil fertility and soil health in sandy cropland.

DATA AVAILABILITY STATEMENT

The datasets generated for this study are available on request to the corresponding author.

AUTHOR CONTRIBUTIONS

SW and XZ conceived and planned the experiment. SW and JL participated in the field and laboratory work. SW performed the experiment and wrote the original manuscript. BS contributed

the data analysis and manuscript editing. All authors contributed to the final manuscript.

FUNDING

This work was financially supported by the National Natural Science Foundation of China (41771117), China National Key Research and Development Plan (2016YFC0500506) from the Northwest Institute of Eco-Environment and Resources, CAS, and collaborative support from CRRP2017-04MY-Balt project by Asia-Pacific Network for Global Change Research (APN).

ACKNOWLEDGMENTS

We thank all the members in Naiman Desertification Research Station and Urat Desert-Grassland Research Station of CAS for their help in field and laboratory work.

REFERENCES

Acostamartínez, V., Burow, G., Zobeck, T. M., and Allen, V. G. (2010). Soil microbial communities and function in alternative systems to continuous cotton. *Soil Sci. Soc. Am. J.* 74, 1181–1192. doi: 10.2136/sssaj2008.0065

Adnan, M., Li, K., Xu, L., and Yan, Y. (2018). X-Shaped ZIF-8 for immobilization *Rhizomucor miehei* lipase via encapsulation and its application toward biodiesel production. *Catalysts* 8:96. doi: 10.3390/catal8030096

Al-Kaisi, M. M., Yin, X., and Licht, M. A. (2005). Soil carbon and nitrogen changes as influenced by tillage and cropping systems in some Iowa soils. *Agric. Ecosyst. Environ.* 105, 635–647. doi: 10.1016/j.agee.2004.08.002

Bancerz, R., Jaroszuk, M. O., Jaszek, M., Janusz, G., Stefaniuk, D., Sulej, J., et al. (2015). New alkaline lipase from *Rhizomucor variabilis*: biochemical properties and stability in the presence of microbial EPS. *Biotechnol. Appl. Biochem.* 63, 67–76. doi: 10.1002/bab.1351

Bancerz, R., Osińska-Jaroszuk, M., Jaszek, M., Sulej, J., Wiater, A., Matuszewska, A., et al. (2018). Fungal polysaccharides as a water-adsorbing material in esters production with the use of lipase from *Rhizomucor variabilis*. *Int. J. Biol. Macromol.* 118, 957–964. doi: 10.1016/j.ijbiomac.2018.06.162

Barnett, H. L., and Hunter, B. B. (1998). *Illustrated Genera of Imperfect Fungi*, 4th Edn. St. Paul: APS Press.

Bayer, E. A., Shoham, Y., and Lamed, R. (2013). "Lignocellulose-decomposing bacteria and their enzyme systems," in *The Prokaryotes: Prokaryotic Physiology and Biochemistry*, eds E. Rosenberg, E. DeLong, S. Lory, E. Stackebrandt, and F. Thompson (Berlin: Springer), 215–266. doi: 10.1007/978-3-642-30141-4_67

Chadha, B. S., Harmeet, G., Mandeep, M., Saini, H. S., and Singh, N. (2004). Phytase production by the thermophilic fungus *Rhizomucor pusillus*. *World J. Microbiol. Biotechnol.* 20, 105–109. doi: 10.1023/b:wibi.0000013319.13348.0a

Chapin, F. S. III, Matson, P. A., and Vitousek, P. M. (2002). *Principles of Terrestrial Ecosystem Ecology*. Berlin: Springer.

Fang, X., Chen, H., Zhao, X., Tao, P., and Xu, H. (2007). Determination of enzyme activity of straw cellulose-decomposing microorganisms. *Lett. Biotechnol.* 18, 628–630.

Guan, S. Y. (1986). *Research Methods on Soil Enzymes*. Beijing: Chinese Agriculture Press.

Institute of Soil Sciences CAS (1978). *Physical and Chemical Analysis Methods of Soils*. Shanghai: Shanghai Science Technology Press.

Jaiswal, D. K., Verma, J. P., and Yadav, J. (2017). *Microbe Induced Degradation of Pesticides in Agricultural Soils*. Berlin: Springer.

Jin, H. (2004). Effect of applying cellulose-decomposing microbes on rice straw decomposition. *Acta Agric. Shanghai* 20, 83–85.

Kassam, A., Friedrich, T., Shaxson, F., and Pretty, J. (2009). The spread of conservation agriculture: justification, sustainability and uptake. *Int. J. Agric. Sustainabil.* 7, 292–320. doi: 10.3763/ijas.2009.0477

Ke, L. N., Hu, Y. H., Gao, H. J., Pan, Z. Z., and Wang, Q. (2016). Antimicrobial activities of cinnamic acid and its derivatives to microorganisms isolated from rotten *Agaricus bisporus*. *J. Xiamen Univ.* 55, 330–335.

Kibblewhite, M. G., Ritz, K., and Swift, M. J. (2008). Soil health in agricultural systems. *Philos. Trans. R. Soc. B Biol. Sci.* 363, 685–701.

Li, Y., Yi, P., Yan, Q., Qin, Z., Liu, X., and Jiang, Z. (2017). Directed evolution of a β-mannanase from *Rhizomucor miehei* to improve catalytic activity in acidic and thermophilic conditions. *Biotechnol. Biofuels* 10:143.

Liu, X., Li, L., Wang, Q., and Mu, S. (2018). Land-use change affects stocks and stoichiometric ratios of soil carbon, nitrogen, and phosphorus in a typical agro-pastoral region of northwest China. *J. Soils Sediments* 18, 3167–3176. doi: 10.1007/s11368-018-1984-5

Liu, Z. W., Gao, W. J., Pan, K. W., Du, H. X., and Zhang, L. P. (2006). Discussion on the study methods and models of litter decomposition. *Acta Ecol. Sin.* 26, 1993–2000.

Livesley, S. J., Ossola, A., Threlfall, C. G., Hahs, A. K., and Williams, N. S. G. (2016). Soil carbon and carbon/nitrogen ratio change under tree canopy, tall grass, and turf grass areas of urban green space. *J. Environ. Qual.* 45, 215–223. doi: 10.2134/jeq2015.03.0121

Lu, G. X., Liu, W., Bian, J., Fu, M. T., and Cheng, X. R. (2011). Study on cultural characteristic of one cellulose-decomposing strains of sungus from alpine grassland soil in eastern Qilian Mountains. *Grassland Turf* 31, 50–55.

Lu, X., Liu, Z., Shen, Y., She, X., Lu, G., Ping, Z., et al. (2009). Primary cutaneous zygomycosis caused by *Rhizomucor variabilis*: a new endemic zygomycosis? A case report and review of 6 cases reported from China. *Clin. Infect. Dis.* 49, e39–e43.

Lynd, L. R., Weimer, P. J., Van Zyl, W. H., and Pretorius, I. S. (2002). Microbial cellulose utilization: fundamentals and biotechnology. *Microbiol. Mol. Biol. Rev.* 66, 506–577. doi: 10.1128/mmbr.66.3.506-577.2002

Millati, R., Edebo, L., and Taherzadeh, M. J. (2005). Performance of Rhizopus, *Rhizomucor*, and Mucor in ethanol production from glucose, xylose, and wood hydrolyzates. *Enzyme Microb. Technol.* 36, 294–300. doi: 10.1016/j.enzmictec.2004.09.007

Nei, M., and Kumar, S. (2000). *Molecular Evolution and Phylogenetics*. Oxford: Oxford University Press.

Nelson, D. W., and Sommers, L. E. (1982). Total carbon, organic carbon and organic matter. *Methods Soil Anal.* 9, 961–1010.

Olson, J. S. (1963). Energy storage and the balance of producers and decomposers in ecological systems. *Ecology* 44, 322–331. doi: 10.2307/1932179

Panagiotou, G., Kekos, D., Macris, B. J., and Christakopoulos, P. (2003). Production of cellulolytic and xylanolytic enzymes by Fusarium oxysporum grown on corn stover in solid state fermentation. *Ind. Crops Prod.* 18, 37–45. doi: 10.1016/s0926-6690(03)00018-9

Patil, A. B., Chandramohan, K., Shivaprakash, M. R., Nadgir, S. D., and Lakshminarayana, S. A. (2013). *Rhizomucor variabilis*: a rare causative agent of primary cutaneous zygomycosis. *Indian J. Med. Microbiol.* 31, 302–305. doi: 10.4103/0255-0857.115662

Qin, H. L., and Wei, W. X. (2007). Ecological significance of microbial biotechnology in modern agroecosystem. *Chinese Agric. Sci. Bull.* 23, 249–253.

Qu, C., Li, B., Wu, H., and Giesy, J. P. (2012). Controlling air pollution from straw burning in china calls for efficient recycling. *Environ. Sci. Technol.* 46, 7934–7936. doi: 10.1021/es302666s

Qu, H., Zhao, X., Zhao, H., Zuo, X., Wang, S., Wang, X., et al. (2011). Litter decomposition rates in Horqin Sandy Land, Northern China: effects of habitat and litter quality. *Fresenius Environ. Bull.* 20, 3304–3312.

Rodrigues, R. C., and Fernandez-Lafuente, R. (2010). Lipase from *Rhizomucor miehei* as an industrial biocatalyst in chemical process. *J. Mol. Catal. B Enzym.* 64, 1–22. doi: 10.1016/j.molcatb.2010.02.003

Roper, M. M., and Gupta, V. (1995). Management-practices and soil biota. *Austral. J. Soil Res.* 33, 321–339. doi: 10.1071/sr9950321

Seabi, B. O., Viljoen, B. C., Roux, C., and Botha, A. (1999). Nitrogen utilization and growth at reduced water activity by mucoralean fungi present in soil. *S. Afr. J. Bot.* 65, 407–413. doi: 10.1016/s0254-6299(15)31031-0

Soltani, M., Sahingil, D., Gokce, Y., and Hayaloglu, A. A. (2019). Effect of blends of camel chymosin and microbial rennet (*Rhizomucor miehei*) on chemical composition, proteolysis and residual coagulant activity in Iranian Ultrafiltered White cheese. *J. Food Sci. Technol.* 56, 589–598. doi: 10.1007/s13197-018-3513-3

Sun, S. C., Nan, H. Y., Wang, Y. G., Leng, F. F., Hu, W., Li, W. X., et al. (2017). Screening and enzymatic productivity of a strain of efficient cellulose hydrolyzing bacteria. *Chinese J. Microbiol.* 29, 1131–1135.

Swangjang, K. (2015). "Soil carbon and nitrogen ratio in different land use," in *Proceedings of the 2015 International Conference on Advances in Environment Research*, Hazratbal, 36–40.

Tomita, H., Muroi, E., Takenaka, M., Nishimoto, K., Kakeya, H., Ohno, H., et al. (2011). *Rhizomucor variabilis* infection in human cutaneous mucormycosis. *Clin. Exp. Dermatol.* 36, 312–314. doi: 10.1111/j.1365-2230.2010.03956.x

Wang, S. K., Zhao, X. Y., Huang, W. D., Li, Y. Q., Yue, X. F., and Zhang, L. M. (2015a). Isolation and identification of cellulose decomposing fungi and their decomposition ability in the Horqin Sandy Grassland. *J. Desert Res.* 35, 1584–1591.

Wang, S. K., Zhao, X. Y., Zhao, H. L., Lian, J., Luo, Y., and Yun, J. (2016a). Impact of sand burial on maize (*Zea mays* L.) productivity and soil quality in Horqin sandy cropland, Inner Mongolia, China. *J. Arid Land* 8, 569–578. doi: 10.1007/s40333-016-0011-1

Wang, S. K., Zhao, X. Y., Zuo, X. A., Liu, X. P., Qu, H., Mao, W., et al. (2015b). Screening of cellulose decomposing fungi in sandy dune soil of Horqin Sandy Land. *Sci. Cold Arid Regions* 7, 74–80.

Wang, S. K., Zuo, X. A., Zhao, X. Y., Li, Y. Q., Zhou, X., Lv, P., et al. (2016b). Responses of soil fungal community to the sandy grassland restoration in Horqin Sandy Land, northern China. *Environ. Monit. Assess* 188, 1–13.

Wei, B., An, J., Zhang, L., Pang, H., Sun, Z., Niu, S., et al. (2017). Improving of soil physical and chemical properties and increasing spring maize yield by straw turnover plus nitrogen fertilizer. *Trans. Chinese Soc. Agric. Eng.* 33, 168–176.

Wei, J. C. (1979). *Manual of Fungi Taxa Identification*. Shanghai: Shanghai Science and Technology Press.

Wen, Z., Liao, W., and Chen, S. (2005). Production of cellulase by Trichoderma reesei from dairy manure. *Bioresour. Technol.* 96, 491–499. doi: 10.1016/j.biortech.2004.05.021

Xu, D. F., Zhang, H. S., Li, T. C., Qi, Y. C., Jiang, C. Q., and Zhou, B. G. (2017). Isolation and identification of the pathogen of maize ear rot in fengyang,anhui province. *J. Anhui Agric. Sci.* 45, 145–150.

Yao, H. Y., and Huang, C. Y. (2006). *Soil Microbial Ecology and Their Research Approaches*. Beijing: Science Press.

Zhang, Y., Wei, D., Xing, L., and Li, M. (2008). A modified method for isolating DNA from fungus. *Microbiology* 35, 466–469.

Zhang, Y., Zang, G. Q., Tang, Z. H., Chen, X. H., and Yu, Y. S. (2014). Burning straw, air pollution, and respiratory infections in China. *Am. J. Infect. Control* 42, 815–815. doi: 10.1016/j.ajic.2014.03.015

Zhao, H. L. (2012). *Desert Ecology*. Beijing: Science Press.

Zhao, H. L., Zhao, X. Y., and Zhang, T. H. (2002). Boundary line on agro-pasture zigzag zone in north China and its problems on eco-environment. *Adv. Earth Sci.* 17, 739–747.

Zhao, H. L., Zhao, X. Y., and Zhang, T. H. (2003). *Desertification processes and its restoration mechanisms in the Horqin Sand Land*. Beijing: Ocean Press.

Zhao, X. Y., Wang, S. K., Luo, Y. Y., Huang, W. D., Qu, H., and Lian, J. (2015). Toward sustainable desertification reversion: a case study in Horqin Sandy Land of northern China. *Sci. Cold Arid Regions* 7, 23–28.

Conflict of Interest: The authors declare that the research was conducted in the absence of any commercial or financial relationships that could be construed as a potential conflict of interest.

frontiers in Environmental Science

ORIGINAL RESEARCH
published: 22 September 2020
doi: 10.3389/fenvs.2020.00152

Multi-Sensor Evaluating Effects of an Ecological Water Diversion Project on Land Degradation in the Heihe River Basin, China

Xiang Song[1,2], Jie Liao[1,2]*, Xian Xue[1,2] and Youhua Ran[2]*

[1] Key Laboratory of Desert and Desertification, Chinese Academy of Sciences, Lanzhou, China, [2] Northwest Institute of Eco-Environment and Resources, Chinese Academy of Sciences, Lanzhou, China

To deal with the increasingly severe land degradation in the downstream of the Heihe River Basin (HRB) in northwest China, an Ecological Water Diversion Project (EWDP) was implemented since 2000. A comprehensive analysis of the effects associated with the project on land degradation is necessary. According to the concept of Land Degradation Neutrality (LDN), multi-sensor data has been used to extract information on Land Use/Land Cover (LULC), Aeolian desertification, and vegetation dynamics, which were chosen as monitoring indices to reveal the process of land degradation in the HRB. Then, these results were combined with meteorological data, socio-economic statistics, and hydrological data to discuss the main driving factors influencing the land degradation process to evaluate the effects of the EWDP on land degradation in the HRB. The results showed that the process of land degradation in the HRB could be divided into two stages, in which the degradation trend was dominant from 1990 to 2000, and the rehabilitation trend was dominant from 2000 to 2015. Although both climate variation and human activities have been favorable to land degradation development in the HRB, climate factors have no significant influence on land degradation in the midstream and downstream in the HRB. The decrease of available water resources is the dominant driving factor of a series of ecological environment problems in the downstream of the HRB, and the land degradation process of the HRB has been stopped and reversed, mainly attributed to the EWDP. The EWDP facilitated the recovery of the deteriorated ecosystem by improving the efficiency of surface water resources reallocation in the downstream. Still, the EWDP indirectly led to the sink of the groundwater table in the midstream, resulting in local vegetation degradation.

Keywords: land degradation, Ecological Water Diversion Project, the Heihe River, multi-sensor, rehabilitation

OPEN ACCESS

Edited by:
Jian Sun,
Institute of Geographic Sciences and Natural Resources Research (CAS), China

Reviewed by:
Kun Jia,
Beijing Normal University, China
Jinyan Zhan,
Beijing Normal University, China

****Correspondence:***
Xiang Song
songxiang@lzb.ac.cn
Jie Liao
liaojie@lzb.ac.cn

Specialty section:
This article was submitted to Land Use Dynamics, a section of the journal Frontiers in Environmental Science

Received: *01 April 2020*
Accepted: *11 August 2020*
Published: *22 September 2020*

Citation:
Song X, Liao J, Xue X and Ran Y (2020) Multi-Sensor Evaluating Effects of an Ecological Water Diversion Project on Land Degradation in the Heihe River Basin, China. Front. Environ. Sci. 8:152. doi: 10.3389/fenvs.2020.00152

INTRODUCTION

Land, as a non-renewable and essential natural resource, is the material basis for human survival, and its rational exploitation and utilization improve social and economic development (Liu, 1995). However, under the background of global warming, population expansion, and rapid growth of the social economy, land degradation, which refers to the decrease of biological productivity of

land (UNCCD, 1994), caused by the excessive and irrational use of land resources, became one of the most pressing problems causing widespread concern in the international community (Romm, 2011; Kakembo et al., 2012).

In arid and semi-arid regions, water is the single most important limiting factor for the growth and productivity of vegetation (Inman-Bamber et al., 2012). Most of those regions have been facing a growing severe shortage of water resources (Zhang and Xia, 2009), especially the inland river basin that is overly sensitive to climate variation and human activities (Mi et al., 2016). In the inland river basin, water resources are essential for maintaining the ecological balance and economic development of oases located in the midstream and downstream (Ma et al., 2005). The upstream inflow is the primary water source available to maintain the ecological environment and for the development of the whole river basin (Zhou et al., 2018). However, because of climate variation and increasing water consumption in the midstream (e.g., increased arable land irrigation, rapid urbanization, economic development, and population expansion, etc.), the amount of water that enters the downstream in many inland rivers has decreased over the past 60 years (Cheng and Li, 2015). As a result, this led to severe eco-environmental problems, such as reducing ecosystem stability, rivers and lakes drying up, declining vegetation cover, severe sandstorms, and land degradation. Therefore, integrated watershed water resource management is the critical solution to the urgent conflict of the regulation between water demand and available water resources in the present and the future in the inland river basin (Pereira et al., 2012), which is vitally essential for the protection of inland river ecosystems and regional sustainable development (Cheng et al., 2014).

The Heihe River Basin (HRB) is the second largest inland river basin in northwestern China and has all the essential characteristics of an inland river in the desert region. In the HRB, the conflict among ecological, societal, and economical water demands is foremost (He et al., 2009; Wang et al., 2009; Zhang et al., 2015). As the center of economic activities in the HRB, more than 95% of the arable land of the whole basin is distributed in the midstream oasis, which consumes about 80% of the water resources over whole HRB (Cheng et al., 2006; Zhang et al., 2006). With the rapid economic development and continuous population boom, the more substantial increase in water consumption in the midstream of the HRB dramatically reduces the discharge entering the downstream used to maintain ecological balance, which results in river breakdown, the lake drying up, groundwater level decline, wetland shrinkage, vegetation degradation, land desertification, etc. (Liu Z. et al., 2002; Xiao and Xiao, 2004; Guo et al., 2009; Cheng et al., 2014). Due to accelerated and sustained deterioration of the ecosystem, the downstream of the HRB has become one of the primary dust storm sources in China (Wang and Cheng, 1998).

In 1997, China's State Council approved the Ecological Water Diversion Project (EWDP) in different water years to ensure that the oasis in the downstream would be restored to the level of the mid 1980s by reasonably allocating the water resources between midstream and downstream. According to the EWDP, when the water quantity of the YLX station reaches 15.8×10^8 m^3, the environmental water supply of the whole basin must be guaranteed to arrive at 7.3×10^8 m^3. As implementation of the EWDP since 2000, responses on the groundwater, lakes, wetlands, evapotranspiration, vegetation, hydrological and environmental process, and socio-economic effects have been reported (Ao et al., 2012; Cheng et al., 2014; Wang et al., 2014; Huang et al., 2016; Luo et al., 2016; Mi et al., 2016; Zhang et al., 2017; Zhou et al., 2018). However, the status and dynamics of land degradation in the HRB after the implementation of the EWDP are still unknown. Therefore, in this study, we used multi-sensor data to assess the effects of the EWDP on land degradation in the HRB.

Land degradation has been monitored via different methodologies through various indicators on regional scales. For example, Wang et al. (2011) used Landsat as the data source to extract the Aeolian desertification data of northern China by a visual interpretation method based on vegetation coverage and sand sheets coverage. Wang et al. (2020) analyzed the patterns of land degradation and restoration during 1990–2015 by using fine-resolution land cover data in Mongolia. Jiang L. et al. (2019) monitored the land degradation according to NDVI and ALBEDO by applying change vector analysis. Duan et al. (2019) identified land degradation based on the Modified Soil Adjusted Vegetation Index (MSAVI), the Fractional Vegetation Cover (FVC), Land Surface Temperature (LST), ALBEDO, and Modified Temperature Vegetation Dryness Index (MTVDI) via the QUEST (quick, unbiased, and efficient statistical tree) classification method. Feng et al. (2016) analyzed the spatial-temporal change of Aeolian desertification in northern China by the Normalized Difference Desertification Index (NDDI).

However, most of these studies on land degradation depend on data with a coarse spatial resolution (e.g., 1 km or 8 km spatial resolution), which cannot provide detailed information on the spatial-temporal patterns of the land degradation. Fewer studies have used higher-resolution images (e.g., Landsat series with 30 m resolution), which focused on one aspect of land degradation. The UNCCD considered Land Degradation Neutrality (LDN) as a Sustainable Development Goal and offered the concept of LDN as a standard quantitative method for determining degradation states in the framework of three aspects that included land cover, land productivity, and carbon storage (Akhtar-Schuster et al., 2017; Cowie et al., 2018). Therefore, we chose Land Use/Land Cover (LULC), vegetation dynamics (reflecting land productivity), and Aeolian desertification (the main form of land degradation in the HRB) as monitoring indices to reveal the process of land degradation in the HRB. The objective of this research included: ① to illuminate the dynamics of land degradation in the HRB by using multi-sensor data; ② to analyze the driving factors behind land degradation; and ③ to discuss the effects of the EWDP on land degradation. The results provide a reference for combating and control land degradation and the basis for regional economic development and economic restructuring as well as promoting basin ecosystem stability and sustainable development.

MATERIALS AND METHODS

Study Region

The HRB, lying between 37.5–43.5°N and 96–104.3°E, is the second largest inland river basin in the arid zone of northwestern China (**Figure 1**), with a total drainage area of 271,000 km^2 and a full length of 821 km. Geographically, the HRB can be divided into three distinct geomorphological units from south to north, including the southern Qilian Mountains in the upstream region, the middle Hexi Corridor, and the northern Alxa Plateau in the downstream. Due to severe elevation fluctuation among the up-, mid-, and downstream (800–5,500 m), the HRB has substantial spatial heterogeneity with diverse ecosystems, including an ice-snow zone, frozen soil, mountain forest, oasis, desert, and desert riparian forest (Kang et al., 2005).

The HRB was situated in the interior of the Eurasian continent and dominated by arid hydrological features. Depending on the location, the temperature, precipitation, and evaporation in the HRB vary dramatically at both temporal and spatial scales. The upstream is in the middle part of the Qilian Mountains, which have an annual mean temperature ranging between 2 and 3°C, and yearly precipitation increased from about 250 mm in the low hill zone to about 500 mm in the high mountain region (Qi and Luo, 2005). The midstream with intense evaporation and little precipitation is in the Hexi Corridor. The annual mean temperature is 6–8°C, and yearly rainfall is 120–200 mm (Qi and Luo, 2005). Oasis agriculture is the main irrigated area and a substantial commodity grain base in China (Xie et al., 2015), which comprises about 97.3% of the population of the HRB and produces most of the GDP of the whole basin (Fang, 2002). The downstream adjacent to the Badain Jaran Desert is the Ejina banner and Alxa right banner, which is mainly covered by the Gobi Desert. Here, the annual mean temperature is 8–10°C, and yearly precipitation is less than 50 mm, but potential annual

FIGURE 1 | Location of the Heihe River Basin.

evaporation is >3000 mm (Liao et al., 2015a). Due to strong wind, the downstream is one primary source of sandstorms in northern China.

By the end of 2014, the total population of the HRB was 2,527,500, with an average population density of 10.64 people/km^2, of which the agricultural population accounted for 56.9% of the total population. The people of the HRB are mainly distributed in the midstream, accounting for 95.3% of the total population. The overall economic development of the HRB is in a backward position. The GDP of the HRB was 115.1 billion yuan in 2014.

Data Acquisition and Pre-processing

Multi-Sensor Data

The Landsat images represent the longest temporal record of space-based land observations; those used in our study included TM (1990, 1995, 2005, and 2010), ETM (2000), and OLI (2015) images with spatial resolutions of 30 m. The principles of image selection included the following: ① the image was acquired from July to September, in which period vegetation typically reaches its maximum extent, and ② the percentage of cloud coverage must be less than 10%. Acquired cloud-free images that encompassed the entire area within a given year were complicated, attributed to the broad field of the study region. Therefore, some images from previous or subsequent years were chosen as replacements for unavailable images in the target years. A total of 132 images were downloaded from the US Geological Survey[1]. All those Landsat images were projected to uniform Albers Conical Equal Area/WGS84 coordinate system and were pre-processed including a radiometric and atmospheric correction to eliminate the radiometric error caused by atmospheric influences. Finally, the Landsat images were clipped and mosaicked to synthesize a cloudy free image covering the HRB.

Due to a fragment of AVHRR data at 1 km, satellite data consisting of a Global Area Coverage (GAC) 4 km AVHRR top of atmosphere reflectance database were chosen for this study. Data between 1990 and 2000 with a temporal resolution of 1 day were processed in this study, which includes AVHRR observations from the NOAA-11 (1990/01/01-1994/12/31) and NOAA-14 (1995/01/01-2000/12/31) satellites. The raw AVHRR images were calibrated following the latest recommendations by NOAA, and atmospheric correction was performed by using the Quick Atmospheric Correction (QUAC) provided by ENVI 5.3. Then, the Minimum red band criterion was used to generate daily composites (Latifovic et al., 2005). After pro-processing, all AVHRR images were reprojected to uniform the Albers Conical Equal Area/WGS84 coordinate system, and the Red band and NIR bands were used to calculate NDVI.

MODIS standard land products provided by NASA and vegetation indices 16-Day L3 Global 1 km (MOD13A2) were used in this study to supplement AVHRR data to cover the entire research period. Data between 2000 and 2015 with a temporal resolution of 16 days and a spatial resolution of 1 km were processed in this study. The MODIS product was downloaded from the NASS's LAADS DAAC[2] and reprojected to the Albers Conical Equal Area/WGS84 coordinate system and resampled to resolutions of 4 km by using MRT (MODIS Reprojection Tool).

The Harmonic Analysis of Time Series (HANTS) method was used to process the NDVI series calculated from AVHRR and MODIS to eliminate the influence of clouds and atmosphere, as well as remove the outliers, smooth the data, and interpolate the missing data. After this process, the mean NDVI in the growing season calculated from 1990 to 2015 was used to extract the information on vegetation dynamics.

Ancillary Data

Meteorological data (1975–2015), including precipitation, annual mean temperature, and annual mean wind velocity were obtained from the China Central Meteorological Bureau[3]. Three weather stations, including Ejina Banner in Alxa League of Inner Mongolia, Zhangye in the Hexi Corridor of Gansu Province, and Qilian in the Qinghai Province, were taken as representative of the climate of the different zone of watersheds. The hydrological data used in this study were collected from the Heihe River Bureau. Three hydrological stations were included in the data set [Yingluoxia (YLX), Zhengyixia (ZYX), and Langxinshan (LXS)].

LULC Classification and Measurement of Changes

Assessing impacts of the EWDP on LULC changes is the basis for watershed management and control land degradation. Dynamic change analysis of LULC is a practical approach to understand the process, extent, and trend of land degradation. In this study, LULC transfer analysis has been used to derive the transition among different LULC classes with the aid of GIS, which provides more details of LULC change information, as well as some necessary data for land degradation process analysis.

According to China Land Cover Classification System and National Land Use Remote Sensing Mapping Classification System (Zhang et al., 2014), a classification system of six primary LULC types (included woodland, grassland wetland, cropland, artificial land, and bare land) was employed in this study, which was divided into 16 secondary types (**Table 1**). The spatial and temporal dynamics of the different LULC classes were investigated using remote the sensing data of the period from 1990 to 2015, covering 25 years. Based on the availability of reliable Landsat data, the study period was divided into five

[1]http://glovis.usgs.gov

[2]https://ladsweb.modaps.eosdis.nasa.gov/

[3]http://data.cma.cn

TABLE 1 | The LULC classification system used in the HRB.

Primary types	Secondary types
Woodland	Forest, Shrubs
Grassland	Dense Grassland, Moderately Grassland, Sparse Grassland
Wetland	Marsh, Water area
Cropland	Paddy field, Non-paddy field
Artificial Land	Residential area, Industrial area, Traffic land, mining land
Bare Land	Bare rock, Bare land, Sandy land

intervals (1990–1995, 1995–2000, 2000–2005, 2005–2010, and 2010–2015). The 2015 LULC Data Set (with a spatial resolution 30 m) of the HRB is produced by using Landsat OLI images, and the Automatic Object-Oriented Classification Based on Decision Tree was used to derive the LULC information. The Dataset in other periods were produced by using the Object-Oriented Vector Similarity Change Detection Method. The details for the Classification and Change Detection Method were described in Song and Yan (2014) and Wu et al. (2014).

Aeolian Desertification Mapping

In the HRB, Aeolian desertification is the dominant form of land degradation. patchy or dispersed vegetation interlace with sand sheets/dune characterizes Aeolian Desertified Land (ADL); the coverage ratios of shifting sand, wind-eroded regions, and vegetation which can be measured not only by field survey but also by remote sensing data were selected as the crucial indices for deriving the severity of ADL. Based on classification criteria proposed in previous studies (Yan et al., 2009; Wang et al., 2012; Song et al., 2015), ADL intensity was classified into four levels: Slight (SL), Moderate (M), Server (S), and Extremely Severe (ES). Details of ADL classification indices are provided in **Table 2**.

Because of excellent flexibility and high precision (Kang and Liu, 2014), we performed a visual interpretation method to generate the ADL status information. When interpreting, we also used TGSI (Topsoil Grain Size Index) (Xiao et al., 2006) and FVC (Fraction of Vegetation Cover) derived by using the Linear Spectral Mixture Model (Li et al., 2013) as auxiliary to identify the degree of ADL. The details of the visual interpretation method are provided in Wang et al. (2013). The spatial resolution of the ADL dataset is 30 m.

TABLE 2 | Indices used for the classification of Aeolian desertified land in the HRB.

Degradation intensity	SSC	FVC	Representative factors
ES	>50	<10	Mobile sand ridges, dunes, and sand sheets cover the whole area. Blowouts are widely distributed. Only sparse xerophytic herbs grow between dunes.
S	25–50	10–30	Sand sheets and coppice dunes are standard. There are some wind-scoured depressions and residual mounds. There is sparse vegetation.
M	5–25	30–60	Semi-anchored dunes cover most of the area, and some scattered mobile dunes or sand sheets are present around the semi-anchored dunes. Blowouts or sand sheets are sparsely distributed. The vegetation areas contain sparse areas of sand sheets, dunes, or blowouts.
SL	<5	>60	Only small, sparse, scattered patches of mobile sand or blowouts are present; most of the area still resembles the original landscape. The whole area is covered by vegetation, but some areas suffer from degradation resulting from a lack of water or human activity.

ES, extremely severe; S, severe; M, moderate; SL, slight; SSC and FVC represent shifting sand cover and fraction of vegetation coverage, respectively.

Vegetation Change Trend Monitoring

Monitoring changes in NDVI induced by land degradation has been widely employed and proven an effective method of identifying land degradation at global, regional, and national scales. In this study, we converted NDVI data into more easily understandable representations of relative greenness (RG) (Burgan and Hartford, 1993), which expresses how green each pixel currently is with the range of greenness observations for that pixel since 1990. It is calculated as:

$$RG = \frac{100 \times (NDVI_o - NDVI_{min})}{(NDVI_{max} - NDVI_{min})}$$

Where,

$NDVI_o$ = mean NDVI values in each growing season.

$NDVI_{min}$ = minimum of mean NDVI in the growth period for that pixel between 1990 and 2015.

$NDVI_{max}$ = maximum of mean NDVI in the growth period for that pixel between 1990 and 2015.

Validation

To obtain the ground validation data for estimating the accuracy of the LUCC and Aeolian desertification database, a field survey was carried out in the HRB from July 20 to August 1 in 2015. Three hundred thirty-four field verification points with landscape photograph accurate positioning by GPS were obtained to assess its accuracy, and coverage photographs obtained with fisheye lenses from 69 samples were used to evaluate the accuracy of FVC calculated by remote sensing. We evaluated the accuracy of the LULC database and the ADL database by combined field verification points and random sampling methods. The results show that the total accuracy of LULC and ADL is more than 95%, the classification performance is satisfactory. Moreover, a significant correlation exists between the measured values and calculated values of FVC (**Figure 2**).

RESULTS

Characteristic of LULC Change in 1990–2015

The status of LULC in 2015 is shown in **Figure 3**. As a result of economic development, changes in the LULC mainly occurred around the oasis in the midstream of the HRB; fewer changes appeared in the upstream, and the downstream only occurred in wetlands surrounding riverbanks and the Ejina oasis. In 1990, bare land was the most significant percentage of the land area throughout the study period, which covered 89.22% of total area (**Table 3**). Although analysis of six time periods (1990–1995–2000–2005–2010–2015) revealed the continuous decline of bare land, it is also the dominant land use type in the HRB. Over the entire study period, the coverage of cropland, forest, shrubs, water area, marsh, and artificial land increased by 28.60, 1.41, 5.92, 36.53, 10.32, and 99.15%, respectively, while grassland and bare land declined by 0.48 and 1.05%, respectively.

To evaluate the land degradation process, we classify the conversion between LULC types into two categories by using

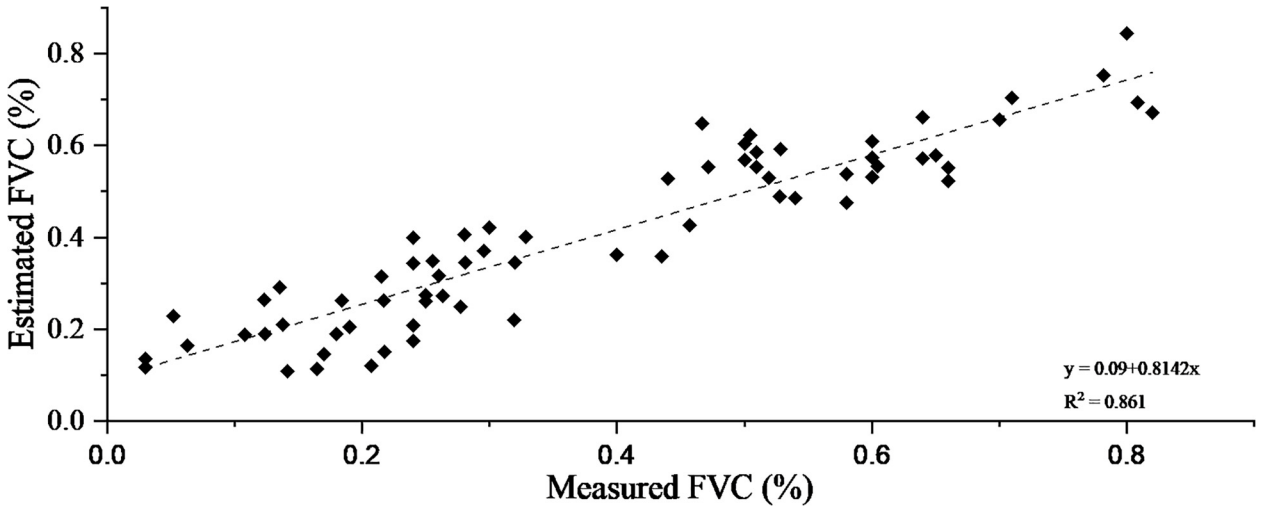

FIGURE 2 | Scatter plot correlation between the field-measured and LSMM-estimated vegetation fraction in 2015.

the transfer matrix. Among them, the land degradation process included a decrease of grassland coverage, grassland turned into bare land, and forest, shrubs, water area, and marsh turned into grassland or bare land; land restoration process included an increase of grassland coverage, bare land turned into grassland, water area, forest and shrubs, and grassland turned into the marsh, forest, and shrubs. **Figure 4** shows the trend of land degradation in the whole basin and each part of the HRB. From the entire basin, the land degradation process was dominant from 1990 to 2000. But since 2000, the land restoration process has changed into the leading process, and land restoration area continued to decrease after reaching its maximum in 2005. Viewed from different parts of the HRB, although the overall trend of degradation and restoration is the same as the whole basin, each part of the basin has its characteristics. Land degradation dominated in the upstream and midstream occurred mainly between 1995 and 2000. However, land degradation in the downstream primarily occurred between 1990 and 1995, but land restoration began to appear since 1995 and became the dominant process until 2000. After land restoration dominated, the midstream and downstream recovered fastest from 2005 to 2010, while the upstream recovered most quickly from 2000 to 2005.

Aeolian Desertification Dynamics

Figure 5 shows the temporal and spatial distribution of ADL in the HRB. Although there was no significant change in the overall location of ADL, the severity of ADL did change over time. The ADL was centrally distributed in areas adjacent to the oasis, areas of sparse vegetation along the river, and areas of the western edge of the Badain Jaran Desert. In 2015 (**Table 4**), ADL covered 11,983.99 km^2, amounting for 4.42% of the total area. Most ADLs were classified as ES and S (34.10%, 43.38% respectively), with a smaller proportion classified as M and SL (12.54%, 9.98%, respectively). ES and S ADL were concentrated and mainly distributed in the Ejina, Gaotai, Jinta, and Yumen. Slight and moderate desertified land was fragmented and mostly in the Suzhou, Linze, Ganzhou, and Minle areas. The ADL in the midstream of the HRB jeopardizes the stability and development of these vital oasis agricultural areas.

From 1990 to 2015, ADL in the HRB declined by 1,038.59 km^2, which is equal to 7.97% of the total ADL in 1990, representing a linear decrease of 64.91 km^2y^{-1}. To analyze the trends of Aeolian desertification, we classified area expansion and degree increase of ADL as desertification development, and area reduction and degree decrease of ADL as desertification recovery, by using the transition matrix (**Figure 6**). From 1990 to 2000, the area of ADL has shown a decreasing trend, but the degree of ADL is aggravated. Therefore, the direction of desertification in the HRB is still a desertification development in this period. From 2000 to 2015, the trend of desertification in the HRB is reversed, which shows not only a decrease of degree but also a reduction of area of ADL. In the midstream, the reason for the reversal of desertification is that it expands the area of ADL which is much smaller than the reduced area of ADL between 1990 and 2000. After 2000, the reversal of desertification is mainly due to the reduction of desertification degrees. In the downstream, the change of desertification degree is the main factor determining the direction of the desertification process. When inflow reduced (1990–2000), vegetation coverage decreased so that desertification presents a trend of development. On the contrary, desertification tends to reverse (2000–2015).

Vegetation Trend

In the arid and semi-arid areas, vegetation is positively generally correlated with precipitation. Therefore, the driving factors of vegetation change can be better explained by combining precipitation change with vegetation trends. **Figures 7**, **8** show the RG (from 1990 to 2015), precipitation, and its change trend (from 1975 to 2015), respectively. Different trend changes are observed in the different parts of the HRB. In the upstream,

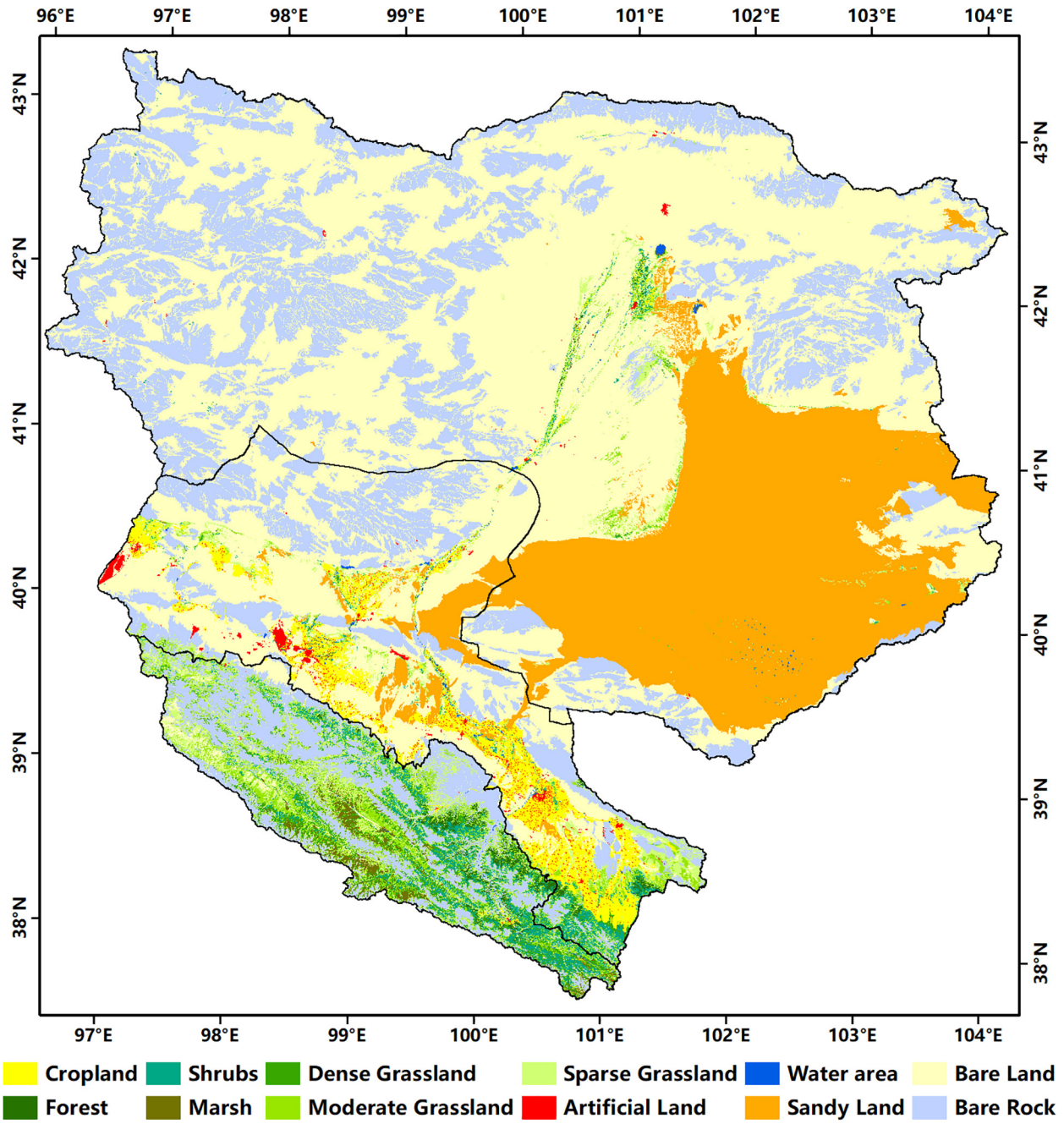

FIGURE 3 | Map of LULC in the HRB in 2015.

the precipitation showed an increasing linear trend with a rate of 1.1 mm/year, which indicated a more wet trend from the last 4 decades, while vegetation also changed from relatively worse to relatively better from 1990 to 2015. Notably, the most massive precipitation appeared in 1998, the plant also was best. In the midstream, worse vegetation areas mainly occurred in oasis agricultural areas and the Shandan County from 1990 to 2001, attributed to less precipitation. However, the natural vegetation around the oasis shows a relatively good trend, which might be due to the increase of groundwater level caused by the rise of irrigation water in the oasis because of drought. From 2002 to 2015, with the rise in precipitation and the implementation of environmental protection projects, vegetation continued to recover in most areas, and the plant was in a relatively better stage, but vegetation around the oasis gradually disappeared. In the downstream, although there is no significant change trend in precipitation, the precipitation in the period from 1990 to 2000 is more than that in the period

TABLE 3 | The area of LULC classes for 1990 and net change of five periods in the HRB (km^2, %).

Land	1990		The net change in area(%)					
Use	Area	%	1990–1995	1995–2000	2000–2005	2005–2010	2010–2015	1990–2015
Upstream								
CL	115.92	0.42	−0.53%	−1.05%	−7.26%	−2.33%	−8.68%	−18.59%
FL	766.03	2.77	−0.17%	−0.11%	0.10%	0.07%	0.10%	−0.01%
SL	2604.06	9.42	−0.07%	−1.05%	2.20%	0.34%	0.17%	1.56%
GL	11326.56	40.95	−0.11%	1.47%	−1.65%	0.19%	−0.18%	−0.31%
WA	52.34	0.19	−0.40%	−0.29%	3.41%	−0.26%	2.37%	4.85%
ML	850.68	3.08	2.07%	−24.18%	45.09%	−0.23%	2.31%	14.63%
AL	10.61	0.04	12.91%	8.76%	15.66%	27.67%	9.36%	98.30%
BL	11927.06	43.13	−0.02%	0.61%	−1.34%	−0.25%	−0.01%	−1.02%
Midstream								
CL	5572.79	10.19	7.12%	4.34%	1.22%	8.51%	5.27%	29.23%
FL	145.75	0.27	−0.98%	0.89%	−0.03%	1.28%	2.94%	4.12%
SL	779.99	1.43	4.08%	−0.88%	6.24%	8.71%	−1.10%	17.84%
GL	3923.31	7.17	−7.17%	−2.64%	4.23%	1.78%	0.23%	−3.90%
WA	94.49	0.17	14.86%	5.20%	−0.58%	16.30%	11.23%	55.39%
ML	101.95	0.19	−42.37%	−23.23%	1.04%	14.77%	−2.41%	−49.94%
AL	519.19	0.95	8.50%	4.03%	10.84%	20.86%	30.48%	97.31%
BL	43544.47	79.63	−0.37%	−0.40%	−0.79%	−1.96%	−1.47%	−4.89%
Downstream								
CL	76.76	0.04	−26.26%	4.56%	76.36%	10.03%	3.07%	54.19%
FL	55.94	0.03	1.50%	1.36%	−1.16%	8.63%	3.06%	13.84%
SL	243.93	0.13	−8.06%	−3.05%	3.93%	15.34%	6.94%	14.27%
GL	1833.66	0.98	−0.85%	3.28%	0.25%	4.74%	−1.58%	5.84%
WA	74.07	0.04	−54.27%	−4.37%	123.46%	29.30%	6.73%	34.86%
ML	11.78	0.01	−98.30%	205.00%	555.74%	130.25%	310.31%	220.80%
AL	42.4	0.02	10.31%	6.97%	2.76%	63.18%	12.18%	121.96%
BL	186343.1	98.76	0.05%	−0.03%	−0.06%	−0.11%	−0.02%	−0.16%
Whole Basin								
CL	5765.47	2.13	6.52%	4.24%	1.77%	8.36%	5.03%	28.60%
FL	967.72	0.36	−0.19%	0.12%	0.01%	0.75%	0.72%	1.41%
SL	3627.98	1.34	0.28%	−1.13%	3.21%	3.18%	0.32%	5.92%
GL	17083.53	6.3	−1.81%	0.77%	−0.21%	1.04%	−0.25%	−0.48%
WA	220.9	0.08	−11.94%	2.06%	20.70%	16.51%	8.02%	36.53%
ML	964.41	0.36	−3.85%	−24.07%	42.71%	0.97%	4.86%	10.32%
AL	572.2	0.21	8.72%	4.34%	10.32%	24.05%	28.30%	99.15%
BL	241814.6	89.22	−0.03%	−0.07%	−0.25%	−0.44%	−0.27%	−1.05%

CL, cropland; FL, forest; SL, shrubs; GL, grassland; WA, water area; ML, marsh; AL, artificial land; BL, bare land.

from 2001 to 2015. However, vegetation change is contrary to precipitation trend, and the vegetation is worse in the period of more precipitation, but better in the period with less precipitation.

DISCUSSION

Natural factors and human activities were the two critical driving forces behind the land degradation process and could both influence land degradation on the regional scale (Dawelbait and Morari, 2012). In this study, we analyzed the driving factors behind the positive and negative process of land degradation from the changes in temperature, precipitation, wind speed, population, cultivated land, livestock, and water use patterns in the HRB.

Effects of Climate Variation on Land Degradation

In this study, because the HRB contains three distinct geographic units, the annual mean temperature, precipitation, and annual mean wind velocity data recorded at Qilian, Zhangye, and Ejina meteorological stations covering the period from 1975 to 2015 in the different parts of the HRB have been selected. Those meteorological data showed the climatic change in the upstream, midstream, and downstream of the HRB, respectively. Furthermore, deviation, 5-year moving average,

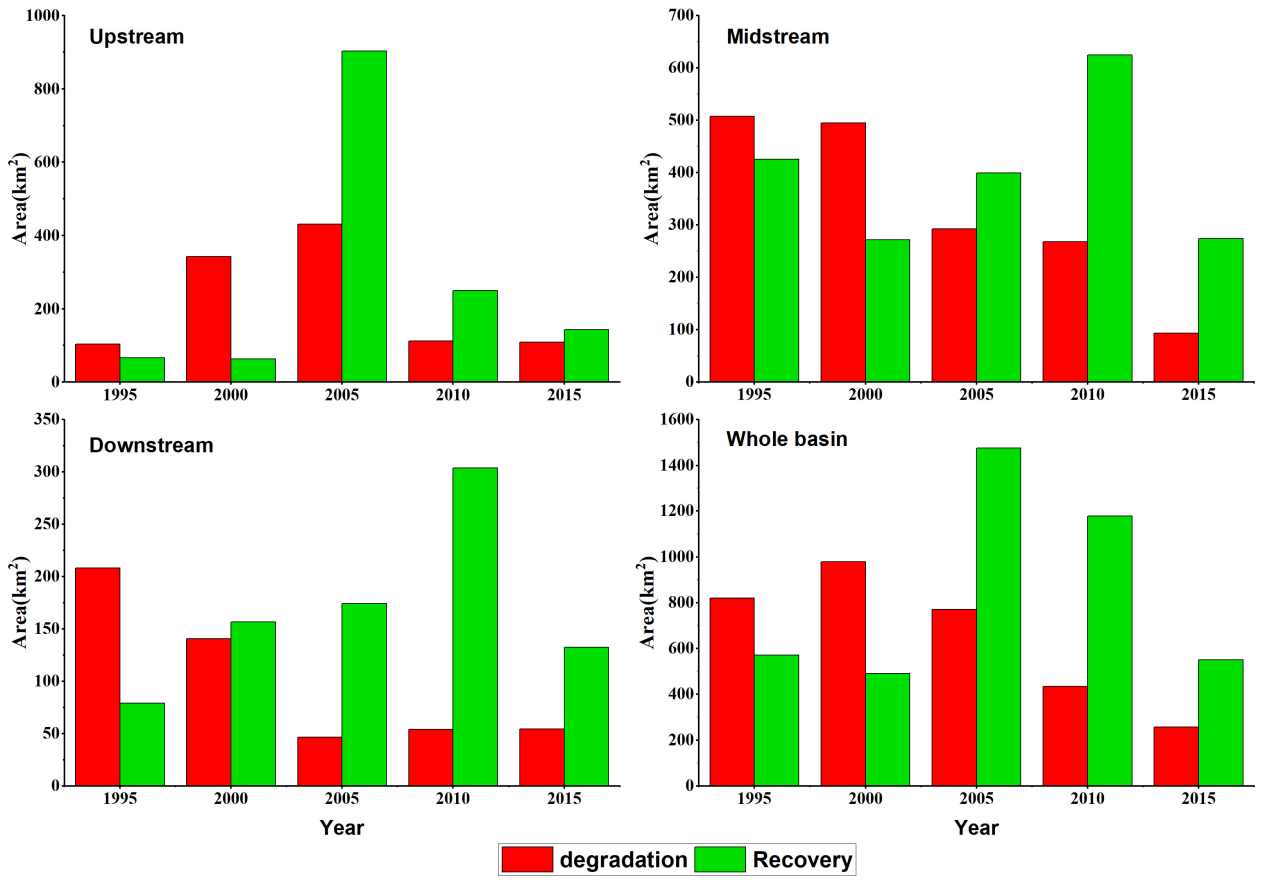

FIGURE 4 | The trend of land degradation process extracted from LULC change in the HRB during 1990–2015.

and linear trend of the relevant variables have been calculated to analyze the climatic variation and the drivers of land degradation (**Figure 8**).

In the upstream of the HRB, the annual mean temperature and precipitation show a significant increasing trend, and the annual mean temperature growth rate was 0.046°C/year. In the upstream, increasing temperature eased thermal constraints on vegetation growth, which was conducive to vegetation growth. Meanwhile, increased precipitation contributes to vegetation growth also. But some scholars considered that increasing temperature is a critical climatic factor responsible for land degradation in cold, high-altitude regions (Xue et al., 2009). As rapidly growing temperature warmed the upper permafrost layers, a large area of permafrost was thawing and even disappeared in some regions, which has decreased water content in vegetation root zone and has led to changes in soil structure and composition. All these changes were the main factor in the degradation of the high cold meadow and swamp meadow (Wang and Cheng, 1999), which is also a significant factor in land degradation from 1995 to 2000 (a dry period, **Figure 8**) in the upstream of the HRB. Therefore, taken together, the process of land degradation is consistent with climate change. This indicates that climate change is the dominant driving factor in land degradation in the upstream of the HRB.

In the midstream and downstream of the HRB, the annual mean temperature also shows a significant increasing trend with a growth rate of more than 0.05°C/year. Every degree of temperature rise can increase potential evapotranspiration by approximately 75 mm/year (Le Houérou, 1996). Thus, a higher temperature could result in increasing topsoil evapotranspiration and decreasing topsoil moisture content. Meanwhile, precipitation not only did not show a significant increasing trend but also showed a slight decrease trend in the midstream of the HRB, which increased the arid conditions of the region. During the study period, the overall aridity of the climate increase attributed to temperature steadily increased while precipitation was not changed throughout the midstream and downstream of the HRB. Therefore, this simultaneous effect of changes in precipitation and temperature created more significant water stress on vegetation, which has worsened the land degradation process. Moreover, because of enhanced irrigation in the oasis agriculture region to address the impact of rising water stress on crops, reduction of ecological water consumption resulted in increased land desertification in the downstream.

Wind also plays a vital role in soil erosion and land degradation in the arid region. Throughout the whole study

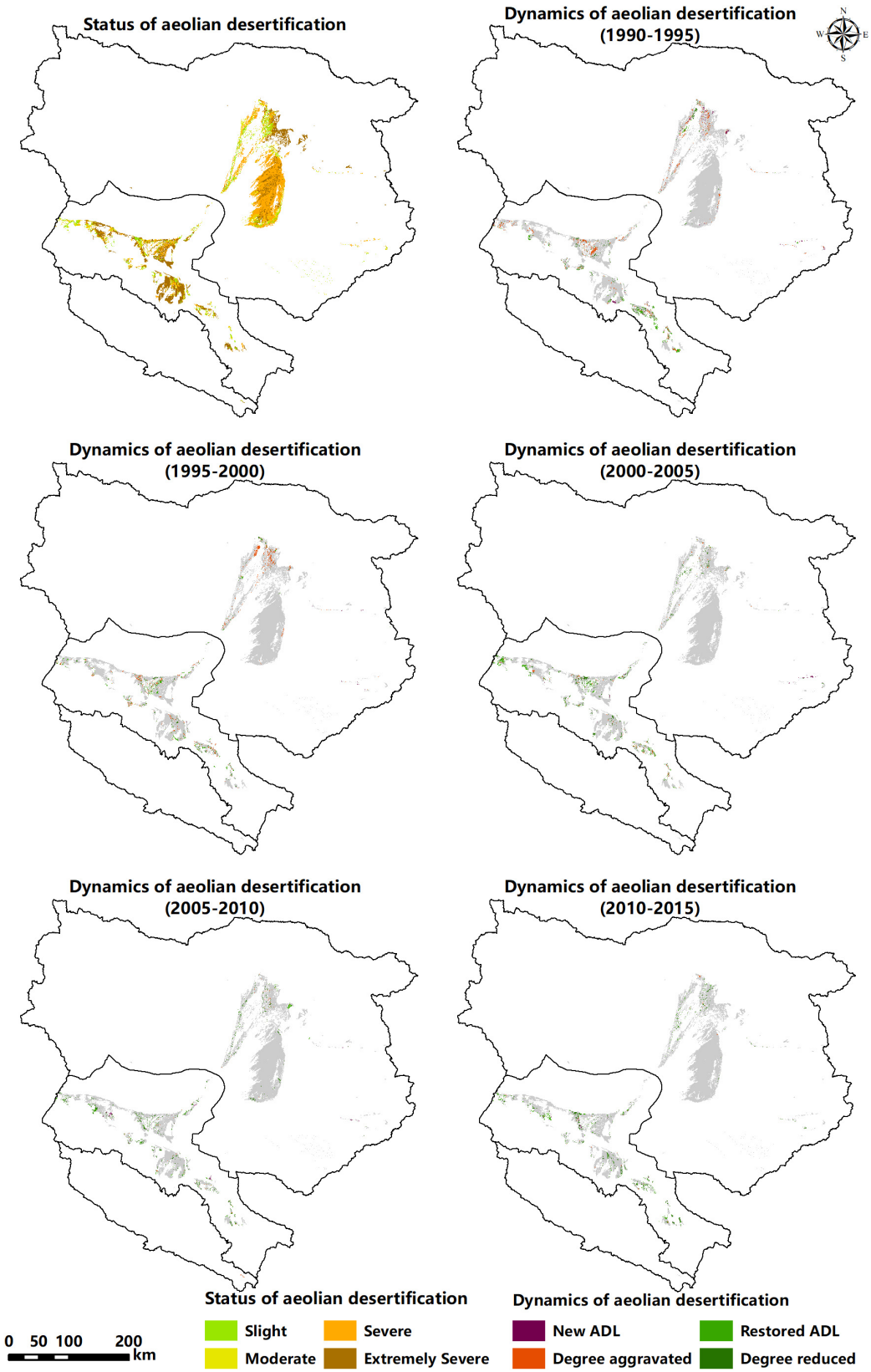

FIGURE 5 | Aeolian desertification monitoring results in the HRB during 1990–2015.

TABLE 4 | The changes in the severity of ADL from 1990 to 2015 in the HRB (km^2, %).

Year	Aeolian desertification intensity								Total ADL	
	Slight		Moderate		Severe		Extremely Severe		Area	Area of the total area
	Area	of ADL	Area	of ADL	Area	of ADL	Area	of ADL		
1990	1172.65	9.00	1642.23	12.61	5486.81	42.13	4720.88	36.25	13022.58	4.81
1995	1102.8	8.58	1558.37	12.12	5520.15	42.93	4675.99	36.37	12857.31	4.74
2000	906.95	7.19	1446.41	11.47	5590.04	44.31	4671.3	37.03	12614.7	4.65
2005	930.46	7.52	1471.8	11.90	5492.51	44.42	4471	36.16	12365.78	4.56
2010	1056.64	8.66	1571.13	12.87	5345.84	43.80	4231.11	34.67	12204.72	4.50
2015	1196.52	9.98	1502.98	12.54	5198.09	43.38	4086.41	34.10	11983.99	4.42

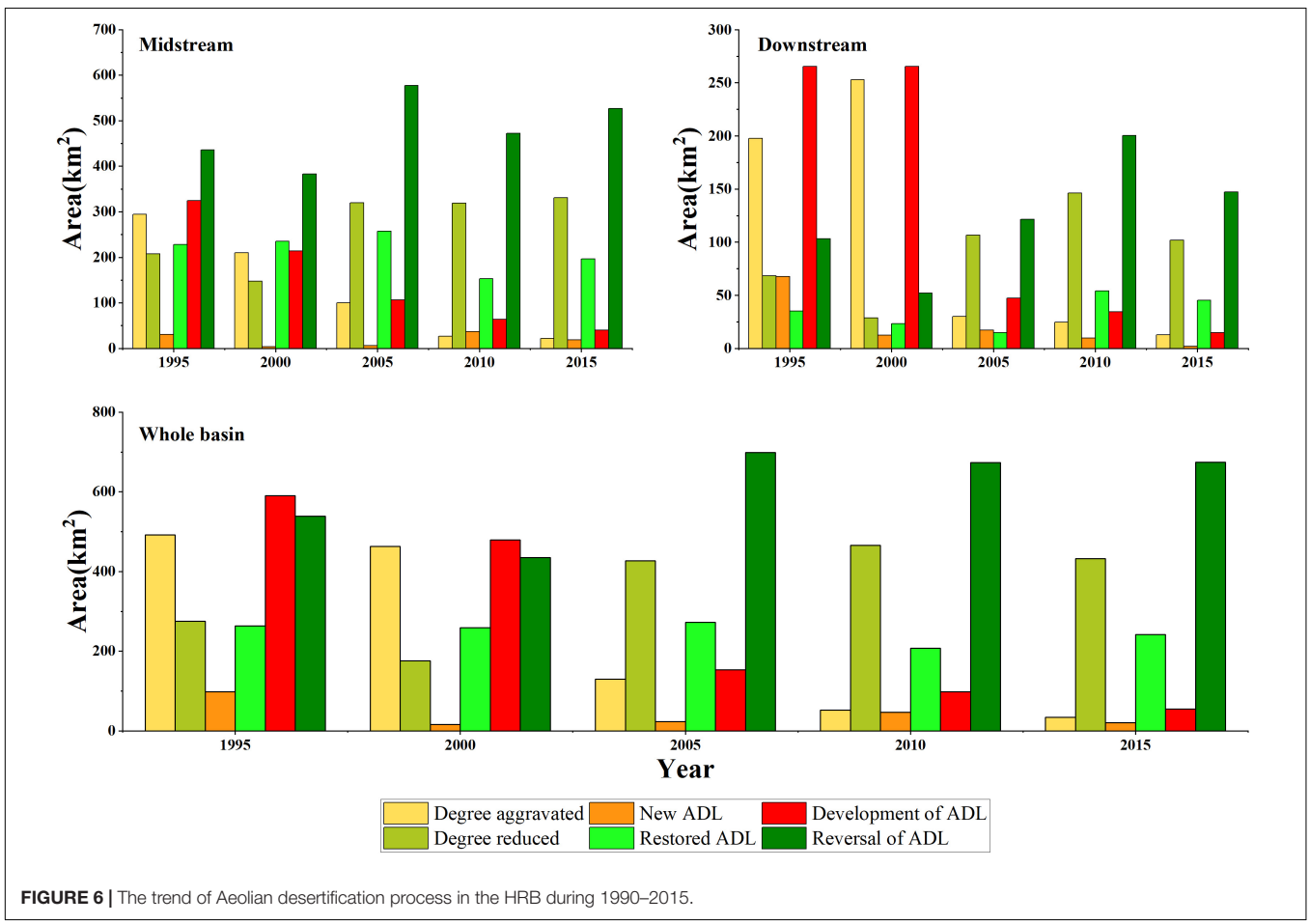

FIGURE 6 | The trend of Aeolian desertification process in the HRB during 1990–2015.

period, the annual mean wind velocity shows a decreasing trend, and only a slightly increasing trend after 2011 in the midstream of the HRB. Such a change could reduce the wind's erosive power and slow down the development of desertification. In conclusion, the trend of climate change is not consistent with that of the land degradation process in the midstream and downstream of the HRB. So, the climate variation was not the main driving force for land degradation in the midstream and downstream of the HRB.

NDVI has been widely used to monitor land degradation (Li et al., 2016). Therefore, we chose 3 × 3 pixel mean-NDVI at three weather stations to do correlation analysis with meteorological elements to reveal the impact of climate factors on land degradation. We found that only the annual mean temperature in the upstream and the annual mean wind speed in the midstream has a significant influence on NDVI ($p < 0.01$; **Table 5**). Generally, the vegetation is sensitive to precipitation

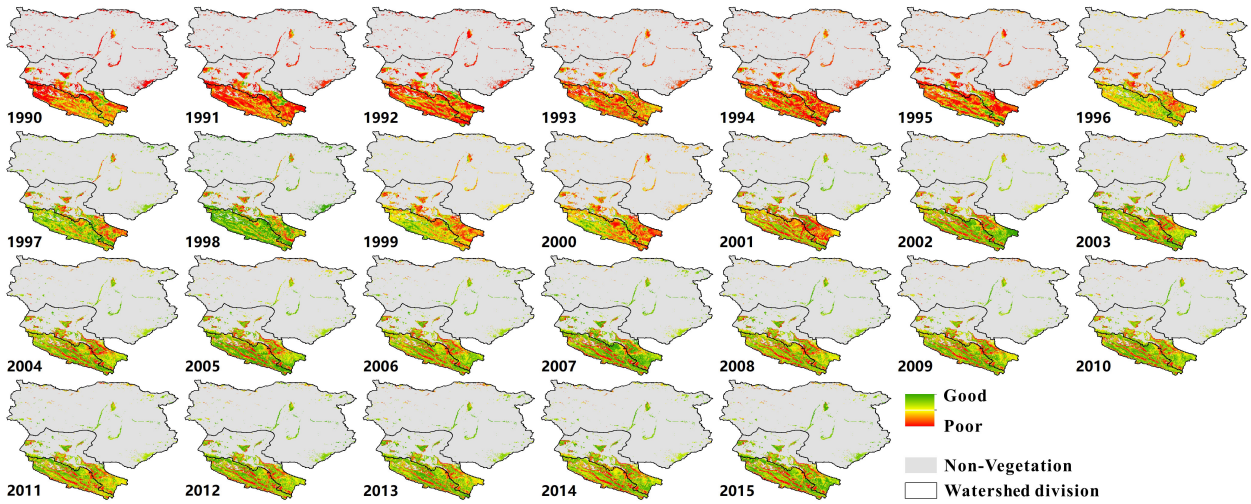

FIGURE 7 | The relative greenness maps portray vegetation greenness in the HRB during 1990–2015.

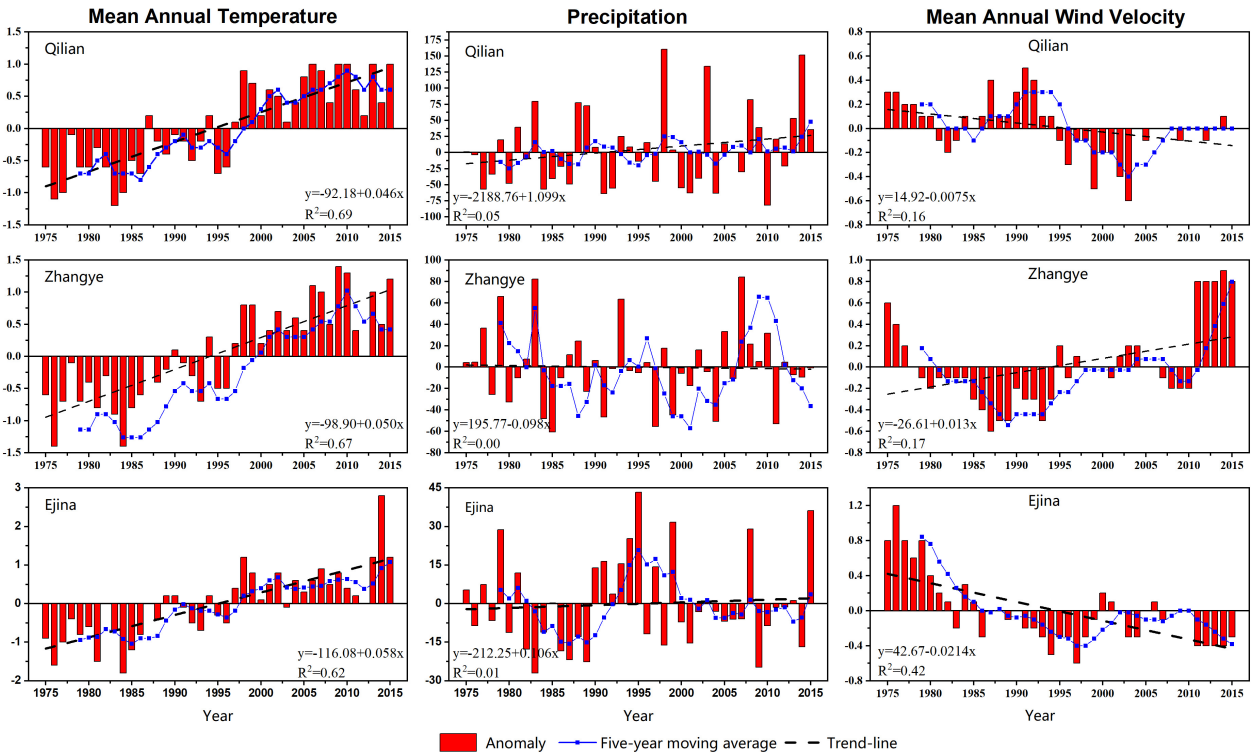

FIGURE 8 | Change in annual temperature, precipitation, and mean wind velocity in the HRB from 1975 to 2015.

in semi-arid and arid areas, but NDVI is not related to precipitation in the midstream and downstream of HRB. In a word, this indicated that climate factors are not the main driving factors of land degradation development and reversion in the midstream and downstream in the HRB.

Effects of Human Activities on Land Degradation

Human activities have two sides to land degradation. On the one hand, unreasonable human activities accelerate or promote the process of land degradation; on the other hand, reasonable human activities contribute to the reversal of land degradation

under adverse natural conditions. In this research, the intensity of human activities was evaluated by using four proxies: the population, the area of arable land, and the numbers of livestock and politic measures, which can be used as an indication of effecting vegetation cover changes.

Rapid population expansion was the root of all irrational human activities, which led to the destruction of the ecological environment. For example (**Figure 9A**), the population of Zhangye City was 549,200 in the 1950s but had increased to 1,213,300 in 2014 (an increase of 221%). The rise in population will inevitably lead to a substantial increase in the area of cultivated land, residential land, industrial land, and traffic land, which is the leading cause of the decrease in Aeolian desertified land after the 1990s. Furthermore, due to the lack of adequate surface protection, the severe destruction of vegetation and soil surface structure caused by population and unreasonable economic activities and the intensification of wind erosion and the accumulation of surface soil salt caused by unreasonable utilization of water resources, were primary factors causing the intensification of land degradation.

Cultivated land in the oasis increased rapidly due to implementation of the "Grain Production Base Policy" in the 1970s and increased by 58.6% in 2010 (Liao et al., 2015b), which led to the oasis in the midstream becoming the major grain production base in Gansu Province and even in China. With the increase of cultivated land, the demand for irrigation water in the midstream continues to increase, which has led to a severe deterioration in the downstream ecosystems, including lakes, rivers drying up, wetlands shrinking, Aeolian desertification, and ecological degradation.

TABLE 5 | The correlation between the NDVI and climatic factors.

Location	Annual mean temperature	Annual Precipitation	Annual mean wind velocity
Qilian	0.64 **	0.23	−0.34
Zhangye	−0.17	0.06	−0.56**
Ejina	0.05	0.04	−0.25

*** Indicates a significant test by 0.01.*

Overgrazing is another main factor in land degradation in the HRB. Since the 1980s, the livestock population in the HRB has increased dramatically. Taking Zhangye City as an example (**Figure 9B**), the sheep population increased by 283.73% from 1984 to 2014. Overgrazing is a common phenomenon in the natural grassland of the HRB. The overloading rate has increased from 21.68% in the early 1990s to 32.1% (Liu J. et al., 2002). At the same time of grazing, over-exploitation of valuable medicinal herbs such as Licorice, Cordyceps, Cynomorium soongaticum, Ephedra, etc. was also one of the main factors causing the extreme desertification of grassland in the HRB.

In response to the expansion of land degradation and the increasing deteriorated ecological environment, a series of environmental protection and restoration projects, including the "Three-North Shelterbelt Project," "Grain for Green," "Grazing Withdrawal Program," "Construction of National Ecological Security Barrier," and others, have been carried out. On the other hand, countermeasures have been adopted to combat land degradation and rehabilitate the deteriorated environment. These include the exclusion of grazing in degraded grassland, closed breeding, aerial sowing of tree and grass, seedings by airplane, etc. These projects and related policy played a vital role in revegetation and land degradation reversal.

Effects of the EWDP on Land Degradation

Figure 10 shows the trend of runoffs from the YLX, water consumption in the midstream, and runoffs to the downstream from 1975 to 2017. Before the EWDP was implemented, the runoffs from YLX have no significant change trend, but the water consumption in the midstream was rising rapidly. In contrast, runoffs to the downstream have declined sharply, and nearly zero, especially in 2001. Combined with the above analysis, we found that the decrease of available water resources is the dominant driving factor of a series of ecological environment problems in the downstream of the HRB.

As **Figure 10** shows, water consumption in the midstream maintained at a stable level, with no significant change trend after 2000. However, the runoffs to the downstream increased dramatically since 2000, and the accumulated actual discharge

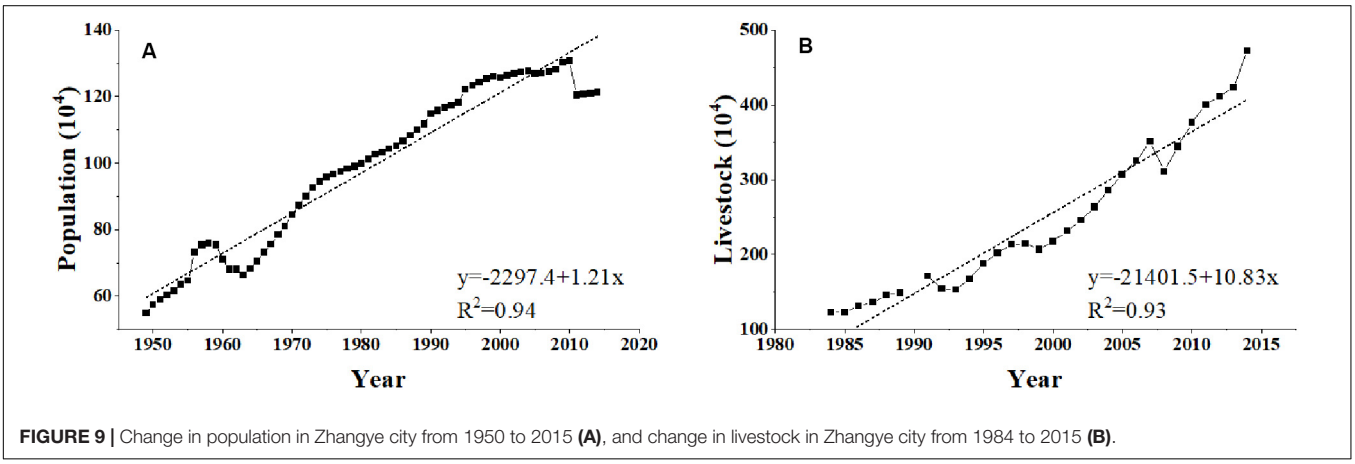

FIGURE 9 | Change in population in Zhangye city from 1950 to 2015 **(A)**, and change in livestock in Zhangye city from 1984 to 2015 **(B)**.

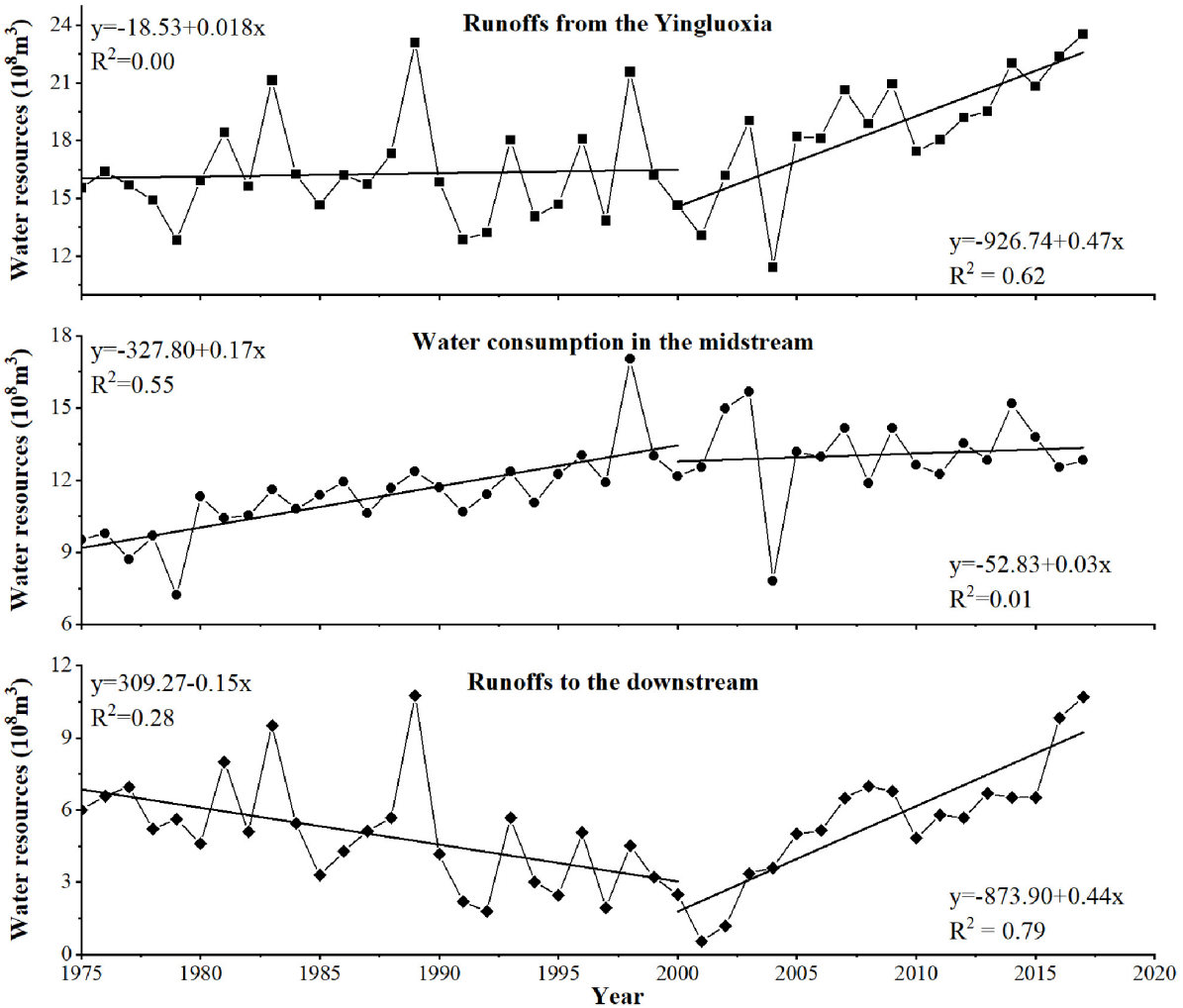

FIGURE 10 | Change in runoffs from the Yingluoxia, water consumption in the midstream, and runoffs to the downstream from 1975 to 2015.

volume of the ZYX section is 13.2 billion m^3 (Jiang X. et al., 2019). The terminal lake of the Heihe River has been recovered, and the area of the East Juyan Lake was up to 59.6 km^2 in 2000, which was greater than in 1958. The West Juyan Lake and the Swan Lake (a residual lake of the ancient Juyan Lake) have also been replenished gradually after 2002 (Liao et al., 2015a). The increased water volume in the terminal lakes of the Heihe River led to increasing groundwater recharge and soil moisture content, which has promoted an increase in native vegetation and the restoration of the ecological environment in the downstream of the HRB. Also, there has been an expansion of downstream vegetation. As **Table 5** shows, environmental rehabilitation has increased vegetation cover of the downstream by 226.7 km^2 during 2000–2015, and the vegetation area in 2015 was much larger than the area in 1990. Attributed to increase in the area of the East Juyan Lake and the recovery of withered forests along the banks, the tourist industry based on the desert lake and a *Populus euphratica* forest has begun to boom, which has promoted the transformation of economic structure in the downstream region to reduce the interference to the ecological environment.

Although the EWDP is a benefit to the restoration of degraded downstream ecological environment, some potential factors which promoted land degradation have also arisen. After the EWDP, the artificial oasis still continuously expanded in the midstream, mainly because desert and ADL are reclaimed for cropland. But due to the shortage of surface water caused by the EWDP, irrigation of most newly reclaimed farmland after 2000 has relied on groundwater. To maintain a more massive increase in water demand for new cropland, groundwater abstraction in the midstream has been intensified further, which was already extensive in the 1980s. Furthermore, to reduce the leakage of ditches and improve the utilization rate of surface water resources, more than 70% of the irrigation system used the waterproof canal, which blocked the groundwater recharge source. So, the combination of farmland expansion in the midstream and the implementation of the water-saving irrigation system were the main reasons for the constant decrease in

the groundwater table, resulting in the deterioration of native grassland around the key irrigation district near the Heihe River, which accounts for land degradation in the midstream after 2000.

CONCLUSION

In this study, LULC, Aeolian desertification, and vegetation change, extracted by using multi-sensor data, were chosen as monitoring indices to illustrate the effects of the EWDP on land degradation in the HRB. Our results reveal that the process of land degradation in the HRB can be divided into two stages, in which the degradation trend was dominant from 1990 to 2000, and the rehabilitation trend was dominant from 2000 to 2015. During the study period, although both climate variation and human activities except political measures have been favorable to land degradation development in the HRB, the land degradation process of the HRB has been stopped and reversed after 2000. The EWDP and the other political measures were benefited to change the land degradation process. Especially in the downstream, the EWDP improving the efficiency of the surface water resources reallocation supplemented groundwater and facilitated the recovery of the deteriorated ecosystem. However, the EWDP indirectly led to the decline of the groundwater table in the midstream caused by the expansion of farmland and completion of the water-saving irrigation system, with resulting local vegetation degradation. Hence, we propose to promote economic restructuring and change the mode of economic growth based on agriculture so as to prevent land degradation caused by the reduction of surface water resources due to the implementation of the EWDP in the midstream of the HRB.

DATA AVAILABILITY STATEMENT

The raw data supporting the conclusions of this article will be made available by the authors, without undue reservation.

AUTHOR CONTRIBUTIONS

XS and JL: methodology. XX: project administration. YHR: hydrological data analysis. JL: socio economic data analysis. XS, JL, and XX: validation. XS: writing—original draft. All authors read and agreed to the published version of the manuscript.

FUNDING

This study was supported by the National Natural Science Foundation of China (Grant No. 41801072), the Project of National Key Research and Development Program of China (2016YFC0500909), and Open Fund Project of the Key Laboratory of Desert and Desertification, Chinese Academy of Sciences (KLDD-2018-001).

REFERENCES

Akhtar-Schuster, M., Stringer, L. C., Erlewein, A., Metternicht, G., Minelli, S., Safriel, U., et al. (2017). Unpacking the concept of land degradation neutrality and addressing its operation through the Rio Conventions. *J. Environ. Manag.* 195, 4–15. doi: 10.1016/j.jenvman.2016.09.044

Ao, F., Jingjie, Y., Pingm, W., and Yichi, Z. (2012). Changing characteristics and influencing causes of groundwater level in the lower reaches of the Heihe River. *J. Nat. Resour.* 27, 686–696. doi: 10.11849/zrzyxb.2012.04.014

Burgan, R. E., and Hartford, R. A. (1993). *Monitoring Vegetation Greenness with Satellite Data*. Ogden, UT: U.S. Department of Agriculture, Forest Service, Intermountain Research Station.

Cheng, G., Li, X., Zhao, W., Xu, Z., Feng, Q., Xiao, S., et al. (2014). Integrated study of the water-ecosystem-economy in the Heihe River Basin. *Nat. Sci. Rev.* 1, 413–428. doi: 10.1093/nsr/nwu017

Cheng, G., Xiao, H., Xu, Z., Li, J., and Lu, M. (2006). Water issue and its countermeasure in the inland river basins of Northwest China: a case study in Heihe river basin. *J. Glaciol. Geocryol.* 28, 406–413. doi: 10.1007/s11442-006-0415-5

Cheng, G. D., and Li, X. (2015). Integrated research methods in watershed science. *Sci. China Earth Sci.* 58, 1159–1168. doi: 10.1007/s11430-015-5074-x

Cowie, A. L., Orr, B. J., Castillo Sanchez, V. M., Chasek, P., Crossman, N. D., Erlewein, A., et al. (2018). Land in balance: the scientific conceptual framework for land degradation neutrality. *Environ. Sci. Policy* 79, 25–35. doi: 10.1016/j.envsci.2017.10.011

Dawelbait, M., and Morari, F. (2012). Monitoring desertification in a Savannah region in Sudan using Landsat images and spectral mixture analysis. *J. Arid Environ.* 80, 45–55. doi: 10.1016/j.jaridenv.2011.12.011

Duan, H., Wang, T., Xue, X., and Yan, C. (2019). Dynamic monitoring of aeolian desertification based on multiple indicators in Horqin Sandy Land China. *Sci. Total Environ.* 650, 2374–2388. doi: 10.1016/j.scitotenv.2018.09.374

Fang, C. (2002). Discrepancy laws of the eco-economic zone in Heihe drainage area and its coupling development pattern. *Acta Ecol. Sin.* 22, 699–708. doi: 10.3321/j.issn:1000-0933.2002.05.012

Feng, L., Jia, Z., and Li, Q. (2016). The dynamic monitoring of aeolian desertification land distribution and its response to climate change in northern China. *Sci. Rep.* 6:39563. doi: 10.1038/srep39563

Guo, Q., Feng, Q., and Li, J. (2009). Environmental changes after ecological water conveyance in the lower reaches of Heihe River, northwest China. *Environ. Geol.* 58:1387. doi: 10.1007/s00254-008-1641-1

He, C., Demarchi, C., Croley, T. E., Feng, Q., and Hunter, T. (2009). Hydrologic modeling of the Heihe watershed by DLBRM in Northwest China. *Sci. Cold Arid Reg.* 1, 432–442. doi: 10.1360/972009-1551

Huang, G., Li, X., Ma, M., Li, H., and Huang, C. (2016). High resolution surface radiation products for studies of regional energy, hydrologic and ecological processes over Heihe river basin, northwest China. *Agric. For. Meteorol.* 230–231, 67–78. doi: 10.1016/j.agrformet.2016.04.007

Inman-Bamber, N. G., Lakshmanan, P., and Park, S. (2012). Sugarcane for water-limited environments: theoretical assessment of suitable traits. *Field Crops Res.* 134, 95–104. doi: 10.1016/j.fcr.2012.05.004

Jiang, L., Jiapaer, G., Bao, A., Li, Y., Guo, H., Zheng, G., et al. (2019). Assessing land degradation and quantifying its drivers in the Amudarya river delta. *Ecol. Indic.* 107:105595. doi: 10.1016/j.ecolind.2019.105595

Jiang, X., Xia, J., Huang, Q., Long, A., Dong, G., and Song, J. (2019). Adaptability analysis of the Heihe River "97" water diversion scheme. *Acta Geogr. Sin.* 74, 103–116. doi: 10.11821/dlxb201901008

Kakembo, V., Ndlela, S., and Cammeraat, E. (2012). Trends in vegetation patchiness loss and implications for landscape function: the case of Pteronia Incana invasion in the eastern cape province, South Africa. *Land Degrad. Dev.* 23, 548–556. doi: 10.1002/ldr.2175

Kang, E., Cheng, G., Song, K., Jin, B., Liu, X., and Wang, J. (2005). Simulation of energy and water balance in Soil-Vegetation-Atmosphere Transfer system in the mountain area of Heihe River Basin at Hexi Corridor of northwest China. *Sci. China Ser. D Earth Sci.* 48, 538–548. doi: 10.1360/02yd0428

Kang, W., and Liu, S. (2014). A review of remote sensing monitoring and quantitative assessment of Aeolian desertification. *J. Desert Res.* 34, 1222–1229. doi: 10.7522/j.issn.1000-694X.2013.00318

Latifovic, R., Trishchenko, A. P., Chen, J., Park, W. B., Khlopenkov, K. V., Fernandes, R., et al. (2005). Generating historical AVHRR 1 km baseline satellite data records over Canada suitable for climate change studies. *Can. J. Remote Sens.* 31, 324–346. doi: 10.5589/m05-024

Le Houérou, H. N. (1996). Climate change, drought and desertification. *J. Arid Environ.* 34, 133–185. doi: 10.1006/jare.1996.0099

Li, J., Yang, X., Jin, Y., Yang, Z., Huang, W., Zhao, L., et al. (2013). Monitoring and analysis of grassland desertification dynamics using Landsat images in Ningxia, China. *Remote Sens. Environ.* 138, 19–26. doi: 10.1016/j.rse.2013.07.010

Li, Q., Zhang, C., Shen, Y., Jia, W., and Li, J. (2016). Quantitative assessment of the relative roles of climate change and human activities in desertification processes on the Qinghai-Tibet Plateau based on net primary productivity. *CATENA* 147, 789–796. doi: 10.1016/j.catena.2016.09.005

Liao, J., Wang, T., and Xue, X. (2015a). Lake's evaporation in the Ejin Basin since transferring water from the Heihe River. *J. Desert Res.* 35, 228–232. doi: 10.7522/j.issn.1000-694X.2013.00448

Liao, J., Wang, T., and Xue, X. (2015b). Oasis evolution in the Heihe River Basin during 1956-2010. *J. Desert Res.* 32, 1426–1441. doi: 10.1007/s11783-011-0280-z

Liu, H. (1995). Types and characteristics of land degradation and countermeasures in China. *Nat. Resour.* 4, 26–32.

Liu, J., Zhang, F., and Xie, X. (2002). The ecological crisis of grassland desertification and the development of Animal husbandry in Hexi corridor. *Agric. Res. Arid Areas* 20, 114–116. doi: 10.3969/j.issn.1674-7240.2002.12.008

Liu, Z., Zhu, Z., and Hao, D. (2002). The mountain-basin complex of Heihe River and resource-environment safety of oasis zone in the lower reaches. *J. Nat. Resour.* 17, 286–293. doi: 10.1007/s11769-002-0026-8

Luo, K., Tao, F., Moiwo, J. P., and Xiao, D. (2016). Attribution of hydrological change in Heihe River Basin to climate and land use change in the past three decades. *Sci. Rep.* 6:33704. doi: 10.1038/srep33704

Ma, J. Z., Wang, X. S., and Edmunds, W. M. (2005). The characteristics of groundwater resources and their changes under the impacts of human activity in the arid Northwest China—a case study of the Shiyang River Basin. *J. Arid Environ.* 61, 277–295. doi: 10.1016/j.jaridenv.2004.07.014

Mi, L., Xiao, H., Zhang, J., Yin, Z., and Shen, Y. (2016). Evolution of the groundwater system under the impacts of human activities in middle reaches of Heihe River Basin (Northwest China) from 1985 to 2013. *Hydrogeol. J.* 24, 971–986. doi: 10.1007/s10040-015-1346-y

Pereira, L. S., Cordery, I., and Iacovides, I. (2012). Improved indicators of water use performance and productivity for sustainable water conservation and saving. *Agric. Water Manag.* 108, 39–51. doi: 10.1016/j.agwat.2011.08.022

Qi, S., and Luo, F. (2005). Water environmental degradation of the Heihe River Basin in arid northwestern China. *Environ. Monit. Assess.* 108, 205–215. doi: 10.1007/s10661-005-3912-6

Romm, J. (2011). Desertification: the next dust bowl. *Nature* 478, 450–451. doi: 10.1038/478450a

Song, X., Wang, T., Xue, X., Yan, C., and Li, S. (2015). Monitoring and analysis of aeolian desertification dynamics from 1975 to 2010 in the Heihe River Basin, northwestern China. *Environ. Earth Sci.* 74, 3123–3133. doi: 10.1007/s12665-015-4350-6

Song, X., and Yan, C. (2014). Land cover change detection using segment similarity of spectrum vector based on knowledge base. *Acta Ecol. Sin.* 34, 7175–7180. doi: 10.5846/stxb201310132458

UNCCD (1994). *United Nations Convention to Combat Desertification in Countries Experiencing Serious Drought and/or Desertification, Particularly in Africa*. Paris: Secretariat of the United Nations Convention to Combat Desertification.

Wang, G., and Cheng, G. (1998). Changes of hydrology and ecological environment during late 50 years in Heihe River Basin. *J. Desert Res.* 18, 233–238. doi: 10.1088/0256-307X/15/11/025

Wang, G., and Cheng, G. (1999). The ecological features and significance of hydrology within arid inland river basins of China. *Environ. Geol.* 37, 218–222. doi: 10.1007/s002540050379

Wang, J., Wei, H., Cheng, K., Ochir, A., Davaasuren, D., Li, P., et al. (2020). Spatio-temporal pattern of land degradation from 1990 to 2015 in Mongolia. *Environ. Dev.* 34:100497. doi: 10.1016/j.envdev.2020.100497

Wang, P., Yu, J., Pozdniakov, S. P., Grinevsky, S. O., and Liu, C. (2014). Shallow groundwater dynamics and its driving forces in extremely arid areas: a case study of the lower Heihe River in northwestern China. *Hydrol. Process.* 28, 1539–1553. doi: 10.1002/hyp.9682

Wang, T., Song, X., Yan, C., Li, S., and Xie, J. (2011). Remote sensing analysis on aeolian desertification trends in Northern China during 1975—2010. *J. Desert Res.* 31, 1351–1356.

Wang, T., Yan, C., Song, X., and Li, S. (2013). Landsat images reveal trends in the aeolian desertification in a source area for sand and dust storms in China's Alashan plateau (1975-2007). *Land Degrad. Dev.* 24, 422–429. doi: 10.1002/ldr.1138

Wang, T., Yan, C., Song, X., and Xie, J. (2012). Monitoring recent trends in the area of aeolian desertified land using Landsat images in China's Xinjiang region. *ISPRS J. Photog. Remote Sens.* 68, 184–190. doi: 10.1016/j.isprsjprs.2012.01.001

Wang, Y., Xiao, H., and Wang, R. (2009). Water scarcity and water use in economic systems in Zhangye city, Northwestern China. *Water Resour. Manag.* 23, 2655–2668. doi: 10.1007/s11269-009-9401-x

Wu, B., Yuan, Q., Yan, C., Wang, Z., Yu, X., Li, A., et al. (2014). Land cover changes of China from 2000 to 2010. *Q. Sci.* 34, 723–731. doi: 10.3969/j.issn.1001-7410.2014.04.04

Xiao, J., Shen, Y., Tateishi, R., and Bayaer, W. (2006). Development of topsoil grain size index for monitoring desertification in arid land using remote sensing. *Intern. J. Remote Sens.* 27, 2411–2422. doi: 10.1080/01431160600554363

Xiao, S., and Xiao, H. (2004). The impact of human activity on the water environment of Heihe water basin in last century. *J. Arid Land Resour. Environ.* 18, 57–62. doi: 10.3969/j.issn.1003-7578.2004.03.011

Xie, Y., Zhao, H., and Wang, G. (2015). Spatio-temporal changes in oases in the Heihe River Basin of China: 1963-2013. *Ecoscience* 22, 33–46. doi: 10.1080/11956860.2015.1047140

Xue, X., Guo, J., Han, B., Sun, Q., and Liu, L. (2009). The effect of climate warming and permafrost thaw on desertification in the Qinghai-Tibetan Plateau. *Geomorphology* 108, 182–190. doi: 10.1016/j.geomorph.2009.01.004

Yan, C. Z., Song, X., Zhou, Y., Duan, H., and Li, S. (2009). Assessment of aeolian desertification trends from 1975's to 2005's in the watershed of the Longyangxia Reservoir in the upper reaches of China's Yellow River. *Geomorphology* 112, 205–211. doi: 10.1016/j.geomorph.2009.06.003

Zhang, A., Zheng, C., Wang, S., and Yao, Y. (2015). Analysis of streamflow variations in the Heihe River Basin, northwest China: trends, abrupt changes, driving factors and ecological influences. *J. Hydrol. Reg. Stud.* 3, 106–124. doi: 10.1016/j.ejrh.2014.10.005

Zhang, G., Nie, Z., and Liu, S. (2006). Threshold of influence of water resources in the Heihe River valley, northwestern Gansu, China on the ecological environment variation of the lower reaches. *Geol. Bull. China* 25, 244–250. doi: 10.1007/s11442-006-0415-5

Zhang, L., Wu, B., Li, X., and Xing, Q. (2014). Classification system of China land cover for carbon budget. *Acta Ecol. Sin.* 34, 7158–7166. doi: 10.5846/stxb201310102431

Zhang, S., Ye, Z., Chen, Y., and Xu, Y. (2017). Vegetation responses to an ecological water conveyance project in the lower reaches of the Heihe River basin. *Ecohydrology* 10:e1866. doi: 10.1002/eco.1866

Zhang, X., and Xia, J. (2009). Coupling the hydrological and ecological process to implement the sustainable water resources management in Hanjiang River Basin. *Sci. China Ser. E-Technol. Sci.* 52, 3240–3248. doi: 10.1007/s11431-009-0363-2

Zhou, Y., Li, X., Yang, K., and Zhou, J. (2018). Assessing the impacts of an ecological water diversion project on water consumption through

high-resolution estimations of actual evapotranspiration in the downstream regions of the Heihe River Basin, China. *Agric. For. Meteorol.* 249, 210–227. doi: 10.1016/j.agrformet.2017.11.011

Conflict of Interest: The authors declare that the research was conducted in the absence of any commercial or financial relationships that could be construed as a potential conflict of interest.

frontiers in Environmental Science

ORIGINAL RESEARCH
published: 26 October 2020
doi: 10.3389/fenvs.2020.534774

Root Features Determine the Increasing Proportion of Forbs in Response to Degradation in Alpine Steppe, Tibetan Plateau

Zhenchao Zhang[1,2] *and Jian Sun*[1]*

[1] Key Laboratory of Ecosystem Network Observation and Modelling, Synthesis Research Centre of Chinese Ecosystem Research Network, Institute of Geographic Sciences and Natural Resources Research, Chinese Academy of Sciences, Beijing, China, [2] School of Soil and Water Conservation, Beijing Forestry University, Beijing, China

Understanding the response of plant community to degradation is fundamentally important for grassland conservation and management. The objective of this study is to examine the changes in soil properties and plant characteristics along a degradation gradient in alpine steppe, and explore the potential mechanisms that biotic and abiotic controls regulate plant community variations. We chose seven sequent degrees of degradation, and conducted a field survey as well as soil and plant samplings in an alpine steppe in Northern Tibet. The results showed that soil water content (SWC), soil compaction (SCOM), soil total carbon (STC), and total nitrogen (STN) dramatically decreased along the degradation gradient. The species richness, overall aboveground biomass (AGB), and AGB of graminoids were apparently reduced with increasing degradation, while AGB of forbs slightly increased. The increasing degradation levels induced a significant increase in the trade-off value of AGB of forbs, which was negatively associated with SWC, SCOM, STC, STN, and soil available nitrogen. The mean root length of forbs was significantly longer than that of graminoids ($P < 0.05$). Moreover, the mean root diameter of the top 1/3 part of forbs was remarkably thicker than that of graminoids ($P < 0.05$). These findings indicate that the degradation-induced cohesionless soils with insufficient water and nutrients together with the divergent root morphological traits of graminoids and forbs determine the plant community structure shift with grassland degradation. This study can improve the understanding of community succession of grassland degradation, and provide guidance for the management of degraded alpine steppe on the Tibetan Plateau.

Keywords: forbs, species richness, plant community structure, root morphological trait, degradation, alpine steppe, Tibetan Plateau

OPEN ACCESS

Edited by:
Xian Xue,
Northwest Institute of Eco-Environment and Resources (CAS), China

Reviewed by:
Shikui Dong,
Beijing Normal University, China
Jessica M. Furrer,
Benedict College, United States

***Correspondence:**
Jian Sun
sunjian@igsnrr.ac.cn

Specialty section:
This article was submitted to Soil Processes, a section of the journal Frontiers in Environmental Science

Received: *14 February 2020*
Accepted: *25 September 2020*
Published: *26 October 2020*

Citation:
Zhang Z and Sun J (2020) Root Features Determine the Increasing Proportion of Forbs in Response to Degradation in Alpine Steppe, Tibetan Plateau. Front. Environ. Sci. 8:534774. doi: 10.3389/fenvs.2020.534774

INTRODUCTION

Grasslands, as the world's most widespread biomes, cover 24% of the total land area (He et al., 2009), store ∼34% of the global terrestrial carbon storage (Cheng et al., 2018), and provide 13.82% of the organic matter supplied by terrestrial ecosystems every year (Zhou et al., 2014). The Tibetan Plateau accounts for ∼44% of China's grasslands, equal to 6% of the world's grasslands (Piao et al., 2012). It is an ideal indicator of global climate change due to the distinctive alpine climate and

severe geographic conditions. With 50.90% covered by alpine grasslands, the Tibetan Plateau not only has important ecosystem service functions (Sun et al., 2019), but also is a vital rangeland for Tibetan herdsmen (Feng et al., 2010). However, the Tibetan Plateau's grassland is highly susceptible to degradation with increasing population, overgrazing, mismanaged feeding, and the effects of natural disaster exacerbated by climate change (Wang et al., 2015). Recently, a considerable portion of the Tibetan Plateau's alpine grasslands has degraded (Harris, 2010; Sun et al., 2019). Particularly, 35% of the alpine grasslands in the source region of the Yangtze have severely degraded to "Black Beach" or "Black Soil," which present land sparsely covered with weedy forbs, poisonous plants, or eroded revealing bare mineral soil (Ma et al., 2002).

Grassland degradation has not only threatened on livestock grazing and limited sustainable development of animal husbandry (Sun et al., 2019), but also resulted in a reduction in ecological functions such as biodiversity provisions, sinks of atmospheric carbon, water and soil conservation, and cultural recreation in the Tibetan Plateau, which has become a global concern in recent years (Harris, 2010; Sun et al., 2019). It is recognized that degradation causes a significant decline in vegetation cover and biodiversity leading to a further decrease in grazing capacity (Cheng et al., 2007). In addition, soil nutrients such as soil organic carbon, total nitrogen, and phosphorus are reduced under the effect of degradation (Wu et al., 2010; Sun et al., 2014; Zhang et al., 2019). Soil water infiltration reduction and soil erosion are accelerated by alpine grassland degradation (Zeng et al., 2013). Consequently, the assessment of soil quality is important for monitoring grassland degradation. In fact, the degradation-induced changes in soils can directly influence the system-level functions and composition of vegetation species (Sun and Wang, 2016).

Plant community composition is a dramatic indicator of environmental change and a key determinant of ecosystem functions (Wang et al., 2007). To date, numerous experiments have been conducted to study the series of impacts of natural and artificial factors on plant community structure on the Tibetan Plateau (Yang et al., 2013). Ganjurjav et al. (2016) predicted that the poisonous forbs would increase possibly covering the entire Tibetan Plateau specially in the alpine steppe under future climate change, which may lead to grassland degradation and aggravate the drought conditions in alpine steppe. It is well-known that soil nutrients are vital abiotic limitations regulating plant community structure, which is ruled by various mechanisms according to initial species composition (Li et al., 2014; Sun et al., 2014). Different plant functional groups may have different responses to nutrient variations within a community (Wang et al., 2010). Graminoids responding quickly to increasing nutrients would exclude other species and dominate the plant community when fertilized (Liu et al., 2013). Other studies emphasized that light availability was more important than nutrient availability in controlling plant community (Liu et al., 2015). Litter that weakens light penetration to lower levels exhibits inhibitory effects on seedling establishment for photophilic plants (Wang et al., 2010). Additionally, water available content could affect the supply of soil nutrients, seed germination, and seedling survival, and thereby determine the plant community structure in the alpine steppe (Yang et al., 2013; Ma et al., 2017).

Various disturbance also plays an important role in the community composition, for instance, fire could constrain the belowground bud density of forbs, while inversely promote graminoids to produce more buds for survival (Wang et al., 2018). Some surveys proved that under grazing pressure, the taller and palatable graminoids favored by livestock declined compared to the lower and unpalatable forbs (Wu et al., 2009; Niu et al., 2010). Nevertheless, graminoids exhibit greater competitive ability than forbs and remarkably increase with grazing exclusion or artificial grassland establishment (Wu et al., 2010; Jing et al., 2014). Unlike large grazing herbivores, small and semi-fossorial herbivores such as *plateau pika* could raise the proportion of graminoids by enhancing the bud density of graminoids vs. forbs, as well as improving the soil physicochemical properties in alpine meadows (Wang et al., 2018). Thus, they are considered to benefit the health of grassland ecosystems (Guo et al., 2012), while high disturbing intensities may lead to alpine meadow deterioration (Wang et al., 2018).

Obviously, the alpine community structure is comprehensively regulated by multifactorial controls of environmental, anthropogenic, and individual biotic effects. However, it is still unclear how grassland degradation alters plant community composition and the underlying mechanism in alpine steppe. Thus, we conducted a field survey in a degraded alpine steppe in Northern Tibet to explore the changes in species richness (SR) and aboveground biomass (AGB) of graminoids and forbs with different degrees of degradation. We hypothesized that the proportion of forbs would increase with increasing degradation, which might be dominated by both degradation-induced changes in soil properties and plant root morphological traits.

To test this hypothesis, we quantified the divergence of AGB and root morphological parameters between graminoids and forbs, and examined the dynamics of soil physicochemical properties at different soil depths along the degradation gradient. We aimed to answer the following questions: (i) How does the plant community structure and SR respond to degradation levels in alpine steppe? (ii) How do plant root morphological traits and degradation-induced changes in soil properties determine the change in plant community composition? The answers can be not only meaningful in theory to improve our understanding on the relationship between grassland degradation and plant community structure, but also valuable in practice to monitor the potential succession direction of alpine steppe worldwide.

MATERIALS AND METHODS

Study Area

The Tibetan Plateau (80°-105°E, 27°-37°N), which is located in southwestern China, covers ∼2.3 × 10^6 km^2 and has a mean altitude of over 4,000 m, as the highest plateau in the world (Sun et al., 2019). All sampled sites belonged to an alpine steppe in Xainza County (88°42′ E, 30°57′ N, 4,675 m.a.s.l.) in Northern Tibet, located in the interior of the Tibetan Plateau, with a

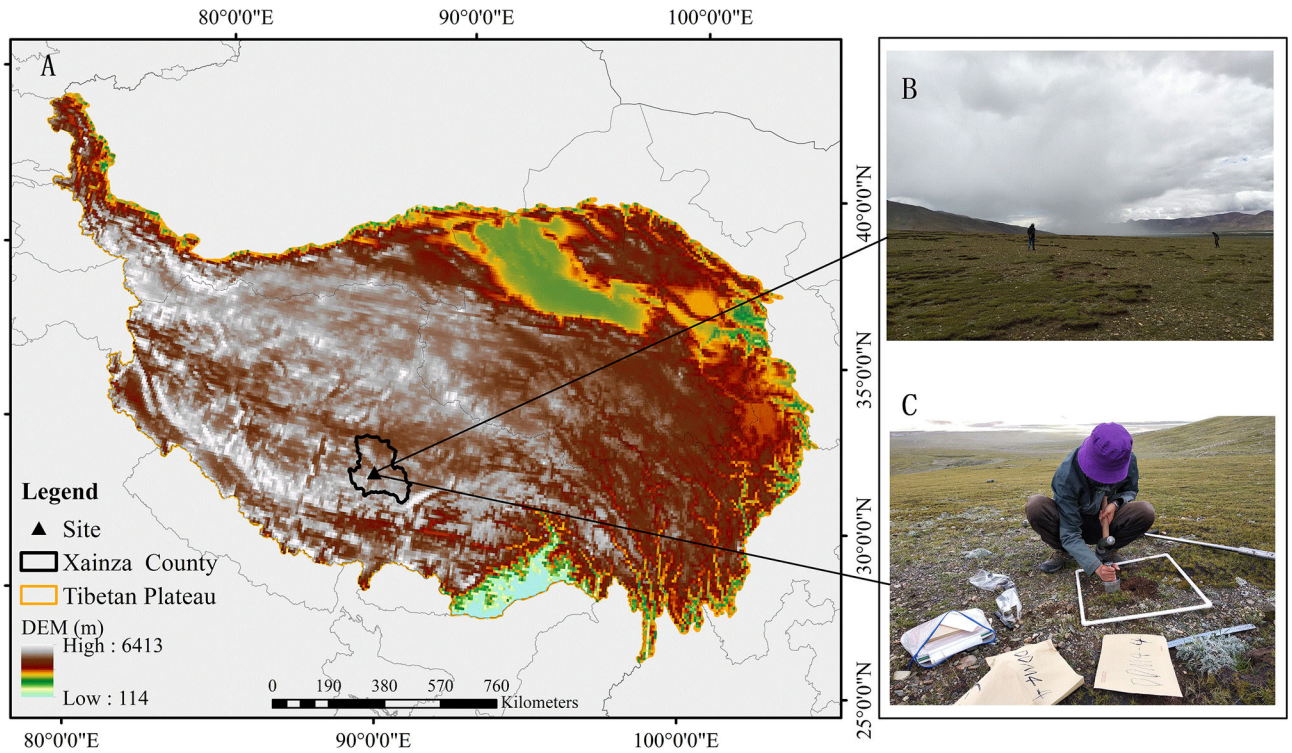

FIGURE 1 | The location of sampled sites in Xainza County on the Tibetan Plateau **(A)**. **(B,C)** presented the landscape of sampled site and sampled quadrat, respectively.

semiarid plateau monsoon climate (**Figure 1**). The mean annual temperature was 0°C at this location over the past 30 years. The mean annual precipitation is 300 mm, which mostly falls from May to September (Zhang et al., 2019). The vegetation is dominated by grasses from *Stipa purpurea*, *Carex thibetica*, and *Leontopodium alpinum*. The main soil category is loam (Zhang et al., 2019).

Data Collection

One typical degraded alpine steppe was chosen as our sample area after wide field surveys in Xainza County. Based on the dividing method by Ma et al. (2002) and Zhang et al. (2019), we divided the degraded grasslands into seven sequent degrees degradation according to vegetation coverage and bare land area. As the seven sites were adjacent, the climatic and topographic conditions were similar. Each site was about 20 m wide and 50 m long where the grasslands were relatively homogeneous with a specific degradation. The transition region between two adjacent sites was excluded when we identified and classified degraded extents, and the conditions of alpine steppes were apparently divergent among different sites. The degraded extents gradually increased from the 1st to the 7th sites of degraded grasslands, and the detailed information were displayed in **Table 1**. The sampling survey was conducted in July and August 2017 during the peak growing season. In order to collect plant and soil samples as well as measure their characteristics, we randomly selected three pairs of 50 × 50 cm quadrats as pseudo replicates within each site, which is a common sampling method for this type of study (Zhang et al., 2019).

The vegetation community characteristics within each quadrat were identified and recorded, including the plant coverage, species, and number. Aboveground plant parts were clipped at the ground level with scissors, while belowground plant parts were directly excavated. The plant samples were separated by plant species and transported to the lab, where they were oven-dried at 65°C for 72 h in the laboratory to determine the plant biomass. Soil water content (SWC) and compactness (SCOM) were measured with portable Time Domain Refectometry equipment (TDR 100, Spectrum Technologies Inc., Chicago, United States) at the soil depth of 0–30 cm with depth intervals of 0–10, 10–20, and 20–30 cm, three replicate soil samples within each quadrat were obtained via soil cores 5 cm in diameter for other soil property measurements.

The three replicate soil samples were mixed thoroughly, air-dried, and sieved through a 2-mm mesh after the visible roots and other debris were removed. Then, we divided the mixed samples into three parts as replicates to determine soil properties. Soil total carbon (STC) and soil total nitrogen (STN) were determined using a vario MACRO cube elemental analyzer (Elementar Analysensysteme GmbH, Germany) (Bao, 2000). Soil total phosphorus content was determined via the $NaHCO_3$ alkali digestion method and molybdenum antimony colorimetric test (Bao, 2000). Soil available nitrogen was measured using the continuous alkali-hydrolyzed reduction-diffusion method (Bao,

TABLE 1 | The information of the seven sites of degraded alpine steppes in our study.

Sites	Coordinate	Altitude (m)	Main species	Coverage (%)
1	30°52′12.78″ N 88°41′25.89″ E	4,812	*Stipa capillata, Kobresia myosuroides, Koeleria cristata, Elymus sibiricus, Oxytropis platysema, Illicium verum, Poa annua, Carex spp.*	86.22
2	30°52′18.67″ N 88°41′34.85″ E	4,784	*Stipa capillata, Kobresia myosuroides, Oxytropis platysema, Illicium verum, Carex spp.*	71.35
3	30°52′22.53″ N 88°41′15.34″ E	4,753	*Stipa capillata, Kobresia myosuroides, Illicium verum, Anaphalis sinica, Carex spp.*	59.43
4	30°52′07.64″ N 88°41′11.59″ E	4,722	*Stipa capillata, Kobresia myosuroides, Oxytropis platysema*	47.11
5	30°52′29.36″ N 88°41′33.55″ E	4,705	*Kobresia myosuroides, Oxytropis platysema; Kobresia setchwanensis, Potentilla anserine*,	38.84
6	30°52′45.56″ N 88°41′36.18″ E	4,681	*Oxytropis kansuensis, Stipa capillata, Artemisia desertorum, Cyperus rotundus*	29.53
7	30°52′59.11″ N 88°41′44.50″ E	4,697	*Carex tristachya, Artemisia desertorum, Cyperus rotundus, Stellera chamaejasme*	14.18

TABLE 2 | Soil properties along the degraded gradient of alpine steppe (mean ± s.e.).

Soil Depths(cm)	Gradient	STC(g/kg)	STN(g/kg)	SAN(mg/kg)	SAP(mg/kg)	STP(g/kg)	SCOM(Pa)	SWC(%)
0–10	1	80.82 ± 64.37^{abc}	7.03 ± 2.68^{a}	9.32 ± 1.22^{a}	3.99 ± 2.87^{ab}	0.18 ± 0.02^{a}	18.56 ± 4.75^{ab}	7.02 ± 0.30^{a}
	2	46.13 ± 1.82^{a}	4.28 ± 0.49^{b}	13.16 ± 2.30^{a}	3.87 ± 4.43^{ab}	0.21 ± 0.03^{ab}	16.19 ± 3.22^{ab}	6.45 ± 0.68^{bd}
	3	42.55 ± 2.62^{a}	4.33 ± 0.39^{b}	10.26 ± 1.72^{a}	6.24 ± 2.06^{ab}	0.20 ± 0.05^{ab}	14.00 ± 1.01^{a}	5.82 ± 2.68^{abc}
	4	41.72 ± 8.83^{ab}	5.52 ± 1.49^{ab}	10.25 ± 2.12^{a}	8.14 ± 2.16^{ab}	0.28 ± 0.04^{b}	15.65 ± 1.73^{a}	6.13 ± 0.40^{bd}
	5	30.13 ± 2.95^{b}	3.52 ± 0.65^{c}	7.93 ± 1.07^{a}	7.41 ± 0.70^{a}	0.22 ± 0.04^{ab}	13.77 ± 1.18^{a}	4.92 ± 0.90^{abc}
	6	29.37 ± 2.76^{b}	5.03 ± 1.20^{b}	8.40 ± 2.52^{a}	7.42 ± 0.94^{a}	0.22 ± 0.06^{ab}	14.75 ± 0.51^{a}	4.42 ± 0.26^{b}
	7	18.73 ± 0.98^{c}	3.81 ± 0.87^{cd}	9.08 ± 4.25^{a}	4.58 ± 1.23^{b}	0.21 ± 0.06^{ab}	11.43 ± 0.65^{b}	3.82 ± 0.26^{cd}
10–20	1	58.57 ± 25.23^{ab}	4.36 ± 0.19^{a}	8.52 ± 2.05^{a}	6.48 ± 1.09^{a}	0.16 ± 0.01^{a}	35.99 ± 7.84^{abd}	9.14 ± 0.22^{a}
	2	36.70 ± 4.78^{ab}	3.78 ± 0.34^{ab}	12.00 ± 2.71^{a}	6.13 ± 2.62^{ab}	0.14 ± 0.01^{b}	33.83 ± 7.52^{abd}	7.94 ± 1.43^{ab}
	3	41.35 ± 4.81^{ac}	4.63 ± 0.97^{a}	8.72 ± 2.71^{a}	3.04 ± 2.62^{ab}	0.19 ± 0.03^{ac}	35.06 ± 7.52^{abd}	7.56 ± 1.43^{ab}
	4	46.67 ± 9.06^{a}	4.97 ± 0.55^{a}	9.56 ± 3.84^{a}	6.83 ± 0.90^{b}	0.21 ± 0.04^{ac}	28.35 ± 0.54^{a}	9.08 ± 0.41^{a}
	5	32.94 ± 2.02^{b}	4.90 ± 1.04^{a}	9.44 ± 2.98^{a}	5.65 ± 0.36^{b}	0.22 ± 0.02^{c}	21.62 ± 0.83^{b}	8.00 ± 0.57^{ab}
	6	32.75 ± 2.71^{bc}	3.51 ± 0.37^{b}	7.58 ± 1.65^{a}	4.71 ± 1.75^{b}	0.22 ± 0.05^{ac}	20.43 ± 1.01^{c}	8.43 ± 1.17^{ab}
	7	20.29 ± 4.25^{c}	2.67 ± 0.11^{b}	6.18 ± 0.73^{a}	3.87 ± 1.77^{ab}	0.25 ± 0.03^{c}	23.38 ± 3.68^{d}	6.57 ± 1.08^{b}
20–30	1	43.58 ± 8.59^{a}	5.28 ± 0.67^{a}	8.53 ± 2.83^{a}	3.40 ± 1.68^{ab}	0.14 ± 0.01^{a}	39.25 ± 2.23^{a}	9.05 ± 1.14^{ac}
	2	25.75 ± 4.30^{bd}	4.47 ± 1.38^{b}	8.86 ± 1.76^{a}	4.20 ± 1.40^{a}	0.18 ± 0.04^{ab}	38.28 ± 3.75^{abe}	8.14 ± 1.91^{abc}
	3	39.59 ± 3.20^{ac}	4.89 ± 0.56^{ab}	8.86 ± 1.76^{a}	5.18 ± 4.04^{ab}	0.20 ± 0.06^{ab}	33.01 ± 3.60^{abce}	7.05 ± 0.26^{b}
	4	54.16 ± 12.53^{a}	3.58 ± 0.45^{b}	9.21 ± 1.76^{a}	4.81 ± 2.68^{ab}	0.19 ± 0.05^{ab}	32.82 ± 1.19^{b}	9.73 ± 0.94^{c}
	5	29.66 ± 2.12^{d}	3.56 ± 0.66^{b}	6.77 ± 2.14^{a}	5.05 ± 2.56^{ab}	0.24 ± 0.05^{b}	28.31 ± 2.16^{c}	9.85 ± 3.27^{abc}
	6	30.99 ± 4.64^{cde}	4.30 ± 1.31^{ab}	6.53 ± 2.84^{a}	6.94 ± 3.21^{b}	0.22 ± 0.05^{b}	22.32 ± 1.31^{d}	8.99 ± 2.12^{abc}
	7	24.63 ± 2.24^{be}	3.36 ± 0.74^{b}	10.13 ± 2.96^{a}	5.54 ± 1.59^{b}	0.26 ± 0.03^{b}	35.02 ± 0.47^{e}	6.75 ± 0.86^{b}

STC, STN, SAN, SAP, STP, SCOM, and SWC represent soil total carbon, soil total nitrogen, soil available nitrogen, soil available phosphorus, soil total phosphorus, soil compactness, and soil water content, respectively. The different letters "a–e" represent significant difference at 0.05 level.

2000). Soil available phosphorus was determined via the Olsen method (Olsen et al., 1954; Bao, 2000). The soil physicochemical properties at 0–30 cm depth were shown in **Table 2**.

Statistical Analyses

The Margalef Index was used to determine SR which was calculated by the following formula (Margalef, 1957):

$$D = (S - 1)/\ln N$$

where D is the Margalef Index, S and N represent the number of objective species and the total number of plant individuals in the ecosystem.

We used a simple approach proposed by previous studies to explore the trade-off between two objectives (graminoids and forbs) by computing the root mean square error of the individual benefits (Bradford and Damato, 2012; Sun et al., 2018). Based on the root mean square error, the distance from the objective point to the zero trade-off line can be quantified, which can represent the extent of overall benefits for graminoids and forbs. The trade-off was decomposed into one of two dimensions tracing the proportion shift of graminoids and forbs in response

to grassland degradation. The benefit for biomass of a single objective plant community defined as the relative deviation from the mean of a given observation is calculated as follows (Bradford and Damato, 2012):

$$B_i = \frac{x_i - x_{min}}{x_{max} - x_{min}}$$

where B_i represents the magnitude of benefit for objective i; x_i, x_{min}, and x_{max} stand for the observed, minimum, and maximum values for objective i. The individual benefits range from 0 to 1 and can be conceptualized as the proportion of possible benefits in objective i (AGB of graminoids or forbs) realized in response to a given degradation. The root mean square error approximates the distance from the "1:1 line" of the zero trade-off and stands for the extent of overall benefits for AGB of graminoids or forbs.

One-way analysis of variance was performed to determine the differences in soil properties along degradation gradient and the differences in root parameters between graminoids and forbs. The least significant difference was used to determine which ingredients differed at the 0.05 significant level. The redundancy analysis was applied based on the data of soil and plant characteristics to detect their cumulative contribution rates on degradation gradient after separately logarithmical and hellinger standardizing treatment, and the packages of "*vegan,*" "*ggrepel,*" and "*ggplot2*" in software R (R Core Team., 2016) were used for the redundancy analysis. Linear regression analysis was used to reveal the tendency of trade-off value of AGB of forbs along the degradation gradient. Correlation analysis and heatmap were carried out the packages of "*corrplot*" in software R (R Core Team., 2016) to explore the relationships among trade-off value of AGB of forbs, SR, and soil physicochemical properties. These analyses were performed by using SigmaPlot for Windows version 14.0 (Systat Software, Inc., Chicago, IL, United States), SPSS 19.0 software (SPSS Inc., Chicago, IL, United States), ArcGIS 10.1 (ESRI, Inc., Redlands, CA, United States), and R software (R Core Team., 2016).

RESULTS

Variations in Soil Physicochemical Properties Along the Degradation Gradient

The redundancy analysis results revealed that the first two axes explained 86.91% of the total variance within the relationship between soil properties and plant characteristics at all seven degraded grasslands (**Figure 2**), of which the eigenvalue of the first and second axis accounted for 68.66% and 18.25% in sequence. For the distribution patterns of soil properties and sites of degraded grasslands, there were stronger relevancies between SCOM with the 7th site, also between STC with the 1st and 3rd sites, while the other sites were more associated with STN, soil available phosphorus, and SWC (**Figure 2**).

The concentrations of STC, STN, SCOM, and SWC consistently decreased with increasing degraded degress, while there was no significant difference in soil available nitrogen, and slight increases in soil available phosphorus and total phosphorus (**Table 2**). The variations occurred most distinctly in the surface soil layer (0–10 cm), and gradually weakened with increasing soil depth. Compared to the potential degraded grassland, the topsoil STC, STN, SCOM, and SWC in the most severe degradation were reduced by 76.8, 45.7, 38.4, and 45.6%, respectively. All the soil elements showed a strong depth dependence except for soil total phosphorus. The amounts of STC, STN, and soil available nitrogen were higher in surface layers (0–10 cm) than these in subsurface layers (10–30 cm), while SCOM and SWC gradually increased with increasing soil depth (**Table 2**).

Variations in Plant Characteristics Along the Degradation Gradient

A comparatively good ranking result was obtained via the redundancy analysis with ranking values of −0.87 for overall AGB, −0.83 for SR of graminoids, −0.76 for AGB of graminoids, −0.38 for overall SR, −0.35 for SR of forbs, and 0.29 for AGB of forbs along the first axis. For the distribution patterns of plant characteristics and sites of degraded grasslands, the 1st, 2nd, and 3rd sites were more correlated to overall AGB and SR, AGB, and SR of graminoids, and SR of forbs. However, the other sites were more relevant to AGB of forbs (**Figure 2**).

The overall and gramineous AGB distinctly decreased with increasing degradation, while a slight increase in the AGB of forbs was observed (**Figure 3**). The overall and forb SR exhibited dramatic declines along the degradation gradient, by contrast, the SR of graminoids slightly decreased (**Figure 3**). As the degradation increased, the trade-off value of AGB of forbs apparently rose turning to positive with R square value of 0.64 ($P < 0.05$; **Figure 4**).

The mean root length of forbs was 16.28 ± 1.18 cm, significantly longer than that of graminoids (13.20 ± 0.78 cm) ($P<0.05$, **Figure 5A**). The root diameter presented no significant difference between graminoids and forbs at the middle and terminal parts, while significantly diverged at the top 1/3 ($P < 0.05$, **Figure 5B**). Specially, the mean root diameter of forbs at the top 1/3 part was 2.82 ± 1.2 cm apparently larger than 0.63 ± 0.34 cm of graminoids ($P<0.05$, **Figure 5B**).

Relationships of Trade-Off Value of AGB of Forbs With Soil Properties and Species Richness

Figure 6 indicates that the trade-off value of AGB of forbs was significantly correlated with most soil factors at the 95% confidence interval level. Specially, the trade-off value of AGB of forbs presented significantly negative associations with SWC, SCOM, STC, STN, and soil available nitrogen in the 0–30 cm soil layer, while positively correlated to soil total phosphorus with $R^2 = 0.65$, 0.92, 0.84, 0.74, 0.71, and 0.69, respectively (**Figure 6**). Additionally, there was a negative relationship between the trade-off value of AGB of forbs with SR ($R^2 = 0.61$).

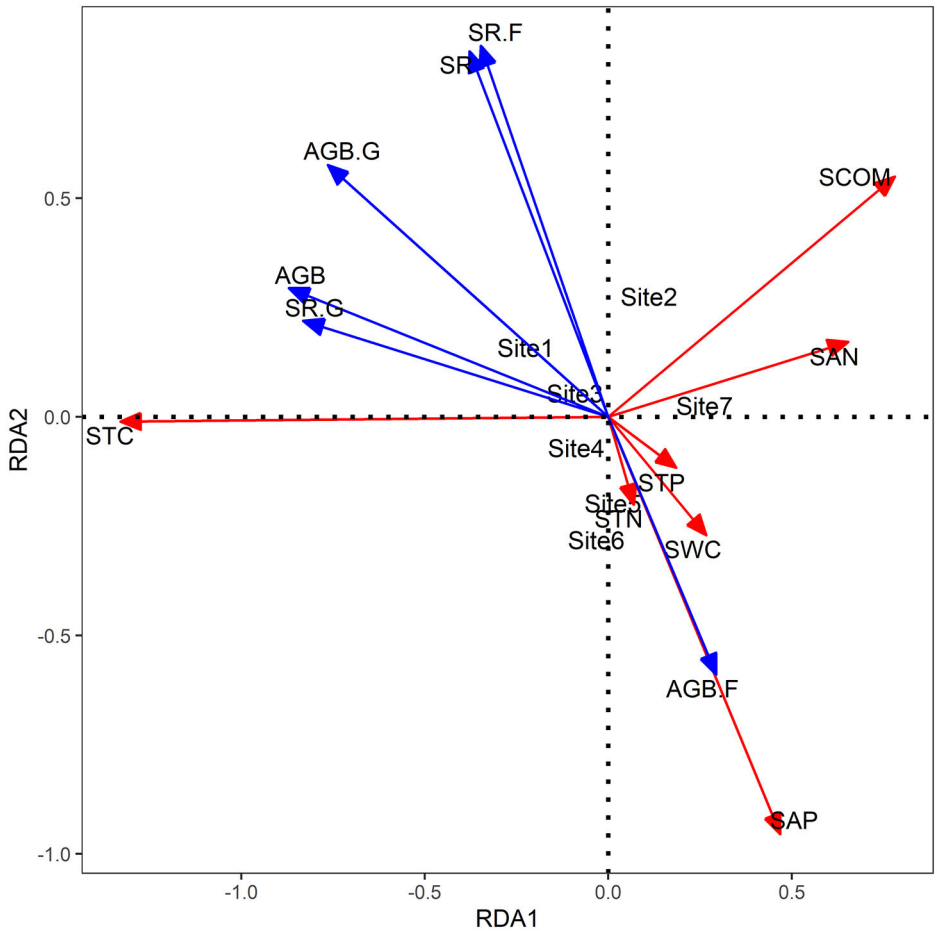

FIGURE 2 | The redundancy analysis of soil variables and vegetation characteristics with different degrees of degradation. The red and blue arrows represent soil variables and vegetation characteristics, respectively. STC, STN, SAN, SAP, STP, SCOM, SWC, AGB, AGB.G, AGB.F, SR, SR.G, SR.F represent soil total carbon, soil total nitrogen, soil available nitrogen, soil available phosphorus, soil total phosphorus, soil compactness, soil water content, overall aboveground biomass, aboveground biomass of graminoids, aboveground biomass of forbs, overall species richness, species richness of graminoids, and species richness of forbs, respectively.

DISCUSSION

Variations of Soil Properties Along the Degradation Gradient

Grassland degradation can affect soil physical properties and nutrition ingredients and thereby result in soil degradation (Zhang et al., 2019). In this study, we found a gradual reduction in SCOM with increasing degradation (**Table 2**), suggesting that degradation contributes to less cohesive soil in alpine steppe. This is consistent with previous studies that degradation leads to decrease in clay but increase in silt content for soil composition, which has a negative impact on SCOM (Yi et al., 2012). Hence, the decline in SCOM may be a powerful indicator of soil degradation in alpine steppe (Feng et al., 2010).

SWC could influence the retention and transfer of available nutrients (Swift et al., 2004). In the present study, we observed a sharp decrease in SWC with enhanced degradation (**Table 1**), which is another major negative influence of degradation on soils, consistent with previous findings (Wang et al., 2009; Yi et al., 2012). It may be because retrogression induces decreases in field capacity and saturated hydraulic conductivity (Pan et al., 2017), which play important positive roles in key hydraulic courses and functions, such as water holding capacity, soil water retention, and infiltration (Fu et al., 2015). Additionally, due to the decline in plant cover, more soil areas are exposed to stronger radiation, which induces an increase in evaporation-reducing SWC (Wang et al., 2009). Meanwhile, due to enhanced soil evaporation and intensified root uptake, SWC in the surface (0–10 cm) layer is lower than that in the subsurface layer (10–30 cm) (**Table 1**). This phenomenon is in accordance with other observations (Wang et al., 2009; Pan et al., 2017).

As expected, STC and STN consistently decreased with increasing degradation in our study (**Table 1**). Similar results were also found by numerous prior studies (Wang et al., 2009; Peng et al., 2018; Zhang et al., 2019). These findings suggested that reduced soil C and N storage are the primary consequence

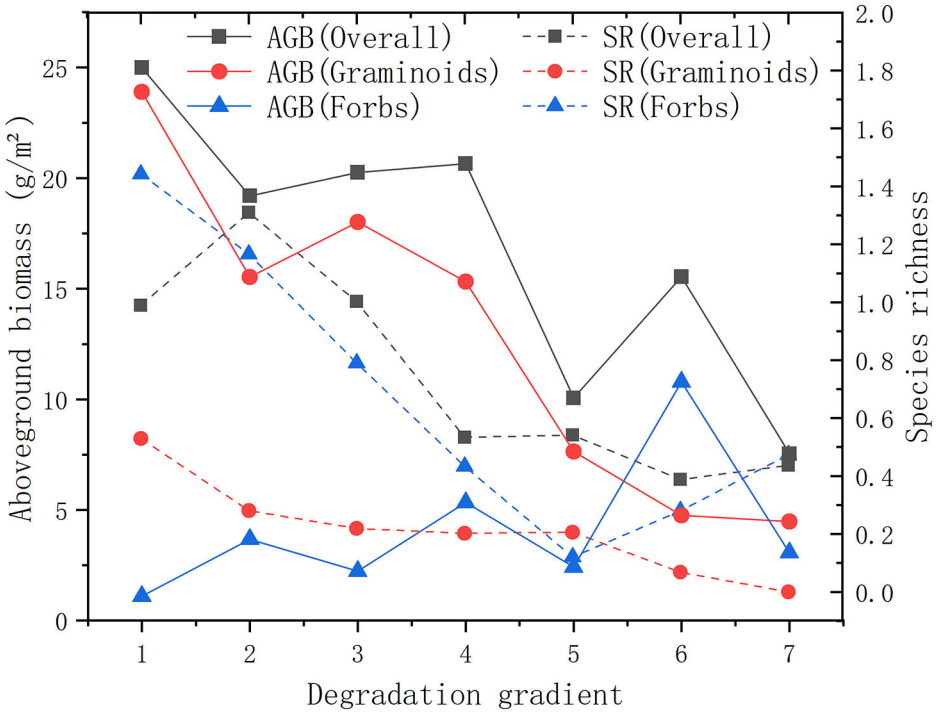

FIGURE 3 | Variations of aboveground biomass (AGB) and species richness (SR) along a degradation gradient. The solid and dashed lines stand for AGB and SR, respectively.

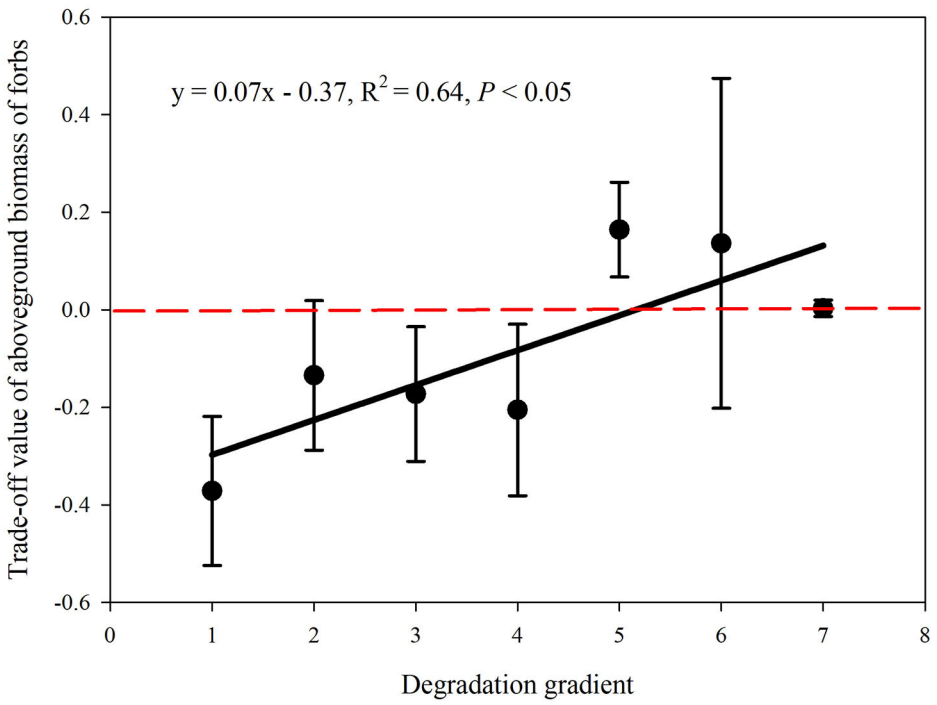

FIGURE 4 | Changes in the trade-off values of aboveground biomass of forbs along a degradation gradient. The red dashed line represents zero value level.

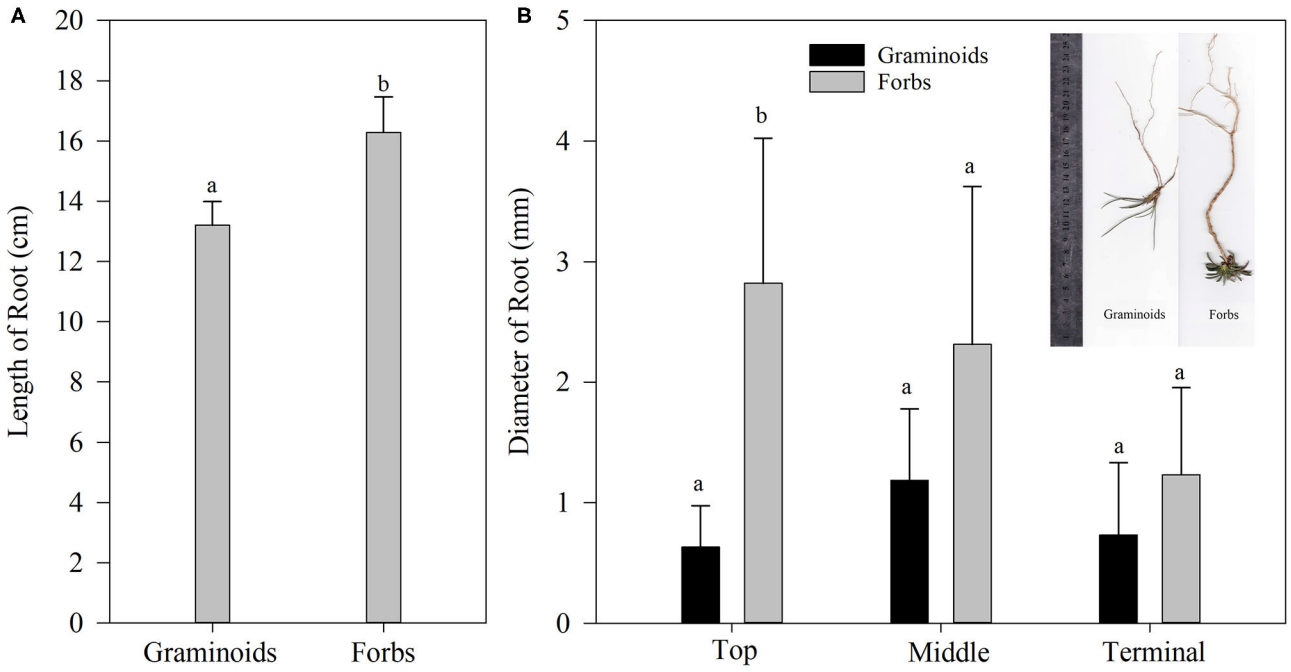

FIGURE 5 | The root morphological traits of graminoids and forbs. **(A)** Length of root; **(B)** diameter of root. Top, middle, and terminal represent the top, middle, and terminal parts (one third) of root. Different letters indicate significant difference at 0.05 level. The photo visually displays the differences of root length and thickness between graminoids and forbs.

of degradation in alpine steppe, which can cause poor soil quality and further accelerate degradation (Dong et al., 2012; Peng et al., 2018). There are a series of reasons for the decreases in STC and STN with the enhanced degradation: First, the distinct reductions in litter input and root activities with increasing degradation level hinder organic matter accumulation (Wang et al., 2010). Second, degradation leads to decrease in vegetation coverage and thereby accelerates water and soil erosion causing nutrient loss (Zhu et al., 2011; Dlamini et al., 2014). Third, degradation causes an increase in bare land area exposed to radiative heating and thus increases soil temperature, which promotes soil respiration leading to rapid consumption of soil organic matters (Wang et al., 2009). Fourth, changes in plant species composition can cause a range of changes in soil biochemical processes. As previous studies have revealed that litter decomposition and nutrient release relatively slowly occur in forbs than graminoids (Li et al., 2014). Finally, degradation worsen the soil microenvironment and induced the reductions of soil microorganisms and enzyme activities (Cai et al., 2014; Zhou et al., 2018) which desirable for the decomposition of organic matter (Zhao et al., 2014). By contrast, there was a slight increase in soil total phosphorus along the degradation gradient (**Table 1**). It can be explained as that soil P with lower diffusivity is primarily derived from rock weathering, which is relatively responsive to climate and parent materials in alpine steppe (Chen et al., 2013).

Our results showed that SCOM, SWC, STC, and STN more strongly responded to degradation in the upper layer (0–10 cm), whereas were less sensitive in the deeper layers (10–30 cm) (**Table 1**). This finding is in agreement with previous studies that the effects of degradation on soil properties are primarily manifested in the top soil (Zeng et al., 2013; Fu et al., 2015; Pan et al., 2017). It is likely due, for the most part, to the degradation-induced declines in plant cover and root grasp. As a result, the topsoil becomes more susceptible to environmental drivers such as wind, raindrops, and surface flow, which directly causes soil erosion, degradation, and even sandification in the alpine steppe (Pan et al., 2017).

Habitat Conditions and Root Morphological Traits Determine Plant Community Shift

Consistent with numerous other reports (Gao et al., 2011; Yang et al., 2013), our results showed that the SR consistently decreased from potentially to severely degraded grassland (**Figure 3**). This result can be explained by a basic ecological theory that the number of plant species is constrained by nutrient availability (Wang et al., 2014). The composition of plant community has important effect on nutrient cycling at ecosystem levels (Epstein et al., 2001; Olofsson et al., 2001). As SR increases, the capacity of a plant community to utilize natural resources improves (Wang et al., 2016). Previous studies have revealed that SR is highest under moderate, rather than high or low nutrient status (Wang et al., 2010). Because a medium disadvantaged condition appears to balance plant abundance for limited resource utilization (Wang et al., 2009). Therefore, the decrease in SR with increasing degradation is expected to occur in nutrient-deficient sites, where degradation decreases fertility falling below the level with

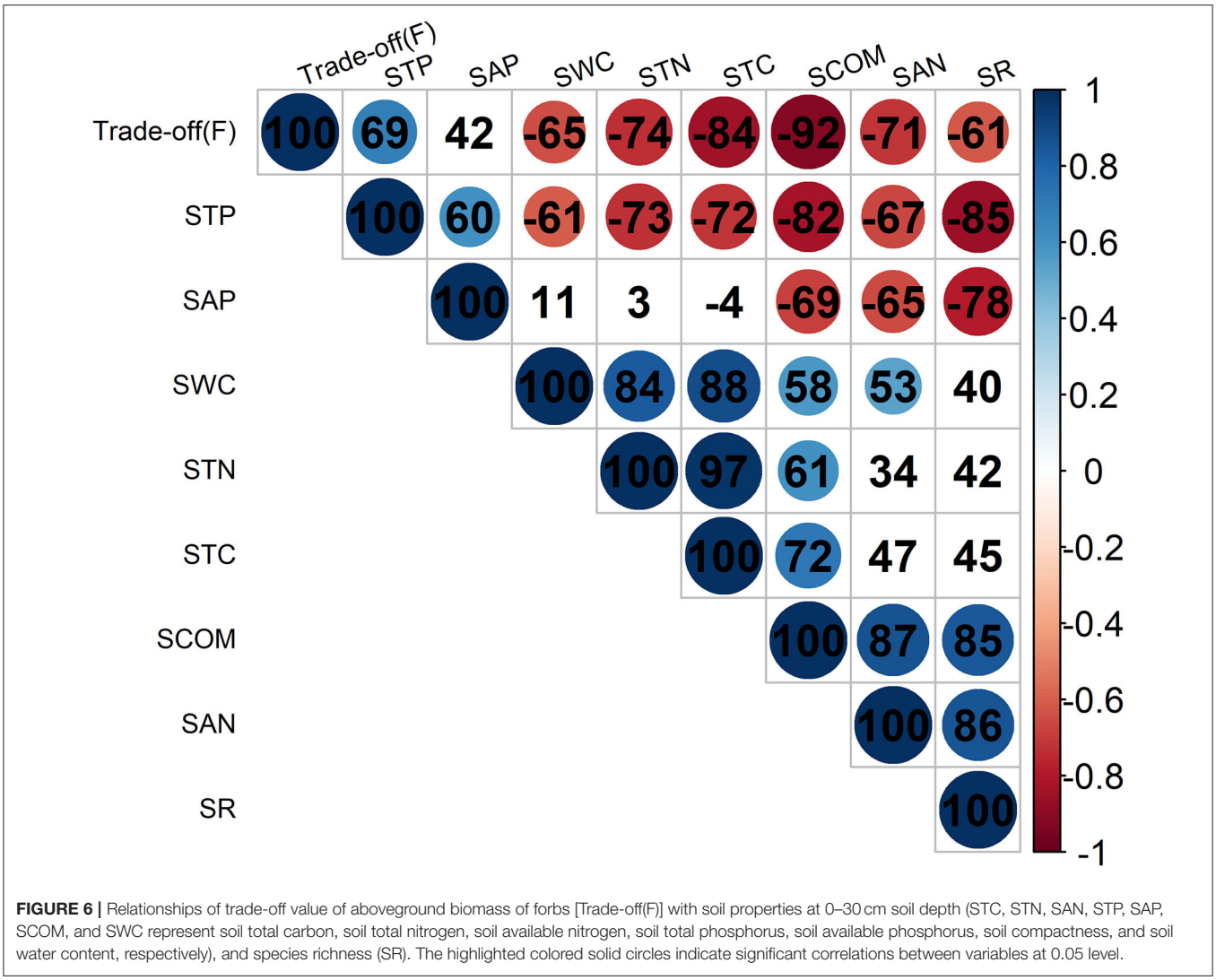

FIGURE 6 | Relationships of trade-off value of aboveground biomass of forbs [Trade-off(F)] with soil properties at 0–30 cm soil depth (STC, STN, SAN, STP, SAP, SCOM, and SWC represent soil total carbon, soil total nitrogen, soil available nitrogen, soil total phosphorus, soil available phosphorus, soil compactness, and soil water content, respectively), and species richness (SR). The highlighted colored solid circles indicate significant correlations between variables at 0.05 level.

potential SR peak. This suggests that grassland degradation might increase the risk of species extinction on the Tibetan Plateau (Lambers, 2015; Urban, 2015).

Community differences in species composition along gradation levels was evident in the varied components of AGB. We found that the trade-off value of AGB of forbs significantly with enhanced degradation (**Figure 4**). Similar observations were obtained by other researchers (Wang et al., 2009; Wu et al., 2009) who reported a shift from palatable grasses to weeds along degradation gradient in alpine grasslands, indicating that degradation is a process of reversed vegetation succession with deterioration of plant community structure. Variations of plant functional groups are closely linked to ecological status shifting toward dominance by competitive exclusion (Wang et al., 2010). Forbs are proved to have higher adaptation to the hostile environmental conditions caused by degradation (Wang et al., 2009). The following several mechanisms maybe contribute to the increase in trade-off value of AGB of forbs with increasing degraded extents observed here.

For habitat conditions, plant growth highly depends on soil nutrients in the infertile alpine steppe (Ganjurjav et al., 2016). In particular, graminoids were more susceptible to soil nutrients due to weak leaf interior self-regulation (Geng et al., 2012). For example, graminoids have relatively high nitrogen requirements, so that their biomass is strongly constrained by nitrogen limitation (Wang et al., 2010). By contrast, forbs exhibit more competitive advantages in soils with limited nutrients, reflected by the negative relationships between trade-off value of AGB of forbs with STC, STN, and soil available nitrogen in this study (**Figure 6**). In addition to the higher requirement of graminoid physiological activities for soil nutrients, it is also because lower nutrients directly hinder the growth of microorganisms and alter their community structure (Breulmann et al., 2012), which is greatly associated with the populations of graminoids (Zhou et al., 2018). Hence, degradation-induced limited soil nutrient availability is a main driver of the increase in forb proportion of the degraded alpine steppe ecosystems (Wang et al., 2010; Wu et al., 2010).

Soil water is another important environmental condition in altering plant colonization and distribution specially in the arid alpine steppe (Sun et al., 2013; Ma et al., 2017). Soil water conditions can affect soil nutrient supply ability and drive plant succession in alpine steppe (Yang et al., 2013; Hou et al., 2018). For example, low SWC is inhospitable to nitrogen uptake for graminoids which is more nitrophilous (Hou et al., 2018). Additionally, even a small variation in SWC may cause a remarkable difference in both seed germination and seedling survival, which consequently affects the individual amount and composition of plant community (Ma et al., 2017). As grassland degradation lead to a dramatic decrease in SWC (**Table 2**), by which graminoids are largely constrained, while forbs inversely dominate the degraded alpine steppe, indicated by the negative correlation between trade-off value of AGB of forbs with SWC (**Figure 6**). This result highlights the vital role of SWC in regulating community composition responding to degradation (Fan et al., 2010; Yang et al., 2013).

For root morphological traits, forbs were found to have remarkably longer roots than graminoids (**Figure 5**). What's more, previous studies have revealed that plant rooting depths varied with different species, which influences the uptake of soil water and the ability to exploit high-nutrient patches (Farley and Fitter, 1999). Specially, forbs root relatively deeper to utilize resources in subsoil when water and nutrients in topsoil sharply decreased, indicated by the slight increase in AGB of forbs with increasing degradation levels (**Figure 3**). However, graminoids produce crowd-short rhizomatous tissues that are shallowly rooted and extends horizontally in the surface soil (Wang et al., 2009). As a result, degradation, which induced sharp declines of topsoil SWC and nutrients (**Table 2**), increases the proportion of deep-rooted and drought resistant forbs, whereas conversely decreases the shallow-rooted graminoids in the alpine steppe (Klein et al., 2008).

In the present study, the trade-off value of AGB of forbs was significantly negatively correlated to SCOM (**Figure 6**), establishing forbs as more plastic in cohesionless soil than graminoids. This result is consistent with previous findings that forbs have greater competitive ability than grasses in severely degraded alpine grassland which leads to less cohesive soil (Gao et al., 2011). It is largely due to that the mean root diameter of forbs is significantly thicker than that of graminoids (**Figure 5B**). Thicker roots provide a better structure to fix the plant against large gale-force winds, increase water storage capacity under arid conditions, and reduce mechanical damage caused by freeze–thaw cycles (Körner, 1999).

However, thick roots help forbs adapt to the harsh environment (e.g., droughts and freeze–thaw cycles) at the cost of efficiency loss in nutrients acquisition (Körner, 1999). As we know, thick roots serve as an excellent way of storage and carriage in alpine grassland, whereas, fine roots are the primary absorptive roots for nutrients (Hong et al., 2018). Alpine plant species thus face a trade-off between tolerance and nutrient absorption. Forbs have fewer fine roots and are mostly axial root species, while graminoids have higher root densities and higher root areas with clustered roots improving the nutritive acquisition rates (Li et al., 2011). Previous studies have demonstrated that graminoids which respond quickly to nutrient increase tend to dominate the plant community and exclude other species when fertilized (Wang et al., 2010). This can explain the low trade-off of forbs in potentially degraded grassland (**Figure 4**), suggesting that graminoids have greater competitive ability than forbs in soils with rich water and nutrients which can satisfy plant growth requirements (Gao et al., 2011).

CONCLUSION

Our results provide strong evidence that grassland degradation results in soil water and nutrient losses, decreasing species richness, and increasing proportion of forbs. The ever-changing habitat condition caused by grassland degradation, together with plant root morphological traits determine the shifting composition of plant community, by which the ecosystem makes full use of limited resources such as water and nutrients to maintain stability and functions. Our findings are of important implications for the conservation and management of alpine grassland ecosystems. The composition of species and their functional traits must be considered to ensure healthy ecosystem function in the process of managing and restoring the degraded grasslands. Intensive management interventions such as weeding may be needed to promote the sustainable development of grasslands in long term. In this study, we only demonstrated the variations of plant community structure along the degradation gradient in alpine steppe from soil and plant morphological traits sides. However, more comprehensive investigation of the potential mechanisms is needed in the future. Hence, plant physiological and genetic methods will be studied in subsequent research.

DATA AVAILABILITY STATEMENT

The datasets generated for this study are available on request to the corresponding author.

AUTHOR CONTRIBUTIONS

ZZ and JS conceived the study, collected and analyzed the data, drew the graphs, and wrote and revised the manuscript.

FUNDING

Funding was provided by the State Key Research Development Program of China (Grant No. 2016YFC0502002), the China Postdoctoral Science Foundation (Grant No. 2017M620889), and the Second Tibetan Plateau Scientific Expedition and Research (Grant No. 2019QZKK0405).

ACKNOWLEDGMENTS

We appreciate the contributions of Ge Hou and Biying Liu in field survey and lab activities.

REFERENCES

Bao, S. D. (2000). *Soil and Agricultural Chenmistry Analysis*. Beijing: China Agriculture Press.

Bradford, J. B., and Damato, A. W. (2012). Recognizing trade-offs in multi-objective land management. *Front. Ecol. Environ.* 10, 210–216. doi: 10.1890/110031

Breulmann, M., Schulz, E., Weishuhn, K., and Buscot, F. (2012). Impact of the plant community composition on labile soil organic carbon, soil microbial activity and community structure in semi-natural grassland ecosystems of different productivity. *Plant Soil* 352, 253–265. doi: 10.1007/s11104-011-0993-6

Cai, X. B., Peng, Y. L., Yang, M. N., Zhang, T., and Zhang, Q. (2014). Grassland degradation decrease the diversity of arbuscular mycorrhizal fungi species in tibet Plateau. *Not. Bot. Horti. Agrobot. Cluj. Napoca*. 42, 333–339. doi: 10.15835/nbha.42.2.9458

Chen, Y. H., Han, W. X., Tang, L. Y., Tang, Z. Y., and Fang, J. Y. (2013). Leaf nitrogen and phosphorus concentrations of woody plants differ in responses to climate, soil and plant growth form. *Ecography* 36, 178–184. doi: 10.1111/j.1600-0587.2011.06833.x

Cheng, J. M., Wu, G. L., Zhao, L. P., Li, Y., Li, W., and Cheng, J. M. (2018). Cumulative effects of 20-year exclusion of livestock grazing on above- and belowground biomass of typical steppe communities in arid areas of the Loess Plateau, China. *Plant Soil Environ.* 57, 40–44. doi: 10.17221/153/2010-PSE

Cheng, X. L., An, S. Q., Chen, J., Li, B., Liu, Y. H., and Liu, S. (2007). Spatial relationships among species, above-ground biomass, N, and P in degraded grasslands in Ordos Plateau, northwestern China. *J. Arid Environ.* 68, 652–667. doi: 10.1016/j.jaridenv.2006.07.006

Dlamini, P., Chivenge, P., Manson, A., and Chaplot, V. (2014). Land degradation impact on soil organic carbon and nitrogen stocks of sub-tropical humid grasslands in South Africa. *Geoderma* 235, 372–381. doi: 10.1016/j.geoderma.2014.07.016

Dong, S. K., Wen, L., Li, Y., Wang, X. X., Zhu, L., and Li, X. Y. (2012). Soil-quality effects of grassland degradation and restoration on the Qinghai-Tibetan Plateau. *Soil Sci. Soc. Am. J.* 76, 2256–2264. doi: 10.2136/sssaj2012.0092

Epstein, H. E., Burke, I. C., and Mosier, A. R. (2001). Plant effects on nitrogen retention in shortgrass steppe 2 years after 15N addition. *Oecologia* 128, 422–430. doi: 10.1007/s004420100670

Fan, J. W., Shao, Q. Q., Liu, J. Y., Wang, J. B., Harris, W. W., Chen, Z. Q., et al. (2010). Assessment of effects of climate change and grazing activity on grassland yield in the three rivers headwaters region of Qinghai–Tibet Plateau, China. *Environ. Monit. Assess* 170, 571–584. doi: 10.1007/s10661-009-1258-1

Farley, R. A., and Fitter, A. H. (1999). The responses of seven co-occurring woodland herbaceous perennials to localized nutrient-rich patches. *J. Ecol.* 87, 849–859. doi: 10.1046/j.1365-2745.1999.00396.x

Feng, R. Z., Long, R. J., Shang, Z. H., Ma, Y. S., Dong, S. K., and Wang, Y. L. (2010). Establishment of Elymus natans improves soil quality of a heavily degraded alpine meadow in Qinghai-Tibetan Plateau, China. *Plant Soil* 327, 403–411. doi: 10.1007/s11104-009-0065-3

Fu, T. G., Chen, H. S., Zhang, W., Nie, Y. P., and Wang, K. L. (2015). Vertical distribution of soil saturated hydraulic conductivity and its influencing factors in a small karst catchment in Southwest China. *Environ. Monitor. Assess.* 187:92. doi: 10.1007/s10661-015-4320-1

Ganjurjav, H., Gao, Q. Z., Gornish, E. S., Schwartz, M. W., Liang, Y., Cao, X. J., et al. (2016). Differential response of alpine steppe and alpine meadow to climate warming in the central Qinghai-Tibetan Plateau. *Agr. Forest Meteorol.* 223, 233–240. doi: 10.1016/j.agrformet.2016.03.017

Gao, Y. H., Zeng, X. Y., Schumann, M., and Chen, H. (2011). Effectiveness of exclosures on restoration of degraded alpine meadow in the eastern Tibetan Plateau. *Arid Soil Res. Rehabil.* 25, 164–175. doi: 10.1080/15324982.2011.554954

Geng, Y., Wang, Z. H., Liang, C. Z., Fang, J. Y., Baumann, F., Kuhn, P., et al. (2012). Effect of geographical range size on plant functional traits and the relationships between plant, soil and climate in Chinese grasslands. *Global Ecol. Biogeogr.* 21, 416–427. doi: 10.1111/j.1466-8238.2011.00692.x

Guo, Z. G., Li, X. F., Liu, X. Y., and Zhou, X. R. (2012). Response of alpine meadow communities to burrow density changes of plateau pika (*Ochotona curzoniae*) in the Qinghai-Tibet Plateau. *Acta Ecol. Sin.* 32, 44–49. doi: 10.1016/j.chnaes.2011.12.002

Harris, R. B. (2010). Rangeland degradation on the Qinghai-Tibetan plateau: a review of the evidence of its magnitude and causes. *J. Arid Environ.* 74, 1–12. doi: 10.1016/j.jaridenv.2009.06.014

He, J. S., Wang, X. P., Flynn, D. F. B., Wang, L., Schmid, B. H., and Fang, J. Y. (2009). Taxonomic, phylogenetic, and environmental trade-offs between leaf productivity and persistence. *Ecology* 90, 2779–2791. doi: 10.1890/08-1126.1

Hong, J. T., Ma, X. X., Yan, Y., Zhang, X. K., and Wang, X. D. (2018). Which root traits determine nitrogen uptake by alpine plant species on the Tibetan Plateau. *Plant Soil* 424, 63–72. doi: 10.1007/s11104-017-3434-3

Hou, G., Sun, J., and Wang, J. N. (2018). Dynamics and controls of carbon use efficiency across China's grasslands. *Pol. J. Environ. Stud.* 27, 1541–1550. doi: 10.15244/pjoes/76912

Jing, Z. B., Cheng, J. M., Su, J. S., Bai, Y., and Jin, J. W. (2014). Changes in plant community composition and soil properties under 3-decade grazing exclusion in semiarid grassland. *Ecol. Eng.* 64, 171–178. doi: 10.1016/j.ecoleng.2013.12.023

Klein, J. A., Harte, J., and Zhao, X. Q. (2008). Decline in medicinal and forage species with warming is mediated by plant traits on the Tibetan Plateau. *Ecosystems* 11, 775–789. doi: 10.1007/s10021-008-9160-1

Körner, C. (1999). *Alpine Plant Life: Functional Plant Ecology of High Mountain Ecosystems*. (Heidelberg: Springer Verlag Berlin).

Lambers, J. H. R. (2015). Extinction risks from climate change. *Science* 348, 501–502. doi: 10.1126/science.aab2057

Li, A., Niu, K. C., and Du, G. Z. (2011). Resource availability, species composition and sown density effects on productivity of experimental plant communities. *Plant Soil* 344, 177–186. doi: 10.1007/s11104-011-0738-6

Li, Y. Y., Dong, S. K., Wen, L., Wang, X. X., and Wu, Y. (2014). Soil carbon and nitrogen pools and their relationship to plant and soil dynamics of degraded and artificially restored grasslands of the Qinghai–Tibetan Plateau. *Geoderma* 213, 178–184. doi: 10.1016/j.geoderma.2013.08.022

Liu, Y. J., Mao, L., Li, J. Y., Shi, G. X., Jiang, S. J., Ma, X. J., et al. (2015). Resource availability differentially drives community assemblages of plants and their root-associated arbuscular mycorrhizal fungi. *Plant Soil* 386, 341–355. doi: 10.1007/s11104-014-2261-z

Liu, Y. W., Xuri, Xu, X., Wei, D., Wang, Y. H., and Wang, Y. S. (2013). Plant and soil responses of an alpine steppe on the Tibetan Plateau to multi-level nitrogen addition. *Plant Soil* 373, 515–529. doi: 10.1007/s11104-013-1814-x

Ma, M. J., Dalling, J. W., Ma, Z., and Zhou, X. H. (2017). Soil environmental factors drive seed density across vegetation types on the Tibetan Plateau. *Plant Soil* 419, 349–361. doi: 10.1007/s11104-017-3348-0

Ma, Y. S., Lang, B. N., Li, Q. Y., Shi, J. J., and Dong, Q. M. (2002). Study on rehabilitating and rebuilding technologies for degenerated alpine meadow in the Changjiang and Yellow river source region. *Pratacult. Sci.* 19, 1–5. doi: 10.3969/j.issn.1001-0629.2002.09.001

Margalef, R. (1957). Information theory in ecology. *Mem. R Acad. Cienc. Artes Barc.* 32, 373–449. doi: 10.1017/S0031819100052062

Niu, K. C., Zhang, S. T., Zhao, B. B., and Du, G. Z. (2010). Linking grazing response of species abundance to functional traits in the Tibetan alpine meadow. *Plant Soil* 330, 215–223. doi: 10.1007/s11104-009-0194-8

Olofsson, J., Kitti, H., Rautiainen, P., Stark, S., and Oksanen, L. (2001). Effects of summer grazing by reindeer on composition of vegetation, productivity and nitrogen cycling. *Ecography* 24, 13–24. doi: 10.1034/j.1600-0587.2001.240103.x

Olsen, S. R., Cole, C. V., Watanabe, F. S., and Dean, L. A. (1954). Estimation of available phosphorus in soils by extraction with sodium carbonate. *USDA Circ.* 939, 1–19.

Pan, T., Hou, S., Wu, S. H., Liu, Y. J., Liu, Y. H., Zou, X. T., et al. (2017). Variation of soil hydraulic properties with alpine grassland degradation in the Eastern Tibetan Plateau. *Hydrol Earth Syst. Sc.* 21, 2249–2261. doi: 10.5194/hess-21-2249-2017

Peng, F., Xue, X., You, Q., Huang, C., Dong, S., Liao, J., et al. (2018). Changes of soil properties regulate the soil organic carbon loss with grassland degradation on the Qinghai-Tibet Plateau. *Ecol. Indic.* 93, 572–580. doi: 10.1016/j.ecolind.2018.05.047

Piao, S. L., Tan, K., Nan, H. J., Ciais, P., Fang, J. Y., Wang, T., et al. (2012). Impacts of climate and CO2 changes on the vegetation growth and carbon balance of Qinghai-Tibetan grasslands over the past five decades. *Glob. Planet Change* 98, 73–80. doi: 10.1016/j.gloplacha.2012.08.009

R Core Team. (2016). *R: A Language and Environment for Statistical Computing*. Vienna, Austria: R Foundation for Statistical Computing. *Available online at: https://www.rproject.org/ (accessed December* 12, 2016).

Sun, J., Cheng, G. W., and Li, W. P. (2013). Meta-analysis of relationships between environmental factors and aboveground biomass in the alpine grassland on the Tibetan Plateau. *Biogeosciences* 10, 1707–1715. doi: 10.5194/bg-10-1707-2013

Sun, J., Ma, B., and Lu, X. (2018). Grazing enhances soil nutrient effects: Trade-offs between aboveground and belowground biomass in alpine grasslands of the Tibetan Plateau. *Land Degrad. Dev.* 29, 337–348. doi: 10.1002/ldr.2822

Sun, J., and Wang, H. M. (2016). Soil nitrogen and carbon determine the trade-off of the above- and below-ground biomass across alpine grasslands, Tibetan Plateau. *Ecol. Indic* 60, 1070–1076. doi: 10.1016/j.ecolind.2015.08.038

Sun, J., Wang, X. D., Cheng, G. W., Wu, J. B., Hong, J. T., and Niu, S. L. (2014). Effects of grazing regimes on plant traits and soil nutrients in an Alpine Steppe, Northern Tibetan Plateau. *PLoS ONE* 9:e108821. doi: 10.1371/journal.pone.0108821

Sun, J., Zhang, Z. C., and Dong, S. K. (2019). Adaptive management of alpine grassland ecosystems over Tibetan Plateau. *Pratacult. Sci.* 36, 933–938.

Swift, M. J., Izac, A., and van Noordwijk, M. (2004). Biodiversity and ecosystem services in agricultural landscapes—are we asking the right questions? *Agrie Ecosyst. Environ.* 104, 113–134. doi: 10.1016/j.agee.2004.01.013

Urban, M. C. (2015). Accelerating extinction risk from climate change. *Science* 348, 571–573. doi: 10.1126/science.aaa4984

Wang, C. T., Long, R. J., Wang, Q. J., Jing, Z. C., and Shi, J. J. (2009). Changes in plant diversity, biomass and soil C, in alpine meadows at different degradation stages in the headwater region of three rivers, China. *Land Degrad. Dev.* 20, 187–198. doi: 10.1002/ldr.879

Wang, C. T., Long, R. J., Wang, Q. L., Liu, W., Jing, Z. C., and Zhang, L. (2010). Fertilization and litter effects on the functional group biomass, species diversity of plants, microbial biomass, and enzyme activity of two alpine meadow communities. *Plant Soil* 331, 377–389. doi: 10.1007/s11104-009-0259-8

Wang, H. M., Sun, J., Li, W. P., Wu, J. B., Chen, Y. J., and Liu, W. H. (2016). Effects of soil nutrients and climate factors on belowground biomass in an alpine meadow in the source region of the Yangtze-Yellow rivers, Tibetan Plateau of China. *J. Arid Land* 8, 881–889. doi: 10.1007/s40333-016-0055-2

Wang, P., James, P., Lassoie, S., Morreale, J., and Dong, S. K. (2015). A critical review of socioeconomic and natural factors in ecological degradation on the Qinghai-Tibetan Plateau, China. *Rangeland J.* 37, 1–9. doi: 10.1071/RJ14094

Wang, Q., Yu, C., Pang, X. P., Jin, S. H., Zhang, J., and Guo, Z. G. (2018). The disturbance and disturbance intensity of small and semi-fossorial herbivores alter the belowground bud density of graminoids in alpine meadows. *Ecol. Eng.* 113, 35–42. doi: 10.1016/j.ecoleng.2018.01.003

Wang, X. X., Dong, S. K., Yang, B., and Li, Y. Y. (2014). The effects of grassland degradation on plant diversity, primary productivity, and soil fertility in the alpine region of Asia's headwaters. *Envir. Mon. Ass.* 186, 6903–6917. doi: 10.1007/s10661-014-3898-z

Wang, Y. F., Yu, S. X., and Wang, J. (2007). Biomass-dependent susceptibility to drought in experimental grassland communities. *Ecol. Lett.* 10, 401–410. doi: 10.1111/j.1461-0248.2007.01031.x

Wu, G. L., Du, G. Z., Liu, Z. H., and Thirgood, S. (2009). Effect of fencing and grazing on a Kobresia-dominated meadow in the Qinghai-Tibetan Plateau. *Plant Soil* 319, 115–126. doi: 10.1007/s11104-008-9854-3

Wu, G. L., Liu, Z. H., Zhang, L., Hu, T. M., and Chen, J. M. (2010). Effects of artificial grassland establishment on soil nutrients and carbon properties in a black-soil-type degraded grassland. *Plant Soil* 333, 469–479. doi: 10.1007/s11104-010-0363-9

Yang, Z. L., Guo, H., Zhang, J. Y., and Du, G. Z. (2013). Stochastic and deterministic processes together determine alpine meadow plant community composition on the Tibetan Plateau. *Oecologia* 171, 495–504. doi: 10.1007/s00442-012-2433-6

Yi, X. X., Li, G. S., and Yin, Y. Y. (2012). The impacts of grassland vegetation degradation on soil hydrological and ecological effects in the source region of the yellow river–a case study in junmuchang region of Maqin country. *Proced. Environ. Sci.* 13, 967–981. doi: 10.1016/j.proenv.2012.01.090

Zeng, C., Zhang, F., Wang, Q., Chen, Y., and Joswiak, D. R. (2013). Impact of alpine meadow degradation on soil hydraulic properties over the Qinghai-Tibetan Plateau. *J. Hydrol.* 478, 148–156. doi: 10.1016/j.jhydrol.2012.11.058

Zhang, Z. C., Hou, G., Liu, M., Wei, T. X., and Sun, J. (2019). Degradation induces changes in the soil C:N:P stoichiometry of alpine steppe on the Tibetan Plateau. *J. Mt. Sci-Engl.* 16, 2348–2360. doi: 10.1007/s11629-018-5346-y

Zhao, C. Z., Zhu, L. Y., Liang, J., Yin, H. J., Yin, C. Y., Li, D. D., et al. (2014). Effects of experimental warming and nitrogen fertilization on soil microbial communities and processes of two subalpine coniferous species in Eastern Tibetan Plateau, China. *Plant Soil* 382, 189–201. doi: 10.1007/s11104-014-2153-2

Zhou, H., Zhang, D. G., Jiang, Z. H., Sun, P., and Xiao, H. L. (2018). Changes in the soil microbial communities of alpine steppe at Qinghai-Tibetan Plateau under different degradation levels. *Sci. Total Environ.* 651, 2281–2291. doi: 10.1016/j.scitotenv.2018.09.336

Zhou, W., Gang, C. C., Zhou, L., Chen, Y. Z., Li, J. L., Ju, W. M., et al. (2014). Dynamic of grassland vegetation degradation and its quantitative assessment in the northwest China. *Acta Oecol.* 55, 86–96. doi: 10.1016/j.actao.2013.12.006

Zhu, M. Y., Tan, S. D., Dang, H. S., and Zhang, Q. F. (2011). Rare earth elements tracing the soil erosion processes on slope surface under natural rainfall. *J. Environ. Radioactiv.* 102, 1078–1084. doi: 10.1016/j.jenvrad.2011.07.007

Conflict of Interest: The authors declare that the research was conducted in the absence of any commercial or financial relationships that could be construed as a potential conflict of interest.

frontiers in Earth Science

BRIEF RESEARCH REPORT
published: 11 November 2020
doi: 10.3389/feart.2020.531104

Reconstructed Aeolian Surface Erosion in Southern Mongolia by Multi-Temporal InSAR Phase Coherence Analyses

Jungrack Kim[1], *Munkhzul Dorjsuren*[2], *Yunsoo Choi*[3]* *and Gomboluudev Purevjav*[2]

[1]RSS Hydro Research and Education Department, RSS-Hydro, Dudelange, Luxembourg, [2]Information and Research Institute of Meteorology, Hydrology and Environment, Ulaanbaatar, Mongolia, [3]Department of Geoinformatics, University of Seoul, Seoul, Korea

The Gobi Desert in southern Mongolia has been identified as the strongest dust storm hot spot threatening public health and socio-economic activities in East Asian countries. Despite its significance, the complete mapping of the aeolian surface erosion in southern Mongolia remains unresolved because of extensive region of interest cannot be interpreted easily by conventional approaches. Therefore, in this study, we built a mapping scheme to define on going aeolian erosion and applied it over the southern Gobi Desert. The remote sensing approach applied here was based on an interferometric synthetic-aperture radar (InSAR) time series technique. A number of Sentinel-1 InSAR pairs that generate phase coherences for a certain period were synthesized via the means of principle component analysis to extract the topographic persistence indicative of surface erosion rates. Validation analyses performed through inter-comparisons of phase coherence signals over landmark areas and residuals between global digital elevation models confirmed the reliability of outputs. The results revealed geological lineaments in southern Mongolia confining sandy deposits and the sediment transportation pathways. Apparently, such bounded eolian deposits and transportation mechanisms within geological structures have significantly contributed to dust generation in the Gobi Desert over southern Mongolia. In addition, this study demonstrated that the newly developed InSAR time series technique has great potential for identifying intensified land erosion and dust sources.

Keywords: land degradation, aeolian erosion, interferometric synthetic-aperture radar, phase coherence, time series analysis

OPEN ACCESS

Edited by:
Atsushi Tsunekawa, Tottori University, Japan

Reviewed by:
Wu Zhu, Chang'an University, China
Mi Jiang, Hohai University, China

***Correspondence:**
YunSoo Choi
choiys@uos.ac.kr

Specialty section:
This article was submitted to Environmental Informatics and Remote Sensing, a section of the journal Frontiers in Earth Science

Received: *31 January 2020*
Accepted: *17 September 2020*
Published: *11 November 2020*

Citation:
Kim J, Dorjsuren M, Choi Y and Purevjav G (2020) Reconstructed Aeolian Surface Erosion in Southern Mongolia by Multi-Temporal InSAR Phase Coherence Analyses. Front. Earth Sci. 8:531104. doi: 10.3389/feart.2020.531104

INTRODUCTION

At present, eolian surface erosion and subsequent dust generation are emerging as serious environmental threats to local communities and the socio-economical aspects of surrounding regions. Therefore, comprehensive mapping of eolian surface erosion is a high priority task in dealing with the threat of such global environmental changes effectively through the use of appropriate countermeasures.

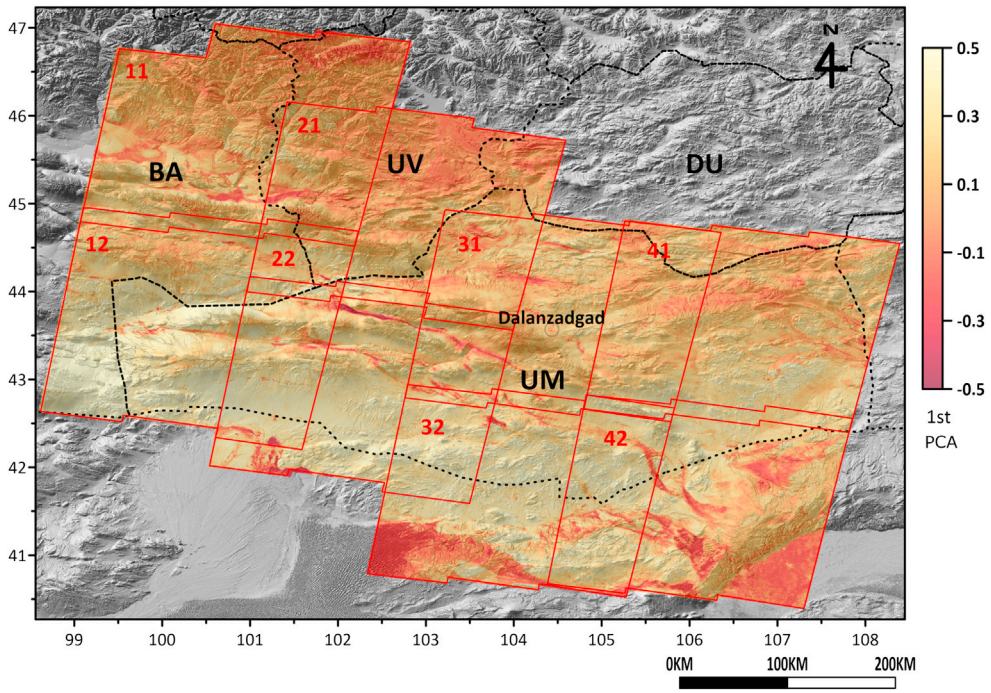

FIGURE 1 | The context of the target area and the InSAR overages analyzed for the mapping of eolian surface erosion together with first PCA PC. Refer to **Supplementary Table S1** for the detailed information of each InSAR coverage.

In regard to all previous research aimed at defining eolian land erosion, it is worth noting that a large number of approaches were based on spatial analysis techniques involving constraints on eolian erosion. For instance, interpretations of vegetation indices, land cover data, and topographic data have often been employed as tools to trace the susceptibility of land to eolian surface erosion and consequent dust generation. However, there have been no exemplary scientific contributions that directly measured the surface erosion rate by means of remote sensing techniques except for a very small number of special cases that were carried out over a limited local scale. In terms of reliability and applications, obviously there are huge differences between approaches that directly measure surface erosion rates and approaches that indirectly synthesize the involved constraints on surface erosion to forecast the erosion rates.

Even though spatial interpretations on the involved constraints have been regarded as an almost unique tool for identifying potential land erosion over an extensive target area, it is highly demanding to explore alternative ways for the direct and quantitative investigation of eolian surface erosion. Thus, given such a background, we developed a strategy to measure eolian surface erosion directly over sufficiently extensive target areas by means of an interferometric synthetic-aperture radar (InSAR) phase coherence time series method with the integration of complementary satellite remote sensing data.

Mongolia, which has undergone long-term desertification in conjunction with eolian land degradation and dust generation, is an ideal area for investigating the methods that can identify dust sources and eolian surface erosion. Therefore, a large number of scientific studies have been carried out in Mongolia, especially within the designated Gobi Desert regions in southern Mongolia, which are a major contributor to eolian erosion and dust generation. However, no previous studies have directly measured the eolian surface changes over the terrain of the target area, probably because of its enormous spatial extent and barren environments that may make it difficult to conduct field work. In that context, the target area to be investigated by the proposed scheme was established on the Gobi Desert in southern Mongolia. Earlier research mainly based on erosol optical depth (AOD) analyses with moderate resolution imaging spectroradiometer (MODIS) data identified this area as an intensified dust generation source (Ginoux et al., 2012; Zhang et al., 2015), where apparent dust hot spots implying significant eolian surface erosion are populated. Besides such research with mid-resolution satellite images to trace the trails of sand dust, the interpretations of the surface conditions regarding ecological/vegetation factors and land cover changes have shown the target area to be a prime contributor to dust storm generation in NE Asia (Eckert et al., 2015; Wu et al., 2016), and therefore, have subsequent surface erosion. The contexts of the target areas are presented in **Figure 1**. The focus here was placed on Bayankhongor (BA), Uvurkhangai (UV), Dundgovi (DU), and Umnugovi (UM) in southeastern Mongolia; wide barren terrains, sporadic sand dunes, grazing enclosures, and very rare villages are distributed throughout this area and add important context to the surface erosion process. Other notable attributes of the target area are as follows: 1) the geomorphic context consists of elongated fault zones and basins (Bayasgalan et al., 1999; Bayasgalan et al.,

2020), which may play a role in dust sediment transportation; 2) the potential fluvial networks either in the forms of seasonal fluvial channels or paleo river beds (Owen et al., 1997). Other interesting geographic features in the target area are the presence of surface coal mines of considerable sizes and artificially planted forests for the purpose of combating desertification. We propose that the above cases have significant potential for the validation of research outcomes.

METHODS

InSAR was devised for the measurement of topography and its deformation (Gabriel et al., 1989). This technology exploits the phase angle difference of electromagnetic waves and has been actively used in various applications. However, InSAR results are frequently marred by various error components including those induced by atmospheric artifacts (Li et al., 2005), the errors of base topography (Kim et al., 2018), and charged space particles that result in delays in InSAR signals (Gomba et al., 2015). Thus, the error of measured deformations needs to be compensated by a time series analyses of InSAR phase angles as shown in Berardino et al. (2002). As the task of splitting the genuine deformations and error components is difficult even with recently improved InSAR time series techniques, the mapping of surface deformations by eolian erosion over extensive arid land has never been the topic of InSAR phase angle analyses. Especially on a surface with constantly and heavily ongoing eolian erosion such as sand dune fields, there is no way to provide an "on-time" base DEM that properly depicts concurrent terrain and reduces the error of the InSAR phase angle approach. However, it is worth noting that there is another approach toward measuring surface erosion that uses another InSAR product, the so-called phase coherence, rather than the phase angle as shown in Liu et al. (2001). With the installment of contemporary InSAR assets such as Terra SAR X, Advanced Land Observing Satellite (ALOS) Phased Array type L-band Synthetic Aperture Radar (PALSAR) 1/2, and Sentinel-1, which have better resolution, revisiting times, and resolving power on the baseline conditions, nowadays some research has begun to establish methods of monitoring sand dune dynamics and eolian migrations as shown in Gaber et al. (2018), Gómez et al. (2018), and Havivi et al. (2018). A detailed study of phase coherence behaviors in arid deserts which may involve eolian erosions was reported by Ullmann et al. (2019) who showed that surface characteristics such as slope and wetness are not crucial for the loss of phase coherence, the so-called decorrelation. Thus, the prime factor affecting decorrelation is the change of topography induced by eolian migrations. This somehow contradicts the early study by Lee and Liu (2001) that stated the decorrelation dependency on the slope but the slope effect must not be an issue in the case of small temporal/spatial baseline observations such as the Sentinel-1 InSAR pair employed in this study. These observations form the basis of the approach of this study. It is also worth noting that such decorrelation effects on the heavy erosion topography is a major hindrance to the application of InSAR phase angle for this study.

The major data set used to accomplish the mapping of eolian erosion in this study was composed of European Space Agency (ESA) Sentinel-1 SAR images. Sentinel-1, which currently consists of two satellite constellations, enables a week of revisiting time that provides excellent temporal and spatial baseline conditions for interferometric analyses. Due to the incomparable spatial observation capabilities organized by its imaging mechanism (Yagüe-Martínez et al., 2016), Sentinel-1 has the potential to become a prime tool for measuring eolian erosion. We employed a total of eight InSAR coverages as presented in **Figure 1** in the target area. Each coverage consisted of 25–80 InSAR image pairs. Although the revisiting time of Sentinel-1 InSAR pairs was very short, empty temporal durations in consecutive InSAR observations occurred frequently. Therefore, we had to choose the time period that had the best density of InSAR pairs. In this study, it was 2017.

The phase coherence of the interferometric SAR pairs representing the major remote sensing information used in this study was useful in the monitoring of the surface change between successful images. The phase coherence of two conjugated complex SAR pixels can be expressed as follows:

$$coh = \frac{\sum_{i=1}^{N} S_{Mi} S_{Si}^{*} e^{j\varnothing(i)}}{\sqrt{\sum_{i=1}^{N} |S_{Mi}|^2} \sqrt{\sum_{i=1}^{N} |S_{Si}|^2}} \quad (1)$$

where S_{Mi} and S^{*}_{Si} are the complex conjugated signals of the master and slave SAR images, N is the total number of signals within the estimated window, and $\varnothing(i)$ is the phase of the ith signal within the moving window for phase coherence extraction and $\varnothing(i)$ is the phase of the ith pixel of the moving window.

Given that phase coherence largely depends on the geometric variation in reflectors, the reflection of radar waves over robust terrain such as barren bedrock, artificial structures, and solidified geomorphic structures produces high phase coherence. However, unstable time varying reflectors such as forestry coverage and materials with changing moistures in consistently eroded surfaces cause weak phase coherence values. Thus, the employment of phase coherences as the signatures for tracing surface erosion require the inspection of such incoherence components. The total coherences can be decomposed as follows:

$$Coh = Coh_{thermal}\, Coh_{spatial}\, Coh_{temporal} \quad (2)$$

Spatial coherence is dependent on the geometry of InSAR observation, implying that the perpendicular baseline (Hoen and Zebker, 2000) and its effect on total decorrelation are usually negligible in the case of small temporal/spatial baseline conditions of employed Sentinel-1 time series (Lee and Liu, 2001). Thermal coherence depends on radar thermal noise and is not related to the observation target (Wang et al., 2009). The parameters of Senitnel-1 InSAR time series observation, including temporal and spatial baselines are stated in **Supplementary Table S1**. Additionally, temporal coherence is a significant parameter in the exploitation of surface migrations. Lee et al. (2012) described the pattern of temporal coherence loss, i.e., temporal decorrelation, as follows:

$$Decorrelation_{temporal} = \exp(-C_t \Delta T) \quad (3)$$

where C_t is the decay constant of temporal coherence that is dependent on the physical and geometric characteristics of the target surface, and ΔT is the time period of InSAR pair observations. Therefore, construction of a phase coherence loss model to simulate surface change is extremely difficult owing to the prerequisites of determination of decay constants in accordance with the target landcover types and imaging conditions. For instance, vegetation usually causes random decreases in the phase coherence in the presence of biomass and the interactions with wind and moisture (Yun et al., 2019). Further, migration on base topography also decreases the phase coherence, however the aforementioned interactions with vegetation produces additional effects on the measured coherence. Our target area in southern Mongolia is characterized by extensive barren territory as well as sparse vegetation and small water bodies. Although we can assume that the major contributions to the decrease in phase coherence are associated with eolian surface erosion, the effects of cover vegetation or other factors such as, surface moisture are not negligible. The mathematical modeling of phase coherence involved with surface characteristics, particularly in vegetation, are described in Santoro et al. (2007, 2010). However, their studies only show the difficulties in vegetation effect modeling relative to temporal phase coherence, particularly due to the necessary complex information on the structures of vegetation canopy as well as the prevalent climatic factors such as, wind and moisture. Wegmuller et al. (2000) presented a phase coherence characteristic over arid topography using simple models and demonstrated the phase coherence associated with surface erosion, however the decomposition of vegetation effects is not feasible. Recent studies of detailed phase coherence modeling in Jiang et al. (2014), Jiang and Guarnieri (2020), and Monti-Guarnieri et al. (2020) demonstrated the mathematical modeling/simulation approaches of phase coherences. However, the results of those studies are not directly applicable to this study because of the modeling complexities of such an extensive target area with a variety of surface conditions exists.

A promising approach to address such problems involves the employment of a time series analysis of phase coherences over a certain time period rather than the mathematical modeling of all coherence components. We addressed these issues using following approach. First, the advantageous time series analysis, specifically that with the principle component analysis (PCA) of phase coherences, was exploited as the outputs of PCA analyses were expected to remove temporal outliers such as the responses of forest cover to the temporal wind and moisture variations and the remnants of thermal/spatial coherence components. In Yun et al. (2019), PCA analysis was successfully applied to suppress random and climatic factor-induced fluctuations and maintain only contributions by the topographic characteristics on phase coherence. Thus, a similar approach to only preserve the surface change component of phase coherence induced by the eolian erosion was employed in this study. Hence, the demand for complicated coherence modeling to decompose the surface change and other contributions could be avoided. The first component of the PCA analysis of phase coherence—called the first PCA hereafter—is proposed to represent the transformed signatures corresponding to eolian surface erosion because it is more consistent than the other components canceled into high-order PCA components (see **Supplementary Table S1**). The effects of such approaches were assessed in *Discussions*. Furthermore, external information was employed to rule out the low phase coherence area, which was not clearly involved with eolian surface erosion, for instance, the topographic slope for excluding high sloped surface creep, the snow cover over high altitude terrain, and the enhanced vegetation index (EVI) for screening out high vegetation areas that clearly do not allow for eolian erosion but result in phase decorrelations. The EVI data set was constructed from MODIS annual mean observations. We used the ALOS Panchromatic Remote-sensing Instrument for Stereo Mapping (PRISM) and Shuttle Radar Topography Mission (SRTM) 30 m DEM. Since we used two DEMs for validation purposes, their accuracies are of prime concern. Among the many accuracy tests of those DEMs, Santillan and Makinano-Santillan (2016) and Zhang et al. (2019)'s works must be noted as they demonstrated the vertical accuracies of two DEMs to be within the submeter range on a flat surface and that other errors mainly originated from the above-surface structures. Therefore, the application of DEMs using the height residual in this study can be justified. The detailed processing flow and the characteristics of the employed data sets are presented in **Supplementary Figure S1**.

RESULTS

The first PCA map is presented in **Figure 1**, and the refined version including only the eolian erosion component is presented in **Figure 2A**. In fact, the processing load to create more than 300 full Sentinel-1 pairs was not tolerable. Thus, we used the processed COMET LICS InSAR phase coherence products (Wright et al., 2016) to compose the time series data. The first PCA maps were mosaicked and controlled to remove the offsets between coverages using the overlapped portions. Following the construction of the first PCA maps over the entire target area, normalization to the 0.0–1.0 range was performed. Thus, the strong first PCA values were mapped to unchanged topography such as robust bedrock or artificial structures. In contrast, the surfaces where the scatterers were consistently changing such as in the vicinity of water bodies and snow had the minimum first PCA values. Meanwhile, the dense vegetation, surface creep in high slope areas, and more importantly, heavy eolian surface erosion in the dune field was close to the minimum value range according to the strength of changes. From the established map, the first things we observed were the thin sand dune elements along with geological lineaments, the highly vegetated areas in UM and UV, and some mountain flank regions where surface creeps and snow covers are populated as shown in **Figure 1**. To mask off the high vegetation canopy, surface creep in sloped terrain and snow cover, the threshold values of EVI (0.1), and slope masks (40°) were determined to decompose the interrelationships between the phase coherence first PCA and EVI/slope. The final products, which represent the eolian surface erosion approximately with 100 m spatial resolution, are shown in **Figure 2A**.

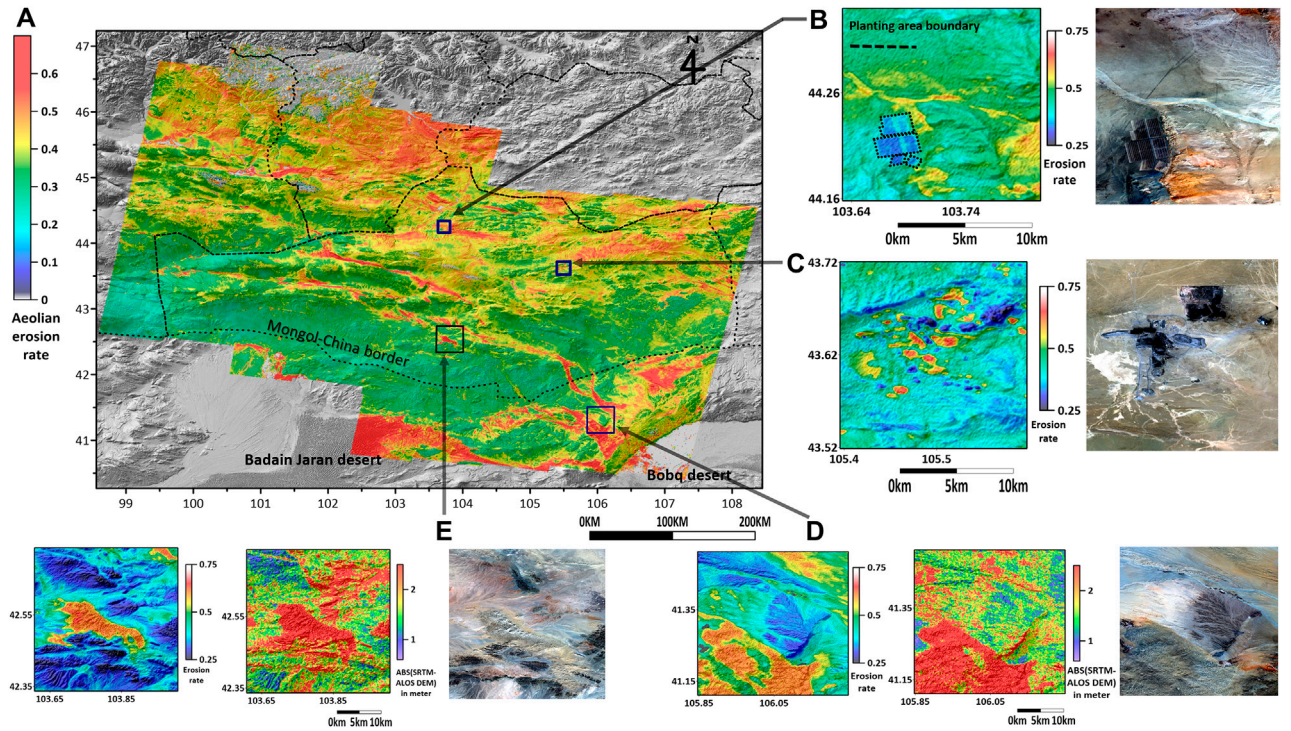

FIGURE 2 | (A) The surface erosion map from the first PCA PC and further data interpretation. The landmark areas over planted area **(B)** and the Tavan Tolgoi coal mine **(C)** proved the reliability of the constructed map. The validations using the DEM residuals are shown in **(D,E)**. The correlation values of those cases are 0.501 and 0.404, respectively.

Various data sources were employed to assess the accuracy and reliability of the constructed eolian erosion map. First of all, the height differences between two global DEMs, namely, the Shuttle Radar Topography Mission (SRTM) DEM and ALOS PRISM DEM, were employed. The height differences between the SRTM DEM, which was constructed based on topography in the 2000s via the C/X band InSAR mission, and the ALOS PRISM DEM, which was extracted from stereo analyses on optical imaging mission data during 2006–2011, naturally imply the surface erosion rate in theory. However, the mismatch of base plane control in the DEMs and the artifacts of data compilations do not allow for the tracing of the entire surface change by means of DEM residuals. Only partial terrain change was occasionally observed, but the morphologies of the height residuals in comparison to the first PCA gave the confidences on the detected eolian erosion as shown in **Figures 2D,E**. Regarding the relatively low correlation value between the first PCA component and height residual (0.501 in area D and 0.404 in area E), it should be noted that the DEM height residual represents the overall topographic change in the period between 1998 and 2006–2011 but the phase coherence only measured the erosion rate during 2017. This implies that erosion occurs consistently but periodical change owing to climatic factors exist. On the other hand, the landmarks areas where we knew clear topographic changes existed or preservation areas were employed. The Tavan Tolgoi coal mine, which is the world's biggest surface coal mine, began to exhibit considerable surface changes from coal production beginning in mid-2010, and these areas were clearly distinguished in the first PCA as shown in **Figure 2C**. The planted areas (44.23 N, 103.69 E) intended as a countermeasure for the undergoing desertification have been subjected to rigorous soil erosion control measures by means of spring cooler irrigation and manned maintenance. The first PCA components over these planted areas were clearly distinguished as high values and prove these features' robustness against surface erosion as demonstrated in **Figure 2B**. Thus, all validations over landmarks demonstrated that the constructed first PCA map had high reliability in terms of being representative of the surface changes induced mainly by eolian erosion.

DISCUSSIONS

On the basis of the eolian erosion map constructed from the InSAR phase coherence time series analysis, which demonstrated unprecedented details, an important observation was that the eolian surface erosion in southern Mongolia coincides with the transportation trails of sedimentary materials through geological structures running NW to SE. The southern Mongolian Gobi consists of stone/pebble covered plains rather than sandy deserts, which is not a conducive environment to intensive dust generation and eolian erosion. The extent of the sand and erodible topsoil areas are limited to only around the sand

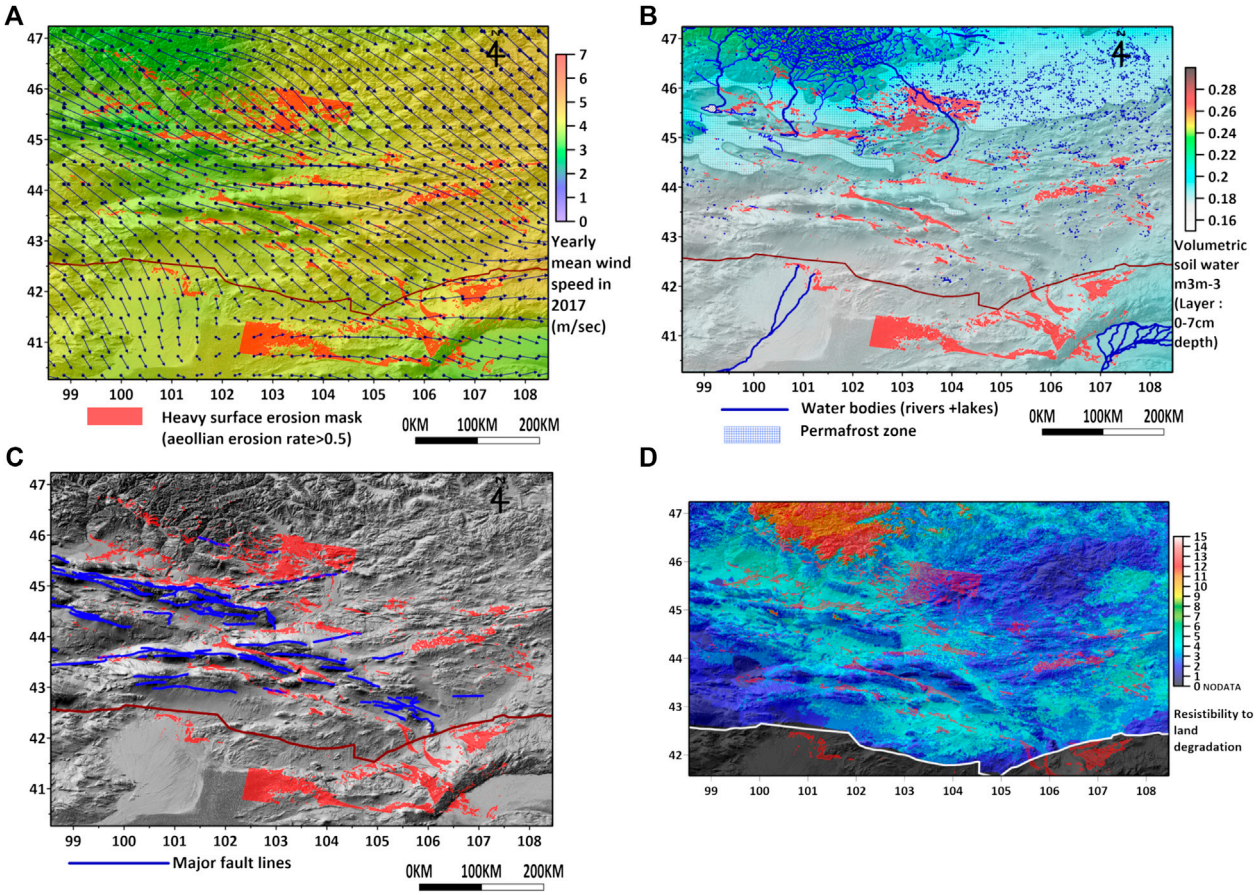

FIGURE 3 | (A) The extent of heavy surface erosion (eolian erosion rate > 0.5) along with the yearly mean ECMWF wind information in 2017, also with **(B)** the hydrological contexts, **(C)** the geological structures (Bayasgalan et al., 2020), and **(E)** the land degradation rate by the empirical analysis with vegetation indexes. The details of comparison data sets were given in the **Supplementary Material**.

dunes concentrated on geological lineaments, the floors of dried seasonal fluvial channels, and the sedimentary deposits within shallow basins and playa, which are connected to the erosion lineaments. After overlying the extracted outlines of intensified surface erosion on the involved contexts such as hill shaded topography, tectonic faults, and European Center for Medium-Range Weather Forecasts (ECMWF) wind direction/velocities as shown in **Figure 3**, we clearly observed that the flows of eolian sediment transportation from the sedimentary deposits run through the corridors in geological structures and are connected to northern Chinese deserts such as the Hobq and Badain Jaran deserts. The presence of active dune fields in the Hobq and Badain Jaran deserts as described in Wang et al. (2009) suggest the important roles of such eolian transportation routes. Thus, we concluded that the coincided wind directions and geological lineaments shown in **Figures 3A,C** are the dominating control factors of the population of eolian surface erosions compared with the effects by hydrological context or vegetation (**Figures 3B,D**). The strengths of surface erosion in the transportation corridors should be incomparable to the background terrains where steep slopes and weakly vegetated stone/pebble areas are present. Thus, the conventional observations employing AOD, in which the majority of southern Mongolia has been assigned as a mineral dust source, need to be reconsidered. The unequally distributed dust generation frequency, which is more obvious in parts of UM and DU (Ginoux et al., 2012), supports our analyses. At the moment, it is proposed that the biggest scientific achievement in this study is the discovery of the potential coupling between the southern Mongolian Gobi and northern Chinese sandy deserts and the roles of geological structures in the transportation mechanism of eolian sediments.

In addition to validation using landmark areas and the inter-comparison with potential driving parameters, we introduced further quantitative analyses as shown in **Figure 4**. First, 150 more major dune fields and dried channels together with playas in southern Mongolia were manually digitized (refer to **Supplementary Figure S3**). On the different landcover types consisting of dune fields, dried channels, rocky surfaces which have minor vegetation cover, water surfaces and vegetated areas (EVI > 0.1) the phase coherences and their PCA components acted as illustrated in **Figure 4A**. The strength of eolian surface migrations can be assumed in the order of the dune, dried channels, and rocky surfaces. The phase coherences in

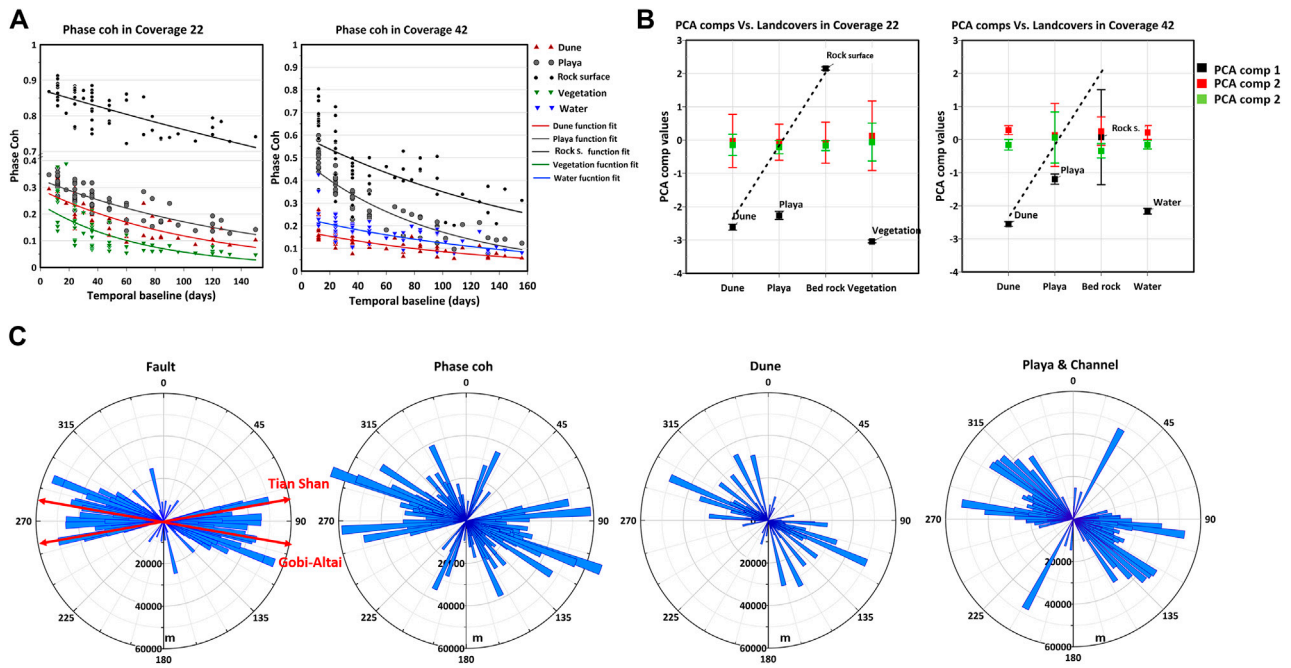

FIGURE 4 | (A) The responses of phase coherences according to temporal baselines and the first PCA components on the different land cover types. Note, the signals are well aligned in a single linear relation (dotted line) on the first PCA and their dispersions (error bars in **(B)**) of the first PCA are very small compared to the second and third PCA components. See **Supplementary Figure S2** to identify the populations employed in landcover parts. **(B)** Polar coordinate representations of low phase coherences, faults, dune, and dried channels. The polar representation of low phase coherence lines was observed to correspond to the sum of dune and dried channel directions.

Figure 4A decrease with the temporal base line represented by **Eq. 3** depending on their landcover types. However, the discrimination between landcover types by phase coherence is made difficult by the mixed signals, as is the assignment of erosion strength. Immediately after taking the first PCA component, the erosion rate according to landcover type can be measured in a single liner relationship. This proved that the feasibility of erosion rate measurement employing the PCA of the phase coherence stack. Second, the spatial correlations between fault structures, low first PCA lineaments, and dune and dried channels have to be verified. All fault lines, dune fields, and dried channels were transferred to linear approximations along major axes. Their polar coordinate representations from central points of every linear approximations are shown in **Figure 4B**. These presentations clearly prove 1) directional populations of low coherence lineaments along with Gobi-Altai (NWW-SEE) and Tian-Shan (NEE-SWW) fault structures which are two major fault directions of southern Mongolia (Lamb et al., 1999); 2) the dune lines are distributed along with the Gobi-Altai structure but the dried channels has dependence on the Tian-Shan structure. However, some spatial disparity between the dune lines and the Gobi-Altai faults were observed because the dune field cannot be located on the fault line but on the basins and graben between faults; 3) the polar coordinate representations of low phase coherence lines are approximated as combinations of dunes and dried channels. In addition, the fact that the morphology of southern Mongolian dune fields which are identified in satellite images are usually oriented along with the direction of Gobi Altai faults, supports our orientation analyses. Therefore, the dependence of the transportation corridor of eolian sediment along with geological strictures has been proven along with the effectiveness of a phase coherence PCA approach. Other validation checks are shown in the **Supplementary Material**.

CONCLUSION

Together with the discovery of regional erosion patterns over southern Mongolia, we have proven the reliability of InSAR phase coherence approaches in the reconstruction of eolian surface erosion. By combining the time series analyses and interpretations with external auxiliary data sources, we successfully defined eolian surface erosion at an unprecedented resolution. As a major scientific outcome, the presence of connecting corridors throughout geological structures as transportation routes of eolian sedimentary materials was identified between the Southern Mongolian basin and the northern Chinese Hobq/Badain Jaran deserts. The overall methodology in this study has the potential to be used as a comprehensive scheme for extensive dust source mapping, which has been an important goal for combating desertification as well as scientific research over arid dry lands. It is still unclear how the strength of the extracted eolian erosion data in this study can be converted into quantized surface erosion metrics. Since the potential applications of this approach are not limited to relatively vegetation-free topography like southern Mongolia, the influence

of vegetation canopy and the climate parameters such as soil moisture and wind which interfere with the precise measurement of eolian erosion must be addressed. We will tackle these issues in future studies employing a combination of InSAR phase angle analyses techniques and/or *in-situ* measurements such as laser scanning or drone stereo imaging perhaps together with prior suppression of vegetation effects using phase coherence modeling.

DATA AVAILABILITY STATEMENT

All datasets generated for this study are included in the manuscript/**Supplementary Material**.

AUTHOR CONTRIBUTIONS

JK conducted the data processing and writing. MD was in charge of collections and the processing of validation and involved in writing. GP and YC contributed to the management of the project and writing.

FUNDING

This work was supported by the Basic Study and Interdisciplinary R&D Foundation Fund of the University of Seoul (2019) and the 2019 Green Tech. Research Fund of the Seoul City government.

ACKNOWLEDGMENTS

InSAR PC data sets were provided by LiCSAR which contains modified Copernicus Sentinel data analyzed by the Center for the Observation and Modeling of Earthquakes, Volcanoes, and Tectonics (COMET). The field work was supported by the Asian Green wall project foundation. The geological fault data were kindly provided by A. Bayasgalan

SUPPLEMENTARY MATERIAL

The Supplementary Material for this article can be found online at: https://www.frontiersin.org/articles/10.3389/feart.2020.531104/full#supplementary-material

REFERENCES

Bayasgalan, A., Jackson, J., Ritz, J.-F., and Carretier, S. (1999). Field examples of strike-slip fault terminations in Mongolia and their tectonic significance. *Tectonics* 18, 394–411. doi:10.1029/1999TC900007.

Bayasgalan, A., Odonbaatar, Ch., and Baasanbat, Ts. (2020). *Termination of gobi-tian Shan fault, southern Mongolia*. Hokudan 2020 Symposium abstract.

Berardino, P., Fornaro, G., Lanari, R., and Sansosti, E. (2002). A new algorithm for surface deformation monitoring based on small baseline differential SAR interferograms. *IEEE Trans. Geosci. Rem. Sens.* 40, 2375–2383. doi:10.1109/TGRS.2002.803792.

Eckert, S., Hüsler, F., Liniger, H., and Hodel, E. (2015). Trend analysis of MODIS NDVI time series for detecting land degradation and regeneration in Mongolia. *J. Arid Environ.* 113, 16–28. doi:10.1016/j.jaridenv.2014.09.001.

Gómez, D., Salvador, P., Sanz, J., Casanova, C., and Casanova, J. (2018). Detecting areas vulnerable to sand encroachment using remote sensing and GIS techniques in nouakchott, Mauritania. *Rem. Sens.* 10, 1541. doi:10.3390/rs10101541.

Gaber, A., Abdelkareem, M., Abdelsadek, I., Koch, M., and El-Baz, F. (2018). Using InSAR coherence for investigating the interplay of fluvial and aeolian features in arid lands: implications for groundwater potential in Egypt. *Rem. Sens.* 10(6), 832. doi:10.3390/rs10060832.

Gabriel, A. K., Goldstein, R. M., and Zebker, H. A. (1989). Mapping small elevation changes over large areas: differential radar interferometry. *J. Geophys. Res.* 94, 9183–9191. doi:10.1029/JB094iB07p09183.

Ginoux, P., Prospero, J. M., Gill, T. E., Hsu, N. C., and Zhao, M. (2012). Global-scale attribution of anthropogenic and natural dust sources and their emission rates based on MODIS Deep Blue aerosol products. *Rev. Geophys.* 50, RG000388. doi:10.1029/2012RG000388.

Gomba, G., Parizzi, A., De Zan, F., Eineder, M., and Bamler, R. (2015). Toward operational compensation of ionospheric effects in SAR interferograms: the split-spectrum method. *IEEE Trans. Geosci. Rem. Sens.* 54, 1446–1461.

Havivi, S., Amir, D., Schvartzman, I., August, Y., Maman, S., Rotman, S. R., et al. (2018). Mapping dune dynamics by InSAR coherence. *Earth Surf. Process. Landforms* 43, 1229–1240. doi:10.1002/esp.4309.

Hoen, E. W., and Zebker, H. A. (2000). Penetration depths inferred from interferometric volume decorrelation observed over the Greenland ice sheet. *IEEE Trans. Geosci. Rem. Sens.* 38(6), 2571–2583. doi:10.1109/36.885204

Jiang, M., Ding, X., Li, Z., Tian, X., Wang, C., and Zhu, W. (2014). InSAR coherence estimation for small data sets and its impact on temporal decorrelation extraction. *IEEE Trans. Geosci. Rem. Sens.* 52(10), 6584–6596. doi:10.1109/TGRS.2014.229840810.1109/tgrs.2013.2261996.

Jiang, M., and Guarnieri, A. M. (2020). Distributed scatterer interferometry with the refinement of spatiotemporal coherence. *IEEE Trans. Geosci. Rem. Sens.* 58 (6), 3977–3987. doi:10.1109/TGRS.2019.2960007.

Kim, J. R., Yun, H., Van Gasselt, S., and Choi, Y. (2018). Error-regulated multi-pass DInSAR analysis for landslide risk assessment. *Photogramm Eng Remote Sensing* 84, 189–202. doi:10.14358/pers.84.4.189.

Lamb, M. A., Hanson, A. D., Graham, S. A., Badarch, G., and Webb, L. E. (1999). Left-lateral sense offset of upper Proterozoic to Paleozoic features across the Gobi Onon, Tost, and Zuunbayan faults in southern Mongolia and implications for other Central Asian faults. *Earth Planet Sci. Lett.* 173 (3), 183–194. doi:10.1016/s0012-821x(99)00227-7.

Lee, C.-W., Lu, Z., and Jung, H.-S. (2012). Simulation of time-series surface deformation to validate a multi-interferogram InSAR processing technique. *Int. J. Rem. Sens.* 33, 7075–7087. doi:10.1080/01431161.2012.700137.

Lee, H., and Liu, J. G. (2001). Analysis of topographic decorrelation in SAR interferometry using ratio coherence imagery. *IEEE Trans. Geosci. Rem. Sens.* 39(2), 223–232. doi:10.1109/36.905230

Li, Z., Muller, J. P., Cross, P., and Fielding, E. J. (2005). Interferometric synthetic aperture radar (InSAR) atmospheric correction: GPS, Moderate Resolution Imaging Spectroradiometer (MODIS), and InSAR integration. *J. Geophys. Res.* 110, B03410. doi:10.1029/2004JB003446.

Liu, J. G., Black, A., Lee, H., Hanaizumi, H., and Moore, J. M. (2001). Land surface change detection in a desert area in Algeria using multi-temporal ERS SAR coherence images. *Int. J. Rem. Sens.* 22, 2463–2477. doi:10.1080/01431160119991.

Monti-Guarnieri, A., Manzoni, M., Giudici, D., Recchia, A., and Tebaldini, S. (2020). Vegetated target decorrelation in SAR and interferometry: models, simulation, and performance evaluation. *Rem. Sens.* 12(16), 2545. doi:10.3390/rs12162545.

Owen, L. A., Windley, B. F., Cunningham, W. D., Badamgarav, J., and Dorjnamjaa, D. (1997). Quaternary alluvial fans in the Gobi of southern Mongolia: evidence for neotectonics and climate change. *J. Quat. Sci.* 12, 239–252. doi:10.1002/(sici)1099-1417(199705/06)12:3<239::aid-jqs293>3.0.co;2-p.

Santillan, J. R., and Makinano-Santillan, M. (2016). Vertical accuracy assessment of 30-M resolution alos, aster, and srtm global dems over northeastern mindanao, Philippines, *Int. Arch. Photogram. Rem. Sens. Spatial Inf. Sci.* XLI-B4, 149–156. doi:10.5194/isprs-archives-XLI-B4-149-2016.

Santoro, M., Askne, J. I. H., Wegmuller, U., and Werner, C. L. (2007). Observations, modeling, and applications of ERS-ENVISAT coherence over land surfaces. *IEEE Trans. Geosci. Rem. Sens.* 45(8), 2600–2611. doi:10.1109/TGRS.2007.897420.

Santoro, M., Wegmuller, U., and Askne, J. I. H. (2010). Signatures of ERS-envisat interferometric SAR coherence and phase of short vegetation: an analysis in the case of maize fields. *IEEE Trans. Geosci. Rem. Sens.* 48(4), 1702–1713. doi:10.1109/TGRS.2009.2034257.

Ullmann, T., Sauerbrey, J., Hoffmeister, D., May, S. M., Baumhauer, R., and Bubenzer, O. (2019). Assessing spatiotemporal variations of sentinel-1 InSAR coherence at different time scales over the atacama desert (Chile) between 2015 and 2018. *Rem. Sens.* 11(24), 2960. doi:10.3390/rs11242960.

Wang, T., Liao, M., and Perissin, D. (2010). InSAR coherence-decomposition analysis. *Geosci. Rem. Sens. Lett. IEEE* 7(1), 156–160. doi:10.1109/LGRS.2009.2029126.

Wang, X., Yang, Y., Dong, Z., and Zhang, C. (2009). Responses of dune activity and desertification in China to global warming in the twenty-first century. *Global Planet. Change* 67(3-4), 167–185. doi:10.1016/j.gloplacha.2009.02.004.

Wegmuller, U., Strozzi, T., Farr, T., and Werner, C. L. (2000). Arid land surface characterization with repeat-pass SAR interferometry. *IEEE Trans. Geosci. Rem. Sens.* 38(2), 776–781. doi:10.1109/36.842006.

Wright, T. J., Gonzalez, P. J., Walters, R. J., Hatton, E. L., Spaans, K., et al. (2016). LiCSAR: Tools for automated generation of Sentinel-1 frame interferograms., In Proceedings of the AGU Fall Meeting. San Francisco, CA, USA December 12–16, 2016.

Wu, J., Kurosaki, Y., Shinoda, M., and Kai, K. (2016). Regional characteristics of recent dust occurrence and its controlling factors in East Asia. *SOLA* 12, 187–191. doi:10.2151/sola.2016-038.

Yagüe-Martínez, N., Prats-Iraola, P., Rodriguez Gonzalez, F., Brcic, R., Shau, R., Geudtner, D., et al. (2016). Interferometric processing of Sentinel-1 TOPS data. *IEEE Trans. Geosci. Rem. Sens.* 54, 2220–2234. doi:10.1109/TGRS.2015.2497902.

Yun, H.-W., Kim, J.-R., Choi, Y.-S., and Lin, S.-Y. (2019). Analyses of time series InSAR signatures for land cover classification: case studies over dense forestry areas with L-band SAR images. *Sensors* 19(12), 2830. doi:10.3390/s19122830.

Zhang, B., Tsunekawa, A., and Tsubo, M. (2015). Identification of dust hot spots from multi-resolution remotely sensed data in eastern China and Mongolia. *Water Air Soil Pollut.* 226, 117. doi:10.1007/s11270-015-2300-2.

Zhang, K., Gann, D., Ross, M., Robertson, Q., Sarmiento, J., Santana, S., et al. (2019). Accuracy assessment of ASTER, SRTM, ALOS, and TDX DEMs for Hispaniola and implications for mapping vulnerability to coastal flooding. *Rem. Sens. Environ.* 225, 290–306. doi:10.1016/j.rse.2019.02.028.

Conflict of Interest: The authors declare that the research was conducted in the absence of any commercial or financial relationships that could be construed as a potential conflict of interest.

frontiers in Environmental Science

ORIGINAL RESEARCH
published: 12 November 2020
doi: 10.3389/fenvs.2020.589104

The Response of Plant and Soil Properties of Alpine Grassland to Long-Term Exclosure in the Northeastern Qinghai–Tibetan Plateau

*Cuihua Huang, Fei Peng, Quangang You, Jie Liao, Hanchen Duan, Tao Wang and Xian Xue**

Drylands Salinization Research Station, Key Laboratory of Desert and Desertification, Northwest Institute of Eco-Environment and Resources, Chinese Academy of Sciences, Lanzhou, China

OPEN ACCESS

Edited by:
Lu-Jun Li,
Northeast Institute of Geography and Agroecology (CAS), China

Reviewed by:
Yangong Du,
Northwest Institute of Plateau Biology (CAS), China
Xuyang Lu,
Institute of Mountain Hazards and Environment (CAS), China

***Correspondence:**
Xian Xue
xianxue@lzb.ac.cn

Specialty section:
This article was submitted to Soil Processes, a section of the journal Frontiers in Environmental Science

Received: *31 July 2020*
Accepted: *13 October 2020*
Published: *12 November 2020*

Citation:
Huang C, Peng F, You Q, Liao J, Duan H, Wang T and Xue X (2020) The Response of Plant and Soil Properties of Alpine Grassland to Long-Term Exclosure in the Northeastern Qinghai–Tibetan Plateau. Front. Environ. Sci. 8:589104. doi: 10.3389/fenvs.2020.589104

Currently, grazing exclosure is one of the most important grassland management measures for restoring all types of degraded alpine grassland in the Qinghai–Tibetan Plateau (QTP). The most widely distributed grassland ecosystems across the northeastern QTP are the alpine meadow (AM), alpine meadow steppe (AMS), and alpine steppe (AS). However, whether the impacts of fencing on vegetation characteristics and soil properties vary among different grassland types remains poorly understood despite that numerous individual studies have been conducted. This study investigated the vegetation characteristics and soil properties in fenced and grazed AM, AMS, and AS in the northeastern QTP. Grazing exclosure significantly increased the vegetation coverage and Shannon–Wiener diversity index in all the three grasslands. Plant species richness was significantly increased in AM, but there were no significant changes in AMS and AS. Aboveground biomass was significantly increased in AMS and AS but not significant in AM. Increase in the percentage of high-quality forage grasses was only observed in AMS. Fencing significantly decreased the soil bulk density (BD) and significantly increased soil organic carbon (SOC) and total nitrogen at a depth of 0–50 cm in AMS and AS but had no effect in AM. Our results indicate that the use of fencing for restoring degraded AM might not achieve the same expected results as in AS and AMS on the QTP.

Keywords: alpine grassland, degradation, fencing, Qinghai–Tibetan plateau, soil organic carbon, species richness

INTRODUCTION

Land degradation has been increasing at an annual rate of 5–10 million ha and affecting about 1.5 billion people globally (Gisladottir and Stocking, 2005; Ilan and Rattan, 2015). The alpine grassland on the Qinghai–Tibetan Plateau (QTP), occupying over 60% total area of the QTP, is proved to be sensitive to climate change and human activities (Wu et al., 2012; Xue et al., 2015; Bakhshi et al., 2019) and has important functions in protecting the headwaters of major rivers in Asia (Yan and Lu, 2015). However, it has severely degraded since the 1980s (Saito et al., 2009; Li et al., 2013; Zhao et al., 2015; Xue et al., 2017)

because of intensification of human activities and climate change (Harris, 2010; Xue et al., 2015; Zeng et al., 2015). The grassland degradation induced 73% reduction in the aboveground biomass, but the amount of poisonous plants almost doubled, which suggests more severe reduction in the palatable grasses. The dramatic reduction in edible biomass accompanied by the sharp increase in livestock number leads to the overgrazing, hence the severe vegetation cover reduction (Wu et al., 2012; Zhao et al., 2015; Lu et al., 2017; Yu et al., 2019; Wang et al., 2020), plant species diversity loss (Chillo et al., 2015), percentage of palatable forage species attenuation (Li et al., 2016), and productivity decrease (Wu et al., 2009). Vegetation degradation will interact with the soil and impose positive feedback to soil degradation (Miao et al., 2015; Tang et al., 2016).

Degraded grassland ecosystems have the capacity for self-recovery if the disturbance ceases for an extended length of time allowing for natural succession (Cheng et al., 2011; Deng et al., 2014). Exclosure is a worldwide management practice, which significantly influences vegetation characteristics (Wu et al., 2009; Deng et al., 2014) and soil properties (Wu et al., 2010a,b; Zhao et al., 2015; Hu et al., 2016), then probably allows for self-recovery of the degradation grassland ecosystem. Realizing the severe alpine grassland degradation and its destructive consequence, the central and local government advocated the use of metal fences in family ranch scale to protect grassland degradation since 2004 in QTP (Yan and Lu, 2015).

The most widely distributed grassland ecosystems across the northeastern QTP are the alpine meadow (AM), alpine meadow steppe (AMS), and alpine steppe (AS) in the northeastern QTP (Wu et al., 2012). AM is a good natural pasture with low layer, soft quality, rich nutrition, strong palatability, and resistance to grazing and trampling. The AM community is simple in structure, not obvious in hierarchy, with dense growth and low plants, sometimes forming a flat planting mat (Wang et al., 2020). An AMS-type rangeland is developed in alpine (or plateau) sub-frigid zones and cold sub-humid regions, with an annual precipitation of 300–400 mm. It is a grassland type mainly composed of hardy perennial arid medium or medium xerophytic herbaceous plants. AS plants are low clustered, with reduced leaf area and shallow roots (Li et al., 2019). The species composition of grassland determines ecosystem stability and resistance to disturbance (Wardle et al., 2000). Different vegetation types have their unique structure composition and stability. Under different environmental conditions, vegetation types with their own unique structural characteristics have different responses to environmental changes (Zhao et al., 2016). So, in different regions or different types of grassland, fencing might result in a wide range of effects on vegetation characteristics and soil properties (Wu et al., 2012; Jing et al., 2014; Cheng et al., 2016). Quantifying the changes in vegetation characteristics and soil properties of different grasslands can help us understand how to carry out land management regimes (Li et al., 2013). Previous studies show different responses of different alpine grasslands to climate warming (Ganjurjav et al., 2016), N addition (Li et al., 2019), and changes in soil properties (Peng et al., 2020a). For example, the plant community of AS shows a stronger association with soil properties than AM alongside degradation (Peng et al., 2020a). Warming did not significantly change the plant composition and species diversity in the AM, but it did cause rapid changes in species diversity (Ganjurjav et al., 2016). Whether the effects of fencing on vegetation and soil properties are consistent among different biomes remains still unclear. To address this scientific gap, we studied the effects of fencing on vegetation and soil properties selected in three typical vegetation types. Each study's grassland type was regarded as a single data point in paired comparisons of grazed vs. fenced sites and then for analysis on the difference in those responses among three alpine grasslands with the vegetation and soil indicators. The results will inform alpine grassland conservation and sustainable management in the future.

MATERIALS AND METHODS

Experimental Design

The climate is characterized by strong solar radiation with short, cool summers and long, cold winters in QTP. The growing season of alpine grasslands lasts from May to September (Gao et al., 2013). We carried out the surveys from July to September 2014 on the QTP. In order to avoid the impact of different fencing durations on the ecosystem, we selected three alpine grassland types (AM, AMS, AS), which was fenced off grazing at the same year. Location, climate, and vegetation information of the three sites can be seen in **Table 1**.

Sampling and Measurements

Vegetation Characteristics

In each site, three plots (30 cm × 30 cm) were selected for vegetation characteristic measurements and soil sampling inside and outside of the fence. A photo was taken for each plot vertically downward by a camera, and the photo was processed by the software CAN-EYE-V6313, developed at the French National Institute of Agricultural Research (INRA) to get the plant coverage (Peng et al., 2018). Plant species identification was done *in situ*. Unidentified specimens were collected and later identified by plant taxonomists. The total species in each plot were counted after the identification of species, and the frequency of each species and coverage were obtained by using a frame with 100 small quadrats (Peng et al., 2017). At the same time, the height of every species was measured *in situ* with a ruler. Species richness is the number of species in each plot (Stirling and Wilsey, 2001). The importance value (IV) of each species was derived by averaging the values of relative frequency, relative coverage, and relative height, which is the ratio of the average value of that species to the summed value of all the species in the plot. The richness index (R) and Shannon–Wiener diversity index (H) of the communities were calculated as follows:

$$R = S$$

$$Pi = \frac{\mathrm{IV}i}{\mathrm{IVtotal}}$$

$$\mathrm{H} = -\sum_{i=1}^{s} PilnPi$$

TABLE 1 | Location, climate, and vegetational information of the three sampling sites.

	AM	AS	AMS
Longitude	101°18′E	102°23′E	100°09′E
Latitude	37°41′N	35°03′N	38°12′N
Altitude/m	3415	2765	3158
Annual precipitation/mm	520	420	516
Average annual temperature/°C	0.8	1.0	2.6
Dominant species (Latin name)	*Kobresia myosuroides (Villars) Foiri*	*Stipa purpurea*	*Elymus nutans Griseb*

where S is the total species numbers of the grassland community, IV_i is the IV of a specific species *i*, and IVtotal is the sum of the IV_i values of all the species.

Plant Biomass Measurement

The aboveground parts of plants, including all litter, for each species, were cut, collected, and put into envelops and tagged for each plot. After the dry-up in the air, the plants were separated into high-quality forage grasses (sedge and grass) and forbs (forbs and shrub). After separation, the biomass was dried in an oven at 65°C for 48 h to a constant weight to obtain the aboveground biomass.

The soil cores were extracted at depths of 0–10, 10–20, 20–30, and 30–50 cm in the center of each plot. The samples were immediately placed in a cooler and then transported to the laboratory. In the laboratory, the soil samples were air-dried and crumbled to pass through a 2-mm diameter sieve to remove large particles from the finer soil. Subsequently, fine living roots were hand-picked based on their color and consistency in a distilled water bath (Peng et al., 2018). The picked fine roots were dried at 65°C for 48 h to a constant weight, and the belowground biomass was obtained. The remaining soil was used for soil organic carbon (SOC) and total N measurement in the lab.

Soil Properties

Soil organic carbon was measured by the potassium dichromate oxidation titration method (Walkley, 1947), and total N was measured by the Kjeldahl method (Bremner, 1996) in the Key Laboratory of Desert and Desertification, Chinese Academy of Sciences (CAS). Other soil samples also were taken at depths of 0–10, 10–20, 20–30, and 30–50 cm to measure soil moisture and bulk density (BD). Soil samples were collected and then put in aluminum boxes (volume, 100 cm^3), then the weight of boxes and wet soil was measured *in situ*. The collected samples were transported and then were dried at 105°C for 48 h in an oven to a constant weight. Then, the BD and soil moisture were calculated as follows:

$$BD = \frac{Weight_{Dry}}{V_{soil\ sampler}}$$

Soil gravimetrical water content was expressed as a percentage of soil water to dry soil weight, and soil moisture was the product of soil gravimetrical water content and BD.

Statistical Analysis

Three-way ANOVA was performed to test the fencing, grassland type, depth, and their interaction effects on vegetation and soil variables. Significant differences were evaluated at the 0.05 level. All statistical analyses were performed using the software program SPSS 19.0 (IBM Corp, 2010). Figures were made by Origin 8.0 (OriginLab Corp, 2007).

RESULTS

Coverage, Biomass, and Diversity

Long-term (8–9 years) fencing significantly increased plant coverage by 32.53, 17.10, and 46.63% in AM, AMS, and AS, respectively (**Table 2**). There was no significant increase in species richness (R) and Shannon–Wiener diversity index (H) after long-term fencing in all three grasslands (**Table 2**). The R and H of AM and AMS were significantly higher than that of AS in either enclosed or grazed sites (**Tables 2**, **3**). Fencing only led to a significant increase in aboveground biomass in AMS and AS (**Table 2** and **Figure 1**). The aboveground biomass of AM in fenced plot was not significantly higher than in grazing plot. Increase in percentage of palatable forage was only observed in AMS (**Table 2**).

Figure 1 shows the biomass distribution in the vertical direction between enclosed and grazed sites in AM, AMS, and AS after long-term fencing. Aboveground biomass was significantly increased after long-term fencing in the three grassland types (**Table 3** and **Figure 1**). Grassland type and soil depth and the interaction between them significantly affected BGB (**Table 3**). Statistical results showed that with the increase in altitude, from AS to AMS and AM, the percentage of BGB at 0–10 cm to the total belowground biomass (0–50 cm) was decreased in the enclosed site, which was 84.5, 81.3, and 73.5%, respectively. The trend of the grazed site was opposite that of the enclosed site at 0–10 cm; it was 57.8, 76.9, and 80.7%, in AS to AMS and AM, respectively.

Soil Bulk Density and Moisture

Bulk density (BD) was significantly affected by fencing, grassland type, soil depth, and their interactions (**Table 3**). With the increase in soil depth, BD was increased in AM both at enclosed and grazed sites (**Figure 2**), but there was no regular change after long-term fencing in AMS and AS (**Figure 2**). The BD in grazed sites was significantly higher than that in enclosed sites in AMS and AS at the soil depths of 0–30 cm, but there were no obvious differences at all the three layers in AM (**Figure 2**).

Grassland type, soil depth, and their interactions significantly affected soil moisture (**Table 3**). Soil moisture was higher in AM and AMS than in AS at all the soil depths (**Figure 3**). Fencing

TABLE 2 | Comparisons of total coverage (TC), species richness (R), Shannon–Wiener diversity index (H), aboveground biomass (AGB), belowground biomass (BGB), percentage of palatable grasses (PPG), between enclosed (In), and grazed (Out) sites with the three vegetation types: alpine meadow (AM), alpine meadow steppe (AMS), and alpine steppe (AS).

Treatments	TC/%	R	H	AGB/g m^{-2}	BGB/g m^{-2}	PPG/%
AM In	77.43a	30a	3.31a	237ab	746a	49.53ab
AM Out	44.90b	22b	2.99ab	183b	975a	41.04b
AMS In	64.40a	30a	3.33a	323a	195b	57.03a
AMS Out	47.30b	29a	3.24a	126bc	147b	41.42b
AS In	77.00a	12b	2.32b	317a	864a	53.74 a
AS Out	30.37c	11b	2.31b	176b	439ab	46.01ab

The different letters in each column mean the biomass or ratios difference was significant at $P < 0.05$.

TABLE 3 | Results (*F* value) of three-way ANOVA analysis about the effect of fencing, depth, grassland type, and interaction of fencing and grassland type, fencing and depth, grassland types and depth, fencing with grassland type and depth on total coverage (Cover.), plant species richness (R), Shannon–Wiener diversity index (H), aboveground biomass (AGB), belowground biomass (BGB), proportion of palatable grasses (PPG), soil organic C (SOC), total nitrogen (TN), soil bulk density (BD), and soil moisture.

Source of variance/df	Fencing /1	Grassland type/2	Soil depth/3	Fencing × grassland type/2	Fencing × depth/3	Grassland type × depth/6	Fencing × Grassland type × depth/6
Cover.	96.12*	1.85	–	6.79*	–	–	–
R	0.998*	0.996*	–	1.001*	–	–	–
H	6.45*	27.11*	–	4.47*	–	–	–
AGB	5.71*	1.54	–	0.81	–	–	–
BGB	0.18	6.14*	22.88*	1.37	0.3	3.17*	1.83
PPG	0.23	0.92	–	0.27	–	–	–
SOC	0.42	111.19*	46.61*	4.89*	0.57	13.73*	0.32
TN	2.3	123.74*	56.81*	7.66*	0.87	13.80*	0.27
BD	27.35*	58.25*	7.61*	5.70*	4.27*	5.72*	3.44*
Soil moisture	0.97	35.22*	1.58	2.46	0.5	2.35*	0.41

*× means interaction effect; * means the difference was significant at $P < 0.05$; – means no data.*

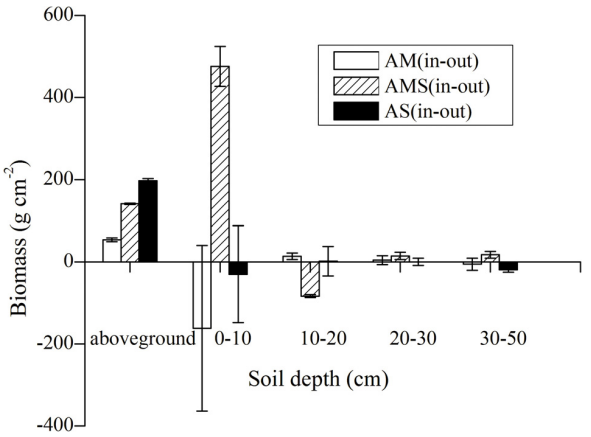

FIGURE 1 | Biomass distribution in the vertical direction between enclosed and grazed sites with three vegetation types: alpine meadow (AM), alpine meadow steppe (AMS), and alpine steppe (AS). Error bars were the standard error of three replicates' biomass difference between enclosed and grazed area at corresponding layers.

increased the soil moisture at the depth 0–20 cm in AM, and it showed no obvious effects at the depth 20–50 cm (**Figure 3**). Soil moisture was decreased at all depths in AMS and AS after long-term fencing, but it was only significant at the depth 0–10 and 20–30 cm in AS (**Figure 3**).

Soil Organic C and Total Nitrogen

With the increase in soil depth, SOC was decreased in all alpine grassland types in either enclosed sites or grazed sites (**Figure 4**). The SOC content varied remarkably among different grassland types (**Table 3** and **Figure 4**). The SOC was higher in AM than in AMS and AS in either enclosed or grazed sites at the depth 0–30 cm (**Figure 4**). Long-term fencing did not have a positive impact on SOC in AM (**Figure 4**). The SOC increased at all depths in AMS and AS after long-term fencing. The increase was only significant in AMS (**Figure 4**). The results of three-way ANOVA analysis showed that grassland type, soil depth, fencing, and their interactions significantly affected SOC. The total soil nitrogen (TN) has a similar pattern with SOC, and their correlation coefficient was 0.99.

DISCUSSION

Vegetation Characteristics

Fencing has a significant effect on plant community structure and composition, which will have feedbacks on ecosystem productivity (Polley et al., 2014). Due to the complexity of the

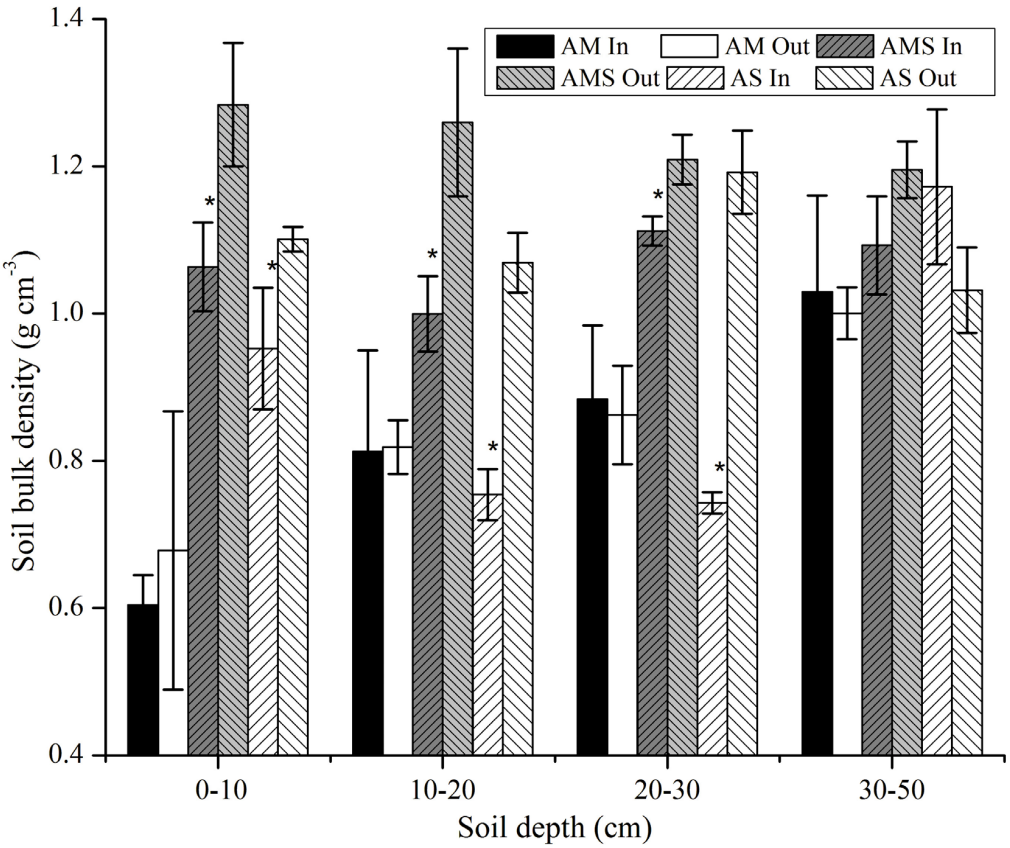

FIGURE 2 | Soil bulk density (BD) in the vertical direction between enclosed (In) and grazed (Out) sites with three vegetation types: alpine meadow (AM), alpine meadow steppe (AMS), and alpine steppe (AS). Error bars were the standard error of three replicates BD between enclosed and grazed sites. *Mean of the change of BD was significant at $P < 0.05$.

growing environment, plants are subjected to different degrees and types of external interference in each stage of plant growth, but plants always adjust their growth strategies through certain traits, such as plant height, leaf size, leaf shape, tiller quantity, biomass allocation (Wu et al., 2009; Li et al., 2019), etc., to ensure the successful completion of their life history. Exclosure is a disturbance to plant growth, and plant community characteristics may change accordingly (Wu et al., 2009; Miao et al., 2015).

Biomass is the basis of the flow of matter and energy in an ecosystem (Yan and Lu, 2015), which is an important quantitative feature of the plant community and can directly reflect the material production of producers in the ecosystem (Spring et al., 1996; Zeng et al., 2015). The AGB of different types of grassland increased to a great extent (**Table 2**) after fencing, which agrees with the results of many studies (Wu et al., 2009; Deng et al., 2014; Zeng et al., 2015; Cheng et al., 2016; Li et al., 2017). The main reason was that foraging was prohibited inside the fences. AGB was significantly increased after long-term exclosure in AMS and AS but not significant in AM. Belowground biomass showed complex responses (**Table 2**) (Milchunas and Lauenroth, 1993; Frank et al., 2002; Miehe et al., 2019). The BGB at 0–10 cm inside fences was lower than that of the corresponding grazed area in AMS and AS, but in AM it is higher (**Figure 1**). Because of the rapid increase of AGB in AS after fencing (Liu et al., 2018), most of the soil nutrients are consumed aboveground, resulting in relatively slow root growth. With the increase in altitude, from AS to AMS and AM, the percentages of 0–10 cm to the total BGB (0–50 cm) were decreased in enclosed sites. The trend of grazed sites was opposite with that in enclosed sites at 0–10 cm. This is because AS recovered at the fastest speed, followed by AMA, and AM at the slowest speed. More than 80% of the species in AM are grasses and sedges (Peng et al., 2020b). Sedge and graminoid species have highly branched fibrous root systems that are mainly distributed near the soil surface, and this leads to a rapid increase near the soil surface biomass of the grasslands during vegetation restoration (Wang et al., 2014). The vegetation composition of AM is dominated by forbs with a deep root system (Liu et al., 2018), and then the AGB increase after fencing is dominated by deep layer (Peng et al., 2020a). In high altitude, the constructive species were rhizome grass which the roots distribute mainly in the upper layer of soil in the enclosed site. With the decrease in altitude, from AM to AMS and AS, the dense cluster type grass was increased, which has more distribution of roots at the depth below 10 cm in the enclosed site (**Figure 1**). Long-term fencing increased AGB and improved the grassland quality especially in AS with lower altitude (**Table 3**). These results support the

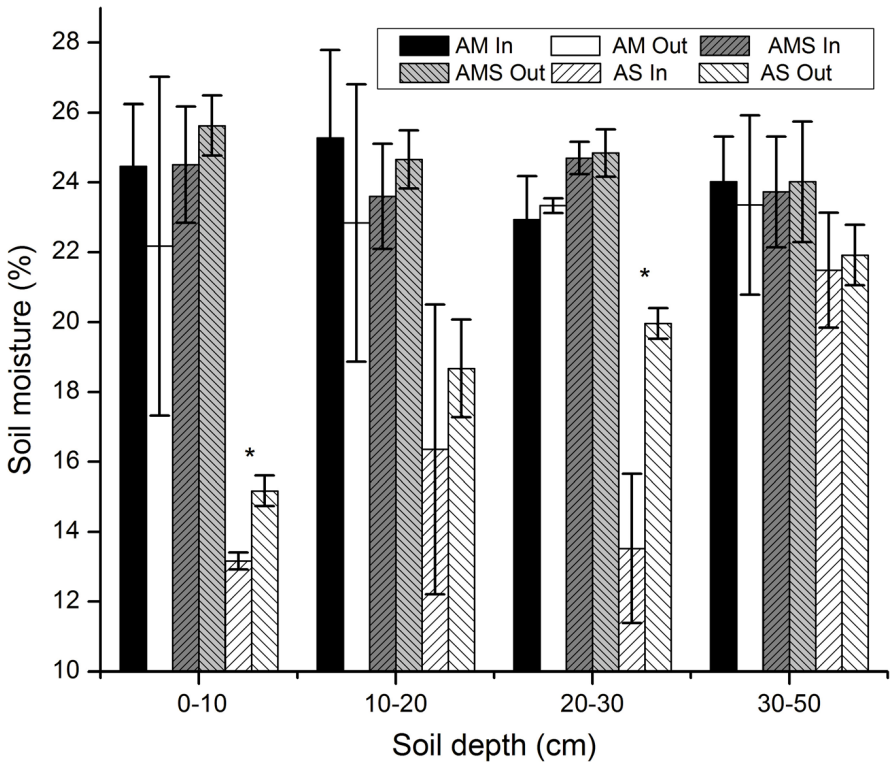

FIGURE 3 | Soil moisture in the vertical direction between enclosed (In) and grazed (Out) sites with three vegetation types: alpine meadow (AM), alpine meadow steppe (AMS), and alpine steppe (AS). Error bars were the standard error of three replicates soil moisture between enclosed and grazed sites; *Mean of the change of soil moisture was significant at $P < 0.05$.

viewpoint that with the fencing the distribution of biomass in the vertical direction was changed: a part of biomass "transfer" from belowground to aboveground.

Communities responded to environmental change by altering the functional characters of some dominant species (Macgillivray et al., 1995; Bakhshi et al., 2019); for example, palatable grasses have greater competitive ability than unpalatable grasses and show an increase (**Table 2**) after long-term fencing (Wu et al., 2009; Deng et al., 2014). Vegetation coverage is an important indicator of land surface vegetation and ecosystem environmental change. The total coverage was significantly increased after long-term fencing in three different alpine grasslands (**Tables 2**, **3**), which were consistent with many other fencing experiment results (Cheng et al., 2011; Mekuria and Veldkamp, 2012). The results support the viewpoint that fencing is a simple and effective measure for restoring degraded grasslands (Wu et al., 2009; Golodets et al., 2010; Deng et al., 2014; Zhao et al., 2015). The species richness (R) in AM (30) and AMS (30) was than twice in AS (12) in an enclosed area, and there was similarity in the grazed area (**Table 2**). It is similar with the results of Wu et al. (2012), which showed that the mean S (R = S) in AM (23.30) was nearly twice as much as in AS (11.80). Previous research has suggested that fencing may improve species richness and diversity index across the QTP (Wu et al., 2012), and our results are similar (**Table 2**). Increasing ranges of species richness and diversity index were bigger in AM than in AMS and AS (**Table 2**). Some experiment results also indicated that fencing might not necessarily increase species richness and diversity index even to decline in species richness and diversity index (Shi et al., 2010; Schultz et al., 2011; Bakhshi et al., 2019) due to differences in the competitive dominance of species (Tilman et al., 1997) and different fencing times (Deng et al., 2014). There is still no consensus on how long-term fencing affects plant species richness and diversity (Zervas, 1998; Schultz et al., 2011; Wu et al., 2012).

The high diversity makes AM more stable and resistant to perturbations than steppes (Kuhsel and Bluthgen, 2015). Species-rich plant communities are relatively more resistant to change in management regimes (Klimes et al., 2013). The sparser canopy of AS relative to that of AM (Zhu et al., 2015) also suggests much easier recruitment and settlement capabilities for grasses. Thus, long-term fencing likely promoted the recruitment and settlement of Stipa species and allowed AS communities to cumulatively benefit from natural conditions. While AM was less sensitive to fencing than AMS and AS (**Figure 2**), a more nuanced management regime should thus be considered in the rehabilitation of AM.

Soil Properties

Soil properties, such as BD, moisture SOC, and TN, directly regulate plant growth (Ganjurjav et al., 2016). BD was found to be lower in fenced grassland compared to grazing grassland. The

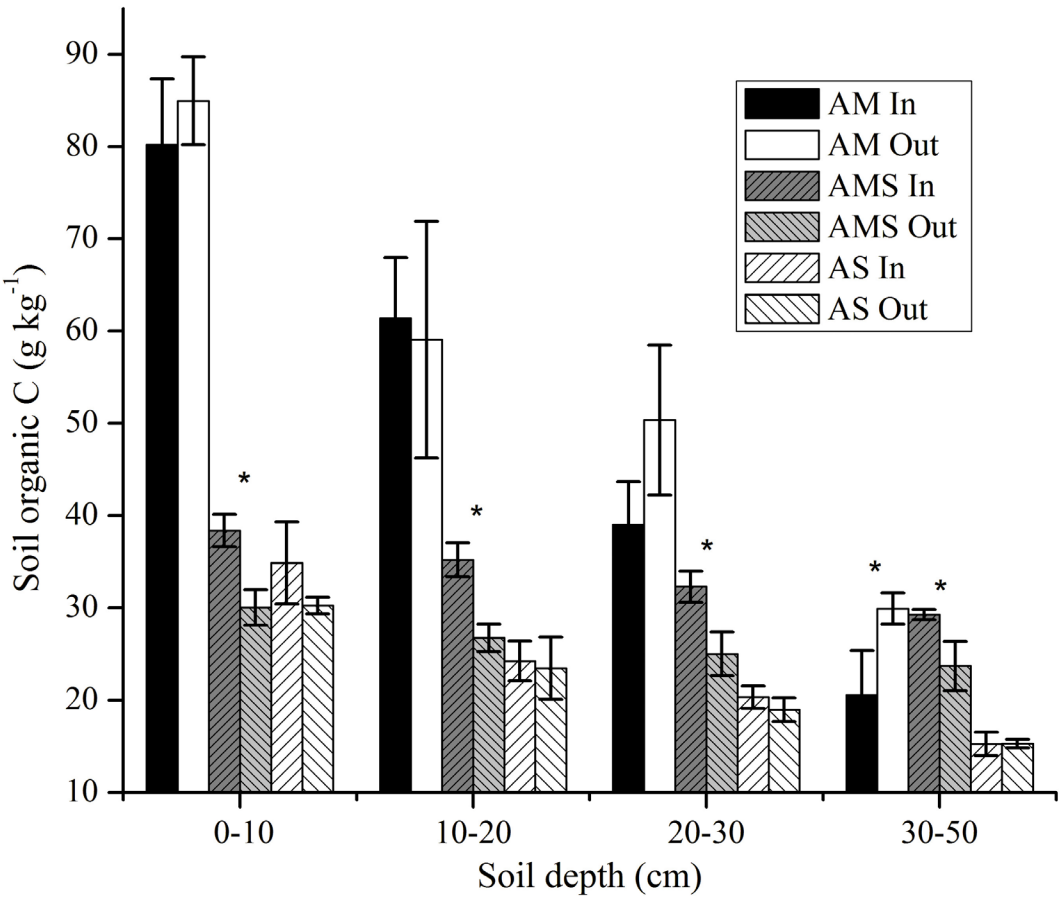

FIGURE 4 | Soil organic C in the vertical direction between enclosed (In) and grazed (Out) sites with three vegetation types: alpine meadow (AM), alpine meadow steppe (AMS), and alpine steppe (AS). Error bars were the standard error of three replicates soil organic C between enclosed and grazed sites. *Mean the change of SOC difference was significant at $P < 0.05$.

reasons included the elimination of soil trampling by livestock, an increase in root biomass accumulation (Yuan et al., 2012), high soil silt and clay content, and presence of extensive shallow root systems in fenced areas (Su et al., 2005). Our results have a similar trend in AMS and AS, but there was almost no change in AM after long-term fencing (**Table 3** and **Figure 2**). The variation of BD of different alpine grassland types was inconsistent, which was mainly caused by the inconsistent increase in BGB of different alpine grassland types after the fencing. The variation of BGB and SOC confirmed this opinion (**Figures 1**, **4**). Long-time fencing leads to the increase in vegetation coverage, which can improve topsoil microhabitats and moisture then prevent the grassland from degradation in alpine grassland (Wu et al., 2011; Deng et al., 2014). On the other hand, increasing coverage also has stronger transpiration, which leads to a decrease in soil moisture. Our results show that soil moisture at the depth of 0–20 cm in AM was increased but in AMS and AS it was decreased at all soil depths (**Figure 3**). Although the coverage of all the three grasslands was increased after fencing (**Table 2**), the transpiration of AMS and AS was stronger than that of AM because of the large leaf area (Li et al., 2020). The stronger transpiration leads to higher water consumption, which decreased the soil moisture in AMS and AS (**Figure 3**).

Soil organic matter is widely recognized to be an important aspect of soil fertility, fulfilling various functions such as improving soil structure, aggregate stability, and water-holding capacity. The SOC at the 0–50 cm depth after long-term fencing in the AS and AMS was increased, but there was no obvious regular change pattern in AM (**Figure 4**). These were consistent with the results of other researches (Wu et al., 2010a; Zhao et al., 2015; Deng and Shangguan, 2017). Vesterdal et al. (2002) thought that the change in land use from grazing to fencing means that the annual cycle of plants was changed by the much longer grassland cycle. Consequently, this enables the development of high net primary productivity and reduces the degree of soil disturbance, leading to increased SOC fractions. TN has a similar, varying pattern with that of SOC (Yu et al., 2019).

As shown throughout this study, the community characteristics and soil properties have different changes after long-time fencing among three different alpine grasslands in northeast QTP. The vegetation coverage, AGB, plant species richness, Shannon–Wiener Diversity index, and proportion of

palatable forage all improved in three alpine grasslands after long-term fencing. With the increase in altitude, from AS to AMS and AM, the percentage BGB at 0–10 cm to the total at 0–50 cm was decreased in the enclosed site, and the change in trend of the grazed site was opposite with that in the enclosed site. BD was obviously decreased in AMS and AS, but there was almost no change in AM after long-term fencing. Fencing increased the SOC and TN at the depth of 0–50 cm in the AS and AMS, but there was no obvious regular change pattern in AM. According to the results, AM was less sensitive to fencing among the three alpine grasslands, so a more nuanced management regime should be considered in the rehabilitation of AM. The similar countermeasures to prevent further degradation and restoration activities of all three alpine grasslands would lead to the failure of some ecological projects.

DATA AVAILABILITY STATEMENT

The raw data supporting the conclusions of this article will be made available by the authors, without undue reservation.

AUTHOR CONTRIBUTIONS

CH contributed to conceptualization, methodology, data curation, and writing – original draft preparation. FP contributed to data curation, investigation, and editing. QY, JL, and HD contributed to data curation and investigation. TW contributed to conceptualization. XX contributed to supervision, funding acquisition, and writing – reviewing and editing. All authors contributed to the article and approved the submitted version.

FUNDING

This work was supported by funds from the National Key R&D Program of China (2016YFC0501803) and the National Natural Science Foundation of China (41771233).

ACKNOWLEDGMENTS

The authors wish to express their gratitude to the reviewers and editor for their time and effort.

REFERENCES

Bakhshi, J., Javadi, S. A., Tavili, A., and Arzani, H. (2019). Study on the effects of different levels of grazing and exclosure on vegetation and soil properties in semi-arid rangelands of Iran. *Acta Ecol. Sin.* doi: 10.1016/j.chnaes.2019.07.003

Bremner, J. M. (1996). "Nitrogen-total," in *Methods of Soil Analysis, Part 3, SSSA Book Series: 5*, ed. D. L. Sparks (Madison: America Society of Agronomy), 1085–1121.

Cheng, J., Wu, G. L., Zhao, L. P., Li, Y., Li, W., and Cheng, J. M. (2011). Cumulative effects of 20-year exclusion of livestock grazing on above- and belowground biomass of typical steppe communities in arid areas of the Loess Plateau, China. *Plant Soil Environ.* 57, 40–44. doi: 10.17221/153/2010-PSE

Cheng, J. M., Jing, G. H., Wei, L., and Jing, Z. B. (2016). Long-term grazing exclusion effects on vegetation characteristics, soil properties and bacterial communities in the semi-arid grasslands of China. *Ecol. Eng.* 97, 170–178. doi: 10.1016/j.ecoleng.2016.09.003

Chillo, V., Ojeda, R. A., Anand, M., and Reynolds, J. F. (2015). A novel approach to assess livestock management effects on biodiversity of drylands. *Ecol. Indic.* 50, 69–78. doi: 10.1016/j.ecolind.2014.10.009

Deng, L., and Shangguan, Z. P. (2017). Afforestation drives soil carbon, and nitrogen changes in China. *Land Degrad. Dev.* 28, 151–165. doi: 10.1002/ldr.2537

Deng, L., Zhang, Z. N., and Shangguan, Z. P. (2014). Long-term fencing effects on plant diversity and soil properties in China. *Soil Till. Res.* 137, 7–15. doi: 10.1016/j.still.2013.11.002

Frank, D. A., Kuns, M. M., and Guido, D. R. (2002). Consumer control of grassland plant production. *Ecology* 83, 602–606. doi: 10.1890/0012-965820 02083

Ganjurjav, H., Gao, Q., Gornish, E. S., Schwartz, M. W., Liang, Y., Cao, X., et al. (2016). Differential response of alpine steppe and alpine meadow to climate warming in the central Qinghai-Tibetan Plateau. *Agric. For. Meteorol.* 223, 233–240. doi: 10.1016/j.agrformet.2016.03.017

Gao, Y. H., Zhou, X., Wang, Q., Wang, C. Z., Zhan, Z. M., Chen, L. F., et al. (2013). Vegetation net primary productivity and its response to climate change during 2001-2008 in the Tibetan Plateau. *Sci. Total Environ.* 444, 356–362. doi: 10.1016/j.scitotenv.2012.12.014

Gisladottir, G., and Stocking, M. (2005). Land degradation control and its global environmental benefits. *Land Degrad. Dev.* 16, 99–112. doi: 10.1002/ldr.687

Golodets, C., Kigel, J., and Sternberg, M. (2010). Recovery of plant species composition and ecosystem function after cessation of grazing in a Mediterranean grassland. *Plant Soil* 329, 365–378. doi: 10.1007/s11104-009-0164-1

Harris, R. B. (2010). Range land degradation on the Qinghai-Tibetan plateau: a review of the evidence of its magnitude and causes. *J. Arid Environ.* 74, 1–12. doi: 10.1016/j.jaridenv.2009.06.014

Hu, Z. M., Li, S. G., Guo, Q., Niu, S. L., He, N. P., Li, L. H., et al. (2016). A synthesis of the effect of grazing exclusion on carbon dynamics in grasslands in China. *Glob. Chang. Biol.* 22, 1385–1393. doi: 10.1111/gcb.13133

IBM Corp (2010). *IBM SPSS Statistics for Windows, Version 19.0*. Armonk, NY: IBM Corp.

Ilan, S., and Rattan, L. (2015). Achieving zero net land degradation: challenges and opportunities. *J. Arid Environ.* 112, 45–51. doi: 10.1016/j.jaridenv.2014.01.016

Jing, Z. B., Cheng, J. M., Su, J. S., Bai, Y., and Jin, J. W. (2014). Changes in plant community composition and soil properties under 3-decade grazing exclusion in semiarid grassland. *Ecol. Eng.* 64, 171–178. doi: 10.1016/j.ecoleng.2013.12.023

Klimes, L., Hajek, M., Mudrak, O., Dancak, M., Preislerova, Z., Hajkova, P., et al. (2013). Effects of changes in management on resistance and resilience in three grassland communities. *Appl. Veg. Sci.* 16, 640–649. doi: 10.1111/avsc.12032

Kuhsel, S., and Bluthgen, N. (2015). High diversity stabilizes the thermal resilience of pollinator communities in intensively managed grasslands. *Nat. Commun.* 6:7989. doi: 10.1038/Ncomms8989

Li, F., Zeng, Y., Luo, J. H., Ma, R. H., and Wu, B. F. (2016). Modeling grassland aboveground biomass using a pure vegetation index. *Ecol. Indic.* 62, 279–288. doi: 10.1016/j.ecolind.2015.11.005

Li, L. J., Song, X. Y., Xia, L., Fu, N., Feng, D., Li, H. Y., et al. (2020). Modelling the effects of climate change on transpiration and evaporation in natural and constructed grasslands in the semi-arid Loess Plateau, China. *Agric. Ecosyst. Environ.* 302:107077. doi: 10.1016/j.agee.2020.107077

Li, S., Dong, S., Shen, H., Han, Y., Zhang, J., Xu, Y., et al. (2019). Different responses of multifaceted plant diversities of alpine meadow and alpine steppe to nitrogen addition gradients on Qinghai-Tibetan Plateau. *Sci. Total Environ.* 688, 1405–1412. doi: 10.1016/j.scitotenv.2019.06.211

Li, W., Cao, W. X., Wang, J. L., Li, X. L., Xu, C. L., and Shi, S. L. (2017). Effects of grazing regime on vegetation structure, productivity, soil quality, carbon and nitrogen storage of alpine meadow on the Qinghai-Tibetan Plateau. *Ecol. Eng.* 98, 123–133. doi: 10.1016/j.ecoleng.2016.10.026

Li, X. L., Gao, J., Brierley, G., Qiao, Y. M., Zhang, J., and Yang, Y. W. (2013). Rangeland degradation on the Qinghai-Tibet plateau: implications for rehabilitation. *Land Degrad. Dev.* 24, 72–80. doi: 10.1002/ldr.1108

Liu, H., Mi, Z., Lin, L., Wang, Y., Zhang, Z., Zhang, F., et al. (2018). Shifting plant species composition in response to climate change stabilizes grassland primary production. *Proc. Natl. Acad. Sci. U.S.A.* 115, 4051–4056.

Lu, X. Y., Kelsey, K. C., Yan, Y., Sun, J., Wang, X. D., Cheng, G. W., et al. (2017). Effects of grazing on ecosystem structure and function of alpine grasslands in Qinghai-Tibetan Plateau: a synthesis. *Ecosphere* 8:e0165610. doi: 10.1002/ecs2.1656

Macgillivray, C. W., Grime, J. P., Band, S. R., Booth, R. E., Campbell, B., Hendry, G. A. F., et al. (1995). Testing predictions of the resistance and resilience of vegetation subjected to extreme events. *Funct. Ecol.* 9, 640–649. doi: 10.2307/2390156

Mekuria, W., and Veldkamp, E. (2012). Restoration of native vegetation following exclosure establishment on communal grazing lands in Tigray, Ethiopia. *Appl. Veg. Sci.* 15, 71–83. doi: 10.1111/j.1654-109X.2011.01145.x

Miao, R. H., Jiang, D. M., Musa, A., Zhou, Q. L., Guo, M. X., and Wang, Y. C. (2015). Effectiveness of shrub planting and grazing exclusion on degraded sandy grassland restoration in Horqin sandy land in Inner Mongolia. *Ecol. Eng.* 74, 164–173. doi: 10.1016/j.ecoleng.2014.10.004

Miehe, G., Schleuss, P. M., Seeber, E., Babel, W., Biermann, T., Braendle, M., et al. (2019). The Kobresia pygmaea ecosystem of the Tibetan highlands - Origin, functioning and degradation of the world's largest pastoral alpine ecosystem Kobresia pastures of Tibet. *SCI Total Environ.* 648, 754–771. doi: 10.1016/j.scitotenv.2018.08.164

Milchunas, D. G., and Lauenroth, W. K. (1993). Quantitative effects of grazing on vegetation and soils over a global range of environments. *Ecol. Monogr.* 63, 327–366. doi: 10.2307/2937150

OriginLab Corp (2007). *The Data Analysis and Graphing Workspace*. Northampton, MA: OriginLab Corporation.

Peng, F., Xue, X., Li, C., Lai, Z., Sun, J., Tsubo, L., et al. (2020a). Plant community of alpine steppe shows stronger association with soil properties than alpine meadow alongside degradation. *Sci. Total Environ.* 733:139048. doi: 10.1016/j.scitotenv.2020.139048

Peng, F., Xue, X., You, Q., Sun, J., Zhou, J., Wang, T., et al. (2020b). Change in the trade-off between aboveground and belowground biomass of alpine grassland: implications for the land degradation process. *Land Degrad. Dev.* 31, 105–117. doi: 10.1002/ldr.3432

Peng, F., Xue, X., Xu, M. H., You, Q. G., Jian, G., and Ma, S. X. (2017). Warming-induced shift towards forbs and grasses and its relation to the carbon sequestration in an alpine meadow. *Environ. Res. Lett.* 12:aa6508. doi: 10.1088/1748-9326/Aa6508

Peng, F., Xue, X., You, Q. G., Huang, C. H., Dong, S. Y., Liao, J., et al. (2018). Changes of soil properties regulate the soil organic carbon loss with grassland degradation on the Qinghai-Tibet Plateau. *Ecol. Indic.* 93, 572–580. doi: 10.1016/j.ecolind.2018.05.047

Polley, H. W., Derner, J. D., Jackson, R. B., Wilsey, B. J., and Fay, P. A. (2014). Impacts of climate change drivers on C4 grassland productivity: scaling driver effects through the plant community. *J. Exp. Bot.* 65, 3415–3424. doi: 10.1093/jxb/eru009

Saito, M., Kato, T., and Tang, Y. (2009). Temperature controls ecosystem CO_2 exchange of an alpine meadow on the northeastern Tibetan Plateau. *Glob. Chang. Biol.* 15, 221–228. doi: 10.1111/j.1365-2486.2008.01713.x

Schultz, N. L., Morgan, J. W., and Lunt, I. D. (2011). Effects of grazing exclusion on plant species richness and phytomass accumulation vary across a regional productivity gradient. *J. Veg. Sci.* 22, 130–142. doi: 10.1111/j.1654-1103.2010.01235.x

Shi, F. S., Chen, H., Wu, Y., and Wu, N. (2010). Effects of livestock exclusion on vegetation and soil properties under two topographic habitats in an alpine meadow on the Eastern Qinghai-Tibetan Plateau. *Pol. J. Ecol.* 58, 125–133. doi: 10.1017/S0032247409008626

Spring, G. M., Priestman, G. H., and Grime, J. P. (1996). A new field technique for elevating carbon dioxide levels in climate change experiments. *Funct. Ecol.* 10, 541–545. doi: 10.2307/2389948

Stirling, G., and Wilsey, B. (2001). Empirical relationships between species richness, evenness, and proportional diversity. *Am. Nat.* 158, 286–299. doi: 10.1086/321317

Su, Y. Z., Li, Y. L., Cui, H. Y., and Zhao, W. Z. (2005). Influences of continuous grazing and livestock exclusion on soil properties in a degraded sandy grassland, Inner Mongolia, northern China. *Catena* 59, 267–278. doi: 10.1016/j.catena.2004.09.00

Tang, J., Davy, A. J., Jiang, D. M., Musa, A., Wu, D. F., Wang, Y. C., et al. (2016). Effects of excluding grazing on the vegetation and soils of degraded sparse-elm grassland in the Horqin Sandy Land, China. *Agric. Ecosyst. Environ.* 235, 340–348. doi: 10.1016/j.agee.2016.11.005

Tilman, D., Knops, J., Wedin, D., Reich, P., Ritchie, M., and Siemann, E. (1997). The influence of functional diversity and composition on ecosystem processes. *Science* 277, 1300–1302. doi: 10.1126/science.277.5330.1300

Vesterdal, L., Ritter, E., and Gundersen, P. (2002). Change in soil organic carbon following afforestation of former arable land. *For. Ecol. Manag.* 169, 137–147. doi: 10.1016/S0378-1127(02)00304-3

Walkley, A. (1947). A critical examination of a rapid method for determining organic carbon in soils - effect of variations in digestion conditions and of inorganic soil constituents. *Soil Sci.* 63, 251–264. doi: 10.1097/00010694-194704000-00001

Wang, J., Wang, X. T., Liu, G. B., Wang, G. L., Wu, Y., and Zhang, C. (2020). Fencing as an effective approach for restoration of alpine meadows: evidence from nutrient limitation of soil microbes. *Geoderma* 363:148. doi: 10.1016/j.geoderma.2019.114148

Wang, X., Dong, S., Yang, B., Li, Y., and Su, X. (2014). The effects of grassland degradation on plant diversity, primary productivity, and soil fertility in the alpine region of Asia's headwaters. *Environ. Monit. Assess.* 186, 6903–6917.

Wardle, D. A., Bonner, K. I., and Barker, G. M. (2000). Stability of ecosystem properties inresponse to above-ground functional group richness and composition. *Oikos* 89, 11–23. doi: 10.1034/j.1600-0706.2000.890102.x

Wu, G. L., Du, G. Z., Liu, Z. H., and Thirgood, S. (2009). Effect of fencing and grazing on a Kobresia-dominated meadow in the Qinghai-Tibetan Plateau. *Plant Soil* 319, 115–126. doi: 10.1007/s11104-008-9854-3

Wu, G. L., Li, W., Zhao, L. P., and Shi, Z. H. (2011). Artificial management improves soil moisture, C, N and Pin an alpine sandy meadow of western China. *Pedosphere* 21, 407–412. doi: 10.1016/S1002-0160(11)60142-2

Wu, G. L., Liu, Z. H., Zhang, L., Chen, J. M., and Hu, T. M. (2010a). Long-term fencing improved soil properties and soil organic carbon storage in an alpine swamp meadow of western China. *Plant Soil* 332, 331–337. doi: 10.1007/s11104-010-0299-0

Wu, G. L., Liu, Z. H., Zhang, L., Hu, T. M., and Chen, J. M. (2010b). Effects of artificial grassland establishment on soil nutrients and carbon properties in a black-soil-type degraded grassland. *Plant Soil* 333, 469–479. doi: 10.1007/s11104-010-0363-9

Wu, J. S., Zhang, X. Z., Shen, Z. X., Shi, P. L., Yu, C. Q., Song, M. H., et al. (2012). Species richness and diversity of alpine grasslands on the Northern Tibetan Plateau: effects of grazing exclusion and growing season precipitation. *J. Resour. Ecol.* 3, 236–242. doi: 10.5814/j.issn.1674-764x

Xue, X., Peng, F., You, Q. G., Xu, M. H., and Dong, S. Y. (2015). Belowground carbon responses to experimental warming regulated by soil moisture change in an alpine ecosystem of the Qinghai-Tibet Plateau. *Ecol. Evol.* 5, 4063–4078. doi: 10.1002/ece3.1685

Xue, X., You, Q. G., Peng, F., Dong, S. Y., and Duan, H. C. (2017). Experimental warming aggravates degradation-induced topsoil drought in alpine meadows of the Qinghai-Tibetan Plateau. *Land Degrad. Dev.* 28, 2343–2353. doi: 10.1002/ldr.2763

Yan, Y., and Lu, X. Y. (2015). Is grazing exclusion effective in restoring vegetation in degraded alpine grasslands in Tibet, China? *Peer J.* 3:e1020. doi: 10.7717/peerj.1020

Yu, L. F., Chen, Y., Sun, W. J., and Huang, Y. (2019). Effects of grazing exclusion on soil carbon dynamics in alpine grasslands of the Tibetan Plateau. *Geoderma* 353, 133–143. doi: 10.1016/j.geoderma.2019.06.036

Yuan, J. Y., Ouyang, Z. Y., Zheng, H., and Xu, W. H. (2012). Effects of different grassland restoration approaches on soil properties in the southeastern Horqin sandy land, northern China. *Appl. Soil Ecol.* 61, 34–39. doi: 10.1016/j.apsoil.2012.04.003

Zeng, C. X., Wu, J. S., and Zhang, X. Z. (2015). Effects of grazing on above- vs. below-ground biomass allocation of alpine Grasslands on the Northern Tibetan Plateau. *PLoS One* 10:e0135173. doi: 10.1371/journal.pone.0135173

Zervas, G. (1998). Quantifying and optimizing grazing regimes in Greek mountain systems. *J. Appl. Ecol.* 35, 983–986. doi: 10.1111/j.1365-2664.1998.tb00019.x

Zhao, F. Z., Kang, D., Han, X. H., Yang, G. H., and Feng, Y. Z. (2015). Soil stoichiometry and carbon storage in long-term afforestation soil affected by understory vegetation diversity. *Ecol. Eng.* 74, 415–422. doi: 10.1016/j.ecoleng.2014.11.010

Zhao, J. X., Li, X., Li, R. C., Tian, L. H., and Zhang, T. (2016). Effect of grazing exclusion on ecosystem respiration among three different alpine grasslands on the central Tibetan Plateau. *Ecol. Eng.* 94, 599–607. doi: 10.1016/j.ecoleng.2016.06.112

Zhu, J. T., Jiang, L., Zhang, Y. J., Jiang, Y. B., Tao, J., Tian, L., et al. (2015). Below-ground competition drives the self-thinning process of Stipa purpurea populations in northern Tibet. *J. Veg. Sci.* 26, 166–174. doi: 10.1111/jvs.12207

Conflict of Interest: The authors declare that the research was conducted in the absence of any commercial or financial relationships that could be construed as a potential conflict of interest.

The reviewer XL declared a past co-authorship with one of the authors FP to the handling editor.

frontiers in Environmental Science

BRIEF RESEARCH REPORT
published: 26 November 2020
doi: 10.3389/fenvs.2020.577406

Dynamics of Soil Water Content Across Different Landscapes in a Typical Desert-Oasis Ecotone

Guohua Wang[1,2,3]*, *Qianqian Gou*[1], *Yulian Hao*[1], *Huimin Zhao*[1] and *Xiafang Zhang*[1]

[1] College of Geographical Sciences, Shanxi Normal University, Linfen, China, [2] Key Laboratory of Desert and Desertification, Northwest Institute of Ecology and Environmental Resources, Chinese Academy of Sciences, Lanzhou, China, [3] Laboratory of Watershed Hydrology and Ecology, Linze Inland River Basin Comprehensive Research Station, Chinese Ecosystem Research Network, Northwest Institute of Ecology and Environmental Resources, Chinese Academy of Sciences, Lanzhou, China

An understanding of soil water content dynamics is important for vegetation restoration in an arid desert-oasis ecotone under different landscapes. In this study, the dynamics of soil water content under three typical landscapes (i.e., desert, sand-binding shrubland, and farmland shelter woodland) were investigated in the Hexi Corridor, northwest China, during the growing season from 2002 to 2013. The results showed that the soil water content in the deep layers decreased from 20–30% to a stable low level of 3–5% in the desert and shrubland. For the farmland shelter woodland, the soil water content at the deep layers also decreased, but the decrease rate was much smaller than the desert and shrubland. The decrease of soil water content in the deep soil layers among desert–shrubland–woodland was strongly associated with the increase of groundwater depths. The greatest increase of groundwater depths mainly occurred during 2008–2011, while the largest decrease of soil water content took place during the years 2009–2011, with a time-lag in response to increase in groundwater depths. This study provides new insight into the long-term dynamics of soil water content in a typical desert oasis ecotone under different landscape components from the influence of overexploiting groundwater that cannot be inferred from a short-term study. The findings demonstrate that the sharp increase of groundwater depths could be the main reason behind the reduction of soil water content in the clay interlayers, and sustainable development of groundwater resources exploitation is very important for the management of desert-oasis ecotone from a long-term perspective.

Keywords: desert-oasis ecotone, vegetation restoration system, soil desiccation, clay inter-layers, textural profile

OPEN ACCESS

Edited by:
Xian Xue,
Northwest Institute of Eco-Environment and Resources (CAS), China

Reviewed by:
Xinping Wang,
Cold and Arid Regions Environmental and Engineering Research Institute (CAS), China
Xueli Chang,
Ludong University, China

***Correspondence:**
Guohua Wang
gimi123@126.com

Specialty section:
This article was submitted to Land Use Dynamics, a section of the journal Frontiers in Environmental Science

Received: *29 June 2020*
Accepted: *20 October 2020*
Published: *26 November 2020*

Citation:
Wang G, Gou Q, Hao Y, Zhao H and Zhang X (2020) Dynamics of Soil Water Content Across Different Landscapes in a Typical Desert-Oasis Ecotone. Front. Environ. Sci. 8:577406. doi: 10.3389/fenvs.2020.577406

INTRODUCTION

Soil water refers to the amount of water stored in the soil unsaturated zone and is often used as an indicator of water limitation in arid and semi-arid regions (Dobriyal et al., 2012). As an important component of the hydrological cycles, soil water is involved in many hydrological processes, such as soil infiltration from precipitation, the formation of runoff, discharge from groundwater, soil evaporation, and plant transpiration (Porporato et al., 2002; Kizito et al., 2012; Li et al., 2014). Soil

water content is better expressed in terms of water availability to plants from an eco-hydrological perspective compared with rainfall or aridity index in dryland systems (Wang et al., 2012). A growing literature has demonstrated that the stability and availability of soil water in root zone is closely associated with the maintenance of arid ecosystem functions and services (Gao et al., 2015). Thus, monitoring soil water content is critical for comprehensively evaluating the benefits and consequences of vegetation restoration and ecosystem sustainable management in dryland ecosystems (Mohanty and Skaggs, 2001; Ruiz-Sinoga et al., 2011; Betti et al., 2016).

In arid northwest China, a defining geomorphologic feature is that many natural or artificial oases of different shapes and sizes are interspersed in widespread sandy deserts (Cheng et al., 1999). Desertification around the edge of these oases is a long-standing environmental problem and is expected to continue in the future due to human activities and climate change (Wang et al., 2015). This makes reestablishment of vegetation (i.e., shrub and tree plantations) a key strategy in ecosystem restorations and provision of ecosystem services in the translated zone between desert and oasis (i.e., desert-oasis ecotone) (Li and Shao, 2013a). However, the stability of artificial vegetation could be threatened by the deterioration of soil water and groundwater due to irrational agricultural irrigation (e.g., over exploitation of groundwater). Meanwhile, the dynamics of soil water content is also considered to differ significantly among components of a disturbed ecosystem (Li and Shao, 2013b). Thus, it is not an easy task to monitoring long-term dynamics of soil water content in a desert oasis ecotone with various soils, topography, vegetation, and land use types (Yi et al., 2014).

The Hexi Corridor is one of the main desert oasis regions in arid northwest China. Most of the oases are established naturally in the inland river deltas or on alluvial–diluvial plains (Zhang et al., 2003). Due to the rapid growing population and intensive demand for food, the conversion of shrubland or grassland to farmland is a recurrent problem in the oasis margins (Su et al., 2007). It has been reported that about 10% of shrubland or grassland previously used for pasture has been converted to cropland within the first half of the twentieth century. This conversion typically results in over exploitation of groundwater

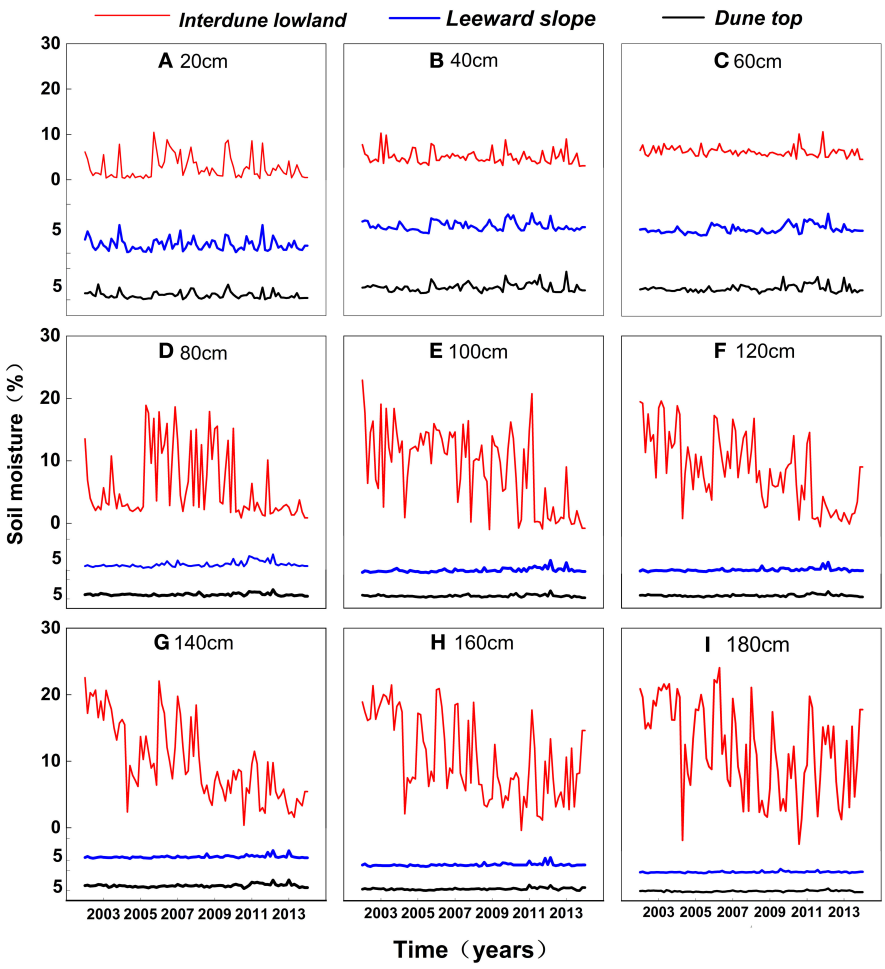

FIGURE 1 | The dynamics of soil water content of different soil layers at **(A)** 20 cm, **(B)** 40 cm, **(C)** 60 cm, **(D)** 80 cm, **(E)** 100 cm, **(F)** 120 cm, **(G)** 140 cm, **(H)** 160 cm, and **(I)** 180 cm in desert.

in the remaining marginal lands and increases groundwater level and shrinks groundwater resource. Understanding the spatial heterogeneity and variables of groundwater and estimating the dynamics of soil water content in different landscapes is crucial for various management and environmental protection in a desert oasis ecotone (Huang et al., 2012). Although many studies have been conducted to examine the temporal and spatial dynamics of soil water content of single landscape, e.g., the farmland (Ji et al., 2007), forest (Knight et al., 2002), and desert (Li et al., 2008), long-term monitoring of the dynamics of soil water content under different landscapes is urgently needed (Hu et al., 2011).

In this study, we considered the desert, shrubland, and woodland as an entire continuum system in the desert oasis ecotone to investigate the soil moisture dynamics, groundwater depths, vegetation conditions and their hydrological relations during the growing season from 2002 to 2013. The main objectives were to: (i) compare the dynamics of soil water content between distinct three landscapes and (ii) investigate the potential hydrological relations between groundwater and soil moisture across different landscapes.

MATERIALS AND METHODS

Study Area

The study area is located in a typical desert–oasis ecotone in Linze County of Gansu province in northwestern China (39° 21′ N, 100° 07′ E and altitude of 1,374 m). The area has a continental temperate desert climate: dry and hot in summer and cold in winter. The mean annual precipitation is only 117 mm. The potential annual evaporation is 2,390 mm, and the dryness index is 20.5. The annual rainfall has no significantly increasing or decreasing trend in the past 40 years (**Supplementary Figure 1A**). The mean annual temperature is 7.6°C, with the highest temperature at 39°C in July and lowest at −27°C in January, respectively. The annual mean and max temperature during the growing season also has no significantly increasing or decreasing trend in the last decade (**Supplementary Figure 1B**). The mean annual wind velocity is 3.2 ms^{-1}, and the wind direction is mainly from the northwest. Gales with wind velocity above 17 m s^{-1} occur about 10–15 days $year^{-1}$.

To curb wind erosion and alleviate its influence on the oasis, a succession of protection measures was implemented from desert to farmland, including fencing natural desert, conversing desert to shrubland and woodland at the edge of the oasis. After several decades, three distinctive landscapes (i.e., desert, sand-binding shrubland, and farmland shelter woodland) have gradually established along unprotected desert to farmland (**Supplementary Figure 2**).

Experimental Design and Measurements

To compare the temporal variation of soil moisture under different landscapes, three replicates of measurement sites for each landscape unit were selected in each landscape to minimize errors due to soil, topography, and vegetation heterogeneity (**Supplementary Table 1**). At the beginning of the soil sampling, the soil texture at the profile of 0–180 cm was determined by pipette method, and the soil is classified as different soil types based on international soil texture classification. The soil water content varied throughout the growing season (April–September), mostly through strong interactions with vegetation and groundwater, and basically remained constant over the winter, due to negligible root activity and human agricultural activity. And thus we considered the growing season to be the study period of interest here. At each site, a composite soil sample at different depths (20, 40, 60, 80, 100, 120, 140, 160, and 180 cm) was randomly collected from three sampling points by using a stainless steel auger (5 cm in diameter) on a sunny day on mid-April, May, June, July, August, and September during the growing season from years 2002 to 2013. Soil water content was then measured gravimetrically and calculated as the ratio of the mass of water to dry soil after drying the samples at 105°C.

Six groundwater depth monitoring wells were established along the desert, shrubland, and woodland at the edge of Linze Oasis (**Supplementary Figure 1**). The groundwater depths were recorded every 10 days from 2002 to 2011. The variation of soil water content was closely related to the local groundwater depths and the irrigation event. The farmland shelter woodland was irrigated once or twice from June to August with an irrigation amount of approximately 100 mm.

TABLE 1 | Mann–Kendall test and field trends of soil water content in desert (red represents sharp decrease rate of soil water content).

Sites	Depths (cm)	ß	Z_C	$Z_{1-\alpha/2}$	Significance	Soil types
Leeward slope	20	–	−1.40	1.96	N	Sand
	40	–	−0.88	1.96	N	Sand
	60	0.01	2.34	1.96	Y	Sand
	80	0.01	4.52	1.96	Y	Sand
	100	0.01	4.94	1.96	Y	Sand
	120	0.01	4.19	1.96	Y	Sand
	140	0.01	3.66	1.96	Y	Sand
	160	0.01	3.80	1.96	Y	Sand
	180	0.01	3.64	1.96	Y	Sand
Dune top	20	−0.01	−2.45	1.96	Y	Sand
	40	–	−0.46	1.96	N	Sand
	60	–	−0.11	1.96	N	Sand
	80	–	−0.55	1.96	N	Sand
	100	–	−0.58	1.96	N	Sand
	120	–	0.04	1.96	N	Sand
	140	–	1.79	1.96	N	Sand
	160	0.01	2.71	1.96	Y	Sand
	180	–	1.51	1.96	N	Sand
Interdune lowland	20	–	−0.19	1.96	N	Sand
	40	–	−1.82	1.96	N	Sand
	60	−0.01	−3.04	1.96	Y	Sand
	80	−0.02	−3.17	1.96	Y	Sand
	100	−0.15	−5.91	1.96	Y	Silty clay loam
	120	−0.15	−7.13	1.96	Y	Silty clay loam
	140	−0.18	−8.20	1.96	Y	Silty clay loam
	160	−0.14	−5.76	1.96	Y	Silty clay loam
	180	−0.11	−3.61	1.96	Y	Silty clay loam

Statistical Analysis

SPSSV15 and Origin 8 were used to estimate the soil moisture variation and trends of six observation sites. Mann-Kendall trend and linear regression analysis methods were performed to show the trend of soil moisture changes in different depths at different landscapes. According to the difference of soil water content, we divided the growing season into three different periods: early growing season (April–May), the middle growing season (June–August), and the late growing season (September–October). Soil water content anomalies during the different periods were used to assess soil moisture stress compared with normal conditions.

RESULTS

Dynamics of Soil Water Content of Different Landscapes

Desert

The vertical distribution of the soil water content could be mainly divided into two-layer types. For the interdune lowland, there was a slight difference between the soil water content of different depths in the upper soil layers, but the soil water content in the deeper layers (i.e., 80–180 cm) (**Figures 1D–I**) was much higher than that of the upper layers (i.e., 20, 40, and 60 cm) (**Figures 1A–C**). The soil water content was relatively stable in the upper layers, but the soil water content at deep layers decreased sharply from an initial 20–24 to 3–5% (**Figures 1D–G**), and the values of ß of Mann–Kendall analyses ranged from −0.11 to −0.18 (**Table 1**). For the leeward slope and dune top, the soil water content at different layers showed a similar pattern, and there was a slight difference among different depths.

Shrubland

In the shrubland of *Elaeagnus angustifolia*, there was also a slight difference between the soil water content of different depths in the upper soil layers, but the soil water content at deep layers of 160–180 cm decreased drastically from an initial 24 to 3%. The decline trend of the soil water content could be well-described by a linear function with a decrease

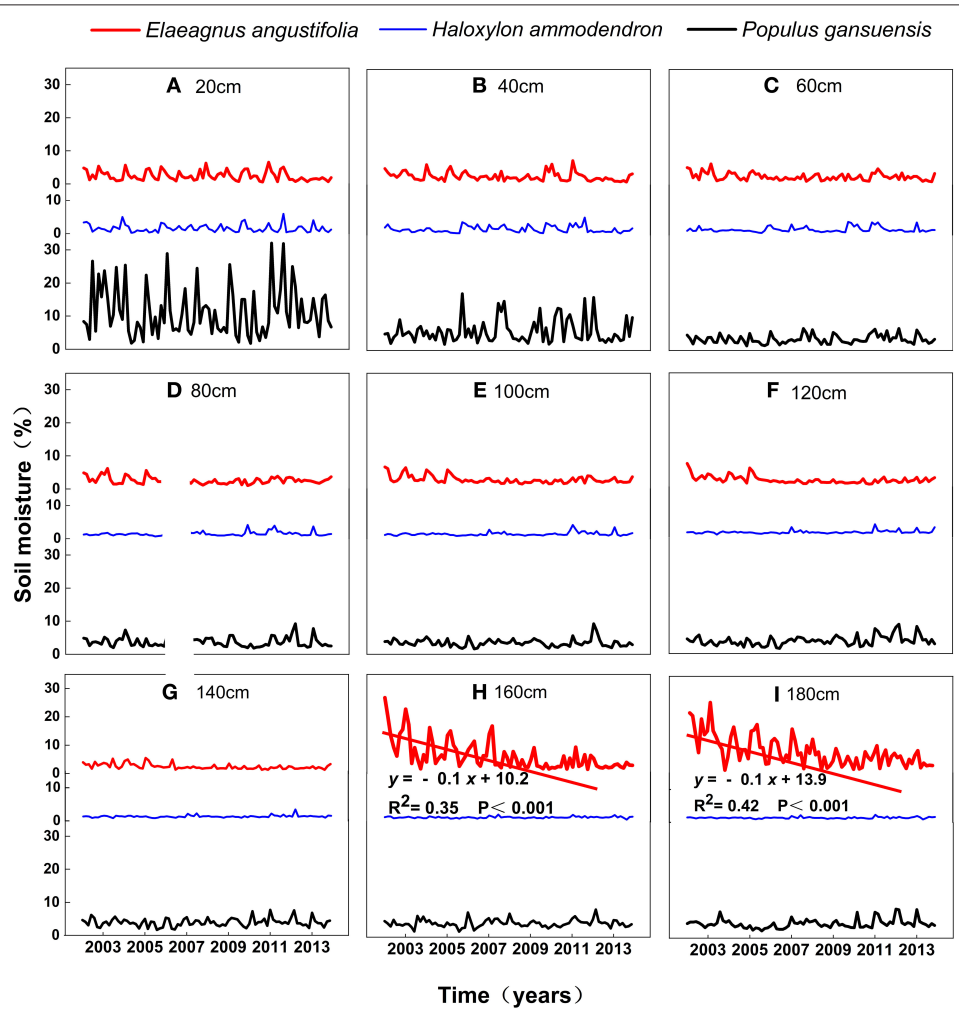

FIGURE 2 | The dynamics of soil water content of different soil layers at **(A)** 20 cm, **(B)** 40 cm, **(C)** 60 cm, **(D)** 80 cm, **(E)** 100 cm, **(F)** 120 cm, **(G)** 140 cm, **(H)** 160 cm, and **(I)** 180 cm in shrubland.

TABLE 2 | Mann–Kendall test and field trends of soil water content in shrubland (red represents sharp decrease rate of soil water content).

Dominant plant species	Depths (cm)	ß	Z_C	$Z_{1-\alpha/2}$	Significance	Soil types
Elaeagnus angustifolia	20	−0.01	−2.14	1.96	Y	Sand
	40	−0.02	−3.62	1.96	Y	Sand
	60	−0.01	−2.00	1.96	Y	Sand
	80	–	−1.40	1.96	N	Sand
	100	−0.01	−3.61	1.96	Y	Sand
	120	−0.02	−4.75	1.96	Y	Sand
	140	−0.02	−5.00	1.96	Y	Sand
	160	−0.10	−6.56	1.96	Y	Silty clay loam
	180	−0.14	−6.65	1.96	Y	Silty clay loam
Haloxylon ammodendron	20	–	−1.67	1.96	N	Sand
	40	–	−0.97	1.96	N	Sand
	60	–	−0.25	1.96	N	Sand
	80	–	1.27	1.96	N	Sand
	100	–	1.53	1.96	N	Sand
	120	0.003	2.41	1.96	Y	Sand
	140	0.001	2.07	1.96	Y	Sand
	160	–	1.34	1.96	N	Sand
	180	–	0.23	1.96	N	Sand
Populus gansuensis	20	–	0.04	1.96	N	**loam**
	40	–	0.05	1.96	N	**loam**
	60	–	0.64	1.96	N	Sand
	80	–	−1.34	1.96	N	Sand
	100	–	−1.73	1.96	N	Sand
	120	–	1.89	1.96	N	Sand
	140	–	0.19	1.96	N	Sand
	160	–	0.58	1.96	N	Sand
	180	-	0.55	1.96	N	Sand

TABLE 3 | Mann–Kendall test and field trends of soil water content in woodland.

Dominant plant species	Depths (cm)	ß	Z_C	$Z_{1-\alpha/2}$	Significance	Soil types
Pinus sylvestris var. *mongolica*	20	–	−0.15	1.96	N	Sandy loam
	40	–	−0.25	1.96	N	Sand
	60	–	−0.16	1.96	N	Sand
	80	–	0.37	1.96	N	Sand
	100	–	0.83	1.96	N	Sand
	120	–	0.67	1.96	N	Sand
	140	−0.02	−2.84	1.96	Y	Sand
	160	−0.02	−2.80	1.96	Y	Sand
	180	−0.03	−4.32	1.96	Y	Sand
Platycladus orientalis	20	–	0.28	1.96	N	Sandy loam
	40	–	−1.38	1.96	N	Sandy loam
	60	–	−1.67	1.96	N	Sand
	80	−0.01	−2.60	1.96	Y	Sand
	100	−0.01	−2.33	1.96	Y	Sand
	120	–	−1.89	1.96	N	Sand
	140	−0.02	−3.17	1.96	Y	Sand
	160	−0.02	−2.30	1.96	Y	Sand
	180	−0.02-	−2.30	1.96	Y	Sand
Pinus tabuliformis	20	–	0.28	1.96	N	Sandy loam
	40	–	1.03	1.96	N	Sand
	60	–	−0.03	1.96	N	Sand
	80	–	0.48	1.96	N	Sand
	100	–	−1.22	1.96	N	Sand
	120	−0.02	−2.87	1.96	Y	Sand
	140	−0.03	−4.04	1.96	Y	Sand
	160	−0.03	−4.84	1.96	Y	Sand
	180	−0.03	−4.97	1.96	Y	Sand

rate of 0.1% every year (**Figures 2H,I**). Meanwhile, the values of ß of Mann-Kendall analyses ranged from m0.10 to −0.14 (**Table 2**). In the shrubland of *Haloxylon ammodendron* and *Populus gansuensis*, the soil water content at different depths was basically at a low level of 2–3%, except for the litter fall layers of *Populus gansuensis* (**Figure 2**).

Woodland

In the farmland shelter woodland, the soil moisture of different depths of three sites show similar temporal trends and decreased uniformly and slightly at deep layers. The soil water content ranged between 4 and 12% at the surface layers (i.e., 20 cm), which was covered by litter falls (**Figure 3**). The soil water content at deeper layers decreased slightly and was basically kept stable (5–8%) (**Figure 3**; **Table 3**).

The Anomalies of Soil Water Content of Different Landscapes

Desert

The anomalies of soil water content clearly varied over the growing season and exhibited strong seasonality in the interdune lowland. The higher values were mainly in early period and lower values were in middle and late period at the deep layers of 100–180 cm (**Figure 4C1**).

Shrubland

In the shrubland of *Elaeagnus angustifolia*, the anomalies of soil water content exhibited similar pattern as desert lowland: the higher values were mainly in early period, but lower values were in middle and late period (**Figure 4A2**).

Woodland

For farmland shelter woodland, the soil water content anomalies of the three sites exhibited similar patterns: higher values are observed in early and middle period, but lower values in late period (**Figures 4A3–C3**).

DISCUSSION

In this study, the differences of soil water content under the three landscapes were compared at several soil layers. Increased variability with soil depth was observed at the desert and shrubland. We found that distinct silty clay layers existed in the deep soil profiles of desert and shrubland. The soil water content in these clay interlayers was more variable than upper soil layers (i.e., sand layers). Consistent with our study, Sun et al. (2018)

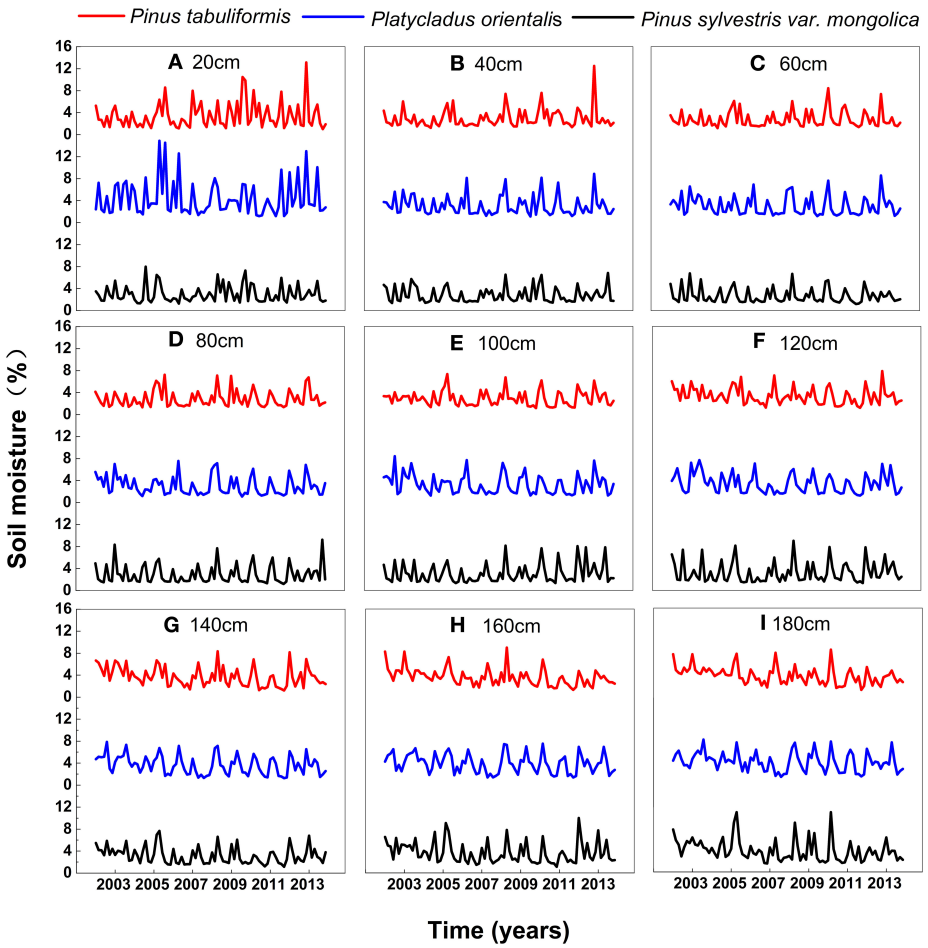

FIGURE 3 | The dynamics of soil water content of different soil layers at **(A)** 20 cm, **(B)** 40 cm, **(C)** 60 cm, **(D)** 80 cm, **(E)** 100 cm, **(F)** 120 cm, **(G)** 140 cm, **(H)** 160 cm, and **(I)** 180 cm in woodland.

also found that clay layers existed at the same study site. Qi et al. (2003) and Gong et al. (2005) also reported that alluvial alluvium or the loess-like parent material was the main soil-forming parent material in the inland river basin of Heihe. Compared with sand layers, these silty clay layers have much stronger water-holding capacity but greater variations (Miller and Franklin, 2002; Su et al., 2004; Betti et al., 2016). In this study, we found that the clay layers could hold more water compared with sand layers, but the soil water content decreased sharply after the year 2009. In desert, the soil water content of sand layers would not change too much due to its limited soil water-holding capacity. This result seemed to support the findings from other similar studies. For instance, Mohanty and Skaggs (2001) reported that the soil water content of sandy loam was more stablethan silty loam in 0–5 cm. Hu et al. (2010) also found that the temporal stability of sandy soils was significantly stronger than that of the sandy loam and silt loam. The inverse texture effects suggest that "taller and denser perennial vegetation" could mainly occur on coarse-textured soils but not fine-textured soils at arid regions with limited precipitation and high evaporation (Noy-Meir, 1973; Sperry and Hacke, 2002). This may be attributed to the soil desiccation at the silty clay layers and its negative effects of preventing root penetration into deeper layers (Li et al., 2013). As such, we predicted that in our study environmental degradation (i.e., significant reduction of soil water content) may lead to a sharp reduction in the biomass and diversity of deep-rooted plants in arid desert ecosystems.

In arid desert ecosystems, the soil water can be replenished by infiltration from rainfall and recharge from groundwater, and the soil water is mainly lost from the soil by evaporation and transpiration of different vegetation types. These inputs and outputs resulted in the changes of soil water content. Surface water in the oasis is very limited and restricted due to rapid population growth, social-economic development, and large-scale expansion of farmland in the recent decades (Liu et al., 2010). Agricultural production therefore heavily relies on groundwater irrigation, and the groundwater irrigation area increased nearly 10 times from 2002 to 2011 in this study area (Wang and Zhao, 2015; Wang et al., 2015).

In this study, we found that the soil water content in the woodland decreased slightly and was apparently more stable than that in the desert and shrubland. Obviously, this was caused by

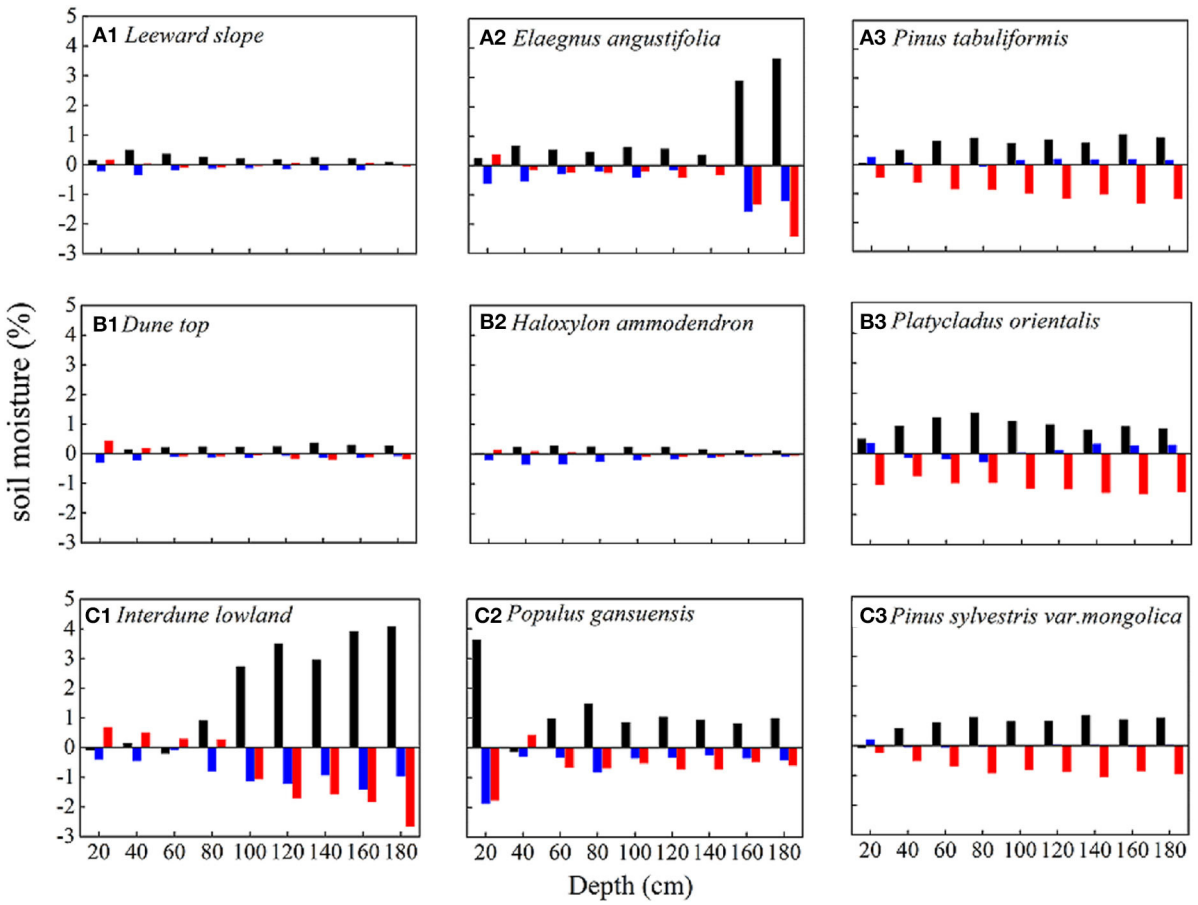

FIGURE 4 | The anomalies of soil water content in desert **(A1, B1,** and **C1)**, shrubland **(A2, B2,** and **C2)**, and woodland **(A3, B3,** and **C3)**. Black represents early period (April–May), blue represents middle period (June–August), and red represents late period (September–October).

the irrigation in the woodland, which could enhance the soil water content in the different soil layers. In contrary to woodland, the soil water content decreased sharply in the interdune lowland with clay interlayers during the years 2008–2010. The decrease of soil water content may be attributed to the increase of groundwater depths, which restricts groundwater access to deep soil layers via capillary transport (**Supplementary Figure 3**). In the natural desert, the groundwater depths ranged from 2 to 5 m, and as the depths of groundwater increased, groundwater could not be transported to plant roots through capillary actions. In the shrubland, we also found that the soil water content in 160–180 cm decreased continually with time. Three major mechanisms may account for the decrease in soil moisture. First, large-area re-vegetation of big shrubs and trees caused high evapotranspiration amount (Chang et al., 2006). Second, the annual precipitation amount is only 110 mm, and the dominant rainfall types are small rainfall events (<5 mm) which can only wet the top soil (0–60 cm) and normally evaporate back quickly after rainfall (Shen et al., 2014; Wang et al., 2019). Furthermore, intensive abstraction of groundwater for farmland irrigation may lead to the increase of groundwater depths, and less groundwater can recharge the soil water content at deep layers.

The low soil water content anomalies at different landscapes were observed mainly around the middle and late period, which coincides well with the increased in groundwater depths (**Supplementary Figure 4**). These results suggest that the groundwater depths have an influence on soil water content at 160–180 cm. The desert-oasis ecotone is a groundwater-dependent system, where groundwater controls the soil water content at deep depths, which directly affects the dynamic of soil water content and vegetation at different temporal and spatial scales (Huang et al., 2012). Normally, the soil water content is much higher under shallower groundwater depths than deeper ones. This may be caused by the effects of capillary actions. In this study area, due to the intensive expanding farmland at the edge of oasis, agricultural irrigation have consumed too much groundwater, and the groundwater depths significantly increased (**Supplementary Figure 3**). When groundwater depths are higher than the capillary rise height, groundwater could not support soil water content at deep soil layers. The intensive expanding of farmland, strong competition

between agricultural and ecological water, intensive pumping of groundwater, and sharp decrease in soil water content have made good water management more important than ever before.

CONCLUSIONS

This study examined the dynamics of soil water content of three different landscapes in a typical desert-oasis ecotone of northwestern China. For desert and sand-fixing shrubland, the soil water content at deeper clay layers decreased sharply due to increased groundwater depths and intensive shrub plantation. For the farmland shelter woodland, the soil water content was relatively stable except for the deep soil layers. The soil water content at deep depths also decreased, but the decrease rate was much smaller than the desert and shrubland due to irrigation. The increase of groundwater depths is the major reason for the decrease of soil water content of desert and shrubland, so a balance between ecological and agricultural water requirement should be considered based on the groundwater storage in the desert-oasis ecotones.

DATA AVAILABILITY STATEMENT

The raw data supporting the conclusions of this article will be made available by the authors, without undue reservation.

AUTHOR CONTRIBUTIONS

GW wrote the manuscript and designed the experiment. QG performed manuscript review. YH, HZ, and XZ provided assistance for data analysis. All authors contributed to the article and approved the submitted version.

FUNDING

This research was funded by Opening Foundation of Key Laboratory of Desert and Desertification, Chinese Academy of Sciences (Grant No. KLDD-2020-05), the National Natural Science Foundation of China (Grant No. 41701045), and Shanxi Provincial Natural Science Foundation of China (Grant No. 201801D221336).

ACKNOWLEDGMENTS

We thank John B. Bradford and Dr. Baoli Liu for giving us so many good suggestions for this study. We also appreciate the guidance of Professor Wenzhi Zhao.

SUPPLEMENTARY MATERIAL

The Supplementary Material for this article can be found online at: https://www.frontiersin.org/articles/10.3389/fenvs.2020.577406/full#supplementary-material

REFERENCES

Betti, G., Grant, C. D., Murray, R. S., and Churchman, G. J. (2016). Size of subsoil clods affects soil-water availability in sand-clay mixtures. *Soil Res.* 54, 276–290. doi: 10.1071/SR15115

Chang, X. X., Zhao, W. Z., Zhang, Z. H., and Su, Y. Z. (2006). Sap flow and tree conductance of shelter-belt in arid region of China. *Agric. For. Meteorol.* 138, 132–141. doi: 10.1016/j.agrformet.2006.04.003

Cheng, G. D., Xiao, D. N., and Wang, G. X. (1999). On the characteristics and building of landscape ecology in arid area. *Adv. Geosci.* 14, 11–15.

Dobriyal, P., Qureshi, A., Badola, R., and Hussain, S. A. (2012). A review of the methods available for estimating soil moisture and its implications for water resource management. *J. Hydrol.* 458–459, 110–117. doi: 10.1016/j.jhydrol.2012.06.021

Gao, X., Zhao, X., Si, B. C., Brocca, L., Hu, W., and Wu, P. (2015). Catchment-scale variability of absolute versus temporal anomaly soil moisture: time-invariant part not always plays the leading role. *J. Hydrol.* 529, 1669–1678. doi: 10.1016/j.jhydrol.2015.08.020

Gong, Z., Ganlin, Z., Jizhi, W., Leide, Z., Dagang, Y., Xinling, R., et al. (2005). Formation and taxonomy of irrigation—silted soils in China. *Arid Zone Res.* 22, 4–10.

Hu, W., Shao, M. A., Han, F., Reichardt, K., and Tan, J. (2010). Watershed scale temporal stability of soil water content. *Geoderma* 158, 181–198. doi: 10.1016/j.geoderma.2010.04.030

Hu, W., Shao, M. A., Han, F. P., and Reichardt, K. (2011). Spatio-temporal variability behavior of land surface soil water content in shrub- and grass-land. *Geoderma* 162, 260–272. doi: 10.1016/j.geoderma.2011.02.008

Huang, Y. L., Chen, L. D., Fu, B. J., Huang, Z. L., Gong, J., and Lu, X. X. (2012). Effect of land use and topography on spatial variability of soil moisture in a gully catchment of the loess Plateau, China. *Ecohydrology* 5, 826–833. doi: 10.1002/eco.273

Ji, X. B., Kang, E. S., Chen, R. S., Zhao, W. Z., Zhang, Z. H., and Jin, B. W. (2007). A mathematical model for simulating water balances in cropped sandy soil with conventional flood irrigation applied. *Agric. Water Manag.* 87, 337–346. doi: 10.1016/j.agwat.2006.08.011

Kizito, F., Dragila, M. I., Senè, M., Brooks, J. R., Meinzer, F. C., Diedhiou, I., et al. (2012). Hydraulic redistribution by two semi-arid shrub species: implications for Sahelian agro-ecosystems. *J. Arid Environ.* 83, 69–77. doi: 10.1016/j.jaridenv.2012.03.010

Knight, A., Blott, K., Portelli, M., and Hignett, C. (2002). Use of tree and shrub belts to control leakage in three dryland cropping environments. *Aust. J. Agric. Res.* 53, 571–586. doi: 10.1071/AR01089

Li, D., and Shao, M. (2013a). One-dimensional Markov chain simulation of vertical change of soil texture in middle reaches of Heihe River, northwest China. *Trans. Chin. Soc. Agric. Eng.* 29, 71–80. doi: 10.3969/j.issn.1002-6819.2013.05.010

Li, D., and Shao, M. (2013b). Simulating the vertical transition of soil textural layers in north-western China with a Markov chain model. *Soil Res.* 51, 182–192. doi: 10.1071/SR12332

Li, X. R., He, M. Z., and Jia, R. L. (2008). The response of desert plant species diversity to the changes in soil water content in the Middle-1ower reaches of the Heihe River. *Adv. Earth Sci.* 23, 685–691.

Li, X. R., Zhang, Z. S., Huang, L., and Wang, X. P. (2013). Review of the ecohydrological processes and feedback mechanisms controlling sand-binding vegetation systems in sandy desert regions of China. *Chin. Sci. Bull.* 58, 1483–1496. doi: 10.1007/s11434-012-5662-5

Li, X. R., Zhang, Z. S., Tan, H. J., Gao, Y. H., Liu, L. C., and Wang, X. P. (2014). Ecological restoration and recovery in the wind-blown sand hazard areas of northern China: relationship between soil water and carrying capacity for vegetation in the tengger desert. *Sci. China* 57, 539–548. doi: 10.1007/s11427-014-4633-2

Liu, B., Zhao, W. Z., Chang, X. X., Li, S. B., Zhang, Z. H., and Du, M. W. (2010). Water requirements and stability of oasis ecosystem in arid region, China. *Environ. Earth Sci.* 59, 1235–1244. doi: 10.1007/s12665-009-0112-7

Miller, J., and Franklin, J. (2002). Modeling the distribution of four vegetation alliances using generalized linear models and classification trees with spatial dependence. *Ecol. Modell.* 157, 227–247. doi: 10.1016/S0304-3800(02)00196-5

Mohanty, B. P., and Skaggs, T. H. (2001). Spatio-temporal evolution and time-stable characteristics of soil moisture within remote sensing footprints with varying soil, slope, and vegetation. *Adv. Water Resour.* 24, 1051–1067. doi: 10.1016/S0309-1708(01)00034-3

Noy-Meir, I. (1973). Desert ecosystems: environment and producers. *Annu. Rev. Ecol. Syst.* 4, 25–51. doi: 10.1146/annurev.es.04.110173.000325

Porporato, A., D'odorico, P., Laio, F., Ridolfi, L., and Rodriguez-Iturbe, I. (2002). Ecohydrology of water-controlled ecosystems. *Adv. Water Resour.* 25, 1335–1348. doi: 10.1016/S0309-1708(02)00058-1

Qi, S., Honglang, X., and Fuxing, L. (2003). Productive potential of soil resources of linze in the heihe corridor. *J. Desert Res.* 23, 182–186.

Ruiz-Sinoga, J. D., Gabarrón Galeote, M. A., Martinez Murillo, J. F., and Marin, R. G. (2011). Vegetation strategies for soil water consumption along a pluviometric gradient in southern Spain. *Catena* 84, 12–20. doi: 10.1016/j.catena.2010.08.011

Shen, Q., Gao, G., Fu, B., and Lü, Y. (2014). Soil water content variations and hydrological relations of the cropland-treebelt-desert land use pattern in an oasis-desert ecotone of the Heihe River Basin, China. *Catena* 123, 52–61. doi: 10.1016/j.catena.2014.07.002

Sperry, J. S., and Hacke, U. G. (2002). Desert shrub water relations with respect to soil characteristics and plant functional type. *Funct. Ecol.* 16, 367–378. doi: 10.1046/j.1365-2435.2002.00628.x

Su, Y. Z., Zhao, H. L., Zhao, W. Z., and Zhang, T. H. (2004). Fractal features of soil particle size distribution and the implication for indicating desertification. *Geoderma* 122, 43–49. doi: 10.1016/j.geoderma.2003.12.003

Su, Y. Z., Zhao, W. Z., Su, P. X., Zhang, Z. H., Wang, T., and Ram, R. (2007). Ecological effects of desertification control and desertified land reclamation in an oasis-desert ecotone in an arid region: a case study in Hexi Corridor, northwest China. *Ecol. Eng.* 29, 117-124. doi: 10.1016/j.ecoleng.2005.10.015

Sun, C. P., Zhao, W. Z., and Yang, Q. Y. (2018). Water retention of the clay interlayer of dunes at the edge of an oasis. *Acta Ecol. Sinica* 38, 3879–3888. doi: 10.5846/stxb201705250970

Wang, G. H., Gou, Q. Q., and Zhao, W. Z. (2019). Effects of small rainfall events on *Haloxylon ammodendron* seedling establishment in Northwest China. *Curr. Sci.* 116, 121–127. doi: 10.18520/cs/v116/i1/121-127

Wang, G. H., and Zhao, W. Z. (2015). The spatiotemporal variability of groundwater depth in a typical desert-oasis ecotone. *J. Earth Syst. Sci.* 124, 799–806. doi: 10.1007/s12040-015-0571-z

Wang, S., Fu, B. J., Gao, G. Y., Yao, X. L., and Zhou, J. (2012). Soil moisture and evapotranspiration of different land cover types in the Loess Plateau, China. *Hydrol. Earth Syst. Sci.* 16, 2883–2892. doi: 10.5194/hess-16-2883-2012

Wang, T., Xue, X., Zhou, L., and Guo, J. (2015). Combating aeolian desertification in Northern China. *Land Degr. Dev.* 26, 118–132. doi: 10.1002/ldr.2190

Yi, J., Zhao, Y., Shao, M., Zhang, J., Cui, L., and Si, B. (2014). Soil freezing and thawing processes affected by the different landscapes in the middle reaches of Heihe River Basin, Gansu, China. *J. Hydrol.* 519, 1328–1338. doi: 10.1016/j.jhydrol.2014.08.042

Zhang, H., Wu, J. W., Zheng, Q. H., and Yu, Y. J. (2003). A preliminary study of oasis evolution in the Tarim Basin, Xinjing, China. *J. Arid Environ.* 55, 520–531 doi: 10.1016/S0140-1963(02)00283-5

Conflict of Interest: The authors declare that the research was conducted in the absence of any commercial or financial relationships that could be construed as a potential conflict of interest.

frontiers in Environmental Science

ORIGINAL RESEARCH
published: 29 January 2021
doi: 10.3389/fenvs.2020.585464

Water Uptake from Different Soil Depths for Desert Plants in Saline Lands of Dunhuang, NW China

*Yong-Qin Cui[1], Li-Qin Niu[1], Jin-Li Xiang[1], Jia-Huan Sun[2], Jian-Hua Xiao[2] and Jian-Ying Ma[3]**

[1]College of Resources and Environment, University of Finance and Economics, Taiyuan, China, [2]Key Laboratory of Desert and Desertification, Chinese Academy of Sciences, Lanzhou, China, [3]School of Geographical Sciences, Northeast Normal University, Changchun, China

Salinization is a major threat to the sustainability of land and water resources, especially in arid and semiarid regions. Understanding the water uptake from different soil depths for desert plants is useful for exploring salinity-tolerance mechanism in desert plants in extremely-arid and salinity-affected area. To understand water uptake from different soil depths for desert plants in Dunhuang, NW China, we used oxygen isotope composition in plant xylem water and soil water to determine the water sources in three different saline sites differing in their degree of soil electrical conductance (site 2 < site 1 < site 3). The co-existing desert plants in each saline site extracted different depth of soil water respectively: *K. foliatum* mainly used shallow soil water (0–20 cm); *H. caspica* and *N. tangutorum* mainly used deep soil water (40–200 cm); *A. sparsifolia* used water from the 120–200 cm soil layers, while *T. ramosissima* and *E. angustifolia* mainly extracted deeper soil water (>200 cm). Compared to that in saline site 2, *Tamarix ramosissima* and *Alhagi sparsifolia* can switch their water sources to deeper soil water when enduring more salt stress. Also, a significant and positive correlation between soil EC and soil water $\delta^{18}O$ values was observed, indicating the evaporation would cause increase in salt concentration and isotopic enrichment in the upper soil profile. Overall, our results suggest that plants may explore deeper soil water to adapt to salt stress under severe salinity. This work may contribute to selecting salt-tolerant plants species which is vital to saline soil rehabilitation and utilization.

Keywords: stable oxygen isotope, desert plants, saline land, soil water utilization, Dunhuang

OPEN ACCESS

Edited by:
Atsushi Tsunekawa, Tottori University, Japan

Reviewed by:
Na Li, Chinese Academy of Science, China
Shaoliang Zhang, Northeast Agricultural University, China
Takeshi Taniguchi, Tottori University, Japan

****Correspondence:***
Jian-Ying Ma
majy652@nenu.edu.cn

Specialty section:
This article was submitted to Soil Processes, a section of the journal Frontiers in Environmental Science

Received: *21 July 2020*
Accepted: *07 December 2020*
Published: *29 January 2021*

Citation:
Cui Y-Q, Niu L-Q, Xiang J-L, Sun J-H, Xiao J-H and Ma J-Y (2021) Water Uptake from Different Soil Depths for Desert Plants in Saline Lands of Dunhuang, NW China. Front. Environ. Sci. 8:585464. doi: 10.3389/fenvs.2020.585464

INTRODUCTION

Saline soil, as an important soil resource, amounts to more than 800 million hectares, which comprises over 6% of the world's total land area (Munns and Tester, 2008). Presently, the total area of saline soil resources is about 1.0×10^8 hm^2 in China (Wang, 1993), and the saline lands account for 7.74% of the total land area in Dunhuang, NW China (Sang, 2006). It is clear that abundant ecological, economic and social benefits could be attained if these saline lands are remedied and developed sufficiently. In recent decades, climate changes have profoundly affected natural and human systems (Field and Barros, 2014). Thereinto, climatic warming has intensified soil moisture evaporation and drives the soil salt to move upward, which exacerbate soil salinization (Xiao et al., 2010). There has been a temporal increase in magnitude and intensity of salt-affected soils (Qadir et al., 2000) because of irrational human practices, such as excessive fertilizer use, irrational irrigation

and deforestation. To date, soil salinization has been a worldwide problem and has attached much significance by governments and scientists (Wang, 2009). Salt accumulation in the soil generally change the soil texture and decrease the soil porosity, and consequently reduce the soil aeration and water conductance, causing differences in water use among plant species.

Soil water is a key restricting factor influencing the survival of desert plants of saline lands in arid regions. Soil depths of water uptake for plants could be determined by comparing the stable isotope hydrogen (D) and oxygen compositions (^{18}O) of soil water and plant xylem water, as the isotope composition of xylem water remains unchanged during water transport from roots to stems (Ehrlinger and Dawson, 1992; Dawson et al., 2002; Šantrůček et al., 2007). In desert ecosystems, coexisting plant species may absorb water from different sources, such as soil water at different depths, groundwater, rain, etc. The differences in root distribution have been considered to be the mechanisms for the coexistence of diversified plant species in desert ecosystems (Zhou et al., 2013; Tiemuerbieke et al., 2018). For example, most shallow-rooted grasses take advantage of water in the shallow soil layers, while shrubs utilize a deeper soil water (Soriano and Sala, 1984). Moreover, some plant species shift soil depth of water uptake under altered environmental conditions. Chen et al. (2017) reported that the main water sources for *Caragana microphylla* shifted from topsoil to deeper soil in the dry season. Zhu et al. (2014) found that the 3-year-old *Tamarix ramosissima Ledeb.* and *Lycium barbarum L.* accessed more water in the deep profile after applying irrigation. Zhai et al. (2016) made a prediction of plant vulnerability to salinity increase in a coastal ecosystem, and found that hammock trees that took up water with higher salinities, had higher $\delta^{18}O$ values of plant stem water. In addition, high soil salinity may make plant water uptake increasingly difficult owing to the changes of soil texture (Mahajan and Tuteja, 2005; Yang et al., 2007). Therefore, plants may switch to more stable water sources under some environmental stress. Thus, plants may access more deeper soil water when suffering from increasingly salinity stress in desert systems.

To date, little is known about the water sources of desert plant species in saline lands in extremely-arid regions. Little rainfall, strong evaporation and rapid groundwater table lowering (Bai, 2009) undoubtedly affects the water utilization of desert plant in saline lands in Dunhuang. Thus, the objectives of the present study are 1) to determine the soil depth of water uptake for coexsiting desert plant species in each saline site; 2) to compare the soil depth of water uptake for common plants (*Tamarix ramosissima* and *Alhagi sparsifolia*) across different saline sites. This study may provide insight into plant-soil water relation of desert plants of saline lands in extremely arid regions and will help us to fully understand the responses of species to ongoing climate changes.

DATA AND METHODS

Study Area

Our study sites were located in the westernmost point of Hexi Corridor of Gansu province, within Dunhuang City (39°40′–41°35′N, 92°13′–95°30′E; average altitude of 1,138 m), northwestern China. The study area is characterized by a typical warm temperate continental arid climate with low rainfall and intense evaporation. The average annual precipitation (1938–2003) was 39.8 mm, with more than 67% occurring from June to August, while the mean annual potential evapotranspiration (PET) was 2,486 mm (Zhang, 2008). The mean annual temperature was 9.8°C, and the minimum and maximum mean monthly temperatures are −15.6°C and 32.8°C, respectively (Zhang, 2008). In the sampling year of 2011, the annual precipitation was 38.3 mm, with 27.3 mm occurring in June-August (Data from the National Meteorological Information Centre, China Meteorological Administration). The predominant soils in study area are salinized silts and sands containing clay interlayers. Vegetation are representative of those occurring throughout Dunhuang area, and are dominated by *T. ramosissima* and *A. sparsifolia*. Water table in this study area is about 60 m below the surface (Cui, 2014). Three saline sites differing in their degree of soil electrical conductance (EC, site 2 < site 1 < site 3) were selected in this study. Detailed site information including locations, dominant species and their life forms, is shown in **Table 1**.

TABLE 1 | Geographic characteristics of study sites, plant species and life form.

Sites	Locations	Altitude(m)	Dominant species	Life form
Saline site 1	40.20°N, 94.72°E	1,110	*Tamarix ramosissima*	Shrub
			Alhagi sparsifolia	Shrub
			Kalidium foliatum	Shrub
			Elaeagnus angustifolia	Arbor
Saline *site 2*	40.21°N, 94.72°E	1,109	*Tamarix ramosissima*	Shrub
			Alhagi sparsifolia	Shrub
Saline *site 3*	40.24°N, 94.63°E	1,105	*Tamarix ramosissima*	Shrub
			Alhagi sparsifolia	Shrub
			Halostachys. caspica	Shrub
			Nitraria. tangutorum	Shrub

Sample Collection

Plant and soil sampling took place in three sites in July 2011. At each site, three plant communities (ca. 5 × 5 m^2) were randomly selected, where all sampling and measurements were conducted. 2-4 dominant plant species present in each community were studied for water uptake. Two common species, *T. ramosissima* and *A. sparsifolia*, were sampled in the three saline sites (**Table 1**).

Plant xylem sample were collected from the non-photosynthetic tissues during the morning period, and were immediately placed in 8 ml glass vials (National Scientific Company, United States) after removing the bark and phloem. The glass vials were sealed by parafilm (Alcan Packaging, WI, United States) and stored in a cool ice chest for delivery to the laboratory. In the laboratory, xylem samples were stored at −20°C before water extraction.

Concurrent with plant xylem sampling, three soil pits per site near studied plants were augured using a hand auger. Soil samples were collected at depths of 0–20 cm, 20–40 cm, 40–60 cm,

60–80 cm, 80–100 cm, 100–120 cm, 120–160 cm and 160–200 cm. Then each soil sample was separated into three parts for measurements for soil water content (SWC), soil EC, pH, ion content and stable isotope composition, respectively. Fresh soil for determination of SWC were sealed in soil tin. The soil samples for measurements of soil EC, pH, ion content were stored in plastic bags, then sieved and air-dried later. The soil samples for stable isotope analysis were immediately put into 10-ml screw-cap glass vials, then sealed with Parafilm and placed in a portable cooler for transporting back to the laboratory. To prevent evaporative isotopic fractionation, the soil samples for stable isotope analysis were stored in a refrigerator (at −20°C) in the laboratory until water extraction.

Isotopic Analyses

Water was extracted from plant stems and soil samples by cryogenic vacuum distillation (Dawson et al., 1993; Ehleringer et al., 2000; Horton et al., 2003). Water samples were measured for isotopic ratios of hydrogen (δD) and oxygen ($\delta^{18}O$) in an isotope ratio mass spectrometer (DELTA V Advantage, Thermo Fisher Scientific, Inc., Waltham, MA, United States) interfaced with an elemental analyzer (Flash EA1112 HT, Thermo Fisher Scientific, Inc., Waltham, MA, United States). The stable hydrogen and oxygen isotope were expressed as delta (δ) values per mil (%) relative to Vienna standard mean ocean water (V-SMOW) (Einbond et al., 1996), as shown in the following equation:

$$\delta = \left(\frac{R_{\text{sample}}}{R_{\text{standard}}} - 1 \right) \times 1,000,$$

where R_{sample} and R_{standard} are the ratio of the heavy to the light isotope in a sample and the standard, respectively. The analytical error for δD and $\delta^{18}O$ were ±1% and ±0.2%, respectively.

Based on the similarities in $\delta^{18}O$ values for the soil water in each layer, and $\delta^{18}O$ values of xylem water, we divided the soil profile into five major sections (0–20 cm, 20–40 cm, 40–60 cm, 60–80 cm and 80–200 cm) in the three saline lands. The isotopic composition for each depth was according to the average value of samples within each interval. The isotope values of each interval and the xylem water were analyzed by the IsoSource software (the multi-source mass balance approach) to evaluate the contribution of each soil depth to xylem water. The IsoSource mixing model (http://www.epa.gov/wed/pages/models/stableIsotopes/isosource/isosource.htm) (Phillips and Gregg, 2003) used stable isotope values to determine the relative contributions of soil water to xylem water. The source increment was defined as 1% and mass balance tolerance was defined as 0.1%.

Measurements of SWC, Soil EC, pH and Ion Content

SWC was determined by a conventional loss-on-drying method and expressed in percentage of gravimetric water content [(g water/g dry soil) × 100%] (Wang and Chen, 2010). Electrical conductivity of 1:5 water extracts, made by adding 25 g of deionized water to 5 g of each sample (Dehaan and Taylor, 2002), were used to reflect soil EC, using a DDS-307 Conductivity Meter (LeiCi Co. Ltd., Shanghai, China). Soil pH was determined by a pH-3D pH meter (ZhiGuang Co. Ltd., Shanghai, China). Ca^{2+} and Mg^{2+} were determined by EDTA complexing titration, and Na^{+} and K^{+} contents were measured with flame spectrometry using a flame photometer (FP640; Shanghai Precision Science Instrument, China). Cl- was determined with $AgNO_3$ titration, HCO_3^{-} and CO_3^{2-} were determined using titration with hydrochloric acid, and SO_4^{2+} was indirectly determined through titration with EDTA (Qadir et al. 2007).

Data Analysis

All statistical analyses were performed with SPSS software (version 17.0, SPSS Inc., Chicago, IL, United States). Multiple comparisons of isotope values for the soil water from all individual layers used a one-way analysis of variance (ANOVA) with Fisher's least significant difference method. Significance was determined at the 95% confidence level ($\alpha = 0.05$). Pearson's correlation was calculated to determine the relationship between $\delta^{18}O$ values, SWC, soil EC, and pH in soil profile. Charting was processed using the software Origin 9.0 (OriginLab Corp., Northampton, MA, United States).

RESULTS

SWC, EC and pH

Soil water content profiles varied significantly in the three saline sites (**Figure 1**). Overall, SWC was higher in the saline site three than that in the saline site one and saline site 2 ($p < 0.05$). In the saline site 1, SWC in 0–80 cm soil profile was significantly higher than that in 80–200 soil profile ($p < 0.05$): SWC varied little in the 0–80 cm soil layers, and showed a little decrease in 80–100 cm soil layers, and then increased in 100–200 cm soil layers. Significant soil profile differences were detected in the saline site 2 ($p < 0.01$): a peak of 11.3% in SWC occurred in 20–40 cm soil layer, and SWC showed little variation in 60–120 cm soil layers, and then increased steadily with depth to 11.3% again in 160–200 cm soil layers. In the saline site 3, SWC showed a decreasing trend from surface soil to deeper soil depths.

Significant site differences were detected in soil EC, especially in 20–100 cm soil layers, with lower soil EC values in the saline site two than that in the saline site one and saline site 3 ($p < 0.05$). Significant variations of soil EC among soil depths were observed in each saline site ($p < 0.05$). Soil EC decreased with soil depth and the highest soil EC was recorded in 0–20 cm soil layer in each saline site (**Figure 1**). Based on the equivalent-ratio of Cl^{-}/SO_4^{2-}, saline soil can be divided into four types of saline soil, which are chlorinate (≥4) sulfate-chlorinate (4–1), chlorinate-sulfate (1–0.5) and sulfate (<0.5) solonchak respectively (Wen, 2014). In this research, the soil salinization type of the three saline sites were the same type of saline soil which was sulfate solonchak (**Figure 2**).

No significant difference in soil pH value was observed across the three saline sites ($p > 0.05$), except that the soil pH in

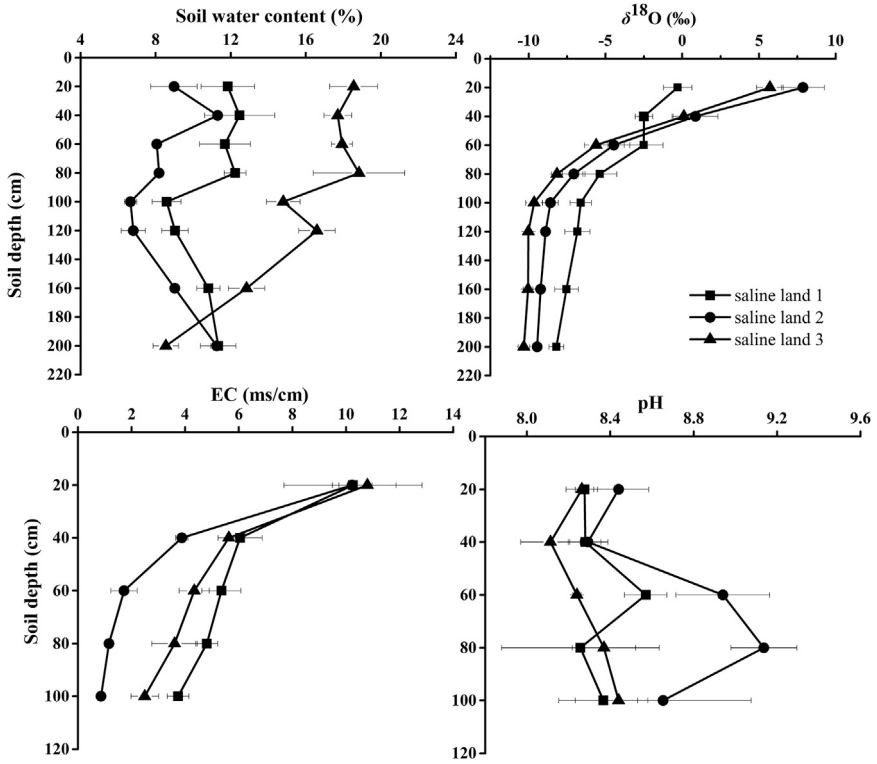

FIGURE 1 | Variation in soil water content, soil water $\delta^{18}O$ values, soil electrical conductivity (EC) and pH along soil profiles in the three saline sites. Data are presented as mean ± 1 SE.

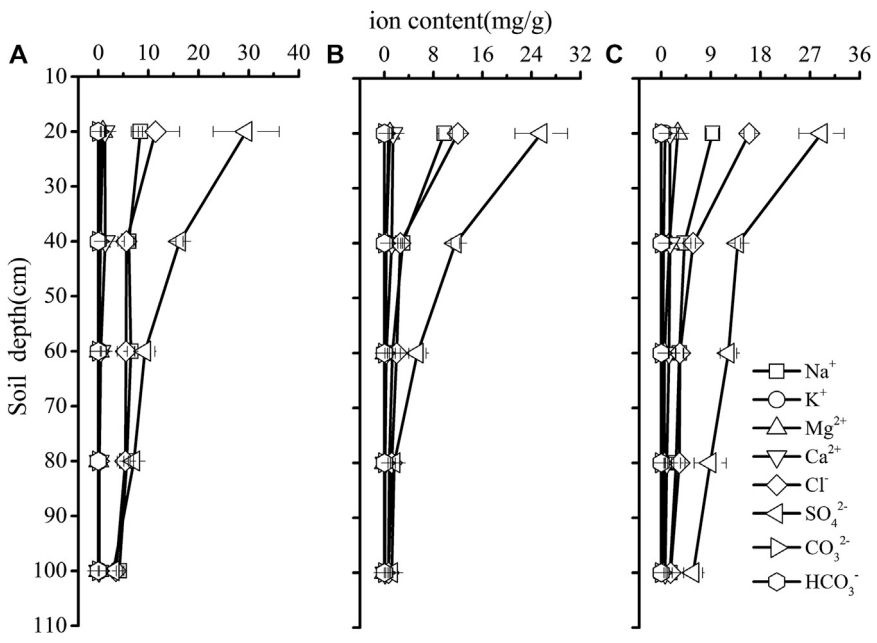

FIGURE 2 | Soil salinity distribution in the saline site 1 **(A)**, saline site 2 **(B)** and saline site 3 **(C)**. Data are presented as mean ± 1 SE.

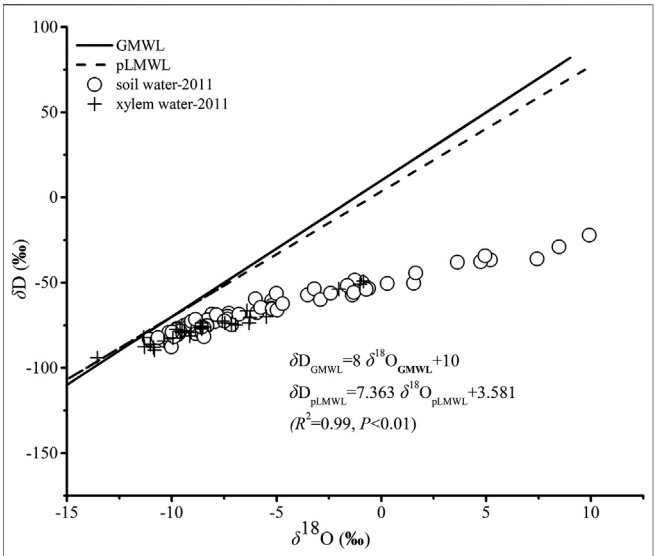

FIGURE 3 | Relationship between δD and $\delta^{18}O$ in soil water and xylem water. The Global Meteoric Water Line (GMWL) and the predicted Local Meteoric Water Line (pLMWL) were also presented.

40–60 cm soil layer was higher significantly in the saline site two than that in the saline site 3 ($p < 0.05$). In each saline site, no apparent variation was found in soil pH value among the soil layers (saline site 1: $p = 0.80$; saline site 2: $p = 0.15$; saline site 3: $p = 0.31$).

$\delta^{18}O$ Values for Soil Water and Xylem Water

There were linear relationships between δD and $\delta^{18}O$ for soil water and xylem water in the study sites (**Figure 3**). δD and $\delta^{18}O$ for Dunhuang were estimated by the Online Isotopes in Precipitation Calculator (OIPC; http://www.waterisotopes.org/) and the predicted Local Meteoric Water Line (pLMWL) was created. All the samples of soil water plotted below the global meteoric water line (GMWL) and pLMWL, indicating the strong evaporation enrichment and the extremely dry conditions. It can be noted that lower δD and $\delta^{18}O$ values were found for xylem water, indicating that the studied plants took up water predominantly from soil water with lower δD and $\delta^{18}O$ values.

The $\delta^{18}O$ values of soil water across the three saline sites differed significantly ($p < 0.05$) in some soil layers (0–20 cm and 80–200 cm) (**Figure 1**). The $\delta^{18}O$ values of soil water in each saline site showed a clear decreasing trend along the soil profile. The $\delta^{18}O$ values of soil water decreased rapidly 6.31, 16.45 and 15.36% from 0 to 100 cm in the saline land 1, saline land two and saline land three, respectively. In contrast, from 100 to 200 cm, no trend in $\delta^{18}O$ values of soil water was observed. The soil water in 0–20 cm soil layer had the highest mean $\delta^{18}O$ value (−0.30, 7.87, and 5.71% for saline site 1, saline site 2 and saline site 3, respectively). The $\delta^{18}O$ values of soil water varied significantly with soil depth, with variation in the upper layers (0–100 cm) greater than in the deep soil layers (>100 cm).

Table 2 summarizes the xylem water $\delta^{18}O$ values collected in the three saline sites. Variations in the $\delta^{18}O$ values of xylem water among plant species were observed in each saline site. In the saline site 1, *K. foliatum* had significantly higher $\delta^{18}O$ values than *A. sparsifolia*, *E. angustifolia* and *T. ramosissima* ($p < 0.01$). In the saline site 2, no apparent variation in the xylem water $\delta^{18}O$ values was observed between *T. ramosissima* and *A. sparsifolia*. In the saline site 3, *T. ramosissima* had significantly lower xylem water $\delta^{18}O$ values than *A. sparsifolia*, *H. capsica* and *N. tangutorum* ($p < 0.01$). For the same plant species, no significant difference in mean xylem water $\delta^{18}O$ values was observed across the different saline sites (*T. ramosissima*: $p = 0.07$; *A. sparsifolia*: $p = 0.66$), whereas multiple comparison tests found that the xylem water of *T. ramosissima* in the saline site two was significantly higher in ^{18}O by −1.41% than that in the saline site 3.

Water Uptake from Different Soil Depths for Desert Plants in the Three Saline Lands

We caculated the contributions of water used by plant species from five ranges of soil depths (0–40 cm, 20–40 cm, 40–60 cm, 60–80 cm and 80–200 cm) by the IsoSource model. The IsoSource outputs showed that, in the saline site 1, *K. foliatum* used average 68.3% soil water from 0 to 20 cm soil layers, and there was no IsoSource solution for *A. sparsifolia*, *E. angustifolia* and *T. ramosissima*, because the mean xylem water $\delta^{18}O$ values were beyond the confine of those of potential water sources (**Table 3**). Then we inferred the soil depth of water extraction by *A. sparsifolia*, *E. angustifolia* and *T. ramosissima* by the overlapping $\delta^{18}O$ values for xylem water and soil water (**Figure 4**). In the saline site 1, *A. sparsifolia* extracted water from the 120–200 cm soil layers, while the $\delta^{18}O$ values of *T. ramosissima* and *E. angustifolia* were more negative than those of 0–200 cm soil water, which indicated that *T. ramosissima* and *E. angustifolia* mainly extracted deeper soil water (>200 cm).

The IsoSource outputs showed that *A. sparsifolia* primarily used soil water from 80 to 200 cm (average 80.2%) and there was no IsoSource solution for *T. ramosissima* in the saline site 2 (**Table 3**). Overlapping $\delta^{18}O$ values for xylem water of *T. ramosissima* and soil water were detected in the saline site 2. We inferred *T. ramosissima* utilized water from 120-200 cm soil layers (**Figure 4**).

TABLE 2 | The $\delta^{18}O$ values of plant xylem water in the three saline *sites*.

Sites	Species	xylem water $\delta^{18}O$ ± SE (%)
Saline site 1	*T. ramosissima*	−9.97 ± 0.49^{a}
	A. sparsifolia	−9.75 ± 1.94^{a}
	E. angustifolia	−10.17 ± 0.59^{a}
	K. foliatum	−1.30 ± 0.37^{b}
Saline site 2	*T. ramosissima*	−9.65 ± 0.38^{a}
	A. sparsifolia	−8.21 ± 0.38^{a}
Saline site 3	*T. ramosissima*	−11.06 ± 0.12^{a}
	A. sparsifolia	−8.61 ± 0.58^{b}
	H. caspica	−6.33 ± 0.04^{c}
	N. tangutorum	−6.98 ± 0.87^{bc}

Data are presented as mean ± 1 SE.

^{a,b,c}Statistically significant differences among different species in each saline site ($p < 0.05$; LSD).

TABLE 3 | Properties of feasible water sources (%) for desert plants in the three saline lands [mean (min-max)].

Sites	Species	Water sources				
		Soil depths (cm)				
		0–20	20–40	40–60	60–80	80–200
Saline land 1	*T. ramosissima*	—	—	—	—	—
	A. sparsifolia	—	—	—	—	—
	E. angustifolia	—	—	—	—	—
	K. foliatum	68.3 (55–85)	11.8 (0–43)	11.7 (0–45)	4.8 (0–19)	3.4 (0–14)
Saline land 2	*T. ramosissima*	—	—	—	—	—
	A. sparsifolia	1 (0–4)	2 (0–8)	4.9 (0–18)	11.9 (0–42)	80.2 (58–94)
Saline land 3	*T. ramosissima*	—	—	—	—	—
	A. sparsifolia	2 (0–8)	3.3 (0–13)	8.3 (0–32)	20.6 (0–76)	65.7 (24–90)
	H. caspica	6.8 (0–23)	10.6 (0–36)	22.6 (0–83)	29.6 (0–86)	30.5 (0–75)
	N. tangutorum	5.1 (0–19)	8.1 (0–30)	18.6 (0–68)	31.7 (0–91)	36.5 (0–80)

Note: Oxygen isotope values were used for the calculations. Average source proportions calculated by the model are shown, as well as range of minimum and maximum source proportions. "–"indicate no IsoSource solution.

The IsoSource outputs showed that average 65.7% of water source of *A. sparsifolia* came from 80 to 200 cm soil layers, *H. caspica* and *N. tangutorum* used little water from depths of 0–20 cm (average 6.8% and 5.1%, respectively), instead derived most of its water from deeper soil layers (40–200 cm) in the saline site 3 (**Table 3**). There was no IsoSource solution for *T. ramosissima*, and the $\delta^{18}O$ values of *T. ramosissima* were more negative than those of 0–200 cm soil water. So, we inferred that *T. ramosissima* mainly extracted soil water at depths of >200 cm in the saline site 3 (**Figure 4**).

Relationship Between SWC, Soil EC and Soil Water $\delta^{18}O$

The relationship between SWC and soil water $\delta^{18}O$ values in 0–200 cm soil profile was analyzed for each saline site, and the result showed that SWC correlated positively with soil water $\delta^{18}O$ values for 0–200 cm soil profile in the saline site 1 ($R = 0.42$, $p > 0.05$) and saline site 3 ($R = 0.49$, $p < 0.05$), while no obvious correlation was observed in the saline site 2 ($R = 0.20$, $p = 0.35$). Whereas, it was found that there was no significant correlation between SWC and soil water $\delta^{18}O$ values in 0–200 cm soil profiles of the whole study area either ($R = 0.18$, $p = 0.13$). The correlations among SWC, soil water $\delta^{18}O$, soil EC, and soil pH values in the 0–100 cm soil profile were also analyzed for each saline site. For the 0–100 cm soil profile, soil EC correlated positively with soil water $\delta^{18}O$ values in each saline site, but no significant correlation was observed between SWC and soil water $\delta^{18}O$ values (**Table 4**).

DISCUSSION

Variations in Soil Water Isotopic Composition

In the three studied saline sites, a vertical isotopic gradient in soil water $\delta^{18}O$ profiles was observed (**Figure 4**), with ^{18}O-enrichment of surface soil water, indicating the occurrence of evaporation. The light isotope is easier to evaporate during evaporation, which makes the liquid water enrich in heavy isotopes, and evaporation mainly occurs in the soil surface layer (Li and Liu, 2008). Therefore, along the soil depths, the enrichment of heavy isotopes decreases (**Figure 4**). Zimmermann et al. (1967) reported the effect of soil water evaporation on hydrogen isotopes. They showed that evaporation at the surface of a saturated soil column leads to D-enrichment near the surface soil layer, which decreases exponentially with soil depths. The enrichment trend may occur as a result of several processes, including evaporation, change in isotopic composition of precipitation and mixing of new and old water. However, the average annual rainfall of Dunhuang is only 39.8 mm (Data from the National Meteorological Information Centre, China Meteorological Administration). Under such extremely arid climate conditions, the rain has evaporated before it infiltrates into the soil. Therefore, in this study, the impact of precipitation on soil water could be ignored. Similar soil water $\delta^{18}O$-profiles were also found in the Heihe Basin (Zhao et al., 2008; Zhou et al., 2011; Zeng and Ma, 2013). Zhao et al. (2008) evaluated water sources of riparian plants in the extremely arid region along the lower reaches of the Heihe River basin by stable isotope technique. They found that soil water isotope concentrations decreased approximately exponentially with depth to a relatively constant concentration. Zhou et al. (2011) used D and ^{18}O to determine the water sources of sand dune plants in middle reaches of Heihe River, and showed δ D and $\delta^{18}O$ values of soil water decreased as a typical exponential function of depth, except that some details of the exponential curve were altered by the infiltration of individual rainfall events. Zeng and Ma (2013) also found that δ D and $\delta^{18}O$ values of soil water soil water decreased along soil depths in two different habitats (oasis-desert transitional zone and desert) in the Heihe River Basin.

In previous studies in arid regions, it was found that soil with less water content in the upper layers usually has more enriched $\delta^{18}O$ values, and soil with more water content in the deeper soil layers has more depleted $\delta^{18}O$ values (Wu et al., 2014; Liu et al., 2015; Zhou et al., 2015). However, no significant and negative correlations between SWC and soil water $\delta^{18}O$ values were

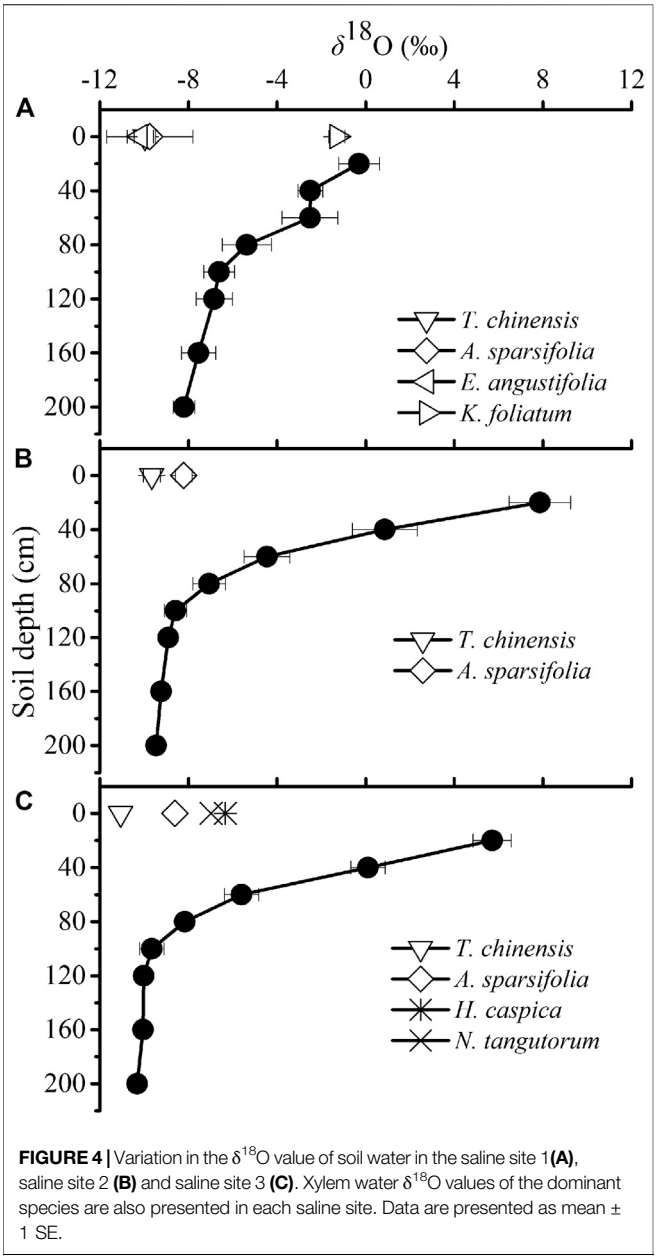

FIGURE 4 | Variation in the $\delta^{18}O$ value of soil water in the saline site 1**(A)**, saline site 2 **(B)** and saline site 3 **(C)**. Xylem water $\delta^{18}O$ values of the dominant species are also presented in each saline site. Data are presented as mean ± 1 SE.

observed in each saline site. It is noted that significantly positive correlation or no obvious correlation were found between SWC and soil water $\delta^{18}O$ values in this study, which is incongruous with previous result that soil water content is negatively correlated with soil water $\delta^{18}O$ values (Zhu et al., 2014; Cui et al., 2017). Whereas, a significant and positive correlation between soil EC and soil water $\delta^{18}O$ values in 0–100 cm soil profile was observed in each saline site (**Table 4**), indicating that intense evaporation exerted significant enrichment effects on soil water $\delta^{18}O$ values in soil profiles and cause more soil salt assembled on soil surface. Zhu et al. (2014) investigated the water uptake for halophyte grown in Northern area of Ningxia plain (China) in contrasted water regimes, and found similar relations that significant and positive correlations between soil salt content and soil water $\delta^{18}O$ values. The positive correlation between salinity and $\delta^{18}O$ was also observed in many field studies on water table, such as Sternberg et al. (1991); Lin and Sternberg (1994), Ewe et al. (2007), which may result from mixing of freshwater with low $\delta^{18}O$ values and saline seawater with high $\delta^{18}O$ values. Zhai et al. (2016) found there was a curvilinear relationship between salinity and the $\delta^{18}O$ values in the vadose zone. However, it was considered that high salinity will significantly restrain the evaporation fractionation of soil water, and thus δ D and $\delta^{18}O$ values will be depleted (Li and Qiu. 2018; Din et al., 2020). In this study, heavy isotopes (^{18}O) were enriched in the liquid phase as water evaporated due to intense soil evaporation (Li and Qiu. 2018). Meanwhile, stronger soil evaporation could cause more salt accumulation and even surface assembled.

Variations in Soil Depth of Water Uptake for Different Desert Plants in Each Saline Site

Co-existing desert plant species in the same saline site exhibited obvious variations in depth of water uptake respectively. In the saline site 1, *K. foliatum* used average 68.3% soil water from 0 to 20 cm soil layers; *A. sparsifolia* extracted water from the 120–200 cm soil layers, while *T. ramosissima* and *E. angustifolia* mainly extracted deeper soil water (>200 cm). In the saline site 2, *A. sparsifolia* primarily used soil water from 80 to 200 cm (average 80.2%) and *T. ramosissima* utilized water from 120–200 cm soil layers. In the saline site 3, *A. sparsifolia* used average 65.7% soil water from 80 to 200 cm soil layers; *H. caspica* and *N. tangutorum* derived most of water from deeper soil layers (40–200 cm); *T. ramosissima* mainly extracted soil water at depths of >200 cm (**Table 3**). The xylem water $\delta^{18}O$ values varied among the studied co-occurring plant species in the studied sites, which indicated that interspecific differences in water absorption. The differences in xylem water $\delta^{18}O$ values is very small, but the water sources may vary among the co-occurring plant species (Min et al. 2019). The variations in soil depth of water uptake for co-occurring plant species would lead to niche segregation and complementary use of limited water resources, and facilitated plant species co-existence (Asbjornsen et al., 2008). In this study, *K. foliatum* depended mainly on shallow soil water, which is in accordance with its root distribution pattern (a relatively shallow root system with taproots penetrate to 20–30 cm deep and spindly adventitious roots) (Shi and Wang, 2003; Yang et al., 2013). *A. sparsifolia* utilized deep soil water in the three saline sites. Wang et al. (2017) got similar result that during the growing season, *A. sparsifolia* acquired soil water stored at 50–200 cm soil depth in the lower reaches of Tarim River. It has been reported that *A. sparsifolia*'s roots could penetrate up to 12–30 m deep (Shi, 2003). In this study *E. angustifolia* extracted soil water below the depth of 200 cm. *E. angustifolia* is a kind of deciduous tree, and it has been reported that their roots can extend into deeper soil layers (Shi and Qu, 2003). *H. caspica* and *N. tangutorum* mainly derived water from 40-200 cm soil depths in saline site 3. This is accordance with their root distribution that their absorbing roots mainly developed in 0–200 cm soil layers (Sun and Yu, 1992). In this study *T. ramosissima* attached soil water of middle

TABLE 4 | Relationship among soil water content (SWC), soil water oxygen composition, soil electrical conductivity (EC) and pH (0–100 cm).

	Saline land 1				Saline land 2				Saline land 3			
	SWC	**$\delta^{18}O$**	**EC**	**pH**	**SWC**	**$\delta^{18}O$**	**EC**	**pH**	**SWC**	**$\delta^{18}O$**	**EC**	**pH**
SWC	1.00				1.00				1.00			
$\delta^{18}O$	0.42	1.00			0.44	1.00			0.29	1.00		
EC	0.60*	0.60*	1.00		0.32	0.94**	1.00		0.48	0.91**	1.00	
pH	−0.31	−0.14	−0.22	1.00	−0.25	-0.53*	−0.43	1.00	−0.65**	−0.36	−0.42	1.00

*Note: Asterisk represents the significance of coefficient, *p < 0.05, **p < 0.01.*

or deep soil layers. There are many literatures on *T. ramosissima*' water sources by stable isotope technique, which got the result that *T. ramosissima* was a facultative phreatophyte and mainly relied on deep soil water and groundwater (Zhou et al., 2013; Wang et al., 2017). For example, Studies in the southeastern Junggar Basin have shown that *T. ramosissima* obtained 90% of its water from deep soil water and groundwater (Zhou et al., 2013). The vertical root distribution seemed determine the soil depth from which plant species can potentially access water (Ehleringer et al., 1991; Xu and Li 2006; Zhou et al., 2015; Zhang et al., 2017). However, some study in the Gurbantonggut desert found that *T. ramosissima* mainly relied on middle to deep soil water (Tiemuerbieke et al., 2018). This inconsistency suggests that plant water uptake was determined by root activity rather than root presence (Dawson and Ehleringer, 1991; Prechsl et al., 2015). Moreover, Imada et al. (2013) reported that *T. ramosissima's* fine root distribution was drastically changed by soil water and nutrient distribution. So, it is indicated that the distribution of active roots showed substantial ecological plasticity in response to soil water and nutrient. Overall, root is an important determinant of the availability of soil water and is closely related with plant–water relations (Nippert et al., 2010).

Variations in Soil Depth of Water Uptake for Common Desert Plants Across the Three Saline Sites

For the common species, despite no habitat effects on xylem water $\delta^{18}O$ values, the depth of water uptake for common species differed across the three saline sites. According to **Figure 4**; **Table 3**, we compared the soil depth from which common plant species may access across the three saline sites, and observed that *T. ramosissima* and *A. sparsifolia* attached more shallow soil water in the saline site 2 than in the saline site 1 and 3. The soil EC in the saline site 2 was the lowest among the three saline sites. This accordance with changes in soil EC suggests that *T. ramosissima* and *A. sparsifolia's* water use could be influenced, to some extent, by soil salinity. Thus, we attempted to propose that it was likely that the widely distributed desert plants exhibited certain plasticity in water use to access deeper water sources to cope with salt stress in the saline habitats. Similar results were reported that woody plants endured salt stress by spatial partitioning and temporal shift in water absorption in the Everglades ecotone and coastal ecosystems (Ewe et al., 1999, Ewe et al., 2007; Ewe and Sternberg 2002). It has been reported that desert plants may shifted to deeper soil water to suffer salt stress in Xinjiang, northwest China (Min et al., 2019). In this study, soil EC, SO_4^{2-}, Cl^- and Na^+ decreased with soil depths (**Figures 1**, **2**), and soil salinity declined with depths. Salt accumulation in the soil generally change the soil texture and decrease the soil porosity, and consequently reduce the soil aeration and water conductance (Min et al., 2019). Moreover, high soil salinity cause plants access water more difficultly (Mahajan and Tuteja 2005; Yang et al., 2007). Therefore, the ability to explore and utilized deeper water sources ensure these desert plants to acclimate to environments stresses.

CONCLUSION

Our research indicated that niche complementarity for water resources among coexisting desert species is the potential mechanism for water-limited and salinity-effected ecosystems, which could maintain a resilient community under drought stress and salt stress. In each saline site, contrasting soil depths of water use for each desert species were mainly determined by their distinct root distributions, which cause water source partitioning. The studied common plant species would access more deeper soil water in more saline habitat, implying *T. ramosissima* and *A. sparsifolia* had the ability to shift to deeper soil water to suffer salt stress. A better understanding of plants physiological responses to different soil salinities would facilitate to rehabilitate saline soil and provide a scientific basis for ecosystem protection and management in arid and semiarid environment.

DATA AVAILABILITY STATEMENT

The raw data supporting the conclusions of this article will be made available by the authors, without undue reservation.

AUTHOR CONTRIBUTIONS

All authors listed have made a substantial, direct and intellectual contribution to the work, and approved it for publication

FUNDING

The work was financially supported by the Opening Foundation of Key Laboratory of Desert and Desertification, Chinese

Academy of Sciences (KLDD-2018–007), the Scientific and Technological Innovation Programs of Higher Education Institutions in Shanxi (2019L0483), National Natural Science Foundation of China (41671207).

ACKNOWLEDGMENTS

We would like to thank Qiao Zeng and Tianyang Fu for help during field and laboratory work.

REFERENCES

Asbjornsen, H., Shepherd, G., Helmers, M. J., and Mora, G. (2008). Seasonal patterns in depth of water uptake under contrasting annual and perennial systems in the Corn Belt Region of the Midwestern. *U.S. Plant and Soil*. 308, 69–92. doi:10.1007/s11104-008-9607-3

Bai, Y. (2009). Assessment on agricultural ecological security in Dunhuang Oasis. MS dissertation. Lanzhou (China): Northwest Normal University.

Chen, D. S., Dong, Z. W., Gao, L., Chen, X. M., Peng, X. H., Si, B. C., et al. (2017). Water-use process of two desert shrubs along a precipitation gradient in Horqin Sandy Land. *Chinese Journal of Plant Ecology* 41 (12), 1262–1272. doi:10.17521/cjpe.2017.0219

Cui, Y.-Q., Ma, J.-Y., Feng, Q., Sun, J.-H., and Sun, W. (2017). Water sources and water-use efficiency of desert plants in different habitats in Dunhuang, NW China. *Ecol. Res.* 32 (2), 243–258. doi:10.1007/s11284-017-1433-8

Cui, Y.-Q. (2014). Water sources and water-use efficiency of desert plants in Dunhuang area, Gansu China. MS dissertation. Beijing (China): Chinese Acadamy of Sciencies.

Dawson, T., Ehleringer, J., Hall, A., and Farquhar, G. (1993). "Water sources of plants as determined from xylem-water isotopic composition: perspectives on plant competition, distribution, and water relations," in *Stable isotopes and plant carbon-water relations*. Editors J. R. Ehleringer and G. D. Farquhar (Cambridge, MA: Academic Press Inc.), 465–496.

Dawson, T., and Ehleringer, J. (1991). Streamside trees that do not use stream water. *Nature* 350 (6316), 335–337. doi:10.1038/350335a0

Dawson, T., Mambelli, S., Plamboeck, A., Templer, P., and Tu, K. (2002). Stable isotopes in plant ecology. *Annu. Rev. Ecol. Systemat.* 33, 507–559. doi:10.1146/annurev.ecolsys.33.020602.095451

Dehaan, R. L., and Taylor, G. R. (2002). Field-derived spectra of salinized soils and vegetation as indicators of irrigation-induced soil salinization. *Remote Sensing of Environment* 80 (3), 406–417. doi:10.1016/S0034-4257(01)00321-2

Din, J., Liu, Y. F., Liu, Q., and Wang, J. J. (2020). Dynamic variation characteristics of hydrogen and oxygen stable isotope composition in soil water after salt water irrigation in arid area. *Saf. Environ. Eng.* 27 (3), 32–39. doi:10.13578/j.cnki.issn.1671-1556.2020.03.005

Ehleringer, J. R., Phillips, S. L., Schuster, W. S. F., and Sandquist, D. R. (1991). Differential utilization of summer rains by desert plants. *Oecologia* 88 (3), 430–434.

Ehleringer, J. R., Roden, J., and Dawson, T. E. (2000). "Assessing ecosystem-level water relations through stable isotope ratio analyses," in *Methods in ecosystem science*. Editors O. E. Sala, R. B. Jackson, H. A. Mooney, and R. W. Howarth (Heidelberg: Springer-Verlag), 181–198.

Ehrlinger, J., and Dawson, T. (1992). Water uptake by plants: perspectives from stable isotope composition. *Plant Cell Environ.* 15 (9), 1073–1082.

Einbond, A., Sudol, M., and Coplen, T. (1996). New guidelines for reporting stable hydrogen, carbon, and oxygen isotope-ratio data. *Geochem. Cosmochim. Acta* 60 (17), 3359–3360.

Ewe, S. M., and Sternberg, D. L. (2002). Seasonal water-use by the invasive exotic, Schinus terebinthifolius, in native and disturbed communities. *Oecologia* 133, 441–448. doi:10.1007/s00442-002-1047-9

Ewe, S. M., Sternberg, Lda. S., and Childers, D. L. (2007). Seasonal plant water uptake patterns in the saline southeast Everglades ecotone. *Oecologia* 152, 607–616. doi:10.1007/s00442-007-0699-x

Ewe, S. M. L., Sternberg, L. D. S. L., and Busch, D. E. (1999). Water-use patterns of woody species in pineland and hammock communities of South Florida. *For. Ecol. Manag.* 118, 139–148.

Field, C. B., and Barros, V. R., and Intergovernmental Panel on Climate Change (2014). *Climate Change 2014: Impacts,Adaptation, and Vulnerability. Part A: Global and Sectoral Aspects. Contribution of Working Group II to the Fifth Assessment Report of the Intergovernmental Panel on Climate Change*. Cambridge, United Kingdom: Cambridge University Press.

Horton, J., Hart, S., and Kolb, T. (2003). Physiological condition and water source use of Sonoran Desert riparian trees at the Bill Williams River, Arizona, United States. *Isot. Environ. Health Stud.* 39 (1), 69–82. doi:10.1080/1025601031000096772

Imada, S., Taniguchi, T., Acharya, K., and Yamanaka, N. (2013). Vertical distribution of fine roots of *Tamarix ramosissima* in an arid region of southern Nevada. *J. Arid Environ.* 92, 46–52. doi:10.1016/j.jaridenv.2013.01.006

Li, J. Z., and Liu, X. Z. (2008). Advances of stable hydrogen and oxygen isotope applied in spac water cycle. *J. Desert Res.* 28 (4), 787–794.

Li, T., and Qiu, G. Y. (2018). Hydrogen and oxygen stable isotope study on the difference of evaporation between salt and pure water. *Trop. Geogr.* 38 (6), 857–865. doi:10.13284/j.cnki.rddl.003084

Lin, G., and Sternberg, L. D. S. L. (1994). Utilization of surface water by red mangrove (*Rhizophora mangle* L.): an isotopic study. *Bull. Mar. Sci.* 54, 94–102.

Liu, S., Chen, Y., Chen, Y., Friedman, J., Hati, J., and Fang, G. (2015). Use of ^{2}H and ^{18}O stable isotopes to investigate water sources for different ages of Populus euphratica along the lower Heihe River. *Ecol. Res.* 30 (4), 581–587. doi:10.1007/s11284-015-1270-6

Mahajan, S., and Tuteja, N. (2005). Cold, salinity and drought stresses: an overview. *Arch. Biochem. Biophys.* 444, 139–158. doi:10.1016/j.abb.2005.10.018

Min, X. J., Zang, Y. X., Sun, W., and Ma, J. Y. (2019). Contrasting water sources and water-use efficiency in coexisting desert plants in two saline-sodic soils in northwest China. *Plant Biol. (Stuttg)* 21 (6), 1150. doi:10.1111/plb.13028

Munns, R., and Tester, M. (2008). Mechanisms of salinity tolerance. *Annu. Rev. Plant Biol.* 59, 651–681. doi:10.1146/annurev.arplant.59.032607.092911

Nippert, J. B., Butler, J. J., Kluitenberg, G. J., Whittemore, D. O., Arnold, D., Spal, S. E., et al. (2010). Patterns of Tamarix water use during a record drought. *Oecologia* 162 (2), 283–292. doi:10.1007/s00442-009-1455-1

Phillips, D., and Gregg, J. (2003). Source partitioning using stable isotopes: coping with too many sources. *Oecologia* 136 (2), 261–269. doi:10.1007/s00442-003-1218-3

Prechsl, U. E., Burri, S., Gilgen, A. K., Kahmen, A., and Buchmann, N. (2015). No shift to a deeper water uptake depth in response to summer drought of two lowland and sub-alpine C_3-grasslands in Switzerland. *Oecologia* 177 (1), 97–111. doi:10.1007/s00442-014-3092-6

Qadir, M., Ghafoor, A., and Murtaza, G. (2000). Amelioration strategies for saline soils: a review. *Land Degrad. Dev.* 11 (6), 501–521. doi:10.1002/1099-145X(200011/12)11:63.0.CO;2-S

Qadir, M., Oster, J. D., Schubert, S., Noble, A. D., and Sahrawat, K. L. (2007). Phytoremediation of sodic and saline-sodic soils. *Adv. Agron.* 96, 197–247. doi:10.1016/S0065-2113(07)96006-X

Sang, X. F. (2006). Visual simulation and management of groundwater in Dunhuang Basin. MS dissertation. Lanzhou (China): Lanzhou University.

Šantrůček, J., Květoň, J., Šetlík, J., and Bulíčková, L. (2007). Spatial variation of deuterium enrichment in bulk water of snowgum leaves. *Plant physiology* 143 (1), 88–97. doi:10.1104/pp.106.089284

Shi, Y. J. (2003). Alhagi sparsifolia. *J. Tradit. Chin. Vet. Med.* 44–45. doi:10.13823/j.cnki.jtcvm.2003.s1.048

Shi, Y. J., and Qu, J. M. (2003). Elaeagnus angustifolia. *J. Tradit. Chin. Vet. Med.* 154–155. doi:10.13823/j.cnki.jtcvm.2003.s1.070

Shi, Y. J., and Wang, C. L. (2003). Kalidium foliatum. *J. Tradit. Chin. Vet. Med.* 142–144. doi:10.13823/j.cnki.jtcvm.2003.s1.047

Soriano, A., and Sala, O. (1984). Ecological strategies in Patagonian arid steppe. *Vegetatio* 56, 9–15.

Sternberg, L. D., Ish-Shalom-Gordon, N., Ross, M., and O'Brien, J. (1991). Water relations of coastal plant communities near the ocean/freshwater boundary. *Oecologia* 88 (3), 305–310. doi:10.1007/BF00317571

Sun, X., and Yu, Z. (1992). A study on root system of *Nitraria Tangutorum*. *J. Desert Res.* 12 (4), 50–54.

Tiemuerbieke, B., Min, X. J., Zang, Y. X., Xing, P., Ma, J. Y., and Sun, W. (2018). Water use patterns of co-occurring C_3 and C_4 shrubs in the Gurbantonggut desert in northwestern China. *Sci. Total Environ*. 634, 341–354. doi:10.1016/j.scitotenv.2018.03.307

Wang, T. (2009). Review and prospect of research on oasification and desertification in arid regions. *J. Desert Res*. 29 (1), 1–9.

Wang, Y. S., and Chen, J. S. (2010). Study of stable isotope model for saturated soil water movement in the condition of evaporation. *J. Sichuan Univ. (engineering science edition)* 42 (1), 10–13. doi:10.3969/j.issn.1002-10.15961/j.jsuese.2010.01.012

Wang, Y. Y., Chen, Y. P., Li, W. H., Wang, R. Z., Zhou, Y. Y., and Zhang, J. P. (2017). Water sources of typial desert riparian plants in the lower reaches of Tarim River. *J. Desert Res*. 37 (6), 1150–1157. doi:10.7522/j.issn.1000-694x.2016.00103

Wang, Z. Q. (1993). *Saline soil in China*. Beijing: Science Press.

Wen, J. (2014). "The present condition and an analysis of control measurements of the secondary salinization of soils in the Bachu county, Xinjiang," in Proceedings of the annual conference of Chinese Society of Water Conservancy, Xuzhou, China, December 29, 2014 (Tianjin, China: Chinese Hydraulic Engineering Society). Editors W. Sui, Y. Sun, and C. Wang, 654–661.

Wu, Y., Zhou, H., Zheng, X.-J., Li, Y., and Tang, L.-S. (2014). Seasonal changes in the water use strategies of three co-occurring desert shrubs. *Hydrol. Process*. 28 (26), 6265–6275. doi:10.1002/hyp.10114

Xiao, G. J., Zhang, Q., Li, Y., Zhang, F. J., Wang, R. Y., and Luo, C. K. (2010). Impact of climatic warming on soil salinity and irrigation amount of Yellow River irrigation areas in Ningxia Hui Autonomous Region. *Transactions of CSAE* 26 (6), 7–13. doi:10.3969/j.issn.1002-6819.2010.06.002

Xu, H., and Li, Y. (2006). Water-use strategy of three central Asian desert shrubs and their responses to rain pulse events. *Plant Soil* 285 (1-2), 5–17. doi:10.1007/s11104-005-5108-9

Yang, C. W., Chong, J. N., Li, C. Y., Kim, C., Shi, D. C., and Wang, D. L. (2007). Osmotic adjustment and ion balance traits of an alkali resistant halophyte Kochia sieversiana during adaptation to salt and alkali conditions. *Plant Soil* 294, 263–276. doi:10.1007/s11104-007-9251-3

Yang, H. T., Li, X. R., Liu, L. C., Jia, R. L., Wang, Z. R., Li, X. J., et al. (2013). Biomass allocation patterns of four shrubs in desert grassland. *J. Desert Res*. 33 (5), 1340–1348. doi:10.7522/j.issn.1000-694x.2013.00197

Zeng, Q., and Ma, J. Y. (2013). Plant water sources of different habitats and its environmental indication in Heihe River basin. *J. Glaciol. Geocryol*. 35 (1), 148–155. doi:10.7522/j.issn.1000-0240.2013.0017

Zhai, L., Jiang, J., DeAngelis, D., and Sternberg, L. D. S. L. (2016). Prediction of plant vulnerability to salinity increase in a coastal ecosystem by stable isotope composition ($\delta^{18}O$) of plant stem water: a model study. *Ecosystems* 285 (19), 32–49. doi:10.1007/s10021-015-9916-3

Zhang, C., Li, X., Wu, H., Wang, P., Wang, Y., Wu, X., et al. (2017). Differences in water-use strategies along an aridity gradient between two coexisting desert shrubs (*Reaumuria soongorica* and *Nitraria sphaerocarpa*): isotopic approaches with physiological evidence. *Plant Soil* 419, 15–25. doi:10.1007/s11104-017-3332-8

Zhang, M. Y. (2008). Study on the carrying capacity of water resources in Dunhuang. MS dissertation. Lanzhou (China): Lanzhou University.

Zhao, L. J., Xiao, H. L., Cheng, G. D., Song, Y. X., Zhao, L., Li, C. Z., et al. (2008). A preliminary study of water sources of riparian plants in the lower reaches of the Heihe basin. *Acta Geosci. Sin*. 29 (6), 709–718. doi:10.1007/s40333-014-0037-1

Zhou, C. X., Sun, Z. Y., and Yu, S. W. (2011). Using D and ^{18}O stable isotopes to determine the water sources of sand dune plants in Linze, middle reaches of the Heihe River. *Geol. Sci. Technol. Inf*. 30 (5), 103–109.

Zhou, H., Zhao, W., Zheng, X., and Li, S. (2015). Root distribution of *Nitraria sibirica* with seasonally varying water sources in a desert habitat. *J. Plant Res*. 128 (4), 613–622. doi:10.1007/s10265-015-0728-5

Zhou, H., Zheng, X. J., Tang, L. S., and Li, Y. (2013). Differences and similarities between water sources of Tamarix ramosissima, Nitraria sibirica and Reaumuria soongorica in the southeastern Junggar Basin. *Chin. J. Plant Ecology* 37 (7), 665–673. doi:10.3724/SP.J.1258.2013.00069

Zhu, L., Wang, Z. H., Mao, G. L., Zheng, S. X., and Xu, X. (2014). Water uptake from different soil depths for halophytic shrubs grown in Northern area of Ningxia plain (China) in contrasted water regimes. *J. Plant Interact*. 9 (1), 26–34. doi:10.1080/17429145.2012.751139

Zimmermann, U., Ehhalt, D., and Muennich, K. O. (1967). "Soil water movement and evapotranspiration: changes in isotopic composition of the water," in *Proceedings of IAEA symposium on Isotope hydrology*. Editor M Knippner (Vienna: Int At. Energy Agency), 567–585.

Conflict of Interest: The authors declare that the research was conducted in the absence of any commercial or financial relationships that could be construed as a potential conflict of interest.

frontiers in Environmental Science

ORIGINAL RESEARCH
published: 01 February 2021
doi: 10.3389/fenvs.2021.589068

Vegetation Restoration Alters Fungal Community Composition and Functional Groups in a Desert Ecosystem

Ying Zhang[1,2], *Hongyu Cao*[1,2,3], *Peishan Zhao*[1,2,3], *Xiaoshuai Wei*[1,2,3], *Guodong Ding*[1,2,3], *Guanglei Gao*[1,2,3]* *and Mingchang Shi*[1,2]*

[1]*Key Laboratory of State Forestry and Grassland Administration on Soil and Water Conservation, Beijing Forestry University, Beijing, China,* [2]*Engineering Research Center of Forestry Ecological Engineering, Ministry of Education, Beijing Forestry University, Beijing, China,* [3]*Yanchi Research Station, School of Soil and Water Conservation, Beijing Forestry University, Beijing, China*

Revegetation is regarded as an effective means to improve the ecological environment in deserts and profoundly influences the potential ecological functions of the soil fungal community. Therefore, Illumina high-throughput sequencing was performed to characterize the soil fungal diversity and community composition at two soil depths (0–10 cm and 10–20 cm) with four revegetation durations (natural grassland, half-mature, nearly mature, and mature *Pinus. sylvestris* var. *mongolica* plantations) in the Mu Us Sandy Land, China. The effects of soil properties on soil fungal communities were also examined to reveal the connection between fungal function and soil environment. The results indicated that 1) soil nutrient content and enzyme activity showed significant differences through the restoration durations, 2) there was no significant effect of soil depth on soil fungal diversity, while the Shannon diversity index of all fungal communities was significantly different among different revegetation durations, 3) compared with grassland, ectomycorrhizal fungi (notably, *Inocybe*, *Tuber*, and *Calostoma*) were abundant in plantations. The endophyte fungus *Mortierella* was among the top 10 genera in all soil samples and arbuscular mycorrhizal fungus *Diversispora* was the indicator genus of the grassland, and 4) catalase and total nitrogen were the main factors affecting fungal community composition and were closely related to saprotrophs and pathotrophs, respectively. This new information indicates the variation of soil fungal communities along revegetation durations and highlights the interaction between fungal functions and desert ecosystems.

Keywords: revegetation duration, soil fungi, temporal variation, soil properties, symbiotrophs

OPEN ACCESS

Edited by:
Xian Xue,
Northwest Institute of Eco-Environment and Resources (CAS), China

Reviewed by:
Na Li,
Chinese Academy of Science, China
Yonglong Wang,
Baotou Teachers' College, China
Peter Edward Mortimer,
Chinese Academy of Sciences, China

***Correspondence:**
Guanglei Gao
gaoguanglei@bjfu.edu.cn
Mingchang Shi
shimc@dtgis.com

Specialty section:
This article was submitted to Soil Processes, a section of the journal Frontiers in Environmental Science

Received: *31 July 2020*
Accepted: *06 January 2021*
Published: *01 February 2021*

Citation:
Zhang Y, Cao H, Zhao P, Wei X, Ding G, Gao G and Shi M (2021) Vegetation Restoration Alters Fungal Community Composition and Functional Groups in a Desert Ecosystem. Front. Environ. Sci. 9:589068. doi: 10.3389/fenvs.2021.589068

INTRODUCTION

Due to long-term and unreasonable land use, the native land has suffered serious ecological degradation and water and soil erosion, which has resulted in the loss of ecological function and services (Nearing et al., 2017; Deng et al., 2019). Revegetation is considered an effective way to impart ecological benefits (Nunez-Mir et al., 2015; Xiao et al., 2015), including improving the quality of soil and vegetation coverage (De Deyn and Van der Putten, 2005; Wang et al., 2012), rehabilitating degraded environments (Jing et al., 2014), and accelerating the recovery of degraded lands (Qin et al.,

2019). Vegetation restoration enhances the ecological stability in restored lands along with the fosterage of soil microbial community succession (Zhang et al., 2017b; Guo et al., 2018).

Soil microbial communities play pivotal roles by maintaining ecosystem functioning and stability in response to changes in soil environment (Kubartova et al., 2012). It is logical that they are expected to be more important than physico-chemical characters and may potentially serve as primary signals for soil health and productivity (Cardinale et al., 2006; Shen et al., 2010). Fungi perform different ecological functions according to certain trophic strategies (Nguyen et al., 2016). Saprotrophs participate in the mineralization of organic matter, while pathotrophs may induce plant diseases (Bardgett and van der Putten, 2014). Symbiotrophs promote plants' ability to absorb nutrients and increase resistance to drought, heavy metals, diseases, and insect pests (Liu et al., 2007; Peay et al., 2013). The diversity and distribution of the functional groups in soil fungi determine the ecological effects of soil fungal communities, which are of great significance for the revegetation process under stress (Jin et al., 2016; Detheridge et al., 2018; Wang et al., 2020).

The temporal variation of the soil fungal community along the revegetation duration is mainly caused by abiotic factors and vegetation characteristics. Soil conditions directly influence soil fungal diversity and community composition (Marín et al., 2017; Nie et al., 2018). For example, in a global context, soil pH is the primary driver of fungal community structure and function (Tedersoo et al., 2014) and water availability may increase soil fungal community diversity and composition (Brockett et al., 2012; Zheng et al., 2017). As key components involved in carbon and nutrient cycling, functional composition of soil fungi is closely related to soil nutrients (Peay et al., 2016; Schlatter et al., 2018). Previous studies have also confirmed that soil fungi are more sensitive to soil enzyme activity than other microbial populations (Stursova et al., 2016).

The vegetation characteristics mainly include aboveground vegetation species (Pickles et al., 2015; Toju et al., 2018), species richness and diversity of vegetation (Chen et al., 2017; Francioli et al., 2020), and stand age (Miao et al., 2019; Guo et al., 2020b). In the early stage, revegetation substantially improves the physiological activities of soil fungi and changes the fungal community structure (Liu et al., 2019a; Yang et al., 2020). With the maturation of vegetation, the compositions of mycorrhizal and saprotrophic fungi are altered due to resource availability that change with plant litter, exudates, and soil properties (Husband et al., 2002; Broeckling et al., 2008; Llado et al., 2018). Therefore, it is important to elucidate the connection between revegetation duration and fungal functional groups and find the role of soil environment in driving fungal community dynamics during revegetation.

The Mu Us Sandy Land is a classical semi-arid region in Northern China, characterized by poor soil, severe nutrient depletion, scarce resources, and limited water availability. It suffers from serious water and soil erosion, hence, ecological revegetation is urgently needed. *Pinus. sylvestris* var. *mongolica* (*P. sylvestris*) originating from the Hulunbuir Sandy Land was successfully introduced into the Mu Us Sandy Land and this contributed significantly to ecological restoration (Lyu et al., 2020). So far, the changes in the below-ground microbial community along revegetation durations, particularly in a desert ecosystem remain unclear, and should be elucidated to generate an understanding of the sustainable development associated with long-term vegetation restoration and natural restoration.

Therefore, to investigate the soil fungal diversity and functional composition responses to revegetation durations, Illumina high-throughput sequencing and FUNGuild platform were used to examine soil fungal taxonomic and functional compositions at different soil depths (0–10 cm and 10–20 cm) during revegetation durations (natural grassland, half-mature, nearly mature, and mature *P. sylvestris* plantations). We hypothesized that the variation in fungal diversity and community composition was largely induced by restoration stages rather than soil depths, and that soil properties may help explain these different responses. In addition, we predicted that the potential ecological functions of some keystone/indicator fungal species were different during the revegetation durations and they further helped to reveal soil conditions and quality. Based on these hypotheses, the objectives of this study were to examine how soil fungal functional groups respond to different revegetation durations and develop their potential functions and to further identify which factors drive the dynamics of the fungal community.

MATERIALS AND METHODS

Study Site

The study site was located in the Hongshixia Sandy Botanical Garden, which is at the southern edge of the Mu Us Sandy Land (38°26′ N, 109°12′ E; 1080 m elevation), Shaanxi Province (**Fig. S1**). The region has a warm temperate continental monsoon climate with an average annual temperature of 9.1°C, average annual precipitation of 385.5 mm, and average annual evaporation of 2502 mm. The soil was classified as an azonal aeolian sandy soil with loose topsoil structure and poor water retention. The predominant vegetation types were *P. sylvestris*, *Artemisia sacrorum*, *Tribulus terrestris*, *Bidens pilosa*, and *Agropyron cristatum*.

Sample Collection

Sample collection was carried out in August 2017, with peak microbial activity in the growth season. Four 50 m × 50 m revegetation duration plots, one grassland plot, and three *P. sylvestris* plantation plots, that did not have significant interference from nurturing practices and human activities were chosen for the study. The grassland plot (natural grassland, MUg) was regarded as a control, where the understory herbs were most similar to plantations. Initially, the three plantation plots were replanted with 3-year-old *P. sylvestris* saplings. With revegetation durations of 23, 29, and 40 years, the stand ages were 26, 32, and 43 years, which represented half-mature (MUh), nearly mature (MUn), and mature (MUm) forests, respectively.

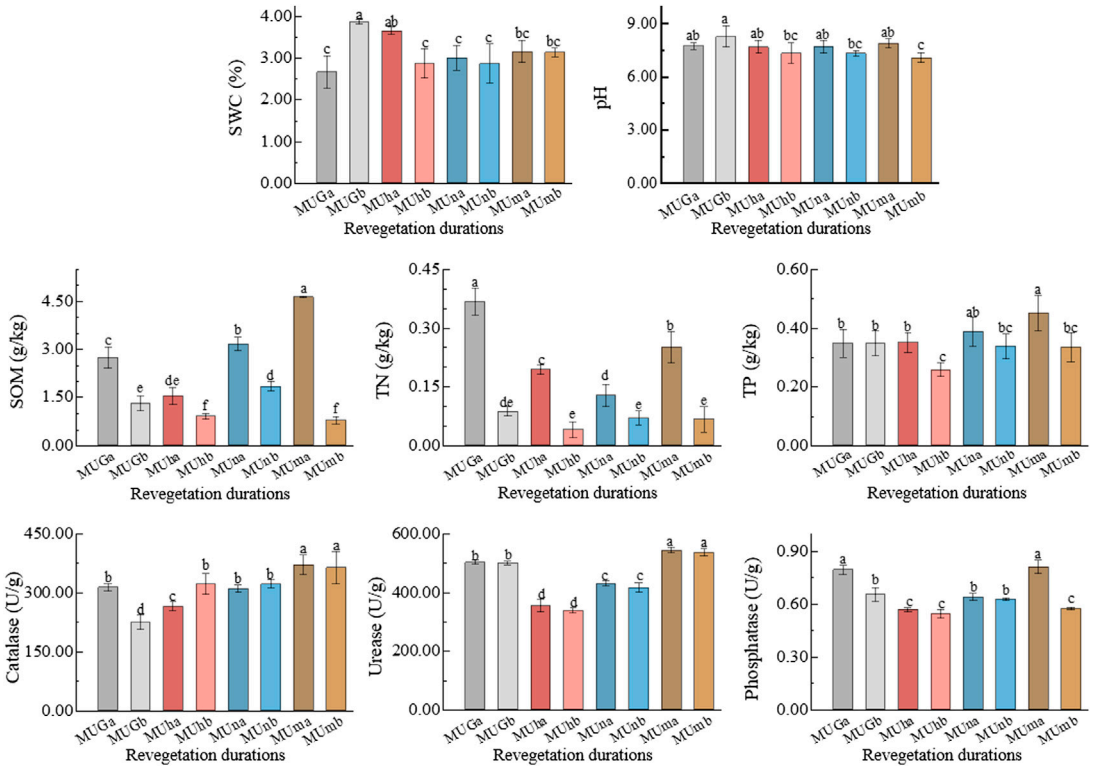

FIGURE 1 | Soil properties in different soil depths trough revegetation durations. Different letters are significantly different ($p < 0.05$).

TABLE 1 | Basic characteristics of sampling plot.

Sample name	Soil depth	Revegetation duration/(a)	Stand age/(a)	Average height/(m)	Average DBH/(cm)	Canopy density	Soil type
MUga	0–10 cm	-	-	-	-	0.78	Aeolian soil
MUgb	10–20 cm						
MUha	0–10 cm	23	26	12.48 ± 3.69	11.76 ± 3.72	0.79	
MUhb	10–20 cm						
MUna	0–10 cm	29	32	13.96 ± 2.38	13.58 ± 2.44	0.86	
MUnb	10–20 cm						
MUma	0–10 cm	40	43	14.14 ± 1.84	19.95 ± 3.03	0.73	
MUmb	10–20 cm						

Values are mean ± standard error. DBH, Diameter at breast height. MUga: 0–10 cm soil depth in grassland; MUgb: 10–20 cm soil depth in grassland; MUha: 0–10 cm soil depth in half-mature forests; MUhb: 10–20 cm soil depth in half-mature forests; MUna: 0–10 cm soil depth in narly-mature forests; MUn: 10–20 cm soil depth in narly-mature forests; MUma: 0–10 cm soil depth in mature forests; MUmb: 10–20 cm soil depth in mature forests.

In grassland, three random 1 m × 1 m quadrats were selected for inventory. In plantations, three standard trees of *P. sylvestris* were randomly chosen after measuring individual tree height, diameter at breast height, and crown width. The sampling points were the center in the quadrats and standard trees, respectively. Each sampling point was at least 10 m from the others. Three composite samples (consisting of four replicate soil samples from four directions at a sampling point) were collected from each plot. The vegetation and litter from the ground were removed to collect soil samples at a depth of 0–10 cm (a) and 10–20 cm (b) (**Table 1**). Therefore, all 24 samples from the plots (four revegetation duration plots × two soil depths × three composite samples) were packaged and labeled. Each soil sample was divided into three parts and subjected to three different procedures: 1) Take back directly to determine soil water content (SWC), soil pH, soil organic matter (SOM), total nitrogen (TN), and total phosphorus (TP). 2) Keep in a portable thermostat at 4–6°C to analyze soil catalase, urease, and phosphatase enzyme activities. 3) Store at −80°C for gene sequencing.

Soil Property Analysis

SWC was measured gravimetrically after drying the soil samples in an oven at 105°C for 12 h. Soil pH was determined from a 1:2.5

mixture of soil and water using a PHS-3E pH meter (INESA, Shanghai, China). SOM was obtained using the $K_2Cr_2O_7$-H_2SO_4 oxidation technique (Walkley and Black, 1934). An automated chemical analyzer (Smartchem 200, Italy) was used to analyze TN and TP based on the indophenol-blue spectrophotometric method and Mo-Sh anti-colorimetric analysis method, respectively (John and Matt, 1970; Mason et al., 1999). All enzyme activities were tested through antitheses, without soil and substrate (Gianfreda et al., 2005). Catalase activity was measured by performing potassium permanganate titration and expressed in milliliters of potassium permanganate devoured per hour per gram of soil. Urease and phosphatase activity were determined using a programmed microplate reader (SpectraMax Paradigm, Molecular Devices, San Jose, CA, United States), and expressed as the sum of the enzyme required to convert 1 mM of substrate in 1 min (Tarafdar and Marschner, 1994).

Sequence Data Analysis

DNA was extracted from 0.4 g soil using the PowerSoil DNA isolation kit (Mo Bio Laboratories, Carlsbad, CA, United States) according to the manufacturer's instructions. DNA concentration was quantified using a Nanodrop spectrophotometer (Thermo Scientific, United States). The fungal ITS1 region was amplified using the primers ITS1F (5'-CTTGGTCATTTAGACGAAGTA A-3') and ITS2 (5'-GCTGCGTTCTTCATCGATGC-3') (Op De Beeck et al., 2014). The AXYGEN Gel Extraction Kit (QIAGEN, Germany) and qPCR were used to detect and quantify the PCR amplification products. After gel imaging, the qualified PCR products were sent to Allwegene Technology Inc. for sequencing using the Illumina MiSeq sequencing system (Illumina, San Diego, CA, United States).

Trimmomatic and FLASH were used to filter the quality and merge the raw fastq files and sequences with quality scores >20 and <50 bp were used for analysis (Zhou et al., 2019; Guo et al., 2020a). Chimeric sequences were removed using the Usearch software package (Version 8.1.1861, http://www.drive5.com/usearch/). Sequences with 97% similarity were classified as operational taxonomic units (OTUs) (Edgar, 2013). To reduce the error caused by the different data sizes, all samples were normalized to 21,260 sequences. The Ribosomal Database Project (RDP) classifier was used to perform taxonomic assignment. Assigned taxa were verified using NCBI BLAST (https://www.ncbi.nlm.nih.gov/). All raw sequence information was deposited in GenBank (SRA accession: PRJNA663124).

Fungal functional guilds were identified using the FUNGuild platform (http://www.stbates.org/guilds/app.php) (Nguyen et al., 2016). Initially, the results with groups "highly probable" or "probable" were accepted and ambiguous groups were confirmed by previous literature findings (He et al., 2017). In this study, the fungal trophic modes were divided into symbiotroph, saprotroph, pathotroph, and combined trophic modes, which included 14 guilds. For combined trophic modes and combined guilds, they were incorporated into "Other fungi" and "Other symbiotroph/saprotroph/pathotroph fungi" groups respectively.

Data Analysis

One-way analysis of variance (ANOVA) with Duncan's multiple range test was used to determine if a significant difference existed among soil variables, while two-way ANOVA with post-hoc Tukey's tests was used to compare soil properties among soil depths and revegetation durations. All analyses were performed using SPSS 20.0 at the 0.05 significance level. Pearson's correlation was used to determine the relationship of soil variables with R-3.6.1.

For the convenience of description, we classified soil fungi according to their relative abundance as follows: dominant (>10.00%), common (10.00%–1.00%), and rare genera (<1.00%). Alpha diversities (richness and Shannon indices) based on OTU data were calculated using the 'vegan' package in R-3.6.1. The soil fungal functional groups and diversity indices were visualized using Origin 2018. Indicator species showed an ecological preference for one or a few habitat types, which were used as a prediction index for environmental changes (Cáceres and Legendre, 2009). The indicator genus of soil fungi was identified to further elucidate the distribution of soil fungi at different soil depths and revegetation durations, which were implemented using the 'indicspecies' and 'labdsv' packages in R-3.6.1. The contribution of soil depth and revegetation duration on fungal functional communities were analyzed by using Permutational multivariate analysis of variance (PERMANOVA) with the 'vegan' package in R-3.6.1.

To explain the relationship between soil properties and soil fungal functional groups, all soil properties were converted to a matrix to perform Mantel test with fungal functional groups and a visual correlation was performed using the 'corrplot' package in R-3.6.1. Subsequently, canonical correlation analysis (CCA) was performed and significance of each environmental variable was analyzed using Canoco 4.5.

RESULTS

Variations in Soil Properties due to Soil Depths and Revegetation Durations

The soil properties varied with soil depth and revegetation duration (**Figure 1**; **Supplementary Table S1**). In the *P. sylvestris* plantation, the SWC and pH in the 0–10 cm layer were higher than those in the 10–20 cm layer, while the opposite results were observed in grasslands (**Figure 1**). According to the two-way ANOVA, soil nutrients (SOM, TN, and TN) and enzyme activities (catalase, urease, and phosphatase) were significantly different among revegetation duration ($p < 0.05$; **Supplementary Table S1**). Between soil depths, significant differences were noted in the content of SOM, TN, and TP (except TP in grassland), with a higher nutrient content observed in upper soil ($p < 0.05$; **Figure 1**). In contrast, the effect of soil depth on catalase and urease activities was not significant ($p > 0.05$), and all enzyme activities had the highest values in mature forests (**Supplementary Table S1**). In addition, a strong positive correlation was observed between phosphatase and TN ($p <$

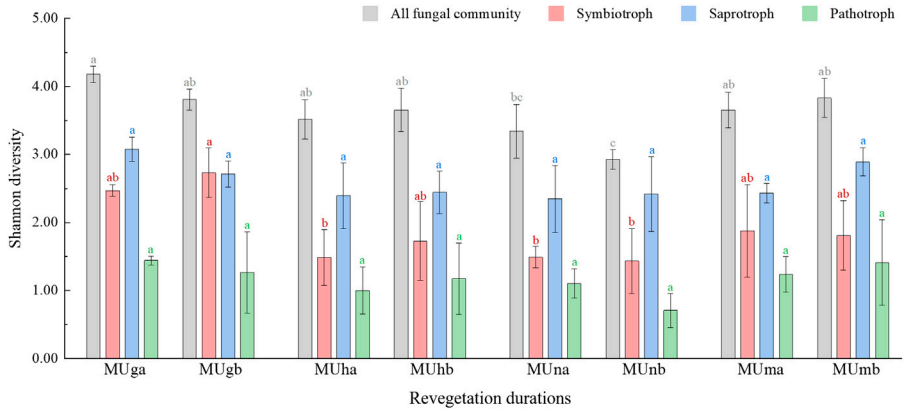

FIGURE 2 | Shannon index of all fungi community and functional groups in different soil depths trough revegetation durations. Different letters are significantly different ($p < 0.05$).

0.05), and a negative correlation was noted between catalase and SWC ($p < 0.05$; **Supplementary Table S2**).

Soil Fungal Community Diversity

In total, 831,489 high-quality sequences were clustered into 1,355 OTUs from all soil samples. There was no significant difference in richness index of all fungal communities, saprotrophs, and pathotrophs at different soil depths or revegetation durations (**Supplementary Table S3**; **Supplementary Table S4**). Soil depth did not have a significant impact on Shannon diversity ($p > 0.05$; **Supplementary Table S4**), and values of Shannon indices first decreased and then increased during restoration durations (**Figure 2**). The Shannon index showed no significant difference between different soil depths ($p > 0.05$; **Supplementary Table S4**), however, it first decreased and then increased during restoration durations (**Figure 2**). The Shannon and richness indices of symbiotrophs significantly correlated with revegetation duration ($p < 0.05$; **Supplementary Table S4**). For the alpha diversity indices of the three trophic modes, the highest values were noted in saprotrophs, followed by symbiotrophs, and lowest in pathotrophs.

The dissimilarities in soil fungal composition among different sampling plots mainly associated with revegetation duration rather than soil depth (**Supplementary Table S5**). Between soil depths, the structure showed no significant difference in all fungal communities or functional groups ($p > 0.05$), while revegetation duration significantly distinguished the fungal community composition ($p < 0.05$; **Supplementary Table S5**).

Soil Fungal Community Composition of Taxonomic and Functional Groups

All fungal OTUs were assigned to 12 phyla, 40 classes, 102 orders, 202 families, and 339 genera. Ascomycota was the dominant phylum with the highest relative abundance (60.32–79.81%), followed by Basidiomycetes (5.33–30.01%) and Mortierellomycota (1.44–10.03%; **Figure 3A**). The proportional distribution of phyla was relatively stable (**Supplementary Table S6**) and their relative abundance between soil depths showed no significant difference ($p > 0.05$); only Basidiomycota showed significant differences through restoration durations ($p < 0.05$; **Supplementary Table S6**).

The composition of functional groups was similar in each soil depth and restoration duration, however, the corresponding relative abundance fluctuated significantly (**Figure 3B**). Soil depths barely affected the relative abundance of functional groups, however, an opposite trend appeared in restoration durations (**Supplementary Table S6**). Compared with plantations, grasslands contained more unassigned fungal functional groups and fewer symbiotrophs. In plantations, saprotrophs were the dominant fungal functional groups in half-mature and mature forests, while symbiotrophs were dominant in nearly mature forests. Ectomycorrhizal (EcM) fungi constituted the most predominant portion of symbiotrophs and a small amount of arbuscular mycorrhizal (AM) and ericoid mycorrhizal fungi were observed. Plant pathogens were the main pathotrophs (**Figure 3B**).

The dominant and common genera in grasslands were different from those observed in plantations (**Supplementary Table S7**). In grasslands, there were no dominant and the common genera mostly belonged to saprotrophs, while the majority of dominant and common genera in plantations possessed symbiotic function. The endophyte fungus *Mortierella* was among the top 10 genera in all soil samples. The plant pathogen *Gibberella* and combined trophic modes fungi *Fusarium* were the top 10 genera only in grasslands and both were identified as indicator genera. In plantations, the relative abundance of *Inocybe* and *Tuber* was greater than 1.00%. In the nearly mature forest, EcM fungi *Inocybe* (14.92%) was the dominant genus and *Tomentella* (1.80%) was a common genus, and both were indicator genera. *Dactylonectria*

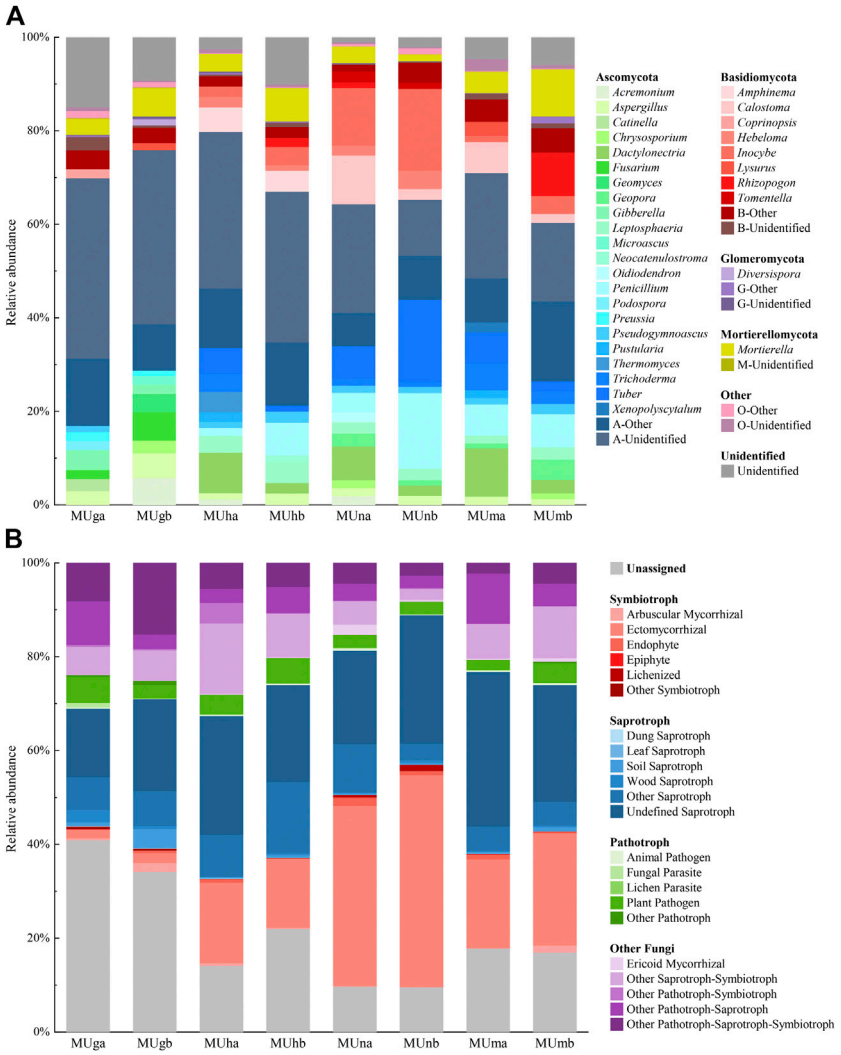

FIGURE 3 | Distribution and relative abundance of soil fungal **(A)** taxonomic and **(B)** functional groups in different soil depths trough revegetation durations. Genera>1.00% were listed.

had a higher relative abundance in topsoil and was regarded as an indicator genus of topsoil.

Relationship Between Fungal Communities and Soil Environment Factors

At different depths, soil fungal community composition through revegetation durations was driven by soil properties (**Figure 4**; **Figure 5**). Soil properties explained 40.7% of the variation in soil fungal distribution (**Figure 4**). Of these, SOM ($p = 0.025$), TN ($p = 0.043$), and phosphatase ($p = 0.003$) had a stronger impact on fungal composition, which was mainly related to topsoil in grassland and subsoil in mature forests. Catalase ($p = 0.012$) played an important role in the composition of topsoil in plantations. Furthermore, saprotrophs were significantly affected by SWC ($p < 0.05$) and catalase ($p < 0.05$; **Figure 5**). Pathotrophs showed a significant positive correlation with TN ($p < 0.05$; **Figure 5**).

DISCUSSION

Revegetation Duration Shaped Fungal Diversity and Composition

Vegetation recovery and reconstruction regulate and control the interactions between microbial communities and forest development, which mainly manifest in the dynamics of microbial diversity and structure (Cavard et al., 2011; Chanthorn et al., 2017). In this study, soil fungal community diversity and structure response to revegetation duration were investigated; these have been confirmed in abandoned farmland (Wang et al., 2020), mining area (Prado et al., 2019), and desert

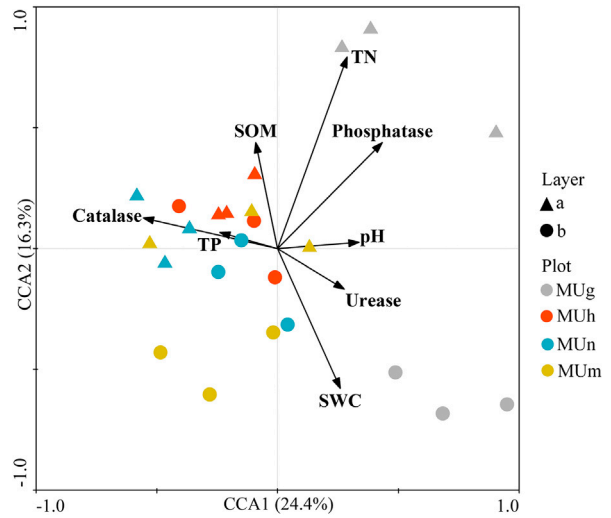

FIGURE 4 | CCA of the soil fungi communities with soil properties in different soil depths through revegetation durations. Each arrow points in the expected direction of the steepest increase of values of environment variable. The angles between arrows indicate correlations between individual environment variable.

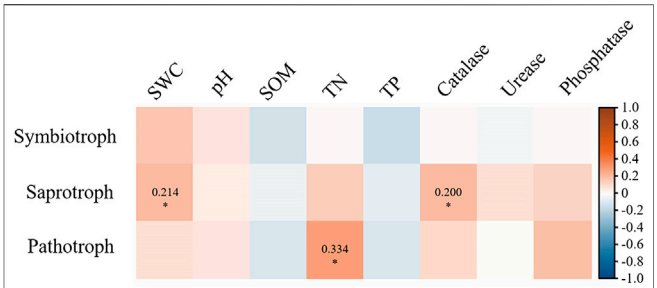

FIGURE 5 | Correlation between soil fungal functional group and soil properties. The color represents Mantel' r value. The * indicates significant correlation, and the Mantel' r values of significant correlation were labeled.

areas (Yu et al., 2017). The variation of Shannon diversities initially decreased and then increased with temporal succession due to two reasons. First, the premier soil fungi existing perpetually find it hard to adapt to the sudden changes in the external conditions when the *P. sylvestris* saplings were replanted, because the dominant plant species and root exudates are different (Jing et al., 2015; Mcdaniel et al., 2016). Second, with the growth of *P. sylvestris* plantations, diversity indices became highest in mature forests. The increase in plant litter and debris provides more diverse habitats and substrates for soil fungal communities to promote fungal diversity (Ren et al., 2019).

In short, the revegetation of *P. sylvestris* in desert areas influenced the soil fungal alpha diversities, even though they decreased at the beginning due to sudden changes in habitats, and then rose gradually after the establishment of a stable interrelation between fungi and plant-soil. In the later stages of *P. sylvestris* plantation development, the increase in diversity confirmed that successional pathways may play a positive role in controlling the development of soil fungi in forest ecosystems (Dang et al., 2017; Shi et al., 2019).

Soil fungal diversity in different trophic modes also varied with vegetation restoration. First, saprotrophs were more diverse than symbiotrophs throughout the whole revegetation period and seemed to remain steady. The higher diversity of saprotrophs may be attributable to their greater adaptability to the external environment (Boddy and Hiscox, 2016) as they participate in the functional traits associated with essential circulation in nature, such as decomposition and nutrient cycling for leaf litter (Ceci et al., 2019; Francioli et al., 2020). Furthermore, the increase in symbiotroph diversity in grasslands may be related to AM fungi, which had the highest proportion in grasslands. Finally, the Shannon diversity of saprotrophs was significantly higher than that of symbiotrophs in grassland, but not in plantations. This confirmed that the AM fungi may not compete as strongly with saprotrophs as EcM fungi (Carteron et al., 2020).

The proportion of the soil fungal functional groups in *P. sylvestris* plantations was influenced by revegetation duration. Due to the poor adaptability to environmental change and the more unstable biological community structure in grassland ecosystems, the unassigned group in grassland had higher relative abundance than in plantation. Symbiotrophs were abundant in *P. sylvestris* plantations as *P. sylvestris* is a classical EcM fungi dependent tree species (Zhu et al., 2008). With the passage of revegetation duration in plantations, the dominant fungal functional group changed from saprotrophs to symbiotrophs and returned to saprotrophs. Following were the main reasons for these dynamic changes: 1) *P. sylvestris* plantations demanded more nutrients when they entered into the vigorous growth period and increase in symbiotrophs was conducive to promote the absorption of nutrients for the host (Kolarikova et al., 2017). With the growth slowing down and litter accumulating, symbiotrophs decreased and saprotrophs increased, which helped to decompose litter and produce available nutrients (Bardgett and van der Putten, 2014; Zhao et al., 2020). 2) The heterogeneity of soil fungal composition may be indirectly caused by root exudates, whose components are related to stand age. Moreover, specific fungal species, with preference for specific components, can be attracted to different root exudates (Llado et al., 2018).

Dynamics of Soil Fungal Ecological Functions in Different Soil Depths Based on Revegetation Durations

In the complicated succession process of soil fungi, some of them appear to flourish or decline as a reciprocation, while others are universal and exist for a long time. In this study, the community composition at the genus level was similar in all soil samples, and the dominant and common genera altered with revegetation duration. *Mortierella* actively participates in soil nutrient transformation and promotes the growth of plants, and its ubiquity may have a positive effect on vegetation restoration in desert areas (Zhang et al., 2011; Walter Osorio and Habte,

2014; Tamayo-Velez and Osorio, 2018). *Gibberella* and *Fusarium* were among the top 10 genera only in grassland. *Gibberella* and the sexual/teleomorphs states of *Fusarium* species are common pathogens causing wilting, root rot, and other diseases (Dumroese and James, 2005; Wollenberg et al., 2019). In contrast, *Penicillium*, the dominant or common genus only in plantations, solubilizes phosphates and excretes antifungal substances that potentially hinder the growth of plant pathogenic fungi (Efthymiou et al., 2018). The increase of *Penicillium* in *P. sylvestris* plantations may contribute to plant health and soil quality.

Diversispora, an AM fungus in Glomeromycota, is an indicator of grassland. This was closely related to vegetation (the herb species in grassland) and host specificity or preference was a key driver of soil fungal community composition (Horn et al., 2017). The top genera in plantations comprise a large proportion of EcM fungi (notably, *Inocybe*, *Tuber*, and *Calostoma*), which have also been identified as common EcM fungi in Pinaceae on a global scale (Hayward et al., 2015; Long et al., 2016; Guo et al., 2020a). EcM fungi facilitate the efficient uptake of nutrients (Rao et al., 2020). They can provide limiting nutrients, including nitrogen, phosphorus, copper, iron, and zinc, and resist disease and drought (van der Heijden et al., 2008). *Inocybe* and *Tomentella* are indicator genera of nearly mature forests. The sudden increase in their relative abundance is responsible for the highest proportion of symbiotrophs in nearly mature forests. In addition, previous studies have confirmed that AM habitats experience greater disturbance from pathotrophs compared with ericoid mycorrhiza (ErM) habitats (Bahram et al., 2020), which may explain the higher number of pathogens in grasslands. Therefore, we reasonably speculated that significant quantity of EcM fungi effectively solved the problem of low soil nutrient content in the desertification area where *P. sylvestris* planted.

It is worth mentioning that some soil fungi were provided with multiple functional groups, such as *Mortierella*, *Fusarium*, *Microascu,* and *Podospora*. The variable trophic modes mean that soil fungi can regulate ecological strategies and behavior to adapt to environmental change (Porras-Alfaro and Bayman, 2011). Some EcM fungi express saprotrophic capacity, even though they usually show a poor competence to decompose carbon compounds (Lindahl and Tunlid, 2015).

Effects of Soil Properties on Fungal Community Composition

In the process of vegetation restoration, soil fungal community was significantly affected by the changing soil properties, which in turn, were most likely affected by vegetation. Soil pH has a ubiquitous impact on soil fungal community composition (Rousk et al., 2011; Tedersoo et al., 2014; Barnes et al., 2018), however, it was not confirmed in this study. This may be because fungi possess a low sensitivity and a wide optimum range of soil environment (Rousk et al., 2010), or the fluctuation of soil pH along vegetation restorations was not significant. It has been demonstrated that vegetation restoration may not be an inevitable factor in changing soil pH in deserts (Zuo et al., 2009).

Moreover, as time of revegetation increased, the accumulation of litter increased the soil nutrients, especially the topsoil. This means that more soil nutrients are present in the topsoil than the subsoil for nutrient leaching, which creates a suitable environment to accommodate eutrophic fungal communities (Liu et al., 2019b; Ren et al., 2019). Another description of revegetation restoration is stand age. The influence of forest development on soil fungal communities has also been reported in evergreen broad-leaved species (Wu et al., 2013) and pine forests (Kyaschenko et al., 2017).

Soil fungi perform important functions in nutrient cycling, while soil nutrients shape soil fungal communities with different functional groups (Peay et al., 2016; Perez-Izquierdo et al., 2017; Li et al., 2018). However, the complex and equivocal interaction between soil nutrients and fungi makes it difficult to generalize the fungi-soil relationship. This explained that no significant correlation was observed between symbiotrophs/saprotrophs and soil nutrients (SOM, TN, and TP), while a variety of mycorrhizal/saprotrophic fungi participate in carbon, nitrogen, and phosphorus cycling (Fujimura and Egger, 2012). In contrast, TN had an important role in the soil fungal community, which was consistent with a previous large-scale research study (Cai et al., 2018; Schappe et al., 2020). In particular, pathotrophs are more susceptible to TN, which has been confirmed to be more inclined to the environment with enriched nutrients (Zhang et al., 2017a; Schappe et al., 2020). However, the type of pathogen determines the different effects of nitrogen, which means that a high nitrogen supply may increase infection by obligate parasites or decrease infection by facultative parasites (Dordas, 2008).

It is worth noting that soil depth did not have an obvious effect on soil fungal diversity and composition in this study, which is in contrast to the conclusions reported previously (Baldrian et al., 2012; Toju et al., 2016; Schlatter et al., 2018). We speculated that a small change in soil depth has a negligible effect on soil fungal diversity and structure. In other words, a small-scale spatial variation cannot be a preponderant trigger for the dynamics of soil fungal diversity and composition under drought and infertile conditions of the desert.

CONCLUSION

Soil nutrient content (SOM, TN, and TP) and enzyme activity (catalase, urease, and phosphatase) showed significant differences among restoration durations, while soil pH and SWC were not affected by soil depth or restoration duration. The alpha diversity of saprotrophs was higher than that of symbiotrophs and pathotrophs. The Shannon diversity index of all fungal communities was significantly different among different revegetation durations, but not soil depth. Heterogeneity was observed in the distribution of fungal taxonomic and functional groups through revegetation duration; grassland contained more unassigned fungal functional groups and fewer symbiotrophs than the plantation. EcM fungi, such as *Inocybe*, *Tuber*, *Geopora*, *Tuber*, *Calostoma*, *Rhizopogon* and *Tomentella* were the primary constituent of symbiotrophs. The endophyte fungus *Mortierella* was a dominant/common genus in all soil samples and AM fungus

Diversispora was the indicator genus of grassland. The soil fungal community was mainly influenced by catalase and TN, which were significantly related to saprotrophs and pathotrophs, respectively.

Therefore, our study outcomes help to understand the conduciveness of soil fungal dynamics to the effect of revegetation and fungal function in deserts. We identified the major determinants affecting soil fungal community composition and discussed their potential functions in different restoration durations. It is important to appreciate the impact of soil fungi on soil quality and plant health. However, soil depth contributed little to soil fungi in the present study and selection of soil depth range should be expanded in future research.

DATA AVAILABILITY STATEMENT

The datasets presented in this study can be found in online repositories. The names of the repository/repositories and accession numbers can be found below: https://www.ncbi.nlm.nih.gov/genbank/, SRA accession: PRJNA663124.

AUTHOR CONTRIBUTIONS

YZ designed and performed the experiments, analyzed the data and wrote paper. HC, PZ, XW performed the investigation and experiments. GG acquired funding, projected administration and wrote paper. GD and MS supervised the whole progress and acquired funding.

FUNDING

This research was funded by the National Natural Science Foundation of China (no. 31700639 and no. 31600583), National Key Research and Development Program of China (no. 2016YFC0500802 and no. 2018YFC0507101) and Fundamental Research Funds for the Central Universities (no. 2017PT03 and no. 2015ZCQ-SB-02).

ACKNOWLEDGMENTS

The authors wish to acknowledge all members of research team for helpful discussions, key laboratory of state forestry and grass land administration on soil and water conservation for technical support and all funding for financial support.

SUPPLEMENTARY MATERIAL

The Supplementary Material for this article can be found online at: https://www.frontiersin.org/articles/10.3389/fenvs.2021.589068/full#supplementary-material.

REFERENCES

Bahram, M., Netherway, T., Hildebrand, F., Pritsch, K., Drenkhan, R., Loit, K., et al. (2020). Plant nutrient-acquisition strategies drive topsoil microbiome structure and function. *New Phytol.* 227 (4), 1189–1199. doi:10.1111/nph.16598

Baldrian, P., Kolarik, M., Stursova, M., Kopecky, J., Valaskova, V., Vetrovsky, T., et al. (2012). Active and total microbial communities in forest soil are largely different and highly stratified during decomposition. *ISME J.* 6 (2), 248–258. doi:10.1038/ismej.2011.95

Bardgett, R. D., and van der Putten, W. H. (2014). Belowground biodiversity and ecosystem functioning. *Nature* 515 (7528), 505–511. doi:10.1038/nature13855

Barnes, C. J., van der Gast, C. J., McNamara, N. P., Rowe, R., and Bending, G. D. (2018). Extreme rainfall affects assembly of the root-associated fungal community. *New Phytol.* 220 (4), 1172–1184. doi:10.1111/nph.14990

Boddy, L., and Hiscox, J. (2016). Fungal ecology: principles and mechanisms of colonization and competition by saprotrophic fungi. *Microbiol. Spectr.* 4 (6), 19. doi:10.1128/microbiolspec

Brockett, B. F. T., Prescott, C. E., and Grayston, S. J. (2012). Soil moisture is the major factor influencing microbial community structure and enzyme activities across seven biogeoclimatic zones in western Canada. *Soil Biol. Biochem.* 44 (1), 9–20. doi:10.1016/j.soilbio.2011.09.003

Broeckling, C. D., Broz, A. K., Bergelson, J., Manter, D. K., and Vivanco, J. M. (2008). Root exudates regulate soil fungal community composition and diversty. *Appl. Environ. Microbiol.* 74 (3), 738–744. doi:10.1128/aem.02188-07

Cáceres, M. D., and Legendre, P. (2009). Associations between species and groups of sites: indices and statistical inference. *Ecology* 90, 3566–3574. 10.1890/08-1823.1

Cai, Z.-q., Zhang, Y.-h., Yang, C., and Wang, S. (2018). Land-use type strongly shapes community composition, but not always diversity of soil microbes in tropical China. *Catena* 165, 369–380. doi:10.1016/j.catena.2018.02.018

Cardinale, B. J., Srivastava, D. S., Emmett Duffy, J., Wright, J. P., Downing, A. L., Sankaran, M., et al. (2006). Effects of biodiversity on the functioning of trophic groups and ecosystems. *Nature* 443 (7114), 989–992. doi:10.1038/nature05202

Carteron, A., Beigas, M., Joly, S., Turner, B. L., and Laliberte, E. (2020). Temperate forests dominated by arbuscular or ectomycorrhizal fungi are characterized by strong shifts from saprotrophic to mycorrhizal fungi with increasing soil depth. *Microb. Ecol.* [Epub ahead of print]. doi:10.1007/s00248-020-01540-7

Cavard, X., Bergeron, Y., Chen, H. Y. H., Paré, D., Laganière, J., and Brassard, B. (2011). Competition and facilitation between tree species change with stand development. *Oikos* 120 (11), 1683–1695. doi:10.1111/j.1600-0706.2011.19294.x

Ceci, A., Pinzari, F., Russo, F., Persiani, A. M., and Gadd, G. M. (2019). Roles of saprotrophic fungi in biodegradation or transformation of organic and inorganic pollutants in co-contaminated sites. *Appl. Microbiol. Biotechnol.* 103 (1), 53–68. doi:10.1007/s00253-018-9451-1

Chanthorn, W., Hartig, F., and Brockelman, W. Y. (2017). Structure and community composition in a tropical forest suggest a change of ecological processes during stand development. *For. Ecol. Manag.* 404, 100–107. doi:10.1016/j.foreco.2017.08.001

Chen, Y.-L., Xu, T.-L., Veresoglou, S. D., Hu, H.-W., Hao, Z.-P., Hu, Y.-J., et al. (2017). Plant diversity represents the prevalent determinant of soil fungal community structure across temperate grasslands in northern China. *Soil Biol. Biochem.* 110, 12–21. doi:10.1016/j.soilbio.2017.02.015

Dang, P., Yu, X., Le, H., Liu, J., Shen, Z., and Zhao, Z. (2017). Effects of stand age and soil properties on soil bacterial and fungal community composition in Chinese pine plantations on the Loess Plateau. *PLoS One* 12 (10), e0186501. doi:10.1371/journal.pone.0186501

De Deyn, G. B., and Van der Putten, W. H. (2005). Linking aboveground and belowground diversity. *Trends Ecol. Evol.* 20 (11), 625–633. doi:10.1016/j.tree.2005.08.009

Deng, J., Yin, Y., Luo, J., Zhu, W., and Zhou, Y. (2019). Different revegetation types alter soil physical-chemical characteristics and fungal community in the Baishilazi Nature Reserve. *PeerJ* 6, e6251. doi:10.7717/peerj.6251

Detheridge, A. P., Comont, D., Callaghan, T. M., Bussell, J., Brand, G., Gwynn-Jones, D., et al. (2018). Vegetation and edaphic factors influence rapid establishment of distinct fungal communities on former coal-spoil sites. *Fungal Ecology* 33, 92–103. doi:10.1016/j.funeco.2018.02.002

Dordas, C. (2008). Role of nutrients in controlling plant diseases in sustainable agriculture. A review. *Agron. Sustain. Dev.* 28 (1), 33–46. doi:10.1051/agro:2007051

Dumroese, R. K., and James, R. L. (2005). Root diseases in bareroot and container nurseries of the Pacific Northwest: epidemiology, management, and effects on outplanting performance. *N. For.* 30 (2–3), 185–202. doi:10.1007/s11056-005-4422-7

Edgar, R. C. (2013). UPARSE: highly accurate OTU sequences from microbial amplicon reads. *Nat. Methods* 10 (10), 996–998. doi:10.1038/nmeth.2604

Efthymiou, A., Jensen, B., and Jakobsen, I. (2018). The roles of mycorrhiza and *Penicillium inoculants* in phosphorus uptake by biochar-amended wheat. *Soil Biol. Biochem.* 127, 168–177. doi:10.1016/j.soilbio.2018.09.027

Francioli, D., van Rijssel, S. Q., van Ruijven, J., Termorshuizen, A. J., Cotton, T. E. A., Dumbrell, A. J., et al. (2020). Plant functional group drives the community structure of saprophytic fungi in a grassland biodiversity experiment. *Plant Soil.* [Epub ahead of print]. doi:10.1007/s11104-020-04454-y

Fujimura, K. E., and Egger, K. N. (2012). Host plant and environment influence community assembly of High Arctic root-associated fungal communities. *Fungal Ecology* 5 (4), 409–418. doi:10.1016/j.funeco.2011.12.010

Gianfreda, L., Rao, M. A., Piotrowska, A., Palumbo, G., and Colombo, C. (2005). Soil enzyme activities as affected by anthropogenic alterations: intensive agricultural practices and organic pollution. *Sci. Total Environ.* 341 (1–3), 265–279. doi:10.1016/j.scitotenv.2004.10.005

Guo, M.-s., Ding, G.-d., Gao, G.-l., Zhang, Y., Cao, H.-y., and Ren, Y. (2020a). Community composition of ectomycorrhizal fungi associated with *Pinus sylvestris* var. *mongolica* plantations of various ages in the Horqin Sandy Land. *Ecol. Indicat.* 110, 105860. doi:10.1016/j.ecolind.2019.105860

Guo, M., Gao, G., Ding, G., and Zhang, Y. (2020b). Drivers of ectomycorrhizal fungal community structure associated with *Pinus sylvestris* var. *Mongolica* differ at regional vs. local spatial scales in northern China. *Forests* 11 (3), 323. doi:10.3390/f11030323

Guo, Y., Chen, X., Wu, Y., Zhang, L., Cheng, J., Wei, G., et al. (2018). Natural revegetation of a semiarid habitat alters taxonomic and functional diversity of soil microbial communities. *Sci. Total Environ.* 635, 598–606. doi:10.1016/j.scitotenv.2018.04.171

Hayward, J., Horton, T. R., and Nunez, M. A. (2015). Ectomycorrhizal fungal communities coinvading with Pinaceae host plants in Argentina: Gringos bajo el bosque. *New Phytol.* 208 (2), 497–506. doi:10.1111/nph.13453

He, J., Tedersoo, L., Hu, A., Han, C., He, D., Wei, H., et al. (2017). Greater diversity of soil fungal communities and distinguishable seasonal variation in temperate deciduous forests compared with subtropical evergreen forests of eastern China. *FEMS (Fed. Eur. Microbiol. Soc.) Microbiol. Ecol.* 93 (7), fix069. doi:10.1093/femsec/fix069

Horn, S., Hempel, S., Verbruggen, E., Rillig, M. C., and Caruso, T. (2017). Linking the community structure of arbuscular mycorrhizal fungi and plants: a story of interdependence? *ISME J.* 11 (6), 1400–1411. doi:10.1038/ismej.2017.5

Husband, R., Herre, E. A., Turner, S. L., Gallery, R., and Young, J. P. W. (2002). Molecular diversity of arbuscular mycorrhizal fungi and patterns of host association over time and space in a tropical forest. *Mol. Ecol.* 11 (12), 2669–2678. doi:10.1046/j.1365-294X.2002.01647.x

Jin, Z., Li, X., Wang, Y., Wang, Y., Wang, K., and Cui, B. (2016). Comparing watershed black locust afforestation and natural revegetation impacts on soil nitrogen on the Loess Plateau of China. *Sci. Rep.* 6, 25048. doi:10.1038/srep25048

Jing, X., Sanders, N. J., Shi, Y. U., Chu, H., Classen, A. T., Zhao, K. E., et al. (2015). The links between ecosystem multifunctionality and above-and belowground biodiversity are mediated by climate. *Nat. Commun.* 6, 8159. doi:10.1038/ncomms9159

Jing, Z., Cheng, J., Jin, J., Su, J., and Bai, Y. (2014). Revegetation as an efficient means of improving the diversity and abundance of soil eukaryotes in the Loess Plateau of China. *Ecol. Eng.* 70, 169–174. doi:10.1016/j.ecoleng.2014.05.011

Johnand Matt, K. J. S. S. (1970). Colorimetric determination of phosphorus in soil and plant materials with ascorbic acid. *Soil Sci.* 109 (4), 214–220. doi:10.1097/00010694-197004000-00002

Kolarikova, Z., Kohout, P., Kruger, C., Janouskova, M., Mrnka, L., and Rydlova, J. (2017). Root-associated fungal communities along a primary succession on a mine spoil: distinct ecological guilds assemble differently. *Soil Biol. Biochem.* 113, 143–152. doi:10.1016/j.soilbio.2017.06.004

Kubartova, A., Ottosson, E., Dahlberg, A., and Stenlid, J. (2012). Patterns of fungal communities among and within decaying logs, revealed by 454 sequencing. *Mol. Ecol.* 21 (18), 4514–4532. doi:10.1111/j.1365-294X.2012.05723.x

Kyaschenko, J., Clemmensen, K. E., Hagenbo, A., Karltun, E., and Lindahl, B. D. (2017). Shift in fungal communities and associated enzyme activities along an age gradient of managed *Pinus sylvestris* stands. *ISME J.* 11 (4), 863–874. doi:10.1038/ismej.2016.184

Li, S., Shakoor, A., Wubet, T., Zhang, N., Liang, Y., and Ma, K. (2018). Fine-scale variations of fungal community in a heterogeneous grassland in Inner Mongolia: effects of the plant community and edaphic parameters. *Soil Biol. Biochem.* 122, 104–110. doi:10.1016/j.soilbio.2018.04.007

Lindahl, B. D., and Tunlid, A. (2015). Ectomycorrhizal fungi - potential organic matter decomposers, yet not saprotrophs. *New Phytol.* 205 (4), 1443–1447. doi:10.1111/nph.13201

Liu, G. y., Chen, L. l., Shi, X. r., Yuan, Z. y., Yuan, L. Y., Lock, T. R., et al. (2019a). Changes in rhizosphere bacterial and fungal community composition with vegetation restoration in planted forests. *Land Degrad. Dev.* 30 (10), 1147–1157. doi:10.1002/ldr.3275

Liu, J., Maldonado-Mendoza, I., Lopez-Meyer, M., Cheung, F., Town, C. D., and Harrison, M. J. (2007). Arbuscular mycorrhizal symbiosis is accompanied by local and systemic alterations in gene expression and an increase in disease resistance in the shoots. *Plant J.* 50 (3), 529–544. doi:10.1111/j.1365-313X.2007.03069.x

Liu, Y., Chen, X., Liu, J., Liu, T., Cheng, J., Wei, G., et al. (2019b). Temporal and spatial succession and dynamics of soil fungal communities in restored grassland on the Loess Plateau in China. *Land Degrad. Dev.* 30 (11), 1273–1287. doi:10.1002/ldr.3289

Llado, S., Lopez-Mondejar, R., and Baldrian, P. (2018). Drivers of microbial community structure in forest soils. *Appl. Microbiol. Biotechnol.* 102 (10), 4331–4338. doi:10.1007/s00253-018-8950-4

Long, D., Liu, J., Han, Q., Wang, X., and Huang, J. (2016). Ectomycorrhizal fungal communities associated with *Populus simonii* and *Pinus tabuliformis* in the hilly-gully region of the Loess Plateau, China. *Sci. Rep.* 6, 24336. doi:10.1038/srep24336

Lyu, Y. L., Shi, P. J., Han, G. Y., Liu, L. Y., Guo, L. L., Hu, X., et al. (2020). Desertification control practices in China. *Sustainability* 12 (8), 15. doi:10.3390/su12083258

Marín, C., Godoy, R., Valenzuela, E., Schloter, M., and Gschwendtner, S. (2017). Functional land-use change effects on soil fungal communities in Chilean temperate rainforests. *J. Soil Sci. Plant Nutr.* 17 (4), 985–1002. doi:10.4067/S0718-95162017000400011

Mason, C. J., Edwards, M., Riby, P. G., and Coe, G. (1999). The use of microwaves in the acceleration of digestion and colour development in the determination of total Kjeldahl nitrogen in soil. *The Analyst* 124 (11), 1719–1726. doi:10.1039/a903623g

Mcdaniel, M. D., Tiemann, L. K., and Grandy, A. S. (2016). Does agricultural crop diversity enhance soil microbial biomass and organic matter dynamics? A meta-analysis. *Ecol. Appl.* 24, 560–570. doi:10.1890/13-0616.1

Miao, Q., Yu, W., Kang, H., and Wang, J. (2019). Prolonging rotation of Chinese fir to over 25 years could maintain a better soil status in subtropical China. *Forests* 10(8), 80629. doi:10.3390/f10080629

Nearing, M. A., Xie, Y., Liu, B., and Ye, Y. (2017). Natural and anthropogenic rates of soil erosion. *International Soil and Water Conservation Research* 5 (2), 77–84. doi:10.1016/j.iswcr.2017.04.001

Nguyen, N. H., Song, Z., Bates, S. T., Branco, S., Tedersoo, L., Menke, J., et al. (2016). FUNGuild: an open annotation tool for parsing fungal community datasets by ecological guild. *Fungal Ecology* 20, 241–248. doi:10.1016/j.funeco.2015.06.006

Nie, S. a., Lei, X., Zhao, L., Brookes, P. C., Wang, F., Chen, C., et al. (2018). Fungal communities and functions response to long-term fertilization in paddy soils. *Appl. Soil Ecol.* 130, 251–258. doi:10.1016/j.apsoil.2018.06.008

Nunez-Mir, G. C., Iannone, B. V., III, Curtis, K., and Fei, S. (2015). Evaluating the evolution of forest restoration research in a changing world: a "big literature" review. *N. For.* 46 (5–6), 669–682. doi:10.1007/s11056-015-9503-7

Op De Beeck, M., Lievens, B., Busschaert, P., Declerck, S., Vangronsveld, J., and Colpaert, J. V. (2014). Comparison and validation of some ITS primer pairs useful for fungal metabarcoding studies. *PLoS One* 9 (6), e97629. doi:10.1371/journal.pone.0097629

Peay, K. G., Baraloto, C., and Fine, P. V. A. (2013). Strong coupling of plant and fungal community structure across western Amazonian rainforests. *ISME J.* 7 (9), 1852–1861. doi:10.1038/ismej.2013.66

Peay, K. G., Kennedy, P. G., and Talbot, J. M. (2016). Dimensions of biodiversity in the Earth mycobiome. *Nat. Rev. Microbiol.* 14 (7), 434–447. doi:10.1038/nrmicro.2016.59

Perez-Izquierdo, L., Zabal-Aguirre, M., Flores-Renteria, D., Gonzalez-Martinez, S. C., Buee, M., and Rincon, A. (2017). Functional outcomes of fungal community shifts driven by tree genotype and spatial-temporal factors in Mediterranean pine forests. *Environ. Microbiol.* 19 (4), 1639–1652. doi:10.1111/1462-2920.13690

Pickles, B. J., Gorzelak, M. A., Green, D. S., Egger, K. N., and Massicotte, H. B. (2015). Host and habitat filtering in seedling root-associated fungal communities: taxonomic and functional diversity are altered in 'novel' soils. *Mycorrhiza* 25 (7), 517–531. doi:10.1007/s00572-015-0630-y

Porras-Alfaro, A., and Bayman, P. (2011). "Hidden fungi, Emergent properties: Endophytes and Microbiomes," in *Annual review of phytopathology, Annual Reviews* Editors N. K. VanAlfen, G. Bruening, and J. E. Leach, 291–315.

Prado, I. G. d. O., da Silva, M. d. C. S., Prado, D. G. d. O., Kemmelmeier, K., Pedrosa, B. G., Silva, C. C. d., et al. (2019). Revegetation process increases the diversity of total and arbuscular mycorrhizal fungi in areas affected by the Fundão dam failure in Mariana, Brazil. *Appl. Soil Ecol.* 141, 84–95. doi:10.1016/j.apsoil.2019.05.008

Qin, M., Shi, G., Zhang, Q., Meng, Y., Liu, Y., Pan, J., et al. (2019). Arbuscular mycorrhizal fungi serve as keystone taxa for revegetation on the Tibetan Plateau. *J. Basic Microbiol.* 59 (6), 609–620. doi:10.1002/jobm.201900060

Rao, M. V., Rice, R. A., Fleischer, R. C., and Muletz-Wolz, C. R. (2020). Soil fungal communities differ between shaded and sun-intensive coffee plantations in El Salvador. *PLoS One* 15 (4), e0231875. doi:10.1371/journal.pone.0231875

Ren, C., Liu, W., Zhao, F., Zhong, Z., Deng, J., Han, X., et al. (2019). Soil bacterial and fungal diversity and compositions respond differently to forest development. *Catena* 181, 104071. doi:10.1016/j.catena.2019.104071

Rousk, J., Bååth, E., Brookes, P. C., Lauber, C. L., Lozupone, C., Caporaso, J. G., et al. (2010). Soil bacterial and fungal communities across a pH gradient in an arable soil. *ISME J.* 4 (10), 1340–1351. doi:10.1038/ismej.2010.58

Rousk, J., Brookes, P. C., and Bååth, E. (2011). Fungal and bacterial growth responses to N fertilization and pH in the 150-year 'Park Grass' UK grassland experiment. *FEMS (Fed. Eur. Microbiol. Soc.) Microbiol. Ecol.* 76 (1), 89–99. doi:10.1111/j.1574-6941.2010.01032.x

Schappe, T., Albornoz, F. E., Turner, B. L., and Jones, F. A. (2020). Co-occurring fungal functional groups respond differently to tree neighborhoods and soil properties across three tropical rainforests in Panama. *Microb. Ecol.* 79 (3), 675–685. doi:10.1007/s00248-019-01446-z

Schlatter, D. C., Kahl, K., Carlson, B., Huggins, D. R., and Paulitz, T. (2018). Fungal community composition and diversity vary with soil depth and landscape position in a no-till wheat-based cropping system. *FEMS (Fed. Eur. Microbiol. Soc.) Microbiol. Ecol.* 94 (7), fiy098. doi:10.1093/femsec/fiy098

Shen, J.-P., Zhang, L.-M., Guo, J.-F., Ray, J. L., and He, J.-Z. (2010). Impact of long-term fertilization practices on the abundance and composition of soil bacterial communities in Northeast China. *Appl. Soil Ecol.* 46 (1), 119–124. doi:10.1016/j.apsoil.2010.06.015

Shi, L., Dossa, G. G. O., Paudel, E., Zang, H., Xu, J., and Harrison, R. D. (2019). Changes in fungal communities across a forest disturbance gradient. *Appl. Environ. Microbiol.* 85 (12), e00080-19. doi:10.1128/AEM.00080-19

Stursova, M., Barta, J., Santruckova, H., and Baldrian, P. (2016). Small-scale spatial heterogeneity of ecosystem properties, microbial community composition and microbial activities in a temperate mountain forest soil. *FEMS Microbiol. Ecol.* 92, fiw185. doi:10.1093/femsec/fiw185

Tamayo-Velez, A., and Osorio, N. W. (2018). Soil fertility improvement by litter decomposition and inoculation with the fungus *Mortierella* sp in avocado plantations of Colombia. *Commun. Soil Sci. Plant Anal.* 49 (2), 139–147. doi:10.1080/00103624.2017.1417420

Tarafdar, J. C., and Marschner, H. (1994). Phosphatase activity in the rhizosphere and hyphosphere of VA mycorrhizal wheat supplied with inorganic and organic phosphorus. *Soil Biol. Biochem.* 26 (3), 387–395. doi:10.1016/0038-0717(94)90288-7

Tedersoo, L., Bahram, M., Polme, S., Koljalg, U., Yorou, N. S., Wijesundera, R., et al. (2014). Global diversity and geography of soil fungi. *Science* 346, 1256688. doi:10.1126/science.1256688

Toju, H., Kishida, O., Katayama, N., and Takagi, K. (2016). Networks depicting the fine-scale co-occurrences of fungi in soil horizons. *PLoS One* 11 (11), e0165987. doi:10.1371/journal.pone.0165987

Toju, H., Tanabe, A. S., and Sato, H. (2018). Network hubs in root-associated fungal metacommunities. *Microbiome* 6, 116. doi:10.1186/s40168-018-0497-1

van der Heijden, M. G., Bardgett, R. D., and van Straalen, N. M. (2008). The unseen majority: soil microbes as drivers of plant diversity and productivity in terrestrial ecosystems. *Ecol. Lett.* 11 (3), 296–310. doi:10.1111/j.1461-0248.2007.01139.x

Walkley, A., and Black, I. A. (1934). An examination of the Degtjareff method for determining soil organic matter,and a proposed modification of the chromic acid titration method. *Soil Sci.* 37 (1), 29–38. doi:10.1097/00010694-193401000-00003

Walter Osorio, N., and Habte, M. (2014). Soil phosphate Desorption induced by a phosphate-solubilizing fungus. *Commun. Soil Sci. Plant Anal.* 45 (4), 451–460. doi:10.1080/00103624.2013.870190

Wang, B., Xue, S., Liu, G. B., Zhang, G. H., Li, G., and Ren, Z. P. (2012). Changes in soil nutrient and enzyme activities under different vegetations in the Loess Plateau area, Northwest China. *Catena* 92, 186–195. doi:10.1016/j.catena.2011.12.004

Wang, C., Zhang, W., Zhao, C., Shi, R., Xue, R., and Li, X. (2020). Revegetation by sowing reduces soil bacterial and fungal diversity. *Ecology and Evolution* 10 (1), 431–440. doi:10.1002/ece3.5906

Wollenberg, R. D., Sondergaard, T. E., Nielsen, M. R., Knutsson, S., Pedersen, T. B., Westphal, K. R., et al. (2019). There it is! *Fusarium pseudograminearum* did not lose the fusaristatin gene cluster after all. *Fungal Biology* 123 (1), 10–17. doi:10.1016/j.funbio.2018.10.004

Wu, Y. T., Wubet, T., Trogisch, S., Both, S., Scholten, T., Bruelheide, H., et al. (2013). Forest age and plant species composition determine the soil fungal community composition in a Chinese subtropical forest. *PLoS One* 8(6), 66829. doi:10.1371/journal.pone.0066829

Xiao, X., Wei, X., Liu, Y., Ouyang, X., Li, Q., and Ning, J. (2015). Aerial seeding: an effective forest restoration method in highly degraded forest landscapes of subtropic regions. *Forests* 6 (6), 1748–1762. doi:10.3390/f6061748

Yang, Y., Cheng, H., Liu, L., Dou, Y., and An, S. (2020). Comparison of soil microbial community between planted woodland and natural grass vegetation on the Loess Plateau. *For. Ecol. Manag.* 460, 117817. doi:10.1016/j.foreco.2019.117817

Yu, J., Xue, Z., He, X., Liu, C., and Steinberger, Y. (2017). Shifts in composition and diversity of arbuscular mycorrhizal fungi and glomalin contents during revegetation of desertified semiarid grassland. *Appl. Soil Ecol.* 115, 60–67. doi:10.1016/j.apsoil.2017.03.015

Zhang, H., Wu, X., Li, G., and Qin, P. (2011). Interactions between arbuscular mycorrhizal fungi and phosphate-solubilizing fungus (*Mortierella* sp.) and their effects on *Kostelelzkya virginica* growth and enzyme activities of rhizosphere and bulk soils at different salinities. *Biol. Fertil. Soils* 47 (5), 543–554. doi:10.1007/s00374-011-0563-3

Zhang, K., Adams, J. M., Shi, Y., Yang, T., Sun, R., He, D., et al. (2017a). Environment and geographic distance differ in relative importance for determining fungal community of rhizosphere and bulk soil. *Environ. Microbiol.* 19 (9), 3649–3659. doi:10.1111/1462-2920.13865

Zhang, Y., Dong, S., Gao, Q., Liu, S., Ganjurjav, H., Wang, X., et al. (2017b). Soil bacterial and fungal diversity differently correlated with soil biochemistry in alpine grassland ecosystems in response to environmental changes. *Sci. Rep.* 7, 1–10. doi:10.1038/srep43077

Zhao, P. S., Guo, M. S., Gao, G. L., Zhang, Y., Ding, G. D., Ren, Y., et al. (2020). Community structure and functional group of root-associated fungi of *Pinus sylvestris* var. *mongolica* across stand ages in the Mu Us Desert. *Ecology and Evolution* 10 (6), 3032–3042. doi:10.1002/ece3.6119

Zheng, Y., Hu, H.-W., Guo, L.-D., Anderson, I. C., and Powell, J. R. (2017). Dryland forest management alters fungal community composition and decouples assembly of root- and soil-associated fungal communities. *Soil Biol. Biochem.* 109, 14–22. doi:10.1016/j.soilbio.2017.01.024

Zhou, H., Zhang, D., Jiang, Z., Sun, P., Xiao, H., Wu, Y., et al. (2019). Changes in the soil microbial communities of alpine steppe at Qinghai-Tibetan Plateau under

different degradation levels. *Sci. Total Environ.* 651, 2281–2291. doi:10.1016/j.scitotenv.2018.09.336

Zhu, J.-j., Li, F.-q., Xu, M.-l., Kang, H.-z., and Wu, X.-y. (2008). The role of ectomycorrhizal fungi in alleviating pine decline in semiarid sandy soil of northern China: an experimental approach. *Ann. For. Sci.* 65 (3), 304. doi:10.1051/forest:2008007

Zuo, X., Zhao, X., Zhao, H., Zhang, T., Guo, Y., Li, Y., et al. (2009). Spatial heterogeneity of soil properties and vegetation-soil relationships following vegetation restoration of mobile dunes in Horqin Sandy Land, Northern China. *Plant Soil* 318 (1–2), 153–167. doi:10.1007/s11104-008-9826-7

Conflict of Interest: The authors declare that the research was conducted in the absence of any commercial or financial relationships that could be construed as a potential conflict of interest.

frontiers in Environmental Science

ORIGINAL RESEARCH
published: 22 February 2021
doi: 10.3389/fenvs.2021.633020

Temporal and Spatial Variations in NDVI and Analysis of the Driving Factors in the Desertified Areas of Northern China From 1998 to 2015

Xuyang Wang[1,2], *Yuqiang Li*[1,2,3]*, *XinYuan Wang*[4,5], *Yulin Li*[1,2,3], *Jie Lian*[1,2] and *Xiangwen Gong*[1,3]

[1]Northwest Institute of Eco-Environment and Resources, Chinese Academy of Sciences, Lanzhou, China, [2]Naiman Desertification Research Station, Northwest Institute of Eco-Environment and Resources, Chinese Academy of Sciences, Tongliao, China, [3]University of Chinese Academy of Sciences, Beijing, China, [4]Gansu Institute of Forestry Survey and Planning, Lanzhou, China, [5]Ecological Environmental Supervision and Administration Bureau of Gansu Province, Lanzhou, China

China faces some of the most serious desertification in the world, leading to many problems. To solve them, large-scale ecological restoration projects were implemented. To assess their effectiveness, we analyzed normalized-difference vegetation index (NDVI) data derived from SPOT VEGETATION and gridded climate datasets from 1998 to 2015 to detect the degrees of desertification and the effects of human and climate drivers on vegetation dynamics. We found that NDVI of desertified areas generally decreased before 2000, then increased. The annual increase in NDVI was fixed dunes (0.0013) = semi-fixed dunes (0.0013) > semi-mobile dunes (0.0012) > gobi (gravel) desert (0.0011) > mobile dunes (0.0003) > saline–alkali land (0.0000). The proportions of the area of each desert type in which NDVI increased were fixed dunes (43.4%) > semi-mobile dunes (39.7%) > semi-fixed dunes (26.7%) > saline–alkali land (23.1%) > gobi desert (14.4%) > mobile dunes (12.5%). Thus, the vegetation response to the restoration efforts increased as the initial dune stability increased. The proportion of the area where desertification was dominated by temperature (1.8%) was far less than the area dominated by precipitation (14.1%). However, 67.6% of the change was driven by non-climatic factors. The effectiveness of the ecological restoration projects was significant in the Loess Plateau and in the Mu Us, Horqin, and Hulunbuir sandy lands. In contrast, there was little effect in the Badain Jaran, Ulan Buh, and Tengger deserts; in particular, vegetation cover has declined seriously in the Hunshandake Sandy Land and Alkin Desert Grassland. Thus, more or different ecological restoration must be implemented in these areas.

Keywords: desert, ecological restoration, desertification, NDVI, climate factors

OPEN ACCESS

Edited by:
Atsushi Tsunekawa, Tottori University, Japan

Reviewed by:
Saumitra Mukherjee, Jawaharlal Nehru University, India
Xinghua Li, Wuhan University, China

***Correspondence:**
Yuqiang Li
liyq@lzb.ac.cn

Specialty section:
This article was submitted to Environmental Informatics and Remote Sensing, a section of the journal Frontiers in Environmental Science

Received: *24 November 2020*
Accepted: *12 January 2021*
Published: *22 February 2021*

Citation:
Wang X, Li Y, Wang X, Li Y, Lian J and Gong X (2021) Temporal and Spatial Variations in NDVI and Analysis of the Driving Factors in the Desertified Areas of Northern China From 1998 to 2015. Front. Environ. Sci. 9:633020. doi: 10.3389/fenvs.2021.633020

1 INTRODUCTION

According to the United Nations Convention to Combat Desertification (UNCCD), the desertification was defined as "land degradation in arid, semi-arid and dry sub-humid areas resulting from various factors, including climatic variations and human activities" (FAO (Food and Agriculture Organization of the United Nations), 1993). And this process can be considered as an important global issue, which is

responsible for the change of the Earth's surface (Tran and Campbell, 2015). Desertification has been threatening millions of people around the world. The 2001 report of the International Fund for Agricultural Development (IFAD), Geneva, Switzerland, showed that one-fourth of the Earth's surface (except Antarctica) has been under threat of desertification, which covers more than 3.6 million hectares, and income losses from this process every year can be estimated to exceed $42 billion (IFAD, 2001). After the International Convention on Desertification of the United Nations has entered into force in 1996 (Jamal, 1997), the need to measure land degradation and desertification processes has substantially increased. While standard ground survey methods for undertaking such measurements are imperfect or expensive, it has been demonstrated that satellite-based and airborne remote sensing systems offer a considerable potential. Earth observation satellites provide significant contributions to desertification assessment and monitoring, particularly by providing the spatial information needed for regional-scale analyses of the relationships between climate change, land degradation and desertification processes. For example, many remotely sensed images of different types and spatial resolutions were adopted to study land cover in arid areas over a time period, such as the high and moderate resolution images like Landsat or SPOT (Wu and Ci, 2002; Alphan and Yilmaz, 2005; Arnous, et al., 2009), or coarse resolution data like MODIS, NOAA imagery (Hoang et al., 2005), or even radar images (Hoang et al., 2003; Del Valle et al., 2010). Such research showed that land degradation in the studied areas tended to increase due to impacts of drought and soil erosion associated with agriculture.

China is one of the countries most seriously affected by desertification due to a combination of increasing frequency and severity of drought caused by climate change and unsustainable human activities such as overgrazing, excessive deforestation, unreasonable reclamation for agriculture, firewood harvesting, and excessive groundwater withdrawal. To monitor desertification in China at frequent intervals, the State Forestry Administration of China organized a national desert survey that is conducted every 5 years. The first monitoring was from 1993–1996 and the fifth was conducted from 2013 to 2016 (Tu et al., 2016). The latter results indicated that the total area of desertified land in China was 2.61×10^6 km^2, accounting for 27.2% of the national land area. Desertification has affected 471 counties in 18 provinces, of which 99% are located in northern China. (We therefore focused on northern China in the present study.) For the desertified land, 1.17×10^6 km^2 are distributed in arid regions (with annual precipitation <200 mm), 0.94×10^6 are in semi-arid regions (350–500 mm), and 0.50×10^6 km^2 are in sub-humid regions (400–800 mm). The area of aeolian desertification (where deserts are created by wind erosion) covers 1.83×10^6 km^2, accounting for 69.9% of the total area of desertified land. Compared with the results from the previous survey, in 2009, the desert area decreased by 12.12×10^3 km^2 over 5 years, with an annual reduction of 2.42×10^3 km^2 (National Desertification Monitoring Data, 2015).

Desertification has many negative effects. First, it damages the ecological environment, thereby threatening human survival, and can even create "ecological refugees". Second, it decreases the productivity of land, thereby decreasing crop and animal production or even totally preventing agriculture and animal husbandry. In addition, desertification degrades ecosystem quality and reduces species diversity and abundance, thereby threatening biodiversity (NEPAPR, 1998). Facing these problems, China's government implemented a range of restoration projects to control desertification. In 1958, the Chinese Communist Party's Central Committee proposed a policy of "marching to the desert", which focused on planting trees and grasses in desert areas. Since 1978, the government has implemented a series of large-scale ecological restoration projects, including the Three-Norths Shelter Forest Construction Program, which constructed large-scale artificial forests in northwestern, northern, and northeastern China. In addition, the 15th National Congress of the Communist Party of China in 1997 proposed a policy of "preventing desertification and improving the ecological environment". Most notably, Vice-Premier Jiang Chunyun proposed a 50 years "building a cross-century ecological project" (Dong et al., 1999) that was divided into an initial stage (1998–2010), a middle stage (2011–2030), and a late stage (2031–2050). The initial stage is now complete, but the effectiveness of the ecological restoration projects implemented during this stage is not yet known. Given the long period covered by this project and the vast sums of money being invested, it's necessary to assess the responses of vegetation cover (a primary indicator of the degree of desertification) to the project.

Vegetation is the main biological component of terrestrial ecosystems and plays an essential role in conserving soil and water, regulating the atmospheric composition, and mitigating the rise of greenhouse gas concentrations (Sun et al., 2015). Changes in vegetation cover will therefore have a huge impact on the environment. Studying changes in the vegetation cover of a site can provide a scientific basis for formulating rational land use patterns (Zhang et al., 2008b). However, surveying vegetation status over an area as large as China is expensive and time-consuming, making it necessary to find less expensive and faster methods, such as satellite remote sensing. The normalized-difference vegetation index (NDVI), which is derived from satellite remote-sensing data in the near-infrared and red bands (Piao et al., 2006), can meet this need. It is a good indicator for evaluating vegetation cover and an effective indicator for monitoring changes in vegetation and the ecological environment over large areas and with sufficient frequency to support monitoring of ecological restoration projects (Paruelo et al., 1997). NDVI datasets have therefore been widely used in ecological research (Fung and Siu, 2000; Pettorelli et al., 2005), studies of vegetation cover (Piao et al., 2003; Lin et al., 2012; Liu et al., 2016), studies of phenology (Clerici et al., 2012; Feng et al., 2017), and in agriculture (Wardlow and Egbert, 2008; Magney et al., 2016).

Climate change, human activities, and CO_2 fertilization effects (increased vegetation growth in response to increasing CO_2 levels) will affect the change in vegetation cover (Piao et al., 2006). Of the abiotic factors that affect plant growth, the effects of temperature and precipitation are the most direct and important (Nemani et al., 2003; Wang et al., 2015). The feedbacks between climate factors and NDVI change have become a key research

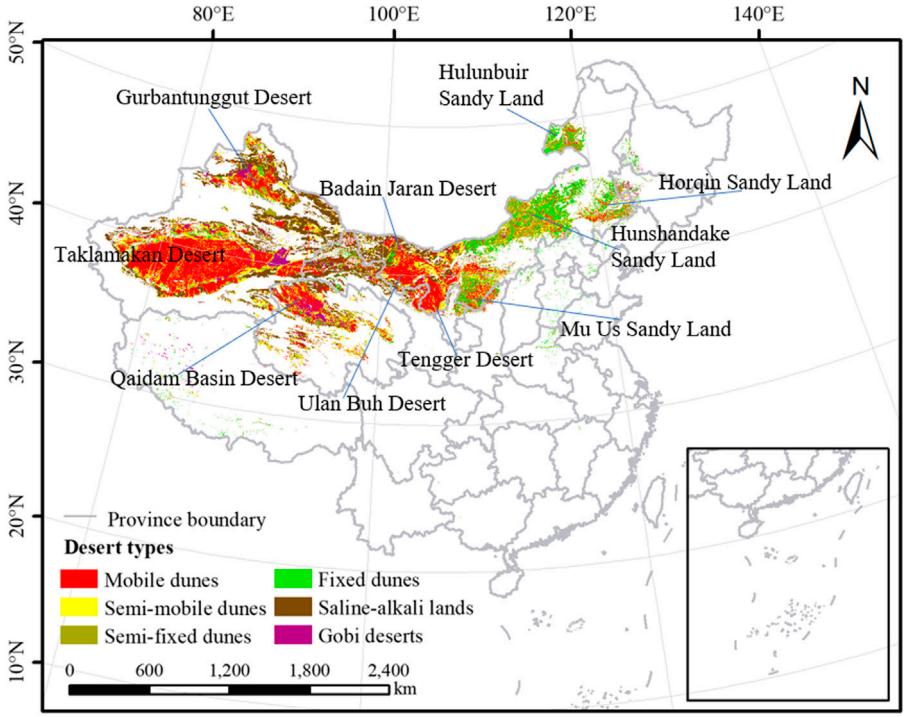

FIGURE 1 | Location of the study area, and the spatial distribution of the desert types in 2000 based on a 1:100,000 scale desert-distribution map of China created from Landsat TM images. The desert types are defined in **Table 1**. Source: Environmental & Ecological Science Data Center for West China, National Natural Science Foundation of China (http://westdc.westgis.ac.cn).

focus around the world, and researchers have shown that temperature, precipitation, and vegetation NDVI are closely related (Nemani et al., 2003; Nie et al., 2012; Nie and Xu, 2015; Nash et al., 2017).

Based on this literature review, we designed the present study to evaluate the effectiveness of China's ecological restoration projects since 1998 for land with different degrees of desertification using NDVI, and examined climate data to identify the driving factors responsible for the vegetation response. The rest of this review is organized as follows. The data and methods are described in Materials and Methods. The temporal and spatial variations of NDVI and its response to changes in temperature and precipitation are presented in Results. Discussion on the impact of climatic factors and ecological restoration on vegetation changes in desertified areas are provided in Discussion, followed by conclusions in Conclusions and Outlook. Our study provides guidance for policy makers to improve the success of their future ecological restoration work.

MATERIALS AND METHODS

Study Area

Figure 1 shows that China's area of desert is mainly distributed in the country's arid and semi-arid northern temperate and warm-temperate zones, between 35°N and 50°N, and between 75°E and 125°E. The elevation of the study area is between −160 to 5,668, and the highest elevation is mainly located in the Qaidam Basin and its surrounding areas (**Supplementary Figure S1**). The region's climate is dry, with annual precipitation less than 250 mm in most parts of the region, and there is a large temperature difference between day and night during the warm season. The maximum summer temperature ranges from 50 to 60°C, and the winter temperature ranges from −20°C to −30°C. According to China's desert classification (Appendix **Table 1**), the desertified land in China can be divided into six different types: mobile dunes (29.3% of the total area in 2000), semi-mobile dunes (17.1%), semi-fixed dunes (14.4%), fixed dunes (9.8%), saline–alkali land (7.4%), and gobi (gravel) desert (22.0%).

There are many deserts and four major sandy lands in the study area: In the west, the Taklamakan Desert covers 337 600 km^2; it is the largest desert in China and the second-largest area of mobile dunes in the world. Northeast of this desert, the Gurbantunggut Desert covers 48 800 km^2, and to the southeast lies the Qaidam Basin, which covers 34,900 km^2; both deserts are dominated by mobile dunes. In the center of the study area, the Badain Jaran Desert covers 44 300 km^2. South of this desert, the Ulan Buh Desert covers 9,900 km^2, and is dominated by mobile dunes, and the Tengger Desert contains the mobile dunes with the fastest migration rate in China, covering an area of 42,700 km^2.In addition, the eastern part of the study area contains four major sandy lands: The Mu Us Sandy land covers

TABLE 1 | Changes in the annual mean normalized-difference vegetation index (NDVI) for different desert types from 1998 to 2015 in China, and statistical measures of their variation.

	NDVI					
Year	**Mobile dunes**	**Semi-mobile dunes**	**Semi-fixed dunes**	**Fixed dunes**	**Gobi desert**	**Saline–alkali land**
1998	0.109	0.179	0.364	0.464	0.112	0.174
1999	0.105	0.166	0.321	0.419	0.105	0.162
2000	0.098	0.156	0.298	0.375	0.099	0.151
2001	0.089	0.144	0.273	0.363	0.088	0.144
2002	0.097	0.162	0.322	0.399	0.099	0.158
2003	0.113	0.180	0.352	0.450	0.112	0.175
2004	0.111	0.175	0.323	0.414	0.111	0.169
2005	0.107	0.170	0.318	0.416	0.109	0.170
2006	0.104	0.170	0.331	0.419	0.103	0.167
2007	0.106	0.172	0.328	0.403	0.108	0.165
2008	0.108	0.180	0.357	0.459	0.102	0.177
2009	0.109	0.172	0.312	0.379	0.105	0.167
2010	0.123	0.202	0.344	0.420	0.136	0.196
2011	0.113	0.182	0.348	0.441	0.110	0.182
2012	0.126	0.211	0.399	0.503	0.124	0.202
2013	0.127	0.206	0.379	0.471	0.127	0.199
2014	0.084	0.153	0.303	0.394	0.076	0.151
2015	0.085	0.154	0.297	0.390	0.081	0.152
Overall mean	0.106	0.174	0.331	0.421	0.106	0.169
Overall SD	0.093	0.139	0.181	0.194	0.067	0.159
Overall CV (%)	87.33	80.15	54.58	45.93	62.99	93.71

SD represents the standard deviation, and CV represents the coefficient of variation.

32,100 km^2 and is dominated by fixed and semi-fixed dunes. The Hunshandake Sandy Land covers 21,400 km^2, but because it has more water than most of the study area, it is covered by lush grassland. The Horqin Sandy Land covers 42,300 km^2, and was once covered by lush vegetation dominated by palatable grasses; however, starting in the 1950s, the region's landscape began to undergo severe desertification and it is now dominated by fixed dunes. The Hulunbuir Sandy Land covers 7,200 km^2, and is dominated by fixed and semi-fixed dunes.

Data Sources

NDVI Data

We used NDVI as an indicator of vegetation cover. NDVI is calculated as follows:

$$NDVI = (NIR - \mathrm{Red}) / (NIR + \mathrm{Red}) \quad (1)$$

Where Red and *NIR* represent the spectral reflectance measurements acquired in the red (visible) and near-infrared regions, respectively (Purevdorj et al., 1998). We used a NDVI dataset for the period from 1998 to 2015 derived from the VEGETATION sensor onboard the SPOT-4 satellite. This data is collected by the Kiruna (Sweden) ground station, and the image quality is controlled by a monitoring center in Toulouse (France), which provides relevant parameters (such as calibration coefficients). The VEGETATION Processing Center of the Flemish Institute for Technological Research is responsible for preprocessing of the global vegetation data at a spatial resolution of 1 km and a temporal resolution of 10 days (Duchemin, 2004). To ensure the data quality, the institute implements simplified methods for atmospheric corrections, radiation corrections, and geometric corrections (Rahman and Dedieu, 1994). We further processed the data using the maximum-value compositing (MVC) algorithm (Holben, 1986) to minimize non-vegetation effects caused by cloud cover, atmospheric interference, and large solar zenith angles (Stow et al., 2007). The SPOT VEGETATION dataset has been widely used by scholars in many countries to study vegetation and the ecological environment (Fraser and Li, 2002; Delbart et al., 2006; Stibig et al., 2007; Zhou et al., 2009; Song et al., 2010).

We obtained monthly NDVI (MNDVI) data using the MVC algorithm, as follows:

$$MNDVI = Max(NDVI_1, NDVI_2, NDVI_3) \quad (2)$$

where $NDVI_1$, $NDVI_2$, and $NDVI_3$ represent the maximum NDVI during the first 10 days, second 10 days, and third 10 days in each month, respectively. We then used the same method (i.e., the MVC algorithm) to process the MNDVI values and calculate the annual NDVI values.

Desert Map of China

The desert area in 2000 was classified into the six major types in Appendix **Table 1** using the 1:100 000 scale desert distribution map of China (http://westdc.westgis.ac.cn), which was created by interpreting Landsat TM data.

Climate Data

We obtained annual average temperature and total precipitation data from 1998 to 2015 from the Data Center for Resources and Environmental Sciences, Chinese Academy of Sciences (http://www.resdc.cn). These gridded datasets (1 km × 1 km) were

interpolated using the ANUSPLIN software (Hutchinson, 1998) based on daily observations from more than 2,400 meteorological stations distributed throughout China. We extracted the gridded datasets for the study area using the Extract by Mask tool provided by version 10.3 of ArcMap (https://desktop.arcgis.com/en/arcmap/).

Analyses

Trend Analysis

We used linear regression analysis to analyze the NDVI trends over time. We calculated the trend for each pixel (the slope) using the Raster Calculator tool provided by version 10.3 of ArcMap using the following formula:

$$Slope = \frac{n*\sum_{i=1}^{n} i*Y_i - \left(\sum_{i=1}^{n} i\right)\left(\sum_{i=1}^{n} Y_i\right)}{n*\sum_{i=1}^{n} i^2 - \left(\sum_{i=1}^{n} i\right)^2} \quad (3)$$

Where i represents the number of the year (i.e., 1998 = 1), and Y_i represents the NDVI value in year i. The vegetation cover increased when slope >0, decreased when slope <0, and was stable when slope ≈0.

Correlation Analysis

The partial correlation coefficient measures the degree of association between two random variables after removing the effects of the set of controlling random variables (Baba et al., 2015). In the present research, we calculated the pixel-based partial correlation between the effects of the two climatic variables (temperature and precipitation) on the NDVI change (i.e., the slope of the trend for each pixel). First, we calculated the linear correlation coefficient using the following formula:

$$R_{xy} = \frac{\sum_{i=1}^{n}\left[(x_i - \overline{x})*(y_i - \overline{y})\right]}{\sqrt{\sum_{i=1}^{n}(x_i - \overline{x})^2}\sqrt{\sum_{i=1}^{n}(y_i - \overline{y})^2}} \quad (4)$$

Where R_{xy} is the linear correlation coefficient for the variables x and y, x_i and y_i are the values of these variables in year i, $\overline{x}$ and $\overline{y}$ represent the average of the two variables during the n years of the study period, and n is the number of years. We then calculated the partial correlation coefficient based on the linear correlation coefficient, as follows:

$$R_{xy,z} = \frac{R_{xy} - R_{xz}*R_{yz}}{\sqrt{(1 - R_{xz}2)}\sqrt{\left(1 - R_{yz}2\right)}} \quad (5)$$

Where $R_{xy,z}$ is the partial correlation coefficient between the dependent variable x and the independent variable y after the independent variable z is fixed. We tested the significance of the partial correlation coefficient using the t test:

$$t = \frac{R_{xy,z}*\sqrt{n - m - 1}}{\sqrt{\left(1 - R_{x,yz}2\right)}} \quad (6)$$

Where n is the number of samples (for the time series from 1998 to 2015, n = 18), and m is the number of independent variables.

In fact, the change of one factor is often affected by the combined effects of multiple factors, and the factors are interrelated. Thus, we calculated the multiple-correlation coefficient based on the correlation and partial correlation coefficients, as follows:

$$R_{x,yz} = \sqrt{1 - \left(1 - R_{xy}2\right)*\left(1 - R_{x,yz}2\right)} \quad (7)$$

Where $R_{x,yz}$ is the multiple-correlation coefficient for the dependent variable x and the independent variables y and z. We used the F-test to identify significant multiple-correlation coefficients, as follows:

$$F = \frac{(n - k - 1)*R_{x,yz}2}{k*\left(1 - R_{x,yz}2\right)} \quad (8)$$

Where n is the number of samples (for the time series from 1998 to 2015, n = 18), and k is the number of independent variables. The specific processing steps of this study are presented in **Supplementary Figure S2**.

RESULTS

The Multi-Year Mean NDVI in the Study Area

Spatial Distribution of the Multi-Year Mean NDVI

The overall regional vegetation cover characteristics can be indicated by the multi-year mean NDVI from 1998 to 2015 (**Figure 2**). Overall, the NDVI values increased from west to east, and ranged from 0 to 0.88. The areas with the highest NDVI were mainly located in the Horqin Sandy Land and the Hulunbuir Sandy Land. The NDVI of the Mu Us Sandy Land and the Hunshandake Sandy Land were mainly between 0.14 and 0.40. Areas with poor vegetation cover, with NDVI <0.13, were common in most parts of the western desert area. However, the values ranged between 0.14 and 0.24 in the Gurbantunggut Desert, which is in the center of the Junggar Basin, in the Xinjiang Uygur Autonomous Region.

The Vegetation Cover of Different Desert Types

The vegetation cover varied greatly for the six desert types during the study period (**Table 1**). For the multi-year mean NDVI, the value decreased in the following order: fixed dunes (0.421) > semi-fixed dunes (0.331) > semi-mobile dunes (0.174) > saline–alkali land (0.169) > mobile dunes (0.106) = gobi desert (0.106). Due to the effects of gradual restoration of desertified land, the coefficient of variation (CV) for each desert type exhibited the following trend: saline–alkaline land (93.7%) > mobile dunes (87.3%) > semi-mobile dunes (80.2%) > gobi desert (63.0%) > semi-fixed dunes (54.6%) > fixed dunes (45.9%). This indicated that the vegetation cover tended to be more variable during the initial stages of vegetation restoration. The CV values of saline-alkali land were higher than those of the other desert types, suggesting that vegetation restoration was most unstable in the saline–alkali land.

Temporal and Spatial Variation of Vegetation Cover for the Different Desert Types

Temporal Variations of NDVI Changes in the Desertified Area of China

Figure 3 shows the temporal variations of NDVI for the six desert types from 1998 to 2015. The annual variation had similar trends for the six desert types, with decreases until 2000 followed by increases from 2001 to 2003. There was little change from 2004 to

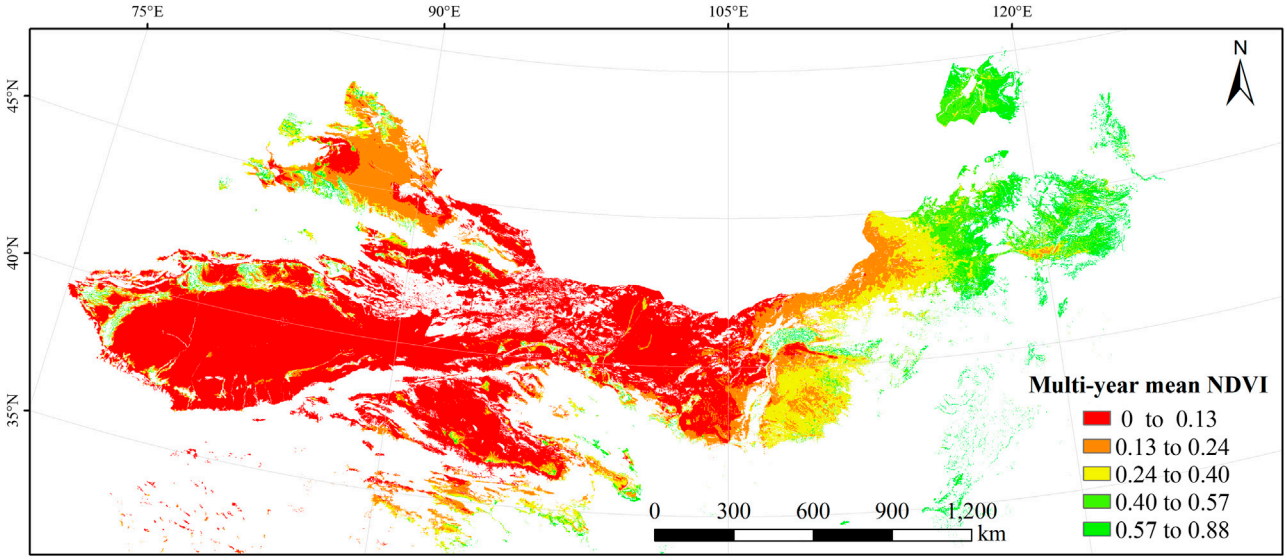

FIGURE 2 | Spatial distribution of the multi-year mean normalized-difference vegetation index (NDVI) of the desertified area of China from 1998 to 2015. The NDVI intervals were calculated using the natural-breaks method provided by ArcMap.

2006, followed by fluctuations after 2007 and a peak in 2012/2013, followed by a decrease until 2015. Fixed and semi-fixed dunes had the highest NDVI values, both of which were much higher than in the other desert types throughout the study period, with a lower NDVI for semi-fixed dunes than for fixed sand dunes. Similarly, mobile and semi-mobile dunes showed very similar NDVI values throughout the study period, as did Gobi desert and saline–alkali land, though NDVI was always lowest for the two latter types.

Spatial Pattern of NDVI Changes in the Desertified Area of China

The NDVI values showed little change in the Badain Jaran, Ulan Buh, and Tengger deserts in the central part of the study area and in many deserts in the western part (**Figure 4**), suggesting that desertification has slowed or stopped in these areas rather than continuing to develop. A large area of light degradation took place in the Gurbantunggut Desert in the northwestern part of the study area. In contrast, areas with increasing vegetation cover were mainly located in the Mu Us, Horqin, and Hulunbuir sandy lands in the eastern part of the study area, as well as around the northern margins of the Taklamakan Desert and southern margins of the Gurbantunggut Desert. The vegetation cover improved particularly greatly in the Mu Us Sandy Land and at the edges of the Horqin Sandy Land. However, not all of these changes were statistically significant (**Figure 5**). Nonetheless, there have been serious decreases of vegetation cover in the Hunshandake Sandy Land and parts of the Horqin Sandy Land.

NDVI Changes for the Six Desert Types

Figure 6 shows the distribution of NDVI changes for the six desert types in the study area from 1998 to 2015. We used these percentages to calculate the proportion of the area of each desert type that changed in different directions. The area where vegetation cover did not change accounted for the largest proportion of the total area, especially for mobile dunes (78.9%), gobi desert (64.0%), semi-mobile dunes (54.4%), and saline–alkali land (54.2%). With increasing or decreasing vegetation cover, the proportion of areas with no NDVI change gradually decreased, so the proportion of the area with changed vegetation cover (including both degradation and restoration) increased. Restoration of vegetation mainly achieved mild to moderate improvement of NDVI. The proportions of the area that showed improved vegetation cover were in the following order: fixed dunes (43.4%) > semi-mobile dunes (39.7%) > semi-fixed dunes (26.7%) > saline–alkali land (23.1%) > gobi desert (14.4%) > mobile dunes (12.5%). The

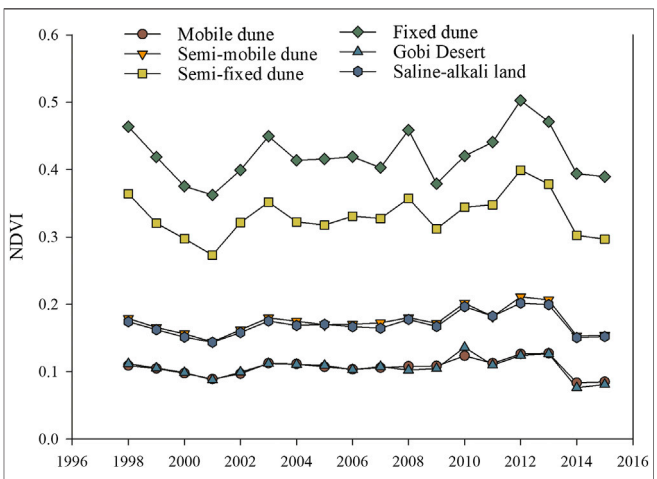

FIGURE 3 | The inter-annual variations of the normalized-difference vegetation index (NDVI) for the six desert types.

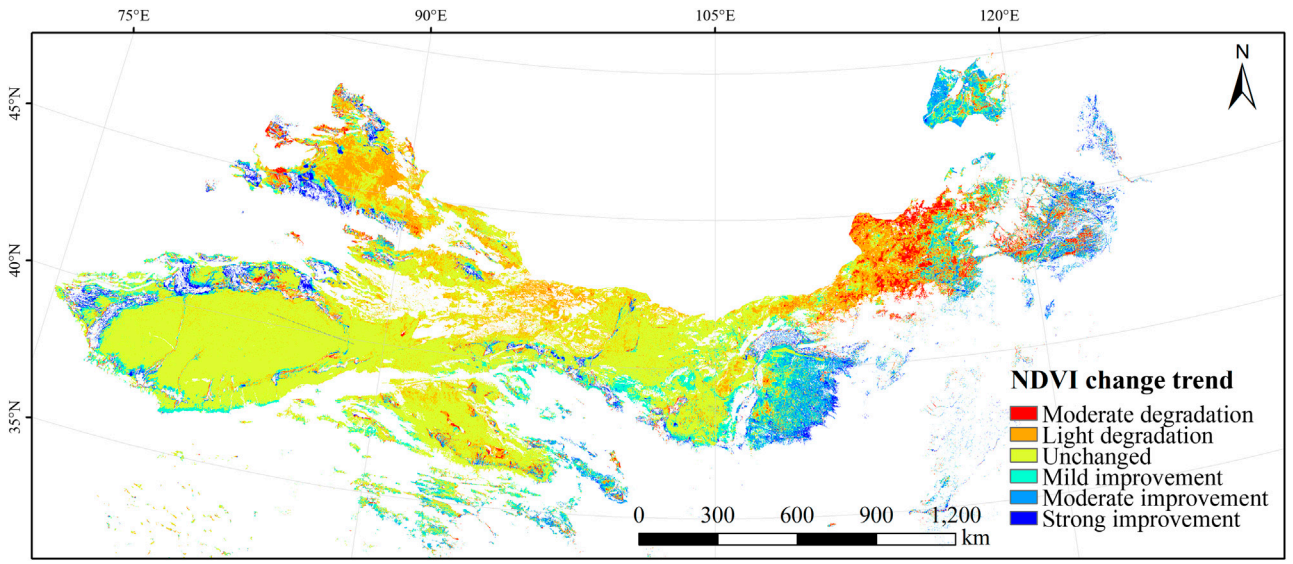

FIGURE 4 | Spatial distribution of the changes in the normalized-difference vegetation index (NDVI) for the six desert types in northern China from 1998 to 2015.

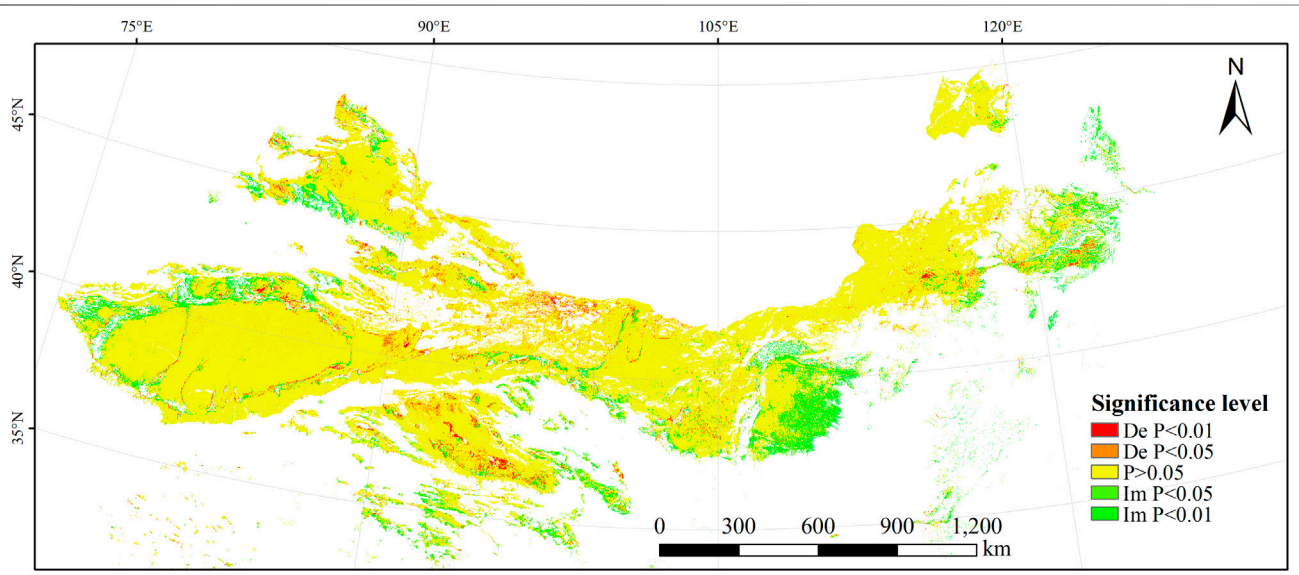

FIGURE 5 | Spatial distribution of statistically significant changes in the annual average normalized-difference vegetation index (NDVI) for the six desert types in northern China from 1998 to 2015. De and Im represent significantly decreasing and increasing NDVI, respectively, and *P* represents the significance level.

proportions of the area that showed decreased vegetation cover were in the following order: fixed dunes (35.1%) > semi-mobile dunes (33.9%) > saline–alkali land (22.7%) > gobi desert (21.6%) > semi-fixed dunes (18.9%) > mobile dunes (8.6%). Only gobi desert showed a greater area of degradation than improvement; this indicated that overall vegetation cover improved in most desert types.

More than half of the total area (56.9%) showed no change in vegetation cover (**Table 2**). For mobile dunes and gobi desert, 24.0 and 14.0% of the area, respectively, showed no NDVI change. The area of light degradation (270.71×10^3 km^2) was larger than that of moderate degradation (68.47×10^3 km^2). The proportion of the area in which vegetation restoration occurred was in the following order: mild improvement (12.6%) > moderate improvement (7.2%) > strong improvement (3.1%). For the total area of desert in China, the proportions of the area that showed improved vegetation cover were in the following order: semi-fixed dunes (5.7%) > semi-mobile dunes (4.4%) > fixed dunes (4.1%) > mobile dunes (3.8%) > gobi desert (3.2%) > saline–alkali land (1.7%). The proportions of the area that showed

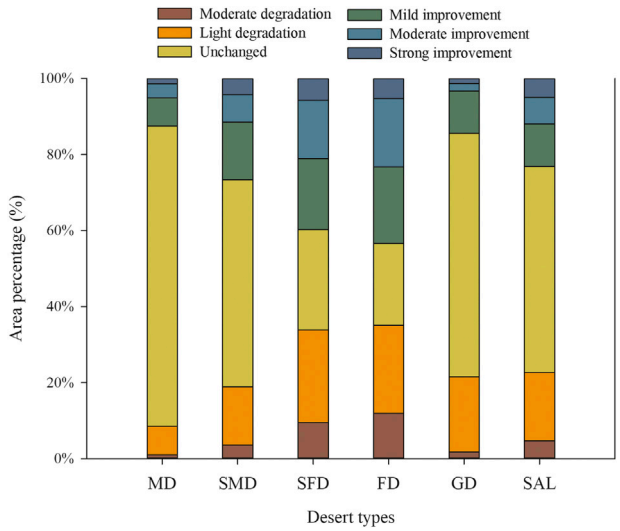

FIGURE 6 | Proportions of the area of each of the six desert types that showed changes in the normalized-difference vegetation index (NDVI) from 1998 to 2015. Desert types: MD, mobile dunes; SMD, semi-mobile dunes; SFD, semi-fixed dunes; FD, fixed dunes; GD, gobi desert; SAL, saline–alkali land.

vegetation degradation were in the following order: semi-fixed dunes (4.9%) > gobi desert (4.7%) > fixed dunes (3.2%) > semi-mobile dunes (3.2%) > mobile dunes (2.6%) > saline–alkali land (1.7%). Of the total desert area in China, 22.8% showed increasing vegetation cover, whereas 20.3% showed decreasing vegetation cover. The areas of vegetation improvement and degradation were both largest for semi-fixed dunes.

Correlations of NDVI With Temperature and Precipitation

Partial Correlations of NDVI With Temperature and Precipitation

Figure 7 shows the spatial distribution of the partial correlations between the multi-year mean NDVI from 1998 to 2015 and the mean annual temperature for the same period. The partial correlation ranged from −0.96 to 0.95. The areas with positive and negative correlations accounted for 66.3 and 33.7% of the study area, respectively. Areas with a positive correlation were mainly distributed in the central and western parts of the study area, whereas negative correlations were mainly located in the four major sandy lands in the eastern part of the study area.

Figure 8 shows the spatial distribution of the partial correlations between the multi-year mean NDVI from 1998 to 2015 and the mean total annual precipitation for the same period. The maximum and minimum values of the correlation coefficient between NDVI and precipitation were 0.95 and −0.90, respectively. The areas with a positive correlation accounted for 81.8% of the total area, and areas with a negative correlation accounted for 18.2% of the study area. The areas with positive correlations were mainly distributed at the western and southern edges of the Taklamakan Desert and in the Gurbantunggut Desert, as well as in the sandy lands in the eastern part of the study area. The negative correlations were mainly located in the Badain Jaran, Ulan Buh, and Tengger deserts in the center of the study area and parts of other deserts in the western part of the study area.

Multiple-Correlation Analysis of NDVI and the Climate Drivers

Figure 9 shows the spatial distribution of the multiple-correlation coefficient between the multi-year mean NDVI from 1998 to 2015 and the climate drivers. The multiple-correlation coefficient ranged from 0 to 0.96. Overall, the areas with a high multiple-correlation coefficient were mainly distributed in the Hunshandake Sandy Land, Hulunbuir Sandy Land, and parts of the Gurbantunggut Desert. The areas with a weak correlation were mainly located in the central area and in the region between the Taklamakan Desert and Gurbantunggut Desert.

Classification of the Driving Factors for NDVI Changes

To further analyze the effects of the driving factors on the dynamic change in NDVI, we defined classification criteria for the dominant driving factors (Appendix **Table 2**) based on previous research on these factors (Mohamed et al., 2004; Liu and Gao, 2009; Wang et al., 2017).

Figure 10 shows the spatial distribution of the driving factors for changes in NDVI in the study area based on the criteria in Appendix **Table 2**. The area where NDVI changes were driven strongly by both precipitation and temperature was very small, accounting for only 0.4% of the total area (**Table 3**); this proportion was <1% for all desert types. In contrast, the area weakly driven by both precipitation and temperature was larger (16.1%) but scattered. The area driven strongly by precipitation (14.1%) was far greater than the area dominated by temperature (1.8%). The areas where precipitation was the major driver were mainly located in the Hunshandake and Hulunbuir sandy lands. NDVI change in rest of the study area was driven primarily by non-climatic factors, which accounted for 67.6% of the study area.

Table 3 shows that the proportion of the area in which the NDVI change was driven primarily by precipitation was in the following order: semi-fixed dunes (30.9%) > fixed dunes (28.5%) > semi-mobile dunes (14.8%) > gobi desert (10.9%) > saline–alkali land (8.9%) > mobile dunes (5.3%). The proportion of the area where NDVI change was driven by non-climate factors was >70% for mobile dunes, gobi desert, and saline–alkali land, and >65% for semi-mobile dunes; this indicates that the effects of the climate drivers on vegetation cover were weak in these areas. Therefore, more vegetation restoration projects are needed in these desert types.

DISCUSSION

NDVI Changes for the Six Desert Types

Overall, NDVI in the desert areas of northern China decreased before 2000, and there was a clear increasing trend after 2000 (**Figure 3**). This result, combined with the strong importance of

TABLE 2 | Changes in the area in which the normalized-difference vegetation index (NDVI) changed from 1998 to 2015 for the six deserttypes.

Change	Mobile dunes		Semi-mobile dunes		Semi-fixed dunes		Fixed dunes		Gobi desert		Saline–alkali land		Total area	
	Area (10^3 km^2)	Proportion of total (%)	Area (10^3 km^2)	Proportion of total (%)	Area (10^3 km^2)	Proportion of total (%)	Area (10^3 km^2)	Proportion of total (%)	Area (10^3 km^2)	Proportion of total (%)	Area (10^3 km^2)	Proportion of total (%)	Area (10^3 km^2)	Proportion of total (%)
Moderate degradation	5.159	0.31	9.939	0.59	22.808	1.36	18.345	1.10	6.379	0.38	5.839	0.35	68.47	4.09
Light degradation	38.65	2.31	42.746	2.56	58.717	3.51	35.785	2.14	72.71	4.35	22.106	1.32	270.71	16.18
Unchanged	401.815	24.02	151.85	9.08	63.395	3.79	33.17	1.98	234.662	14.03	66.824	3.99	951.72	56.89
Mild improvement	37.94	2.27	42.259	2.53	44.775	2.68	31.075	1.86	40.636	2.43	13.808	0.83	210.49	12.58
Moderate improvement	18.859	1.13	20.374	1.22	36.967	2.21	27.776	1.66	7.532	0.45	8.565	0.51	120.07	7.18
Strong improvement	7.065	0.42	11.741	0.70	13.797	0.82	8.149	0.49	4.678	0.28	6.133	0.37	51.56	3.08

The percentages represent the proportion of the total area of desertin China accounted for by the area of each deserttype

non-climate factors (**Table 3**), demonstrated that the improvement of vegetation cover occurred as a result of the initial stage (1998–2010) of the ecological restoration projects implemented by the Chinese government, although precipitation also had a significant effect in some areas. However, the NDVI change differed among the six desert types. Of the total area of fixed dunes, 43.4% showed increased vegetation cover (**Figure 6**); this was the highest percentage for the six desert types, and suggested that fixed dunes responded best to vegetation restoration. In contrast, the effects of restoration were worst for mobile dunes, with only 12.5% of the area of this type showing improved vegetation cover. Similarly, the most and least degradation appeared in areas of fixed dunes and mobile dunes, respectively. This contradicts a previous study in which the restoration was most effective in mobile dunes (Zhang et al., 2012). The difference may be mainly due to the differences in the study areas, since Zhang et al. only studied the Horqin Sandy Land. There are 0.43×10^6 km^2 of mobile sand dunes in the Horqin Sandy Land, accounting for 15.8% of its area, and soil degradation has been greatly reduced by planting sand scrubs on mobile dunes. This would reduce wind speeds (thus, wind erosion) and improve the microclimate around the plants, creating conditions more conducive to vegetation growth (Gagnaire-Renou et al., 2001; Zhao et al., 2007). Unfortunately, mobile dunes accounted for more than half of the total area of desert in our study area (**Table 1**). Such a large proportion would increase the difficulty of vegetation restoration. However, both Zhang et al.'s study and the present study showed that fixed dunes responded strongly to restoration, with greatly increased vegetation cover.

The mean NDVI increased at a rate of 0.013 per year for semi-fixed dunes and fixed dunes, vs. only 0.0003 for mobile dunes (**Table 4**). The vegetation therefore showed an increased response to restoration as dune stability increased. Thus, future vegetation restoration should pay more attention to desert types with low vegetation cover, such as mobile dunes, saline–alkali land, and gobi desert, with the goal of restoring them to a condition that will let them respond more strongly to subsequent restoration efforts.

Spatial Pattern of NDVI Changes in the Desert Area

A large area of light degradation took place at the edges of the Gurbantunggut Desert and Taklamakan Desert. This may be because both deserts are located in an arid zone, and desertification control measures in such arid areas mainly included establishing belts of sand-fixing grasses at the edge of oases and planting sand-fixing plants in mobile sand dunes near these oases. In contrast, vegetation cover decreased seriously in the Hunshandake Sandy Land, a region with strong winds that is an important source of blowing sand in Beijing and Tianjin. Here, desert expanded greatly from 1960 to 1987, with the area of desertified land reaching its maximum by 2000. The Beijing–Tianjin Sandstorm Source Project, implemented between 2000 and 2005, caused initial restoration of the severely desertified land, but only about 65 km^2 of desertified land was restored in the Hunshandake Sandy Land; given the

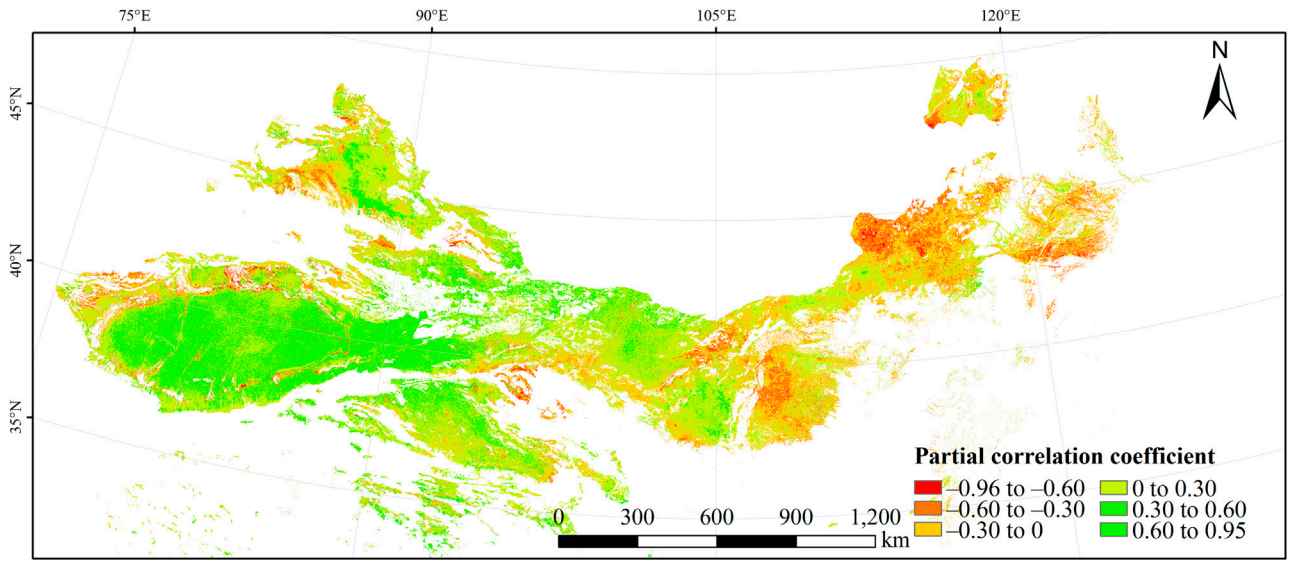

FIGURE 7 | Spatial distribution of partial correlations between the multi-year mean normalized-difference vegetation index (NDVI) from 1998 to 2015 and the mean annual temperature for the same period in the desert area of northern China.

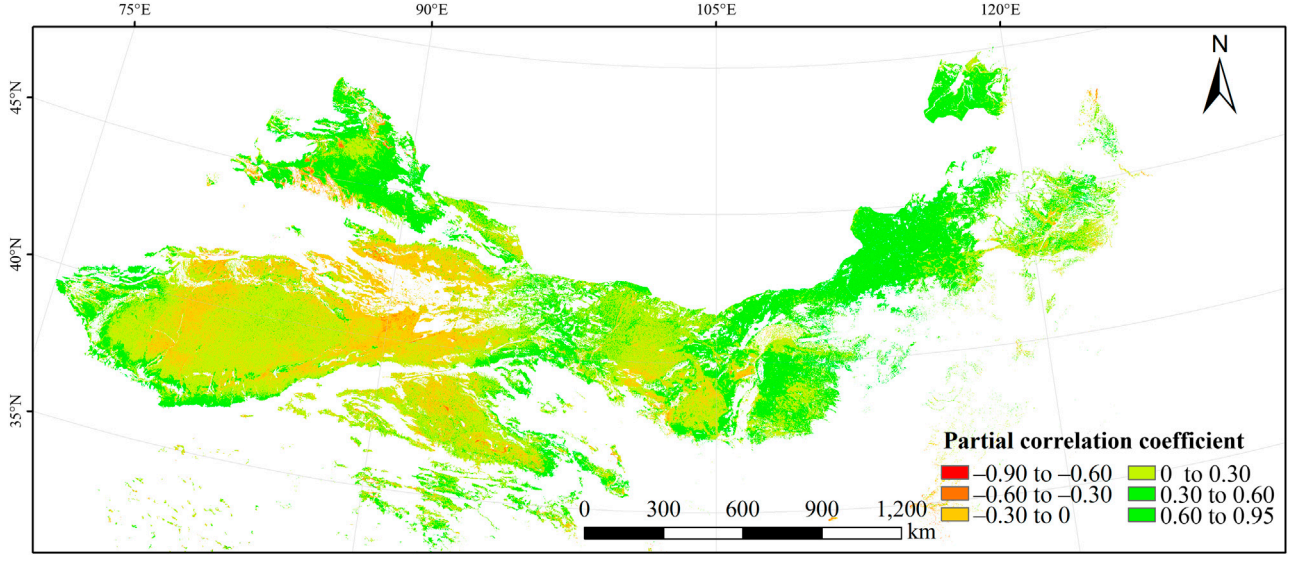

FIGURE 8 | Spatial distribution of partial correlations between the multi-year mean normalized-difference vegetation index (NDVI) from 1998 to 2015 and the mean total annual precipitation for the same period in the desert area of northern China.

large size of this area, restoration of its desertified land will be a long-term process (Liu and Wang, 2007). The areas with improved vegetation cover were mainly located in the Mu Us Sandy Land, Horqin Sandy Land, and Hulunbuir Sandy Land, which is consistent with previous results (Li et al., 2007; Wang et al., 2010; Yan and Bo, 2013). These three sandy lands, which are located in moister parts of our study area, were located in an area where NDVI changes were strongly driven by precipitation (**Figure 10**). Thus, the effectiveness of ecological restoration projects was greater in areas where changes were driven by precipitation.

The Effects of Climate Factors on NDVI Change

On a global scale, Schultz and Halpert (1995) reported that the time variation of NDVI is not highly correlated with climate variation. Whereas Ichii et al. (2002) found that NDVI trends are

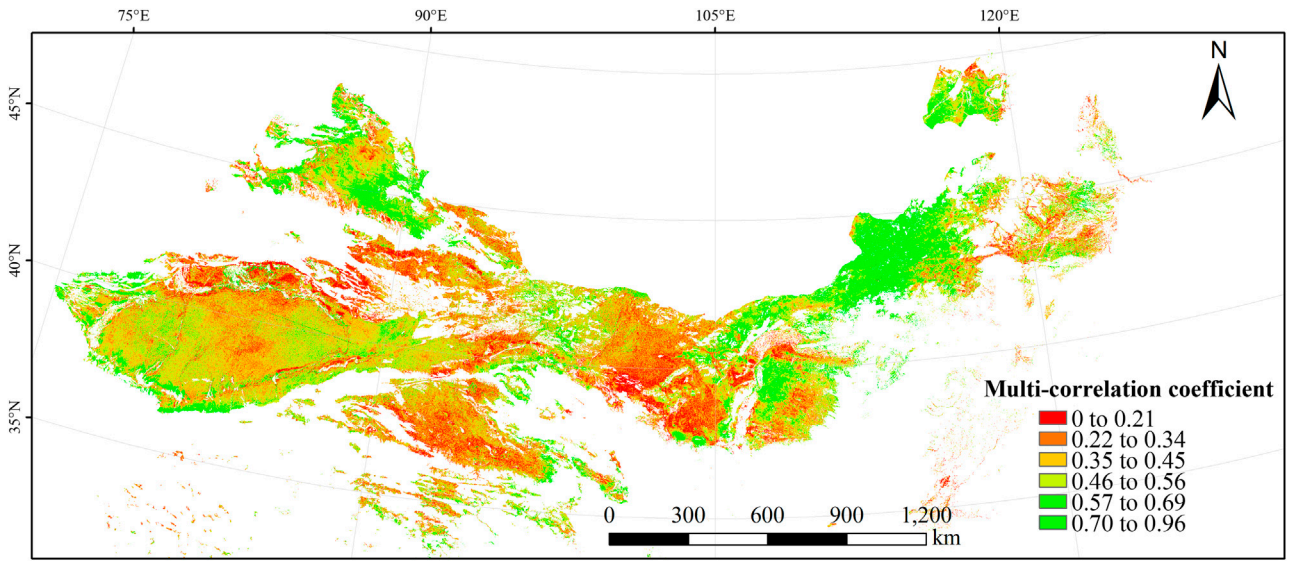

FIGURE 9 | Spatial distribution of the multiple-correlation coefficient between the multi-year mean normalized-difference vegetation index (NDVI) from 1998 to 2015 and the two climate drivers (temperature and precipitation) for the same period in the desert area of northern China.

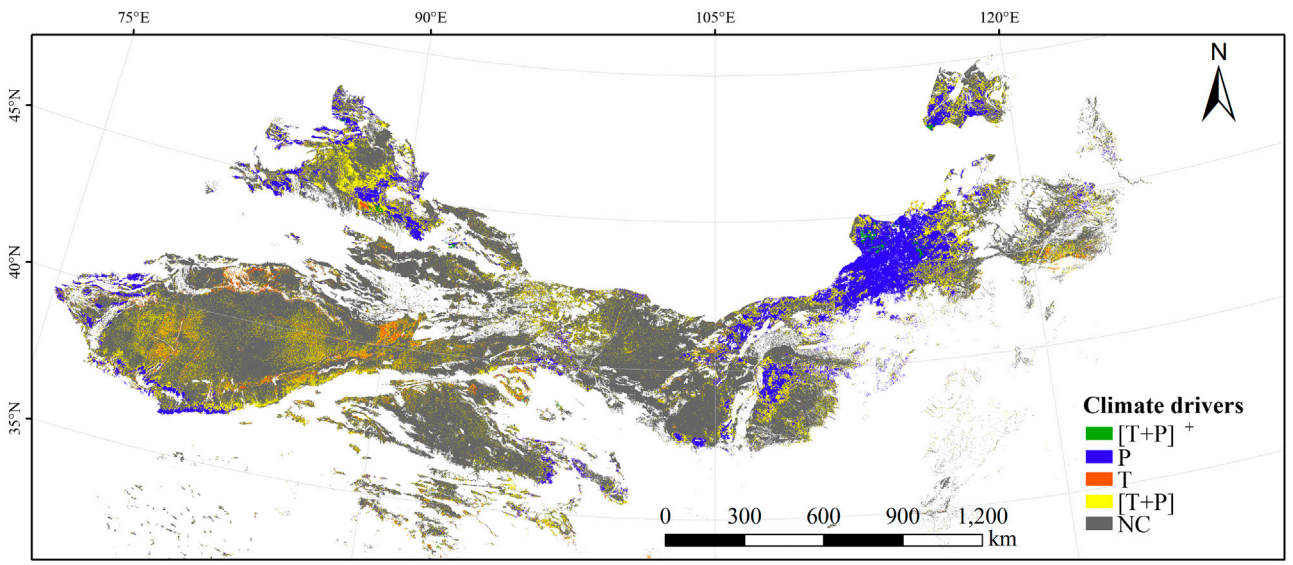

FIGURE 10 | Spatial distribution of the effects of the driving factors on changes in the multi-year normalized-difference vegetation index (NDVI) in the desert area of China from 1998 to 2015. $[T + P]^+$ represents changes driven strongly by temperature and precipitation, P represents changes driven mainly by precipitation, T represents changes driven mainly by temperature, [T + P] represents changes driven weakly by temperature and precipitation, and NC represents changes driven by non-climate factors.

mainly controlled by temperature rise in the northern mid- and high latitudes and precipitation decrease in the semiarid regions of the Southern Hemisphere. On a regional scale, Djebou et al. (2015) found that the long-term trends in vegetation dynamics may not be a direct consequence of precipitation in the southwestern United States. However, the factors sustaining trends in NDVI are complex (Barbosa et al., 2006). For instance, in northern Patagonia's arid and semi-arid ecosystems, Fabricante et al. (2009) highlighted that precipitation may not be the main driver of NDVI fluctuations during certain periods of the year. Piao et al. (2006) found a relationship between the NDVI trend and air temperature. Furthermore, the relationship between vegetation change and climate variables in the dry climate region was notable. It was reported that there is a strong relationship between the magnitude of vegetation response to precipitation and the

TABLE 3 | The proportion of the study area in which NDVI changes from 1998 to 2015 were dominated by different driving factors for the six desert types.

	Proportion (%) of total desert area						
Driving factor	**Mobile dunes**	**Semi-mobile dunes**	**Semi-fixed dunes**	**Fixed dunes**	**Gobi desert**	**Saline–alkali land**	**Total area**
$[T+P]^+$	0.11	0.37	0.83	0.98	0.22	0.32	0.38
P	5.26	14.77	30.87	28.54	10.92	8.86	14.10
T	1.87	2.29	1.67	1.29	0.95	3.51	1.78
[T+P]	14.57	16.20	18.45	20.58	15.40	14.56	16.13
NC	78.19	66.36	48.18	48.61	72.51	72.75	67.61

$[T+P]^+$ represents changes driven strongly by temperature and precipitation, P represents changes driven mainly by precipitation, T represents changes driven mainly by temperature, [T+P] represents changes driven weakly by temperature and precipitation, and NC represents changes driven by non-climate factors.

aridity gradient in several dry climate regions of the globe, such as Inner Mongolia (Chuai et al., 2013), the Tibetan Plateau (Ding et al., 2007), the African Sahel (Schmidt et al., 2014; Fensholt et al., 2013), northern Patagonia (Fabricante et al., 2009), and the northeast region of Brazil (Barbosa et al., 2006). In 66.3% of the study area, we found a positive correlation between temperature and NDVI, primarily in the central and western parts (**Figure 7**). This may be mainly due to increased photosynthesis at higher temperatures, which promotes vegetation growth so long as the rainfall is relatively stable and does not become a limiting factor (Diao and Xia, 2016). Similarly, 81.8% of the study area showed a positive correlation between NDVI and precipitation (**Figure 8**), mainly distributed in the semi-arid areas. This result was consistent with previous research in the Horqin Sandy Land, where precipitation was positively correlated with increased vegetation cover, and where this correlation was stronger than that for temperature (Huang et al., 2016).

The area in which NDVI changes were driven primarily by temperature (1.8%) was far less than the area dominated by precipitation (14.1%), largely because the areas driven by temperature were mainly located in the arid parts of our study area, and higher temperatures would increase evapotranspiration, thereby increasing stress on the vegetation and restricting the vegetation cover (Cao et al., 2011). This would also reduce the correlation between NDVI and temperature (Zhang et al., 2008a). In contrast, the areas driven by precipitation were mainly in the moister Hunshandake, Horqin, and Hulunbuir sandy lands. In recent years, the amount of precipitation has decreased continuously in this region, and sandy grassland is highly sensitive to changes in precipitation; thus, precipitation is a dominant factor influencing the growth of vegetation in these sandy lands (Mao et al., 2012).

Effectiveness of Ecological Restoration Projects in Desert Areas

The natural and socioeconomic conditions in desertified areas in China are complex and diverse, and the resource advantages or disadvantages and the direction of regional economic development differ among these regions. Therefore, the measures that have been adopted for desertification control also differed. To control the expansion of desert as soon as possible, Ecological Function Reserves have been established in areas with serious desertification (**Figure 11**). These reserves are areas in which activities such as agriculture and livestock grazing have been prohibited or greatly reduced to mitigate the pressure on the ecosystem, and in which intensive vegetation restoration has been conducted. The ecological functions and restoration measures for these protected areas are summarized in Appendix **Table 3**.

We estimated the annual change rate of the NDVI from 1998 to 2015 for the Ecological Function Reserves in Appendix **Table 3**. The mean NDVI increased in most ecological protection zones, but decreased in the Alkin Desert Grassland Ecological Function Reserve and the Hunshandake Sandy Land Ecological Function Reserve (Appendix **Table 3**). Outside of these reserves, the mean NDVI increased at a rate of 0.0005 per year. In contrast, annual NDVI in some Ecological Function Reserves was far larger than this value: Eight times this rate in the Yili Ecological Function Reserve, more than 15 times this rate in the Songnen Plain Wetland Ecological Function Reserve, more than five times this rate in the Horqin Sandy Land Ecological Function Reserve, three times this rate in the Yangtze River Source Ecological Function Reserve, more than five times this rate in the Yellow River Source Ecological Function Reserve, more than 10 times this rate in the Mu Us Sandy Land Ecological Function Reserve, and 20 times this rate in the Loess Plateau Ecological Function Reserve. These results strongly suggest that desertification has been mitigated by the ecological restoration measures that were implemented in these areas.

However, NDVI did not increase much faster than the rate for the overall study region in several of the reserves: the Tianshan Mountain Ecological Function Reserve, Tarim River Basin Ecological Function Reserve, Heihe River Basin Ecological Function Reserve, and Altai Mountain Ecological Function Reserve. This indicates that the ecological restoration effects were weak in these western desert areas, possibly because precipitation is a greater constraint in this region. In addition, the sensitivity of the Alkin Desert Grassland to desertification was very high due to the extremely arid climate and the scarcity of vegetation. To promote NDVI growth, it will be necessary to stop all development activities in this region, and especially any human activities that damage the reserve's ecological functions; for example, it will be necessary to establish more sustainable levels for the grassland's livestock carrying capacity, return grazing areas to protected grassland, ban grazing during periods when the grassland is most vulnerable, establish grazing exclosures and implement rotation grazing, and implement

TABLE 4 | The annual mean rate of increase of the normalized-difference vegetation index (NDVI) from 1998 to 2015 for the six desert types.

	Desert type					
	Mobile dunes	**Semi-mobile dunes**	**Semi-fixed dunes**	**Fixed dunes**	**Saline–alkali land**	**Gobi desert**
Increase in NDVI (per year)	0.0003	0.0012	0.0013	0.0013	0.0000	0.0011

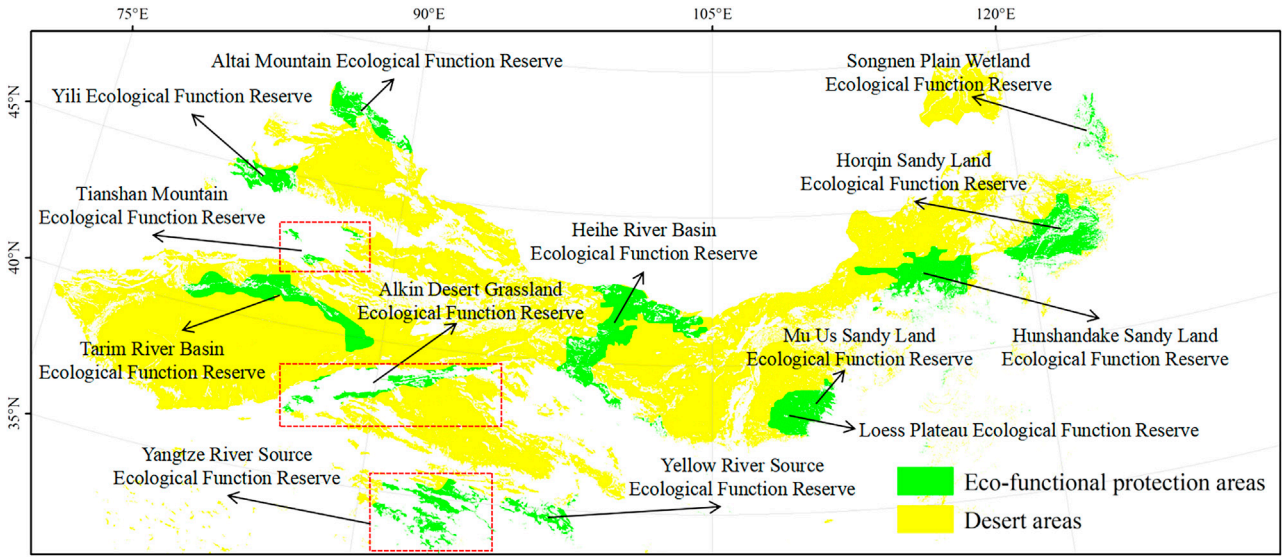

FIGURE 11 | The Ecological Function Reserves that have been established in northern China's desert areas.

ecological migration (i.e., relocation of farmers and herders to more suitable areas where their activities can be sustained) in severely degraded areas. In the Hunshandake Sandy Land, degradation of the grassland ecosystem by unsustainable development and utilization of the grassland resources has been occurring for a long time, leading to the development of a large area of degraded grassland, serious desertification, decreasing soil fertility in cultivated land, loss of forests caused by firewood production, and drought and water shortages, which together threaten the region's ecological security. To mitigate these problems, the government should take aggressive measures to stop the land-use practices that are responsible for degradation, restore the native ecosystems, and promote changes to the traditional energy structure in rural areas by encouraging the adoption of alternative energy sources such as natural gas that would reduce the need to harvest trees to provide firewood. In addition, efforts must be made to adopt agricultural methods to use water more efficiently, such as the implementation of mulches to reduce evaporation of water from the soil surface and the use of drip irrigation rather than flooding for agricultural irrigation.

CONCLUSIONS AND OUTLOOK

Based on satellite NDVI data and gridded climate datasets from 1998 to 2015, we assessed the effectiveness of the large-scale ecological restoration projects that have been implemented in northern China, and analyzed the effect of the two main climate drivers (precipitation and temperature) on the region's vegetation dynamics and the spatial distribution of NDVI and changes in NDVI. We found that vegetation covers generally increased as a result of the restoration projects, but that the change in NDVI differed among the six desert types. The most and least improvement in vegetation cover appeared in fixed and mobile dunes, respectively. The vegetation covers also increased more as dune stability increased. Thus, more efforts should be paid to restoration of desert types with low vegetation cover and unstable dunes in future vegetation restoration projects; by increasing their stability, this will also increase their ability to respond to future restoration efforts.

The effectiveness of ecological restoration projects was strongest in areas where NDVI change was driven by precipitation, such as the Loess Plateau and the Mu Us, Horqin, and Hulunbuir sandy lands. In contrast, ecological restoration projects in the Badain Jaran, Ulan Buh, and Tengger deserts were ineffective, and there has been a serious decrease in vegetation cover in the Hunshandake Sandy Land and the Alkin Desert Grassland. Thus, more or different ecological restoration efforts must be implemented in these areas.

This study aimed to employ remote sensing and geographic information system (GIS) to examine the relationship between NDVI and climate drivers. The following recommendations are

made to upgrade the methodology described in this study as an effective tool desertification monitoring.

(1) NDVI on its own is a crude mean of vegetation changes. It must therefore be related and integrated to biophysical data (such as soil type, evapotranspiration etc.) in order to determine areas at risk, and other socio-economic information, in order to determine groups at risk of desertification. GIS is an essential tool for integration of such diverse data sets, in order to facilitate timely decision making.
(2) The NDVI was used to reflect vegetation dynamics of desert areas in the present study, to achieve the assessment goal of desertification in future research, it is necessary to compare the sensitivity of various indices to desertification, e.g. Modified Soil-adjusted vegetation index (MSAVI), Normalized Difference Water Index (NDWI), Soil brightness Index (SBI), Wetness vegetation index (WVI) etc.
(3) NDVI time-series data sets have been widely used in vegetation dynamic change monitoring. However, the significant residual effects and noise levels impede the application of NDVI time-series data in environmental change research. Although the maximum-value compositing (MVC) technique (Holben, 1986) has been widely used to eliminate the effect of cloud contamination and the residual atmosphere, it is necessary to reconstruct high-quality NDVI time series by novel and robust filter method, e.g., the moving weighted harmonic analysis (MWHA) method (Yang et al., 2015), the iterative interpolation for data reconstruction (IDR) method (Julien and Sobrino, 2010), the mean value iteration filter (MVI) method (Ma and Veroustraete, 2006), changing weight filter (CWF) method (Zhu et al., 2012), etc.
(4) Assessment of wind (direction and speed) in the study area.
(5) Changes in the non-climate environment, such as changes in the groundwater level and soil matrix, will affect the NDVI-climate relationship (Lv et al., 2013; Liang and Yang, 2016). Therefore, to improve the prediction of NDVI response to future climate change, we should consider all kinds of uncertainty factors when analyzing the NDVI-climate relationship.

DATA AVAILABILITY STATEMENT

The raw data supporting the conclusions of this article will be made available by the authors, without undue reservation.

AUTHOR CONTRIBUTIONS

XuW organized and wrote the paper. XiW, XG and JL assisted in processing the data. XuW did this paper under the guidance of QYL and LYL. All authors reviewed the manuscript.

FUNDING

This research was supported by the National Key R & D Program of China (2017YFA0604803), the National Natural Science Foundation of China (31971466 and 32001214), the National Natural Science Foundation of Gansu Province (20JR5RA089), and the Strategic Priority Research Program of the Chinese Academy of Sciences (XDA23060404).

SUPPLEMENTARY MATERIAL

The Supplementary Material for this article can be found online at: https://www.frontiersin.org/articles/10.3389/fenvs.2021.633020/full#supplementary-material.

REFERENCES

Alphan, H., and Yilmaz, K. T. (2005). Monitoring environmental changes in the Mediterranean coastal landscape: the case of Cukurova, Turkey. *Environ. Manage.* 35 (5), 607–619. doi:10.1007/s00267-004-0222-7

Arnous, M. O., Cheikh, M. A. S., Mongi, B. Z., Aliout, R., and Muntoni, F. (2009). "Remote sensing technology application for desertification mapping a case study, Oudia, Tunisia," in *Desertification and risk analysis using high and medium resolution satellite data*. Editors Marini, A., and Talbi, M., Dordrecht: Springer, 183–197.

Baba, K., Shibata, R., and Sibuya, M. (2015). Partial correlation and conditional correlation as measures of conditional independence. *Aust. N. Z. J. Stat.* 46, 657–664. doi:10.1111/j.1467-842X.2004.00360.x

Barbosa, H. A., Huete, A. R., and Baethgen, W. E. (2006). A 20-year study of NDVI variability over the Northeast Region of Brazil. *J. Arid Environ.* 67 (2), 288–307. doi:10.1016/j.jaridenv.2006.02.022

Cao, X. M., Chen, X., Bao, A. M., and Wang, Q. (2011). Response of vegetation to temperature and precipitation in xinjiang during the period of 1998-2009. *J. Arid Land.* 3 (2), 94–103. doi:10.3724/SP.J.1227.2011.00094

Chuai, X. W., Huang, X. J., Wang, W. J., and Bao, G. (2013). NDVI, temperature and precipitation changes and their relationships with different vegetation types during 1998–2007 in Inner Mongolia, China. *Int. J. Climatol.* 33 (7), 1696–1706. doi:10.1002/joc.3543

Clerici, N., Weissteiner, C. J., and Gerard, F. (2012). Exploring the use of MODIS NDVI-based phenology indicators for classifying forest general habitat categories. *Remote Sens.* 4, 1781–1803. doi:10.3390/rs4061781

Del Valle, H. F., Blanco, P. D., Metternicht, G. I., and Zinck, J. A. (2010). Radar remote sensing of wind-driven land degradation processes in northeastern Patagonia. *J. Environ. Qual.* 39 (1), 62–75. doi:10.2134/jeq2009.0071

Delbart, N., Toan, T. L., Kergoat, L., and Fedotova, V. (2006). Remote sensing of spring phenology in boreal regions: a free of snow-effect method using NOAA-AVHRR and SPOT-VGT data (1982–2004). *Remote Sens. Environ.* 101, 52–62. doi:10.1016/j.rse.2005.11.012

Diao, M., and Xia, C. (2016). Analysis on the change of vegetation growth in Junggar Basin during 1982-2013. *For. Resour. Manage.* 5, 39–46. doi:10.13466/j.cnki.lyzygl.2016.05.008

Ding, M. J., Zhang, Y. L., Liu, L. S., Zhang, W., Wang, Z. F., and Bai, W. Q. (2007). The relationship between NDVI and precipitation on the Tibetan Plateau. *J. Geogr. Sci.* 17 (3), 259–268. doi:10.1007/s11442-007-0259-7

Djebou, D. C. S., Singh, V. P., and Frauenfeld, O. W. (2015). Vegetation response to precipitation across the aridity gradient of the southwestern United States. *J. Arid Environ.* 115, 35–43. doi:10.1016/j.jaridenv.2015.01.005

Dong, G. R., Wu, B., Ci, L. J., Zhou, H. S., Lu, Q., and Luo, B. (1999). Present situation, cause and control way of desertification in China. *J. Desert Res.* 4, 22–36.

Duchemin, B. (2004). VEGETATION/SPOT: an operational mission for the Earth monitoring; presentation of new standard products. *Int. J. Remote Sens.* 25, 9–14. doi:10.1080/0143116031000115265

Fabricante, I., Oesterheld, M., and Paruelo, J. M. (2009). Annual and seasonal variation of NDVI explained by current and previous precipitation across Northern Patagonia. *J. Arid Environ.* 73 (8), 745–753. doi:10.1016/j.jaridenv.2009.02.006

FAO (Food and Agriculture Organization of the United Nations) (1993). Sustainable development of dry lands and combating desertification: Definition and general approach to the problem. Available at: http://www.fao.org/3/V0265E/V0265E01.htm#How%20to%20define%20desertification (Accessed January 8, 2021).

Feng, L., Guo, S., Zhu, L., Zhou, Y., and Lu, D. (2017). Urban vegetation phenology analysis using high spatio-temporal NDVI time series. *Urban For. Urban Greening.* 25, 43–57. doi:10.1016/j.ufug.2017.05.001

Fraser, R. H., and Li, Z. (2002). Estimating fire-related parameters in boreal forest using SPOT VEGETATION. *Remote Sens. Environ.* 82, 95–110. doi:10.1016/S0034-4257(02)00027-5

Fung, T., and Siu, W. (2000). Environmental quality and its changes, an analysis using NDVI. *Int. J. Remote Sens.* 21, 1011–1024. doi:10.1080/014311600210407

Gagnaire-Renou, E., Benoit, M., and Forget, P. (2001). Degradation of sandy arid shrubland environments: observations, process modelling, and management implications. *J. Arid Environ.* 47, 123–144. doi:10.1006/jare.2000.0711

Hoang, V. A., Meredith, W., and David, M. (2005). *Remote Sensing for desertification mapping: case study in the coastal area of Vietnam*. 11. Available at: http://www.mekonginfo.org/assets/midocs/0002592-environment-remote-sensing-for-desertification-mapping-case-study-of-vietnam.pdf (Accessed January 6, 2021).

Hoang, V. A., Meredith, W., and David, M. (2003). *A Multi-sensor approach for desertification monitoring in the coastal of Vietnam*, Tyne: School of Civil Engineering and Geosciences University of Newcastle upon Tyne, 16.

Holben, B. N. (1986). Characteristics of maximum-value composite images from temporal AVHRR data. *Int. J. Remote Sens.* 7, 1417–1434. doi:10.1080/01431168608948945

Huang, H. T., Chang, X. L., Yue, X. Y., and Lv, D. Y. (2016). Responses of NDVI changes to air temperature and precipitation of different sandy landscape areas in the Horqin Sandy Land. *J. Desert Res.* 1, 40–49. doi:10.7522/j.issn.1000-694X.2015.00087

Hutchinson, M. F. (1998). Interpolation of rainfall data with thin plate smoothing splines - part i: two dimensional smoothing of data with short range correlation. *J. Geogr. Inf. Decis. Anal.* 2, 153–167.

Ichii, K., Kawbata, A., and Yamaguchi, Y. (2002). Global correlation analysis for NDVI and climatic variables and NDVI trends: 1982–1990. *Int. J. Remote Sens.* 23 (18), 3873–3878. doi:10.1080/01431160110119416

IFAD (2001). Desertification as a global problem. Geneva, Switzerland: Conference of the parties, COP-V, UNCCD: 2.

Jamal, A. (1997). United Nations convention to Combat desertification in those countries experiencing serious drought and/or desertification. *particularly Africa.* 6 (1), 1–6.

Julien, Y., and Sobrino, J. A. (2010). Comparison of cloud-reconstruction methods for time series of composite NDVI data. *Remote Sens. Environ.* 114 (3), 618–625. doi:10.1016/j.rse.2009.11.001

Li, A. M., Han, Z. W., Huang, C. H., and Tan, Z. H. (2007). Remote sensing monitoring on dynamic of sandy desert degree in Horqin Sandy land at the beginning of 21st century. *J. Desert Res.* 4, 546–551. doi:10.3321/j.issn:1000-694X.2007.04.004

Liang, P., and Yang, X. P. (2016). Landscape spatial patterns in the Maowusu (Mu Us) Sandy Land, northern China and their impact factors. *Catena.* 145, 321–333. doi:10.1016/j.catena.2016.06.023

Lin, L., Ma, A. Q., and Ma, Q. M. (2012). Spatial and temporal variations of vegetation coverage in coastal peri-urban area: a case study of Laoshan District, Qingdao. *Environ. Sci. Technol.* 35, 178–185. doi:10.3969/j.issn.1003-6504.2012.01.037

Liu, J. H., and Gao, J. X. (2009). Effects of climate and land use change on the changes of NPP in the farming-pastoral ecotone of Northern China. *Resour. Sci.* 31 (3), 493–500. doi:10.3321/j.issn:1007-7588.2009.03.021

Liu, S. L., and Wang, T. (2007). Study on land desert process in Hunshandake sandy land. *J. Desert Res.* 27 (5), 719–724. CNKI:SUN:ZGSS.0.2007-05-001

Liu, X., Zhou, W., and Bai, Z. (2016). Vegetation coverage change and stability in large open-pit coal mine dumps in China during 1990–2015. *Ecol. Eng.* 95, 447–451. doi:10.1016/j.ecoleng.2016.06.051

Lv, J. J., Wang, X. S., Zhou, Y. X., Qian, K. Z., Wan, L., Eamus, D., et al. (2013). Groundwater-dependent distribution of vegetation in Hailiutu River catchment, a semi-arid region in China. *Ecohydrology.* 6, 142–149. doi:10.1002/eco.1254

Ma, M., and Veroustraete, F. (2006). Reconstructing Pathfinder AVHRR land NDVI time-series data for the Northwest of China. *Adv. Space Res.* 37 (4), 835–840. doi:10.1016/j.asr.2005.08.037

Magney, T. S., Eitel, J. U. H., Huggins, D. R., and Vierling, L. A. (2016). Proximal NDVI derived phenology improves in-season predictions of wheat quantity and quality. *Agr. Forest Meteorol.* 217, 46–60. doi:10.1016/j.agrformet.2015.11.009

Mao, D., Wang, Z., Luo, L., and Yang, G. (2012). Correlation analysis between NDVI and climate in northeast China based on AVHRR and GIMMS data sources. *Remote Sens. Technol. Appli.* 27, 81–89. doi:10.11873/j.issn.1004-0323.2012.1.77

Mohamed, M. A., Babiker, I. S., Chen, Z. M., Ikeda, K., Ohta, K., and Kato, K. (2004). The role of climate variability in the inter-annual variation of terrestrial net primary production (NPP). *Sci. Total Environ.* 332, 123. doi:10.1016/j.scitotenv.2004.03.009

Nash, M., Wickham, J., Christensen, J., and Wade, T. (2017). Changes in landscape greenness and climatic factors over 25 years (1989-2013) in the USA. *Remote Sens.* 9, 295. doi:10.3390/rs9030295

National Desertification Monitoring Data, (2015). *The desert and Sandification State of China*. Available at: http://124.205.185.8/lysjk/indexJump.do?url=view/moudle/searchData/showDetail&keyid=1003491&search= (Accessed 8 April, 2019)

Nemani, R. R., Keeling, C. D., Hashimoto, H., Jolly, W. M., Piper, S. C., Tucker, C. J., et al. (2003). Climate-driven increases in global terrestrial net primary production from 1982 to 1999. *Sci.* 300, 1560–1563. doi:10.1126/science.1082750

NEPAPR (1998). *China National Biodiversity Research Report*. Beijing: China Environmental Science Press.

Nie, Q., Xu, J., Ji, M., Cao, L., Yang, Y., and Hong, Y. (2012). The vegetation coverage dynamic coupling with climatic factors in Northeast China transect. *Environ. Manage.* 50, 405–417. doi:10.1007/s00267-012-9885-7

Nie, Q., and Xu, J. (2015). The relationship between vegetation coverage and climate elements in Yellow River Basin, China. doi:10.7287/peerj.preprints.153v1

Paruelo, J. M., Epstein, H. E., Lauenroth, W. K., and Burke, I. C. (1997). ANPP estimates from NDVI for the central grassland region of the United States. *Ecol.* 78, 953–958. doi:10.1890/0012-9658(1997)078[0953:AEFNFT]2.0.CO;2

Pettorelli, N., Vik, J. O., Mysterud, A., Gaillard, J. M., Tucker, C. J., and Stenseth, N. C. (2005). Using the satellite-derived NDVI to assess ecological responses to environmental change. *Trends Ecol. Evolution.* 20, 503–510. doi:10.1016/j.tree.2005.05.011

Piao, S., Fang, J., Zhou, L., Guo, Q., Henderson, M., Ji, W., et al. (2003). Interannual variations of monthly and seasonal normalized difference vegetation index (NDVI) in China from 1982 to 1999. *J. Geophys. Res.* 108 (D14), 4401. doi:10.1029/2002JD002848

Piao, S. L., Mohammat, A., Fang, J. Y., Cai, Q., and Feng, J. M. (2006). NDVI-based increase in growth of temperate grasslands and its responses to climate changes in China. *Glob. Environ. Change Human Policy Dimens.* 16 (4), 340–348. doi:10.1016/j.gloenvcha.2006.02.002

Purevdorj, T., Tateishi, R., Ishiyama, T., and Honda, Y. (1998). Relationships between percent vegetation cover and vegetation indices. *Int. J. Remote Sens.* 19, 3519–3535. doi:10.1080/014311698213795

Rahman, H., and Dedieu, G. (1994). SMAC: a simplified method for the atmospheric correction of satellite measurements in the solar spectrum. *Int. J. Remote Sens.* 15, 123–143.

Schmidt, M., Klein, D., Conrad, C., Dech, S., and Paeth, H. (2014). On the relationship between vegetation and climate in tropical and northern Africa. *Theor. Appl. Climatol.* 115 (1e2), 341–353. doi:10.1007/s00704-013-0900-6

Schultz, P. A., and Halpert, M. S. (1995). Global analysis of the relationships among a vegetation index, precipitation, and land surface temperature. *Int. J. Remote Sens.* 16, 2755–2777. doi:10.1080/01431169508954590

Song, Y., Ma, M. G., and Veroustraete, F. (2010). Comparison and conversion of AVHRR GIMMS and SPOT VEGETATION NDVI data in China. *Int. J. Remote Sens.* 31, 2377–2392. doi:10.1080/01431160903002409

Stibig, H. J., Belward, A. S., Roy, P. S., Rosalina-Wasrin, U., Agrawal, S., Joshi, P. K., et al. (2007). A land cover map for south and southeast Asia derived from SPOT-4 VEGETATION data. *J. Biogeogr.* 34 (4), 625–637. doi:10.111/j.1365-2699.2006.01637.x

Stow, D., Petersen, A., Hope, A., Engstrom, R., and Coulter, L. (2007). Greenness trends of Arctic tundra vegetation in the 1990s: comparison of two NDVI data sets from NOAA AVHRR systems. *Int. J. Remote Sens.* 28, 4807–4822. doi:10.1080/01431160701264284

Sun, W., Song, X., Mu, X., Gao, P., and Zhao, G. (2015). Spatiotemporal vegetation cover variations associated with climate change and ecological restoration in the Loess Plateau. *Agr. Forest Meteorol.* 209 (1), 87–99. doi:10.1016/j.agrformet.2015.05.002

Tran, H., and Campbell, J. B. (2015). Detecting sand movement: a NDVI time series analysis (Binh Thuan case study). *Conference on Scientific Research Cooperation between Vietnam and Poland in Earth Sciences*. Vietnam: Hanoi university of Mining and Geology.

Tu, Z. F., Li, M. X., and Sun, T. (2016). The status and trend analysis of desert and sandification. *For. Resour. Manage.* 1, 1–5. doi:10.13466/j.cnki.lyzygl.2016.01.001

Wang, A. H., Li, L. I., Chi, Y. B., Wang, Z. Y., and Zhou, H. Z. (2010). Study on monitoring of desert and sandy desert land in China using images of Beijing-1 small satellite. *Sci. Geogr. Sin.* 30, 409–414. doi:10.13249/j.cnki.sgs.2010.03.006

Wang, H. S., Liu, D. S., Lin, H., Montenegro, A., and Zhu, X. L. (2015). NDVI and vegetation phenology dynamics under the influence of sunshine duration on the Tibetan Plateau. *Int. J. Climatol.* 35, 687–698. doi:10.1002/joc.4013

Wang, Q. W., Zhang, T. B., Yi, G. H, Chen, T. T., Bie, X. J., and He, Y. H. (2017). Tempo-spatial variations and driving factors analysis of net primary productivity in the Hengduan mountain area from 2004 to 2014. *Acta Ecol. Sin.* 37 (9), 3084–3095. doi:10.5846/stxb201602030248

Wardlow, B. D., and Egbert, S. L. (2008). Large-area crop mapping using time-series MODIS 250m NDVI data: an assessment for the U.S. Central Great Plains. *Remote Sens. Environ.* 112, 1096–1116. doi:10.1016/j.rse.2007.07.019

Wu, B., and Ci, L. J. (2002). Landscape change and desertification development in the Mu Us Sandland, Northern China. *J. Arid Environ.* 50 (3), 429–444. doi:10.1006/jare.2001.0847

Yan, F., and Bo, W. U. (2013). Desert progress in Mu Us sandy land over the past 40 years. *Arid. Land Geogr.* 36 (6), 987–996.

Yang, G., Shen, H., Zhang, L., He, Z., and Li, X. (2015). A moving weighted harmonic analysis method for reconstructing high-quality SPOT VEGETATION NDVI time-series data. *IEEE T. Geosci. Remote.* 53 (11), 6008–6021. doi:10.1109/TGRS.2015.2431315

Zhang, G., Dong, J., Xiao, X., Hu, Z., and Sheldon, S. (2012). Effectiveness of ecological restoration projects in Horqin Sandy Land, China based on SPOT-VGT NDVI data. *Ecol. Eng.* 38, 20–29. doi:10.1016/j.ecoleng.2011.09.005

Zhang, K., Si, J. H., Wang, R. Y., Wang, X. P., Han, H. T., and Guo, N. (2008a). Impact of climate change on Desert vegetation in alxa region. *J. Desert Res.* 5, 879–885. doi:10.1098/rstb.2012.0074

Zhang, Y., Zhao, Z., Li, S., and Meng, X. (2008b). Indicating variation of surface vegetation cover using SPOT NDVI in the northern part of North China. *Geogr. Res.* 27, 745–477. doi:10.3321/j.issn:1000-0585.2008.04.003

Zhao, H. L., Su, Y. Z., Zhang, H., Zhao, L. Y., and Zhou, R. L. (2007). Multiple effects of shrub on soil properties and understory vegetation in Horqin Sand Land, Inner Mongolia. *J. Desert Res.* 27, 385–390. doi:10.3321/j.issn:1000-694X.2007.03.007

Zhou, H. J., Rompaey, A. V., and Wang, J. A. (2009). Detecting the impact of the "Grain for Green" program on the mean annual vegetation cover in the Shaanxi Province, China using SPOT-VGT NDVI data. *Land Use Pol.* 26, 954–960. doi:10.1016/j.landusepol.2008.11.006

Zhu, W., Pan, Y., Hao, H., Wang, L., Mou, M., and Liu, J. (2012). A changing-weight filter method for reconstructing a high-quality NDVI time series to preserve the integrity of vegetation phenology, *IEEE T. Geosci. Remote.* 50 (4), 1085–1094. doi:10.1109/TGRS.2011.2166965

Conflict of Interest: The authors declare that the research was conducted in the absence of any commercial or financial relationships that could be construed as a potential conflict of interest.

frontiers in Earth Science

ORIGINAL RESEARCH
published: 23 February 2021
doi: 10.3389/feart.2021.609916

A New Automatic Statistical Microcharcoal Analysis Method Based on Image Processing, Demonstrated in the Weiyuan Section, Northwest China

Yaguo Zou[1,2], *Yunfa Miao*[1,2,3]*, *Shiling Yang*[4,5,6], *Yongtao Zhao*[1], *Zisha Wang*[1,2], *Guoqian Tang*[7] *and Shengli Yang*[7]

[1]Key Laboratory of Desert and Desertification, Northwest Institute of Eco-Environment and Resources, Chinese Academy of Sciences, Lanzhou, China, [2]College of Resources and Environment, University of Chinese Academy of Sciences, Beijing, China, [3]Center for Excellence in Tibetan Plateau Earth Sciences, Institute of Tibetan Plateau Research, Chinese Academy of Sciences, Beijing, China, [4]Key Laboratory of Cenozoic Geology and Environment, Institute of Geology and Geophysics, Chinese Academy of Sciences, Beijing, China, [5]CAS Center for Excellence in Life and Paleoenvironment, Beijing, China, [6]College of Earth and Planetary Sciences, University of Chinese Academy of Sciences, Beijing, China, [7]Key Laboratory of Western China's Environmental Systems (Ministry of Education), College of Earth and Environmental Sciences, Lanzhou University, Lanzhou, China

OPEN ACCESS

Edited by:
Atsushi Tsunekawa, Tottori University, Japan

Reviewed by:
Li Wu, Anhui Normal University, China
Jun Inoue, Osaka City University, Japan

***Correspondence:**
Yunfa Miao
miaoyunfa@lzb.ac.cn

Specialty section:
This article was submitted to Quaternary Science, Geomorphology and Paleoenvironment, a section of the journal Frontiers in Earth Science

Received: *24 September 2020*
Accepted: *08 January 2021*
Published: *23 February 2021*

Citation:
Zou Y, Miao Y, Yang S, Zhao Y, Wang Z, Tang G and Yang S (2021) A New Automatic Statistical Microcharcoal Analysis Method Based on Image Processing, Demonstrated in the Weiyuan Section, Northwest China. Front. Earth Sci. 9:609916. doi: 10.3389/feart.2021.609916

Microcharcoal is a proxy of biomass burning and widely used in paleoenvironment research to reconstruct the fire history, which is influenced by the climate and land cover changes of the past. At present, microcharcoal characteristics (amount, size, shape) are commonly quantified by visual inspection, which is a precise but time-consuming approach. A few computer-assisted methods have been developed, but with an insufficient degree of automation. This paper proposes a new methodology for microcharcoal statistical analysis based on digital image processing by ImageJ software, which improves statistical efficiency by 80–90%, and validation by manual statistical comparison. The method is then applied to reconstruct the fire-related environmental change in the Weiyuan loess section since about 40 thousand years before present (ka BP), northwest China with a semi-arid climate, found that the microcharcoal concentration is low in cold and dry climate and high in warm and humid climate. The two main contributions of this study are: 1) proposal of a new, reliable and high efficient automatic statistical method for microcharcoal analysis; and 2) using the new method in a semi-arid section, revealing the paleofire evolution patterns in the semi-arid region was mainly driven by the biomass rather than the aridity degree found in humid regions.

Keywords: microcharcoal, paleofire, automatic statistics, vegetation, Late Pleistocene, loess

INTRODUCTION

Fire is an important ecological factor that can indicate changes of climate, vegetation and human activities. In recent years, with the frequent occurrence of extreme weather events, the incidence of biomass burning has increased (Jolly et al., 2015). This has had significant impacts: ecological damage, economic costs, and human casualties (Ashe et al., 2009; Goldammer et al., 2013), for

example, the 2019–2020 Australian bushfire season (colloquially known as the Black Summer) (Campbell et al., 2020; Lindenmayer and Taylor, 2020). Therefore, it is of practical significance to understand the processes controlling wildfires. However, climate dynamics and vegetation variations operate at relatively larger scales than fire processes (Macias Fauria et al., 2011), which are considered to be the primary control factors of the fire (Moritz et al., 2005). Hence, understanding past fire dynamics and their relationship to environmental factors is a key aspect of preserving and managing present-day ecosystem functions and fire occurrence (Conedera et al., 2009).

An effective method to obtain paleofire data is from sedimentary records (Miao et al., 2016b; Han et al., 2020), using pyrogenic carbon as a proxy of paleofire, since this is produced by the incomplete combustion of organic matter during biomass burning or fossil fuel consumption (Goldberg, 1985). Microcharcoal is an indicator of pyrogenic carbon, and in palynological studies it is also extracted during the pollen extraction process. Microcharcoal can be characterized by its jet-black, opaque, angular particles in samples; otherwise, the clear or brown, amorphous, weakly -structured particles are considered as vegetal matter (Patterson et al., 1987).

At present, the statistical analysis of microcharcoal is mainly based on visual inspection, which is accurate in identifying the microcharcoal characteristics but time-consuming: the manual measurement of the size of each microcharcoal grain is not conducive to improving work efficiency. In terms of our work experience, it takes 2–8 h to count each sample depending on the impurity content, for instance, this study (Weiyuan loess section) includes 76 samples, it will take about 19–76 working days (8 h per working day) to complete the statistics. Therefore, an automatic approach would clearly be advantageous, by increasing the speed at which samples could be analyzed and allowing the analysis of larger numbers of samples (Rhodes, 1998). Automatic counting of microcharcoal is an area that has long been proposed, following the studies of MacDonald et al., (1991) and Horn et al., (1992). However, research in this field is restricted by the development of computer performance and microscopic imaging technology, and has only progressed slowly. In 2004, ImageJ, an open-source, high-performance and lightweight biological image processing software was proposed (Abràmoff et al., 2004). ImageJ was used in microcharcoal analysis for the first time in 2005 (Stevenson and Haberle, 2005), and the procedure has also been used by Hawthorne and Mitchell (2016), but the method is only suitable for a small sample amount (e.g., in a petri dish) and large microcharcoal particle size (>125 μm), and the automation is still inadequate. Another independent study on the automatic analysis of microcharcoal (Thevenon and Anselmetti, 2007) found a method that can be applied to a large number of samples, however, due to the lack of accurate assessment, the results cannot be used directly and still need manual verification. Therefore, the method can only be regarded as computer-aided analysis, rather than automatic analysis.

In this study, we firstly proposed a new automatic statistical method for microcharcoal analysis, based on ImageJ software (Abràmoff et al., 2004). We then applied the new method to the Weiyuan loess section in the semi-arid area of northwest China, to analyze environmental changes in this area since about 40 ka BP. As part of the second-largest arid to semi-arid area in the world, northwestern China is a unique location for studying fire history, along with vegetation and aridity evolution (Miao et al., 2016a); in addition, arid and semi-arid regions are also more vulnerable to global climate change (Prospero and Lamb, 2003; Cook et al., 2004; Sankaran et al., 2005). Therefore, studying the past fire evolution in this region (Huang et al., 2006; Tan et al., 2015; Han et al., 2020; Miao et al., 2020) is helpful to understand the impacts of future climate changes on the incidence and intensity of fire.

MATERIALS AND METHODS

Study Site

The Weiyuan section (Yang S et al., 2015) (104.25°E, 35.13°N) is located in the west of the Loess Plateau, northwest China, at the boundary of the monsoon zone and non-monsoon zone. This region has a semi-arid and typical temperate continental climate, with an annual average temperature of about 6.8°C, and annual average precipitation of around 363 mm (Yang X et al., 2015; **Figure 1A**).

The section is located on a fluvial terrace of the upper Weihe River, and contains typical loess-paleosol sediment. The sampled section thickness is 6.8 m, with a sampling interval of 5–10 cm. The Weiyuan section can be divided into the following several layers (**Figure 1B**) (Yang X et al., 2015): 1) 0–20 cm: cultivated layer, disturbed by human planting activities; 2) 20–135 cm: paleosol (S0), developed under a warm and wet climate during the Holocene (11.7-0 ka BP), corresponding to marine isotope stage 1 (MIS 1); 3) 135–555 cm: loess (L1-1), developed under a cold and dry climate during the Last Glacial Maximum (26.5-20 ka BP, MIS2); 4) 555–680 cm: loess (L1-2), a weak paleosol developed during an interstadial of the Last Glacial Period (MIS 3, 57–32 ka BP), under a warmer and wetter climate. Two AMS ^{14}C dates have been obtained for the L1-1 and S0 units in the Weiyuan section (Yang S et al., 2015) (**Figure 1B**).

Microcharcoal Extraction and Identification

The sediment samples of the Weiyuan section were extracted following standard palynological methodology (Miao et al., 2017) as follows. 1) One tablet of *Lycopodium* (each one containing about 27, 600 *Lycopodium* spores) was initially added to each weighted sample as a reference for the calculation of concentration (Maher, 1981); 2) acid digestion with 10% HCl removed carbonates; 3) acid digestion with 40% HF removed silicates; 4) fine sieving (10 μm mesh) to enrich the microcharcoal particles (as well as pollen grains); 5) microscope slides of each sample were prepared for identification.

The microcharcoal concentration can be calculated according to the following formula:

$$Charcoal\ concentration_x = C_x / L_x \times 27600 / W_x$$

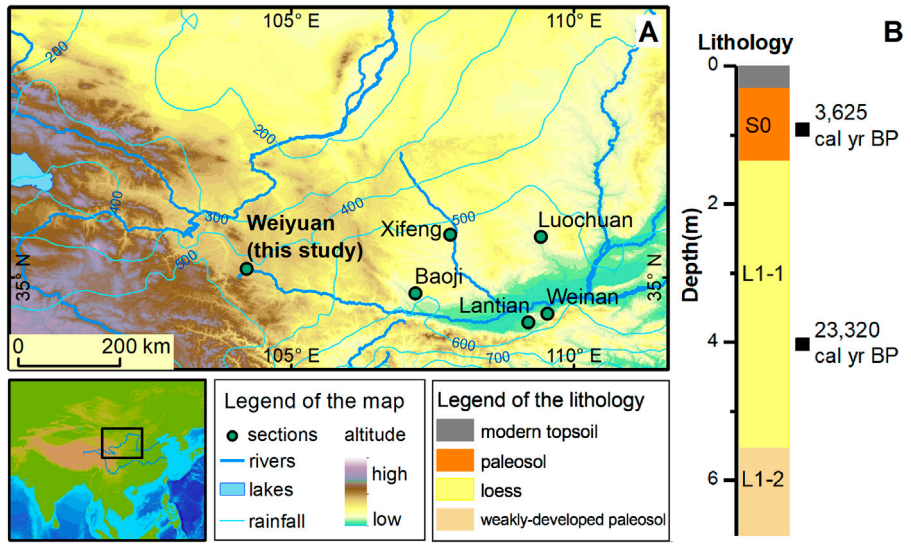

FIGURE 1 | Overview of the Weiyuan section. **(A)**: Location of the Weiyuan section and other sections; **(B)**: the stratigraphic column with the Accelerator Mass Spectrometry (AMS) radiocarbon ages of the Weiyuan section (Yang S et al., 2015).

where: x is sample number; C is the identified number of microcharcoals; L is the identified number of *Lycopodium* spores; and W is the sample dry weight.

Image Processing and Statistics

To apply the image processing method, scanned RGB digital images were acquired from the microslides by the Zeiss slide scanner Axio Scan. Z1, a 10× magnification objective lens was used with a CCD camera with an imaging accuracy of 0.44 μm/pixel. For a standard slide of 26 mm × 76 mm in size, a 1.5 GB image file in Zeiss CZI format was generated and converted in Zeiss Zen software to the more common TIFF format for analysis in ImageJ. Note that converting to TIFF will increase the size of the file to about 5GB, which is very demanding for computer performance, therefore, the minimum performance recommendations of computer processor are 3 GHz of clock rate, eight cores, and 32 GB of RAM, moreover, cropping the image into subsets for processing is also a remedy. an example image, is shown in **Figure 2A**. The RGB color model is an additive color model applied to display images in electronic systems, based on human perception of colors. All other colors are then defined as mixtures of the three additive primary colors, red, green, and blue, in different proportions (Hirsch, 2004). In the commonly adopted 8-bit storage format, its mathematical representation is:

$$Color = (R, G, B),\ \ R, G, B \in (0 - 255)$$

Here, the range 0–255 represents the resolution of typical 8-bit binary storage ($2^8 = 256$), for instance, (0, 0, 0) represents pure black and (255, 255, 255) represents pure white. Considering that microcharcoal is mainly characterized by being black in color, when image processing we convert RGB color to grayscale images in ImageJ (Ferreira and Rasband, 2012), using the formula:

$$Grayscale = (R + G + B)/3$$

The converted grayscale image is shown in **Figure 2B**. The automated method needs to distinguish both microcharcoal and *Lycopodium* spores; however, testing showed the microcharcoal particles were successfully separated from microcharcoal-like particles, while no efficient method was found to distinguish the *Lycopodium* spores from the *Lycopodium*-like particles. Therefore, the statistics for the *Lycopodium* spores were determined manually. Fortunately, counting the *Lycopodium* spores is a relatively easy task, because according to Wang et al., (2020), a minimum count of 300 *Lycopodium* spores will enable stable microcharcoal results.

The key to automatic analysis of microcharcoal samples is to convert the human eye identification criteria described in natural language into computer image processing criteria described in mathematical language. First of all, the most intuitive criterion is that the grayscale values of microcharcoal particles are low, and we suggest this as the basic standard. Furthermore, as shown in **Figure 2B**, the grayscale values of microcharcoal-like particles are also low, and these are hard to distinguish based only on the grayscale value. Further observations showed that the range of grayscale values of microcharcoal particles is smaller than that of the microcharcoal-like particles: this is because of the grayscale color of microcharcoal particles is relatively consistent, while that of microcharcoal-like particles may have some variability. Therefore, we propose the median grayscale value or the standard deviation of a single particle as a further distinguishing criterion.

RESULTS

Image Interpretation by ImageJ

Microcharcoal image automatic recognition consists of two steps: training a classification model and testing the classification model.

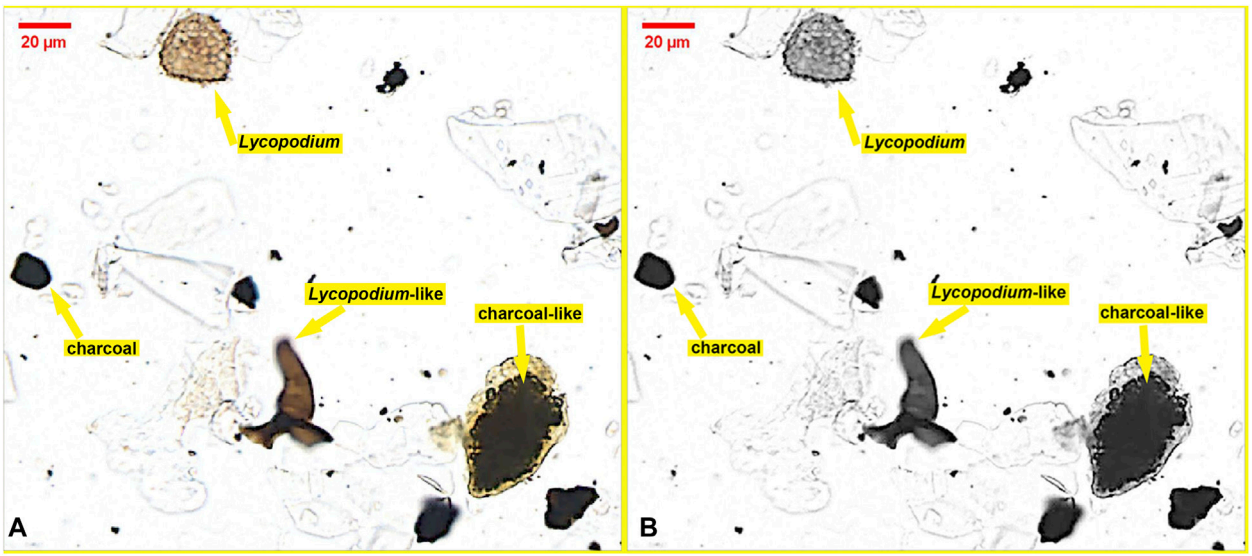

FIGURE 2 | Spectral and morphological characteristics of microcharcoal, microcharcoal-like, *Lycopodium* spores, and *Lycopodium*-like objects in a RGB color model **(A)** and gray scale image **(B)**. *Lycopodium*-like means that its spectral signature is similar to *Lycopodium* when classified by computer, although they can be easily distinguished manually.

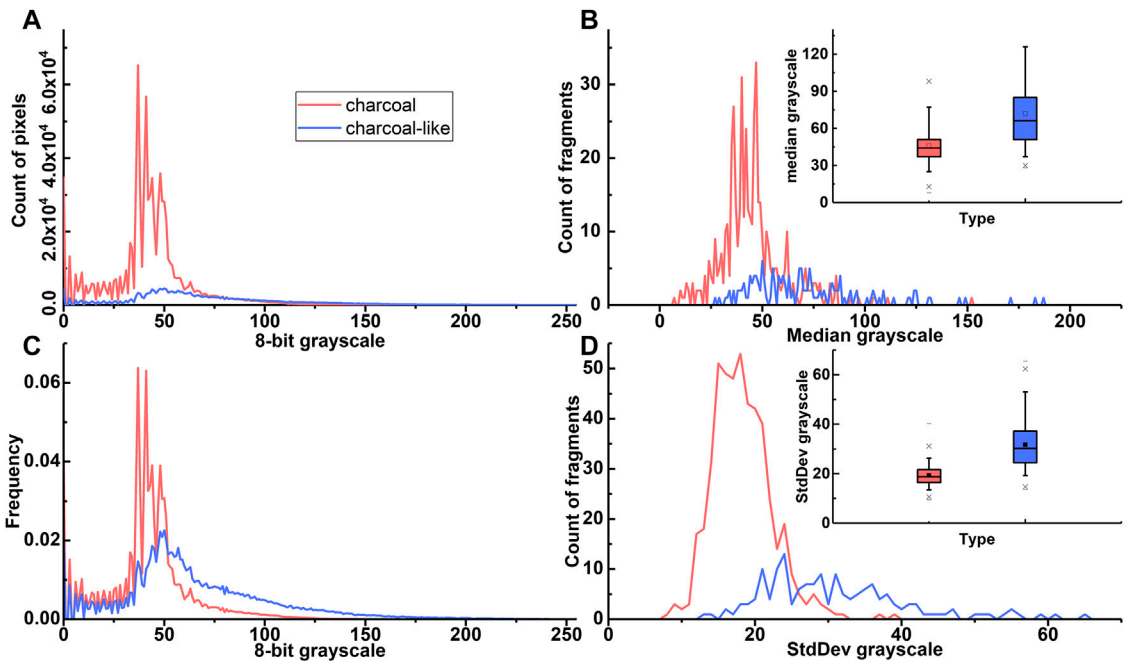

FIGURE 3 | The distinction between microcharcoal and microcharcoal-like particles in a training set was manually selected from sample Nos. 10, 20, 30, 40, 50, 60, and 70. **(A)**: histograms of grayscale values of microcharcoal and microcharcoal-like pixels; **(B)**: the frequency distributions of the grayscale values of microcharcoal and microcharcoal-like pixels; **(C)**: the distribution of median grayscale values of microcharcoal and microcharcoal-like particles; **(D)**: the standard deviations of grayscale values of microcharcoal and microcharcoal-like particles.

To train the classification model, we compiled a training set from sample Nos. 10, 20, 30, 40, 50, 60, and 70 to avoid individual samples introducing errors in the imaging system. We manually selected microcharcoal and microcharcoal-like particle samples from the seven test sets and calculated their statistical characteristics. **Figure 3A** shows histograms of the grayscale

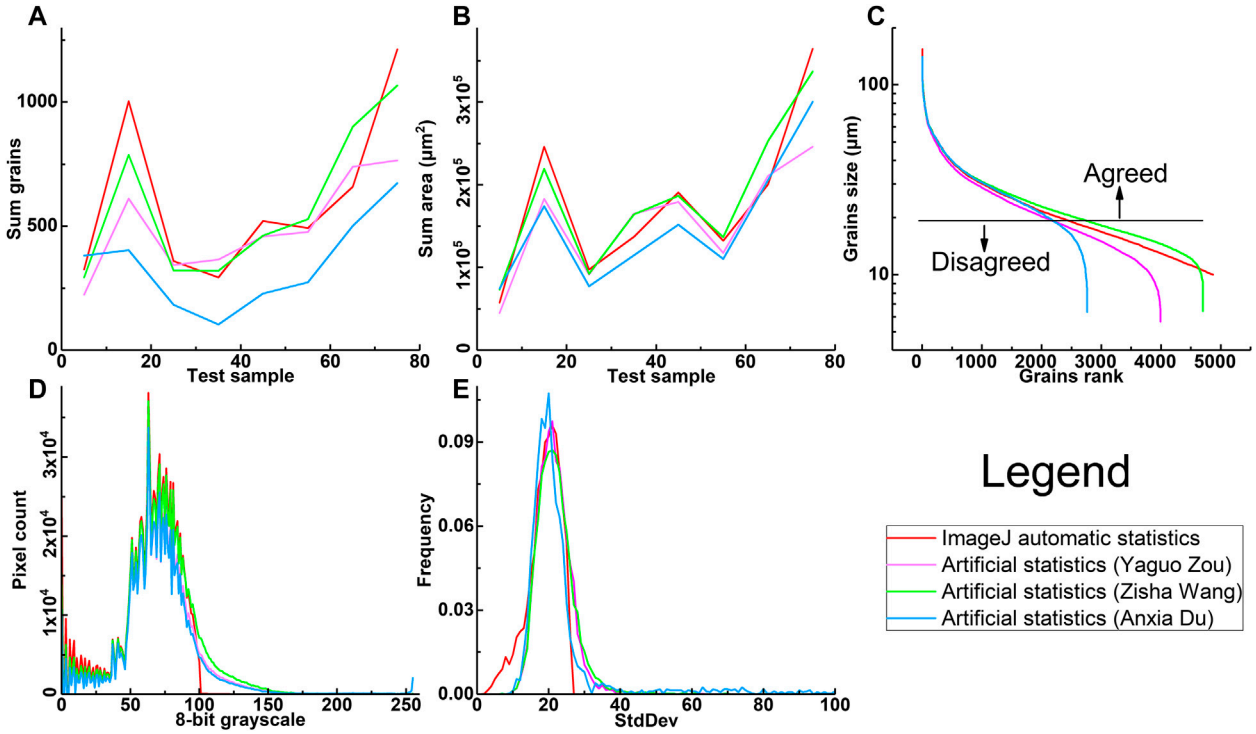

FIGURE 4 | Comparison of automatic (ImageJ) and manual statistical analysis. **(A)**: the total number of counted particles. **(B)**: the total area of counted particles. **(C)**: the rank-size distribution of counted particles; **(D)**: the distributions of grayscale values of counted pixels; **(E)**: the standard deviation of grayscale values of counted particles.

values of microcharcoal and microcharcoal-like pixels, and **Figure 3B** shows the frequency distributions; the grayscale value distributions of microcharcoal and microcharcoal-like particles are not clearly distinguishable, making it is difficult to simply set a threshold on a grayscale image and conclude that any pixel value less than that is definitely microcharcoal. However, the amount of microcharcoal is far greater than the amount of microcharcoal-like material, which supports the opinion that most of the black particles identified during pollen analysis could be regarded as microcharcoal (Sun et al., 2000). Therefore, further distinguishing strategies are needed. We calculated the median and standard deviation of the grayscale value of each selected particle (see **Figures 3C,D**); both achieve a better differentiation than the grayscale value alone, with the standard deviation performing better than the median. Therefore, we decided to use the standard deviation as a further distinction criterion.

Based on the above discussion, we propose the following distinguishing procedure based on ImageJ software. 1) Grayscale threshold: the image is converted from RGB to grayscale, and pixels with grayscale values of 100 or less are retained for the next step. According to the training set, the grayscale values of 98.28% of microcharcoal pixels and 84.41% of microcharcoal-like pixels meet this criterion. 2) Noise reduction: the selected results are processed in ImageJ to remove small patches and to fill holes. 3) Vector graph generation: raster images of individual pixels are converted to vector images of individual particles, using the ImageJ particle analysis tool. 4) Parameter analysis: required spectral and shape parameters can be calculated by ImageJ, such as median grayscale value, standard deviation of grayscale value, length, width, area, perimeter, etc. 5) Standard deviation threshold: objects with a grayscale standard deviation greater than 26 were excluded, because they were more likely to be not microcharcoal. 6) Removal of particles smaller than 10 microns in length, following standard palynological practice (Miao et al., 2017), because a 10 μm mesh is adopted for fine sieving of samples to remove the impurities. In addition, particles smaller than 10 microns are more difficult to identify, regardless of whether using computers or human eyes.

Evaluation by Comparison With Manual Analysis

Next, we manually tested the classification accuracy by selecting test samples. To avoid choosing samples from the training data, we selected test sets from sample Nos. 5, 15, 25, 35, 45, 55, 65, and 75 in a random position, each test sample size is approximately 1/9 to the result sample size. The results of ImageJ automatic analysis based on the above procedures were compared with the results of manual statistical analysis by three people: Yaguo Zou, Zisha Wang and Anxia Du (see **Figure 4**). The microcharcoal identification experience of the three people is 2 years, 3 years and 1 year respectively. The identification was done in ImageJ based on the cropped test sample from the scanned image under 400×

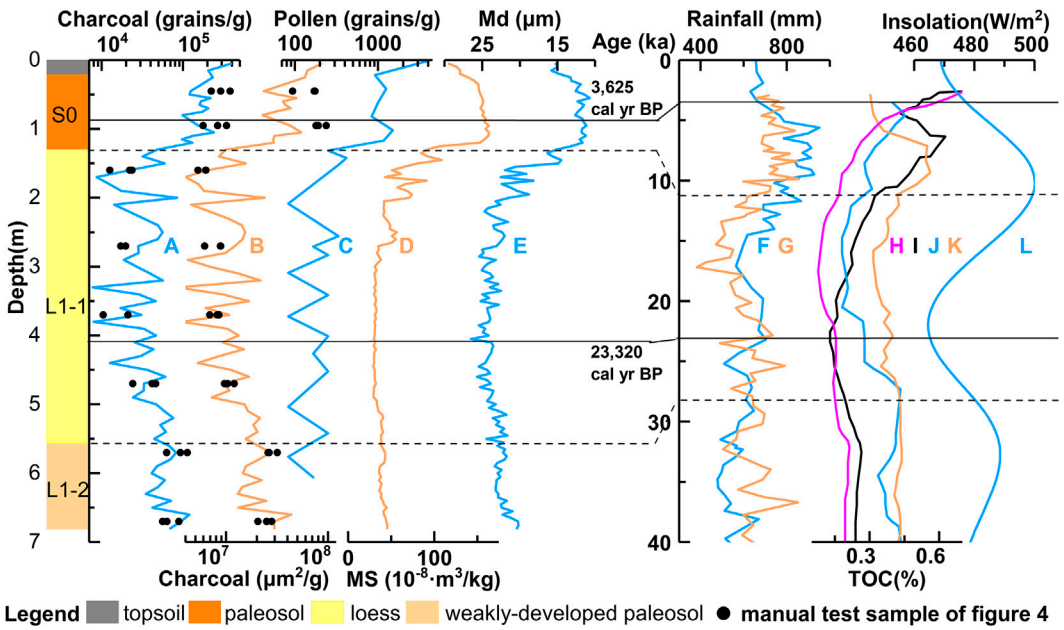

FIGURE 5 | Comparison between the microcharcoal concentration in the Weiyuan section and other environmental indexes nearby. **(A)**: particle concentration of microcharcoal in Weiyuan (this study); **(B)**: area concentration of microcharcoal in Weiyuan (this study); **(C)**: pollen concentration in the Weiyuan section (Yang X et al., 2015); **(D)**: magnetic susceptibility (MS) in the Weiyuan section (Yang S et al., 2015); **(E)**: median grain size (Md) in the Weiyuan section (Yang S et al., 2015); **(F)**: ^{10}Be based rainfall in the Baoji section (Beck et al., 2018); **(G)**: phytoliths based mean annual precipitation (MAP) in the Weinan section (Lu et al., 2007); **(H–K)**: Total organic carbon (Grant et al., 2019) (Grant et al.) content in Luochuan **(H)**, Xifeng **(I)**, Weinan **(J)**, and Lantian **(K)** respectively (Lu et al., 2019). **(L)**: summer insolation in 35°N (Laskar et al., 2004). The black dots in **(A)** and **(B)** are the results analyzed manually by 3 people in **Figure 4** as a reference for the accuracy of the automatic method; however, we note that the test sample size in **Figure 4** is only 1/9 to the result sample size in **(A)** and **(B)**.

magnification (the original image is scanned by 10× objective lens and CCD camera into an image with a resolution of 0.44 um/pixel, and can be further enlarged in ImageJ, similar to the function of the eyepiece), and the black, opaque, angular particles (Patterson et al., 1987) were identified as microcharcoal. **Figure 4A** shows the total number of counted particles, and reveals that the automatic statistical results are close to those of Yaguo Zou and Zisha Wang, but higher than those of Anxia Du; however, the trends of all four sets of results are consistent. It is interesting that anomalous values were produced by human analysis, not by the machine analysis, for the reasons explained below. **Figure 4B** shows the total area of counted particles, and unlike the number of particles, this is consistent across all four cases (3 humans, 1 machine). One obvious possibility to explain the statistical difference appeared in particle count but not in particle area, is that the smaller particles were overlooked: as a result, the number of particles recorded by Anxia Du was smaller but the total area was still similar. This is confirmed in **Figure 4C**, where the rank-size distributions of counted particles show that the four statistical sequences are broadly consistent in the large size particles range, but as the grain size gets smaller, the differences increase. This is easy to understand because our statistical rule requires that microcharcoal particles above 10 microns should be counted, but the visual implementation of this threshold requires experience – unless every particle is measured, which is time-consuming. Overall, the grayscale value distributions of counted pixels (**Figure 4D**) and the standard deviations of counted particles (**Figure 4E**) show that the four sets of results for manual and machine analysis are generally consistent with each other.

In conclusion, the results of the machine and manual statistical analysis achieve high levels of consistency in their distributions of pixel grayscale values (**Figure 4D**), particle grayscale standard deviations (**Figure 4E**), and particle rank-size distribution greater than 20 microns (**Figure 4C**). The main divergence occurs at around the 5–20 microns grain size (**Figure 4C**), because the visual measurement is needed in the manual statistical analysis to determine whether or not a microcharcoal particle is larger than 10 microns. Therefore, the results are consistent in the total area counted (**Figure 4B**), but not in the number of particles counted (**Figure 4A**), however, the trends are still consistent.

Statistical Results

The results of analyzed microcharcoal concentrations in the Weiyuan section are shown in **Figure 5**. Note that we provide the traditional particle concentration (**Figure 5A**), but for the convenience of comparing image processing with the manual statistics, the area concentration (**Figure 5B**) is also given. We believe that the area concentration is more accurate than the particle concentration in reflecting the amount of microcharcoal; however, the high correlation coefficient (0.97) between the two curves shows that the particle concentration and area concentration are closely matched. In addition, the results analyzed manually in **Figure 4** are dotted on the curves in

Figures 5A,B as a reference for the accuracy of the automatic method; however, we note that the test sample size in **Figure 4** is only 1/9 to the result sample size in **Figure 5**; Nevertheless, we still find a good correlation between the manual and automatic analysis methods.

As the trend shown in the microcharcoal results, from the L1-2 layer (MIS 3) to the L1-1 layer (MIS2), along with the climate changed from cool and wet to dry and cold in the Last Glacial Period, it shows a low values state and a slowly decreasing trend in microcharcoal content. The S0 layer (MIS 1, Holocene), deposited during a warm and wet climate, shows three clear stages in its microcharcoal content: first, a rapid increase during the early Holocene, then a fluctuating state from ~4 to 2 ka BP, and finally an increase since 2 ka BP. This pattern indicates that fire events in the region were weaker during the Last Glacial Period and stronger during the Holocene, which is inconsistent with the commonly recognized trends that fires occur more frequently in glacial periods and less frequently in interglacial periods.

DISCUSSION

Comparison of Microcharcoal Statistical Methods

As an important proxy reflecting the occurrence of fire events, microcharcoal has a unique research value; however, manual statistical analysis of microcharcoal contents is time-consuming, which hinders the application and development of this method. Based on previous research on the automatic analysis of microcharcoal, this paper proposed and verifies a new automatic statistical method, our method reduce the time to count a sample from 2–8 h to 20–30 min, and there was no reduction in accuracy compared with manual statistics, which is more convenient and greatly improves the statistical efficiency of microcharcoal.

Scientific statistical work needs comprehensive evaluation in terms of both accuracy and efficiency. The automatic statistical analysis of microcharcoal is a long-standing but rarely discussed problem, first addressed by MacDonald et al., (1991) in their study using a transmitted light microscope and an image analysis system designed for optical densitometry; in their method, microcharcoal was identified according to its optical density (opacity). A more complete automatic statistical system was proposed by Horn et al., (1992), based on statistical characteristics such as grayscale and its standard deviation. However, due to the limited computer performance and at that time, these early explorations were not developed further, and their methods were not widely adopted.

With the continuous development of computer technology, and successive improvements in image processing software, automatic pattern recognition has become widely used in many fields: for example, ImageJ in biology, metallographic analyzer in materials science, ENVI and Erdas in remote-sensing. These image processing packages are also often used by other disciplines, including in research on computer-aided microcharcoal analysis (Stevenson and Haberle, 2005; Thevenon and Anselmetti, 2007; Lu et al., 2009; Tan et al., 2014; Hawthorne and Mitchell, 2016). However, many studies simply apply the software directly, without discussing the software's statistical basis and without a thorough evaluation of its accuracy.

This study further analyzed the problem of microcharcoal statistics from the perspective of methodology, yielding preliminary results as described above. However, there are still many deficiencies in this study: for example, we are not sure whether the threshold chosen in this paper is applicable to other sedimentary sections, because of their different sedimentary environments and soil textures. In addition, the problem with the automatic statistical analysis of *Lycopodium* spores has not been satisfactorily resolved, although this may be addressed by using the WEKA (Hall et al., 2009) expansion package in ImageJ, which is an image classification algorithm based on training samples and machine learning; however, this algorithm requires high-performance computer, because the microscope images are too large. Alternatively, more recognisable markers may be used for instead of the *Lycopodium* spores, such as plastic markers (Ogden and Gordon, 1986). In this sense, automated statistical algorithms are evaluated not only for their accuracy, but also for their achievement of the same accuracy but with the consumption of fewer computational resources. Therefore, we suggest strengthening research efforts in this field in the future, not only the address the automatic statistical analysis of microcharcoal and *Lycopodium* spores, but also to extend the method to the analysis of all spores and pollen species encountered in palynological studies.

Spatial Heterogeneity of Fire Event Controlling Factors

In combustion theory, the fire triangle (Countryman, 1972) is a simple model for understanding the three necessary ingredients for ignition and combustion: heat, fuel, and an oxidizing agent (usually oxygen). This is a microscopic model from a chemical perspective, then Moritz et al., (2005) extended it to different scales of time and space, including the large scale which vegetation, climate, and ignition sources constitute the three vertices of the triangle. Among them, vegetation conditions and extreme weather (Miao et al., 2020) are considered to be two basic factors to control the production of microcharcoal (Herring, 1985; Clark, 1988; Whitlock and Larsen, 2002; Huang et al., 2006; Adolf et al., 2018). More specifically, the solar insolation drives the terrestrial temperature changes (Bond et al., 1997; Chen et al., 1997; Petit et al., 1999; Sun et al., 2012), and the moisture (precipitation) is coevolved with the temperature (Miao et al., 2012), moreover, the burning of the biomass is more easily in dry conditions (Huang et al., 2006; Pechony and Shindell, 2010; Miao et al., 2019; Han et al., 2020).

Based on the above discussion, we selected the environmental indexes related to fire activities for comparative analysis (**Figure 5**): 1) the pollen concentration (Yang X et al., 2015; **Figure 5C**) as a proxy for plant species richness; 2) the magnetic susceptibility (Yang S et al., 2015; **Figure 5D**) as a proxy for East Asian Summer Monsoon strength; 3) median grain size (Yang S et al., 2015; **Figure 5E**) as a proxy for East Asian Winter Monsoon; 4) the reconstructions of rainfall based on ^{10}Be in

the Baoji section (Beck et al., 2018; **Figure 5F**); 5) mean annual precipitation based on phytoliths in the Weinan section (Lu et al., 2007) (**Figure 5G**); 6) total organic carbon content in Luochuan (**Figure 5H**), Xifeng (**Figure 5I**), Weinan (**Figure 5J**), and Lantian (**Figure 5K**) respectively (Lu et al., 2019); 7) summer insolation in 35°N (Laskar et al., 2004; **Figure 5L**).

Based on the information in **Figure 5**, we interpret the paleofire characteristics in this section, since about 40 ka BP, as follows.

Fire activity during the Last Glacial Period was significantly reduced relative to that in the Holocene, which is contrary to the usual view of wildfire being more prevalent in cold and dry climates, leading to more microcharcoal in associated sediments (Kaars et al., 2000; Luo et al., 2001; Wang et al., 2005; Wang et al., 2012; Zhao et al., 2019; Xiao et al., 2020; Zhang et al., 2020). We speculate that the reason for this difference is that the above records are all from humid regions, while this study was located in a semi-arid region. Here, although the climate of the Last Glacial Period was dry and conducive to the occurrence of fire, the vegetation coverage in Weiyuan was low, as supported by palynological records (Yang X et al., 2015; **Figure 5C**), total organic carbon content (Lu et al., 2019) (**Figures 5H–K**) and model simulation (Liu et al., 2002; Ni et al., 2010). This would have limited the development of wildfire. Paleofire studies in other arid areas, for example, Sierra Leone in sub-Saharan Africa, have found similar patterns (Bird and Cali, 1998). However, long time-scale paleofire records in arid and semi-arid areas remain sparse, and often show strong spatial heterogeneity (Wang et al., 2005; Wang et al., 2012), so this hypothesis needs to be verified by additional microcharcoal studies in arid areas in the future.

The first significant increase of fire was from 12 ka BP to 5 ka BP, this period can be further divided into two stages. At the earlier stage, summer insolation was at a high level (Laskar et al., 2004; **Figure 5L**), which is considered as a contributing factor to the occurrence of wildfires (Whitlock et al., 2010), and it was confirmed by sedimentary records (Millspaugh et al., 2000; Brunelle and Whitlock, 2003; Whitlock et al., 2008; Gil-Romera et al., 2014; Inoue et al., 2018) and simulation results (Hély et al., 2010). At the later stage, summer insolation has decreased, but the rainfall began to increase (Beck et al., 2018; Lu et al., 2007; **Figures 5F,G**), which promoted plant growth (Yang X et al., 2015; Lu et al., 2019; **Figures 5C,H–K**) and resulted in an abundant fuel supply.

The second significant increase of fire, since 2 ka BP, is more likely to be associated with human activity. Weiyuan section is located near the center of early ancient China, and thus lies in a region with strong ancient human activities (Dong et al., 2013; An et al., 2017). Wang et al., (2003) suggest that human activity is the strongest additional factor superimposed on the natural background trend. With the development of human productivity, anthropogenic influence on natural processes has gradually strengthened: in areas where early human activity was intense, the increase in microcharcoal over the last few thousand years is often explained as a result of human use of fire, and this is more evident in the Holocene microcharcoal record (Xue et al., 2018).

CONCLUSION

(1) In this study, an automatic statistical method for microcharcoal was proposed, based on ImageJ software. The microcharcoal was identified using the pixel grayscale value threshold and the particle grayscale standard deviation threshold. Results from the statistical method were compared with manual analysis to demonstrate the method's statistical effectiveness. This method is efficient and accurate, and provide a powerful tool for microcharcoal analysis.

(2) We applied the new automatic statistical method to reconstruct paleofire activity since ~40 ka BP in the Weiyuan loess section, which is located in semi-arid northwest China. We compared this record with other related records, and revealed the spatial heterogeneity of factors controlling paleofire. We speculated that differences in vegetation coverage caused fire events in arid and humid areas to show opposing patterns. This is related to the contrasting abundance of fuel in arid and humid areas, but because of the lack of fire records in arid and semi-arid areas, more research is needed on the paleofire evolution in this area to verify this hypothesis.

DATA AVAILABILITY STATEMENT

The raw data supporting the conclusions of this article will be made available by the authors, without undue reservation.

AUTHOR CONTRIBUTIONS

YZ designed the experiment and wrote the manuscript, YM, YZ, and SY guided the work and modify the paper, SY collected samples and provided guidance, ZW and GT participated in the experiment.

FUNDING

The project is supported by NSFC (41772181, 41888101, 41807440, 42030505), the Strategic Priority Research Program of CAS (No. XDA20070200); Young Top Talents Project of the "Ten Thousand Youth Program" of the Organization Department of the Central Committee of the CPC; Youth Innovation Promotion Association, CAS (2014383); "Light of West China" Program, CAS; NSF of Gansu Province (18JR3RA395) and State Key Laboratory of Loess and Quaternary Geology, Institute of Earth Environment, CAS (SKLLQG1515).

ACKNOWLEDGMENTS

We are grateful to Yindi Duan, Xicai Zheng, Hongjie Yan helped in lab, Anxia Du contributed in manual statistical check. We thank the anonymous reviewers for their constructive suggestions.

REFERENCES

Abràmoff, M. D., Magalhães, P. J., and Ram, S. J. (2004). Image processing with ImageJ. *Biophot. Int.* 11 (7), 36–42.

Adolf, C., Wunderle, S., Colombaroli, D., Weber, H., Gobet, E., Heiri, O., et al. (2018). The sedimentary and remote-sensing reflection of biomass burning in Europe. *Global Ecol. Biogeogr.* 27 (2), 199–212. doi:10.1111/geb.12682

An, C.-B., Tang, L., Barton, L., and Chen, F.-H. (2017). Climate change and cultural response around 4000 cal yr B.P. in the western part of Chinese Loess Plateau. *Quat. Res.* 63 (3), 347–352. doi:10.1016/j.yqres.2005.02.004

Ashe, B., McAneney, K. J., and Pitman, A. J. (2009). Total cost of fire in Australia. *J. Risk Res.* 12 (2), 121–136. doi:10.1080/13669870802648528

Beck, J. W., Zhou, W., Li, C., Wu, Z., White, L., Xian, F., et al. (2018). A 550,000-year record of East Asian monsoon rainfall from ^{10}Be in loess. *Science* 360 (6391), 877–881. doi:10.1126/science.aam5825

Bird, M. I., and Cali, J. A. (1998). A million-year record of fire in sub-Saharan Africa. *Nature* 394 (6695), 767–769. doi:10.1038/29507

Bond, G., Showers, W., Cheseby, M., Lotti, R., Almasi, P., deMenocal, P., et al. (1997). A pervasive millennial-scale cycle in North Atlantic Holocene and glacial climates. *Science* 278 (5341), 1257. doi:10.1126/science.278.5341.1257

Brunelle, A., and Whitlock, C. (2003). Postglacial fire, vegetation, and climate history in the Clearwater Range, Northern Idaho, United States. *Quat. Res.* 60 (3), 307–318. doi:10.1016/j.yqres.2003.07.009

Campbell, S. L., Jones, P. J., Williamson, G. J., Wheeler, A. J., Lucani, C., Bowman, D. M. J. S., et al. (2020). Using digital technology to protect health in prolonged poor air quality episodes: a case study of the AirRater app during the Australian 2019–20 fires. *Fire* 3 (3), 40. doi:10.3390/fire3030040

Chen, F. H., Bloemendal, J., Wang, J. M., Li, J. J., and Oldfield, F. (1997). High-resolution multi-proxy climate records from Chinese loess: evidence for rapid climatic changes over the last 75 kyr. *Palaeogeogr. Palaeoclimatol. Palaeoecol.* 130 (1), 323–335. doi:10.1016/S0031-0182(96)00149-6

Clark, J. S. (1988). Particle motion and the theory of charcoal analysis: source area, transport, deposition, and sampling. *Quat. Res.* 30 (1), 67–80. doi:10.1016/0033-5894(88)90088-9

Conedera, M., Tinner, W., Neff, C., Meurer, M., Dickens, A. F., and Krebs, P. (2009). Reconstructing past fire regimes: methods, applications, and relevance to fire management and conservation. *Quat. Sci. Rev.* 28 (5–6), 555–576. doi:10.1016/j.quascirev.2008.11.005

Cook, E. R., Woodhouse, C. A., Eakin, C. M., Meko, D. M., and Stahle, D. W. (2004). Long-term aridity changes in the Western United States. *Science* 306 (5698), 1015–1018. doi:10.1126/science.1102586

Countryman, C. M. (1972). *The fire environment concept*. Berkeley, CA: U.S. Department of Agriculture Forest Service Pacific Southwest Forest and Range Experiment Station.

Dong, G., Jia, X., Elston, R., Chen, F., Li, S., Wang, L., et al. (2013). Spatial and temporal variety of prehistoric human settlement and its influencing factors in the upper Yellow River valley, Qinghai Province, China. *J. Archaeol. Sci.* 40 (5), 2538–2546. doi:10.1016/j.jas.2012.10.002

Ferreira, T., and Rasband, W. (2012). *ImageJ user guide*. Bethesda: National Institutes of Health.

Gil-Romera, G., González-Sampériz, P., Lasheras-Álvarez, L., Sevilla-Callejo, M., Moreno, A., Valero-Garcés, B., et al. (2014). Biomass-modulated fire dynamics during the last glacial-interglacial transition at the central pyrenees (Spain). *Palaeogeogr. Palaeoclimatol. Palaeoecol.* 402, 113–124. doi:10.1016/j.palaeo.2014.03.015

Goldammer, J. G., Justice, C., Center, G. F. M., Unides, N., Csiszar, I., Reduction, U. N. O. f. D. R., et al. (2013). *Vegetation fires and global change: challenges for concerted international action. A white paper directed to the United Nations and International Organizations*. Remagen-Oberwinter: Kessel.

Goldberg, E. (1985). *Black carbon in the environment*. New York: John Wiley & Sons.

Grant, G. R., Naish, T. R., Dunbar, G. B., Stocchi, P., Kominz, M. A., Kamp, P. J. J., et al. (2019). The amplitude and origin of sea-level variability during the Pliocene epoch. *Nature* 574 (7777), 237–241. doi:10.1038/s41586-019-1619-z

Hall, M., Frank, E., Holmes, G., Pfahringer, B., Reutemann, P., and Witten, I. H. (2009). The WEKA data mining software: an update. *SIGKDD Explor. Newsl.* 11 (1), 10–18. doi:10.1145/1656274.1656278

Han, Y., An, Z., Marlon, J. R., Bradley, R. S., Zhan, C., Arimoto, R., et al. (2020). Asian inland wildfires driven by glacial-interglacial climate change. *Proc. Natl. Acad. Sci. U.S.A.* 117 (10), 5184–5189. doi:10.1073/pnas.1822035117

Hawthorne, D., and Mitchell, F. J. G. (2016). Identifying past fire regimes throughout the Holocene in Ireland using new and established methods of charcoal analysis. *Quat. Sci. Rev.* 137, 45–53. doi:10.1016/j.quascirev.2016.01.027

Hély, C., Girardin, M. P., Ali, A. A., Carcaillet, C., Brewer, S., and Bergeron, Y. (2010). Eastern boreal North American wildfire risk of the past 7000 years: a model-data comparison. *Geophys. Res. Lett.* 37 (14), L14709. doi:10.1029/2010GL043706

Herring, J. R. (1985). "Charcoal fluxes into sediments of the North Pacific Ocean: the cenozoic record of burning," in *The carbon cycle and atmospheric CO2: natural variations Archean to present*. Washington, D.C.: American Geophysical Union, 419–442.

Hirsch, R. (2004). *Exploring colour photography: a complete guide*. London: Laurence King.

Horn, S. P., Horn, R. D., and Byrne, R. (1992). An automated charcoal scanner for paleoecological studies. *Palynology* 16 (1), 7–12. doi:10.1080/01916122.1992.9989403

Huang, C., Pang, J., Chen, S. e., Su, H., Han, J., Cao, Y., et al. (2006). Charcoal records of fire history in the Holocene loess–soil sequences over the southern Loess Plateau of China. *Palaeogeogr. Palaeoclimatol. Palaeoecol.* 239 (1–2), 28–44. doi:10.1016/j.palaeo.2006.01.004

Inoue, J., Okuyama, C., and Takemura, K. (2018). Long-term fire activity under the East Asian monsoon responding to spring insolation, vegetation type, global climate, and human impact inferred from charcoal records in Lake Biwa sediments in central Japan. *Quat. Sci. Rev.* 179, 59–68. doi:10.1016/j.quascirev.2017.11.007

Jolly, W. M., Cochrane, M. A., Freeborn, P. H., Holden, Z. A., Brown, T. J., Williamson, G. J., et al. (2015). Climate-induced variations in global wildfire danger from 1979 to 2013. *Nat. Commun.* 6, 7537. doi:10.1038/ncomms8537

Kaars, S. v. d., Wang, X., Kershaw, P., Guichard, F., and Setiabudi, D. A. (2000). A Late Quaternary palaeoecological record from the Banda Sea, Indonesia: patterns of vegetation, climate and biomass burning in Indonesia and northern Australia. *Palaeogeogr. Palaeoclimatol. Palaeoecol.* 155 (1), 135–153. doi:10.1016/S0031-0182(99)00098-X

Laskar, J., Robutel, P., Joutel, F., Gastineau, M., Correia, A. C. M., and Levrard, B. (2004). A long-term numerical solution for the insolation quantities of the Earth. *Astron. Astrophys.* 428 (1), 261–285. doi:10.1051/0004-6361:20041335

Lindenmayer, D. B., and Taylor, C. (2020). New spatial analyses of Australian wildfires highlight the need for new fire, resource, and conservation policies. *Proc. Natl. Acad. Sci. U.S.A.* 117 (22), 12481. doi:10.1073/pnas.2002269117

Liu, J., Yu, G., and Chen, X. (2002). Palaeoclimate simulation of 21 ka for the Tibetan Plateau and Eastern Asia. *Clim. Dynam.* 19 (7), 575–583. doi:10.1007/s00382-002-0248-6

Lu, A., Li, Z., Li, J., Xuan, P., and Matsumoto, E. (2009). Comparative experiment of extracting charcoal from sediment with microscope in the Red River basin, Vietna. *Quartenary Sci.* 29 (4), 825–830. doi:10.3969/j.issn.1001-7410.2009.04.1 [in Chinese].

Lu, H.-Y., Wu, N.-Q., Liu, K.-B., Jiang, H., and Liu, T.-S. (2007). Phytoliths as quantitative indicators for the reconstruction of past environmental conditions in China II: palaeoenvironmental reconstruction in the Loess Plateau. *Quat. Sci. Rev.* 26 (5), 759–772. doi:10.1016/j.quascirev.2006.10.006

Lu, H., Liu, W., Yang, H., Wang, H., Liu, Z., Leng, Q., et al. (2019). 800-kyr land temperature variations modulated by vegetation changes on Chinese Loess Plateau. *Nat. Commun.* 10 (1), 1958. doi:10.1038/s41467-019-09978-1

Luo, Y., Chen, H., Wu, G., and Sun, X. (2001). Records of natural fire and climate history during the last three glacial-interglacial cycles around the South China Sea. *Sci. China Earth Sci.* 44 (10), 897. doi:10.1007/BF02907081

MacDonald, G. M., Larsen, C. P. S., Szeicz, J. M., and Moser, K. A. (1991). The reconstruction of boreal forest fire history from lake sediments: a comparison of charcoal, pollen, sedimentological, and geochemical indices. *Quat. Sci. Rev.* 10 (1), 53–71. doi:10.1016/0277-3791(91)90030-X

Macias Fauria, M., Michaletz, S. T., and Johnson, E. A. (2011). Predicting climate change effects on wildfires requires linking processes across scales. *WIREs Clim. Change.* 2 (1), 99–112. doi:10.1002/wcc.92

Maher, L. J. (1981). Statistics for microfossil concentration measurements employing samples spiked with marker grains. *Rev. Palaeobot. Palynol.* 32 (2), 153–191. doi:10.1016/0034-6667(81)90002-6

Miao, Y., Fang, X., Song, C., Yan, X., Zhang, P., Meng, Q., et al. (2016a). Late Cenozoic fire enhancement response to aridification in mid-latitude Asia: evidence from microcharcoal records. *Quat. Sci. Rev.* 139, 53–66. doi:10.1016/j.quascirev.2016.02.030

Miao, Y., Herrmann, M., Wu, F., Yan, X., and Yang, S. (2012). What controlled Mid–Late miocene long-term aridification in Central Asia? — global cooling or Tibetan Plateau uplift: a review. *Earth Sci. Rev.* 112 (3), 155–172. doi:10.1016/j.earscirev.2012.02.003

Miao, Y., Jin, H., and Cui, J. (2016b). Human activity accelerating the rapid desertification of the Mu us Sandy Lands, North China. *Sci. Rep.* 6 (1), 23003. doi:10.1038/srep23003

Miao, Y., Song, Y., Li, Y., Yang, S., Li, Y., Zhao, Y., et al. (2020). Late Pleistocene fire in the Ili Basin, Central Asia, and its potential links to paleoclimate change and human activities. *Palaeogeogr. Palaeoclimatol. Palaeoecol.* 547, 109700. doi:10.1016/j.palaeo.2020.109700

Miao, Y., Wu, F., Warny, S., Fang, X., Lu, H., Fu, B., et al. (2019). Miocene fire intensification linked to continuous aridification on the Tibetan Plateau. *Geology* 47 (4), 303–307. doi:10.1130/g45720.1

Miao, Y., Zhang, D., Cai, X., Li, F., Jin, H., Wang, Y., et al. (2017). Holocene fire on the northeast Tibetan Plateau in relation to climate change and human activity. *Quat. Int.* 443, 124–131. doi:10.1016/j.quaint.2016.05.029

Millspaugh, S. H., Whitlock, C., and Bartlein, P. J. (2000). Variations in fire frequency and climate over the past 17 000 yr in central Yellowstone National Park. *Geology* 28 (3), 211–214. doi:10.1130/0091-7613(2000)28<211:VIFFAC>2.0.CO;2

Moritz, M. A., Morais, M. E., Summerell, L. A., Carlson, J. M., and Doyle, J. (2005). Wildfires, complexity, and highly optimized tolerance. *Proc. Natl. Acad. Sci. U.S.A.* 102 (50), 17912. doi:10.1073/pnas.0508985102

Ni, J., Yu, G., Harrison, S. P., and Prentice, I. C. (2010). Palaeovegetation in China during the late Quaternary: biome reconstructions based on a global scheme of plant functional types. *Palaeogeogr. Palaeoclimatol. Palaeoecol.* 289 (1), 44–61. doi:10.1016/j.palaeo.2010.02.008

Ogden, I., and Gordon, J. (1986). An alternative to exotic spore or pollen addition in quantitative microfossil studies. *Can. J. Earth Sci.* 23 (1), 102–106. doi:10.1139/e86-010

Patterson, W. A., Edwards, K. J., and Maguire, D. J. (1987). Microscopic charcoal as a fossil indicator of fire. *Quat. Sci. Rev.* 6 (1), 3–23. doi:10.1016/0277-3791(87)90012-6

Pechony, O., and Shindell, D. T. (2010). Driving forces of global wildfires over the past millennium and the forthcoming century. *Proc. Natl. Acad. Sci. U.S.A.* 107 (45), 19167. doi:10.1073/pnas.1003669107

Petit, J. R., Jouzel, J., Raynaud, D., Barkov, N. I., Barnola, J. M., Basile, I., et al. (1999). Climate and atmospheric history of the past 420,000 years from the Vostok ice core, Antarctica. *Nature* 399 (6735), 429–436. doi:10.1038/20859

Prospero, J. M., and Lamb, P. J. (2003). African droughts and dust transport to the Caribbean: climate change implications. *Science* 302 (5647), 1024–1027. doi:10.1126/science.1089915

Rhodes, A. N. (1998). A method for the preparation and quantification of microscopic charcoal from terrestrial and lacustrine sediment cores. *Holocene* 8 (1), 113–117. doi:10.1191/095968398671104653

Sankaran, M., Hanan, N. P., Scholes, R. J., Ratnam, J., Augustine, D. J., Cade, B. S., et al. (2005). Determinants of woody cover in African savannas. *Nature* 438 (7069), 846–849. doi:10.1038/nature04070

Stevenson, J., and Haberle, S. G. (2005). Macro charcoal analysis: a modified technique used by the department of archaeology and natural history. Canberra University.

Sun, X., Li, X., and Chen, H. (2000). Evidence for natural fire and climate history since 37 ka Bp in the northern part of the South China Sea. *Sci. China Earth Sci.* 43 (5), 487–493. doi:10.1007/BF02875310

Sun, Y., Clemens, S. C., Morrill, C., Lin, X., Wang, X., and An, Z. (2012). Influence of Atlantic meridional overturning circulation on the East Asian winter monsoon. *Nat. Geosci.* 5 (1), 46–49. doi:10.1038/ngeo1326

Tan, Z., Han, Y., Cao, J., Chang Huang, C., and An, Z. (2015). Holocene wildfire history and human activity from high-resolution charcoal and elemental black carbon records in the Guanzhong Basin of the Loess Plateau, China. *Quat. Sci. Rev.* 109, 76–87. doi:10.1016/j.quascirev.2014.11.013

Tan, Z., Huang, C. C., Pang, J., and Ding, M. (2014). Wild fire history and human landuse over Weihe River Basin since Holocene: evidence from charcoal records. *J. Jilin Univ.(Earth Sci. Ed.)* 44 (4), 1297–1306. doi:10.13278/j.cnki.jjuese.201404208 [in Chinese].

Thevenon, F., and Anselmetti, F. S. (2007). Charcoal and fly-ash particles from Lake Lucerne sediments (Central Switzerland) characterized by image analysis: anthropologic, stratigraphic and environmental implications. *Quat. Sci. Rev.* 26 (19), 2631–2643. doi:10.1016/j.quascirev.2007.05.007

Wang, X., Ding, Z., and Peng, P. a. (2012). Changes in fire regimes on the Chinese Loess Plateau since the last glacial maximum and implications for linkages to paleoclimate and past human activity. *Palaeogeogr. Palaeoclimatol. Palaeoecol.* 315–316, 61–74. doi:10.1016/j.palaeo.2011.11.008

Wang, X., Peng, P. A., and Ding, Z. L. (2005). Black carbon records in Chinese Loess Plateau over the last two glacial cycles and implications for paleofires. *Palaeogeogr. Palaeoclimatol. Palaeoecol.* 223 (1), 9–19. doi:10.1016/j.palaeo.2005.03.023

Wang, Y., Xu, X., and Li, F. (2003). Geologist's concern over environmental effect of human activities—with reference to charcoal fragment analysis for the Yellow River Delta. *Adv. Mar. Sci.* 21 (3), 251–258. doi:10.3969/j.issn.1671-6647.2003.03.002

Wang, Z., Zhao, Y., Miao, Y., Zou, Y., and Tang, G. (2020). A study of the statistical problem of microcharcoal in loess sediments based on the pollen methodology. *Arid. Land Geogr.* 43 (3), 661–670. doi:10.12118/j.issn.1000-6060.2020.03.12 [in Chinese].

Whitlock, C., Higuera, P. E., McWethy, D. B., and Briles, C. E. (2010). Paleoecological perspectives on fire ecology: revisiting the fire-regime concept. *Open Ecol. J.* 3 (1), 6–23. doi:10.2174/1874213001003020006

Whitlock, C., and Larsen, C. (2002). Charcoal as a fire proxy. 3, 75–97. doi:10.1007/0-306-47668-1_5

Whitlock, C., Marlon, J., Briles, C., Brunelle, A., Long, C., and Bartlein, P. (2008). Long-term relations among fire, fuel, and climate in the north-western US based on lake-sediment studies. *Int. J. Wildland Fire.* 17 (1), 72–83. doi:10.1071/WF07025

Xiao, X., Yao, A., Hillman, A., Shen, J., and Haberle, S. G. (2020). Vegetation, climate and human impact since 20 ka in central Yunnan Province based on high-resolution pollen and charcoal records from Dianchi, southwestern China. *Quat. Sci. Rev.* 236, 106297. doi:10.1016/j.quascirev.2020.106297

Xue, J., Zhong, W., Li, Q., Cheng, R., You, A., Wei, Z., et al. (2018). Holocene fire history in eastern monsoonal region of China and its controls. *Palaeogeogr. Palaeoclimatol. Palaeoecol.* 496, 136–145. doi:10.1016/j.palaeo.2018.01.029

Yang, S., Ding, Z., Li, Y., Wang, X., Jiang, W., and Huang, X. (2015). Warming-induced northwestward migration of the East Asian monsoon rain belt from the Last Glacial Maximum to the mid-Holocene. *Proc. Natl. Acad. Sci. U.S.A.* 112 (43), 13178. doi:10.1073/pnas.1504688112

Yang, X., Jiang, W., Yang, S., Kong, Z., and Luo, Y. (2015). Vegetation and climate changes in the western Chinese Loess Plateau since the Last Glacial Maximum. *Quat. Int.* 372, 58–65. doi:10.1016/j.quaint.2014.06.065

Zhang, X., Zheng, Z., Huang, K., Yang, X., and Tian, L. (2020). Sensitivity of altitudinal vegetation in southwest China to changes in the Indian summer monsoon during the past 68000 years. *Quat. Sci. Rev.* 239, 106359. doi:10.1016/j.quascirev.2020.106359

Zhao, Z., Shi, S., Yin, J., Chen, Z., Qin, Q., and Liu, A. (2019). Fire history can be obtained from the charcoal record on the southwest plateau of Guizhou. *Acta Eclogica Sinica.* 39 (2), 507–517. [in Chinese].

Conflict of Interest: The authors declare that the research was conducted in the absence of any commercial or financial relationships that could be construed as a potential conflict of interest.

frontiers in Environmental Science

ORIGINAL RESEARCH
published: 08 June 2021
doi: 10.3389/fenvs.2021.589896

Considerations on Forest Changes of Northwest China in Past Seven Decades

Yang Guojing[1], *Li Junhao*[1] *and Zhou Lihua*[2,3]*

[1]Key Laboratory of Eco-Hydrology of Inland River Basin, Northwest Institute of Eco-Environment and Resources, Chinese Academy of Sciences, Lanzhou, China, [2]Institutes of Science and Development, Chinese Academy of Sciences, Beijing, China, [3]School of Public Policy and Management, University of Chinese Academy of Sciences, Beijing, China

Forests cover four billion hectares (31%) of the Earth's landmass and contain over 75% of all carbon in vegetation. They provide renewable raw materials and natural amenities, protect land and water resources, harbor biological diversity, and mitigate climate change. However, due to less precipitation, the forest coverage rate is only 5.86% in Northwest China. The forests in these arid areas are mainly distributed in alpine areas, which play a key role in runoff regulation and ensure the ecological and economic development of the middle and lower reaches of the inland basins. In the past several decades, China had experienced large-scale deforestation and reforestation. What were the changes of the few forest areas and growing stock in arid Northwest China? Has forest quality been restored? Changes of that had been analyzed in this article. The results showed that the forest area and growing stock decreased greatly from the 1950s to 1970s; the artificial forest area increased clearly; the natural forest area stabilized from the 1980s, growing stock of forest per unit area was still lower than that in the 1950s; and the forest quality had not yet been restored. Results of the analysis of influencing factors showed that the policy-led human activities in different periods were the efficient cause of forest changes in Northwest China. With the development of forestry science, more and more attention has been paid to forest ecological restoration. "Three-North Shelter Forest Program (TNSFP)" in 1978 had made great progress on forest areas by afforestation, and the ecological benefits and economic benefits also increased remarkably owing to the increase in the artificial forest area. In recent years, great progress on forest areas has been made by afforestation, and the forests also contribute significantly to the ecology and economy. However, large-scale afforestation in the Loess Plateau had caused a phenomenon of large investment and little effect on water conservation in some afforestation areas, which showed that afforestation initiated under different polices, which were not always scientifically based, resulted in unintended consequences. Clear ecological principles should be used to ensure best environmental and forest ecology outcomes.

Keywords: forest changes, forest area, forest growing stock, arid Northwest China, forest structure, forest function, ecological principles

OPEN ACCESS

Edited by:
Atsushi Tsunekawa, Tottori University, Japan

Reviewed by:
Elzbieta Antczak, University of Łódź, Poland
Neil A. Coles, University of Leeds, United Kingdom

****Correspondence:***
Zhou Lihua
lhzhou@casisd.cn

Specialty section:
This article was submitted to Land Use Dynamics, a section of the journal Frontiers in Environmental Science

Received: *31 July 2020*
Accepted: *04 May 2021*
Published: *08 June 2021*

Citation:
Guojing Y, Junhao L and Lihua Z (2021) Considerations on Forest Changes of Northwest China in Past Seven Decades. Front. Environ. Sci. 9:589896. doi: 10.3389/fenvs.2021.589896

INTRODUCTION

Forests are the main body and important resource of terrestrial ecosystem, which cover four billion hectares (31%) of the Earth's landmass and contain over 75% of carbon in vegetation (F.A.O, 2010). Forests not only provide humans many material products, such as wood, food, energy, and medicinal materials, but also provide abundant ecological services such as carbon sequestration, oxygen release, water conservation, soil and water conservation, air purification, wind and sand fixation, and protection of biological diversity (Shi L. et al, 2011). They could offer humans an important place to enjoy leisure and vacation, ecotourism, and cultural heritage. Therefore, survival, development, and prosperity of mankind can never be separated from the protection and support of forests. Forests are vital to humanity.

The forest coverage rate of China is 22.96%, while the forest coverage rate of Northwest China is only 5.86% (F.M.O.C, 2019), and it is the lowest compared with northeast, north, south, and southwest China. The forests in Northwest China are mainly concentrated in a few high-altitude areas. In fact, it is because of these forests that the plain areas have a unique and stable water supply, thus ensuring the ecological and economic development of the northwest region, so the forest is the "foundation" of ecological balance and economic development of Northwest China (Wang et al., 2011).

China had experienced large-scale deforestation, reforestation, and afforestation over the past several decades (Wang et al, 2007), and the same happened in Northwest China. From the early 1950s to the late 1970s, the forest in Northwest China suffered deforestation and unreasonable exploitation and utilization, which resulted in the continuous reduction of the forest area, the sharp reduction of forest growth, and even serious ecological disaster. Since the 1980s, the leaders at all levels and government departments have attached great importance to the cultivation of forest resources and vigorously implemented the policies of afforestation and forest retreat. Especially since the implementation of the "Three-North Shelter Forest Program (TNSFP)" in 1978, the forest area and growing stock have increased for nearly 30 years, which had greatly improved the ecological and economic benefits of local areas. The changes of the forest area and growing stock had been analyzed, and the forest quality changes had also been analyzed in this study. The results indicated that growing stock per unit area of natural forest was lower than that in the 1950s. Limited by the precipitation conditions and other factors in Northwest China, the forests are still in the situation of "increasing quantity and unsatisfactory quality." In this study, we used the national forest inventory data of ten time periods (1950–1962, 1973–1976, 1977–1981, 1984–1988, 1989–1993, 1994–1998, 1999–2003, 2004–2008, 2009–2013, and 2014–2018) to evaluate the status and change of the forests in Northwest China over the past seven decades (F.M.O.C, 2004, 2009, 2014, 2019). The results would be conducive to understanding of the dynamic and multifaceted state of forests in Northwest China, which would be of great significance to the development of macro-policy and environmental monitoring.

We knew that forests contribute significantly to the ecology and economy, but it does not mean that the larger the forest area, the more beneficial it is. In the Loess Plateau, the cost of afforestation is too high due to topography and limited precipitation. In recent years, although extensive afforestation in the Loess Plateau has some benefits for soil erosion, it also has adverse effects, resulting in local water shortage in some areas. Therefore, the scientific nature of large-scale afforestation policies in some areas should be carefully considered, and clear ecological principles should be used to ensure best environmental and forest ecology outcomes.

FOREST DISTRIBUTION AND STRUCTURAL CHARACTERISTICS IN NORTHWEST CHINA

Small Forest Area and Lower Forest Coverage in Northwest China

In Northwest China, the annual average precipitation is not more than 400 mm, which seriously limits the growth and development of forests in this region. As we all know, the demand for forest tree species for environmental temperature and water supply is high, forests are generally distributed in the areas where the hottest monthly mean temperature is not less than 10°C and the annual precipitation is not less than 400 mm (He. Q.T. 1999). In Northwest China, although the heat conditions are sufficient, water availability is not enough to make the forests grow. Therefore, most of the forests in Northwest China are distributed in high mountains and abundant river valleys, or in areas with sufficient groundwater supply. In Northwest China, there is only about 27.18 million ha of the forest area, and the forest coverage rate is 8.72%. Among them, there are more than 70% of natural forests distributed in a few mountainous areas with much precipitation (F.M.O.C. 2009). **Figure 1** and **Table 1** clearly show the characteristics of forest distribution in Northwest China.

From the perspective of each administrative region, the forest coverage rate of Shaanxi Province is higher than the national average, and all other northwest provinces and regions have lower than 12% of forest coverage rate (**Table 1**). Especially, the forest coverage rate of Xinjiang is only 4.87%, which is the lowest in China (F.M.O.C. 2009).

Natural Forests Distributed in High Mountain Areas With High Growing Stock

The natural forests in the northwestern region are mainly distributed in the southern slopes of the Qinling Mountains (Hanzhong Prefecture, Bailong River Basin), Mount Tianshan, the Altai Mountains, Qilian Mountains, and the southeastern part of Qinghai. These are the original alpine forest areas and are distributed by the state-owned forestry bureaus (**Table 2**). Secondary forest areas include Shaanxi, Ganzi East (Xiaolong Mountain, Ziwuling), Huanglong Mountain, and Bridge Mountain. Natural forests account for the largest proportion of middle-aged forests (29.90%), followed by near-mature

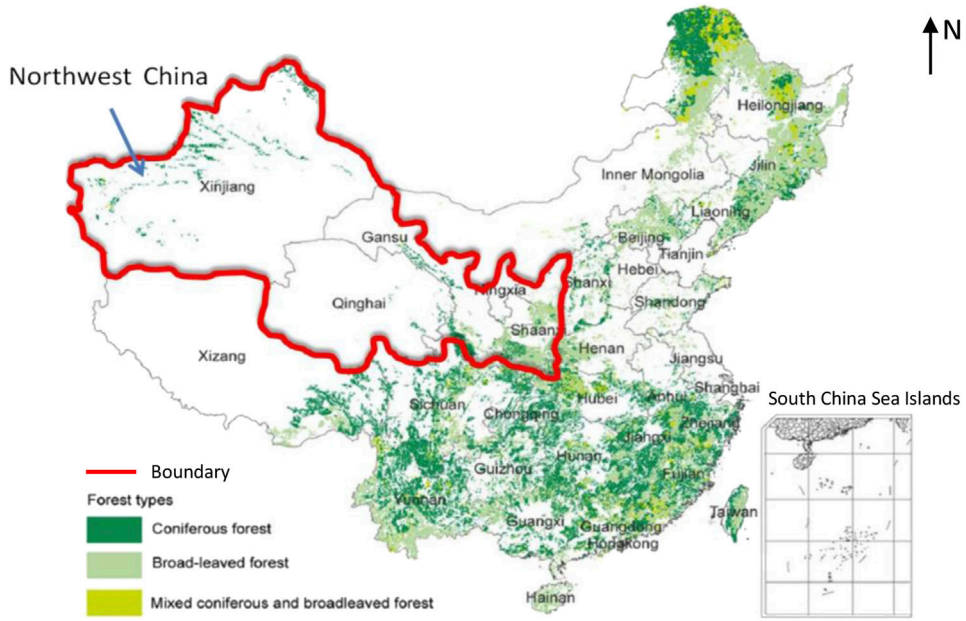

FIGURE 1 | Forest distribution in Northwest China based on the data of the sixth forest inventory (1999–2003). Forests are grouped into three types: coniferous forest, broad-leaved forest, and coniferous and broad-leaved mixed forest. The background map shows the administrative divisions of China. doi:10.1371/journal.pone.0020778.g001.

TABLE 1 | Forest area and growing stock in Northwest China.

Province	Land area [1×10^6 ha (F. M. O. C. (2019))]	Forest area [1×10^6 ha (F. M. O. C. (2019))]	Forest growing stock [1×10^8 m (Chen, 2007)]	Forest coverage rate (%)
Shaanxi	20.58	8.86	5.10	43.06
Ningxia	6.64	0.84	1.11	12.63
Gansu	45.37	5.14	2.84	11.33
Qinghai	73.10	4.25	0.56	5.82
Xinjiang	166	8.08	4.65	4.87
Northwest China	311.69	27.18	14.26	8.72
China	960	220.44	190.07	22.96

Data from the ninth forest inventory (2014–2018).

TABLE 2 | Major alpine forest areas and forest types in Northwest China.

Main mountain natural forest area	Forest area [1×10^4 ha (Huang. 2012)]	Altitude distribution of forests (m)	Precipitation in the forest regions (mm)	Main dominant species
Coniferous forest on the northern slope of Tianshan Mountain	253	1,600 ~ 2,700	420	*P. schrenkiana Fischet Mey*
Coniferous forest on the southwest slope of the Altai Mountains	225	1,500 ~ 600	470	*Abies sibirica, Larix sibirica Ledeb*
Coniferous forest on the northern slope of Qilian Mountain	43.6	2,300 ~ 3,600	500	*Picea crassifolia Kom, Sabina przewalskii Komr*
Coniferous and broad-leaved mixed forest in Qinling Mountain	317	600 ~ 3,500	800 ~ 1,200	*Quercus acutissima Carruth, Quercus variabilis Bl, Betula albosinensis Burk, Abies fargesii Franch, Larix olgensis Henry,* bamboo grove
Holan mountain forest area	22.9	2,000 ~ 3,000	420	*Pinus tabuliformis Carr, Picea crassifolia Kom*

forests (19.45%). The forest area with the medium canopy closure (0.5–0.7) is the largest in the forest canopy closure, accounting for 56.76%, followed by sparse forest (0.2–0.4), accounting for 31.50%; the natural forest also has relatively high accumulations per unit area (125.56 m^3 ha) and has strong ecological functions such as carbon sequestration and oxygen release, and and soil and water conservation.

Riparian Forests Along Inland Rivers With Simple Structure and Dominant Species of Sandy and Halophytes

There are large areas of *Populus euphratica* forest or *Haloxylon ammodendron* forest along the inland river in Northwest China. The riverside *Populus euphratica* forests were concentrated along the Tarim and Heihe rivers in southern Xinjiang, forming corridor-like riparian forests. Its climate is characterized by extreme drought in the middle temperate zone and warm temperate zone. The average annual temperature is 10–11°C, which is greater than or equal to the accumulated annual temperature of 10°C 4,000–4,300°C, and the annual precipitation is 25–50 mm, and the evaporation is 2,000–3,000 mm. The growth of *Populus euphratica* forest is basically separated from the effects of natural precipitation and surface water, mainly relying on flooding and groundwater to survive. *Populus euphratica* forest is simple in composition, simple in structure, and characterized by the Central Asian desert. They are dominated by xerophytes, psammophytes, and halophytes (Wu, 1980). Common vegetation types are *Populus euphratica*, gray willows, *Tamarix* multibranched, *Elaeagnus angustifolia*, licorice, camel thorn, *Nitraria*, *Lycium ruthenicum*, and *Halostachys caspica*, among which Compositae is the most common, followed by Leguminosae, *Tamarix*, Chenopodiaceae, etc. In addition to a large area of alpine forests and riparian forests along the inland rivers, the area of artificial forest is also increasing under the development of the TNSFP in the northwestern region, mainly distributed around the cultivated land, with the main purpose acting as wind breaks and stabilizing the soils.

FOREST CHANGES IN NORTHWEST CHINA IN RECENT SEVEN DECADES

Forest Area and Growing Stock Decreasing From the 1950 to 1970s and Increasing After 1980s

It was reported that from the early 1950s to the late 1970s, the policies of "steel-making" and "seeking grain from barren mountains" during the historical period of "the Great Leap Forward" resulted in the rush of deforestation and grassland reclamation for many years in Northwest China, resulting in the loss of natural forest resources in Northwest China (Li B.C. 2000). And then, in the past few decades since the 1980s, driven by the economic interests, deforestation and grassland destruction had begun in some provinces, again leading to a reduction in the forest area. Inappropriate policies led to a variety of irrational forest development, leading to a decline in the forest area and growing stock, reaching the lowest level in the early 1980s (**Figures 2**, **3**).

On the basis of previous analysis of national forest inventory data, the area of forest in Northwest China decreased from 11.87 million ha (F. M. O. C. 2004) in the 1950s to 10.8 million ha (F. M. O. C. 2009) in the late 1970s, and decreased by nearly 1.1 million hm in 30 years. The growing stock also decreased from 6.5×10^8 m^3 in the 1950s to 5.3×10^8 m^3 in the late 1970s and decreased 1.2×10^8 m^3 in the past 30 years. Compared with the economic value of forests, forests in Northwest China played a more significant role in maintaining ecological balance and ensuring the safety of environment security in Northwest China. The loss of forest resources had aggravated soil erosion, water shortage, climate deterioration, desert expansion, landslides, and debris flow disasters in Northwest China. The comprehensive effect of these factors made the social economy and culture of Northwest China more backward and posed a great challenge to the living environment of the people of all nationalities in Northwest China. The ecology and economics in Northwest China had paid a huge price for these policies.

Since the 1980s, the absolute amount of the forest area and growing stock in Northwest China has increased in the past 40 years of reform and opening up. The forest area increased from 10.9×10^6 ha in 1977 to 26.8×10^6 ha (F. M. O. C. 2019) in 2018 and increased by 15.9×10^6 ha in 40 years (**Figure 2**). The growing stock also increased from 5.07×10^8 m^3 in 1977 to 13.21×10^8 m^3 in 2018 and increased by 8.14×10^8 m^3 in 40 years. However, in terms of the proportion of natural forests and artificial forests, the main reason for the increase in the forest area in the recent 40 years was the increase in the proportion of artificial forest. The results of the forestry inventory in the early days of the founding of New China showed that the areas and growing stock proportion of natural forests in the northwestern region were 95.3 and 99.5%. By 2018, the proportion of natural forests decreased to 64.1 and 91.3%, and the proportion of area and growing stock continued to decline, and the proportion of artificial forest areas and growing stock continued to rise (**Figures 4**, **5**). Therefore, the increase in the forest area and growing stock were mainly caused by large-scale afforestation after the 1980s.

Un-Restored Quality and Ecological Benefits of Forest in Northwest Chinese

The quality of forest is essential for maintaining and increasing forest resources, and the forest quality status is directly related to the effectiveness of forests, which is as important as forest coverage. According to the changes of the forest structure in Northwest China, before the 1970s, the area and growing stock proportion of coniferous forests were 72.8 and 77.3%, respectively, which were higher (**Figures 6**, **7**); From the 1980s to 2003, the area ratio of coniferous and broad-leaved forest was close to 1:1, the stock volume of coniferous forest was dominant, but the proportion decreased from 77.3 to 53.9%; after that, the

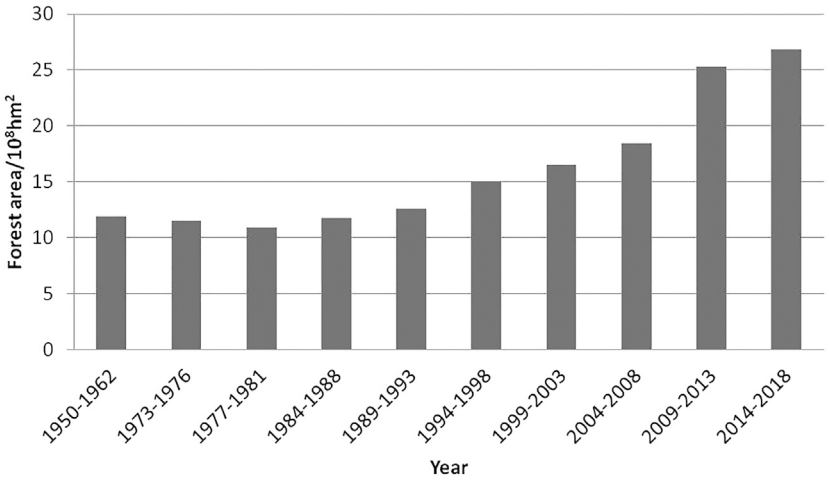

FIGURE 2 | Forest area changes in Northwest China.

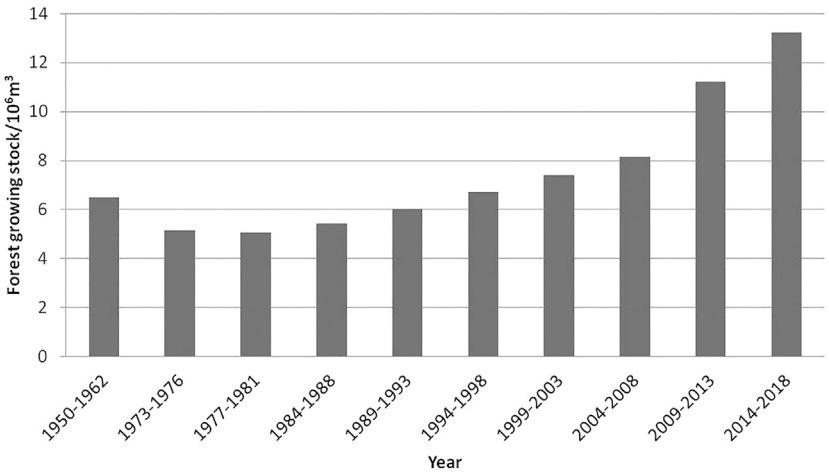

FIGURE 3 | Forest growing stock changes in Northwest China.

proportion rose slowly to 59.03% in 2018. It can be observed that the coniferous forest harvesting significantly reduced the forest area during the period from 1977 to 1981. And after the 1980s, the conservation policies had the coniferous forest gradually restored.

In terms of the actual change areas of forest age-groups, the area of young and medium forest basically showed a trend of increasing. By 2018, the area of sapling and half-mature forests was 1.5 and 2.9 times that in 1950, respectively. The area of mature/ancient forests decreased significantly from 1950 to 1981, which was only 61% of that in 1950. From 1982 to 2018, the area of mature/ancient forests increased gradually. Compared with 1950, the proportion of the sapling forest area changed slightly in 2018, from 34.4 to 33.6%; the proportion of the half-mature forest area increased from 18.6 to 38.3%; the proportion of the mature/ancient forest area decreased significantly from 46.9 to 28.1%, and the lowest value was 28.8% in 1989 (**Figure 8**). This indicated that artificial afforestation and natural regeneration had ensured that the area of sapling forests was not reduced, while the cutting speed of mature/ancient forests was obviously higher than the natural ripening speed of half-mature forests. The change trends of forest growing stock of different age-groups were similar to the change trend of forest area, but the growing stock of forest per unit area was lower than that in 1950s. From the analysis of the proportion of the growing stock of each age-group of the forests, the growing stock of mature/ancient forests was always accounted for the main part of the growing stock of the forests, which was 81.3% in 1950 and reduced to 58.7% in 2018. The proportion of growing stock of sapling forests and half-mature forests increased significantly, from 5.7 to 13% in 1950 to 12.1 and 32.7% in 2009, respectively (**Figure 9**). Obviously, after 1981, the forest area and total growing stock in Northwest China increased greatly, but the main reason was the increase in the plantation area, and mainly

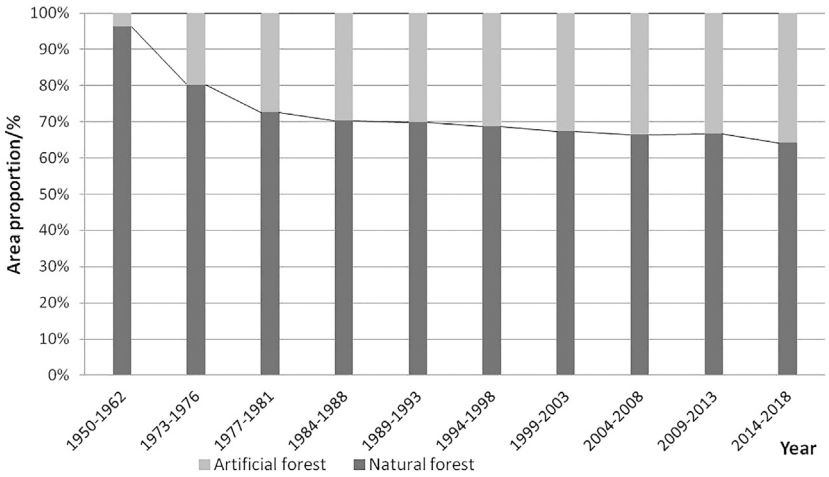

FIGURE 4 | Forest area proportion of artificial forest and natural forest.

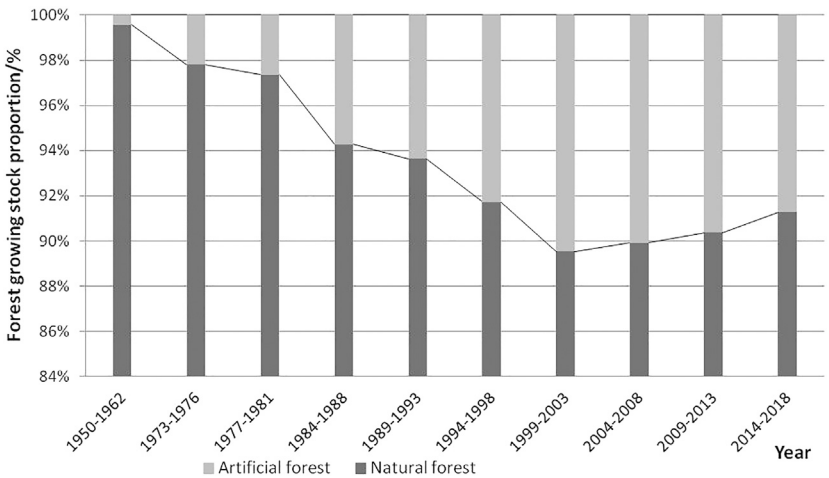

FIGURE 5 | Forest growing stock proportion of artificial forest and natural forest.

the increase of sapling forests and half-mature forests area and growing stock.

INFLUENCING FACTORS OF FOREST CHANGES IN NORTHWEST CHINA

Impact of Misguided Policies on Forests

In the mid-1950s, the "grain-based" approach to development had resulted in extensive deforestation and wasteland reclamation, seriously destroying the national forest resources, including the forests in Northwest China. And after that, in 1960s, large-scale immigration activities such as excessive agricultural reclamation and forestry development greatly destroyed the well-preserved natural forests. The series of misguided development policies had lasted almost 20 years and directly led the reduction of forest areas and growing stock. It was not until the late 1970s that the national forestry sector realized the mistakes and began to protect forests and plant trees, which resulted in the increase of forests. Therefore, the implementation of different policies was the main direct cause of the forest changes in past several decades.

Impact of Rapid Population Growth on Forest Resources

The explosive growth of population had brought a series of difficulties to mankind and also brought serious harm to the ecological environment. It was manifested in the continuous reclamation of wasteland and deforestation in order to meet the needs of food, housing, and fuel under the pressure of population explosion. Population growth showed constant negative pressure, population density was significantly

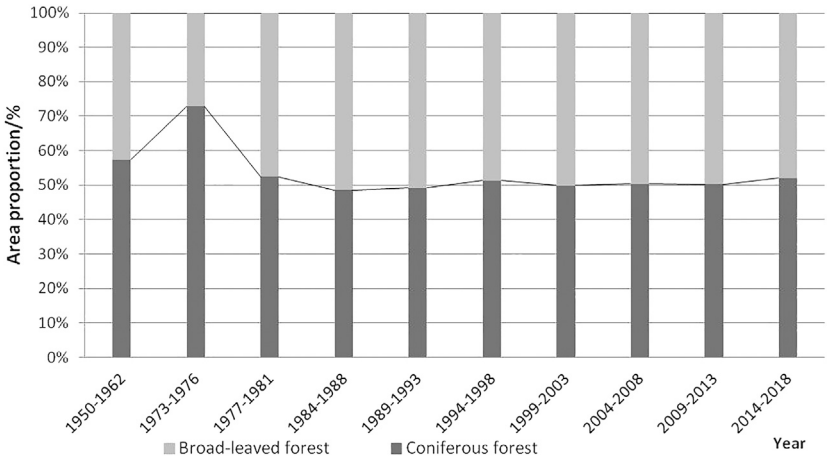

FIGURE 6 | Forest area proportion of broad-leaved forest and coniferous forest.

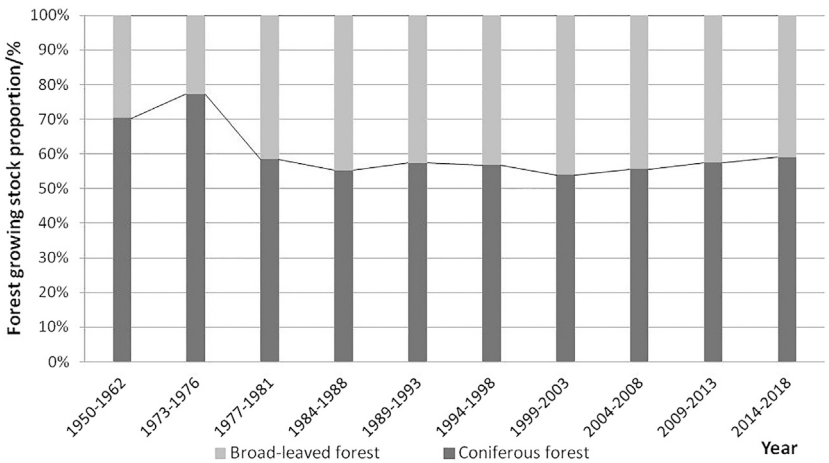

FIGURE 7 | Forest growing stock proportion of broad-leaved forest and coniferous forest.

correlated with deforestation rate, and the correlation coefficient was 0.65 in China (Chen X.Q. 2007). The social burden of state-owned forest industry enterprises and large-scale land development were the leading factors causing the destruction of natural forests (Li L.P. 2011; Bie Q. et al., 2013).

Impact of Forest Property Right and Management Systems on Forest Resources

In the past 30 years, the state-owned forest areas had changed slowly in the process of economic system reform. The rigid system of forest land property rights restricted the effective utilization of the most abundant capital elements in the state-owned forest areas, and the industrial structure was too concentrated on the utilization of forest products. Furthermore, there were no practical measures to evaluate the restoration and protection of forest resources (Wang and LI., 2010; Wang et al., 2014). All these limited the further development of forest resources.

Impact of Education, Science, and Technology on Forest Resources

The education level of the people in a country or region also affects the development of forestry, which has a great relationship with the scientific education environment. Advances in science and technology would contribute to improve the efficiency of forest resources utilization and would also improve the level of forest management and protection, thereby improving the quantity and quality of forest resources. However, the level of science and technology education in Northwest China was generally backward, and the arid climate itself was not conducive to the restoration and development of forest vegetation, and the high investment cost of forestry

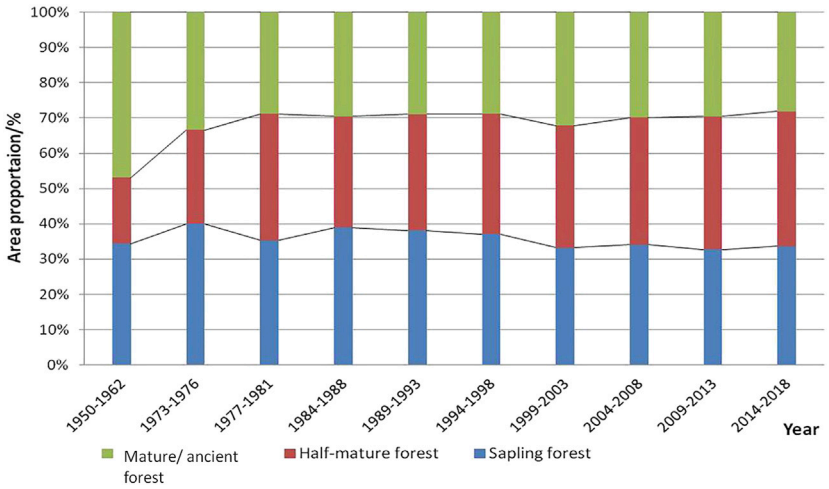

FIGURE 8 | Forest area proportion of different age-groups.

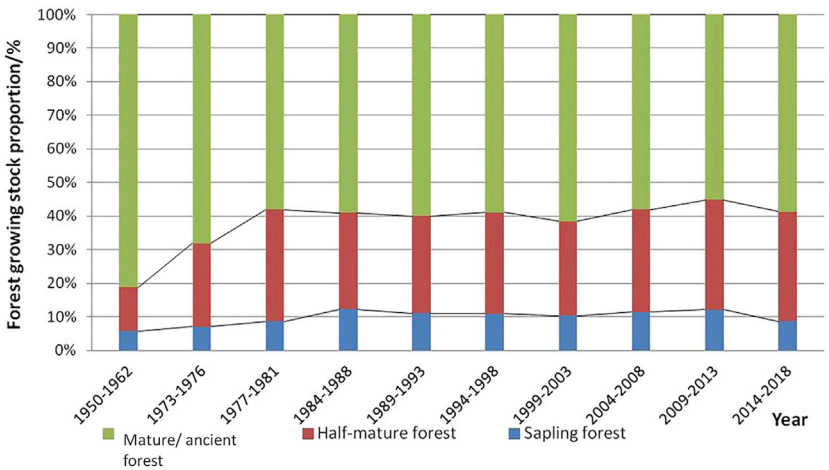

FIGURE 9 | Forest growing stock proportion of different age-groups.

development was also not conducive to the active participation of social forces. These directly affected the prevention of forest fires and forest pest control, and thus affected the normal growth of forests.

CONSIDERATIONS ON FOREST DEVELOPMENT IN NORTHWEST CHINA

Large-scale afforestation might bring some advantages and also had adverse effects. On the one hand, the increase of the forest area would be beneficial to improve the ecological environment to a certain extent, which could be demonstrated by the TNSFP. On the other hand, unreasonable afforestation in large areas would cause economic waste and even lead to other ecological problems.

Ecological Benefit From the "Three-North Shelter Forest Program"

Average annual precipitation is below 400 mm in most areas of Northwest China, which is not conducive to forest growth. In these areas, forests suffered damage as a result of some natural forces and unreasonable human activities in the past decades, which caused a series of ecological problems, such as desertification, aggravated soil erosion, increasing dust weather, and so on. In Northwest China, the total area of desert and desertification land is 1.49 million km^2 (Huang. 2012), and 90% of the serious soil erosion areas of Loess Plateau are distributed in this region. Chinese government departments attached great importance to improving this situation and economic conditions and approved the major strategic decisions for the development of large-scale shelterbelts, in Northeast, Northwest, and North China in

November 1978, which was the TNSFP. From then on, there was a great increase in the forest area and growing stock in Northwest China. The area of trees increased from 3.80 million ha (Huang. 2012) in 1977 to 6.43 million ha (Huang. 2012) in 2007, and shrubs increased from 3.38 million ha (Huang. 2012) to 10.14 million ha (Huang. 2012), increasing by 0.7 and 20 times, respectively (S.F.A.C. 2008). The growing stock of forest trees also increased from 370 million m^3 in 1977 to 660 million m^3 in 2007, an increase of nearly 0.8 times. Forest coverage increased from 2.62% in 1977 to 6.28% in 2007 (Ma G.Q. & Song F., 2015). Over the past decades, the implementation of this measure has significantly increased forest coverage in Northwest China, effectively controlled soil desertification, improved soil erosion and air quality in some areas, and protected biodiversity, which has also brought about certain economic benefits.

Reflections From Afforestation in the Loess Plateau

In the past ten years, the Loess Plateau, as a key area of soil and water conservation in China, has invested a huge amount of funds, and the local people have also invested in hard-to-measure labor, which has made certain achievements in soil conservation. The latest investigation on soil and water conservation ecology in the Loess Plateau of China showed that the vegetation coverage on the Loess Plateau had increased from 31.6% in 1999 to 59.6% in 2013 through vegetation restoration and reconstruction. The average annual sediment discharge of the Yellow River had decreased from 1.6 billion ton to about 300 million ton in 2015, with a reduction of 80%. Despite that the sediment discharge decreased significantly, the modulus of soil erosion on the Loess Plateau remained between 4,000 and 6,000 t/[km·a], and the amount of soil erosion was still more than four times of the allowable value of maintaining ecological security (Zhang S. 2015). The erosion modulus of the Loess Plateau was still not up to the standard, and the problem of soil erosion was still serious. Moreover, after large-scale afforestation in the Loess Plateau, the soil became dry and the runoff decreased (Huang et al, 2012), which may further aggravate the local water shortage, increase the scarcity of already scarce water resources, and may threaten the local and downstream water supply security (Wang Y.H. et al., 2011). Therefore, it was urgent to assess the impact of afforestation on regional water production in the Loess Plateau and to determine reasonable forest coverage in the region (basin) in order to ensure the coordinated development of the region.

Reflection 1: Forest Role in Soil Erosion Control in the Loess Plateau Had Been Overestimated

With the strengthening of the study on the control of the Loess Plateau, the role of forests in maintaining the ecological balance and preventing soil erosion had been discussed. Some scholars believed that the Loess Plateau originally had dense primitive forests in history, and it was only because the deforestation and land reclamation had destroyed the ecological balance, resulting in the uncontrollable soil erosion. Therefore, they vigorously advocated large-scale afforestation. In fact, according to the geographical location of the Loess Plateau, the zonal law, and the characteristics of the monsoon climate in China, the Loess Plateau is mostly in the transition zone from semiarid to arid areas. Except for the eastern edge of the Loess Plateau and some mountainous areas in the central and western regions, there are small areas of forest due to the influence of topography and much precipitation; most of the other areas belong to semiarid grassland landscape. The annual precipitation in semiarid area is less than 400 mm, which cannot meet the needs of forest growth. The water consumption of artificial forest vegetation reduces the soil moisture content of 3–8 m soil layers in some areas of the Loess Plateau, which is close to or lower than wilting humidity for a long time, forming a deep dry soil layer which is difficult to restore, which would lead to the instability of artificial forest vegetation ecosystem. Some studies had found that afforestation on the Loess Plateau reduced the annual runoff depth by an average of 23 mm. Although the value was not very large, it accounted for 58% of the annual runoff depth of non-forest land, indicating that large-scale afforestation would cause a significant decrease in runoff yield in the watershed (Mu X. M. et al., 2007). Therefore, a large amount of afforestation investment cannot achieve the function of water conservation but reduced the runoff, making the local water supplies even more strained.

Reflection 2: Machine-Building Terraces Were More Effective in Soil and Water Conservation than Afforestation or Grass Planting in the Loess Plateau

Mechanized terracing is a method of building terraced fields with bulldozers, requiring less investment and short period, with a quick, effective, and obvious effect of soil and water conservation, and is generally selected for gentle slopes with better site conditions. The investigation showed that the investment of machine-building terraced fields is ￥20–30 per ha, the grain yield per ha would be increased 2–3 times than that of sloping fields, and the investment could be recovered in 4–5 years. The economic benefits and water and soil conservation benefits were more significant than those of afforestation and grass planting (Yang et al, 2014). At the same time, due to the increase in the yield per ha, 1 ha of terraced fields could be transformed into 1–2 ha of steep slope land accordingly, which could not only improve agricultural productivity but also obtain a good soil and water conservation effect. It is a more effective way of soil and water conservation than afforestation. Besides, in the process of water circulation, the terraced fields make the infiltration of rainfall strengthen rapidly and even make all the rainfall infiltrate into terraced fields *in situ*. Due to the inherent characteristics of high permeability and high water storage in the Loess Plateau, it would provide a smooth passage for rainfall infiltration. Therefore, the terraced fields could provide abundant water factors for vegetation growth and support the benign development of "hydrology and ecology" (Li S. H. 2011).

CONCLUSION AND ENLIGHTENMENT

The status and changes of forests in Northwest China had been assessed on the basis of national forest inventory data of a 10-year period over the past seven decades. From the 1950s to 2018, forests in Northwest China experienced large-scale deforestation and afforestation in the past several decades. The area, growing stock, and structure of forest had changed a lot. The forest area and growing stock decreased pre-1970s and increased significantly since the 1980s due to artificial forest. However, the growing stock of forest per unit area is still lower than that in the 1950s, meaning that the quality of forests and their ecological benefits has not been restored. However, some recent studies showed that large-scale afforestation had also caused other ecological effects. Excessive afforestation in the Loess Plateau had led to soil drying and runoff reduction, threatening water security in local and downstream areas. Main conclusions were as follows:

1) In the past 70 years, the forest area and growing stock in the northwest region had decreased pre 1980s and increased significantly since the 1980s mainly due to the increase of artificial forest. Another reason was that there were different standards of forest canopy cover in forest inventory data in different periods. In order to keep the data consistent, we visited the forestry departments of the counties in study areas and accessed historical information about forest inventory, with their help, the additional forest area and corresponding growing stock added under the new definition for forest were removed. The forest data in this paper were based on the forest canopy cover definition of 1978 (canopy cover ≥30% for forest; canopy cover ≥40% for shrub lands). Although we had tried to remove the impact of the data because of different definition of forest, there must be some influence on the analysis results.

2) "Increasing quantity and unsatisfactory quality" has been the general situation of forest in Northwest China at present. The change of forest composition and structure in Northwest China over the past 70 years showed that the loss of forest in the early stage was mainly caused by the loss of coniferous forest in mountainous areas. The cutting intensity of mature/ancient forests was obviously higher than the natural maturity speed of middle-aged forests, which led to the low growing stock of forest per unit area, single species, poor diversity, and no restoration of forest quality and ecological benefits. Therefore, the protection of natural forests in mountain areas should continue to be strengthened in the future.

3) The ecological benefits of the construction of the "Three-North Shelter Forest Program" project in Northwest China were remarkable. It not only controlled the sandstorm damage in the key control areas but also effectively controlled the serious soil erosion areas in the Loess Plateau. At the same time, it brought some economic benefits. However, recent studies showed that large-scale afforestation on the Loess Plateau had led to soil drying and runoff reduction, threatening water security in local and downstream areas. In the Loess Plateau, the influence of afforestation on regional water production should be evaluated. Clear ecological principles should be used to ensure best environmental and forest ecology outcomes.

4) Although the forest area in Northwest China was small, the effects of water conservation, acting as wind breaks and stabilizing soil, are remarkable. Site conditions, soil environment, and climatic factors suitable for stable forests growth were very restrictive in arid Northwest China. In order to realize the sustainability of forest vegetation restoration, the clear ecological construction principle of "soil and water determine vegetation" must be implemented. In Northwest China, it is urgent to develop forestry development policies adapted to local conditions. Therefore, the scientific nature of large-scale afforestation should be considered.

DATA AVAILABILITY STATEMENT

The original contributions presented in the study are included in the article/Supplementary Material. Further inquiries can be directed to the corresponding author.

AUTHOR CONTRIBUTIONS

Conceptualization: YG and ZL. Data curation: YG and LJ. Formal analysis: YG and ZL. Funding acquisition: YG. Methodology: YG. Writing—original draft: YG and LJ. Writing—review and editing: YG and ZL. All authors contributed critically to the drafts and gave final approval for publication.

FUNDING

This study was financially supported by the Strategic Priority Research Program of the Chinese Academy of Sciences (XDA20020401); the National Natural Science Foundation of China (41671187); the National Key Research and Development Program of China (2018YFA0606402); and the Second Tibetan Plateau Scientific Expedition and Research Program (STEP) (2019QZKK0404).

REFERENCES

Bie, Q., Zhao, C. Y., and Qiang, W. L. (2013). Dynamic Change of *Picea Crassifolia* in Qilian Mountain in Recent 40 Years. *J. Arid Land Resour. Environ.* 27 (4), 176–180. doi:10.13448/j.cnki.jalre.2013.04.020

Carle, J., Vuorinen, P., and Del Lungo, A. (2002). Status and Trends in Global Forest Plantation Development. *For. Prod. J.* 52, 12–23. doi:10.1007/s00226-002-0143-7

Chen, X. Q. (2007). *The Study on Influence Factors of Regional Forest Resources Fluctuation in China*. [dissertation/master's thesis]. [Beijing: Beijing Forestry University].

F.A.O. (2010). *Food and Agriculture Organization of the United Nations Global Forests Resources Assessment 2010: Country Report*. Rome: Food and Agriculture Organization of the United Nations. Forestry Paper No.163.

F.M.O.C (2004). *China's Forest Resources 1999-2003 Report*. Beijing: China's Forestry Publishing House. (Chinese Ministry of Forestry) (In Chinese).

F.M.O.C (2014). *China's Forest Resources 2009-2013 Report*. Beijing: China's Forestry Publishing House. (Chinese Ministry of Forestry) (In Chinese).
F.M.O.C (2019). *China's Forest Resources 2014-2018 Report*. Beijing: China's Forestry Publishing House. (Chinese Ministry of Forestry) (In Chinese).
F.M.O.C. (2009). *Chinese Ministry of Forestry China's Forest Resources 2004-2008 Report*. Beijing: China's Forestry Publishing House. (In Chinese).
He, Q. T. (1999). *Forest Environment*. Beijing: Higher Education Press.
Huang, S. W., Li, X. S., Wu, B. F., et al. (2012). The Distribution and Drivers of Land Degradation in the Three-North Shelter Forest Region of china during 1982-2006. *Acta Geographica Sinica* 67 (5), 589–598. doi:10.11821/xb201205002
Li, L.-p., Liu, Y.-n., Tang, Z.-y., Guo, Z.-d., and Fang, J.-y. (2011). Community Structure and its Affecting Factors of Mountain Coniferous Forests in Xinjiang, China. *Arid Zone Res.* 28 (1), 31–39. doi:10.3724/sp.j.1148.2011.00031
Li, B. C. (2000). A Study on the Destruction and Change of Forests in Qilian Mountain Area in History. *Collections essays Chin. Hist. Geogr.* 1, 1–16.
Li, S. H. (2011). *Study on Terraced Hydrological Ecology and its effects* [dissertation/doctor's Thesis]. Xi'an: Chang'an University.
Ma, G. Q., and Song, F. (2015). Assessment on the Forest Condition of "Three North" Shelter Forest Area. *J. Arid Land Resour. Environ.* 18 (5), 108–111.
Mu, X. M., Ba, S. C. L., and Zhang, L. (2007). Impact of Soil Conservation Measures on Runoff and Sediment in Hekou-Longmen Region of the Yellow River. *J. Sediment Res.* 4 (2), 36–41. doi:10.16239/j.cnki.0468-155x.2007.02.006
Shi, L., Zhao, S., Tang, Z., and Fang, J. (2011). The Changes in China's Forests: An Analysis Using the Forest Identity. *PLoS ONE* 6 (6), e20778. doi:10.1371/journal.pone.0020778
The state forestry administration of the People's Republic of China (2008). 30-year Development Report on the Construction of the Three-North Shelterbelt System (1978—2008). Beijing: China Forestry Publishing House.
Wang, D. Q., and Li, G. Q. (2010). Development and Changes of Forest Resources of Ningxia in Nearly Thirty Years. *For. Inventory Plann.* 35 (5), 98–102. doi:10.3374/014.051.0103
Wang, G., Innes, J. L., Lei, J., Dai, S., and Wu, S. W. (2007). ECOLOGY: China's Forestry Reforms. *Science* 318, 1556–1557. doi:10.1126/science.1147247
Wang, Y., Yu, P., Feger, K.-H., Wei, X., Sun, G., Bonell, M., et al. (2011). Annual Runoff and Evapotranspiration of Forestlands and Non-forestlands in Selected Basins of the Loess Plateau of China. *Ecohydrol.* 4, 277–287. doi:10.1002/eco.215
Wang, Y. K., Yang, Q. S., and Guo, S. X. (2014). Changes of Forest Resources in North Slope of Qilian Mountains. *Arid Land Geogr.* 37 (5), 966–979. doi:10.13826/j.cnki.cn65-1103/x.2014.05.013
Wang, Y. H., Yu, P. T., Karl-Heinz, F., Wei, X, Sun, G, et al. (2011). Annaual Runoff and Evapotranspiration of Forestlands and Non-Forestlands in Selected Basins of the Loess Plateau of China. *Ecohydrology*. 4 (2), 277–287. doi:10.1002/eco.215
Wu, Y. Z. (1980). *Vegetations in China*. Beijing: Science Press. (In Chinese).
Yang, T. B., Wang, S. L., and Yang, W. H. (2014). Construction Organization Design and Cost Estimation of Machine Repair Terraces. *Soil and Water Conservation in China* 1, 25–27. doi:10.14123/j.cnki.swcc.2014.01.014
Zhang, S. (2015.11.08). *The Average Annual Sediment Transport of the Yellow River Is Reduced, and the Water and Soil Loss of the Yellow River Plateau Is Still Serious*. Available at: http://www.powerfoo.com/news/sdkx/sdkx2/2015/1110/15111084 31072C19H4IDF8F6DA61120.html. [OL]

Conflict of Interest: The authors declare that the research was conducted in the absence of any commercial or financial relationships that could be construed as a potential conflict of interest.

frontiers in Environmental Science

ORIGINAL RESEARCH
published: 30 June 2021
doi: 10.3389/fenvs.2021.580775

Dynamics of Community Biomass and Soil Nutrients in the Process of Vegetation Succession of Abandoned Farmland in the Loess Plateau

Menghe Gu[1], *Shulin Liu*[1], *Hanchen Duan*[1], *Tao Wang*[1]* *and Zhong Gu*[2]

[1]*Key Laboratory of Desert and Desertification, Drylands Salinization Research Station, Northwest Institute of Eco-Environment and Resources, Chinese Academy of Sciences, Lanzhou, China,* [2]*College of Agriculture, Fujian Agriculture and Forestry University, Fuzhou, China*

The interaction between vegetation and soil is important for vegetation restoration and reconstruction during the succession of abandoned farmland. We chose four kinds of abandoned farmlands with the time of 1, 6, 12, and 22 years to experiment in the Loess Plateau. The community composition, community biomass, and soil nutrients of the four kinds of abandoned farmlands were studied by the method of temporal–spatial alternation, and the interaction effects among vegetation, biomass, soil nutrients, and abandonment time were analyzed. The results showed there were 33 species belonging to 13 families during the succession and 15 species of Gramineae and Compositae, accounting for 47% of the total community species. The succession trend of abandoned farmland was as follows: The vegetation was the weed community of *Heteropappus altaicus* + *Artemisia capillaris* in the beginning of the abandonment stage and became the weed community of *Tragus racemosus* + *Enneapogon borealis* after 6 years of abandonment. Then, *Leymus secalinus* became the dominant population in the community after 12 years of abandonment. When the succession lasted for 22 years, the vegetation became a common advantageous community of *Stipa breviflora* and *Cleistogenes songorica*. Soil moisture (SM) was positively correlated with soil nutrients and negatively correlated with abandonment time and community biomass. Soil organic matter (SOM), soil total nitrogen (STN), and alkali hydrolyzable nitrogen (AHN) were the highest in 0–10 cm soil layer, showing obvious surface accumulation. The three decreased with the soil layer, and there was a positive correlation among them. The abandonment time had a positive effect on the above-ground biomass (AGB) and below-ground biomass (BGB) and a negative effect on the SOM, STN, and AHN. The root/shoot ratio (R/S) was positively correlated with SOM and negatively correlated with abandonment time. With the progress of succession, the hierarchical differentiation of the community was gradually obvious, and the community structure begun to complicate. The community better adapted to the arid environment and toward the local top community succession.

Keywords: abandoned farmland, community biomass, Loess Plateau, root/shoot ratio, soil nutrients

OPEN ACCESS

Edited by:
Atsushi Tsunekawa, Tottori University, Japan

Reviewed by:
Wang Xiukang, Yan'an University, China
Xiliang Song, Shandong Agricultural University, China

***Correspondence:**
Tao Wang
wangtao@lzb.ac.cn

Specialty section:
This article was submitted to Land Use Dynamics, a section of the journal Frontiers in Environmental Science

Received: *07 July 2020*
Accepted: *08 June 2021*
Published: *30 June 2021*

Citation:
Gu M, Liu S, Duan H, Wang T and Gu Z (2021) Dynamics of Community Biomass and Soil Nutrients in the Process of Vegetation Succession of Abandoned Farmland in the Loess Plateau. Front. Environ. Sci. 9:580775. doi: 10.3389/fenvs.2021.580775

INTRODUCTION

In the soil–vegetation system, vegetation and soil are unified organisms, which depend on each other and restrict each other. Soil affects the individual development and growth dynamics of plants and determines the type and distribution of plant community. Vegetation is an important soil-forming factor and also the basis of sustainable utilization of soil. In the process of growth, plants gradually improve the physical and chemical properties of soil by absorption and utilization of soil nutrients (Jiang, 2007; Chang et al., 2008; Jia et al., 2011; Hou and Fu, 2014; Kämpf et al., 2016; Yang et al., 2018; Li et al., 2019; Shang et al., 2019; Hou et al., 2020). Community biomass, as an important measure of ecosystem productivity, reflects the growth and development of plants and changes in their morphological characteristics and is also one of the important indicators to describe the community structure and function, which is a comprehensive reflection of the mutual competition between species and the mutual adaptation between species and the environment (Yan et al., 2006; Wang et al., 2009; Costa et al., 2014; Hou et al., 2020). Abandonment succession is the process of vegetation succession recovering to the top community after farmland abandonment. Many studies had shown that, during the vegetation succession after farmland abandonment, the species diversity and community productivity increased gradually, and the community structure tended to be complicated, which better improved the regional ecological environment (Jiang, 2007; Hou and Fu, 2014; Hülber et al., 2017; Du et al., 2020). There is a close relationship between vegetation restoration and soil nutrients. In the early stage of vegetation restoration, the regressive effect of community litter is weak, and the soil nutrient pool is in a state of loss. With the progress of vegetation restoration and community succession, vegetation litter gradually increases, supplementing the soil nutrient pool. At the same time, the increase in vegetation productivity also increases the soil nutrients; with the improvement of soil's physical and chemical properties, the productivity of vegetation is further improved, which promotes the process of vegetation succession (Yan et al., 2006; Du et al., 2009; Martinez et al., 2010; Fayez, 2012; Yang et al., 2018; Shang et al., 2019; Hou et al., 2020; Liu et al., 2020).

The Loess Plateau was once a major agricultural region in China. However, poor soil water conservation performance, serious soil erosion because of its special loess parent material, and reduced agricultural production had caused vegetation degradation and ecological environment deterioration, which seriously affect and restrict the local economic development and sustainable development of ecological environment (Jiang, 2007; Wang et al., 2009; Jia et al., 2011; Fang et al., 2018; Zhang et al., 2018; Li et al., 2019; Ge et al., 2020). In 1999, the Chinese government launched the "returning farmland to forest and grassland" ecological project, hoping to improve the deteriorating ecological environment by increasing the natural vegetation coverage. Therefore, researchers had done lots of research works on the succession process and the interaction between vegetation and soil of abandoned farmland. To study vegetation succession dynamics, it was necessary to clarify the allocation strategy of community biomass. The research in this area was still relatively weak for the reason that the research on below-ground biomass (BGB) was time-consuming and laborious. Jiang (2007) had found that the soil nutrient showed the fluctuation change of decreasing first and then rising during the succession of abandoned farmland. Liu (2008) had showed the opposite fluctuation trend. However, Du et al. (2008) found that the nutrient loss was serious in the few years after abandonment, and soil organic carbon, soil organic nitrogen, and soil microorganisms began to increase after 29 years of abandonment. The study of Mu et al. (2016) and Liu et al. (2020) showed that pioneer species plants invaded after farmland abandonment, the constructive species and dominant species were replaced constantly, and species abundance, coverage, and community biomass showed a fluctuating trend during the process of vegetation succession. Community biomass was an important parameter of plant community characteristics, and the root/shoot ratio (R/S) reflected the distribution ratio of community biomass in the process of plant growth (Tang et al., 2015; Du et al., 2020). Tang et al. (2015) showed that the R/S of plants was positively correlated with soil organic matter (SOM) and soil total nitrogen (STN) in the degraded grassland. Du et al. (2020) also showed soil nutrients were important factors affecting biomass distribution in the shrub grass community.

In this study, we selected the abandoned farmland in the hilly area of the Loess Plateau of Gansu Province as the research object. We studied the dynamic changes of vegetation, community biomass and its distribution proportion, and soil nutrients according to combined field investigation and indoor analysis by the method of spatial sequence instead of time sequence in the succession process of abandoned farmland vegetation. We tried to answer the following questions: 1) In the process of vegetation succession of abandoned farmland in the Loess Plateau, how vegetation adapted and responded to soil environmental changes? 2) How did the change in soil nutrients affect the allocation of community biomass?

METHODS AND EXPERIMENT DESIGN

Study Site

The study area lies at the Gaolan ecological and agricultural comprehensive test station of the Northwest Institute of Eco-Environment and Resources, CAS, in the Loess Plateau of China (36°13′N, 103°47′E). The site has an altitude of 1780–1820 m a.s.l. and an average annual temperature of 6.3°C. The average annual precipitation is 263 mm, 70% concentrated in May to September, and the annual evaporation is 1785 mm. The soil type of the experimental site is calcic soil (Wei et al., 2006). And the natural vegetation belongs to temperate desertification grassland. The main species are *Reaumuria songarica*, *Ajania fruticulosa*, *Stipa breviflora*, *Lycium barbarum*, *Limonium sinense*, *Cleistogenes songorica*, *Salsola collina*, *Leymus secalinus*, *Artemisia sacrorum*, *Acroptilon repens*, *Peganum harmala*, *Artemisia capillaris*, and *Linum pallescens*.

Methods and Experiment Design

We chose four kinds of abandoned farmlands with the time of 1, 6, 12, and 22 years to experiment. The community composition, community biomass, and soil nutrients of the four kinds of abandoned farmlands were studied by the method of space–time alternation. A 100 m × 500 m experiment plot was selected for each kind of abandoned farmland. In 2011 and 2012, from May to August, a vegetation survey was carried out monthly, and five quadrats (repeats) were randomly selected in each experimental plot. Quadrats of 1 m × 1 m were selected in the 1-, 6-, and 12-year abandoned farmlands (herbaceous vegetation), and 4 m × 4 m was selected in the 22-year abandoned farmland (herbaceous and shrubby vegetation). The survey contents included species abundance, species coverage, and species frequency. In August, soil samples were taken by digging the profile to test soil moisture (SM, %), soil pH value (pH), SOM ($g{\cdot}kg^{-1}$), soil total nitrogen (STN, $g{\cdot}kg^{-1}$), and alkali hydrolyzable nitrogen (AHN, $mg{\cdot}kg^{-1}$). The depths of soil layers were 0–10 cm, 10–20 cm, 20–30 cm, 30–40 cm, 40–50 cm, and 50–60 cm, totally six layers. In each experiment plot, nine points were selected by the S-type to take samples according to six soil layers, and then each three points was mixed into one, so each plot had 3 × 6 soil samples, with a total of 72 soil samples in our experiment. The soil cores were oven-dried to determine SM. Other soil samples were to be tested after air-drying for 4–5 days. The pH was determined by the glass electrode method (water: soil = 5:1). SOM was tested by the potassium dichromate volumetric method, STN was tested by semimicro-Kjeldahl, and AHN was tested by the alkaline diffusion method (Bao, 1986). In September, the above-ground biomass (AGB) was harvested in all quadrats and got constant weight after drying (85°C, 48 h). The BGB was obtained by the excavation method. The soil mass of 1 m × 1 m × 0.6 m and 4 m × 4 m × 1 m under the quadrats was excavated, and the movable roots were picked up, washed, dried, and weighed (105°C, 48 h).

Data Analysis

Microsoft Excel 2010 and statistical package SPSS 21.0 were used to analyze the data and results. Microsoft Excel statistical software was used to calculate the species importance value, Simpson index of species diversity, community biomass, and root/shoot ratio (R/S) of abandoned farmland. SPSS was used for one-way ANOVA, correlation analysis, and linear simulation analysis. We used one-way ANOVA (type III sum of squares) to analyze the significance of abandonment time on community biomass, SM, R/S, SOM, STN, and AHN. The significant differences were further analyzed by multiple comparisons (LSD). Correlation analysis was used to analyze the relationship among community biomass, abandonment time, SM, R/S, and soil nutrient indexes. The relationship between AGB and BGB was analyzed by linear regression.

The calculation formula of species importance value is as follows:

$$\text{Importance value} = \text{Relative abundance} + \text{Relative frequency} + \text{Relative coverage}.$$

The Simpson index was used for species diversity, and the formula is as follows:

TABLE 1 | Important value of species in four kinds of abandoned farmlands.

Latin name of species	Abandonment time			
	1 year	6 years	12 years	22 years
Heteropappus altaicus	86.15	23.80	–	51.11
Artemisia capillaris	116.96	35.03	26.52	52.52
Tragus racemosus	27.76	107.06	–	42.06
Enneapogon borealis	25.32	104.07	–	61.05
Halogeton arachnoideus	30.11	–	–	17.41
Euphorbia humifusa	9.61	33.58	–	28.26
Leymus secalinus	37.56	33.75	190.08	–
Cirsium setosum	31.29	–	–	–
Heteropappus altaicus	21.38	8.04	30.61	6.78
Taraxacum officinale	20.91	21.57	–	–
Cynanchum chinense	20.06	–	–	–
Setaria viridis	27.96	–	–	33.03
Convolvulus arvensis	6.78	13.68	–	–
Plumbagella micrantha	6.78	19.55	–	–
Eragrostis minor	14.96	–	–	–
Lycium barbarum	20.92	–	–	14.89
Medicago sativa	6.83	–	–	–
Chenopodium acuminatum	–	13.89	26.35	6.69
Sonchus oleraceus	–	24.29	32.36	–
Acroptilon repens	–	–	27.59	–
Stipa breviflora	–	–	–	51.22
Cleistogenes songorica	–	–	–	55.79
Salsola collina	–	–	–	7.77
Peganum nigellastrum	–	–	–	23.07
Caragna fruten	–	–	–	9.01
Ajania fruticulosa	–	–	–	10.06
Peganum harmala	–	–	–	11.08
Linum pallescens	–	–	–	8.15
Reaumuria songarica	–	–	–	11.76
Limonium sinense	–	–	–	18.90
Allium japonicum	–	–	–	23.81
Astragalus membranaceus	–	–	–	7.80

$$D = 1 - \sum (N_i/N)^2,$$

where N_i is the number of individuals of species i and N is the sum of individuals of all species.

RESULTS

Vegetation Characteristics of Abandoned Farmlands

The species importance values of abandoned farmlands are shown in **Table 1**. The Simpson diversity indexes were as follows: 12 years (0.36) < 6 years (0.60) < 1 year (0.64) < 22 years (0.79). In the early stage of abandonment, the species diversity was high because many opportunists began to invade at the early stage of abandonment. According to the importance value of species, the dominant species were *Artemisia capillaris* and *Artemisia sacrorum* of Asteraceae in the beginning of farmland abandonment. The other species were *Tragus racemosus*, *Enneapogon borealis*, *Cirsium setosum*, *Lycium barbarum*, *Medicago sativa*, *Heteropappus altaicus*, *Halogeton arachnoideus*, *Eragrostis minor*, *Setaria viridis*, *Leymus secalinus*, *Cynanchum chinense*, *Taraxacum officinale*, *Convolvulus arvensis*, *Euphorbia humifusa*, and *Plumbagella*

TABLE 2 | Community composition of four abandoned farmlands.

Family	Latin name	Life type
Asteraceae	*Artemisia capillaris*	Perennial herb
	Artemisia sacrorum	Perennial herb
	Heteropappus altaicus	Perennial herb
	Ajania fruticulosa	Small semi-shrub
	Sonchus oleraceus	One-year or biennial herb
	Acroptilon repens	Perennial herb
	Cirsium setosum	Perennial herb
	Taraxacum officinale	One-year or biennial herb
	Acroptilon repens	Perennial herb
Poaceae	*Eragrostis minor*	Annual herb
	Setaria viridis	Annual herb
	Tragus racemosus	Annual herb
	Enneapogon borealis	Annual herb
	Leymus secalinus	Perennial herb
	Stipa breviflora	Perennial herb
	Cleistogenes songorica	Perennial herb
Leguminosae	*Caragna fruten*	Deciduous shrub
	Astragalus membranaceus	Perennial herb
	Medicago sativa	Annual or perennial herb
Plumbaginaceae	*Limonium sinense*	Perennial herb
	Plumbagella micrantha	Annual herb
Chenopodiaceae	*Salsola collina*	Annual herb
	Halogeton arachnoideus	Annual herb
	Chenopodium acuminatum	Annual herb
Tamaricaceae	*Reaumuria songarica*	Shrub
Zygophyllaceae	*Peganum harmala*	Perennial herb
	Peganum nigellastrum	Semi-shrub herb
Convolvulaceae	*Convolvulus arvensis*	Perennial herb
Apocynaceae	*Cynanchum chinense*	Perennial herb
Solanaceae	*Lycium barbarum*	Deciduous shrub
Liliaceae	*Allium japonicum*	Perennial herb
Vitaceae	*Euphorbia humifusa*	Annual herb
Linaceae	*Linum pallescens*	Perennial herb

micrantha. After 6 years of abandonment, *Tragus racemosus* and *Enneapogon borealis* of Poaceae became the dominant species in the community. The other species were *Artemisia capillaris*, *Artemisia sacrorum*, *Chenopodium acuminatum*, *Cirsium setosum*, *Sonchus oleraceus*, *Heteropappus altaicus*, *Enneapogon borealis*, *Tragus racemosus*, *Taraxacum officinale*, *Convolvulus arvensis*, *Euphorbia humifusa*, and *Plumbagella micrantha. Leymus secalinus* was a common species in the early stage of abandonment and became the dominant species in the community after 12 years of abandonment. The other species were *Artemisia capillaris*, *Chenopodium acuminatum*, *Heteropappus altaicus*, *Sonchus oleraceus*, and *Acroptilon repens*. In this succession stage, the Simpson index was the lowest. With the progress of succession, *Stipa breviflora* and *Cleistogenes songorica* gradually became the dominant group of the community; at the same time, *Artemisia capillaris*, *Artemisia sacrorum*, *Tragus racemosus*, and *Enneapogon borealis* played an important role in the community after 22 years of abandonment. The other species were *Allium japonicum*, *Euphorbia humifusa*, *Plumbagella micrantha*, *Chenopodium acuminatum*, *Setaria viridis*, *Salsola collina*, *Lycium barbarum*, *Linum pallescens*, *Peganum harmala*, *Peganum nigellastrum*, *Astragalus membranaceus*, *Heteropappus altaicus*, *Caragna fruten*, *Reaumuria songarica*, *Ajania fruticulosa*, and *Limonium sinense*. In this period of succession, the Simpson index was the highest, and some drought-tolerant species began to emerge in the community, such as *Caragna fruten*, *Reaumuria songarica*, *Ajania fruticulosa*, and *Limonium sinense*.

Vegetation investigation showed that there were 33 species in the experimental area, which belong to 13 families, respectively (**Table 2**). They were Asteraceae, Poaceae, Leguminosae, Plumbaginaceae, Chenopodiaceae, Tamaricaceae, Zygophyllaceae, Convolvulaceae, Apocynaceae, Solanaceae, Liliaceae, Vitaceae, and Linaceae. There were 15 species of plants in Gramineae and Compositae, which occupied 47% of the total community species. There were two species of plants in Plumbaginaceae and Zygophyllaceae, respectively, and three species of plants in Chenopodiaceae and Leguminosae, respectively. There was only one species of plant in other families. The order of species abundance of the four abandoned farmlands was 12 years (6 species) < (12 species) < 1 year (17 species) < 22 years (22 species), showing the trend of decreasing first and then increasing. The species of Compositae and Gramineae accounted for the largest proportion in the community in the whole experimental area. It showed that species of Compositae and Gramineae played an important role in the natural restoration of abandoned farmland vegetation in the experimental area.

Dynamics of Community Biomass and R/S During Vegetation Succession

The AGB of the four kinds of abandoned farmlands was 691 $g{\cdot}m^{-2}$, 1,036 $g{\cdot}m^{-2}$, 2,145 $g{\cdot}m^{-2}$, and 2,566 $g{\cdot}m^{-2}$, respectively, in 2011 and was 707 $g{\cdot}m^{-2}$, 847 $g{\cdot}m^{-2}$, 1957 $g{\cdot}m^{-2}$, and 2,495 $g{\cdot}m^{-2}$, respectively, in 2012 (**Figure 1A**). The BGB of the four kinds of abandoned farmlands was 309 $g{\cdot}m^{-2}$, 402 $g{\cdot}m^{-2}$, 604 $g{\cdot}m^{-2}$, and 535 $g{\cdot}m^{-2}$, respectively, in 2011 and was 334 $g{\cdot}m^{-2}$, 424 $g{\cdot}m^{-2}$, 659 $g{\cdot}m^{-2}$, and 466 $g{\cdot}m^{-2}$, respectively, in 2012 (**Figure 1B**). The AGB and BGB increased with the abandonment time. The one-way ANOVA showed that there was no significant difference in AGB ($F = 0.343$, $p > 0.05$) and BGB ($F = 0.022$, $p > 0.05$) between 2011 and 2012. There were significant differences in AGB ($F = 81.862$, $p < 0.001$) and BGB ($F = 21.727$, $p < 0.001$) among four kinds of abandoned farmlands. Multiple comparisons (LSD) of AGB showed that there were significant differences between that of 1-year abandoned farmland and that of 12-year and 20-year abandoned farmlands ($p < 0.001$). There were significant differences between that of 6-year abandoned farmland and that of 12-year and 20-year abandoned farmlands ($p < 0.001$). Multiple comparisons (LSD) of BGB showed that there were significant differences between that of 1-year abandoned farmland and that of other three abandoned farmlands ($p < 0.01$). There was a significant difference between that of 6-year and 12-year abandoned farmlands ($p < 0.001$) and between that of 12-year and 20-year abandoned farmlands ($p < 0.01$).

To illustrate the contributions to plant species from AGB and BGB, we evaluated the relationship between AGB and BGB of all samples using the linear fitting method (**Figure 2**). A positive

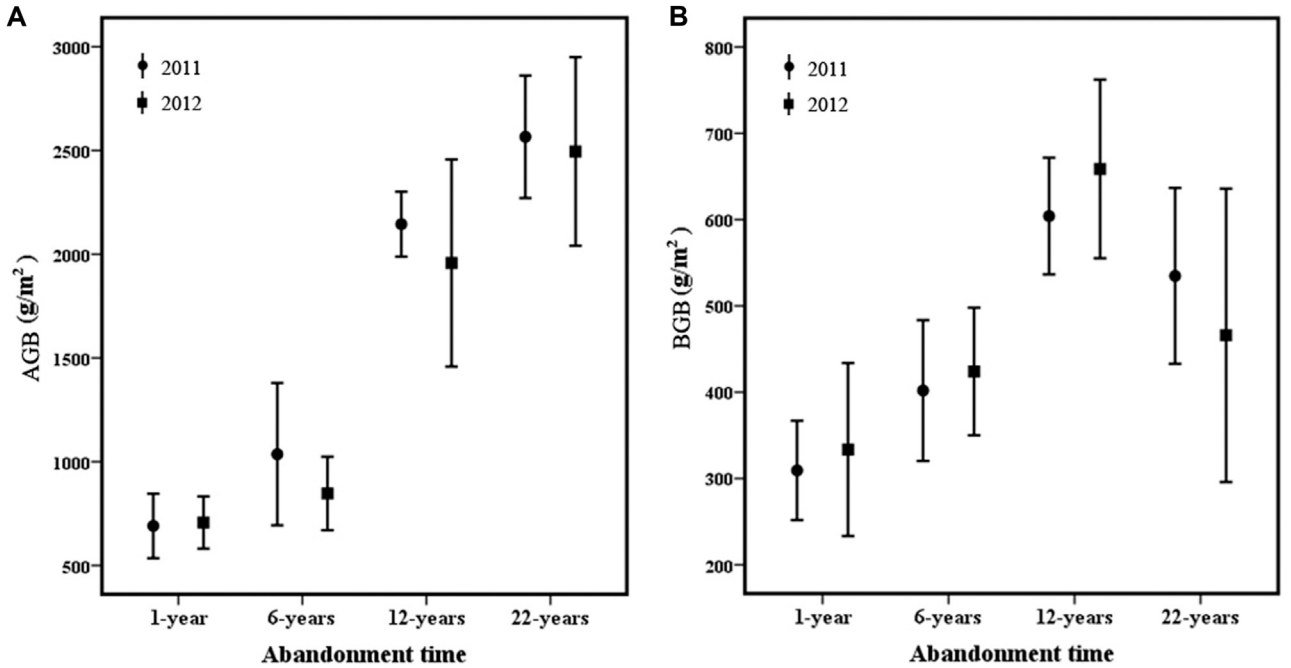

FIGURE 1 | AGB and BGB of four abandoned farmlands. **(A)** AGB in 2011 and 2012. **(B)** BGB in 2011 and 2012.

linear relationship between AGB and BGB ($R^2 = 0.426$, $p < 0.01$) indicates that the BGB could be estimated based on AGB.

The R/S of the four kinds of abandoned farmlands was 0.47, 0.43, 0.28, and 0.25 in 2011 and was 0.48, 0.51, 0.35, and 0.22 in 2012 (**Figure 3**). The R/S decreased with the abandonment time. The ANOVA showed that there was no significant difference in R/S between 2011 and 2012 (F = 0.004, $p > 0.05$) and were significant differences among four kinds of abandoned farmlands (F = 5.820, $p < 0.01$). The multiple comparisons (LSD) showed that there was a significant difference between that of 1-year and 20-year abandoned farmlands ($p < 0.05$). There were significant differences between that of 6-year abandoned farmland and that of 12-year and 20-year abandoned farmlands ($p < 0.05$).

Dynamics of pH, SM, SOM, STN, and Alkali Hydrolyzed Nitrogen During Vegetation Succession

The pH of the four kinds of abandoned farmlands was 8.69 ± 0.09, 8.55 ± 0.12, 8.56 ± 0.04, and 8.53 ± 0.20, respectively. The soil appeared weakly alkaline, and pH decreased gradually with the abandonment time in the Loess Plateau. The SM of the four kinds of abandoned farmlands was 55.19, 43.52, 39.36, and 44.53% in 2011 and was 38.14, 36.00, 31.29, and 33.67% in 2012. It showed a trend of decreasing first and then increasing. The abandonment time and soil layer all had significant effect on SM (F = 15.31, $p < 0.001$; F = 8.29, $p < 0.001$). Multiple comparisons (LSD) of four abandonment times showed that there was a significant difference between the SM of 1-year abandoned farmland and that of the other three abandoned farmlands ($p < 0.001$) and between that of the 6-year and 12-year abandoned farmlands.

The SOM of the four kinds of abandoned farmlands was 63.57 g·kg^{-1}, 64.88 g·kg^{-1}, 43.76 g·kg^{-1}, and 53.25 g·kg^{-1} in 2011 and was 61.87 g·kg^{-1}, 67.02 g·kg^{-1}, 48.18 g·kg^{-1}, and 50.66 g·kg^{-1} in 2012. SOM of four abandoned farmlands in different soil layers is shown in **Figure 4A**. SOM decreased with the soil layer in 0–60 cm, with surface accumulation. SOM increased first and then decreased with the abandonment time, and the highest SOM was found in the 6-year abandoned land. The one-way ANOVA of SOM showed that there was no significant difference between 2011 and 2012 (F = 0.24, $p > 0.05$). The soil layer and abandonment time had significant effect on SOM (F = 77.21, $p < 0.001$; F = 62.58, $p < 0.001$), and the interaction between the two had significant effect on SOM (F = 2.43, $p < 0.05$). Multiple comparisons (LSD) of SOM in six soil layers showed that there were significant differences among all soil layers ($p < 0.001$) except between 40–50 cm and 50–60 cm soil layers. Multiple comparisons (LSD) of SOM in four abandonment times showed that there was a significant difference between 1-year and 6-year abandonment times ($p < 0.05$), and the rest all had significant differences ($p < 0.01$).

The STN of the four kinds of abandoned farmlands was 4.18 g·kg^{-1}, 4.07 g·kg^{-1}, 3.55 g·kg^{-1}, and 3.23 g·kg^{-1} in 2011 and was 3.67 g·kg^{-1}, 3.91 g·kg^{-1}, 3.36 g·kg^{-1}, and 3.08 g·kg^{-1} in 2012. As shown in **Figure 4B**, STN in 2011 and 2012 decreased with the soil layer in 0–60 cm, with surface accumulation, similar to the SOM. With the abandonment time, STN continued to decline, except for the 6-year abandoned farmland in 2012. The one-way ANOVA of STN showed there was a significant

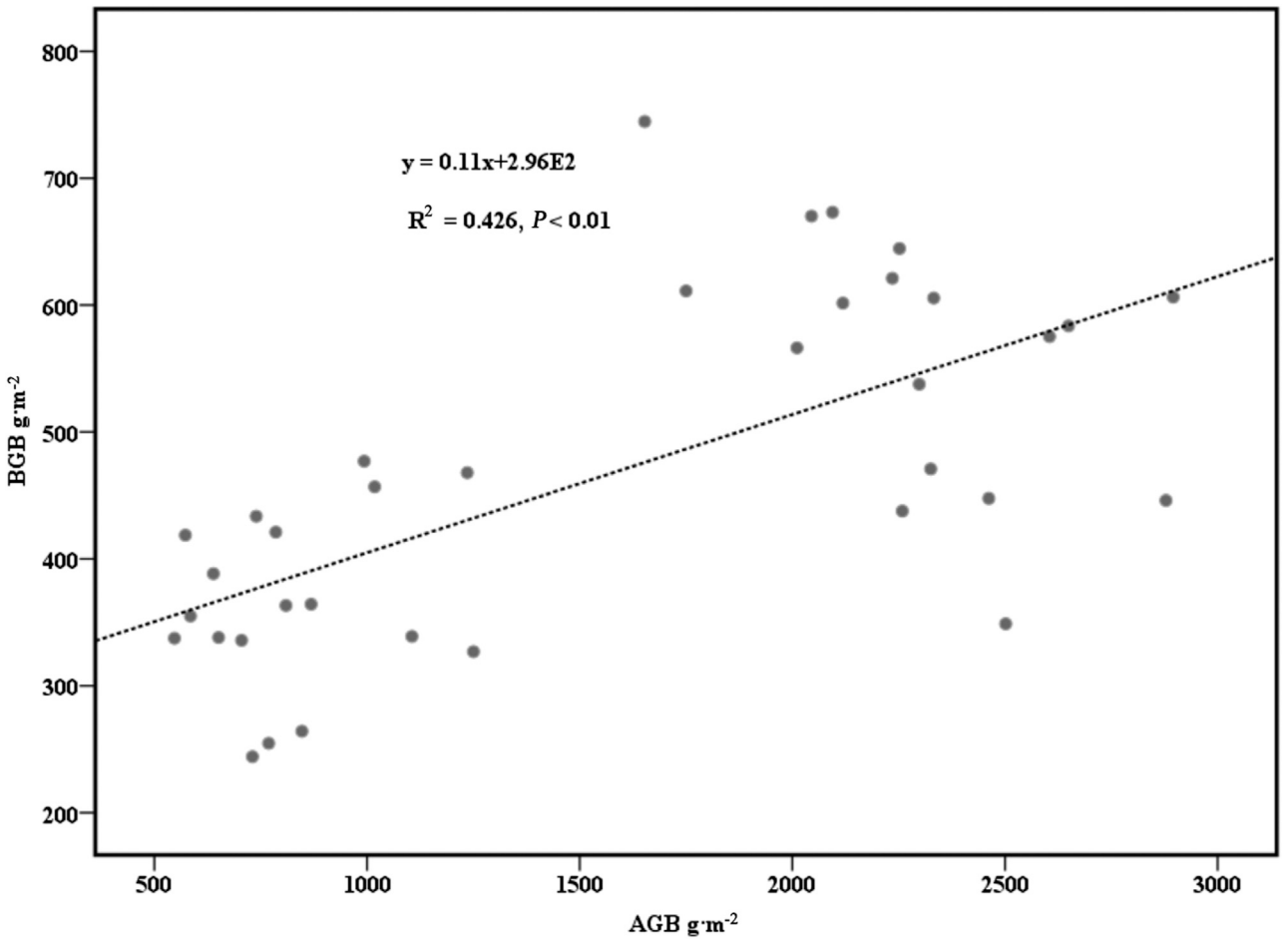

FIGURE 2 | Relationships between AGB and BGB in the Loess Plateau.

difference between 2011 and 2012 (F = 12.02, $p < 0.05$). The soil layer and abandonment time had significant effect on STN (F = 57.62, $p < 0.001$; F = 29.31, $p < 0.001$), and the interaction between the two had significant effect on STN (F = 2.84, $p < 0.05$). Multiple comparisons (LSD) of STN in six soil layers showed that there were significant differences among all soil layers ($p < 0.05$) except between 40–50 cm and 50–60 cm soil layers. Multiple comparisons (LSD) of STN in four abandonment times showed that there were significant differences among all abandonment times ($p < 0.001$) except between 1-year and 6-year abandonment times.

The AHN of the four kinds of abandoned farmlands was 25.89 mg·kg^{-1}, 25.17 mg·kg^{-1}, 21.44 mg·kg^{-1}, and 12.67 mg·kg^{-1} in 2011 and was 21.39 mg·kg^{-1}, 23.28 mg·kg^{-1}, 18.44 mg·kg^{-1}, and 12.83 mg·kg^{-1} in 2012. As shown in **Figure 4C**, AHN decreased with the soil layer in 0–60 cm in 2011 and 2012, with surface accumulation, similar to the SOM and STN. With the abandonment time, AHN continued to decline, except for the 6-year abandoned farmland in 2012. The one-way ANOVA of AHN showed there was a significant difference between 2011 and 2012 (F = 12.49, $p < 0.05$). The soil layer and abandonment time had significant effect on AHN (F = 88.49, $p < 0.001$; F = 62.95, $p < 0.001$), and the interaction between the two had significant effect on AHN (F = 5.61, $p < 0.001$). Multiple comparisons (LSD) of AHN in six soil layers showed that there were significant differences among all soil layers ($p < 0.05$). Multiple comparisons (LSD) of AHN in four abandonment times showed that there were significant differences among all abandonment times ($p < 0.001$) except between 1-year and 6-year abandonment times.

Correlation Analysis of Abandonment Time, AGB, BGB, R/S, SOM, STN, AHN, and SM

The results of correlation analysis among AGB, BGB, R/S, abandonment time, SOM, STN, AHN, and SM are shown in **Table 3**. The abandonment time showed a significant correlation with the seven indexes measured ($p < 0.01$), among which it showed a positive correlation with the AGB and BGB. AGB was shown to have a positive correlation with BGB ($p < 0.01$) and a negative correlation with other indexes. BGB was shown to have a negative correlation with SOM, STN, and SM ($p < 0.01$). SOM was shown to have a positive correlation with STN, AHN, R/S ($p < 0.01$), and SM ($p < 0.05$). STN was shown to have a positive

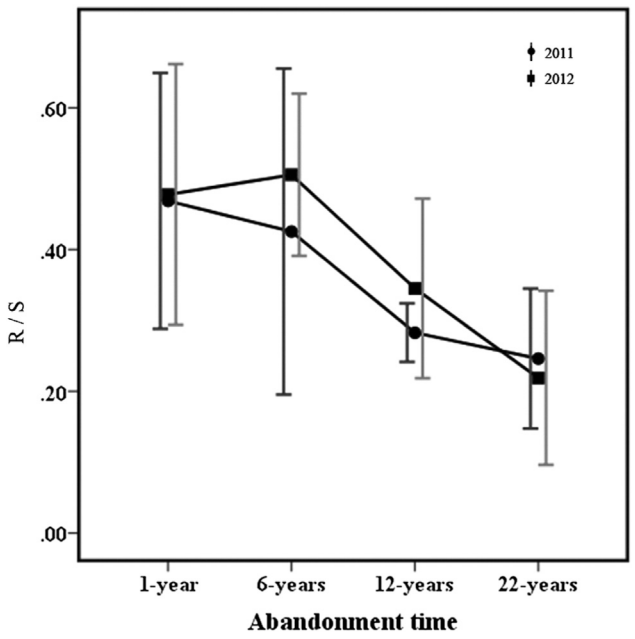

FIGURE 3 | R/S of four abandoned farmlands.

correlation with AHN and SM ($p < 0.01$). R/S was shown to have a positive correlation with AHN ($p < 0.05$).

DISCUSSION

Many studies had shown that the annual herbaceous plants would invade after farmland is abandoned. With the succession progress, the constructive species and dominant species of the plant community would change, and the richness and coverage of the community would show a fluctuating trend (Jiang, 2007; Chang et al., 2008; Kämpf et al., 2016; Hülber et al., 2017; Shang et al., 2019; Liu et al., 2020). In the early stage of abandonment, many free niches provided opportunities for pioneer species to invade and survive and species diversity was higher in the community. With the invasion of a large number of annual weeds, interspecific competition began to become fierce, leading to the withdrawal of some less competitive species from the weed community. As abandoned up to 12 years, the rhizomatous grass, *Leymus secalinus*, became the dominant population. Its strong tillering ability, big individuals, early turning green, and strong competitiveness, which inhibited the growth and reproduction of many annual and perennial herbs, resulted in the decline of the survival of some species in the

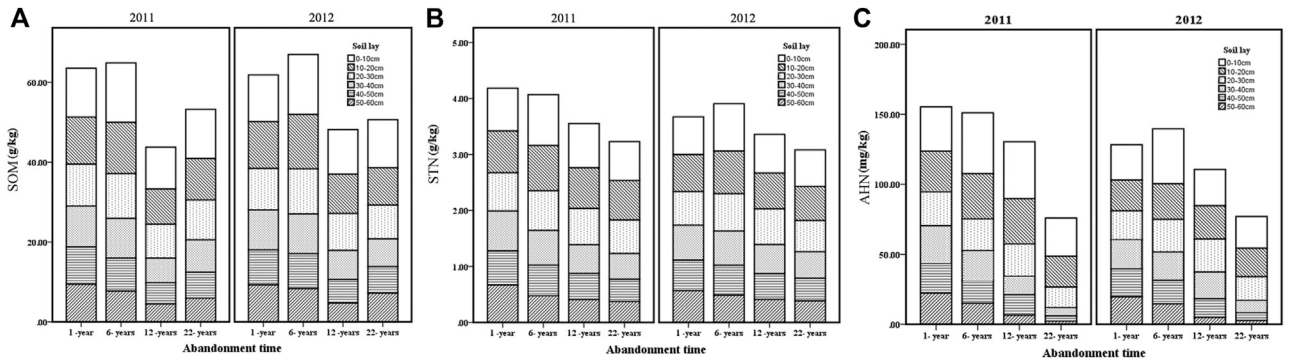

FIGURE 4 | SOM **(A)**, STN **(B)**, and AHN **(C)** of four abandoned farmlands in different soil layers.

TABLE 3 | Correlation analysis among abandonment time, AGB, BGB, R/S, SOM, STN, AHN, and SM.

	AT	AGB	BGB	SOM	STN	R/S	AHN	SM
AT	1							
AGB	0.940[b]	1						
BGB	0.603[b]	0.653[b]	1					
SOM	−0.629[b]	−0.729[b]	−0.624[b]	1				
STN	−0.732[b]	−0.721[b]	−0.521[b]	0.679[b]	1			
R/S	−0.683[b]	−0.788[b]	−0.235	0.585[b]	0.404	1		
AHN	−0.853[b]	−0.784[b]	−0.444	0.556[b]	0.897[b]	0.467[a]	1	
SM	−0.481[b]	−0.448[a]	−0.482[b]	0.411[a]	0.583[b]	0.299	0.490[a]	1

[a]p < *0.05*.
[b]p < *0.01*.

community and even death and emigration (Liu et al., 2007; Shi et al., 2008). Therefore, the community diversity decreased during this succession stage. After 22 years of abandonment succession, the *Leymus secalinus* community was replaced by a co-dominant community formed by *Cleistogenes songorica* and *Stipa breviflora*, more species survived, and species richness and vegetation coverage gradually increased. The co-dominant community had a stable structure, and the ecological environment gradually improved. Some more drought-tolerant shrubs, such as *Reaumuria songarica* and *Ajania fruticulosa*, began to emerge in the community. So far, the vegetation succession process of the herbaceous stage of abandoned farmland in the Loess Plateau had been completed. The results of this study were consistent with those of many previous studies. Many studies had shown that annual herbaceous plants invaded after farmland abandonment. With the succession of abandoned farmland, the constructive species and dominant species of the plant community were replaced, and the richness, coverage, and biomass of the community showed a fluctuating trend (Liu et al., 2007; Mu et al., 2016; Liu et al., 2020). Studies on abandoned farmland in the Loess Plateau by Du et al. (2008) showed that 6 years after abandonment, the community diversity of the mono-dominant community formed by *Artemisia gmelinii* or *Artemisia giraldii* decreased. After 15 years, the mono-dominant community was replaced by the drought-tolerant co-dominant community of *Lespedeza davurica* and *Bothriochloa ischaemum*, and the community diversity increased. Zhang et al. (2018) also found that species diversity had changed with abandonment time in the process of abandoning farming in the Loess Plateau. Our results were also similar to those of Jiang (2007) studies in the Loess Plateau. His results showed that species richness decreased to the lowest level seven years after abandonment. After 20 years of abandonment, species richness increased significantly to 26 species. Species richness changed with the abandonment time in the process of vegetation restoration. With the process of succession, the differentiation of community hierarchy was gradually obvious, and the community structure was becoming more and more complex, which can accommodate the coexistence of more species of multiple ecological types, and the succession had developed toward the local top community.

Many studies on abandoned farmland had found that AGB and BGB fluctuated with abandonment time during the process of vegetation restoration (Du et al., 2008; Wang et al., 2009; Martinez et al., 2010; An et al., 2011; Costa et al., 2014; Yang et al., 2018). During the process of community succession, the change of community biomass is closely related to the community structure and dominant community. AGB distribution mainly relates to the competition for light resources, while BGB distribution mainly relates to the competition for soil nutrients (Du et al., 2008; An et al., 2011; Jia et al., 2011; Hou and Fu, 2014; Mu et al., 2016; Zhang et al., 2018). In this study, there were many vacant niches during the early stage of succession, and the competition was not fierce. A large number of annual herbs invaded, most of them were individually small and short-lived species, and they found it difficult to accumulate high AGB and BGB in a short growth period. *Leymus secalinus*, as a dominant population, replaced the previous weed community after 12 years of abandonment. It relied on its vigorous vegetative reproduction to expand its population, extended and expanded outward in space, and increased its quantity and volume in time through clonal tillers. So, it could obtain higher AGB and BGB in resource competition during this succession stage. This was also the main reason why *Leymus secalinus* became a dominant species in many grassland types (Liu et al., 2007; Shi et al., 2008). Du et al. (2008) and An et al. (2011) showed that the biomass of abandoned farmland decreased at first and then increased, while our results showed that biomass continued to increase in the whole succession process. The reason why our research results were not completely consistent with others was because of *Leymus secalinus*. In the middle stage of abandonment, it became the dominant species and obtained high biomass maintained the continuous increase of abandoned farmland biomass. After 22 years of abandonment, the dominant species of the community changed, gradually from the herbaceous community to the shrub community. More drought-tolerant species, such as *Ajania fruticulosa*, *Lycium barbarum*, and *Reaumuria songarica*, appeared in the community. The distribution proportion of AGB increased, while that of BGB decreased. The community contained multiple ecotypes of species to coexist, and the community structure tended to be stable. The community succession developed toward the local top community.

In the Loess Plateau, SM is the primary factor affecting vegetation restoration and reconstruction. Different species can obtain water from different depths of soils. Conversely, the distribution, storage, and change of water resources determine the species type and distribution (Jiang, 2007; Chang et al., 2008; Du et al., 2008; Yang et al., 2018). In this study, SM showed a downward trend, biomass continued to increase, and the two showed a negative correlation. The SM was higher during the early stage of abandonment due to the previous agricultural measures, and pioneer species could obtain higher biomass. The SM was consumed continuously during abandonment, and it reached the lowest level after abandonment for 12 years. However, the dominant species *Leymus secalinus* was not limited by SM. It could obtain deeper soil water for its well-developed root system and obtain high AGB and BGB. When abandoned for 22 years, higher community biomass was accumulated because of community diversity and vegetation coverage increased gradually. Wei et al. (2006) research also showed that, in the early stage of abandonment, loose soil could maintain high SM. With succession, SM decreased, and *Leymus secalinus* became an important factor affecting SM. SM fluctuated during the succession, and other researchers have similar results in the Loess Plateau (Jiang, 2007; Du et al., 2008).

The succession of community is a process of interaction between vegetation and soil. Vegetation affects the accumulation and distribution of soil nutrients through litter and root exudates, and soil nutrient content in turn affects the growth of vegetation (Du et al., 2009; Fayez, 2012; Li et al., 2019; Shang et al., 2019; Du et al., 2020; Ge et al., 2020; Liu et al., 2020). Jiang (2007) and Liu (2008) had found that the soil nutrient showed the fluctuation change of decreasing first and then

increasing during the succession in the hilly area of the Loess Plateau. In this study, the SOM and STN decreased with the increase of abandonment time, which was not completely consistent with that reported in other studies. When abandoned after 12 years, the rhizomatous grass *Leymus secalinus* had gradually became the dominant species; its developed roots had strong competitiveness and effectively utilized and absorbed soil nutrients, causing soil nutrients to decline. At the same time, the decreased SOM and STN may be related to the soil nutrient loss caused by soil erosion in the Loess Plateau. In addition, the time series of the study was not long enough in this study. At 22 years of succession, the organic matter began to increase. With the increase of abandonment time, the total nitrogen content of soil is likely to increase. In the abandoned farmland in the Loess Plateau, Du et al. (2008) had found when the abandoned farmland was disturbed in the first few years, it showed obvious nutrition loss, and the growth of the below-ground part of the vegetation was limited. With the succession going on, SOM, STN, and soil microorganisms gradually increased, which was conducive to promoting the succession of the plant community. Hou (2012), Zhang et al. (2018), and Ge et al. (2020) also had similar research results in the Loess Plateau. The results had shown that the physical and chemical properties of the soil were gradually optimized and tended to benign development with the recovery of vegetation during the succession of abandoned farmland.

The R/S reflects the distribution ratio of photosynthesis products in plants. Its change is a response strategy for plants to environmental changes. Soil nutrient is one of the factors affecting the R/S (Yan et al., 2006; Du et al., 2008; Costa et al., 2014; Tang et al., 2015; Fang et al., 2018; Yang et al., 2018). The results of Tang et al. (2015) had shown that the R/S of plants was positively correlated with SOM and STN in the degraded grassland of Yanchi County in Ningxia. Fang et al. (2018) had found that higher soil nutrients played an important role in promoting the growth of fine roots and increasing the distribution of BGB in the loess hilly area of Shanxi. Du et al. (2020) had found there was a significant correlation between soil available phosphorus and community biomass, and between SOM and R/S, indicating that soil factors were important factors affecting biomass distribution in the shrub grass community in Northwest Hebei Province. Our study found that the R/S was positively correlated with SOM, but not with STN, which was consistent with the previous results. When plants distribute biomass in different organs, they will adopt the survival strategy of absorbing soil water, soil nutrients, and light resources to the maximum extent, so as to achieve the maximum growth rate during the process of growth (Yan et al., 2006; Wang et al., 2009; Costa et al., 2014). When the soil nutrient resources are insufficient, plants will adjust their growth strategies to adapt to environmental changes by changing the AGB and BGB allocation.

CONCLUSION

In this experiment, the succession trend of abandoned farmland was as follows: The vegetation was the weed community of *Heteropappus altaicus* + *Artemisia capillaris* in the beginning of the abandonment stage and became the weed community of *Tragus racemosus* + *Enneapogon borealis* after 6 years of abandonment. Then, *Leymus secalinus* became the dominant population in the community after 12 years of abandonment. With the succession time reaching 22 years, the vegetation of abandoned farmland became a common advantageous community of *Cleistogenes songorica* + *Stipa breviflora*. The AGB and BGB of abandoned farmland increased gradually with the abandonment time. The growth rate of AGB and BGB reached 118 and 53%, respectively, during 6–12 years of abandonment. The R/S of the abandoned farmland was less than 1 and decreased during the process of succession. The pH was more than 8, and the soil appeared weak alkaline in the Loess Plateau. SM decreased gradually with the succession time and reached the lowest level after 12 years of abandonment. SOM showed a trend of increasing first and then decreasing, and STN and AHN were decreased during the process of succession.

DATA AVAILABILITY STATEMENT

The raw data supporting the conclusions of this article will be made available by the authors, without undue reservation.

AUTHOR CONTRIBUTIONS

MG designed and arranged the experiment and wrote the manuscript. SL modified the manuscript. HD participated in the field experiment. TW is our project leader, who was in charge of the experiment in general. ZG participated in data collation and statistics analysis.

FUNDING

This study was supported by the Project of National Key Research and Development Program of China "Assessment on evolution trend and stability of desertified land in the semiarid region of northern China."

REFERENCES

An, H., Yang, X. G., Liu, B. R., Li, X. B., He, X. Z., and Song, N. P. (2011). [Changes of Plant Community Biomass and Soil Nutrients during the Vegetation Succession on Abandoned Cultivated Land in Desert Steppe Region]. *Ying Yong Sheng Tai Xue Bao.* 22 (12), 3145–3149. doi:10.13287/j.1001-9332.2011.0467

Bao, S. D. (1986). *Soil Agrochemical Analysis [M]*. Beijing: China Agricultural Publishing House.

Chang, J. F., Liu, H. J., Zhao, M., Han, F. G., Zhong, S. N., and Tang, J. N. (2008). Three Stages of Degeneration Succession of Desert Vegetation in Minqin. *Chin. Agric Sci Bull.* 24 (6), 389–395.

Costa, T. L., Sampaio, E. V. S. B., Sales, M. F., Accioly, L. J. O., Althoff, T. D., Pareyn, F. G. C., et al. (2014). Root and Shoot Biomasses in the Tropical Dry

forest of Semi-arid Northeast Brazil. *Plant Soil*. 378, 113–123. doi:10.1007/s11104-013-2009-1

Du, F., Liang, Z. S., Xu, X. X., Zhang, X. C., and Shan, L. (2008). Spatial Heterogeneity of Soil Nutrients and Above-Ground Biomass in Abandoned Old-fields of Loess Hilly Region in Northern Shaanxi, China. *Acta Ecol. Sinica*. 28 (1), 13–22. doi:10.1016/s1872-2032(08)60017-7

Du, J. H., Yan, P., Ding, L. G., Er, Y. H., and Zhu, M. J. (2009). Soil Physical and Chemical Properties of Nitraria Tangutorun Nebkhas Surface an Different Development Stages in Minqin Oasis. *J. Desert Res.* 29 (2), 248–253.

Du, M. Q., Zhang, H. S., Peng, D., and Zha, T. G. (2020). Distribution of Shrub-Herb Community Biomass and its Relationship with Soil Factors in Middle and Low Mountainous Areas of Northwest Hebei Province. *Pratac Sci.* 37 (1), 1–9. doi:10.11829/j.issn.1001-0629.2019-0227

Fang, Z., Zhang, S. K., Liu, H. W., Jiao, F., and Zhang, J. (2018). Distribution of Herbaceous Community Biomass and its Relationship with Influencing Factors in the Loess Hilly Region. *Acta Pratac Sinica*. 27 (2), 26–35. doi:10.11686/cyxb2017152

Fayez, R. (2012). Soil Properties and C Dynamics in Abandoned and Cultivated Farmlands in a Semi-arid Ecosystem. *Plant Soil*. 351, 161–175. doi:10.1007/s11104-011-0941-5

Ge, J. M., Wang, S., Fan, J., Gongadze, K., and Wu, L. H. (2020). Soil Nutrients of Different Land-Use Types and Topographic Positions in the Water-Wind Erosion Crisscross Region of China's Loess Plateau. *Catena*. 184, 1–10. doi:10.1016/j.catena.2019.104243

Hou, D., Bolan, N. S., Tsang, D. C. W., Kirkham, M. B., and O'Connor, D. (2020). Sustainable Soil Use and Management: An Interdisciplinary and Systematic Approach. *Sci. Total Environ.* 729, 138961. doi:10.1016/j.scitotenv.2020.138961

Hou, J., and Fu, B. (2014). Vegetation Dynamics during Different Abandoned Year Spans in the Land of the Loess Plateau of China. *Environ. Monit. Assess.* 186, 1133–1141. doi:10.1007/s10661-013-3444-4

Hou, X. R. (2012). *The Spatial Distribution and Storage of Soil Organic Carbon and Nitrogen of Hilly Region of Loess Plateau*. Yangling: Northwest Agriculture & Forestry University

Hülber, K., Moser, D., Sauberer, N., Maas, B., Staudinger, M., Grass, V., et al. (2017). Plant Species Richness Decreased in Semi-natural Grasslands in the Biosphere Reserve Wienerwald, Austria, over the Past Two Decades, Despite Agri-Environmental Measures. *Agric. Ecosyst. Environ.* 243, 10–18. doi:10.1016/j.agee.2017.04.002

Jia, X., Shao, M., and Wei, X. (2011). Richness and Composition of Herbaceous Species in Restored Shrubland and Grassland Ecosystems in the Northern Loess Plateau of China. *Biodivers Conserv.* 20, 3435–3452. doi:10.1007/s10531-011-0130-0

Jiang, J. P. (2007). *Co-variation of Vegetation and Soil Quality during Ecosystem Restoration in the Hilly Region of the Semiarid Loess Plateau*. Lanzhou: Lanzhou University

Kämpf, I., Mathar, W., Kuzmin, I., Hölzel, N., and Kiehl, K. (2016). Post-soviet Recovery of Grassland Vegetation on Abandoned fields in the forest Steppe Zone of Western Siberia. *Biodivers Conserv*. 25, 2563–2580. doi:10.1007/s10531-016-1078-x

Li, J. W., Liu, Y. L., Hai, X. Y., Shangguan, Z. P., and Deng, L. (2019). Dynamics of Soil Microbial C:N:P Stoichiometry and its Driving Mechanisms Following Natural Vegetation Restoration after farmland Abandonment. *Sci. Total Environ.* 693, 1–11. doi:10.1016/j.scitotenv.2019.133613

Liu, W. H., Zhou, Q. P., and Yan, H. P. (2007). Research Progress on the Propagation Path of Rhizome Grasses. *Chin. Qinghai J. Anim. Veter Sci* 37 (2), 46–49.

Liu, Y. (2008). *Effects of Vegetation Restoration on Soil Quality in Yangou Catchment in Hilly-Gully Region of the Loess Plateau*. Xi'an: Northwest Agriculture & Forestry University

Liu, Y., Zhu, G., Hai, X., Li, J., Shangguan, Z., Peng, C., et al. (2020). Long-term forest Succession Improves Plant Diversity and Soil Quality but Not Significantly Increase Soil Microbial Diversity: Evidence from the Loess Plateau. *Ecol. Eng.* 142, 105631. doi:10.1016/j.ecoleng.2019.105631

Martinez, D. E., Ferrandis, P., and Escudero, A. (2010). Secondary Old-Field Succession in an Ecosystem with Restrictive Soils: Does Time from Abandonment Matter? *Appl. Veg Sci.* 13, 234–248. doi:10.1111/j.1654-109X.2009.01064.x

Mu, L., Zhang, P. J., Liu, Y. H., Liu, X. C., Ren, Y. F., Wang, B., et al. (2016). Effect of Restoration Measures on Herbaceous Community Characteristics of Abandoned Land in Desert Steppe of Inner Mongolia. *Chin. Agric Sci Bull.* 32 (16), 110–116.

Shang, Z. H., Cao, J. J., Degen, A. A., Zhang, D. W., and Long, R. J. (2019). A Four Year Study in a Desert Land Area on the Effect of Irrigated, Cultivated Land and Abandoned Cropland on Soil Biological, Chemical and Physical Properties. *Catena*. 175, 1–8. doi:10.1016/j.catena.2018.12.002

Shi, H. X., Zhou, Q. P., Yan, H. P., Liu, W. H., and Yang, Y. L. (2008). Preliminary Study on the Space and Time Expanding of Three Rhizometype Grasses in Clonal Reproduction Stage. *Pratac Sci.* 25 (5), 127–132.

Tang, Z. S., An, H., and Shang Guan, Z. P. (2015). Effects of Desertification on Soil Nutrients and Root-Shoot Ratio in Desert Steppe. *Acta Agrestia Sinica*. 23 (3), 463–468. doi:10.11733/j.issn.1007-0435.2015.03.005

Wang, G., Liu, G., and Xu, M. (2009). Above- and Belowground Dynamics of Plant Community Succession Following Abandonment of farmland on the Loess Plateau, China. *Plant Soil*. 316, 227–239. doi:10.1007/s11104-008-9773-3

Wei, X. H., Xie, Z. K., and Duan, Z. H. (2006). Vegetation Rehabilitation and Soil Moisture Control in Abandoned Plowlands on Western Loess Plateau. *J. Desert Res.* 26 (4), 590–595.

Yan, E.-R., Wang, X.-H., and Huang, J.-J. (2006). Shifts in Plant Nutrient Use Strategies under Secondary forest Succession. *Plant Soil*. 289, 187–197. doi:10.1007/s11104-006-9128-x

Zhang, W., Ren, C., Deng, J., Zhao, F., Yang, G., Han, X., et al. (2018). Plant Functional Composition and Species Diversity Affect Soil C, N, and P during Secondary Succession of Abandoned farmland on the Loess Plateau. *Ecol. Eng.* 122, 91–99. doi:10.1016/j.ecoleng.2018.07.031

Conflict of Interest: The authors declare that the research was conducted in the absence of any commercial or financial relationships that could be construed as a potential conflict of interest.

frontiers in Environmental Science

ORIGINAL RESEARCH
published: 05 August 2021
doi: 10.3389/fenvs.2021.574883

Simulated Experiment on Wind Erosion Resistance of *Salix* Residual in the Agro-Pastoral Ecotone

Qiang Li[1,2]*, *Furen Kang*[2], *Zheng Zhang*[1,2], *Chunyan Ma*[2] *and Weige Nan*[3]

[1]*Shaanxi Key Laboratory of Ecological Restoration in Shaanbei Mining Area, Yulin University, Yulin, China,* [2]*State Key Laboratory of Soil Erosion and Dryland Farming on the Loess Plateau, Institute of Soil and Water Conservation, Northwest A&F University, Yangling, China,* [3]*Shaanxi Normal University, Xi'an, China*

Plant residual is of great importance in retarding soil wind erosion in the agro-pastoral ecotone. However, few studies have determined the effects of sand plant residual on wind erosion resistance. Based on field surveys, the influences of *Salix* residual biomass of 200, 400, 600, and 800 g m^{-2}, soil incorporated with a residual thickness of 0.5, 1.0, and 2.0 cm, and typical proportion of residual branches and leaves (2:1, 1:1, and 1:2) on wind erosion resistance were investigated using a simulated wind tunnel. The results showed the following: 1) The soil loss amount ranged from 1.56 to 40.8 kg m^{-2} as *Salix* residual biomass decreased from 800 to 0 g m^{-2}, with a critical residual biomass value of 400 g m^{-2}. 2) As the thickness of soil-incorporated residual increased, the soil loss amount reduced rapidly, especially for 0–9 cm above the surface accounting for 84.6% of the total. 3) *Salix* branch residual is more important in resisting soil wind erosion as compared with its leaves. This kind of study may provide theoretical explanations for the optimal reconstruction of sandy vegetation in the northern wind-sand regions.

Keywords: wind tunnel, soil loss amount, simulated wind erosion, *Salix* litter, Mu Us sandy land

OPEN ACCESS

Edited by:
Xian Xue,
Northwest Institute of Eco-Environment and Resources (CAS), China

Reviewed by:
Na Li,
Northeast Institute of Geography and Agroecology (CAS), China
Jianjun Qu,
Northwest Institute of Eco-Environment and Resources (CAS), China

***Correspondence:**
Qiang Li
mr.li_qiang@163.com

Specialty section:
This article was submitted to Soil Processes, a section of the journal Frontiers in Environmental Science

Received: *30 June 2020*
Accepted: *28 June 2021*
Published: *05 August 2021*

Citation:
Li Q, Kang F, Zhang Z, Ma C and Nan W (2021) Simulated Experiment on Wind Erosion Resistance of Salix *Residual in the Agro-Pastoral Ecotone. Front. Environ. Sci. 9:574883. doi: 10.3389/fenvs.2021.574883*

INTRODUCTION

Wind erosion is an environmental concern in arid and semi-arid regions due to the emission of particulates into the atmosphere (He, 2014; Tuo et al., 2016; Zhang et al., 2018). Decades of practice showed that sandy vegetation construction is an effective method of ecological reconstruction in the northern wind-sand regions (Yu et al., 2017; Zhang et al., 2019). Most recently, research has been focused on the interactions between sandy vegetation and its influence on the soil quality in the agro-pastoral ecotone of northern China (Zhang and Zhao, 2015; Wang et al., 2020) and the relationship between plant distribution patterns and wind erosion resistance (He, 2014; Li et al., 2016, Li et al., 2017). The redistribution of leaves and fruits caused by the northwest wind is the main reason for the formation of different plant residual patterns (Zhao et al., 2003; Li et al., 2020). However, few studies have determined the effects of sand plant residual on wind erosion resistance.

Salix (*Salix psammophila*) is typical vegetation in the Mu Us Sandy Land, which is one of the first choices of the "Three-North Shelter Forest Program" in China. The Three-North Shelter Forest Program is a large-scale artificial forestry ecological project in the three northern areas of China (northwest, north, and northeast) (Li et al., 2016). Previous studies related to wind erosion have shown that *Salix* residual community can form obvious patterns in the dune slope; the spatial and temporal variation of this could strongly influence the vegetation species composition, community structure, and soil quality development due to the long-term effects of wind (Sun et al., 2016b; Liu

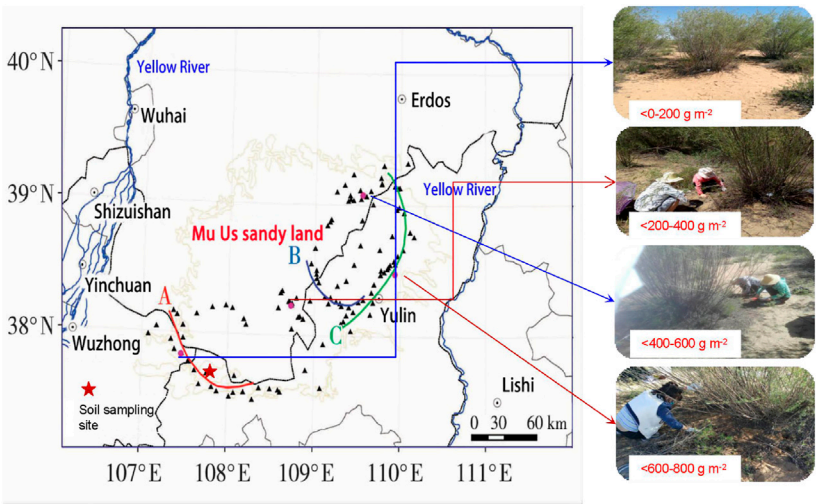

FIGURE 1 | Distribution of residual samples of *Salix* residual in the southeastern margin of the Mu Us Sandy Land [the survey route includes A, B, and C lines].

TABLE 1 | Biomass of different parts of *Salix* and residual thickness in 36 *Salix* sites.

Component	NO.1	NO.2	NO.3	NO.4	NO.5	NO.6	NO.7	NO.8	NO.9	NO.10	NO.11	NO.12
Branches (g m^{-2})	186.49	133.07	24.59	184.98	163.11	123.67	298.49	88.18	211.11	53.89	56.15	100.74
Leaves (g m^{-2})	73.69	54.67	62.96	143.82	141.00	107.78	72.78	105.16	206.22	36.00	17.33	97.19
Fruits (g m^{-2})	15.44	11.78	5.78	19.29	25.19	17.33	11.85	11.22	33.33	51.85	1.78	24.00
Others (g m^{-2})	13.93	11.00	0.00	15.82	20.74	10.52	11.11	18.07	28.89	48.89	13.63	2.22
Residual thickness (mm)	16.0	13.1	19.0	10.0	10.1	7.1	11.2	9.1	12.3	6.8	3.3	5.5
Component	**NO.13**	**NO.14**	**NO.15**	**NO.16**	**NO.17**	**NO.18**	**NO.19**	**NO.20**	**NO.21**	**NO.22**	**NO.23**	**NO.24**
Branches (g m^{-2})	62.81	27.11	26.22	80.59	105.33	5.63	62.81	27.11	26.22	57.33	45.19	68.22
Leaves (g m^{-2})	105.48	57.93	19.56	84.89	87.11	16.11	105.48	57.93	19.56	40.11	33.78	39.11
Fruits (g m^{-2})	19.85	16.74	3.33	20.15	25.04	16.89	19.85	16.74	3.33	21.78	17.19	7.78
Others (g m^{-2})	26.22	4.15	5.11	17.04	12.15	8.89	26.22	4.15	5.11	4.15	7.70	1.11
Residual thickness (mm)	14.0	24.5	33.0	19.1	6.9	19.0	28.0	16.0	9.7	14.2	25.0	8.1
Component	**NO.25**	**NO.26**	**NO.27**	**NO.28**	**NO.29**	**NO.30**	**NO.31**	**NO.32**	**NO.33**	**NO.34**	**NO.35**	**NO.36**
Branches (g m^{-2})	195.33	123.11	45.56	271.11	194.44	182.22	96.30	50.22	98.96	161.33	86.89	71.22
Leaves (g m^{-2})	45.33	31.33	12.11	44.22	21.00	22.22	66.52	22.67	9.78	76.67	40.44	25.22
Fruits (g m^{-2})	20.00	15.56	9.44	21.48	15.33	11.56	10.22	14.07	4.00	16.30	7.89	10.78
Others (g m^{-2})	2.07	5.19	6.07	3.33	9.78	5.78	7.56	51.70	4.89	6.52	4.33	13.89
Residual thickness (mm)	17.0	14.5	18.0	16.0	10.0	26.5	17.0	14.0	8.5	26.5	10.0	8.0

et al., 2017). In addition, the accumulation and redistribution process of plant residual can cause significant biological effects on the surface micro-environment and is an important factor affecting soil–plant nutrient cycling as well as wind erosion resistance (Sun et al., 2016; Parwada, 2017).

The present study undertook a simulated experiment using a wind tunnel, analyzing the amount of soil loss and its characteristics under simulated wind erosion. The main objective of this study was to quantitatively explore the effects of *Salix* residual on wind erosion resistance. This type of study may provide theoretical explanations for the optimal reconstruction of sandy vegetation in the agro-pastoral ecotone of northern China.

MATERIALS AND METHODS

Experimental Design

A simulated experiment was carried out in the simulation hall of the State Key Laboratory of Soil Erosion and Dryland Farming on the Loess Plateau at the Institute of Soil and Water Conservation, CAS. The soil used in the experiment was a typical silt loam soil with 0.9% clay, 8.3% silt, and 80.8% sand, collected from the top 20 cm soil in the *Salix* land at Dingbian County, Shaanxi Province (37°50.188′N, 107°28.941′E), China (**Figure 1**). The key hypothesis of this study is that wind erosion resistance of residual can be achieved by adjusting biomass, the soil–residual thickness, and the ratio of branches and leaves.

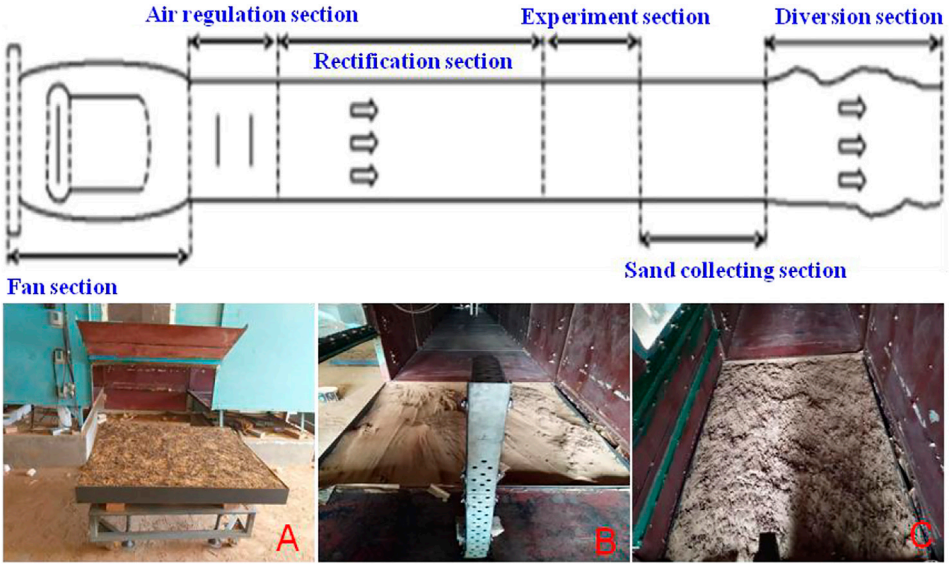

FIGURE 2 | Schematic diagram of the experiment wind tunnel structure and entity: **(A)** experiment slot; **(B)** sand collection; **(C)** status after simulated wind erosion.

According to the field investigation of 36 *Salix* sites in study areas (**Table 1**), the simulated experimental treatments examined in the present study were four residual biomass treatments of 200, 400, 600, and 800 g m^{-2}, three soil–residual thickness treatments of 0.5, 1.0, and 2.0 cm, and three ratios of branches and leaves of 2:1, 1:1, and 1:2, which derived from true conditions in the field as shown in **Figure 2**. In total, 22 experiment slots (10 treatments and 1 control, with 2 repetitions) were used in the present study. The experiment treatments were arranged on April 5–9, 2017. Then, the prepared experiment slots were sprayed with 3 L tap water three times at intervals of 10 days in order to eliminate the soil water effect. After that, the experiment slots were placed for 3 months in order to provide a similar environment to the field, and the simulated experiment was carried between August 2–15, 2017.

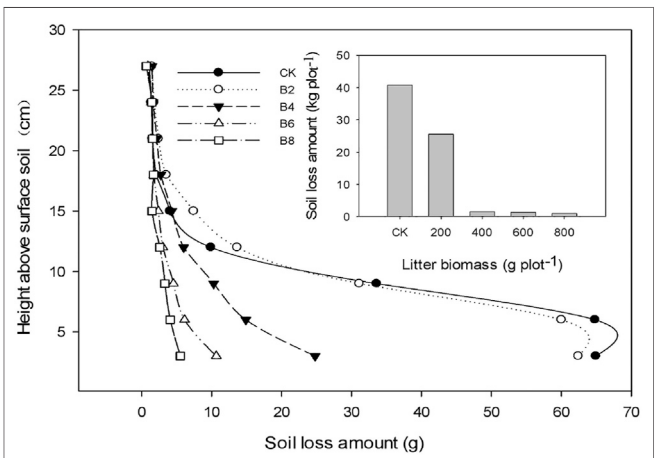

FIGURE 3 | Soil loss amount under different residual biomass.

Simulated Wind Tunnel and Experiment Process

The soil sample was passed through a 5-mm sieve after the removal of root fragments and was then air-dried. The wind tunnel came from the simulation hall of the State Key Laboratory of Soil Erosion and Dryland Farming on the Loess Plateau at the Institute of Soil and Water Conservation, CAS. The wind tunnel measured 24 × 1.2 × 1.0 m (length × width × height) and included a fan section, sections for wind regulation and rectification, an experimental section, and sections for sand collection and diversion (**Figure 2**). The regulation section could produce airflow with a stable field free of turbulence. The uniformity of airflow velocity was >99%, and the gradient of axial static pressure was <0.005. The wind speed could continuously vary from 0 to 15 m s^{-1} using a coordinated inverter in the fan section (Tuo et al., 2016). A vane anemometer, installed 0.2 m from the experimental section and 0.2 m above the tunnel floor, accurately (±0.2 m s^{-1}) adjusted the wind speed. The diversion section evacuated the airflow to maintain a clean laboratory environment. Soil loss above the surface was calculated as the ratio of the horizontal sediment flux to the length of the soil surface upwind of the sampler. The wind speed of 11 m s^{-1} and blow period of 15 min were used, which could represent a typical wind event in the Mu Us Sandy Land, China (Tuo et al., 2018). Soil collected in the sand collecting section from the surface soil to the height of the 0–30 cm wind tunnel at intervals of 3 cm collected from the bottom total amount of wind erosion. The soil loss amount was calculated by the weight difference of the experiment slot before/after simulated wind erosion. The advantage of this method is that it simulates environmental factors such as wind speed and representative composition and properties; however, the disadvantage is that the

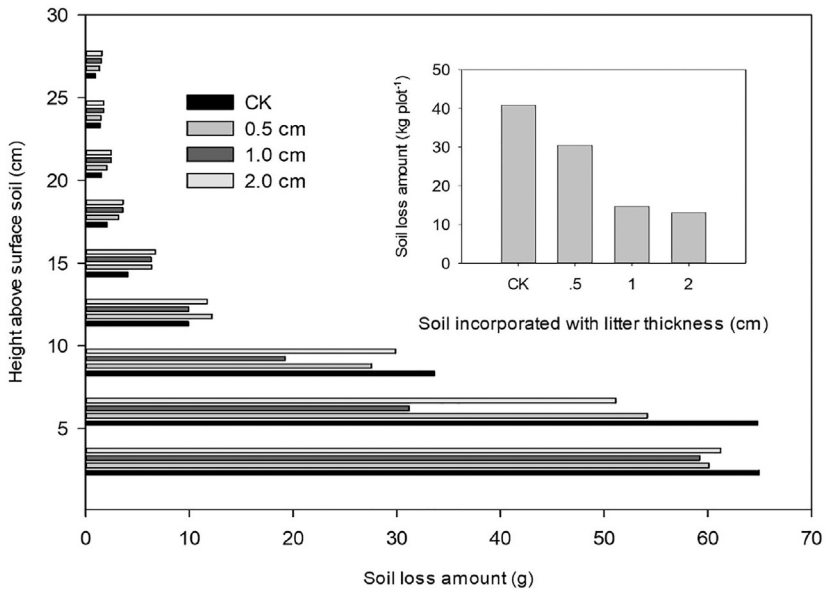

FIGURE 4 | Soil loss amount under soil incorporated with different residual thickness.

experimental plot area is limited and the marginal effect is large. This problem can be solved by increasing the sample size in the future.

Statistical Analysis

The mean of two repetitions for each treatment in the present study was used for data analysis. The effects of *Salix* residual biomass, the thickness of soil-incorporated residual, and the different ratios of *Salix* residual branches and leaves on wind erosion resistance were analyzed with Office 2017 and SigmaPlot 18.0.

RESULTS AND DISCUSSION

Effect of *Salix* Residual Biomass on Wind Erosion Resistance

Soil covered with plant residual could be especially valuable in the semi-arid regions (Zhang et al., 2017). **Figure 3** shows the relationship between soil loss amount and *Salix* residual biomass. Compared with CK, the soil loss amount ranged from 1.56 to 40.8 kg m^{-2} as *Salix* residual biomass increased from 200 to 800 g m^{-2}. Interestingly, there is a great difference in soil loss amount between treatments from 200 to 400 g m^{-2}, while little difference was observed among the treatments when residual biomass increased from 400 to 800 g. These observations suggest that the natural residual biomass status (400 g m^{-2}) may be notable for retarding soil wind erosion in study regions. Relative to the original surface soil, the soil loss amount was reduced at 37.4, 96.2, 96.6, and 97.5%, respectively, for treatments of 200, 400, 600, and 800 g m^{-2}. These results were in agreement with those of the latest studies which found that the thick, intact litter layer is an important agent for soil protection (Liu et al., 2017). For example, He et al. (2017) studied the effect of plant residue removal at 0, 25, 50, 75, and 100% of initial height on soil wind erosion and found that crop residual removal can affect the susceptibility to soil wind erosion in Kansas. Besides, **Figure 3** shows the soil loss amount was focused on 0–9 cm above the soil surface when the soil was incorporated with lower plant residual biomass (less than 400 g m^{-2}). Therefore, as *Salix* residual biomass decreased from 800 to 0 g m^{-2}, the soil loss amount ranged from 1.56 to 40.8 kg m^{-2}, and the critical residual biomass value was 400 g m^{-2}.

Effect of Soil Incorporated With *Salix* Residual on Wind Erosion Resistance

Plant residual is of great importance in retarding soil wind erosion in the agro-pastoral ecotone (Abdourhamane et al., 2019). Soil incorporated with plant residual is an important part of the ecological system, and its accumulation and redistribution could significantly affect soil surface soil–plant nutrient cycling and soil erosion resistance (Kamota et al., 2014; Guo et al., 2017). **Figure 4** shows that the soil loss amount reduced rapidly with the increment of soil-incorporated residual thickness. Compared with CK, the soil loss amount was reduced at 25.3, 63.9, and 67.8%, respectively, for treatments of soil-incorporated residual at the height of 0.5, 1, and 2 cm. For different layers above the soil surface, the soil loss amount of vertical 0–9 cm accounts for 81.2–89.2% of the total soil loss amount. In addition, the soil loss amount at the layers of 12–30 cm above the surface was similar among the treatments in the present study. This result was in agreement with the fact that the application of plant residual to soil can stabilize soil against soil erosion (He et al., 2017; Pi et al., 2018). Thus, as the thickness of soil incorporated residual increased, the soil loss amount reduced rapidly, especially for 0–9 cm above the surface, accounting for 84.6% of the total.

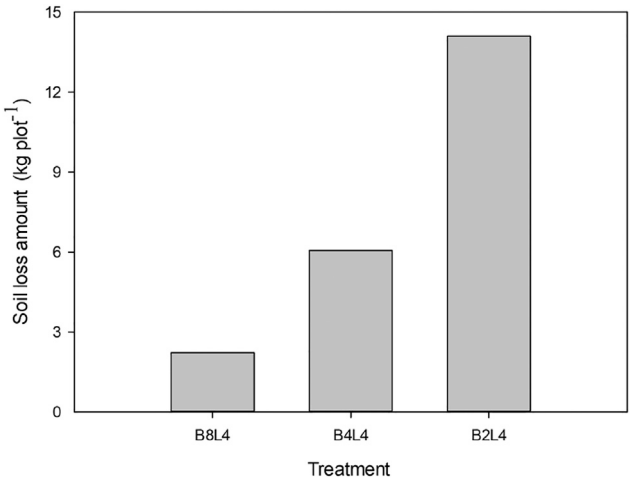

FIGURE 5 | Soil loss amount under different ratios of *Salix* residual branches and leaves.

Effect of *Salix* Residual Branches and Leaves on Wind Erosion Resistance

Plant residual could influence soil erosion resistance as it can alter the chemical and/or biological composition of the soil, which may influence soil's physical properties and/or plant growth and thus soil erosion resistance (He et al., 2017). For this reason, it is necessary to explore the contribution to retarding soil wind erosion between plant branches and leaves. **Figure 5** indicates that with the increasing ratios of *Salix* branches and leaves, the soil loss amount showed an increasing trend. By contrast, *Salix* branches are the key point in resisting soil wind erosion as compared with leaves in the present study. Such results may be ascribed to the larger wind speed of 11 m s^{-1}. Further study of the influence of near-surface wind speed on wind erosion (Li et al., 2014; Jiang et al., 2018) and the sustainability of the ecological benefits of sand plant residual needs to be conducted (Wu et al., 2019).

CONCLUSION

Based on field surveys, the influences of *Salix* residual biomass of 200, 400, 600, and 800 g m^{-2}, soil incorporated with residual thickness of 0.5, 1.0, and 2.0 cm, and typical proportion of residual branches and leaves (2:1, 1:1, and 1:2) on wind erosion resistance were investigated in silt loam by a wind tunnel experiment. The results showed that, in the simulated experiment, the soil loss amount ranged from 1.56 to 40.8 kg m^{-2} as *Salix* residual biomass decreased from 800 to 0 g m^{-2}, and a sharp decrease in the soil loss amount was found from treatments of 200 to 400 g m^{-2}. In addition, the soil loss amount reduced rapidly as the thickness of soil-incorporated residual increased, and the soil loss amount of 0–9 cm above the surface soil accounts for 84.6% of the total. Compared with *Salix* leaves, the branches are more important in resisting soil wind erosion in the agro-pastoral ecotone.

DATA AVAILABILITY STATEMENT

The original contributions presented in this study are included in the article/Supplementary Material, and further inquiries can be directed to the corresponding author.

AUTHOR CONTRIBUTIONS

QL designed and wrote this article, FK and ZZ conducted the experiment, and CM and WN analyzed the data.

FUNDING

Financial assistance for this study was provided by the projects of the National Natural Science Foundation of China (Grant Nos. 41807521, 41867015, 41661101), the Open Program of the State Key Laboratory of Soil Erosion and Dryland Farming on the Loess Plateau, Institute of Soil and Water Conservation, CAS and MWR (A314021402-1801), and young technology stars in Shaanxi Province (2020KJXX-037).

ACKNOWLEDGMENTS

We also express our gratitude to the reviewers and editors for their constructive comments and suggestions.

REFERENCES

Abdourhamane Touré, A., Tidjani, A. D., Rajot, J. L., Marticorena, B., Bergametti, G., Bouet, C., et al. (2019). Dynamics of Wind Erosion and Impact of Vegetation Cover and Land Use in the Sahel: A Case Study on sandy Dunes in southeastern Niger. *Catena* 177, 272–285. doi:10.1016/j.catena.2019.02.011

Guo, Z., Chang, C., Wang, R., and Li, J. (2017). Comparison of Different Methods to Determine Wind-Erodible Fraction of Soil with Rock Fragments under Different Tillage/management. *Soil Tillage Res.* 168, 42–49. doi:10.1016/j.still.2016.12.008

He, W. (2014). *Vegetation Characteristics and its Response to Soil Erosion in Mu Us Desert*. Hohhot, China: Inner Mongolia Agricultural University.

He, Y., Presley, D. A. R., Tatarko, J., and Blanco-Canqui, H. (2017). Crop Residue Harvest Impacts Wind Erodibility and Simulated Soil Loss in the central Great plains. *GCB Bioenergy* 10, 3–10. doi:10.1111/gcbb.12483

Jiang, Y., Gao, Y., Dong, Z., Liu, B., and Zhao, L. (2018). Simulations of Wind Erosion along the Qinghai-Tibet Railway in north-central Tibet. *Aeolian Res.* 32, 192–201. doi:10.1016/j.aeolia.2018.03.006

Kamota, A., Muchaonyerwa, P., and Mnkeni, P. N. S. (2014). Decomposition of Surface-Applied and Soil-Incorporated Bt Maize Leaf Litter and Cry1Ab Protein during Winter Fallow in South Africa. *Pedosphere* 24, 251–257. doi:10.1016/s1002-0160(14)60011-4

Li, J., Jia, H., Han, X., Zhang, J., Sun, P., and Lu, M. (2016). Selection of Reliable Reference Genes for Gene Expression Analysis under Abiotic Stresses in the

Desert Biomass Willow, salix Psammophila. *Front. Plant Sci.* 7, 11–13. doi:10.3389/fpls.2016.01505

Li, Q., Liu, G.-B., Zhang, Z., Tuo, D.-F., Bai, R.-r., and Qiao, F.-f. (2017). Relative Contribution of Root Physical Enlacing and Biochemistrical Exudates to Soil Erosion Resistance in the Loess Soil. *Catena* 153, 61–65. doi:10.1016/j.catena.2017.01.037

Li, Q., Liu, G., Zhang, Z., Tuo, D., and Miao, X. (2016). Structural Stability and Erodibility of Soil in an Age Sequence of Artificial Robinia Pseudoacacia on a Hilly Loess Plateau. *Pol. J. Environ. Stud.* 25, 1595–1601. doi:10.15244/pjoes/62390

Li, Q., Liu, N., Zhang, Z., Ma, C. Y., Yu, W. J., and Nan, W. G. (2020). Features of the Distribution of Salix Residual in the South Edge of Mu Us Sandy Land of China. *Drought meteorology* 38 (2), 313–318.

Li, X., Niu, J., and Xie, B. (2014). The Effect of Leaf Residual Cover on Surface Runoff and Soil Erosion in Northern China. *Plos One* 9, 77–89. doi:10.1371/journal.pone.0107789

Liu, W., Luo, Q., Lu, H., Wu, J., and Duan, W. (2017). The Effect of Litter Layer on Controlling Surface Runoff and Erosion in Rubber Plantations on Tropical Mountain Slopes, SW China. *Catena* 149, 167–175. doi:10.1016/j.catena.2016.09.013

Parwada, C. (2017). *Residual Quality Effects on Soil Stability and Erodibility*.

Pi, H., Sharratt, B., Schillinger, W. F., Bary, A. I., and Cogger, C. G. (2018). Wind Erosion Potential of a winter Wheat-Summer Fallow Rotation after Land Application of Biosolids. *Aeolian Res.* 32, 53–59. doi:10.1016/j.aeolia.2018.01.009

Sun, L., Zhang, G.-h., Liu, F., and Luan, L.-l. (2016). Effects of Incorporated Plant Litter on Soil Resistance to Flowing Water Erosion in the Loess Plateau of China. *Biosyst. Eng.* 147, 238–247. doi:10.1016/j.biosystemseng.2016.04.017

Sun, L., Zhang, G.-h., Luan, L.-l., and Liu, F. (2016). Temporal Variation in Soil Resistance to Flowing Water Erosion for Soil Incorporated with Plant Litters in the Loess Plateau of China. *Catena* 145, 239–245. doi:10.1016/j.catena.2016.06.016

Tuo, D., Xu, M., and Gao, G. (2018). Relative Contributions of Wind and Water Erosion to Total Soil Loss and its Effect on Soil Properties in Sloping Croplands of the Chinese Loess Plateau. *Sci. Total Environ.* 633, 1032–1040. doi:10.1016/j.scitotenv.2018.03.237

Tuo, D., Xu, M., Gao, L., Zhang, S., and Liu, S. (2016). Changed Surface Roughness by Wind Erosion Accelerates Water Erosion. *J. Soils Sediments* 16, 105–114. doi:10.1007/s11368-015-1171-x

Wang, Y., Dong, Y., Su, Z., Mudd, S. M., Zheng, Q., Hu, G., et al. (2020). Spatial Distribution of Water and Wind Erosion and Their Influence on the Soil Quality at the Agropastoral Ecotone of North China. *Int. Soil Water Conservation Res.* 8, 253–265. doi:10.1016/j.iswcr.2020.05.001

Wu, Z., Wang, M., Zhang, H., and Du, Z. (2019). Vegetation and Soil Wind Erosion Dynamics of Sandstorm Control Programs in the Agro-Pastoral Transitional Zone of Northern china. *Front. Earth Sci.* 13 (2), 430–443. doi:10.1007/s11707-018-0715-y

Yu, X., Huang, Y., Li, E., Li, X., and Guo, W. (2017). Effects of Vegetation Types on Soil Water Dynamics during Vegetation Restoration in the Mu Us sandy Land, Northwestern China. *J. Arid Land* 9, 188–199. doi:10.1007/s40333-017-0054-y

Zhang, G., Azorin-Molina, C., Shi, P., Lin, D., Guijarro, J. A., Kong, F., et al. (2019). Impact of Near-Surface Wind Speed Variability on Wind Erosion in the Eastern Agro-Pastoral Transitional Zone of Northern China, 1982-2016. *Agric. For. Meteorology* 271, 102–115. doi:10.1016/j.agrformet.2019.02.039

Zhang, J.-Q., Zhang, C.-L., Chang, C.-P., Wang, R.-D., and Liu, G. (2017). Comparison of Wind Erosion Based on Measurements and Sweep Simulation: a Case Study in Kangbao County, Hebei Province, china. *Soil Tillage Res.* 165, 169–180. doi:10.1016/j.still.2016.08.006

Zhang, J., Yang, M., Deng, X., Liu, Z., Zhang, F., and Zhou, W. (2018). Beryllium-7 Measurements of Wind Erosion on Sloping fields in the Wind-Water Erosion Crisscross Region on the Chinese Loess Plateau. *Sci. Total Environ.* 615, 240–252. doi:10.1016/j.scitotenv.2017.09.238

Zhang, Y., and Zhao, W. (2015). Vegetation and Soil Property Response of Short-Time Fencing in Temperate Desert of the Hexi Corridor, Northwestern China. *Catena* 133, 43–51. doi:10.1016/j.catena.2015.04.019

Zhao, H., Wu, Q., and Liu, G. (2003). Studies on Soil and Water Conservation Functions of Residual in Chinese pine Stand on Loess Plateau. *Scientia Silvae Sinicae* 39, 168–172.

Conflict of Interest: The authors declare that the research was conducted in the absence of any commercial or financial relationships that could be construed as a potential conflict of interest.

Publisher's Note: All claims expressed in this article are solely those of the authors and do not necessarily represent those of their affiliated organizations, or those of the publisher, the editors and the reviewers. Any product that may be evaluated in this article, or claim that may be made by its manufacturer, is not guaranteed or endorsed by the publisher.

Advantages of publishing in Frontiers

OPEN ACCESS
Articles are free to read for greatest visibility and readership

FAST PUBLICATION
Around 90 days from submission to decision

HIGH QUALITY PEER-REVIEW
Rigorous, collaborative, and constructive peer-review

TRANSPARENT PEER-REVIEW
Editors and reviewers acknowledged by name on published articles

Frontiers
Avenue du Tribunal-Fédéral 34
1005 Lausanne | Switzerland

Visit us: www.frontiersin.org
Contact us: frontiersin.org/about/contact

REPRODUCIBILITY OF RESEARCH
Support open data and methods to enhance research reproducibility

DIGITAL PUBLISHING
Articles designed for optimal readership across devices

FOLLOW US
@frontiersin

IMPACT METRICS
Advanced article metrics track visibility across digital media

EXTENSIVE PROMOTION
Marketing and promotion of impactful research

LOOP RESEARCH NETWORK
Our network increases your article's readership